EMERGING INFECTIOUS DISEASES®

U.S. CENTERS FOR DISEASE CONTROL AND PREVENTION

Vaccine-Preventable Diseases

October 2026

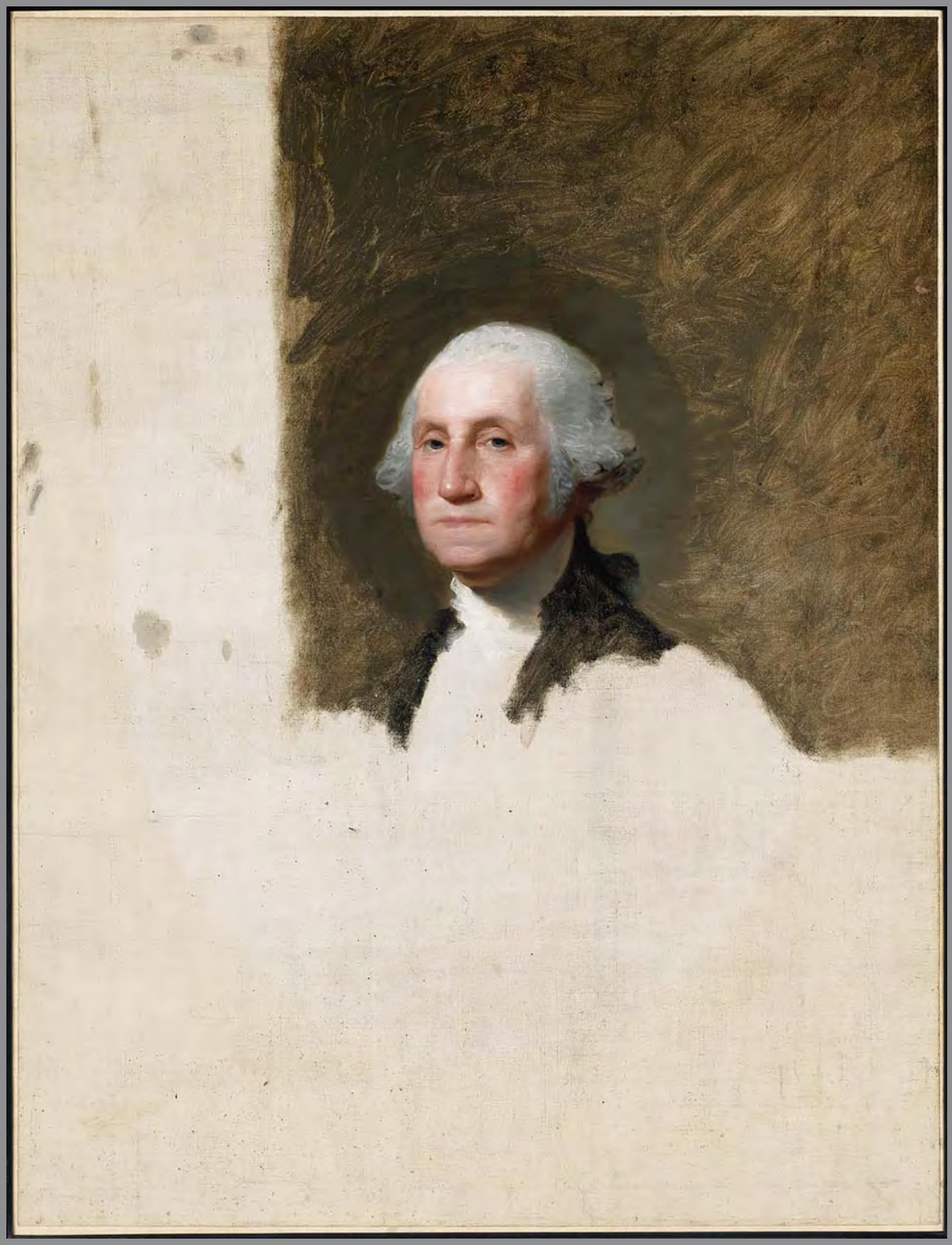

Gilbert Stuart, George Washington, 1796. Oil on canvas. 121.9 cm × 94 cm (48 in × 37 in). Museum of Fine Arts, Boston, Massachusetts, USA. Co-owned by the National Portrait Gallery, Washington, DC, USA.

Pages 1537–1776

EMERGING INFECTIOUS DISEASES

A Peer-Reviewed Journal Tracking and Analyzing Disease Trends

Emerging Infectious Diseases is published monthly by the Centers for Disease Control and Prevention, 1600 Clifton Rd NE, Mailstop H16-2, Atlanta, GA 30329-4018, United States. Telephone 404-639-1960; email eideditor@cdc.gov

EMERGING INFECTIOUS DISEASES®

Vaccine-Preventable Diseases **October 2026**

On the Cover

Gilbert Stuart, George Washington, 1796. Oil on canvas. 121.9 cm × 94 cm (48 in × 37 in). Museum of Fine Arts, Boston, Massachusetts, USA. Co-owned by the National Portrait Gallery, Washington, DC, USA.

About the Cover p. 1772

Perspective

Synopses

Medscape EDUCATION ACTIVITY

Research

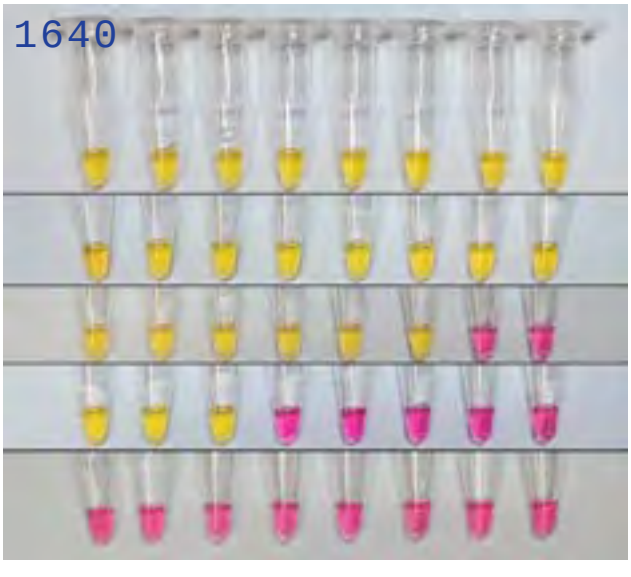

Historical Review

Dispatches

EMERGING INFECTIOUS DISEASES®
October 2026

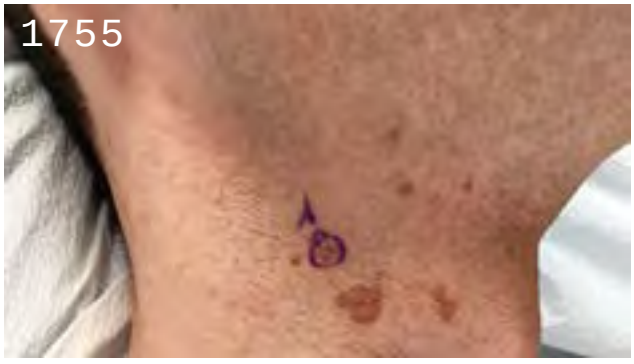

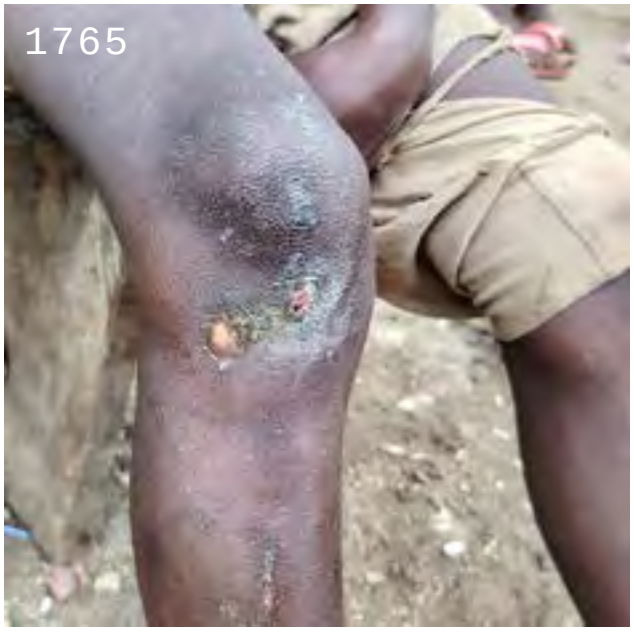

1680

Research Letters

EMERGING INFECTIOUS DISEASES®

October 2026

In Memoriam

About the Cover

1769

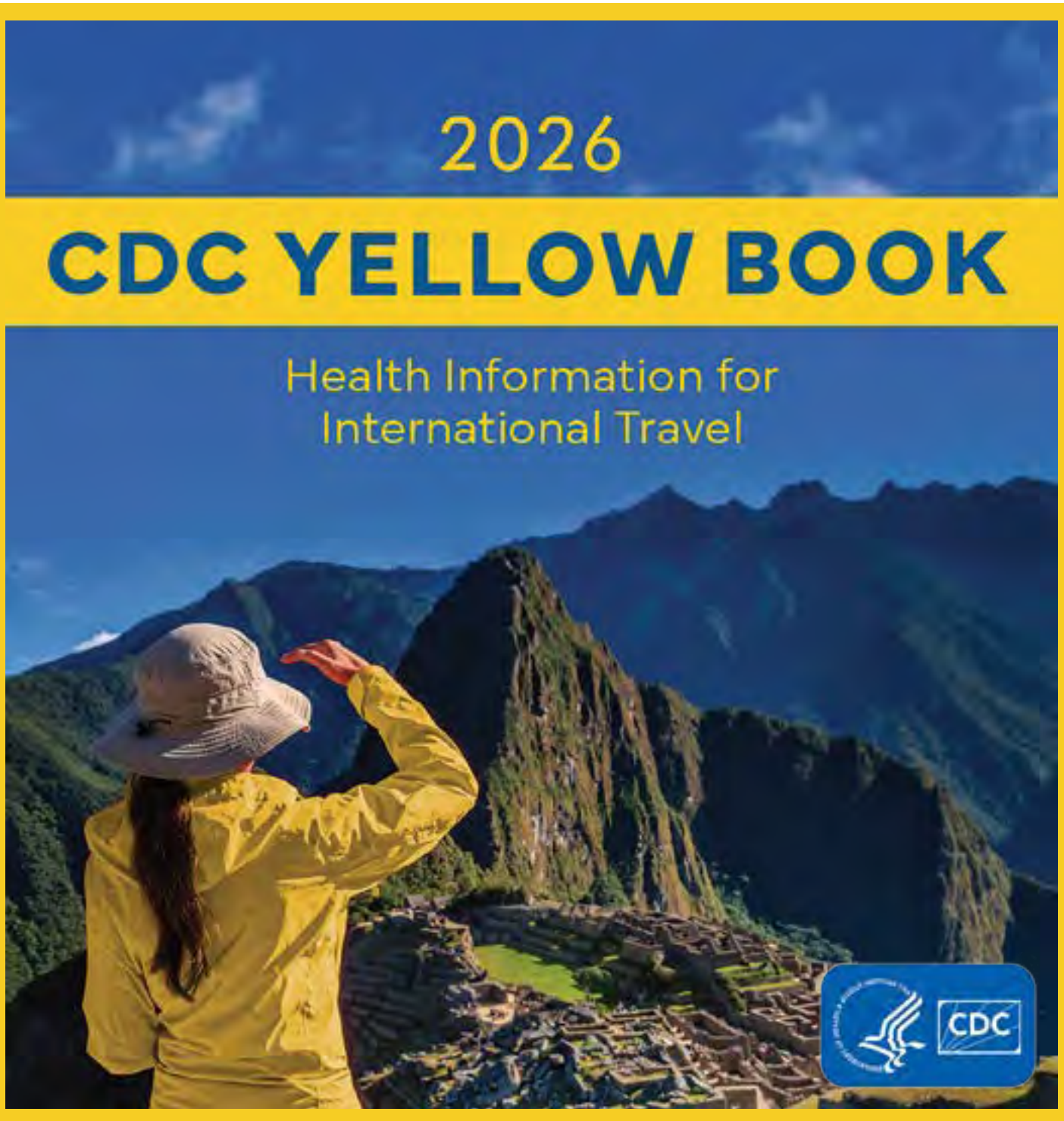

Launch of CDC Yellow Book 2026– A Trusted Travel Medicine Resource

CDC is pleased to announce the launch of the **CDC Yellow Book 2026**. The CDC Yellow Book is a resource containing the U.S. government's travel medicine recommendations and has been trusted by the travel medicine community for over 50 years. Healthcare professionals can use the print and digital versions to find the most up-to-date travel medicine information to better serve their patients' healthcare needs.

The CDC Yellow Book is available online now at www.cdc.gov/yellowbook and in print starting in June 2025 through Oxford University Press and other major online booksellers.

Reassortment of Highly Pathogenic Avian Influenza as a Driver for Zoonotic Spillover, Asia

Alexander M.P. Byrne,[1] Lorcan Carnegie,[1] Nicola S. Lewis, Ian G. Barr, Erik A. Karlsson, Michelle Wille

Highly pathogenic avian influenza H5Nx viruses remain a major zoonotic threat, yet global attention has focused largely on clade 2.3.4.4b, potentially overlooking major changes within long-endemic H5N1 lineages in Asia. Recent reports from South and Southeast Asia describe the emergence of reassortant clade 2.3.2.1 viruses alongside renewed human infections after apparent prolonged epidemiologic stability. Collectively, those events suggest a regional pattern rather than isolated anomalies. In this article, we argue that reassortment, rather than point mutation alone, might be an underrecognized driver of zoonotic risk in endemic H5N1 lineages and is reshaping those lineages. We examine why such events might be underrecognized in settings with entrenched poultry influenza, identify limitations of current surveillance systems, and call for integrated, real-time approaches linking genomic detection with phenotypic assessment across animal and human health sectors to enable timely risk assessment and coordinated public health action.

Avian influenza viruses (AIVs) remain among the most identifiable but unpredictable threats to both public health and food security (*1*–*4*). Since their emergence in 1996, highly pathogenic avian influenza (HPAI) H5Nx viruses of the A/goose/Guangdong/1/1996 lineage have spread globally, heavily devastating poultry production and repeatedly spilling over into mammals, including humans, often with fatal outcomes. As of August 30, 2025, the World Health Organization (WHO) has reported 990 laboratory-confirmed H5N1 human cases across ≥25 countries, including 475 deaths (*5*). Since the onset of the HPAI H5Nx panzootic in 2021, the global focus has been on clade 2.3.4.4b, given its dramatic global spread. The focus on clade 2.3.4.4b is warranted given the spillover to and circulation in dairy cattle and the increase in human cases associated with those outbreaks, because those issues raise substantial concerns that the viruses might emerge as a future human pandemic. However, the focus on clade 2.3.4.4b risks obscuring major evolutionary and zoonotic changes within more ancestral but persistent H5N1 clade 2.3.2.1 lineages, which remain enzootic in parts of Asia and receive limited global attention.

Evolutionary Diversification and Resurgence of Zoonotic Infections in Clade 2.3.2.1 Viruses

HPAI H5N1 clade 2.3.2.1 emerged in 2007 and subsequently spread across Asia and into Europe (*6*,*7*). Continued circulation in Asia led to further classification into subclades 2.3.2.1a, 2.3.2.1b, and 2.3.2.1c in 2014. Because the viruses have continued to evolve, 2.3.2.1c has been further reclassified into subclades 2.3.2.1d–g (*6*,*8*). That diversification reflects regional geography and poultry production systems, such that at present those viruses predominately circulate in live bird markets; clade 2.3.2.1a has predominately been detected in poultry in Bangladesh and India, and 2.3.2.1e circulates in Cambodia, Laos, and Vietnam (*1*,*9*–*11*; A.A. Raut et al., unpub. data, https://www.biorxiv.org/content/10.1101/2025.02.23.638954v1). Beyond 2.3.2.1a and 2.3.2.1e, the only other subclade that continues to be detected (2.3.2.1g) is restricted to poultry in Indonesia (*12*; T.T. Lam et al., unpub. data, https://www.biorxiv.org/content/10.1101/2025.11.23.690055v1). The remaining 2.3.2.1 subclades were previously found to have circulated

Author affiliations: Worldwide Influenza Centre, The Francis Crick Institute, London, UK (A.M.P. Byrne, N.S. Lewis); Food and Agriculture Organization of the United Nations, Rome, Italy (L. Carnegie); World Health Organization Collaborating Centre for Reference and Research on Influenza, Peter Doherty Institute for Infection and Immunity, University of Melbourne, Melbourne, Victoria, Australia (I.G. Barr, M. Wille); Institut Pasteur du Cambodge, Phnom Penh, Cambodia (E.A. Karlsson); Environment and Infectious Risks Unit, Laboratory for Urgent Response to Biological Threats, Institut Pasteur, Paris, France (E.A. Karlsson)

DOI: https://doi.org/10.3201/eid3210.260067

[1]These first authors contributed equally to this article.

predominantly in poultry in Asia; China (2.3.2.1b, 2.3.2.1d, and 2.3.2.1f), Hong Kong (2.3.2.1b and 2.3.2.1c), India (2.3.2.1f), Mongolia (2.3.2.1c), Nepal (2.3.2.1c), Japan (2.3.2.1c), Vietnam (2.3.2.1b), the Middle East (2.3.2.1f), Africa (2.3.2.1f), and Europe (2.3.2.1c), but very few cases have been detected since 2020 (T.T. Lam et al., unpub. data).

Before 2015, HPAI H5N1 virus clade 2.3.2.1 caused 1 human infection across Cambodia, India, and Bangladesh; in subsequent years, the clade became enzootic and ecologically stable in poultry within those countries but was associated with relatively few reported human infections (Figure 1). Since 2023, a measurable rise in human infections caused by clade 2.3.2.1 virus has been observed. During February 2023–November 19, 2025, Cambodia reported 34 HPAI H5N1 cases after nearly a decade without confirmed infections, based on notifications to WHO and sequence data from GISAID (*13*) and GenBank (*14*). In parallel, 6 HPAI H5N1 human cases were reported in India and Bangladesh in 2025 alone (*15*).

Alarmingly, all HPAI H5N1 human infections since October 2023 were caused by reassortants from viral backgrounds with distinct ecologic and evolutionary characteristics: long-circulating enzootic clade 2.3.2.1 lineages, HPAI H5N1 clade 2.3.4.4b, and low pathogenicity avian influenza (LPAI). Specifically, in Cambodia, all recent human infections have involved reassortant viruses containing hemagglutinin (HA), neuraminidase (NA), and nucleoprotein (NP) gene segments from clade 2.3.2.1e viruses and internal gene segments likely derived from clade 2.3.4.4b (polymerase basic [PB] 2, matrix protein [MP], nonstructural [NS]) and LPAI (PB1 and polymerase acidic [PA]) viruses (Figure 2) (*11*). This genotype is now dominant in poultry in Cambodia (*11*). In parallel, reassortant clade 2.3.2.1a viruses have caused 2 human cases in India (*15*) and 4 cases in Bangladesh in 2025 (*5*,*15*,*16*) and was detected in a person traveling from India to Australia in 2024 (*9*). Those viruses retained the clade 2.3.2.1a HA, NA, NP, and NS gene segments but had internal gene segments likely derived from a combination of clade 2.3.4.4b (PB2 and MP) or LPAI (PB1 and PA) viruses (Figure 2).

Possible Increased Zoonotic Risk for Clade 2.3.2.1 Viruses from Underdetected Reassortments

Reassortment is well recognized as the mechanism underlying all human influenza pandemic viruses in the 20th Century (*4*,*17*–*19*). In the context of HPAI

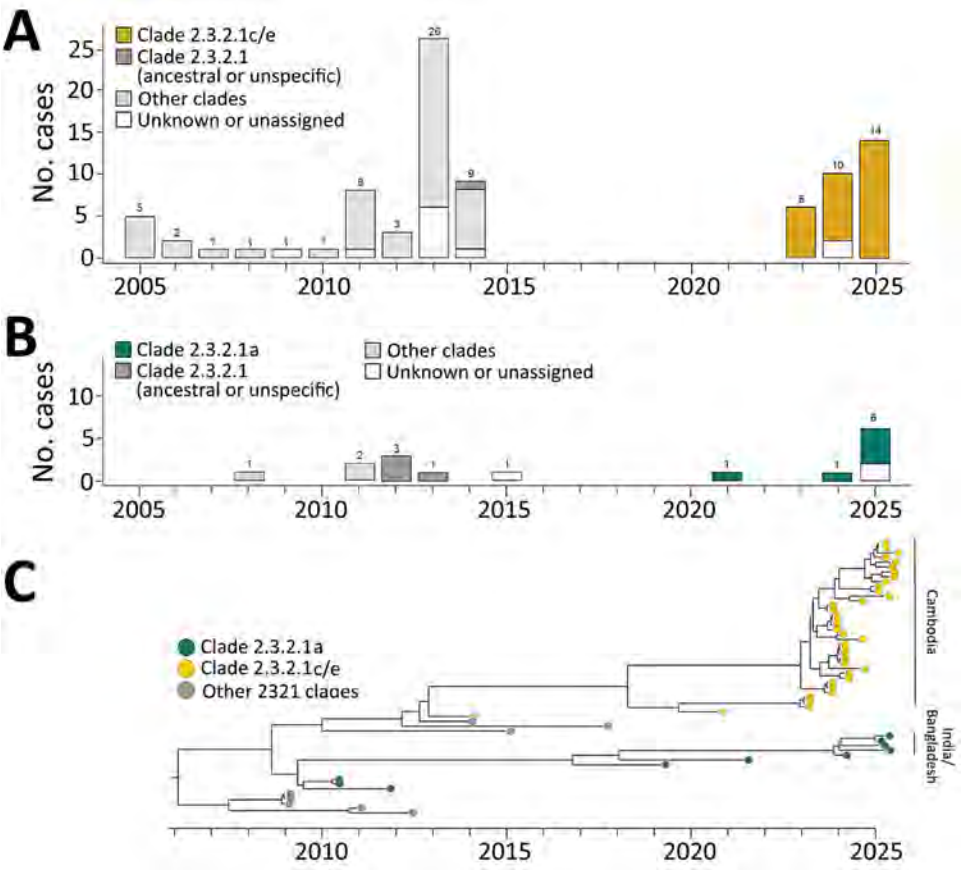

Figure 1. Emergence and human case trends of highly pathogenic avian influenza (HPAI) H5N1 clade 2.3.2.1 viruses in study of reassortment of HPAI as a driver for zoonotic spillover, Asia. A, B) Case notification data of HPAI H5N1 in Cambodia (A) and India and Bangladesh (B), demonstrating the clear resurgence of zoonotic spillover occurring in 2023, driven by reassortant clade 2.3.2.1c/e and 2.3.2.1a viruses. C) Time-scaled phylogeny of the H5 hemagglutinin gene for clade 2.3.2.1 viruses, highlighting the divergence of clade 2.3.2.1a and clade 2.3.2.1c/e.

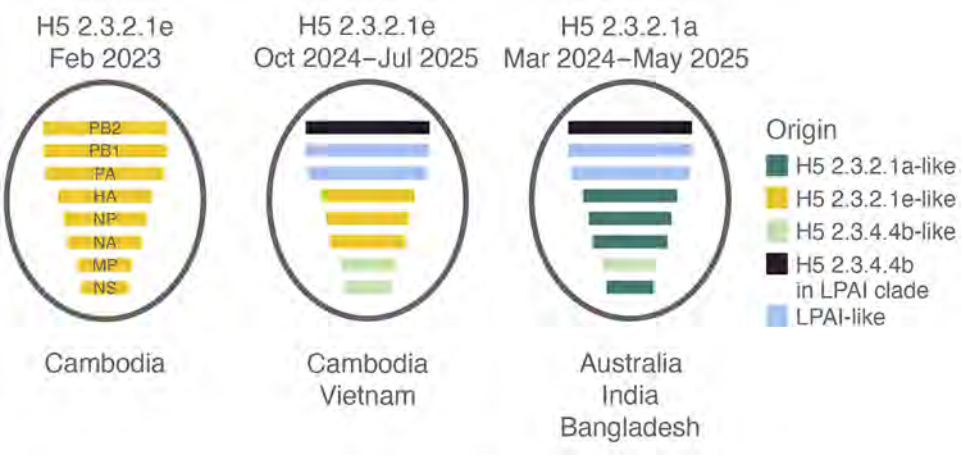

Figure 2. Simplified schematic of the segment constellations of identified human reassortant viruses in study of reassortment of highly pathogenic avian influenza as a driver for zoonotic spillover, Asia. Figure demonstrates the origin of each genomic segment (H5 clade 2.3.2.1a, 2.3.2.1e, 2.3.4.4b, LPAI, or H5 clade 2.3.4.4b within an LPAI clade 2.3.4.4b) by country of detection. Australia detection was in a person traveling to Australia from India. HA, hemagglutinin; LPAI, low pathogenicity avian influenza; MP, matrix protein; NA, neuraminidase; NP, nucleoprotein; NS, nonstructural; PA, polymerase acidic; PB, polymerase basic.

H5N1 clade 2.3.2.1, both 2.3.2.1a and 2.3.2.1e clades have undergone reassortment in the past, but available data suggest that, in the decade before the recent reassortants emerged, they were characterized by relatively stable gene constellations (*20*,*21*). In contrast, clade 2.3.4.4b viruses have been marked by frequent reassortment (*22*,*23*; J. Baxter et al., unpub. data, https://www.biorxiv.org/content/10.1101/2025.07.19.665680v2). The emergence of reassortants between clades 2.3.4.4b and 2.3.2.1 viruses might therefore reshape the epidemiology of clade 2.3.2.1 viruses, challenging long-held assumptions about their behavior in poultry systems and their associated zoonotic risk (*11*; W.T. Harvey, unpub. data, https://www.biorxiv.org/content/10.1101/2025.08.20.670882v1).

We hypothesize that the potential epidemiologic changes in HPAI H5N1 clade 2.3.2.1a/e viruses, coinciding with phenotypic changes from the reassortment, might have increased opportunities for zoonotic spillover in Asia. Specifically, we propose that those reassortants emerged and circulated in poultry before they were detected in humans and that they might have gained a fitness or transmission advantage in poultry that increased human exposure. Testing for those potential changes is currently constrained by a key knowledge gap: the gene constellations of viruses circulating in poultry in Asia before the human detections have not been systematically characterized. That gap means neither the origin nor the prevalence of the reassortants can be comprehensively established. Resolving the gap in the short term will require retrospective testing of archived poultry samples collected before the recognized human cases (where available) and, in the longer term, improved surveillance systems. Detecting the reassortant constellations in such samples would support previous circulation in poultry; its absence would instead point to a fitness advantage for mammalian adaptation rather than poultry transmission. To our knowledge, no such systematic retrospective screening has yet been reported, and it should be prioritized to clarify the directionality of spillover.

Key research in epidemiology and phenotypic characterization is needed to test our hypotheses. So far, we have not observed a rise in poultry prevalence before human infections caused by the reassortants; however, in the HPAI H5N1 enzootic poultry systems where outbreaks are often underreported, confirming whether the true prevalence has increased is challenging. To understand that question, more timely and sensitive surveillance and phylogenetic and epidemiologic analyses are needed. We also do not know whether reassortment itself caused a phenotypic advantage in causing zoonotic infections. Further phenotypic characterization is needed to elucidate the potential mechanisms through which these reassortants gained the ability to cause zoonotic infections.

Although a direct causal link between those specific reassortment events and the increase in recent human infections in Asia has not yet been demonstrated, current research in Cambodia and available sequence data from other countries, such as Bangladesh, demonstrate a clear association (*9*,*11*). It is of particular concern that those reassortants combine gene segments from viral backgrounds with distinct ecologic and evolutionary characteristics. Therefore, we argue that, in general, reassortment is a key evolutionary mechanism shaping zoonotic risk for HPAI H5N1. Accordingly, we highlight the gap in current surveillance systems and propose an improved system to detect and interpret avian influenza virus strains of zoonotic risk.

Limited Real-Time, Integrated Approach to Detecting and Interpreting Risk

Current surveillance systems have key limitations in detecting and interpreting reassortment events. The issue is not only whether a reassortant virus is detected but whether its significance is recognized early enough to enable appropriate mitigation strategies to be implemented. In many endemic poultry settings, surveillance still relies heavily on clade-level reporting and targeted monitoring of known mammalian-adaptive mutations or antigenic markers (*24*–*27*), rather than routine whole-genome sequencing (WGS) and integrated genotype-level analysis. That factor can obscure substantial underlying genetic change, creating a false impression of continuity even when viruses have acquired novel internal gene constellations with considerable phenotypic consequences. Reassortants might therefore be underdetected or detected only after they are associated with human cases. Even when WGS data are available, genetic constellations alone rarely reveal when reassortment occurred, how long the reassortant has circulated, or whether it has altered viral fitness, host range, transmissibility, or antigenicity. Those questions require timely phylogenetic analysis, phenotypic characterization, antigenic testing, and epidemiologic investigation. Strengthened surveillance capacity after the COVID-19 pandemic might partly explain increased detection of human infections but does not remove the need for systems capable of identifying sustained influenza reassortment events earlier and assessing whether they represent a meaningful change in zoonotic risk.

Improved Surveillance for Detecting, Analyzing, and Interpreting Reassortment

A reimagined approach to monitoring zoonotic risk requires real-time tracking of major and sustained reassortment events, supported by systems that can detect, share, and interpret genomic, phenotypic, and epidemiologic data as those events unfold. Near–real-time WGS and data sharing are essential for identifying emerging reassortant viruses, particularly at high-risk interfaces where wild and domestic birds interact, including live bird markets, backyard poultry systems, farms, and wetlands. Those steps would improve on current systems by moving beyond clade-level reporting and targeted screening for known mammalian-adaptive markers, which can miss key changes in internal gene constellations. Newly emerging genotypes should be assessed through phylogenetic analysis, epidemiologic investigation, and routine phenotypic characterization. In addition, emerging computational approaches, such as CoalRe (*28*) and TreeSort (*29*), could help reconstruct the evolutionary history of reassortment events, estimate their timing and persistence, and guide surveillance and control strategies to assist with detecting emerging novel genotypes. However, the outputs of such tools must be evaluated in the context of epidemiologic and phenotypic data.

Once sustained reassortment is identified, phenotypic testing is needed to evaluate the biological risk posed by the viruses, assess whether they remain matched to existing candidate vaccine viruses, and contextualize the genomic data. Ideally, that step should occur even in the absence of recognized human cases, enabling timely risk interpretation before zoonotic infections are detected. This factor is particularly key because available evidence suggests that reassortant viruses might already have been circulating in poultry in Bangladesh and Cambodia (*11*) before the first recognized reassortant-associated human cases. Testing whether reassortment increases zoonotic risk would require comparisons with other circulating poultry genotypes, estimates of how frequently similar reassortants arise, mammalian infection data, phenotypic characterization, and analyses of when reassortment occurred and how long reassortant viruses circulated before detection. Those tactics could help determine whether reassortment has altered viral fitness, host range, transmissibility, antigenicity, or zoonotic risk.

To summarize, surveillance for reassortants with potential zoonotic risk should be structured as a linked and sometimes iterative pathway: sample collection; laboratory testing, including PCR, WGS, data sharing, virus isolation, and phenotypic characterization; data collation and analysis to enable risk interpretation; and wider data sharing to the scientific community and public detailing the perceived risk and appropriate mitigation measures. Systematic sampling across high-risk interfaces would improve the chance of detecting reassortants before they are recognized through human infections. PCR and WGS would enable novel gene constellations to be identified and compared with other circulating poultry genotypes, whereas virus isolation and phenotypic characterization would help determine whether those viruses show altered replication, host range, antigenicity, vaccine–virus match, or other traits relevant to zoonotic risk. Data collation and WGS phylogenetic/phylodynamic analyses that have been designed to track reassortment patterns should then be used to estimate how frequently similar reassortants arise, when reassortment occurred, how long reassortant viruses have circulated, and

whether they are associated with mammalian infections or changes in poultry virus dynamics. For that process to work, surveillance systems need sustained sampling, sequencing capacity, virus isolation facilities, standardized phenotypic assays, analytical tools, trained personnel, interoperable databases, and timely data-sharing mechanisms. In that framework, the hypothesis that reassortment has increased the zoonotic capacity of circulating viruses can be tested directly, rather than suggested only after an increase in human infections is detected.

Ultimately, achieving this vision requires integrated cross-sector systems rather than isolated or duplicated efforts. To enable timely phenotypic analyses, laboratory access to viruses is essential and should be supported by routine peacetime virus-sharing frameworks and predefined decision points for triggering further investigation that can feed into existing initiatives such as the WHO Tool for Influenza Pandemic Risk Assessment (*30*). Those activities, from field surveillance to phenotypic characterization, must also be conducted in a coordinated manner across multiple stakeholders to prevent unnecessary duplication, particularly given the limited resources available, while also ensuring rapid identification and assessment of novel and emerging viruses. Effective mechanisms for joint risk assessment and 2-way genomic data exchange between animal and public health authorities are essential to ensure that emerging genetic findings trigger proportionate and coordinated One Health responses, including clarity on whether the genotypes or amino acid changes detected in human outbreaks reflect those circulating in animal populations. Ideally, surveillance systems would be integrated across animal, human and environmental sectors through interoperable platforms with standardized metadata, enabling rapid identification of emerging genomic constellations and direct comparison with zoonotic cases. Without systems that connect animal and human data streams in real time, reassortant or adaptive events will continue to be detected retrospectively or with substantial delay, increasing the risk for onward human transmission.

In conclusion, the perceived resurgence of HPAI H5N1 infections in humans caused by reassortant clade 2.3.2.1 viruses in South and Southeast Asia is more than an epidemiologic footnote; it is a warning. Such events illustrate how reassortment within long-overlooked Asia HPAI H5N1 lineages is reshaping zoonotic risk, potentially driven by intensifying poultry production, shifting wild bird migration patterns, and intensively shared human–animal interfaces. Yet current surveillance systems are not configured to detect such evolutionary shifts in real time. Unless surveillance is reimagined to capture and interpret reassortment as it occurs through integrated One Health approaches that connect animal, environmental, and human data streams and translate genomic signals into coordinated action, the next warning might not appear in a dataset or sequence repository, but instead as an outbreak already beyond our control.

Acknowledgments

We thank everyone involved in the critical discussions and review of this manuscript, as well as all those contributing to live bird market and influenza surveillance and response globally. We gratefully acknowledge all data contributors (i.e., the authors and their originating laboratories responsible for obtaining the specimens and their submitting laboratories for generating the genetic sequence and metadata and sharing through the GISAID Initiative on which this research is based). The text as published does not necessarily represent the official views of the Food and Agriculture Organization of the United Nations, the World Organisation for Animal Health, or OFFLU.

A.M.P.B., L.C., and M.W. performed bioinformatics analysis, data curation and validation, data visualization and manuscript writing. All authors conceptualized the study and reviewed/edited the manuscript. All authors substantially contributed to the discussion of content.

About the Author

Dr. Byrne is the senior bioinformatician at the Worldwide Influenza Centre, WHO Collaborating Centre for Reference and Research on Influenza at the Francis Crick Institute. His research focuses on understanding influenza evolution and factors involved in cross-species transmission.

References

1. Charostad J, Rezaei Zadeh Rukerd M, Mahmoudvand S, Bashash D, Hashemi SMA, Nakhaie M, et al. A comprehensive review of highly pathogenic avian influenza (HPAI) H5N1: an imminent threat at doorstep. Travel Med Infect Dis. 2023;55:102638. https://doi.org/10.1016/j.tmaid.2023.102638
2. Krammer F, Hermann E, Rasmussen AL. Highly pathogenic avian influenza H5N1: history, current situation, and outlook. J Virol. 2025;99:e0220924. https://doi.org/10.1128/jvi.02209-24
3. Peacock THP, James J, Sealy JE, Iqbal M. A global perspective on H9N2 avian influenza virus. Viruses. 2019;11:11. https://doi.org/10.3390/v11070620
4. Wang L, Gao GF. A brief history of human infections with H5Ny avian influenza viruses. Cell Host Microbe. 2025;33:176–81. https://doi.org/10.1016/j.chom.2025.01.010

5. Surveillance Division of the Communicable Disease Branch of the Centre for Health Protection Hong Kong. Avian influenza report, volume 21, number 35 [cited 2025 Jul 25]. https://www.chp.gov.hk/files/pdf/2025_avian_influenza_report_vol21_wk35.pdf
6. World Health Organization/World Organisation for Animal Health/Food and Agriculture Organization (WHO/OIE/FAO) H5N1 Evolution Working Group. Revised and updated nomenclature for highly pathogenic avian influenza A (H5N1) viruses. Influenza Other Respir Viruses. 2014;8:384–8. https://doi.org/10.1111/irv.12230
7. WHO/OIE/FAO H5N1 Evolution Working Group. Continued evolution of highly pathogenic avian influenza A (H5N1): updated nomenclature. Influenza Other Respir Viruses. 2012;6:1–5.
8. Ort JT, Shepard SS, Zolnoski SA, Lam TT-Y, Davis CT, Neher RA, et al. Development of avian influenza A(H5) virus datasets for Nextclade enables rapid and accurate clade assignment. Virus Evol. 2025;11:veaf058. https://doi.org/10.1093/ve/veaf058
9. Deng Y-M, Wille M, Dapat C, Xie R, Lay O, Peck H, et al. Influenza A(H5N1) virus clade 2.3.2.1a in traveler returning to Australia from India, 2024. Emerg Infect Dis. 2025;31:135–8. https://doi.org/10.3201/eid3101.241210
10. Hassan MM, Hoque MA, Debnath NC, Yamage M, Klaassen M. Are poultry or wild birds the main reservoirs for avian influenza in Bangladesh? EcoHealth. 2017;14:490–500. https://doi.org/10.1007/s10393-017-1257-6
11. Siegers JY, Xie R, Edwards KM, Byrne AMP, Hu S, Wang R, et al. Resurgence of zoonotic highly pathogenic avian influenza A(H5N1) virus in Cambodia. N Engl J Med. 2025;393:1650–2. https://doi.org/10.1056/NEJMc2504302
12. OFFLU. OFFLU avian influenza data package: WHO VCM February 2026 [cited 2026 Jun 23]. https://offlu.org/technical-activities/february-2026-avian-influenza
13. Shu Y, McCauley J. GISAID: global initiative on sharing all influenza data—from vision to reality. Euro Surveill. 2017;22:22. https://doi.org/10.2807/1560-7917.ES.2017.22.13.30494
14. Sayers EW, Cavanaugh M, Clark K, Ostell J, Pruitt KD, Karsch-Mizrachi I. GenBank. Nucleic Acids Res. 2020;48(D1):D84–6.
15. Centers for Disease Control and Prevention. Global summary of recent human cases of H5N1 bird flu [cited 2025 Aug 6]. https://www.cdc.gov/bird-flu/spotlights/h5n1-summary-08042025.html
16. World Health Organization. Influenza at the human-animal interface: Summary and risk assessment, from 28 May to 1 July 2025 [cited 2025 Jul 25]. https://eswi.org/education-hub/influenza-human-animal-interface-summary-and-risk-assessment-28-may-1-july-2025
17. Smith GJD, Vijaykrishna D, Bahl J, Lycett SJ, Worobey M, Pybus OG, et al. Origins and evolutionary genomics of the 2009 swine-origin H1N1 influenza A epidemic. Nature. 2009;459:1122–5. https://doi.org/10.1038/nature08182
18. Kilbourne ED. Influenza pandemics of the 20th century. Emerg Infect Dis. 2006;12:9–14. https://doi.org/10.3201/eid1201.051254
19. Lycett SJ, Duchatel F, Digard P. A brief history of bird flu. Philos Trans R Soc Lond B Biol Sci. 2019;374:20180257. https://doi.org/10.1098/rstb.2018.0257
20. Marinova-Petkova A, Shanmuganatham K, Feeroz MM, Jones-Engel L, Hasan MK, Akhtar S, et al. The continuing evolution of H5N1 and H9N2 influenza viruses in Bangladesh between 2013 and 2014. Avian Dis. 2016;60:108–17. https://doi.org/10.1637/11136-050815-Reg
21. Suttie A, Tok S, Yann S, Keo P, Horm SV, Roe M, et al. Diversity of A(H5N1) clade 2.3.2.1c avian influenza viruses with evidence of reassortment in Cambodia, 2014–2016. PLoS One. 2019;14:e0226108–0226108. https://doi.org/10.1371/journal.pone.0226108
22. Kandeil A, Patton C, Jones JC, Jeevan T, Harrington WN, Trifkovic S, et al. Rapid evolution of A(H5N1) influenza viruses after intercontinental spread to North America. Nat Commun. 2023;14:3082. https://doi.org/10.1038/s41467-023-38415-7
23. Graziosi G, Lupini C, Catelli E, Carnaccini S. Highly pathogenic avian influenza (HPAI) H5 clade 2.3.4.4b virus infection in birds and mammals. Animals (Basel). 2024;14:14. https://doi.org/10.3390/ani14091372
24. Capelastegui F, Goldhill DH. H5N1 2.3.4.4b: a review of mammalian adaptations and risk of pandemic emergence. J Gen Virol. 2025;106:002109. https://doi.org/10.1099/jgv.0.002109
25. Peacock TP, Moncla L, Dudas G, VanInsberghe D, Sukhova K, Lloyd-Smith JO, et al. The global H5N1 influenza panzootic in mammals. Nature. 2025;637:304–13. https://doi.org/10.1038/s41586-024-08054-z
26. Li H, Amaral K, Tugg Y, Fletcher C, Surendran V, Palladino E, et al. Molecular signatures of mammalian adaptation of avian influenza viruses [cited 2025 Sep 9]. https://www.mcmasterforum.org/docs/default-source/product-documents/rapid-responses/molecular-signatures-of-mammalian-adaptation-of-avian-influenza-viruses.pdf
27. Ríos Carrasco M, Lin T-H, Zhu X, Gabarroca García A, Uslu E, Liang R, et al. The Q226L mutation can convert a highly pathogenic H5 2.3.4.4e virus to bind human-type receptors. Proc Natl Acad Sci U S A. 2025;122:e2419800122. https://doi.org/10.1073/pnas.2419800122
28. Müller NF, Stolz U, Dudas G, Stadler T, Vaughan TG. Bayesian inference of reassortment networks reveals fitness benefits of reassortment in human influenza viruses. Proc Natl Acad Sci U S A. 2020;117:17104–11. https://doi.org/10.1073/pnas.1918304117
29. Markin A, Macken CA, Baker AL, Anderson TK. Revealing reassortment in influenza A viruses with TreeSort. Mol Biol Evol. 2025;42:msaf133. https://doi.org/10.1093/molbev/msaf133
30. World Health Organization. Tool for Influenza Pandemic Risk Assessment (TIPRA) 2nd edition: version 2 release [cited 2026 May 22]. https://www.who.int/publications/i/item/tool-for-influenza-pandemic-risk-assessment-(tipra)-2nd-edition

Address for correspondence: Erik Karlsson, Institut Pasteur du Cambodge, 5 Monivong Blvd., PO Box #983, Phnom Penh, Cambodia; email: ekarlsson@pasteur-kh.org; or Michelle Wille, WHO Collaborating Centre for Reference and Research on Influenza, Peter Doherty Institute for Infection and Immunology, 792 Elizabeth St, Melbourne, VIC 3000, Australia; email: michelle.wille@unimelb.edu.au

Early Action Review of Detection, Notification, and Response Timeliness during Cross-Border Bundibugyo Virus Disease Outbreak, Uganda, 2026

Joshua Kayiwa, Mudarshiru Bbuye, Ritah Atuhaire, Doreen Nyakato, Mathew Tut, Bayad Nozad, Jovan Baryamujura, Bernard Lubwama, Solome Okware, Pamela Kajumba, Grace Akello, Bonny Kintu, Rebecca Kahunde, Dativa Aliddeki, Motuma Guyassa, Lydia Nakiire, Felix Ocom, Paul Mbaka, Peter Elyanu, Allan Muruta, Atek Kagirita, Charles Olaro

Bundibugyo virus disease (BVD), an Ebola virus species with no licensed vaccine or therapeutic, reemerged in May 2026 as a cross-border outbreak in Uganda and the Democratic Republic of the Congo. During a 2-day workshop, July 8–9, 2026, we conducted an early action review of the outbreak response using the 7-1-7 framework (7 days to detect, 1 day to notify, 7 days to complete early response actions) to assess timeliness and identify bottlenecks and enablers across 9 response pillars. Uganda declared its outbreak on May 15, 2026; by July 8, the country had recorded 20 confirmed cases (15 imported, 5 locally transmitted) and a case-fatality rate of 15%. Uganda met all 3 targets: detection in 6 days, notification in <1 day, and response completion in 2 days. Low clinical suspicion, cross-border data-sharing gaps, fragmented digital systems, and delayed community engagement were common bottlenecks; strong leadership and coordination structures were most cited enablers.

Bundibugyo virus disease (BVD) is a severe viral hemorrhagic fever caused by *Orthoebolavirus bundibugyoense*, a documented Ebola virus species. The virus was first identified during a 2007 outbreak in Bundibugyo District, western Uganda (*1*); that outbreak ultimately comprised 131 cases, including 56 laboratory-confirmed cases and a case-fatality rate (CFR) of 40% among confirmed cases (*2*–*4*). Bundibugyo virus subsequently caused a second confirmed outbreak, in the Democratic Republic of the Congo (DRC) in 2012, comprising 62 cases, including 36 laboratory-confirmed cases and a CFR of 33% among confirmed cases (*5*). Reported CFRs for BVD are generally lower than for Ebola caused by Zaire ebolavirus (*6*). Unlike other Ebola virus species, no licensed vaccine or approved specific therapeutic currently exists for BVD, although licensed Zaire ebolavirus vaccines show early evidence of partial cross-reactive immunogenicity, and candidate BVD-specific vaccines and therapeutics are undergoing World Health Organization (WHO)–led prioritization (*7*–*11*).

On May 15, 2026, both Uganda and the DRC declared separate outbreaks, a transboundary BVD event, from which cases were epidemiologically linked to Ituri Province, DRC (*12*). Uganda's index case, a 59-year-old DRC national, sought care at a private hospital in Kampala on May 11, 2026, and died on May 14, 2026 (*13*). On May 17, 2026, WHO determined the event constituted a Public Health Emergency of International Concern under the International

Author affiliations: National Public Health Emergency Operations Centre, Ministry of Health, Kampala, Uganda (J. Kayiwa, M. Bbuye, R. Atuhaire, D. Nyakato, J. Baryamujura, B. Lubwama, P. Kajumba, G. Akello, F. Ocom, A. Kagirita); Africa Centres for Disease Control and Prevention, Addis Ababa, Ethiopia (M. Tut, D. Aliddeki); UK Health Security Agency, London, UK (B. Nozad, M. Guyassa); World Health Organization, Kampala (S. Okware); Department of Integrated Epidemiology, Surveillance and Public Health Emergencies, Ministry of Health, Kampala (B. Kintu, A. Muruta); National Health Laboratory and Diagnostic Services, Ministry of Health, Kampala (R. Kahunde); Baylor Foundation Uganda, Kampala (L. Nakiire, P. Elyanu); Ministry of Health, Kampala (P. Mbaka, C. Olaro)

DOI: https://doi.org/10.3201/eid3210.261411

Health Regulations 2005 (*14*), and on May 18, 2026, the Africa Centres for Disease Control and Prevention declared the outbreak a Public Health Emergency of Continental Security (*15*). By July 8, 2026, Uganda had recorded 20 confirmed cases, of which 15 were directly imported from the DRC, underscoring the cross-border nature of the outbreak and the need for sustained joint surveillance and coordinated screening along the Uganda–DRC corridor.

The 7-1-7 target, defined as ≤7 days to detect a suspected outbreak, ≤1 day to notify relevant public health authorities, and ≤7 days to complete essential early response actions, was jointly developed by WHO and Resolve to Save Lives, a nongovernmental global public health organization (*16*). The 7-1-7 target has been adopted by dozens of countries and institutions worldwide as a standardized, real-world performance benchmark for outbreak detection and response (*16*,*17*). Retrospective, multicountry evidence indicates substantial variation in how consistently those targets are met in practice (*18*,*19*), and Uganda has since institutionalized 7-1-7 monitoring as part of its national outbreak coordination platform (*20*); subsequent applications have been documented across other outbreak types in the country (*21*). WHO recommends that an early action review (EAR), an agile, structured methodology for assessing timeliness and identifying bottlenecks and enablers using the 7-1-7 tool, be conducted for all outbreaks of public health significance (*22*). The EAR formally assesses the timeliness of detection, notification, and response against the 7-1-7 targets, while enabling countries to evaluate coordination effectiveness within and across response pillars, identify pillar-level bottlenecks and enablers, and document emerging good practices.

Uganda conducted its EAR ≈8 weeks into the BVD response, as both an operational necessity and a formal obligation under the International Health Regulations 2005 Monitoring and Evaluation Framework (*23*). The process further assisted with development of actionable, time-bound recommendations to strengthen the ongoing response and inform national preparedness and readiness planning, in line with Uganda's National Action Plan for Health Security (NAPHS), 2024–2029. In this article, we present the process, results, and lessons learned from that review.

Methods

Study Design and Setting

We conducted a retrospective, multipillar programmatic review using WHO's standardized EAR methodology and 7-1-7 assessment tool (*22*). Nine response pillars were scoped for review under Uganda's incident management system (IMS) structure: coordination; surveillance; laboratory; case management; risk communication and community engagement (RCCE); water, sanitation, and hygiene (WASH); logistics; strategic information, research, and innovation (SIRI); and continuity of essential health services (CEHS). We convened a 2-day workshop during July 8–9, 2026, bringing together participants from the Uganda Ministry of Health (MoH) and implementing and development partners, as well as experts from WHO, Africa Centres for Disease Control and Prevention, and the UK Health Security Agency.

The 7-1-7 Framework

The 7-1-7 tool defines 3 sequential intervals: detection, the interval from the date of disease emergence (here defined as the earliest date on which a confirmed BVD case crossed the border into Uganda, thereby introducing the risk) to the date the event was first recorded by any source, against a target of ≤7 days; notification, the interval from the date of detection to formal notification of the public health authority responsible for action, against a target of ≤1 day; and response, the interval from notification to completion of the last of 7 defined early response actions (investigation, epidemiologic and risk assessment, laboratory confirmation, case management and infection prevention and control (IPC) measures, public health countermeasures, risk communication, and establishment of a coordination mechanism) against a target of ≤7 days (*16*,*17*).

Data Collection and Synthesis

A total of 74 participants—38 from MoH, 12 from development, and 24 implementing partners—convened in 9 IMS pillar-based breakout groups, each supported by a trained facilitator and note-taker. Using the 7-1-7 standardized tool, each group reconstructed its pillar's timeliness of detection, notification, and response actions; calculated interval timeliness against target; identified bottlenecks and enablers; and proposed immediate and longer-term remedial actions. On the second day, pillar findings were presented and discussed in plenary, enabling cross-pillar validation, consensus-building, and refinement of the consolidated bottlenecks, enablers, and recommendations. We subsequently consolidated findings centrally across all 9 pillars, and tagged each item to its source pillar for traceability.

Ethics Considerations

This review constituted a programmatic evaluation of routine public health outbreak response activities

using non–patient-identifiable process data. It was conducted under the MoH's standing mandate for outbreak response and quality improvement and did not constitute human subjects research requiring separate ethical review.

Results

Outbreak Overview

By July 8, 2026, Uganda had confirmed 20 BVD cases: 15 imported from the DRC and 5 arising from secondary transmission within the country. The CFR stood at 15% among confirmed cases. Of the 831 contacts identified by then, 6 seroconverted, 4 died of causes unrelated to BVD, 1 was repatriated to DRC on request, and the remainder completed the standard 21-day follow-up according to existing guidelines. The country had tested ≥2,337 persons from 106 districts who were suspected of having any viral hemorrhagic fever (VHF), including samples from mortality surveillance. Case accrual slowed markedly as the response advanced. Uganda's confirmed case count rose only marginally, from 19 cases as of June 17, 2026, to 20 by July 8, 2026, consistent with effective containment of secondary transmission following the initial response.

7-1-7 Timeliness

We summarized interval timeliness of the BVD response against the 7-1-7 targets (Table 1). Uganda's earliest cross-border BVD case was traced to May 8, 2026 (date of emergence). The event was first recorded by the health system on May 14, 2026, when a community leader alerted the Director General of Health Services, giving a detection interval of 6 days (target ≤7 days). Formal notification occurred the same day, a notification interval of ≤1 day (target ≤1). The last of the 7 early response actions was completed on May 16, 2026, two days after notification (target ≤7). Uganda therefore met all 3 of the 7-1-7 targets for this event.

Enablers by Pillar

We consolidated the enablers identified across all 9 pillar breakout groups, organized by pillar (Table 2). Three cross-pillar enablers were consistently cited: presence of strong senior leadership, reinforced by existing coordination architecture such as the National Task Force, the IMS, and the National Public Health Emergency Operations Centre, underpinning rapid activation across nearly every pillar; Uganda's past experience in managing similar outbreaks, coupled with existing digital systems; and a trained, well-experienced, and ready-to-deploy workforce.

Bottlenecks and Action Matrix–Proposed Immediate and Longer-Term Recommendations

We compiled a list of bottlenecks identified for each pillar (Table 3, https://wwwnc.cdc.gov/EID/article/32/10/26-1411-T3.htm). Two major cross-cutting patterns emerged. First, a low index of clinical suspicion, attributable to the nonclassical, symptom-predominant manifestations of the BVD strain rather than the classic hemorrhagic symptoms (*24*), recurred as a root cause in both the surveillance and case management pillars. Those bottlenecks contributed to delayed recognition, referral, and IPC uptake, especially in private healthcare facilities. Second, fragmentation of digital and information systems recurred across the surveillance, logistics, and SIRI pillars, manifesting as parallel electronic information systems, limited real-time stock visibility, and poor interoperability between reporting platforms.

For each bottleneck identified during the review, the corresponding pillar group proposed a remedial action, distinguishing actions for immediate implementation from actions requiring longer-term planning and funding, for example, through the NAPHS (2024–2029) or partner-funded programs (Table 3). All actions were validated in plenary on the second day of the workshop and discussed critically for feasibility and ownership by the respective pillar group.

Discussion

This EAR found that Uganda met all 3 of the 7-1-7 targets during the 2026 cross-border BVD outbreak: detection achieved within 6 days, notification within 1 day, and completion of early response actions within 2 days. Meeting all 3 of the 7-1-7 targets simultaneously is an excellent finding in practice; a 5-country

Table 1. Interval timeliness for World Health Organization 7-1-7 response target during cross-border Bundibugyo virus disease outbreak, Uganda, 2026*

Interval	Definition (dates)	Timeliness	Target	Target met
Detection	Emergence (May 8) → detection (May 14)	6 d	≤7 d	Y
Notification	Detection (May 14) → notification (May 14)	<1 d	≤1 d	Y
Response	Notification (May 14) → completion of last early response action (May 16)	2 d	≤7 d	Y

*7-1-7, ≤7 days to detect a suspected outbreak, ≤1 day to notify relevant public health authorities, and ≤7 days to complete essential early response actions.

retrospective assessment of 41 public health events found that only 54% of events met the detection targets, 71% the notification targets, and 49% the response targets (*18*). Our results are thus consistent with Uganda's early gains reported from its national 7-1-7 rollout (*20,21*). Similar EARs conducted for a

Table 2. Enablers of 7-1-7 timeliness during cross-border Bundibugyo virus disease outbreak, Uganda, 2026*

Response pillars	Actions
Coordination	
Detection	Proactive engagement from senior MoH leadership (Director General of Health Services) ensured rapid triage and verification of the initial signal, accelerating response actions.
Notification	The MoH officially declared the outbreak on May 15, 2026.
Response	Operationalization of the existing multihazard preparedness and response framework, which activated the National Task Force and IMS, enabling appointment of the Incident Commander by the DGHS within 3 h of confirmation. Presence of the National Public Health Emergency Operations Centre facilitated initial IMS activation and coordination mechanisms, including strategic, partner, pillar-specific, and daily IMS meetings.
Surveillance	
Detection	Community vigilance and involvement in surveillance enabled quicker identification and reporting of suspected cases.
Notification	A Kampala-based community leader from DRC was cooperative in reporting unusual health events, enabling early recognition and escalation of the initial signals.
Laboratory	
Response	Trained laboratory staff and adequate supplies and reagents for PCR testing and genomic sequencing enabled timely identification of BVD and correlation of the index case with the ongoing DRC outbreak. An efficient specimen referral hub network facilitated smooth transportation of suspected-outbreak samples to reference testing laboratories. Activation of district and regional laboratory pillar coordination for sample collection, transport, and reporting.
Case management	
Response	A well-equipped, established 84-bed ETU at Mulago National Referral Hospital plus a pool of ready-to-deploy trained staff supported swift admission and care.
RCCE	
Response	Availability of a central repository of English and translated Information Education and Communication materials, EVD-tailored messages, and guidelines for the public. Existing community structures including village health teams, community development officers, parish chiefs, and cultural and local council leaders were used for swift social mobilization and community-based surveillance. Strong collaboration between the MoH and the media network enabled timely dissemination of accurate messages.
WASH	
Response	Existing service contract frameworks for waste collection and management between the MoH and private service providers operating in the mapped high-risk districts. Inclusion of emergency personal protective equipment as a requirement in preexisting framework contracts/emergency procurement procedures. Adoption of a clustered deployment strategy at regional level to optimize team coverage.
Logistics	
Response	Pre-positioned emergency commodities at national medical stores, Mulago ETU, and Entebbe Isolation Unit, which were redistributed to the subnational level for immediate patient care.
SIRI	
Response	Availability of preprocured and functional ICT equipment, including internet and tablets for immediate deployment.
Cross-cutting	
Response	Readily available, competent national and subnational multidisciplinary rapid response teams deployed to high-risk districts. Previous national EVD response plans facilitated swift compilation of the current BVD response plan, accelerating prompt mobilization of resources by government and partners and operationalizing initial response mechanisms. Availability of existing and functional digital systems and dashboards, including ePHEM (https://pheoc.health.go.ug), eIDSR (https://eidsr.health.go.ug), Go.Data (https://vhf.health.go.ug), IRRDS (https://irrds.cphl.go.ug), the Uganda Health Alert System (https://alerts.health.go.ug), RESTRACK (https://restrack.cphl.go.ug), LIMS (https://rds.cphluganda.org), Action Tracker (https://actiontracker.health.go.ug), the Partner 4W matrix (https://partners.health.go.ug), and IORS (https://dashboards.health.go.ug), among others, which supported prompt data capture, analysis, and presentation, enabling rapid decision-making.

*7-1-7, ≤7 days to detect a suspected outbreak, ≤1 day to notify relevant public health authorities, and ≤7 days to complete essential early response actions. BVD, Bundibugyo virus disease; DGHS, Director General of Health Services; DRC, Democratic Republic of the Congo; ETU, Ebola treatment unit; EVD, Ebola virus disease; ICT, information and communication technologies; IMS, incident management system; MoH, Ministry of Health; RCCE, risk communication and community engagement; SIRI, strategic information, research, and innovation; WASH, Water, Sanitation and Hygiene.

cholera outbreak in Kenya (N. Roosevelt et al., unpub. data, https://doi.org/10.1101/2025.07.29.25332335) and a measles outbreak in Sierra Leone (*25*) have also identified actionable, pillar-specific bottlenecks, suggesting that the EAR methodology yields consistently useful operational insight across pathogens and settings. The low proportion of cases attributable to secondary transmission (5 of 20) further suggests that timeliness translated into a real reduction in onward transmission of a pathogen for which no licensed vaccine or therapeutic currently exists (*7*).

Despite the strong aggregate timeliness of the early BVD response, the review identified concrete opportunities for improvement. Generally, the ongoing transboundary BVD outbreak has illustrated the persistent clinical and public health challenges posed by filovirus disease outbreaks in resource-limited settings, including diagnostic delay and the demands of a coordinated field response (*26*). The recurrence of low clinical suspicion across both the surveillance and case management pillars is a notable finding; the clinical manifestation of cases in this outbreak was characterized predominantly by fever and gastrointestinal symptoms, rather than overt hemorrhage (*24*). Therefore, frontline health workers trained on a classic hemorrhagic case definition might have underrecognized the disease clinically, delaying isolation, IPC measures, and referral, particularly in private healthcare facilities. That initial gap in suspicion was rapidly narrowed by public awareness campaigns, intensified contact tracing, mortality surveillance, and point of entry (PoE) screening. We attribute the limited secondary transmission (5 of 20 cases) chiefly to those fast-follow interventions, rather than to missed cases during the outbreak's earliest, low-suspicion phase. That finding further suggests that case definition training and job aids should explicitly incorporate the nonhemorrhagic manifestation of BVD as documented in this outbreak, rather than relying solely on generic Ebola virus disease case definitions. Similarly, the recurrence of digital and information-system fragmentation across the surveillance, laboratory, logistics, and SIRI pillars, including suboptimal electronic laboratory information system use, limited stock visibility, and poor system interoperability, points to a structural rather than pillar-specific weakness in Uganda's outbreak information architecture. Such shortfalls are likely to recur in future events unless they are addressed at the systems level, rather than pillar by pillar.

The cross-border nature of this outbreak also foregrounded the need for real-time information-sharing with the DRC. Limited cross-border surveillance data-sharing was cited as a bottleneck despite the outbreak's clear epidemiologic linkage to the parallel event in Ituri Province, DRC (*12*). That finding is further underscored by the fact that 15 of Uganda's 20 confirmed cases were directly imported from the DRC, principally among persons in search of specialized medical care. Strengthening routine institutionalized cross-border collaboration, joint investigations, harmonized PoE screening, and regular bilateral coordination meetings were accordingly among the most frequently proposed immediate actions (Table 3), consistent with prior calls for stronger DRC–Uganda border health cooperation, given the recurring risk of spillover along this corridor (*19*). Such bidirectional dependence also means a well-prepared country can strengthen its neighbor's early warning. Uganda's own detection benefited from informal advanced notice of suspected Ituri Province cases, and the country has since extended preparedness support to healthcare facilities along the shared corridor.

The strong response-interval performance we identified also reflects a third cross-cutting pattern (Table 2): decisive senior leadership operating through existing coordination architecture. An incident commander was appointed within 3 hours of the initial case confirmation, and the National Task Force, IMS, and National Public Health Emergency Operations Centre were activated immediately, consistent with WHO's requirement that a public health emergency operations center be fully activated within 120 minutes of detecting any public health event (*27*). The MoH was also able to make a public declaration of the event within the same day that the laboratory confirmed the index case. Of note, however, the coordination pillar's own submission also reported a bottleneck of the opposite character: continued partner implementation of some response activities outside pillar coordination structures, leading to inconsistent response coordination. That finding indicates that strong central leadership did not, by itself, guarantee full coordination of all actors at the response start phase and that institutionalizing the coordination structures themselves, rather than relying on the persons who led this particular response, warrants continued attention (*28*).

Many of the enablers we identified reflect capacities built over nearly 2 decades of response to recurrent filovirus outbreaks in Uganda, including the 2007 BDV event (*2*–*4*). Those events catalyzed sustained investment in ready-to-deploy rapid response teams, national and regional public health emergency operations centers, mobile laboratory capacity, prepositioned emergency stocks, and predeveloped risk communication materials, among other capacities.

Countries lacking such infrastructure might need to apply a narrower subset of the enablers to achieve comparable 7-1-7 performance.

Beyond the specific bottlenecks discussed above, the pillar-generated action matrix (Table 3) warrants critical comment on implementation feasibility. Surveillance alone accounts for 5 of the 17 immediate actions, raising a practical question about parallel implementation capacity within an already-stretched pillar team. Second, several longer-term actions, such as the proposed salary approval for permanent PoE staffing through the NAPHS (2024–2029), depend on external budget cycles beyond MoH's direct control. Third, although digital and information-system fragmentation was identified as a single, cross-cutting problem, the proposed actions remain pillar-siloed (e.g., electronic laboratory information system training, a logistics tracker, and SIRI interoperability) rather than converging on 1 cross-pillar strategy that Uganda's post-EAR action tracker should pursue. Finally, several of the identified bottlenecks, including inconsistent mortality surveillance, limited community leader familiarity with community-based surveillance, and constrained cross-border data-sharing, have also recurred across other unpublished Uganda-specific EARs, reflecting structural rather than outbreak-specific weaknesses that warrant systemwide remediation.

The first limitation of this review is that it was conducted during the eighth week after outbreak declaration rather than within the recommended first or second week (*22*), limiting the extent to which findings could inform real-time course correction of the still-active readiness and response efforts. That delay was deliberate; convening the same response staff in a 2-day workshop earlier, while case counts were still rising, risked distracting from active outbreak control, a tradeoff likely more acute in settings with larger or still-escalating caseloads, such as the concurrent DRC response. Second, although the health system director and other senior leaders credited as enablers did not personally attend EAR discussions, social-desirability bias among participants cannot be excluded; anonymized feedback channels could mitigate that effect in future EARs. Third, the CEHS and WASH pillar actions were documented within other pillars' submissions, including surveillance and logistics, explaining why some of their input is not separately visible (Table 3). That limitation further reflects the interlinked, complementary nature of response activities and that no single pillar can mount a response action in isolation from others (*29*). Finally, as a single-country case study of an outbreak consisting of predominantly imported cases, findings on absolute timeliness might not generalize to settings with different surveillance infrastructure or to outbreaks driven primarily by endemic in-country transmission. However, the recurring bottleneck themes, including clinical suspicion, information-system fragmentation, and cross-border data-sharing, could plausibly extend to other Ebola-endemic contexts within the Great Lakes region of Africa.

In conclusion, this EAR found that Uganda met all 3 of the 7-1-7 targets during the 2026 cross-border BVD outbreak: detection in 6 days, notification in <1 day, and completion of early response actions in 2 days. That result outperforms published multicountry benchmarks and was associated with limited secondary transmission. Those gains reflect the value of proactive leadership and coordination architecture in this response, backed by capacities built over nearly 2 decades of prior filovirus responses. The review further identified actionable, pillar-specific opportunities: reinforcing clinical suspicion for atypical disease manifestations, institutionalizing cross-border surveillance collaboration with the DRC, integrating fragmented digital and laboratory information systems, and accelerating community engagement. Incorporating those recommendations into Uganda's NAPHS (2024–2029), and conducting future EARs earlier in an outbreak course where feasible, can further strengthen national capacity to detect, notify, and respond to high-consequence pathogens.

Acknowledgments

We acknowledge the Uganda MoH leadership and the input of all pillar leads, facilitators, and note-takers who contributed to the success of the EAR process. We also thank Africa Centres for Disease Control and Prevention (Africa CDC), the UK Health Security Agency, and WHO for assisting in the review process and for continued technical partnership in strengthening Uganda's public health emergency preparedness and response. We also individually acknowledge the following persons, within their respective institutions, for their participation in the EAR exercise: MoH Integrated Epidemiology Surveillance and Public Health Emergencies (Hariet Mayinja, Irene Urinzihiwe, Hilda Barbra Wesonga, Stella Lunkuse); other MoH departments (Tonny Tindyebwa, Maureen Amutuhaire, Doreen Nabasirye, Ambrose Jakira, Catherine Kembabazi, Martin Lukwago, Philip Katabarwa, Aviva Ingrid Ampeire, Wilfred Opeli, Joanitah Namuyaba, Siliver Maniraguha, Abraham Byomugabe, Edward Katto, Jane Basirika, Kenneth Kalani); Uganda National Institute of Public Health (Daniel Kadobera, Benon Kwesiga,

Regina Nanyunja); Africa CDC (Nasreldin Mehad, Paidamoyo Magaya); UK Health Security Agency (Tebit Assefa, Liz McGinley, Edmund Newman); Foreign, Commonwealth and Development Office (Joan Wilson); Medical Teams International (Jacob Oluma); United Nations Children's Fund (Martin Ngolobe); Kampala City Council Authority (Amabel Ayebare); FHI360/STRIDES (Nathan Tumwesigye); World Vision International (Benon Musasizi); US Centers for Disease Control and Prevention (Brittany Gianetti, Sandra Nabatanzi, Enos Sande); European Centre for Disease Prevention and Control (Agorista Baka); Uganda Health Activity (Wilberforce Owembabazi); Palladium-TADDAP II (Judith Nanyondo, Herbert Bakiika); Uganda Red Cross Society (Suudhi Bamutya, Eric Ofwono); Baylor Uganda (Bernadette Basuta Mirembe); African Epidemiology Network (Ben Masiira); World Health Organization (Benjamin Bodo, Immaculate Atuhaire, Linda Phionah Lilian, Chris Opesen, Esther Muwanguzi, Robert Musoke, Richard Ssekitoleko); and International Rescue Committee (Jude Senkuwu).

The pillar-level 7-1-7 assessment tools and the post-EAR action tracker underlying this report are held by the Uganda Ministry of Health National Public Health Emergency Operations Centre and are available from the corresponding author on reasonable request.

This early action review was implemented by the Uganda Ministry of Health and partners. Africa CDC provided financial support for the 2-day workshop described in this manuscript, including venue, participant travel, and per diem costs for the participants, and provided technical staff who cofacilitated the review. WHO and the UK Health Security Agency provided technical facilitation support. The funders had no role in the analysis or interpretation of findings, or in the decision to publish.

The authors used an AI writing assistant (Claude; Anthropic, https://www.anthropic.com) to assist with manuscript formatting, reference list formatting and renumbering, structural reorganization to conform to journal style, and language/copyediting. It was not used to generate, analyze, or interpret study data, and it did not contribute original scientific content. The corresponding author reviewed and verified all AI-assisted edits and takes full responsibility for the accuracy and integrity of the manuscript's content.

All participating pillar teams consented to becoming co-authors after fully participating in the data collection, timeline reconstruction, and identification of bottlenecks, enablers, and recommendations during the EAR workshop; the review secretariat consolidated findings and drafted the manuscript on behalf of the team.

About the Author

Mr. Kayiwa currently heads the Public Health Threat Intelligence unit at the National Public Health Emergency Operations Centre, Uganda Ministry of Health, Kampala. His research interests include public health emergency management, information systems for outbreak surveillance and response, early warning and response performance, and postevent learning reviews, such as after-action and early action reviews.

References

1. Towner JS, Sealy TK, Khristova ML, Albariño CG, Conlan S, Reeder SA, et al. Newly discovered Ebola virus associated with hemorrhagic fever outbreak in Uganda. PLoS Pathog. 2008;4:e1000212. https://doi.org/10.1371/journal.ppat.1000212
2. Wamala JF, Lukwago L, Malimbo M, Nguku P, Yoti Z, Musenero M, et al. Ebola hemorrhagic fever associated with novel virus strain, Uganda, 2007–2008. Emerg Infect Dis. 2010;16:1087–92. https://doi.org/10.3201/eid1607.091525
3. MacNeil A, Farnon EC, Wamala J, Okware S, Cannon DL, Reed Z, et al. Proportion of deaths and clinical features in Bundibugyo Ebola virus infection, Uganda. Emerg Infect Dis. 2010;16:1969–72. https://doi.org/10.3201/eid1612.100627
4. MacNeil A, Farnon EC, Morgan OW, Gould P, Boehmer TK, Blaney DD, et al. Filovirus outbreak detection and surveillance: lessons from Bundibugyo. J Infect Dis. 2011; 204:S761–7. https://doi.org/10.1093/infdis/jir294
5. Kratz T, Roddy P, Tshomba Oloma A, Jeffs B, Pou Ciruelo D, de la Rosa O, et al. Ebola virus disease outbreak in Isiro, Democratic Republic of the Congo, 2012: signs and symptoms, management and outcomes. PLoS One. 2015;10:e0129333. https://doi.org/10.1371/journal.pone.0129333
6. Jacob ST, Crozier I, Fischer WA II, Hewlett A, Kraft CS, Vega MA, et al. Ebola virus disease. Nat Rev Dis Primers. 2020;6:13. https://doi.org/10.1038/s41572-020-0147-3
7. Feldmann H, Sprecher A, Geisbert TW. Ebola. N Engl J Med. 2020;382:1832–42. https://doi.org/10.1056/NEJMra1901594
8. Africa Centres for Disease Control and Prevention. Bundibugyo virus disease fact sheet. Addis Ababa: The Centres; 2026 [cited 2026 Jul 13]. https://khub.africacdc.org/records/resource/bundibugyo-virus-disease-fact-sheet
9. Lhomme E, Wiedemann A, Ayouba A, Ben-Farhat S, Thaurignac G, Roy C, et al.; PREVAC Study Team. Cross-reactive Bundibugyo antibody responses after receipt of licensed Ebola vaccines. N Engl J Med. 2026;395:612–5. https://doi.org/10.1056/NEJMc2608018
10. World Health Organization. WHO Technical Advisory Group on candidate vaccine prioritization: meeting report, 19 and 25 May 2026. Geneva: The Organization; 2026.
11. World Health Organization. WHO Technical Advisory Group on Therapeutics Prioritization for Bundibugyo virus disease: meeting report, 20 and 26 May 2026. Geneva: The Organization; 2026.
12. Zomahoun DL, Boyd MA, Honein MA, Montgomery JM, Zielinski-Gutierrez E, Meites E, et al.; CDC 2026 Ebola Response. Notes from the field: outbreak of Ebola disease caused by Bundibugyo virus—Democratic Republic of the Congo and Uganda, May 2026. MMWR Morb Mortal Wkly Rep. 2026;75:293–4. https://doi.org/10.15585/mmwr.mm7522e3

13. Uganda Ministry of Health. Ebola Bundibugyo virus disease outbreak 2026. Kampala: The Ministry; 2026 [cited 2026 Jul 13]. https://evd-daily.health.go.ug
14. World Health Organization. Disease outbreak news: epidemic of Ebola disease in the Democratic Republic of the Congo and Uganda determined a Public Health Emergency of International Concern. Geneva: The Organization; 2026 May 17 [cited 2026 Jul 13]. https://www.who.int/emergencies/disease-outbreak-news
15. Africa Centres for Disease Control and Prevention. Africa CDC declares the ongoing Bundibugyo Ebola outbreak a Public Health Emergency of Continental Security. Addis Ababa: The Centres; 2026 May 18 [cited 2026 Jul 13]. https://africacdc.org/news-item/africa-cdc-declares-the-ongoing-bundibugyo-ebola-outbreak-a-public-health-emergency-of-continental-security
16. Frieden TR, Lee CT, Bochner AF, Buissonnière M, McClelland A. 7-1-7: an organising principle, target, and accountability metric to make the world safer from pandemics. Lancet. 2021;398:638–40. https://doi.org/10.1016/S0140-6736(21)01250-2
17. Resolve to Save Lives. The 7-1-7 target: early disease detection & outbreak response. New York: Resolve to Save Lives; 2026 [cited 2026 Jul 13]. https://resolvetosavelives.org/how-we-save-lives/epidemic-prevention/7-1-7
18. Bochner AF, Makumbi I, Aderinola O, Abayneh A, Jetoh R, Yemanaberhan RL, et al. Implementation of the 7-1-7 target for detection, notification, and response to public health threats in five countries: a retrospective, observational study. Lancet Glob Health. 2023;11:e871–9. https://doi.org/10.1016/S2214-109X(23)00133-X
19. Jean Louis F, Nichols L, de la Torre C, Dahourou AG. Strengthening outbreak detection in Africa to achieve the 7-1-7 global framework: challenges and opportunities. Public Health Rev. 2025;46:1608039. https://doi.org/10.3389/phrs.2025.1608039
20. Nakiire L, Bochner AF, Nabatanzi M, Kisakye AK, Kayiwa J, Lee C, et al. Implementing the 7-1-7 target to improve epidemic preparedness and response in Uganda. BMJ Glob Health. 2025;10:e018207. https://doi.org/10.1136/bmjgh-2024-018207
21. Katumba H, Migisha R, Mutesi C, Ainembabazi B, Naiga HN, Namakula LO, et al. Application of the 7-1-7 framework in a prototypical anthrax outbreak: identifying missed opportunities for early detection in southwestern Uganda, September 2024. IJID One Health. 2026;12:100136. https://doi.org/10.1016/j.ijidoh.2026.100136
22. World Health Organization. Guidance and tools for conducting an Early Action Review (EAR): rapid performance improvement for outbreak detection and response. Report no. WHO/WPE/HSP/CER/2023.1. Geneva: The Organization; 2023.
23. World Health Organization. International health regulations (2005). 3rd edition. Geneva: The Organization; 2016.
24. Akilimali P, Ebengo DM, Scarpino SV, Amuri-Aziza A, Wawina-Bokalanga T, Matondo-Mbundu P, et al. Clinical characteristics of patients infected with Bundibugyo virus, DRC, 2026. N Engl J Med. 2026;395:610–2. https://doi.org/10.1056/NEJMc2608070
25. Eleeza O, Barrera-Cancedda AE, Mutebi RR, Njenga A, Vandi MA, Mearns S, et al. Epidemic-ready primary healthcare and the application of 7-1-7 metrics: a case study on a measles outbreak in Sierra Leone, January to March 2024. Health Secur. 2025;23:369–75. https://doi.org/10.1177/23265094251384635
26. Sullivan NJ. Bundibugyo virus disease in 2026—clinical and public health responses. N Engl J Med. 2026;395:278–89. https://doi.org/10.1056/NEJMra2607216
27. Fekadu ST, Gebrewahid AL, Mankoula W, Eteng W, Lokossou V, Kawe Y, et al. Public health emergency operations centres in Africa: a cross-sectional study assessing the implementation status of core components and areas for improvement, December 2021. BMJ Open. 2023;13:e068934. https://doi.org/10.1136/bmjopen-2022-068934
28. Mayigane LN, Vedrasco L, Chungong S. 7-1-7: the promise of tangible results through agility and accountability. Lancet Glob Health. 2023;11:e805–6. https://doi.org/10.1016/S2214-109X(23)00167-5
29. Agbo S, Gbaguidi L, Biliyar C, Sylla S, Fahnbulleh M, Dogba J, et al. Establishing national multisectoral coordination and collaboration mechanisms to prevent, detect, and respond to public health threats in Guinea, Liberia, and Sierra Leone 2016–2018. One Health Outlook. 2019;1:4. https://doi.org/10.1186/s42522-019-0004-z

Address for correspondence: Joshua Kayiwa, National Public Health Emergency Operations Centre, Ministry of Health, PO Box 7272, Plot 6 Lourdel Rd, Nakasero, Kampala, Uganda; email: joshua.kayiwa@uniph.go.ug

Meta-analysis of Maternal and Fetal Outcomes of Crimean-Congo Hemorrhagic Fever during Pregnancy

Bahar Donk, Deniz Güllü, Ahmet Mirhan Cırık, Handan Alay, Faruk Karakeçili, Kemalettin Özden, Fatma Kesmez Can, Orçun Barkay, Natalia Pshenichnaya, Önder Ergönül

In support of improving patient care, this activity has been planned and implemented by Medscape, LLC and Emerging Infectious Diseases. Medscape, LLC is jointly accredited with commendation by the Accreditation Council for Continuing Medical Education (ACCME), the Accreditation Council for Pharmacy Education (ACPE), and the American Nurses Credentialing Center (ANCC), to provide continuing education for the healthcare team.

Medscape, LLC designates this Journal-based CME activity for a maximum of 1.00 ***AMA PRA Category 1 Credit(s)™***. Physicians should claim only the credit commensurate with the extent of their participation in the activity.

Successful completion of this CME activity, which includes participation in the evaluation component, enables the participant to earn up to 1.0 MOC points in the American Board of Internal Medicine's (ABIM) Maintenance of Certification (MOC) program. Participants will earn MOC points equivalent to the amount of CME credits claimed for the activity. It is the CME activity provider's responsibility to submit participant completion information to ACCME for the purpose of granting ABIM MOC credit.

All other clinicians completing this activity will be issued a certificate of participation. To participate in this journal CME activity: (1) review the learning objectives and author disclosures; (2) study the education content; (3) take the post-test with a 75% minimum passing score and complete the evaluation at http://www.medscape.org/journal/eid; and (4) view/print certificate. For CME questions, see page 1776.

NOTE: It is the policy of Medscape Education to avoid the mention of brand names or specific manufacturers in accredited educational activities. However, trade and manufacturer names in this activity are provided in an effort to provide clarity. The use of brand or manufacturer names should not be viewed as an endorsement by Medscape of any specific product or manufacturer.

Release date: September 29, 2026; Expiration date: September 29, 2027

Learning Objectives

Upon completion of this activity, participants will be able to:

- Assess the epidemiology of Crimean-Congo hemorrhagic fever (CCHF) during pregnancy
- Distinguish the most common presenting symptom of CCHF during pregnancy in the current case series
- Evaluate variables associated with a higher risk for maternal mortality with CCHF
- Evaluate variables associated with a higher risk for fetal demise with CCHF

CME Editor

Amy J. Guinn, BA, MA, Technical Writer/Editor, Emerging Infectious Diseases. *Disclosure: Amy J. Guinn, BA, MA, has no relevant financial relationships.*

CME Author

Charles P. Vega, MD, Health Sciences Clinical Professor of Family Medicine, University of California, Irvine School of Medicine, Irvine, California. *Disclosure: Charles P. Vega, MD, has the following relevant financial relationships: served as consultant or advisor for: Boehringer Ingelheim; Exact Sciences; GlaxoSmithKline.*

Authors

Bahar Donk, BSc; Deniz Güllü, BSc; Ahmet Mirhan Cırık, BSc; Handan Alay, MD; Faruk Karakeçili, MD; Kemalettin Özden, MD; Fatma Kesmez Can, MD; Orçun Barkay, MD; Natalia Pschenichaya, MD; Onder Ergonul, MD, MPH.

Crimean-Congo hemorrhagic fever (CCHF) during pregnancy is associated with severe maternal and fetal complications, but evidence remains limited to heterogeneous case reports. We synthesized patient-level data from published and unpublished cases identified through systematic database searches and direct collaboration with centers in CCHF-endemic areas. We harmonized patient-level clinical, laboratory, obstetric, treatment, and outcome data for 55 pregnancies. The maternal mortality rate was 28.8% (15/52), and fetal loss occurred in 57.4% (31/54) of cases. Maternal mortality rates increased with advancing gestation, reaching 31.3% in the third trimester, but fetal loss was highest (85.7%) in the first trimester. Ribavirin treatment during the third trimester was associated with lower observed maternal mortality rates (odds ratio 0.33, 95% CI 0.13–0.84; p = 0.031). Our findings highlight gestational age–specific risks of CCHF and support the need for standardized management protocols and strengthened CCHF surveillance during pregnancy in endemic regions.

Crimean-Congo hemorrhagic fever (CCHF) is a life-threatening tickborne disease caused by CCHF virus (CCHFV) (*1*). CCHF is endemic across Africa, Asia, Eastern Europe, and the Middle East and is expanding geographically toward historically nonendemic regions, including Western and Southern Europe (*2*–*5*). Transmission occurs primarily through bites of infected *Hyalomma* spp. ticks but also through contact with the blood or tissues of viremic livestock or, less commonly, through healthcare-related exposure (*6*). Clinical manifestations typically appear after a short incubation period and begin with a nonspecific febrile prodrome, which progresses to hemorrhagic manifestations and multiorgan system failure in some patients (*1*). Reported case-fatality rates vary from 5% to 40% depending on the setting, outbreak dynamics, and access to supportive care (*7*).

Pregnancy represents a uniquely vulnerable physiologic state in the context of viral hemorrhagic fevers because of pregnancy-associated immunologic modulation, altered coagulation pathways, and the fetoplacental unit (*8*,*9*). Although data remain limited, CCHF during pregnancy has consistently been associated with disproportionately high maternal and fetal mortality rates, as well as severe obstetric complications including massive hemorrhage, disseminated intravascular coagulation, spontaneous abortion, intrauterine fetal demise, and preterm delivery (*10*,*11*). Vertical CCHFV transmission has also been reported, raising additional concerns regarding neonatal outcomes and postnatal transmission risk (*12*).

Despite those severe outcomes, evidence-based management of CCHF during pregnancy is not well-established. Most published data consist of isolated case reports or small case series, often lacking detailed clinical timelines or consistent reporting of maternal, fetal, and neonatal outcomes. As a result, key clinical questions, including predictors of maternal death, determinants of fetal loss, and the potential role of antiviral therapy, remain unclear. In addition, pregnant persons are routinely excluded from clinical trials, including those evaluating antiviral agents such as ribavirin, further limiting evidence-based guidance in this population.

We conducted a meta-analysis of published cases of CCHF during pregnancy and integrated newly identified, previously unpublished cases from endemic regions. By combining detailed clinical, laboratory, obstetric, and outcome data at the patient level, we aimed to characterize maternal, fetal, and neonatal outcomes; identify clinical and laboratory predictors of adverse outcomes; and provide comprehensive evidence to inform clinical management and risk stratification in this neglected but high-risk population.

Methods

Study Design and Reporting

We designed a study to synthesize patient-level data from published and unpublished cases of CCHF during pregnancy. We conducted and reported this study in accordance with PRISMA-IPD guidelines (*13*). We did not prospectively register a formal study protocol and did not register the review in PROSPERO or any other registry.

Search Strategy

We searched for reported CCHF cases published from database inception through October 31, 2025, from the PubMed Ovid MEDLINE, Scopus, Web of Science, and Cochrane Library databases. We conducted the search on October 31, 2025, by using keywords related to pregnancy and CCHF (Appendix 1, https://wwwnc.

Author affiliations: Graduate School of Health Sciences, Koç University, Istanbul, Turkey (B. Donk, D. Güllü); School of Medicine, Koç University, Istanbul (B. Donk, D. Güllü, Ö. Ergönül); Koç University—İşBank Center for Infectious Diseases (KUISCID), Istanbul (B. Donk, D. Güllü, Ö. Ergönül); School of Medicine, Marmara University, Istanbul (A.M. Cırık); School of Medicine, Atatürk University, Erzurum, Turkey (H. Alay, K. Özden, F.K. Can); School of Medicine, Binali Yıldırım University, Erzincan, Turkey (F. Karakeçili, O. Barkay); Central Research Institute of Epidemiology, Moscow, Russia (N. Pshenichnaya) ; Russian Medical Academy of Continuous Professional Education, Moscow, Russia (Ö. Ergönül)

DOI: https://doi.org/10.3201/eid3210.260383

cdc.gov/EID/article/32/10/26-0383-App1.pdf). We imported all records identified through the database search into EndNote for macOS (Clarivate Analytics) and removed duplicates. We performed screening and full-text assessment for studies published in English and manually screened reference lists in eligible studies to identify additional relevant articles.

Inclusion and Exclusion Criteria

We included studies that described ≥1 pregnant patient who had clinically confirmed or laboratory-confirmed CCHF and that included individual patient-level clinical or outcome data. Study types included case reports, case series, observational studies, and review articles. We excluded review articles without primary patient-level data. We retrieved full-text articles meeting the inclusion criteria and assessed articles in detail. In addition to published studies, we incorporated unpublished cases that met the inclusion criteria.

Study Selection

Two independent reviewers (B.D. and A.M.C.) screened titles and abstracts for eligibility. We then assessed full-text articles by using predefined inclusion criteria. We resolved disagreements through consultation with a third reviewer (D.G.).

Case Identification and Data Collection

Two reviewers (B.D. and A.M.C.) independently extracted patient data from included studies by using a standardized prepared form in Excel (Microsoft). For unpublished cases, we put out a call through the CCHF Consortium in Turkey. Participating centers provided eligible cases by using a prepared Excel data collection sheet. In addition, we directly contacted 1 collaborator in Russia to identify potential eligible cases. We reviewed all contributed cases for completeness, internal consistency, and adherence to study inclusion criteria.

Variables and Outcomes

Extracted variables included maternal demographic characteristics, exposure history, diagnostic methods, clinical manifestations, laboratory parameters at admission, gestational age at infection, treatment, and maternal and fetal outcomes.

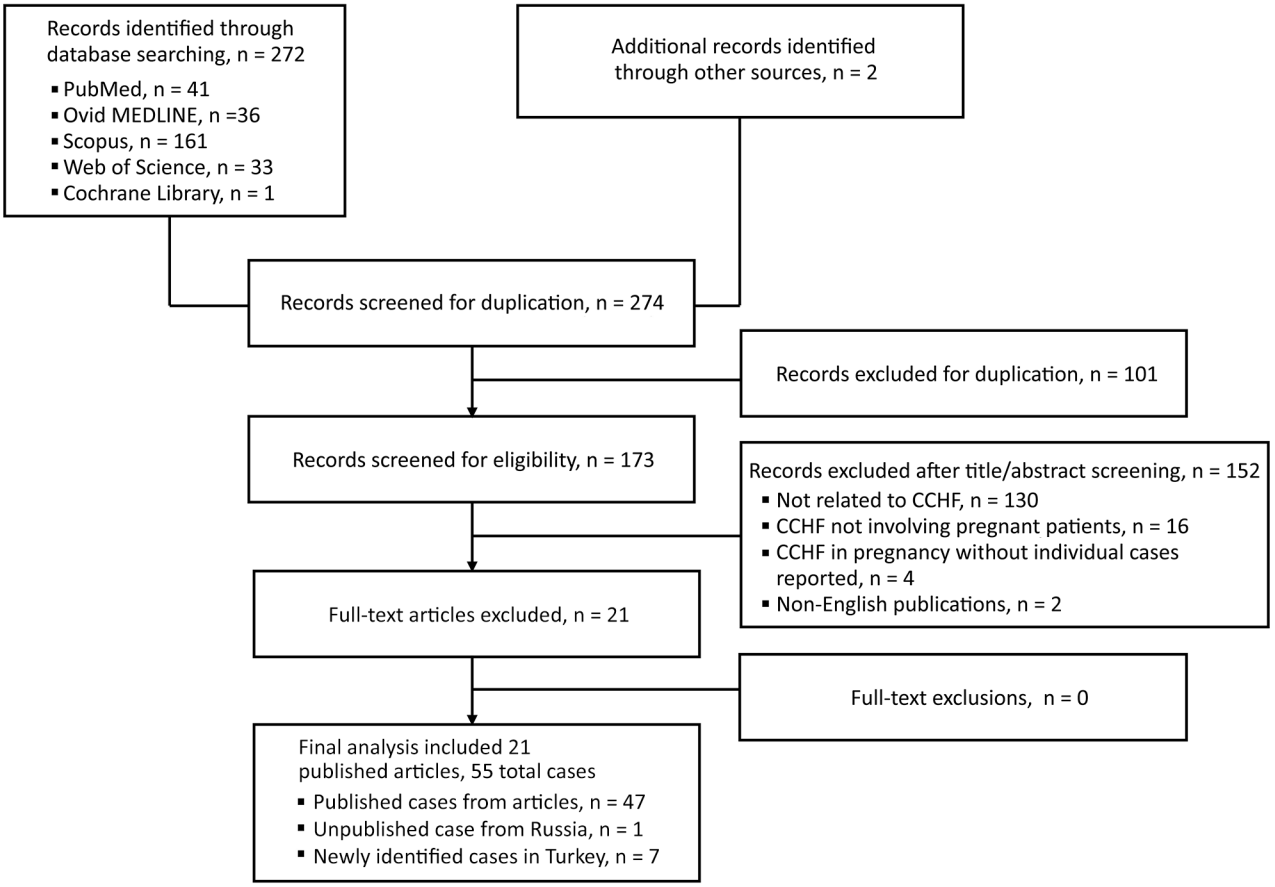

Figure 1. Flowchart of literature search and study inclusion for meta-analysis of maternal and fetal outcomes of CCHF during pregnancy. CCHF, Crimean-Congo hemorrhagic fever.

Figure 2. Geographic distribution of cases identified from a meta-analysis of maternal and fetal outcomes of Crimean-Congo hemorrhagic fever during pregnancy. Countries are shaded according to the number of cases; case counts are labeled on each country. Map generated by using R version 4.5.2 (The R Project for Statistical Computing).

The primary maternal outcome was maternal death. The primary fetal outcome was fetal loss, including spontaneous abortion, intrauterine fetal demise, and neonatal death. Secondary analyses evaluated trimester-specific outcomes and explored associations between ribavirin exposure and maternal death.

Missing Data

We did not impute missing data. We performed all analyses by using available data only and explicitly reported the denominator for each analysis to reflect the number of cases with complete information for the relevant variable.

Risk of Bias Assessments

Because most included studies were case reports or small case series without comparator groups, formal risk of bias tools were not applicable. Potential sources of bias included selective reporting and incomplete clinical data. We considered those limitations in the interpretation of findings.

Statistical Analyses

We used SPSS Statistics 31.0.1 for macOS (IBM Corp.) for all statistical analyses. We summarized continuous variables as median (IQR) because of nonnormal distribution and limited sample size. We presented categorical variables as frequency (%). We conducted maternal mortality analyses using χ^2 test for categorical comparisons and applied Fisher exact test when expected frequency in any cell was <5. We used univariate logistic regression analysis to assess associations between ribavirin use and maternal death. We reported results as odds ratios (ORs) with 95% CIs and corresponding p values. All tests were 2-sided, and we considered $p<0.05$ statistically significant. We used R version 4.5.2 (The R Project for Statistical Computing) to generate geographic distribution maps and related figures. To assess the robustness of the findings, we performed a sensitivity analysis that included only laboratory-confirmed cases determined by PCR, ELISA, or both.

Results

Study Selection

The database search identified a total of 274 articles. After removing duplicates, 173 unique records remained, from which 19 articles met our inclusion criteria. We identified 2 additional articles, 1 from a journal published in Turkey and 1 located through reference screening but not found in our initial database search. We also incorporated 1 unpublished case from Russia and 7 newly identified cases from Turkey, resulting in a total of 55 included cases (Figure 1) (Appendix 2, https://wwwnc.cdc.gov/EID/article/32/10/26-0383-App2.xlsx). We did not identify any major discrepancies or data integrity concerns.

Demographic Characteristics

All reported cases were described from Eastern Europe, the Middle East, and Africa. Turkey had the most (43.6%, 24/55) reported cases, followed by Iran (18.2%, 10/55) and Russia (14.5%, 8/55) (Figure 2). Maternal age was reported for 37 cases; median age was 26 (IQR 20.5–30) years. Gestational age at infection was reported for 40 cases; median gestational age was 21 (IQR 16–34) weeks, distributed across the first (n = 7), second (n = 16), and third (n = 17) trimesters. Tick exposure was reported in 20/30 (66.7%) women. Laboratory-confirmed diagnosis was available for 72.7% (40/55) of cases (Table 1).

Clinical Manifestations and Initial Laboratory Results

Fever (74.5%), mucosal bleeding (40%), myalgia

Table 1. Characteristics of patients from a meta-analysis of maternal and fetal outcomes of Crimean-Congo hemorrhagic fever during pregnancy*

Characteristics	Value
Reported country, n = 55	
Turkey	24 (43.6)
Iran	10 (18.2)
Russia	8 (14.5)
Iraq	5 (9.1)
Kazakhstan	3 (5.4)
Mauritania	2 (3.6)
South Africa	1 (1.8)
Bulgaria	1 (1.8)
Kosovo	1 (1.8)
Tick bite history, n = 30	
Y	20 (66.7)
N	10 (33.3)
Median (IQR) maternal age at infection, y; n = 37	26 (20.5–30)
Median (IQR) gestational age at infection, wks; n = 40	21 (16–34)
Trimester at infection, n = 40	
First	7 (17.5)
Second	16 (40.0)
Third	17 (42.5)
Clinical signs and symptoms at initial admission, n = 55	
Fever	41 (74.5)
Myalgia	21 (38.2)
Abdominal pain	4 (7.3)
Nausea and vomiting	11 (20.0)
Headache	15 (27.3)
Rash	10 (18.2)
Malaise	9 (16.4)
Chills	11 (20.0)
Loss of appetite	8 (14.5)
Somnolence	1 (1.8)
Vaginal bleeding	13 (23.6)
Mucosal hemorrhage other than vaginal bleeding	22 (40.0)
Free fluid on abdominal ultrasonography	2 (3.6)
Diagnostic method, n = 47	
PCR	20 (42.6)
ELISA	3 (6.4)
PCR and ELISA	17 (36.2)
Clinical	3 (6.4)
Autopsy	3 (6.4)
Maternal death by trimester, n = 52	15 (28.8)
First	0
Second	3 (18.8)
Third	5 (31.3)
Unknown	7 (53.8)
Fetal death by trimester, n = 54	31 (57.4)
First, n = 7	5 (71.4)
Second, n = 16	5 (31.3)
Third, n = 17	9 (52.9)
Unknown, n =14	12 (85.7)
Concurrent maternal and fetal death, n = 33	11 (33.3)
Median (IQR) gestational age at delivery, wks; n = 19	38 (37–40)
CCHF status of fetus, no.	
IgM-negative	4
IgM-positive	1
PCR-positive	4
PCR-negative	3

*Values are no. (%) except as indicated. CCHF, Crimean-Congo hemorrhagic fever; IQR, interquartile range.

Table 2. Laboratory parameters of pregnant patients from a meta-analysis of maternal and fetal outcomes of Crimean-Congo hemorrhagic fever during pregnancy

Parameter	No. patients	Median patient value (IQR)	Reference range
Leukocytes, × 10^3 cells/mL	34	3.7 (2.8–5.1)	4–11
Hemoglobin, g/dL	17	10.0 (9.0–11.1)	12–16
Platelet count, × 10^3/μL	35	58 (24–115)	150–400
Alanine aminotransferase, U/L	22	80 (25–190)	0–40
Aspartate aminotransferase, U/L	22	226.5 (56–448.5)	0–37
Lactate dehydrogenase, U/L	18	473.5 (262.5–1,004)	120–250
Creatinine phosphokinase, U/L	12	90 (70.8–962)	30–200
Prothrombin time, s	26	13.25 (11.4–15.0)	8.9–11.1
Activated partial thromboplastin time, s	26	43.5 (30.9–53.8)	24–35
International normalized ratio	13	1.07 (1.00–1.22)	0.8–1.2

(38.2%), headache (27.3%), and vaginal bleeding (23.6%) were the most frequently reported signs and symptoms (Table 1). Laboratory evaluations demonstrated marked cytopenia and coagulation abnormalities and median values were as follows: platelet count (n = 35 patients) 58 × 10^3/μL (IQR 24–115 ×10^3), leukocytes (n = 34) 3,700 cells/mL (IQR 2,825–5,075/mL), aspartate aminotransferase (n = 22) 226 U/L (IQR 56–449 U/L), lactate dehydrogenase (n = 18) 474 U/L (IQR 263–1,004 U/L), and prothrombin time (n = 26) 44 seconds (IQR 31–54 seconds) (Table 2).

Outcome Analysis

Maternal outcomes were reported for 52 women, among whom 15 (28.8%) died. Fetal outcomes were reported in 54 pregnancies, 31 (57.4%) of which resulted in fetal loss. Maternal case-fatality rates (CFRs) increased with gestational age at infection: CFRs were 0 (0/7) for first trimester, 18.8% (3/16) for the second trimester, and 31.3% (5/16) for third trimester. Fetal loss was variable across trimesters. First trimester pregnancies had the highest fetal CRF, 85.7% (12 deaths in 14 cases). We noted a sharp decrease in fetal CFR for the second trimester, with a 31.3% (5/16) fatality rate. However, we observed an increasing trend in the third trimester, for which the fetal CFR was 52.9% (9/17) cases (Table 1; Figure 3).

We performed a sensitivity analysis restricted to laboratory-confirmed cases, excluding 3 cases diagnosed by autopsy, 3 by clinical criteria alone, and 9 without available diagnostic information. In that restricted cohort, maternal CFR was 13.2% (5/38) and

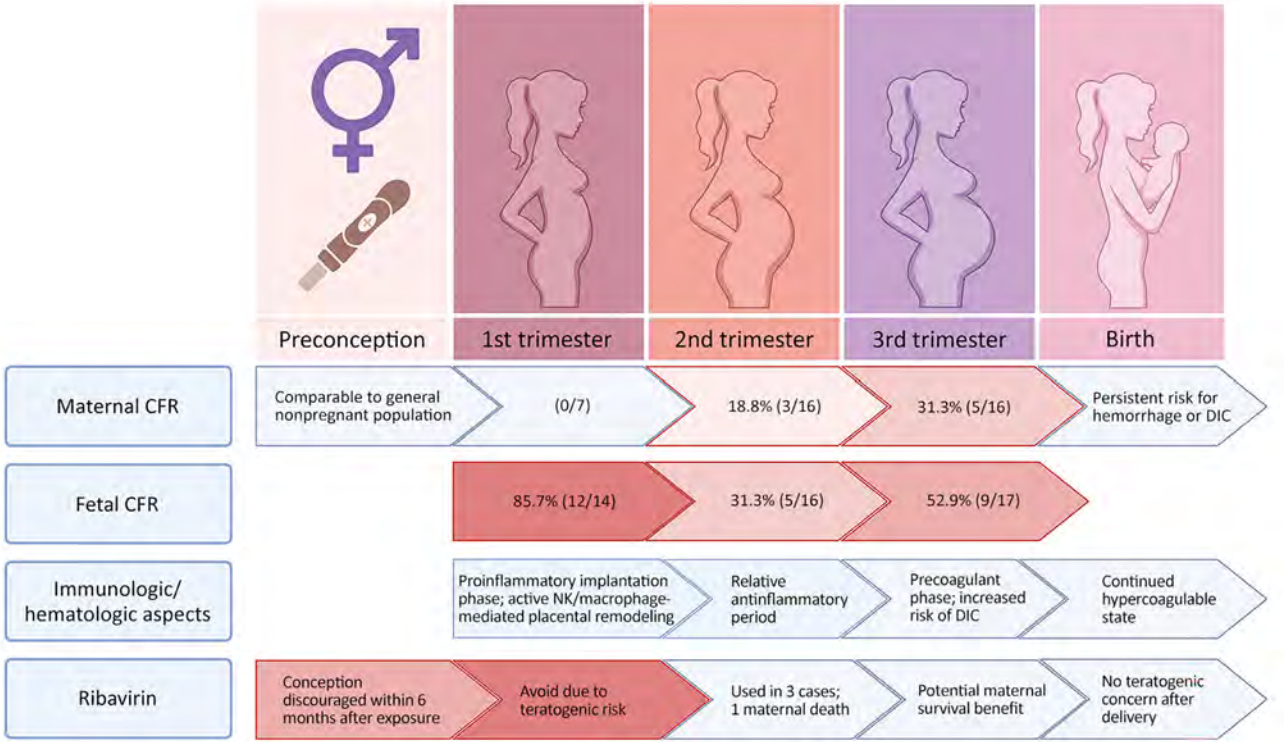

Figure 3. The summary of the maternal and fetal outcomes from a meta-analysis of maternal and fetal outcomes of Crimean-Congo hemorrhagic fever during pregnancy. Graphic shows transmission risk and the role of ribavirin by trimester. CFR, case-fatality rate; DIC, disseminated intravascular coagulation.

Table 3. Association of ribavirin usage with maternal death from a meta-analysis of maternal and fetal outcomes of Crimean-Congo hemorrhagic fever during pregnancy*

Cohort	Outcomes reported, no. (%)	Maternal death		p value
		No. (%)	Odds ratio (95% CI)	
Total cohort, n = 55	52 (94.5)	15 (28.8)		
Ribavirin treatment reported†	43 (82.7)		0.171 (0.019–1.513)	0.112
No ribavirin	29 (67.4)	9 (20.9)	Referent	
Ribavirin	14 (32.6)	1 (2.3)		
First trimester	6 (11.5)		NA	NA
No ribavirin	6 (100)	0		
Ribavirin	0	0		
Second trimester	16 (30.8)	3 (18.8)	2.750 (0.162–46.8)	0.489
No ribavirin	13 (81.2)	2 (66.7)	Referent	
Ribavirin	3 (18.8)	1 (33.3)		
Third trimester	14 (26.9)	5 (35.7)	0.333 (0.132–0.840)	**0.031**
No ribavirin	8 (57.1)	5 (100)	Referent	
Ribavirin	6 (42.9)	0		

*Bold font indicates statistical significance. NA, not applicable.
†Includes case reports of determination of whether to administer ribavirin. Trimester at ribavirin administration was not reported for 5 patients, none of whom died.

fetal CFR was 47.5% (19/40). Although both of those CFRs were lower than in the full cohort, trimester-specific patterns were similar; we observed no maternal deaths in the first trimester and persistently high fetal loss throughout pregnancy.

Ribavirin use (received or not) was reported for 43 pregnancies, among which 32.6% (14/43) patients received ribavirin. Maternal outcome was available for 33 of 43 cases with known ribavirin therapy (received or not). Only 1 (7.1%; 1/14) patient who received ribavirin died, whereas the CFR was 31% (9/29) for mothers who did not receive ribavirin (OR 0.17 [95% CI 0.02–1.51]; p = 0.128). We performed a subgroup analysis for the association between ribavirin and maternal death per trimester. No patients received ribavirin therapy during the first trimester. Among 3 patients treated with ribavirin during the second trimester, 1 (33.3% CFR) died. Of 11 other patients who received ribavirin, no deaths were reported for 6 treated during the third trimester nor for 5 whose trimester at ribavirin administration was not reported. We noted a statistically significant difference in maternal death between groups who did and did not received ribavirin in third trimester (OR 0.33 [95% CI: 0.13–0.84]; p = 0.031) (Table 3).

Discussion

In this meta-analysis integrating published and previously unpublished cases, we applied a patient-level analytical framework to examine CCHF during pregnancy. By harmonizing clinical manifestations, laboratory parameters, gestational timing, treatment exposure, and maternal and fetal outcomes at the patient level, we were able to explore trimester-specific risk patterns and treatment associations. Our findings suggest that CCHF in pregnancy is associated with substantial maternal mortality rates and high rates of fetal loss, highlighting pregnancy as a clinically relevant modifier of disease course and outcome.

The overall maternal CFR of 28.8% observed in our cohort exceeds that reported in most contemporary nonpregnant CCHF cohorts, where the fatality rate typically ranges from 5% to 20% (*7*). Of note, the patient-level approach enabled stratification by gestational age, revealing a clear increase in maternal mortality rates with advancing pregnancy. We observed no maternal deaths for first-trimester infection, whereas mortality rates rose substantially in the second and third trimesters (Table 1). That gestational gradient might reflect the cumulative physiologic burden of pregnancy, including increasing plasma volume, progressive cardiopulmonary demands, and heightened vulnerability to hemorrhage in late gestation (*14*,*15*). In contrast, fetal loss was most pronounced for first-trimester infection; >80% of CCHFV infections during early pregnancies resulted in fetal demise. That finding is biologically plausible because early gestation is characterized by rapid placental development and heightened susceptibility to systemic inflammation and maternal viremia (*16*,*17*).

In sensitivity analyses restricted to laboratory-confirmed cases, rates of both maternal death and fetal loss were lower. However, trimester-specific patterns of maternal and fetal outcomes remained similar. The observed reduction in absolute maternal mortality rates likely reflects differences in case ascertainment, including exclusion of postmortem diagnoses and cases without confirmed testing, as well as variability in clinical management and supportive care. The persistence of trimester-specific trends supports the robustness of the observed gestational risk gradient.

Consistent with prior reports (*10*), the most frequent clinical features included fever, mucosal

bleeding, myalgia, and headache (Table 1). Vaginal bleeding was observed in nearly one quarter of cases, underscoring the dual obstetric and infectious risk profile of CCHF in pregnancy. Laboratory evaluation demonstrated profound thrombocytopenia, leukopenia, transaminase elevation, and coagulation abnormalities (Table 2), which are hallmarks of severe CCHF. Pregnancy-associated hemostatic changes likely amplify those imbalances, contributing to the high incidence of hemorrhagic complications observed. The association between maternal death and laboratory abnormalities could not be performed because so few cases were available.

The relatively high frequency of vaginal bleeding in our cohort demonstrates a crucial bedside challenge. In pregnant patients, hemorrhagic manifestations of CCHF can overlap with obstetric emergencies, such as placental abruption, placenta previa, miscarriage, or postpartum hemorrhage. Placental abruption is particularly relevant in the second half of pregnancy, where vaginal bleeding, abdominal pain, uterine tenderness, and fetal distress can dominate the clinical presentation (*18*). However, those findings might be difficult to distinguish from systemic viral hemorrhage in patients with CCHF, where thrombocytopenia, coagulopathy, and endothelial dysfunction are prominent features (*1*). As a result, vaginal bleeding in endemic settings should prompt consideration of both obstetric and infectious etiologies, particularly when accompanied by systemic symptoms, such as fever and myalgia.

Beyond obstetric causes of bleeding, HELLP (hemolysis, elevated liver enzymes, and low platelets) syndrome represents a key diagnostic mimic. Thrombocytopenia and elevated liver enzymes are central features of both HELLP syndrome and severe CCHF. Hemolysis can further complicate laboratory interpretation, particularly in patients receiving ribavirin, which is known to induce hemolytic anemia (*19*). In that context, distinguishing between pregnancy-specific disorders and viral hemorrhagic disease can be challenging. Therefore, in patients with thrombocytopenia, transaminase elevation, and bleeding, especially in endemic regions or with relevant exposure history, CCHF should be considered alongside HELLP syndrome and other hypertensive disorders of pregnancy (*20*). Early multidisciplinary assessment is essential because delays in recognizing either condition could adversely affect maternal and fetal outcomes.

Pregnancy is characterized by complex, stage-dependent immunologic adaptations aimed at maintaining fetal tolerance while preserving antimicrobial defense (*21*). Those changes include modulation of innate immune responses, shifts in T-cell polarization, altered interferon signaling, and dynamic cytokine regulation (*21*,*22*). Although such adaptations are physiologically essential, they could impair effective antiviral immunity and permit higher or more sustained viral replication during infections like CCHF (*23*). The placenta plays a central role in that interaction. Increasing evidence from viral hemorrhagic fevers suggests that the placenta might serve as a site of viral persistence, immune activation, and endothelial injury (*24*). Placental infection can result in local inflammation, microvascular damage, and disruption of the maternal–fetal barrier, predisposing to fetal hypoxia, intrauterine fetal demise, and preterm labor (*25*). In advanced gestation, the highly vascularized placental bed could also act as a source of ongoing viral replication and hemorrhage, potentially exacerbating maternal disease severity.

Vertical transmission of CCHF virus has been reported in several cases, but its true incidence remains unknown because of inconsistent neonatal testing and follow-up (*12*,*26*). Potential routes include transplacental transmission during maternal viremia, exposure to infected maternal blood during delivery, and postnatal contact with infectious bodily fluids. Of note, we found 4 PCR-positive and 1 IgG-positive cases reported in the literature (Table 1). In our dataset, neonatal outcomes were inconsistently documented, reflecting a critical gap in the literature and highlighting the need for standardized neonatal evaluation in future cases.

Although direct evidence for CCHFV transmission through breast milk is limited (*27*), viral RNA has been detected in blood and body fluids during acute infection, as well as in the convalescent phase (*28*). In 1 reported case, breast milk was CCHFV IgM-positive despite being PCR-negative (*29*). Therefore, temporary avoidance of breastfeeding during the viremic phase is prudent, particularly in cases of maternal bleeding or severe disease.

Ribavirin remains the most widely used antiviral agent for CCHF. Recent observational studies have suggested a potential positive role in reducing risk for death, particularly when initiated early in the disease course (*30*,*31*). However, its clinical application in obstetric populations is complicated by its classification as a category X drug. That designation stems from its potent teratogenic and embryocidal effects documented across multiple animal models, where even low-dose exposure resulted in substantial craniofacial, skeletal, and ocular malformations (*19*,*32*). In our meta-analysis, no patients infected during the

first trimester received ribavirin, reflecting prevailing concerns regarding fetal toxicity and the absence of safety data in early pregnancy. Of note, ribavirin use was associated with lower observed maternal mortality rates, particularly in the third trimester, during which no deaths occurred among treated patients, and we observed a statistically significant difference in maternal deaths compared with untreated patients (Table 3). However, the number of patients who received ribavirin in the third trimester was limited. Thus, those findings must be interpreted cautiously and considered hypothesis-generating. Because treatment decisions were made across diverse clinical settings, differences in disease severity, timing of clinical manifestations, and overall clinical management might have influenced outcomes. Nevertheless, the lower maternal mortality observed among ribavirin-treated patients in later gestational periods aligns with clinical practice in several endemic regions, where maternal survival is prioritized once fetal organogenesis is complete.

The major strength of this study lies in its patient-level design, which enabled standardized variable definitions, gestational age–specific analyses, and direct comparison of treated and untreated patients. The inclusion of unpublished cases further enhances representativeness and mitigates publication bias toward unusually severe CCHF manifestations. Limitations include the retrospective nature of included data, incomplete reporting of outcomes, and heterogeneity in diagnostic and treatment practices across regions and decades. Variations in supportive care, including transfusion strategies, management of hemorrhagic manifestations, and access to intensive care, might have contributed to outcome variability. Laboratory confirmation was unavailable for some historical cases, and detailed timing of ribavirin initiation was missing for nearly all cases.

In conclusion, CCHF during pregnancy represents a critical clinical challenge characterized by a high maternal CFR and devastating neonatal outcomes. The unique immunologic environment of pregnancy, together with the placenta's role as a potential viral reservoir, exacerbates disease severity and creates a substantial risk for vertical transmission. Our findings suggest that although CCHFV infection during the first trimester is associated with the highest rates of fetal loss, advanced gestation carries a higher risk for maternal hemodynamic collapse and catastrophic hemorrhage. Despite its known teratogenic risks, ribavirin could be considered in selected cases as part of life-saving maternal management. The small number of laboratory-confirmed neonatal CCHFV infections and inconsistent reporting of outcomes limit our understanding; further research into the long-term outcomes of survivors is needed to address the current gaps in obstetric and pediatric CCHF care. Ultimately, the high mortality rates observed in this cohort underscore the urgent need for standardized clinical protocols and for more structured CCHF surveillance and follow-up strategies in endemic regions.

Acknowledgments

We thank Ertaç Nebioğlu for his valuable contributions to the literature review for our study.

About the Author

Ms. Donk is an MD-PhD student at Koç University School of Medicine in Istanbul and a research intern at the Koç University İşbank Center for Infectious Diseases. Her research interests include immunology and infectious diseases.

References

1. Ergönül O. Crimean-Congo haemorrhagic fever. Lancet Infect Dis. 2006;6:203–14. https://doi.org/10.1016/S1473-3099(06)70435-2
2. Spengler JR, Bergeron É, Spiropoulou CF. Crimean-Congo hemorrhagic fever and expansion from endemic regions. Curr Opin Virol. 2019;34:70–8. https://doi.org/10.1016/j.coviro.2018.12.002
3. Lorenzo Juanes HM, Carbonell C, Sendra BF, López-Bernus A, Bahamonde A, Orfao A, et al. Crimean-Congo hemorrhagic fever, Spain, 2013–2021. Emerg Infect Dis. 2023;29:252–9. https://doi.org/10.3201/eid2902.220677
4. Zé-Zé L, Nunes C, Sousa M, de Sousa R, Gomes C, Santos AS, et al. Fatal case of Crimean-Congo hemorrhagic fever, Portugal, 2024. Emerg Infect Dis. 2025;31:139–43. https://doi.org/10.3201/eid3101.241264
5. Pervanidou D, Georgiadou S, Stavropoulou E, Stefos A, Tsioka K, Kefaloudi CN, et al. Two autochthonous cases of Crimean-Congo haemorrhagic fever and the One Health response, Thessaly, Greece, 2025. Euro Surveill. 2025;30:50. https://doi.org/10.2807/1560-7917.ES.2025.30.50.2500717
6. Karanam SK, Nagvishnu K, Uppala PK, Edhi S, Varri SR. Crimean-Congo hemorrhagic fever: pathogenesis, transmission and public health challenges. World J Virol. 2025;14:100003. https://doi.org/10.5501/wjv.v14.i1.100003
7. World Health Organization. Crimean-Congo haemorrhagic fever. 2025 Feb 20 [cited 2025 Dec 29]. https://www.who.int/news-room/fact-sheets/detail/crimean-congo-haemorrhagic-fever
8. Cornish EF, Filipovic I, Åsenius F, Williams DJ, McDonnell T. Innate immune responses to acute viral infection during pregnancy. Front Immunol. 2020;11:572567. https://doi.org/10.3389/fimmu.2020.572567
9. Sayres L, Hughes BL. Contemporary understanding of Ebola and Zika virus in pregnancy. Clin Perinatol. 2020;47:835–46. https://doi.org/10.1016/j.clp.2020.08.005
10. Pshenichnaya NY, Leblebicioglu H, Bozkurt I, Sannikova IV, Abuova GN, Zhuravlev AS, et al. Crimean-Congo hemorrhagic fever in pregnancy: a systematic

review and case series from Russia, Kazakhstan and Turkey. Int J Infect Dis. 2017;58:58–64. https://doi.org/10.1016/j.ijid.2017.02.019
11. Kahraman E, Celina SS. Crimean-Congo haemorrhagic fever in pregnancy: clinical outcomes and public health implications. Front Public Health. 2026;13:1722564. https://doi.org/10.3389/fpubh.2025.1722564
12. Ergonul O, Celikbas A, Yildirim U, Zenciroglu A, Erdogan D, Ziraman I, et al. Pregnancy and Crimean-Congo haemorrhagic fever. Clin Microbiol Infect. 2010;16:647–50. https://doi.org/10.1111/j.1469-0691.2009.02905.x
13. Stewart LA, Clarke M, Rovers M, Riley RD, Simmonds M, Stewart G, et al.; PRISMA-IPD Development Group. Preferred reporting items for systematic review and meta-analyses of individual participant data: the PRISMA-IPD statement. JAMA. 2015;313:1657–65. https://doi.org/10.1001/jama.2015.3656
14. Soma-Pillay P, Nelson-Piercy C, Tolppanen H, Mebazaa A. Physiological changes in pregnancy. Cardiovasc J S Afr. 2016;27:89–94. https://doi.org/10.5830/CVJA-2016-021
15. Ren D, Fu S, Yan T, Ni T, Zhang Z, Zhang M, et al. The clinical characteristics and outcomes of hemorrhagic fever with renal syndrome in pregnancy. Front Med (Lausanne). 2022;9:839224. https://doi.org/10.3389/fmed.2022.839224
16. Mor G, Cardenas I, Abrahams V, Guller S. Inflammation and pregnancy: the role of the immune system at the implantation site. Ann N Y Acad Sci. 2011;1221:80–7. https://doi.org/10.1111/j.1749-6632.2010.05938.x
17. Auriti C, De Rose DU, Santisi A, Martini L, Piersigilli F, Bersani I, et al. Pregnancy and viral infections: mechanisms of fetal damage, diagnosis and prevention of neonatal adverse outcomes from cytomegalovirus to SARS-CoV-2 and Zika virus. Biochim Biophys Acta Mol Basis Dis. 2021;1867:166198. https://doi.org/10.1016/j.bbadis.2021.166198
18. Schneider E, Kinzler WL. Placental abruption: pathophysiology, diagnosis, and management. Clin Obstet Gynecol. 2025;68:98–104. https://doi.org/10.1097/GRF.0000000000000903
19. US Food and Drug Administration. Content and format of labeling for human prescription drug and biological products; requirements for pregnancy and lactation labeling. Report no. NDA 021511. Silver Spring (MD): The Administration; 2014.
20. Frank MG, Weaver G, Raabe V; State of the Clinical Science Working Group of the National Emerging Pathogens Training Education Center's Special Pathogens Research Network. Crimean-Congo hemorrhagic fever virus for clinicians—epidemiology, clinical manifestations, and prevention. Emerg Infect Dis. 2024;30:854–63. https://doi.org/10.3201/eid3005.231647
21. Mor G, Aldo P, Alvero AB. The unique immunological and microbial aspects of pregnancy. Nat Rev Immunol. 2017;17:469–82. https://doi.org/10.1038/nri.2017.64
22. Sykes L, MacIntyre DA, Yap XJ, Teoh TG, Bennett PR. The Th1:Th2 dichotomy of pregnancy and preterm labour. Mediators Inflamm. 2012;2012:967629. https://doi.org/10.1155/2012/967629
23. Sappenfield E, Jamieson DJ, Kourtis AP. Pregnancy and susceptibility to infectious diseases. Infect Dis Obstet Gynecol. 2013;2013:752852. https://doi.org/10.1155/2013/752852
24. Bebell LM, Oduyebo T, Riley LE. Ebola virus disease and pregnancy: a review of the current knowledge of Ebola virus pathogenesis, maternal, and neonatal outcomes. Birth Defects Res. 2017;109:353–62. https://doi.org/10.1002/bdra.23558
25. Racicot K, Mor G. Risks associated with viral infections during pregnancy. J Clin Invest. 2017;127:1591–9. https://doi.org/10.1172/JCI87490
26. Ajazaj-Berisha L, Halili B, Ndrejaj V, Sherifi K, Jakupi X, Priesnitz S, et al. Crimean-Congo hemorrhagic fever mimicking HELLP syndrome in a pregnant woman and her infant in Kosovo: a case report. Viruses. 2025;17:178. https://doi.org/10.3390/v17020178
27. Erbay A, Çevik MA, Önguru P, Gözel G, Akinci E, Kubar A, et al. Breastfeeding in Crimean-Congo haemorrhagic fever. Scand J Infect Dis. 2008;40:186–8. https://doi.org/10.1080/00365540701649554
28. Yagci-Caglayik D, Kayaaslan B, Yapar D, Kocagul-Celikbas A, Ozkaya-Parlakay A, Emek M, et al. Monitoring Crimean-Congo haemorrhagic fever virus RNA shedding in body secretions and serological status in hospitalised patients, Turkey, 2015. Euro Surveill. 2020;25:10. https://doi.org/10.2807/1560-7917.ES.2020.25.10.1900284
29. Dizbay M, Aktas F, Gaygisiz U, Ozger HS, Ozdemir K. Crimean-Congo hemorrhagic fever treated with ribavirin in a pregnant woman. J Infect. 2009;59:281–3. https://doi.org/10.1016/j.jinf.2009.08.004
30. Arab-Bafrani Z, Jabbari A, Mostakhdem Hashemi M, Arabzadeh AM, Gilanipour A, Mousavi E. Identification of the crucial parameters regarding the efficacy of ribavirin therapy in Crimean-Congo haemorrhagic fever (CCHF) patients: a systematic review and meta-analysis. J Antimicrob Chemother. 2019;74:3432–9. https://doi.org/10.1093/jac/dkz328
31. Güllü D, Yigci D, Baykam N, Çelikbaş AK, Yapar D, Akdoğan Ö, et al. Key predictors of mortality in Crimean-Congo haemorrhagic fever: a retrospective multicentre cohort study. Clin Microbiol Infect. 2025;31:2056–62. https://doi.org/10.1016/j.cmi.2025.08.009
32. Sinclair SM, Jones JK, Miller RK, Greene MF, Kwo PY, Maddrey WC. The Ribavirin Pregnancy Registry: an interim analysis of potential teratogenicity at the mid-point of enrollment. Drug Saf. 2017;40:1205–18. https://doi.org/10.1007/s40264-017-0566-6

Address for correspondence: Önder Ergönül, Topkapı, Koç Üniversitesi Hastanesi, Davutpaşa Cd no. 4, Zeytinburnu/İstanbul 34010, Turkey; email: oergonul@ku.edu.tr

Detection of *Anaplasma capra* in Patients with Suspected Crimean-Congo Hemorrhagic Fever, Turkey, 2022

Kursat Altay,[1] Nazif Elaldi,[1] Ufuk Erol, Binnur Koksal, Omer Faruk Sahin, Ayse Nur Pektas, Seyit Ali Buyuktuna, Murtaza Oz, Yasemin Cakır Kıymaz, Tuba Nur Tasseten, Husnu Furkan Sakar, Mehmet Bakir

Anaplasma capra is a recently discovered bacterial tickborne pathogen that was first identified in goats in 2012 and later in humans in China in 2015. We detected and genetically characterized *A. capra* in adult patients with suspected Crimean-Congo hemorrhagic fever (CCHF) in Turkey during the 2022 outbreak. We screened all patients for *A. capra* by using nested PCR targeting the *gltA* and *groEL* genes. We confirmed CCHF by molecular and serological tests. Of 263 patients, 6 (2.28%) were positive for *A. capra*. Sequence analysis revealed 84.16%–100% *gltA* gene similarity and 90.24%–100% *groEL* gene similarity with GenBank entries. Phylogenetic analysis confirmed all *A. capra* gene sequences belonged to genotype 1. Our results demonstrate clinical evidence of genotype 1 *A. capra* infection in humans. Our findings highlight the need for clinicians to consider *A. capra* in the differential diagnosis of CCHF-like symptoms, especially in endemic areas.

Ticks are hematophagous ectoparasites of the subclass Acari, comprising ≈900 species worldwide. Ticks act as vectors for >200 human and animal pathogens, including bacteria such as the rickettsiae and viruses (*1*). The incidence and effect of tickborne diseases have risen globally because of environmental and weather changes (*2*). Tickborne infections impose a substantial global burden, with hundreds of thousands of human cases reported annually; Lyme disease alone is estimated to cause ≈450,000 cases each year in the United States (*3*,*4*). Turkey, situated at the crossroads of Europe and Asia, is epidemiologically critical for zoonotic infections, with 107 zoonoses reported and 21 classified as high priority by European health authorities (*5*,*6*). In Turkey, ticks serve as major vectors for various zoonotic diseases, including anaplasmosis and Crimean-Congo hemorrhagic fever (CCHF) (*5*–*7*).

Currently, CCHF is the most prevalent tickborne viral disease in humans and is endemic in parts of Africa, Asia, the Middle East, and southeastern Europe. Turkey has reported the highest number of CCHF cases globally (*8*–*10*). The first CCHF cases were documented in 2002 in the Middle Anatolia–Black Sea region, a hyperendemic area for the disease, and ≈1,000 cases have been reported annually since (*10*,*11*). The causative agent, CCHF virus (CCHFV), a member of the Nairoviridae family within the Bunyavirales order, is primarily transmitted by *Hyalomma marginatum* ticks. No licensed vaccine or effective antiviral treatment is available for CCHF (*12*). The disease typically manifests nonspecific symptoms such as fever, fatigue, myalgia, and gastrointestinal complaints but can progress to severe hemorrhagic manifestations. Case-fatality rates (CFRs) vary geographically, reaching up to 30% in some regions; in Turkey, the CFR is ≈5% (*12*,*13*).

Anaplasmosis, caused by *Anaplasma marginale*, *A. centrale*, *A. phagocytophilum*, *A. bovis*, *A. ovis*, and *A. platys* bacteria, is one of the consequential tickborne zoonotic bacterial infections and is transmitted to vertebrate hosts mainly by *Ixodid* species ticks.

Author affiliations: Sivas Cumhuriyet University Faculty of Veterinary Medicine, Sivas, Turkey (K. Altay, U. Erol, O.F. Sahin, H.F. Sakar); Sivas Cumhuriyet University Faculty of Medicine, Sivas (N. Elaldi, S.A. Buyuktuna, M. Oz, Y. Cakır Kıymaz); Sivas Cumhuriyet University Faculty of Health Sciences, Sivas (B. Koksal); Sivas Cumhuriyet University Advanced Technology Application and Research Center, Sivas (A.N. Pektas); Sivas Cumhuriyet University Institute of Science, Sivas (T.N. Tasseten); Medicana Sivas Hospital, Sivas (M. Bakir).

DOI: https://doi.org/10.3201/eid3210.251049

[1]These first authors contributed equally to this article.

A. phagocytophilum is the etiologic agent of anaplasmosis in humans, dogs, horses, and ruminants (*14*). Advances in nucleic acid amplification tests and phylogenetic studies in comparing the DNA sequences of pathogens have enabled the detection of new genotypes and species of tickborne pathogens, revealing the necessity of reinterpreting the etiology of cases (*14*–*18*). In 2012, a study designed to detect *Anaplasma* bacteria in goats (*Capra aegagrus hircus*) in northern China revealed a new *Anaplasma* bacterial gene sequence (*19*). In 2015, the same gene sequence was detected in humans in China and was subsequently named *A. capra*. *A. capra* DNA was detected by nested PCR for the *gltA* gene in 28 (5.9%) of 477 patients who had a tick-bite history (*20*). Symptoms manifested as influenza-like illness, including fever, headache, malaise, dizziness, chills, gastrointestinal symptoms, and elevated hepatic enzyme concentrations. Leukopenia and thrombocytopenia were reported only in a limited number of cases (*20*).

Of note, ≈24% of patients with suspected CCHF in Turkey were found to be negative for CCHFV by molecular and serological tests, suggesting alternative tickborne etiologies (*21*). In addition, *A. capra* has been detected in domestic ruminants and water buffalo in the Middle Anatolia–Black Sea region of Turkey, supporting its tickborne nature and suggesting possible human infection in the same area (*15*,*18*). Our aim is to investigate the presence and molecular characteristics of *A. capra* in hospitalized patients with suspected CCHF in a hyperendemic region of Turkey.

Material and Methods

Study Design and Patient Selection

This retrospective study included 263 adult patients (≥18 years of age) who were hospitalized with suspected CCHF at the clinical ward of the Department of Infectious Diseases and Clinical Microbiology, Sivas Cumhuriyet University Hospital (SCUH), Sivas, Turkey, during a CCHF outbreak in 2022. SCUH is a tertiary referral hospital designated by the Turkish Ministry of Health for CCHF case management, serving a population of ≈1.5 million and located in the hyperendemic Middle Anatolia region. At admission, patients underwent a thorough physical examination and clinical history assessment by ward clinicians.

We included patients in our study on the basis of previously established case definitions (*22*). Study patients had ≥2 clinical manifestations: fever, headache, diffuse body pain, arthralgia, weakness, diarrhea, or bleeding. In addition, patients had to meet ≥1 criteria: residence in or recent travel to a CCHF-endemic region within the previous 2 weeks, a history of tick bite, thrombocytopenia ($<1.5 \times 10^5$ platelets/mm^3), or leukopenia ($<4 \times 10^3$ leukocytes/mm^3).

Sample Collection and CCHF Diagnosis

Three blood samples were collected from each patient. One sample was sent to the SCUH central laboratory for routine biochemical and hematological analysis; a second, 2 mL EDTA-treated (BD, https://www.bd.com) whole blood sample, was processed at the university's Biosafety Level 2 CCHF Research Laboratory for DNA extraction; and the third sample was forwarded to the Turkish Ministry of Health's Central Reference Virology Laboratory in Ankara for confirmation of CCHF via molecular and serologic testing.

The EDTA-treated whole blood samples were anonymized and stored in a deep freezer at –80°C) until DNA extraction. CCHF diagnosis was confirmed by a positive commercial CCHFV qualitative reverse transcriptase PCR (qRT-PCR) test kits (Bioeksen, https://www.bioeksen.com) or commercial CCHFV IgM indirect immunofluorescence test kits (Euroimmun, https://www.euroimmun.com).

We obtained epidemiologic data, including age, sex, place of residence (village, district, and city), occupation, tick exposure history, date of symptom onset, hospitalization, and sample collection via face-to-face interview records. We retrieved clinical findings, laboratory values, and outcomes (fatal or nonfatal) from the hospital's electronic medical record system. All patients were managed by the same clinical team and received standard supportive care, including fluid resuscitation, blood product transfusions (fresh frozen plasma, packed red cells, and apheresis platelets), and cardiovascular and respiratory support as needed (*22*). Oral ribavirin therapy was administered at the discretion of the clinician according to a standard protocol (30 mg/kg loading dose, then 15 mg/kg/6 h for 4 d, then 7.5 mg/kg/8 h for 6 d). Patients were discharged when afebrile, without bleeding, with platelet counts >100,000/mm^3, and with unremarkable coagulation parameters.

Routine microbiological testing included blood and urine cultures at admission. Complete blood count, serum biochemical tests (aspartate aminotransferase, alanine aminotransferase, creatine phosphokinase, lactate dehydrogenase), and coagulation parameters (prothrombin time and activated partial thromboplastin time) were assessed at baseline and monitored as needed during hospitalization.

Brucella spp. Bacteria Testing

In the clinical ward, testing for brucellosis is routinely performed on samples from patients with suspected CCHF (*23*). Diagnostic procedures include the Rose Bengal test, Wright serum agglutination test, Coombs antiglobulin test, and automated blood cultures. Clinicians interpreted the Rose Bengal test as positive or negative on the basis of visible agglutination. They performed Wright and Coombs tests by incubating patient serum at serial dilutions (≥1:20) at 37°C for 48–72 hours; titers of ≥1:160 were considered diagnostically notable. Clinicians processed blood cultures by using BD BACTEC Plus Aerobic/F and Peds Plus/F bottles in the BD BACTEC 9120 automated system (BD). They confirmed positive cultures by using matrix-assisted laser desorption/ionization time-of-flight mass spectrometry with the MALDI Biotyper Microflex LT system (Bruker, https://www.bruker.com).

Molecular Detection of *A. capra* DNA

We performed nested PCR targeting the *gltA* gene to detect *A. capra* DNA in EDTA-treated blood samples. We extracted genomic DNA by using the GeneAll Exgene Clinic SV kit (GeneAll, https://geneall.com), according to the manufacturer's protocol. In the first round of PCR, we amplified 1031 bp of the *gltA* gene, and in the nested PCR step, we amplified 594 bp fragments of the *gltA* gene by using previously described primers (Table 1). We adapted PCR protocols from previously published methods (*20*,*24*). We included positive and negative controls in each PCR run to ensure accuracy and specificity.

Genotyping of *A. capra* Strains

We obtained partial sequences of the *gltA* and *groEL* genes from all PCR-positive samples by using various primers (Table 1). We analyzed the nucleotide sequences by using BLAST (https://blast.ncbi.nlm.nih.gov) to determine their similarity to previously published *A. capra* sequences in GenBank. We submitted all the sequences generated to GenBank and obtained accession numbers for each sequence. We constructed phylogenetic trees for *A. capra gltA* and *groEL* sequences by using the maximum-likelihood method in MEGA 11 software (*25*). We determined the best-fit evolutionary model by using the Find Best-Fit Substitution Model tool in MEGA 11. We selected the Kimura 2-parameter model with gamma-distributed rates and invariant sites for the *gltA* gene (*26*), and we used the Tamura-Nei (TN93) model with gamma distribution among sites for the *groEL* gene (*27*). We performed bootstrap analysis with 1,000 replicates to assess tree robustness.

Data Collection and Statistical Methods

We retrospectively extracted epidemiologic, clinical, laboratory, and outcome data from the electronic medical records of SCUH and entered the data into Microsoft Excel (Microsoft, https://www.microsoft.com). Collected data included patient demographics, symptoms, physical findings, laboratory values, and outcomes (fatal vs. nonfatal). Because this was a descriptive study, we did not perform inferential statistical analyses. We have presented our results as raw counts and percentages where applicable.

Ethics Approval

The study was conducted in accordance with the Declaration of Helsinki and was approved by the research ethics committee of Sivas Cumhuriyet University (protocol no. 2022–12/16). Written informed consent was obtained from all participants.

Results

Diagnosis of CCHF, *A. capra* Infection, and Brucellosis

A total of 263 patients with suspected CCHF were enrolled in the study (100 female and 163 male). Among them, 206 (78.3%) patients were confirmed to have CCHF, diagnosed via CCHFV qRT-PCR (n = 197) or CCHFV IgM serology (n = 9). Nested PCR targeting a 594-bp fragment of the *A. capra gltA* gene identified 6 patients (2.28%) as positive for *A. capra.* All 6 patients were also positive for the *groEL* gene. Two patients were found to have co-infections with both *A. capra*

Table 1. Primers used for amplification of the *gltA* and *groEL* genes of *Anaplasma capra* recovered from patients with anaplasmosis, Turkey

Target gene	Primer name	Primer sequence, 5′ → 3′	Amplified product size, bp	Reference
gltA	Outer-f	GCGATTTTAGAGTGYGGAGATTG	1,031	(*19*)
	Outer-r	TACAATACCGGAGTAAAAGTCAA		
	Inner-f	TCATCTCCTGTTGCACGGTGCCC	594	(*23*)
	Inner-r	CTCTGAATGAACATGCCCACCCT		
groEL	Outer-f	GCG AGG CGT TAG ACA AGT CCATT	1,129	(*19*)
	Outer-r	TCC AGA GAT GCA AGC GTG TATAG		
	Inner-f	TGA AGA GCA TCA AAC CCG AAG	874	(*23*)
	Inner-r	CTG CTC GTG ATG CTA TCG G		

Table 2. Demographic characteristics, clinical symptoms, and physical findings of patients diagnosed with anaplasmosis caused by *Anaplasma capra*, Turkey*

Characteristic	Patient 1	Patient 2	Patient 3	Patient 4	Patient 5	Patient 6
Infectious agent	*A. capra* and CCHFV	*A. capra*	*A. capra*	*A. capra* and *Brucella* sp.	*A. capra* and CCHFV	*A. capra*
Age, y/sex	83/F	30/F	39/F	60/F	48/M	58/F
History of tick bite	No	Unknown	Yes	Unknown	Yes	Yes
Symptoms						
Weakness	Yes	Yes	Yes	Yes	Yes	Yes
Musculoskeletal pain	Yes	No	Yes	No	Yes	Yes
History of fever	Yes	No	No	Yes	Yes	Yes
Headache	No	Yes	No	Yes	Yes	Yes
Nausea and/or vomiting	Yes	No	No	No	No	No
Signs						
Splenomegalia	Yes	No	No	Yes	No	No
Fever, ≥38°C	Yes	No	No	No	No	No
Bleeding events†	No	No	No	No	No	No
Petechia	No	No	No	No	No	No
Hypotension, <90 mm Hg	Yes	No	No	No	No	No
Ecchymosis	Yes	No	No	No	No	No
Confusion	Yes	No	No	No	No	No
Co-infection	CCHFV	No	No	Brucellosis	CCHFV	No
Fatal outcome	Yes	No	No	No	No	No

*CCHFV, Crimean-Congo hemorrhagic fever virus.
†At least 1 of epistaxis, bleeding gum, hemoptysis, hematuria, melena, and vaginal bleeding other than menstrual cycle.

and CCHFV. One patient had a dual infection with *A. capra* and *Brucella* sp., which was confirmed by positive blood culture.

Among the *A. capra*-positive patients without co-infections, we performed an extended diagnostic workup for alternative infectious, autoimmune, and inflammatory etiologies, including viral hepatitis panels, HIV, COVID-19, Epstein-Barr virus, cytomegalovirus, *Rickettsia conorii*, Q fever, autoimmune antibodies (antinuclear, dsDNA, antineutrophil cytoplasmic, cyclic citrullinated peptide, rheumatoid factor, anticardiolipin), antistreptolysin O titer, and thyroid function tests. All test results were negative or unremarkable.

Demographics and Characteristics of *A. capra* Infection

We summarized demographic, clinical, and laboratory characteristics of the 6 patients with anaplasmosis (Table 2). Patients were 30–83 years of age; 5 were female and 1 was male. Three (50%) patients reported

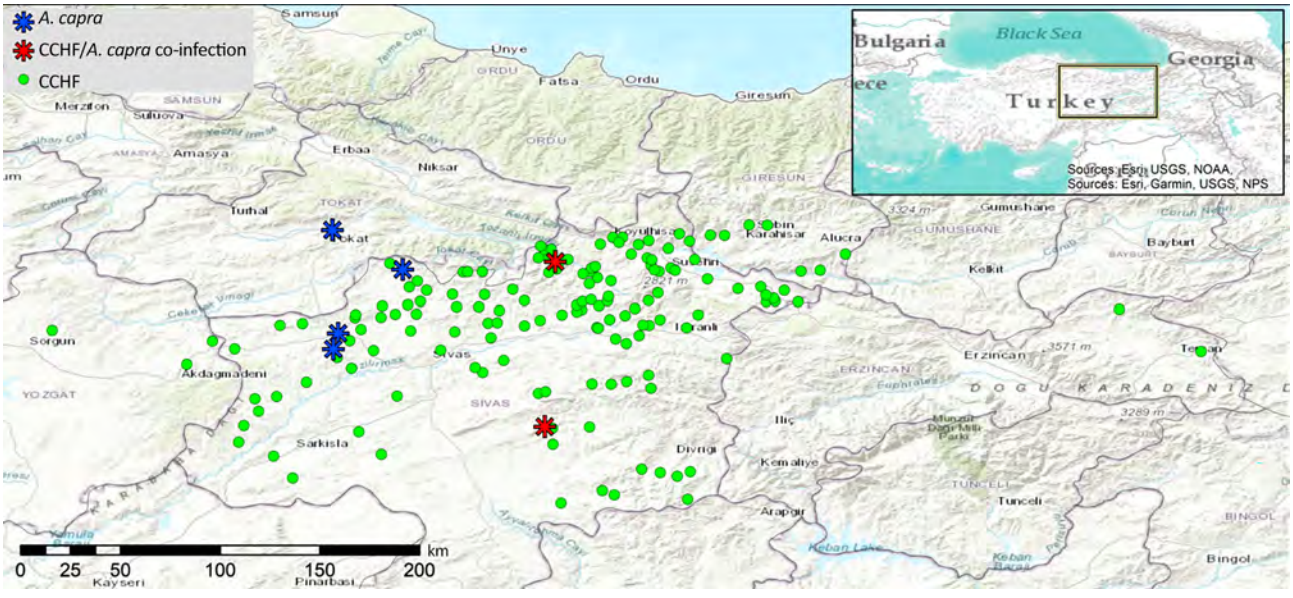

Figure 1. Geographic distribution of patients with suspected or confirmed CCHF in rural areas of Sivas, Tokat, Giresun, Yozgat, Erzincan, and Ordu Provinces, Turkey, 2022. Green dots represent confirmed CCHF patients (n = 206), blue asterisks represent *Anaplasma capra*–only cases, red asterisks represent *A. capra* and CCHF co-infections. Inset shows study area within Turkey. Map reproduced with permission from Zati Vatansever. CCHF, Crimean-Congo hemorrhagic fever.

Table 3. Laboratory testing results of patients diagnosed with anaplasmosis caused by *Anaplasma capra*, Turkey*

Characteristic	Patient 1	Patient 2	Patient 3	Patient 4T	Patient 5	Patient 6
Infectious agent	*A. capra* and CCHFV	*A. capra*	*A. capra*	*A. capra* and *Brucella* sp.	*A. capra* and CCHFV	*A. capra*
Laboratory testing (reference range)						
Leukocytes, cells/mm^3 (4,000–10,500)	3,280	1,750	5,490	2,770	5,640	4,690
Platelets, 10^3/mm^3 (150–450)	20	46	207	74	87	158
Hemoglobin, g/dL (13.5–18.0 [M], 12.5–16.0 [F])	11.1	10.1	15.6	9.7	14.3	12.4
AST, IU/L (0–40)	1,549	78	28	219	362	27
ALT, IU/L (0–40)	476	103	29	95	216	20
CPK, µg/mm^3 (0–190)	4,386	69	297	210	658	63
LDH, IU/L (135–225)	2,303	182	240	895	586	237
PT, seconds (8.4–10.6)	21.4	11.4	8.47	10.4	9.32	8.44
aPTT, seconds (23.6–30.6)	75.8	34.2	24.8	29.5	24.6	25

*ALT, alanine aminotransferase; aPTT, activated partial thromboplastin time; AST, aspartate aminotransferase; CCHFV, Crimean-Congo hemorrhagic fever virus; CPK, creatine phosphokinase; LDH, lactate dehydrogenase; PT, prothrombin time.

a history of tick exposure. All 6 were residents in rural areas of Sivas (n = 5) and Tokat (n = 1) provinces (Figure 1). Common symptoms were fatigue (100%, n = 6), musculoskeletal pain (66.7%, n = 4), headache (66.7%, n = 4), and fever history (66.7%, n = 4). Physical examination revealed splenomegaly in 2 patients (33.3%) and current fever (38.3°C) in 1 patient (16.7%). No bleeding manifestations were observed in any of the cases. Leukopenia was observed in 3 patients (50%, n = 3), including 1 co-infected with *Brucella* sp. (patient 4) and another with CCHFV. Thrombocytopenia was observed in 4 patients (66.7%, n = 4), 2 of whom had co-infection with CCHFV and 1 with *Brucella* sp. (Table 3). One patient who was co-infected with CCHFV died (Table 2).

Antimicrobial Drug Treatment for *A. capra*

Because of the retrospective nature of our study, patients did not receive targeted treatment for anaplasmosis during hospitalization. One surviving patient co-infected with *Brucella* sp. was successfully treated with a 42-day regimen of oral rifampin and doxycycline. Among the remaining patients, 1 (co-infected with CCHFV) died without receiving doxycycline therapy. The other 4 survivors were contacted and invited for postdischarge doxycycline treatment; however, they did not return for follow-up.

A. capra gltA and *groEL* Sequencing and Phylogenetic Analyses

We submitted the *gltA* and *groEL* gene sequences obtained from all 6 *A. capra*–positive patients to GenBank (accession nos. OQ819441–6 [*gltA*] and OQ819447–52 [*groEL*]). Nucleotide similarity analysis of the *gltA* sequences revealed 84.16%–100% identity with previously published *A. capra* sequences in GenBank. The sequences exhibited high similarity (98.11%–100%) to strains from cattle, sheep, goats, and wild animals across various geographic regions. In addition, our human *A. capra* sequences revealed 100% identity with *A. capra* strains previously detected in water buffalo (GenBank accession nos. ON783817–9) in Turkey, as well as with sequences from sheep (accession no. MW930534), goats (accession no. MW930535), red deer (accession no. MH084720), and swamp deer (accession no. MH084719) in France and sheep in Kyrgyzstan (accession nos. OM100820–40).

Alignment of the *gltA* sequences revealed 0–8 nucleotide substitutions compared with 58 *A. capra* sequences from domestic and wild animals. In contrast, comparisons with 158 *A. capra* sequences from humans, animals, and ticks showed greater genetic diversity (84.16%–88.05% similarity), with 65–67 nucleotide differences observed (Appendix Figure 1, http://wwwnc.cdc.gov/EID/article/32/10/25-1049-App1.pdf). The phylogenetic tree created on the basis of *gltA* sequences indicated that the sequences clustered into 2 distinct genotypes (Figure 2).

Similarly, the *groEL* gene sequences from the study samples showed 90.24%–100% identity with *A. capra* sequences in GenBank. We observed high nucleotide similarity (97.91%–100%) between our human *A. capra* sequences and those from water buffalo, sheep, goats, red deer, swamp deer, Korean water deer, roe deer, and ticks such as *Dermacentor everestianus* and *Haemaphysalis qinghaiensis*. Specifically, we noted 100% sequence identity with sequences from water buffalo in Turkey (GenBank accession nos. ON783820–2) and a sequence from a sheep in France (accession no. MW930531). Between our sequences and 26 closely related *A. capra* sequences, we found 0–17 nucleotide substitutions. However, we observed major differences (71–72 nucleotide substitutions) when sequences were compared with 138 *A. capra* sequences from domestic and wild animals, ticks, and humans (Appendix Figure 2). The phylogenetic tree we constructed from *groEL* sequences further supported the classification of sequences into 2 clades (Figure 3).

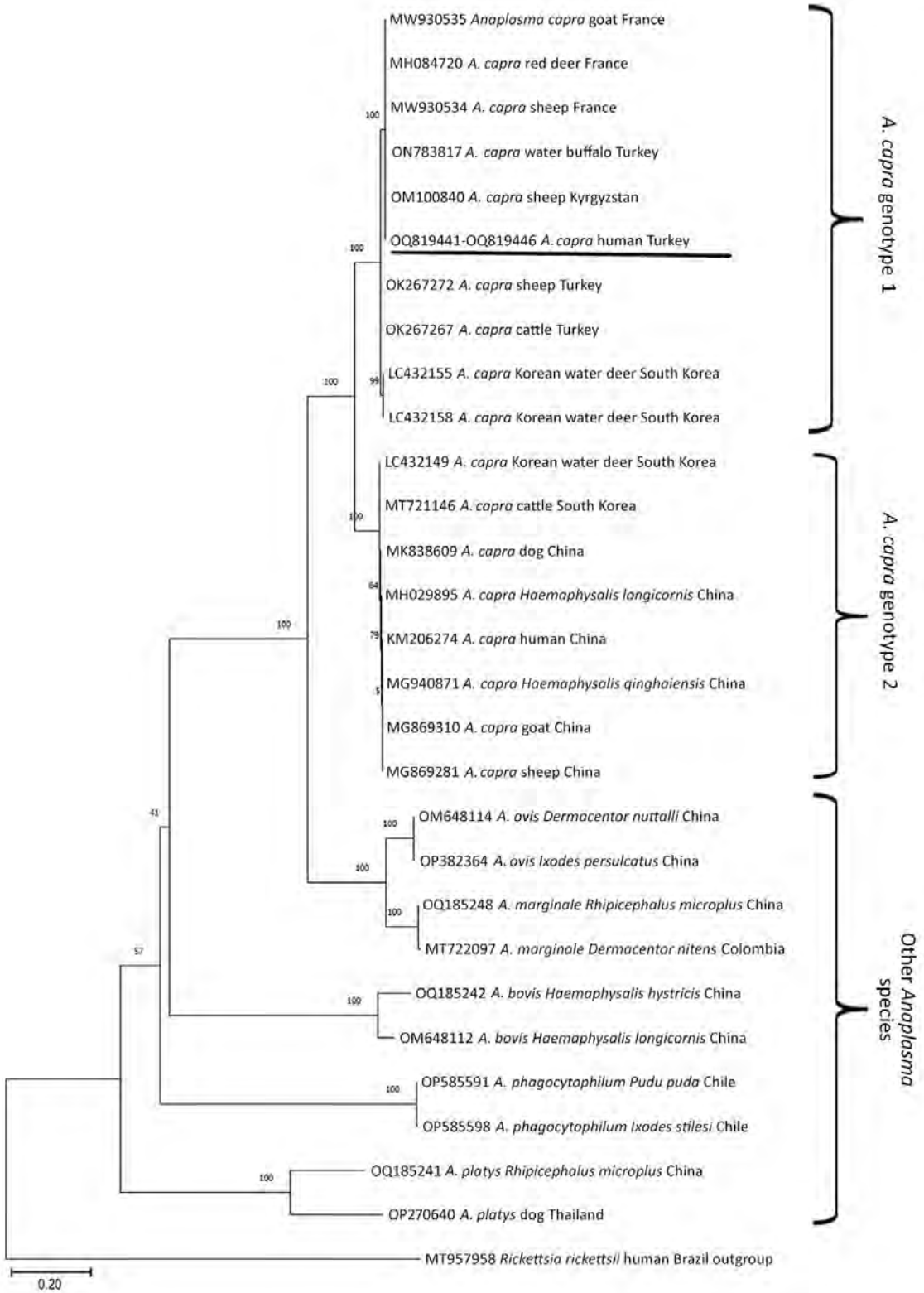

Figure 2. Phylogenetic tree of *gltA* gene sequences from *Anaplasma capra* genotype 1, genotype 2, and related species from patients with suspected or confirmed Crimean-Congo hemorrhagic fever, Turkey, 2022. We constructed the tree by using the maximum-likelihood method in MEGA 11 (*25*). *Rickettsia rickettsii* was used as the outgroup. Study sequences are underlined. GenBank accession numbers are provided. Scale bar represents nucleotide substitutions per site.

Discussion

To date, multiple studies have demonstrated that *A. capra* can infect a wide range of hosts and might have a global distribution. The bacterium has been identified in various animal species, including goats, sheep (*28*), cattle (*29*), dogs (*30*), and yaks (*31*), and in multiple tick speciesm such as *Haemaphysalis qinghaiensis* (*31*), *H. longicornis* (*32*), *Rhipicephalus microplus* (*33*), *Dermacentor abaensis*, and *D. nuttalli* (*34*) in China. Beyond China, *A. capra* was first detected in cattle in Malaysia (*35*) and later in sheep in Sweden in 2018 (*36*), marking its identification in Europe. In 2021, it was also detected in cattle and ticks in Angola, establishing its presence in Africa (*37*). In Turkey, *A. capra* has been identified in cattle, sheep (*15*), and water buffalo (*18*).

Most previous studies have focused on animal hosts and the molecular characterization of *A. capra.* However, we detected *A. capra* in 6 (2.28%) of 263 adult patients who were hospitalized for suspected CCHF. This study provides clinical evidence of *A. capra* infection in humans outside of China, confirming its zoonotic potential and geographic spread.

Anaplasma spp. bacteria are known to infect various blood cells, including monocytes, platelets, and granulocytes, where they replicate intracellularly (*14*). *A. capra* has been shown to infect erythrocytes under in vitro conditions, forming dark vacuolar inclusions or corpuscles in the cytoplasm (*38*). Clinically, CCHFV infection is known to range from mild illness to severe disease with multiorgan involvement and death. In contrast, human infections with *A. capra* have so far been associated with milder clinical manifestations, with no reported fatalities to date. Shared clinical and laboratory features include fever, malaise, headache, myalgia, and elevated hepatic enzyme levels, whereas leukopenia and thrombocytopenia have been reported only in a limited number of *A. capra* cases (*10*,*13*,*20*). In a previous study, 5 (17.9%) of 28 patients with *A. capra* infection were hospitalized for 11–21 days because of severe illness characterized by lymphadenopathy and elevated liver enzymes (*20*). Because of the shared transmission routes and overlapping clinical features, persons living in rural areas or involved in animal husbandry are at high risk for both CCHF and anaplasmosis. The CFR for anaplasmosis is typically low (<1%); doxycycline is the drug of choice for the treatment of anaplasmosis (*20*,*39*). One study reported that all 28 patients in their cohort were successfully treated with doxycycline with no fatalities (*20*). In our study, 1 of the 6 patients (16.7%) died; the patient was co-infected with CCHFV.

Because CCHFV is well-established as causing death and ticks can harbor multiple pathogens (*6*), the specific contribution of *A. capra* infection to disease severity or mortality cannot be determined. However, we cannot determine whether *A. capra* and CCHFV and *A. capra* and *Brucella* sp. can be transmitted together by a single tick bite. This study and a previous one showed co-infections with CCHFV and other pathogens (*21*). Despite ticks having the potential capacity of *Brucella* spp. transmission, we found limited literature on tickborne brucellosis in humans (*40*). Because some patients are residents in rural areas and perform animal husbandry, they have risks for both CCHFV and *Brucella* spp. transmission.

Our findings highlight the diagnostic challenges in patients with a history of tick exposure seeking care for nonspecific clinical manifestations. Therefore, diagnostic approaches should be guided by clinical evaluation and the limitations of available laboratory tests rather than focusing on a single etiologic agent. In such settings, empiric treatment with doxycycline might be considered when clinically indicated, particularly in endemic areas for tickborne diseases.

After the recognition of *A. capra*'s zoonotic potential, several molecular studies have investigated its genetic characteristics. Analyses of the 16S rRNA, *gltA*, and *groEL* genes have revealed substantial genetic variation across sequences (*15*–*18*,*20*). Research conducted in Turkey has identified 2 distinct genotypes of *A. capra*, genotype 1 and genotype 2. Although prior studies found no strong correlation between genotype and host species or geographic origin, all previously reported human cases in China were associated with genotype 2 (*15*,*17*,*18*). In our study, both *gltA* and *groEL* gene analyses confirmed that the human *A. capra* sequences clustered within genotype 1 (Appendix Figures 1,2). Although genotypes and 2 can be distinguished on the basis of gene sequencing, their roles in host specificity and disease manifestations remain unclear. Further studies are needed to better characterize those genotypes and clarify their clinical and epidemiologic significance.

The first limitation of this study is that serologic testing for *A. capra* was not performed because of the lack of validated and widely available assays, which limits our ability to support the molecular findings with serologic evidence. Second, the small number of cases restricts the generalizability of our findings. Finally, our study population might be subject to selection bias, because our inclusion criteria required the presence of leukopenia or thrombocytopenia (because of suspected CCHF).

In conclusion, the public health significance of tickborne pathogens continues to grow because of expanding interactions between humans and tick

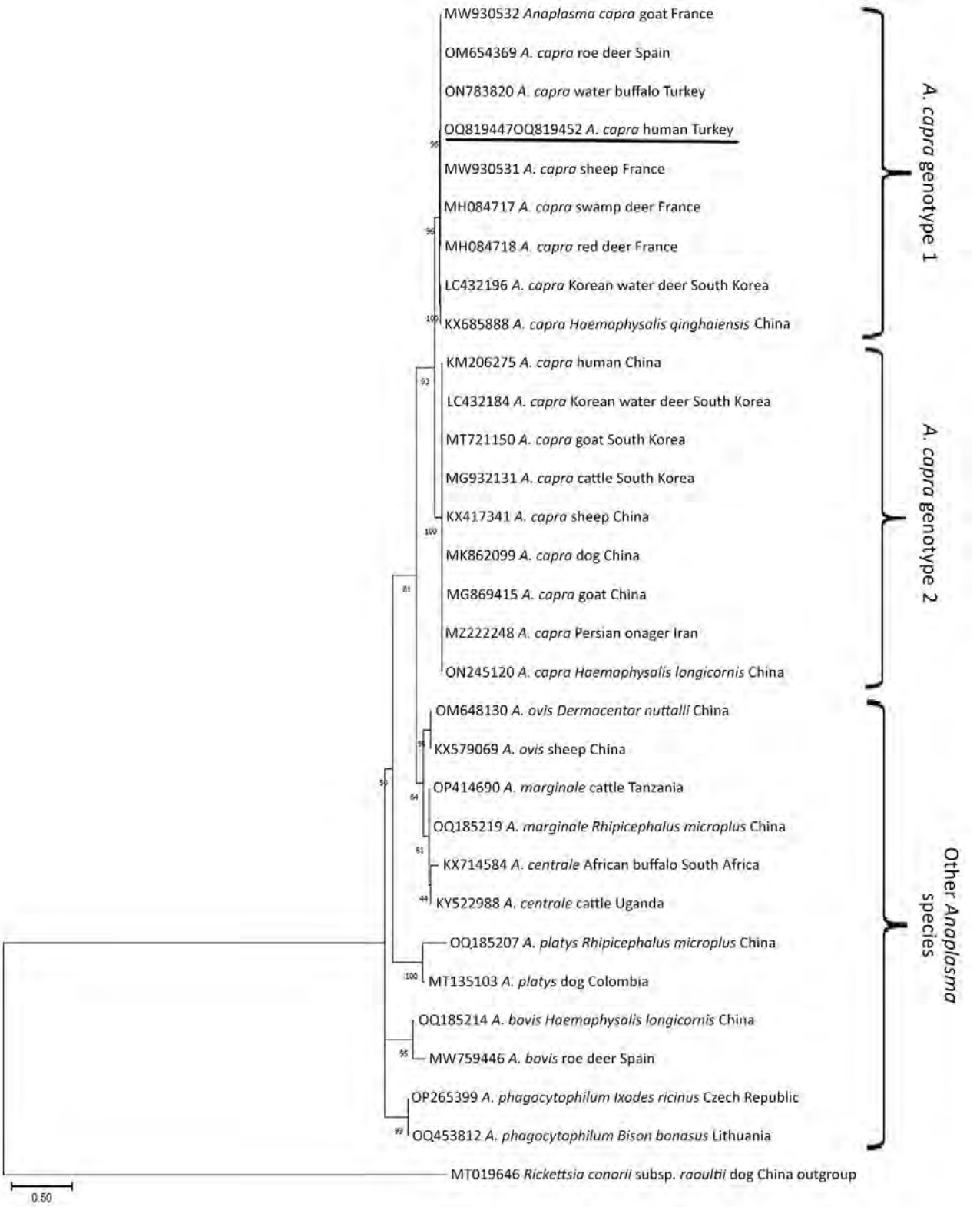

Figure 3. Phylogenetic tree of *groEL* gene sequences from *Anaplasma capra* genotype 1, genotype 2, and other *Anaplasma* species from patients with suspected or confirmed Crimean-Congo hemorrhagic fever, Turkey, 2022. We constructed the tree by using the maximum-likelihood method in MEGA 11 (*25*). *Rickettsia conorii* subspecies *raoultii* was used as the outgroup. Study sequences are underlined. GenBank accession numbers are provided. Scale bar represents nucleotide substitutions per site.

habitats. We found molecular evidence of *A. capra* infection in humans in Turkey. Our findings demonstrate that *A. capra* is circulating not only in domestic and wild animals but also in humans in the Middle Anatolia/Black Sea region, a known hyperendemic area for CCHF. Those results confirm the zoonotic potential of *A. capra* genotype 1 and highlight the need for further research to identify its biologic vectors and better understand its epidemiology in CCHF-endemic areas. Clinicians working in such regions should be aware of *A. capra* as a differential diagnosis in patients with a history of tick exposure and suspected CCHF, especially with negative CCHFV test results.

Acknowledgments

The authors gratefully acknowledge the Central CCHF Reference Virology Laboratory of the Turkish Ministry of Health, Ankara, Turkey, for providing diagnostic testing for CCHFV.

Author contributions: conceptualization, methodology, formal analysis, original draft, and review and editing of draft, K.A. and N.E.; methodology and formal analysis, U.E., B.K., O.F.S., and A.N.P.; methodology and resources, S.A.B., M.O., Y.C.K., T.N.T., H.F.S., and M.B.

About the Author

Dr. Elaldi is a professor at the Sivas Cumhuriyet University, Sivas, Turkey. His research focuses on emerging and reemerging infections and molecular surveillance with particular emphasis on vectorborne pathogens, including Crimean-Congo hemorrhagic fever virus.

References

1. Negi T, Kandari LS, Arunachalam K. Update on prevalence and distribution pattern of tick-borne diseases among humans in India: a review. Parasitol Res. 2021;120:1523–39. https://doi.org/10.1007/s00436-021-07114-x
2. Sonenshine DE. Range expansion of tick disease vectors in North America: implications for spread of tick-borne disease. Int J Environ Res Public Health. 2018;15:478. https://doi.org/10.3390/ijerph15030478
3. de la Fuente J, Estrada-Pena A, Venzal JM, Kocan KM, Sonenshine DE. Overview: ticks as vectors of pathogens that cause disease in humans and animals. Front Biosci. 2008;13:6938–46. https://doi.org/10.2741/3200
4. Centers for Disease Control and Prevention. Lyme disease surveillance and data, 2025 [cited 2026 Mar 23]. https://www.cdc.gov/lyme/data-research/facts-stats/index.html
5. Düzlü Ö, İnci A, Yıldırım A, Doğanay M, Özbel Y, Aksoy S. Vector-borne zoonotic diseases in Turkey: rising threats on public health. Turkiye Parazitol Derg. 2020;44:168–75. https://doi.org/10.4274/tpd.galenos.2020.6985
6. Inci A, Yildirim A, Duzlu O, Doganay M, Aksoy S. Tick-borne diseases in Turkey: a review based on one health perspective. PLoS Negl Trop Dis. 2016;10:e0005021. https://doi.org/10.1371/journal.pntd.0005021
7. Aydin L, Bakirci S. Geographical distribution of ticks in Turkey. Parasitol Res. 2007;101(Suppl 2):S163–6. https://doi.org/10.1007/s00436-007-0694-5
8. Sorvillo TE, Rodriguez SE, Hudson P, Carey M, Rodriguez LL, Spiropoulou CF, et al. Towards a sustainable One Health approach to Crimean-Congo hemorrhagic fever prevention: focus areas and gaps in knowledge. Trop Med Infect Dis. 2020;5:113. https://doi.org/10.3390/tropicalmed5030113
9. Shahhosseini N, Wong G, Babuadze G, Camp JV, Ergonul O, Kobinger GP, et al. Crimean-Congo hemorrhagic fever virus in Asia, Africa and Europe. Microorganisms. 2021;9:1907. https://doi.org/10.3390/microorganisms9091907
10. Bente DA, Forrester NL, Watts DM, McAuley AJ, Whitehouse CA, Bray M. Crimean-Congo hemorrhagic fever: history, epidemiology, pathogenesis, clinical syndrome and genetic diversity. Antiviral Res. 2013;100:159–89. https://doi.org/10.1016/j.antiviral.2013.07.006
11. Gunes T, Engin A, Poyraz O, Elaldi N, Kaya S, Dokmetas I, et al. Crimean-Congo hemorrhagic fever virus in high-risk population, Turkey. Emerg Infect Dis. 2009;15:461–4. https://doi.org/10.3201/eid1503.080687
12. Hawman DW, Feldmann H. Crimean-Congo haemorrhagic fever virus. Nat Rev Microbiol. 2023;21:463–77. https://doi.org/10.1038/s41579-023-00871-9
13. Yilmaz GR, Buzgan T, Irmak H, Safran A, Uzun R, Cevik MA, et al. The epidemiology of Crimean-Congo hemorrhagic fever in Turkey, 2002–2007. Int J Infect Dis. 2009;13:380–6. https://doi.org/10.1016/j.ijid.2008.07.021
14. Dumler JS, Barbet AF, Bekker CP, Dasch GA, Palmer GH, Ray SC, et al. Reorganization of genera in the families *Rickettsiaceae* and *Anaplasmataceae* in the order *Rickettsiales*: unification of some species of *Ehrlichia* with *Anaplasma, Cowdria* with *Ehrlichia* and *Ehrlichia* with *Neorickettsia*, descriptions of six new species combinations and designation of *Ehrlichia equi* and 'HGE agent' as subjective synonyms of *Ehrlichia phagocytophila.* Int J Syst Evol Microbiol. 2001;51:2145–65. https://doi.org/10.1099/00207713-51-6-2145
15. Altay K, Erol U, Sahin OF. The first molecular detection of *Anaplasma capra* in domestic ruminants in the central part of Turkey, with genetic diversity and genotyping of *Anaplasma capra.* Trop Anim Health Prod. 2022;54:129. https://doi.org/10.1007/s11250-022-03125-7
16. Altay K, Erol U, Sahin OF, Aytmirzakizi A. First molecular detection of *Anaplasma* species in cattle from Kyrgyzstan; molecular identification of human pathogenic novel genotype *Anaplasma capra* and *Anaplasma phagocytophilum* related strain. Ticks Tick Borne Dis. 2022;13:101861. https://doi.org/10.1016/j.ttbdis.2021.101861
17. Altay K, Erol U, Sahin OF, Aytmirzakizi A, Temizel EM, Aydin MF, et al. The detection and phylogenetic analysis of *Anaplasma phagocytophilum*-like 1, *A. ovis* and *A. capra* in sheep: *A. capra* divides into two genogroups. Vet Res Commun. 2022;46:1271–9. https://doi.org/10.1007/s11259-022-09998-1
18. Sahin OF, Erol U, Altay K. Buffaloes as new hosts for *Anaplasma capra*: Molecular prevalence and phylogeny based on *gtlA, groEL,* and *16S rRNA* genes. Res Vet Sci. 2022;152:458–64. https://doi.org/10.1016/j.rvsc.2022.09.008
19. Liu Z, Ma M, Wang Z, Wang J, Peng Y, Li Y, et al. Molecular survey and genetic identification of *Anaplasma* species in

goats from central and southern China. Appl Environ Microbiol. 2012;78:464–70. https://doi.org/10.1128/AEM.06848-11
20. Li H, Zheng YC, Ma L, Jia N, Jiang BG, Jiang RR, et al. Human infection with a novel tick-borne *Anaplasma* species in China: a surveillance study. Lancet Infect Dis. 2015;15:663–70. https://doi.org/10.1016/S1473-3099(15)70051-4
21. Fırtına Topcu K, Sümer Z. Investigation of the Crimean-Congo hemorrhagic fever virus and the seropositivity of *Coxiella burnetii, Borrelia burgdorferi* in patients with a history of tick bites. Turk Mikrobiyol Cemiy Derg. 2022;52:265–73. https://doi.org/10.54453/TMCD.2022.78557
22. Leblebicioglu H, Bodur H, Dokuzoguz B, Elaldi N, Guner R, Koksal I, et al. Case management and supportive treatment for patients with Crimean-Congo hemorrhagic fever. Vector Borne Zoonotic Dis. 2012;12:805–11. https://doi.org/10.1089/vbz.2011.0896
23. Öz M, Çubuk F, Çakır Kıymaz Y, Öksüz C, Hasbek M, Büyüktuna SA, et al. Hidden threats: brucellosis diagnosis and co-infection patterns in Crimean-Congo hemorrhagic fever suspects. Diagn Microbiol Infect Dis. 2025;111:116724. https://doi.org/10.1016/j.diagmicrobio.2025.116724
24. Yang J, Liu Z, Niu Q, Liu J, Han R, Liu G, et al. Molecular survey and characterization of a novel *Anaplasma* species closely related to *Anaplasma capra* in ticks, northwestern China. Parasit Vectors. 2016;9:603. https://doi.org/10.1186/s13071-016-1886-6
25. Tamura K, Stecher G, Kumar S. MEGA11: molecular evolutionary genetics analysis version 11. Mol Biol Evol. 2021;38:3022–7. https://doi.org/10.1093/molbev/msab120
26. Kimura M. A simple method for estimating evolutionary rates of base substitutions through comparative studies of nucleotide sequences. J Mol Evol. 1980;16:111–20. https://doi.org/10.1007/BF01731581
27. Tamura K, Nei M. Estimation of the number of nucleotide substitutions in the control region of mitochondrial DNA in humans and chimpanzees. Mol Biol Evol. 1993;10:512–26.
28. Yang J, Liu Z, Niu Q, Liu J, Han R, Guan G, et al. A novel zoonotic *Anaplasma* species is prevalent in small ruminants: potential public health implications. Parasit Vectors. 2017;10:264. https://doi.org/10.1186/s13071-017-2182-9
29. Guo WP, Huang B, Zhao Q, Xu G, Liu B, Wang YH, et al. Human-pathogenic *Anaplasma* spp., and *Rickettsia* spp. in animals in Xi'an, China. PLoS Negl Trop Dis. 2018;12:e0006916. https://doi.org/10.1371/journal.pntd.0006916
30. Shi K, Li J, Yan Y, Chen Q, Wang K, Zhou Y, et al. Dogs as new hosts for the emerging zoonotic pathogen *Anaplasma capra* in China. Front Cell Infect Microbiol. 2019;9:394. https://doi.org/10.3389/fcimb.2019.00394
31. Wang Y, Zhang Q, Han S, Li Y, Wang B, Yuan G, et al. *Ehrlichia chaffeensis* and four *Anaplasma* species with veterinary and public health significance identified in Tibetan sheep (*Ovis aries*) and yaks (*Bos grunniens*) in Qinghai, China. Front Vet Sci. 2021;8:727166. https://doi.org/10.3389/fvets.2021.727166
32. Zhang H, Sun Y, Jiang H, Huo X. Prevalence of severe febrile and thrombocytopenic syndrome virus, *Anaplasma* spp. and *Babesia microti* in hard ticks (Acari: Ixodidae) from Jiaodong Peninsula, Shandong Province. Vector Borne Zoonotic Dis. 2017;17:134–40. https://doi.org/10.1089/vbz.2016.1978
33. Guo WP, Zhang B, Wang YH, Xu G, Wang X, Ni X, et al. Molecular identification and characterization of *Anaplasma capra* and *Anaplasma* platys-like in *Rhipicephalus microplus* in Ankang, Northwest China. BMC Infect Dis. 2019;19:434. https://doi.org/10.1186/s12879-019-4075-3
34. Han R, Yang JF, Mukhtar MU, Chen Z, Niu QL, Lin YQ, et al. Molecular detection of *Anaplasma* infections in ixodid ticks from the Qinghai-Tibet Plateau. Infect Dis Poverty. 2019;8:12. https://doi.org/10.1186/s40249-019-0522-z
35. Koh FX, Panchadcharam C, Sitam FT, Tay ST. Molecular investigation of *Anaplasma* spp. in domestic and wildlife animals in Peninsular Malaysia. Vet Parasitol Reg Stud Reports. 2018;13:141–7. https://doi.org/10.1016/j.vprsr.2018.05.006
36. Grandi G, Aspán A, Pihl J, Gustafsson K, Engström F, Jinnerot T, et al. Detection of tick-borne pathogens in lambs undergoing prophylactic treatment against ticks on two Swedish farms. Front Vet Sci. 2018;5:72. https://doi.org/10.3389/fvets.2018.00072
37. Barradas PF, Mesquita JR, Ferreira P, Gärtner F, Carvalho M, Inácio E, et al. Molecular identification and characterization of *Rickettsia* spp. and other tick-borne pathogens in cattle and their ticks from Huambo, Angola. Ticks Tick Borne Dis. 2021;12:101583. https://doi.org/10.1016/j.ttbdis.2020.101583
38. Peng Y, Lu C, Yan Y, Song J, Pei Z, Gong P, et al. The novel zoonotic pathogen, *Anaplasma capra*, infects human erythrocytes, HL-60, and TF-1 cells in vitro. Pathogens. 2021;10:600. https://doi.org/10.3390/pathogens10050600
39. MacQueen D, Centellas F. Human granulocytic anaplasmosis. Infect Dis Clin North Am. 2022;36:639–54. https://doi.org/10.1016/j.idc.2022.02.008
40. Ma R, Li C, Gao A, Jiang N, Feng X, Li J, et al. Evidence-practice gap analysis in the role of tick in brucellosis transmission: a scoping review. Infect Dis Poverty. 2024;13:3. https://doi.org/10.1186/s40249-023-01170-4

Address for correspondence: Nazif Elaldi, Sivas Cumhuriyet University Faculty of Medicine, Department of Infectious Diseases and Clinical Microbiology, 58140, Sivas, Turkey; email: nelaldi@cumhuriyet.edu.tr

Systematic Review and Meta-analysis of Group B *Streptococcus* Rectovaginal Colonization Rates and Serotype Distribution among Pregnant Women, Asia-Pacific Region, 2014–2025

Zheng Quan Toh, Lien Anh Ha Do, Darren Suryawijaya Ong, Claire von Mollendorf,[1] Fiona M. Russell[1]

We conducted a systematic review and meta-analysis of group B *Streptococcus* (GBS) rectovaginal colonization prevalence, serotype distribution, and antimicrobial drug resistance (AMR) rates among pregnant women in the Asia-Pacific region. We included articles published in the MEDLINE, Embase, and PubMed databases during January 2014–October 2025. Overall, 1,623 studies were identified; 98 of those were included in the meta-analysis. Of 978,150 pregnant women, 172,973 were colonized with GBS; pooled estimated prevalence was 18.0% (95% CI 12%–23%). Studies from Southeast Asia were limited. GBS serotype distributions were reported in 24 studies; serotype III was the most common (range 5.0%–100.0%). Thirty studies included AMR rates; low (0%–2.0%) AMR rates were found for β-lactams. GBS colonization is common among pregnant women in the Asia-Pacific region. Continued surveillance of GBS prevalence will be needed, particularly in Pacific and Southeast Asian countries, to guide effective GBS prevention and treatment programs.

Group B *Streptococcus* (GBS), also known as *Streptococcus agalactiae*, is a gram-positive bacterium that causes substantial infant illness and death worldwide (*1*). Approximately 400,000 cases of neonatal invasive GBS disease and >90,000 deaths associated with GBS infections occur globally each year (*2*–*4*). Most GBS cases and associated deaths occur in low- and middle-income countries, where access to antenatal screening and treatment is limited (*2*–*4*).

Maternal rectovaginal GBS colonization is a major risk factor for invasive GBS disease in pregnant women and neonates (*5*). Pregnant women who have rectovaginal GBS colonization can transfer bacteria to their fetuses or newborn infants during delivery, causing early onset of neonatal invasive GBS disease. To reduce GBS transmission, most high-income countries offer intrapartum antibiotic prophylaxis (IAP) to GBS-positive pregnant women, screened at 35–37 weeks' gestation, or to women who have established risk factors for GBS colonization. Risk factors include prolonged rupture of amniotic membranes, GBS bacteriuria during pregnancy, intrapartum maternal fever, and having previously delivered an infant who had early-onset GBS disease (*6*). Penicillin or ampicillin is the first-line antimicrobial treatment for GBS infection; clindamycin or vancomycin is used for persons who are allergic to penicillin (*7*). However, low-income countries face major challenges in implementing GBS screening and IAP, including lack of national GBS screening guidelines and programs, limited access to prenatal care, lack of laboratory resources for testing, and high prevalences of home births (*8*,*9*). Furthermore, frequent use of antimicrobial drugs has raised concerns regarding the emergence of antimicrobial drug resistance (AMR) (*10*).

Systematic reviews of global maternal rectovaginal GBS colonization up to January 2020 reported the average colonization rate to be 14%–18%; the highest

Author affiliation: Murdoch Children's Research Institute and University of Melbourne, Parkville, Victoria, Australia

DOI: https://doi.org/10.3201/eid3210.260687

[1]These authors contributed equally to this article.

prevalences occurred in Africa and central and South Asia (*2*,*11*,*12*). Those reviews contained limited data from the Asia-Pacific region, particularly the Oceania subregion (*2*,*11*,*12*). Maternal GBS colonization rates were used to estimate global and regional prevalence of invasive GBS in infants; estimates for the Oceania subregion were extrapolated from other regional data (*2*). Among the 10 GBS serotypes, Ia, III, and V were the most common serotypes found in maternal colonization and accounted for >60% of invasive GBS disease in infants (*13*), although serotype distribution varied by region. Serotypes VI–IX were more common in Asia (6%–16%) and West Africa (15%) than in Europe (<2%) or North America (<1%) (*11*,*13*). To inform public health policy and develop preventive and treatment strategies against invasive GBS, we conducted a systematic review and meta-analysis to assess maternal rectovaginal GBS colonization rates, serotype distribution, and AMR rates among pregnant women in the Asia-Pacific region.

Methods

We registered our systematic review protocol at PROSPERO (https://www.crd.york.ac.uk; registration no. CRD42024535368). We followed the PRISMA (Preferred Reporting Items for Systematic reviews and Meta-Analyses) 2020 guidelines (https://www.prisma-statement.org) for reporting systematic review data.

Search Strategy and Selection Criteria

We included articles published during January 1, 2014, to October 31, 2025, in MEDLINE (https://www.nlm.nih.gov/medline) and Embase (https://www.embase.com) using the OVID platform (https://www.ovid.com). We used Medical Subject Headings and thesaurus terms and keywords. We searched PubMed (https://pubmed.ncbi.nlm.nih.gov) for articles not yet indexed. We used search terms related to *Streptococcus agalactiae*, carriage, mothers, pregnancy, and Asia-Pacific. We limited our search to studies published in English (Appendix, https://wwwnc.cdc.gov/EID/article/32/10/26-0687-App1.pdf). We included studies reporting GBS colonization rates in pregnant and postpartum women and those reporting samples obtained from vaginal, rectal, or perianal regions. We included all observational and case studies reporting GBS prevalence in pregnant women from East Asia, South Asia, Southeast Asia, and Oceania.

We excluded studies of pregnant women when GBS prevalence estimates were derived from <50 women or when rates could not be ascertained from laboratory sample data. We also excluded modeling, ecologic, and qualitative studies; systematic reviews; opinion-based pieces; and animal studies.

We uploaded the search results to Covidence systematic review management software (https://www.covidence.org) for screening. Two authors independently screened the titles and abstracts of the studies; Z.Q.T. screened 100% and L.A.H.D. screened 10% of randomly selected papers. We excluded duplicate articles during the Covidence uploading and screening stages. Z.Q.T. and L.A.H.D. each independently performed 100% of full-text study screening. The 2 reviewers resolved any disagreements at the screening or full-text stages through mutual consensus.

Data Extraction and Quality Assessment

One reviewer (Z.Q.T.) extracted data by using Covidence and Microsoft Excel (https://www.microsoft.com) tables. Extracted data included country, study period, study design, study population, gestational age at time of sampling, number of pregnant women tested, number of women with detected GBS, method of detection (culture or molecular, with or without enrichment), sampling site (vagina, rectum, or perianal region at any time during pregnancy), serotype distribution, serotyping methods, AMR rates, and AMR testing method.

We used the Joanna Briggs Institute Critical Appraisal Tool (https://jbi.global/critical-appraisal-tools) for analytical cross-sectional studies to assess the risk of bias scores in the studies; Z.Q.T. performed the assessment. We selected that risk of bias tool because our review focused on the prevalence of GBS colonization, and most studies were observational. We addressed 8 criteria (Appendix Table 1). A yes response received a score of 1, whereas a no or unclear response received a score of 0. We considered a total score of 6–8 as low risk, 3–5 as moderate risk, and 0–2 as high risk for bias.

Data Analysis

We generated data by using Microsoft Excel and analyzed those data by using Stata version 19.0 (StataCorp LLC, https://www.stata.com). We excluded studies from the meta-analysis that had a high risk for bias (score <3). We pooled GBS prevalences by using a random-effects inverse variance model, weighted by sample size. This model assumed that studies included in the meta-analysis were a random sample from a larger population of studies and that prevalences varied across those studies. We pooled GBS prevalences according to country income levels by using 2026 World Bank country income

classifications (https://datahelpdesk.worldbank.org/knowledgebase/articles/906519-world-bank-country-and-lending-groups) and visualized those data on Forrest plots and line graphs; we expressed prevalence as percentage (95% CI). We performed analyses for East Asia, South Asia, Southeast Asia, and Oceania subgroups. We assessed heterogeneity between studies by using an I^2 test. We summarized GBS serotype distribution and AMR rates for studies that reported those outcomes. We generated figures for GBS colonization prevalence rates according to detection methods and serotype distribution, as well as descriptive statistics by using GraphPad Prism version 10 (GraphPad Software, Inc., https://www.graphpad.com).

Results

Study Characteristics

We identified 1,623 studies from the literature search; 106 of those met the inclusion criteria (Figure 1). The interrater agreements were 83.4% for title and abstract screening and 88.2% for full-text reviews.

We summarized study details and participant characteristics for the 106 included studies (Table 1; Appendix Tables 2, 3). Of those studies, 42.5% (45/106) were cross-sectional, 28.3% (30/106) were prospective cohort, and 28.3% (30/106) were retrospective studies; 1 was a case-control study (Appendix Table 3). We found 38 studies reported data from high-income countries (HICs), 38 from upper-

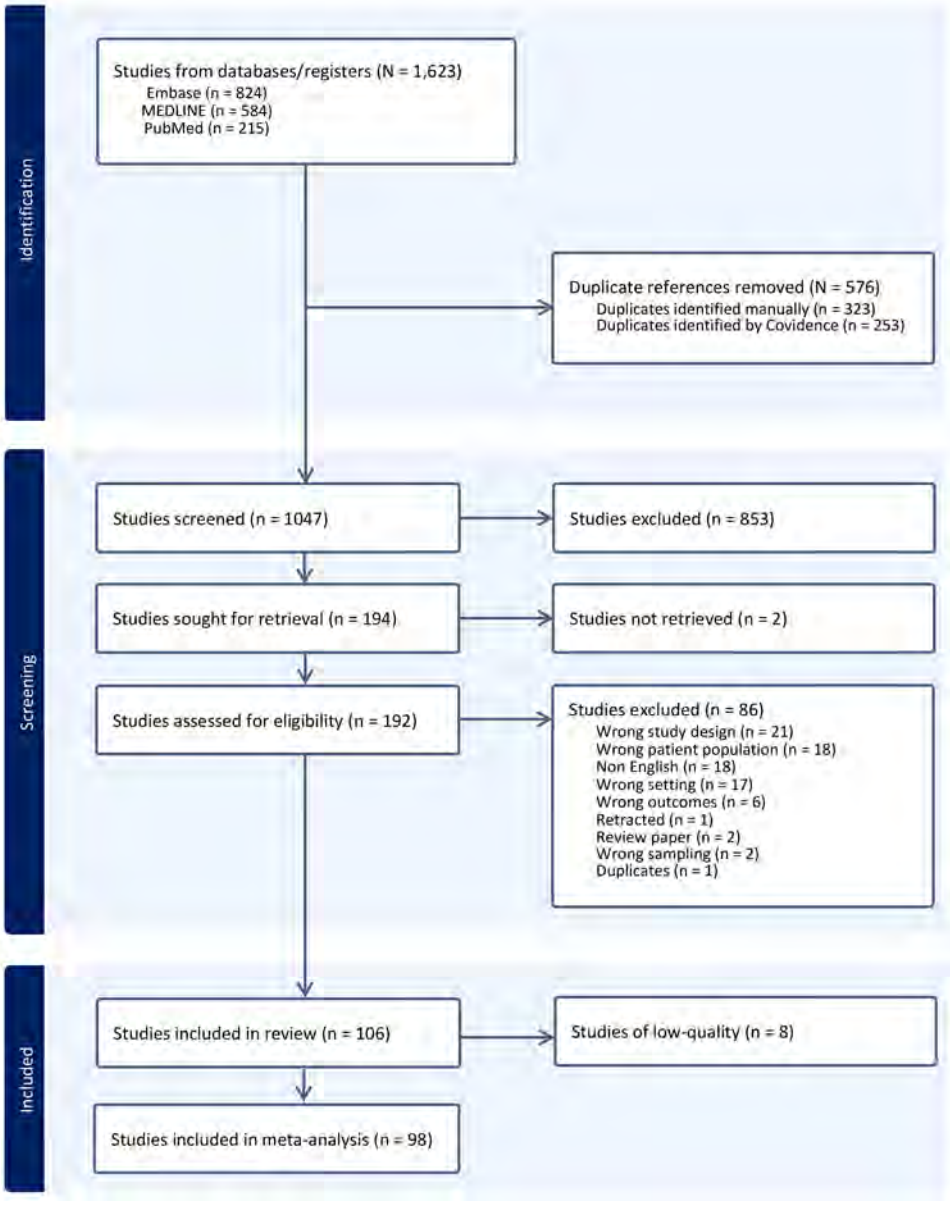

Figure 1. Flow diagram of selection criteria in study of rectovaginal colonization rates and serotype distribution among pregnant women, Asia-Pacific region, 2014–2025. We followed the 2020 Preferred Reporting Items for Systematic reviews and Meta-Analyses guidelines (PRISMA; https://www.prisma-statement.org) and used MEDLINE (https://www.nlm.nih.gov/medline), Embase (https://www.embase.com), and PubMed (https://pubmed.ncbi.nlm.nih.gov) databases to identify included studies. Covidence systematic review management software (https://www.covidence.org) was used to screen and identify duplicate studies.

Table 1. Summary of included studies, according to country-income status, in study of group B *Streptococcus* rectovaginal colonization rates and serotype distribution among pregnant women, Asia-Pacific region, 2014–2025*

Country income level	No. studies	Asia-Pacific region	Pregnant women tested, no. (range†)	Women with GBS colonization, no. (range†)	Studies with GBS serotyping data, no. (%)	Studies with AMR data, no. (%)	ROB score, median (IQR)
High income	38		758,701 (79–318,740)	149,899 (17–30,176)	7 (18.4)	10 (28.9)	5 (4–6)
Australia	10	Oceania	89,828 (531–60,674)	19,253 (106–13,058)	1 (10.0)	1 (10.0)	5 (3.3–6)
Hong Kong, China	6	East Asia	435,391 (134–318,740)	89,173 (63–63,767)	0	1 (16.7)	5.5 (3.5–6.8)
Japan	9	East Asia	6870 (79–1,957)	1162 (17–423)	4 (44.4)	2 (22.2)	6 (4–6)
South Korea	6	East Asia	36,182 (150–33,721)	3,856 (23–3,578)	2 (33.3)	3 (50.0)	5.5 (5–6.8)
Taiwan	7	East Asia	190,430 (519–154,088)	36,455 (113–30,176)	0	3 (42.9)	5 (4–6.5)
Upper-middle income	38		210,333 (100–49,908)	22,058 (19–5,902)	10 (25.6)	13 (33.3)	5 (4–6)
China	33	East Asia	208,819 (116–49,908)	21,668 (18–5,902)	9 (26.5)	11 (32.4)	5 (4–6)
Indonesia	2	Southeast Asia	336 (159–177)	79 (26–53)	1 (50.0)	1 (50.0)	5.5 (4.3–6.8)
Malaysia	1	Southeast Asia	573	235	0	0	7
Thailand	2	Southeast Asia	605 (100–505)	76 (19–57)	0	1 (50.0)	6 (5.5–6.5)
Low and middle income	31‡		13,727 (50–3,863)	1,688 (0–310)	8 (25.8)	11 (35.5)	5 (4–6)
Bangladesh	3	South Asia	1,375 (224–1,151)	356 (46–172)	2 (66.7)	1 (33.3)	5 (5–6.5)
India	13	South Asia	4,687 (50–966)	402 (0–174)	2 (15.4)	5 (38.5)	5 (4–6)
Pakistan	5	South Asia	839 (78–261)	136 (18–48)	1 (20.0)	0	5 (4–6)
Sri Lanka	4	South Asia	825 (150–250)	142 (28–45)	1 (25.0)	3 (75.0)	5 (4.5–5.3)
Vietnam	6	Southeast Asia	6,001 (50–3,863)	652 (3–310)	2 (33.3)	2 (33.3)	6 (4.5–6.5)
Total	106‡		982,761	173,645	25 (23.5)	34 (32.1)	5 (4–6)

*Expanded data are provided in Appendix Table 2 (https://wwwnc.cdc.gov/EID/article/32/10/26-0687-App1.pdf). AMR, antimicrobial drug resistance; ANC, antenatal clinic; IQR, interquartile range; ROB, risk of bias.
†Range indicates the number of persons included in each study.
‡One study contributed data to both Bangladesh and India; therefore, country-specific counts exceed the total number of included studies.

middle–income countries (UMICs), and 30 from low-middle–income countries (LMICs) (Table 1); 1 study was a multi-country study that included data from both Bangladesh and India (Appendix Table 3). The studies reported data from a total of 13 countries; 33 (31.1%) studies reported data from China. Most (62 [58.5%]) studies reported data from East Asia, whereas 24 (22.4%) reported data from South Asia, 11 (10.3%) from Southeast Asia, and 10 (9.3%) from Oceania (all from Australia). A total of 25 (23.5%) studies reported serotype distribution, and 34 (32.1%) reported AMR rates.

Most (101 [95.3%]) studies included pregnant women who received GBS screening as part of their antenatal care visit or during labor; 3 of those studies also enrolled women experiencing preterm labor (Appendix Table 3). Data from 29 studies, predominately from Australia, Japan, Hong Kong, and Taiwan, were derived from routine antenatal screening programs. Three studies included pregnant women with preterm prelabor rupture of membranes or term premature rupture of membranes (Appendix Table 3); 2 studies included pregnant women with risk factors for GBS infection (Appendix Table 3). For GBS testing, samples were obtained from the vagina and rectum (71 [66.0%] studies), vagina only (27 [25.5%]), and vagina and cervix (2 [1.9%]); 7 (6.6%) studies did not specify the sampling site.

GBS Colonization Prevalence

Of the 106 studies, 8 were removed from meta-analysis because of a high risk of bias score (<3) (Appendix Table 3). The 98 remaining studies in the meta-analysis included 978,150 pregnant women; 172,973 of those had GBS colonization. Overall, the pooled estimated GBS prevalence was 18.0% (95% CI 12%–23%); significant interstudy heterogeneity was observed ($p = 0.001$; $I^2 = 99.8\%$) (Appendix Figure 1). Pooled estimated prevalences were 20.0% (95% CI 16.0%–24.0%; n = 149,539/757,142) in HICs, 11.0% (95% CI 7.0%–14.0%; n = 21,814/207,412) in UMICs, and 12.0% (95% CI 7.0%–17.0%; n = 1,579/13,462) in LMICs (Appendix Figure 1). By subregion, pooled estimated prevalences were 21.0% (95% CI 20.0%–23.0%) in Oceania, 17.0% (95% CI 12.0%–23.0%) in East Asia, 14.0% (95% CI 4.0%–24.0%) in Southeast Asia, and 13.0% (95% CI 8.0%–17.0%) in South Asia (Appendix Figure 2). We also estimated country-specific prevalences

(Appendix Figure 3). We observed considerable between-study heterogeneity within countries; prevalence estimates for countries with <4 studies had wide CIs, reflecting the limited available data.

Microbiologic culture methods for GBS detection were used in 73 (74.5%) of the 98 studies; 43 (58.9%) of those 73 studies reported using enrichment or selective media. PCR alone was used in 9 (9.2%) of the 98 studies, mass spectrophotometry in 2 (2.0%) studies, and immunochromatography in 1 (1.0%) studies; GBS detection methods were not specified in 13 (13.3%) studies (Appendix Table 3). A trend toward higher GBS colonization was observed when enrichment and microbiologic culture methods were used compared with culture alone for both HICs and LMICs, but not UMICs, whereas the number of studies that used PCR was limited (Appendix Figures 4, 5).

Vaginal sampling was reported in 24 (24.5%) of the 98 studies (most were from UMICs and LMICs), whereas both vaginal and rectal samplings were reported in 65 (66.3%) studies. Two (2.0%) studies reported samples from the cervix and vagina; 7 (7.1%) did not report the sampling site. A trend toward higher GBS colonization was observed when sampling sites included both the vagina and rectum than the vagina alone for both HICs and LMICs, but not UMICs (Appendix Figures 4, 6).

GBS Serotype Distribution

Of 98 studies included in the meta-analysis, 24 (24.5%) from 10 countries reported serotype distributions of GBS isolates (*14*–*36*) (Figure 2); 8 of those studies reported data from China. Fourteen (58.3%) of the 24 studies used multiplex PCR, and 10 (41.6%) used latex agglutination serotyping kits as their serotyping method. Six (25.0%) studies each reported serotyping data for <30 isolates, 7 (29.1%) each reported 50–100 isolates, and 11 (45.8%) each reported >100 isolates (Appendix Table 3). The 5 most reported serotypes were III (range 5.0%–100.0%), Ia (range 0%–61.0%), V (range 0.5%–32.0%), Ib (range 0.5%–22.8%), and II (range 1.5%–32.1%) (Figure 2).

GBS AMR Patterns

A total of 30 (30.6%) of 98 studies reported GBS AMR patterns; one third of those were from China (Appendix Table 3). AMR testing varied across studies (Table 2); 12 of the 30 studies tested <50 GBS strains (Appendix Table 3). Sixteen studies reported AMR rates for both ampicillin and penicillin, the first-line antimicrobial drugs used to treat GBS infections (Table 2); an additional 11 studies reported rates only for penicillin. Overall, AMR rates were low for both penicillin and ampicillin (Table 2). Among antimicrobial drugs tested in ≥10 studies, tetracycline had the highest (median 77.7%, range 19.3%–90%) maximum AMR rate, followed by erythromycin (median 40.7%, range 5.2%–78.6%), clindamycin (median 35.7%, range 0%–77.1%), and levofloxacin (median 26.9%, range 0%–68.4%).

Quality of Included Studies

We determined the risk of bias scores for all 106 included studies and summarized details of the risk of bias assessment (Appendix Tables 3, 4). High risk for bias was observed in 8 (7.5%) studies, moderate risk in 53 (50.0%) studies, and low risk in 45 (42.5) studies (Appendix Table 3). Thirty (28.3%) of the 106 studies did not provide sufficient information about the study population (e.g., retrospective design or data derived from laboratory samples); 51 (48.1%) studies did not sufficiently describe the participants or settings, and 48 (45.3%) did not use appropriate methods for sample collection or GBS detection. Most (91 [85.8%]) studies used appropriate statistical methods.

Discussion

By conducting a systematic review and meta-analysis, we estimated that the prevalence of GBS colonization among pregnant women in the Asia-Pacific region was 18.0% (95% CI 12%–23%). Approximately one third of studies reported data from China, and the remainder reported data from 12 other countries in the region. We did not find studies from the Oceania region apart from Australia, and no studies reported data for island countries within the Pacific region. We included only 8 studies from countries in Southeast Asia, and no data were reported on GBS colonization rates among pregnant women in high neonatal mortality settings (>20 deaths/1,000 live births) (*37*).

Our findings were consistent with a systematic review published in 2017, which reported a global maternal GBS colonization prevalence of 18% (95% CI 17%–19%) (*11*). Our regional estimates were also broadly consistent with those reported previously, including 21.0% in our study versus 23% for Oceania (Australia/New Zealand), 17.0% versus 11% for East Asia, 14.0% versus 14% for Southeast Asia, and 13.0% versus 13% for South Asia (*11*). However, we demonstrated higher rates of GBS colonization than has been previously used to estimate the global burden of invasive GBS disease (*2*). Data on invasive GBS disease remain limited across many countries in Southeast Asia and the Pacific regions, and accurate ascertainment of neonatal GBS disease rates is challenging because of

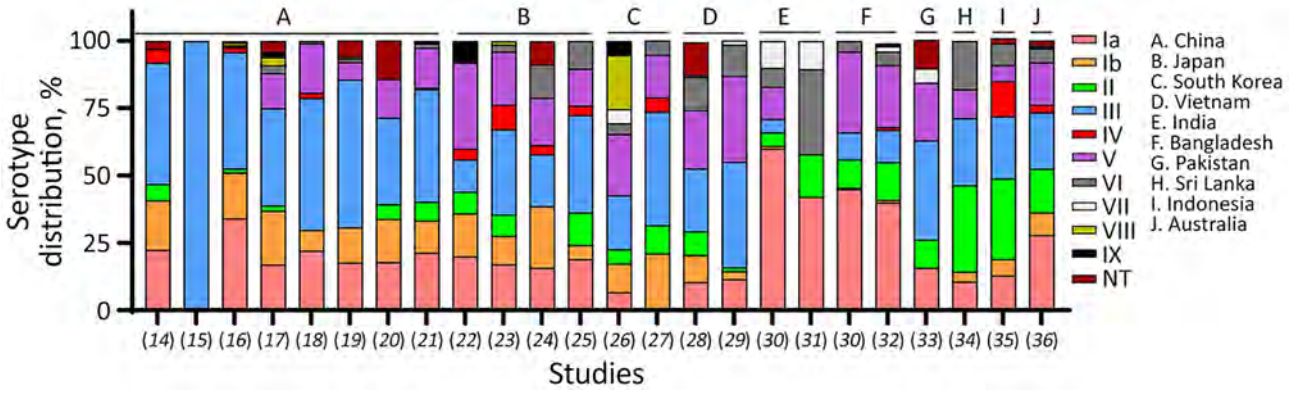

Figure 2. Serotype distribution of group B *Streptococcus* isolates among pregnant women, Asia-Pacific region, 2014–2025. Data are expressed as stacked bars. Colors indicate distribution of serotypes I–IX reported from 10 countries. Study reference numbers are indicated on the x-axis. NT, not typed.

limited access to sensitive microbiologic diagnostics, incomplete case capture, and the use of IAP, which reduces culture sensitivity. Hence, many LMICs rely on modeled estimates. The most recent estimates of invasive GBS were obtained by using maternal GBS colonization prevalences of 10.4% for Southeast Asia and 18.6% for Oceania (2). In our review, we found higher rates of maternal colonization, indicating the prevalence of invasive GBS in the Asia-Pacific region might have been underestimated.

Table 2. Antimicrobial drug resistance rates for group B *Streptococcus* isolates in study of rectovaginal colonization rates and serotype distribution among pregnant women, Asia-Pacific region, 2014–2025*

Antimicrobial drugs	No. (%) studies reporting AMR†	No. isolates tested	% AMR rate, median (range)
Aminoglycosides			
Amikacin/gentamicin	2 (6.7)	74	73.2 (46.4–100)
Amphenicols			
Chloramphenicol	9 (26.5)	6,596	9.2 (2.6–52.4)
β-lactams			
Ampicillin	16 (53.3)	6,521	0 (0–2.0)
Penicillin	27 (90.0)	10,474	0 (0–2.9)
Carbapenems			
Meropenem	6 (20.0)	3,903	0 (0–2.6)
Cephalosporins			
Cefepime	3 (10.0)	3,776	2.6 (0–7.1)
Cefotaxime	15 (50.0)	5,078	0 (0–6.7)
Cefazolin	1 (3.3)	189	0
Fluoroquinolones			
Ciprofloxacin	4 (13.3)	613	8.8 (3.3–67.4)
Levofloxacin	20 (66.7)	8,919	26.9 (0–68.4)
Lincosamides			
Clindamycin	29 (96.7)	10,812	35.7 (0–77.1)
Glycopeptides			
Vancomycin	22 (73.3)	9,461	0 (0–3.3)
Teicoplanin	1 (3.3)	25	0
Macrolides			
Azithromycin	2 (6.7)	132	69.4 (51.3–87.5)
Clarithromycin	2 (6.7)	132	64.3 (50–78.6)
Erythromycin	29 (96.7)	10,348	40.7 (5.2–78.6)
Telithromycin	1 (3.3)	56	3.6
Oxazolidinone			
Linezolid	8 (26.7)	1,710	0 (0–0.8)
Streptogramin			
Quinupristin	1 (3.3)	509	0.2
Tetracyclines			
Doxycycline	2 (6.7)	74	46.2 (35.7–56.7)
Minocycline	1 (3.3)	28	56.7
Tetracycline	14 (46.7)	7,714	77.7 (19.3–90.0)

*AMR, antimicrobial drug resistance.
†N = 30. Countries included in studies reporting AMR: Australia (n = 1); Bangladesh (n = 1); China (n = 10); Hong Kong, China (n = 1); India (n = 3); Indonesia (n = 1); Japan (n = 2); Taiwan (n = 3); Thailand (n = 1); South Korea (n = 3); Sri Lanka (n = 3); and Vietnam (n = 1).

Overall, we found that GBS colonization prevalence appeared slightly higher in HICs than in UMICs or LMICs within the Asia-Pacific region. Our findings remained consistent when we stratified studies according to GBS detection methods and sampling sites within each income group. Differences across settings might partly reflect variations in laboratory testing methods (e.g., using different types of enrichment broth and blood agar plates), sampling sites, and identification methods or, more broadly, population differences in antimicrobial drug use (*38*), intestinal microbiomes (*39*), and sexual behaviors (*40*). Our findings should be interpreted with caution because substantially more study participants from HICs were included than those from UMICs and LMICs. Furthermore, a large proportion of studies of UMICs and LMICs were conducted in China (UMICs) and India (LMICs); the high number of those studies might produce bias in the overall estimate. More studies are needed to better characterize maternal GBS prevalence, particularly in LMICs, which have the highest GBS disease prevalence.

Only 19 studies have been reported from 10 countries in the Asia-Pacific region in the past 10 years. The 5 most common GBS serotypes (Ia, Ib, II, III, and V) identified in our review were consistent with other reports of global GBS serotype distribution among pregnant women (*11*,*41*). Those 5 serotypes accounted for 97% of invasive isolates causing infant GBS disease globally. Serotype III was the most common cause of disease worldwide (*41*) and the major serotype causing invasive infant GBS disease in the Asia-Pacific region, although data have only been available for this region from China, Japan, and Australia (*41*). Sequence type 283 of serotype III has been linked to ongoing outbreaks of invasive adult GBS disease associated with consumption of raw fish in nonpregnant women within Asia (*42*). Although human shedding and human-to-human transmission are possible, sequence type 283 was not identified in any of the studies included in this review that reported multilocus sequence typing data (12 studies). Both trivalent and hexavalent vaccine candidates undergoing phase III clinical trials target serotypes III, Ia, and Ib, whereas hexavalent vaccines also target serotypes II, IV, and V (*43*,*44*). Those vaccines have the potential to reduce infant and maternal GBS invasive disease. Countries with the highest prevalence of invasive GBS disease and death among young infants are likely to benefit most from maternal GBS vaccination. Ongoing monitoring and serotype surveillance will be essential to ensure vaccine effectiveness and to detect potential shifts in GBS serotype distribution.

AMR is one of the top 10 global health threats identified by the World Health Organization; an estimated 5 million annual deaths have been associated with bacterial AMR (*45*). Antimicrobial drug use during labor is common (≈40% of patients) to treat or prevent urogenital infections, chorioamnionitis, and GBS colonization (*46*). Most studies included in our review demonstrated that a high proportion of GBS strains remained susceptible to the first-line antimicrobial drugs, penicillin and ampicillin, as well as second-line drugs, such as vancomycin. However, our review found high rates of resistance to clindamycin (up to 75%) and erythromycin (up to 80%), which are the drugs typically used for persons who are allergic to penicillin; we also found high rates of tetracycline resistance (up to 90%), likely resulting from treatment of other bacterial diseases (*47*). Antimicrobial drug–resistant GBS strains are an increasing global concern; rising resistance potentially compromises the prevention and treatment of invasive GBS disease and increases the potential for these strains to spread AMR to other pathogenic bacteria (*48*–*50*).

In HICs, established national GBS IAP programs (i.e., IAP given to pregnant women with risk factors for GBS disease development or for those with confirmed disease) are associated with lower rates of invasive GBS disease in neonates and GBS-related deaths in infants (*2*). In contrast, in most UMICs and LMICs that have no national IAP programs, invasive GBS disease and GBS-related deaths in infants are higher than in HICs, even with a lower overall prevalence of maternal GBS colonization (*2*). IAP programs have been associated with reduced risk for early-onset GBS disease, without evidence of increasing antimicrobial drug resistance (*6*). Our findings support the implementation of IAP programs, where feasible, in UMICs and LMICs. In settings where IAP is not feasible, maternal GBS vaccination might offer an alternative strategy for preventing neonatal GBS disease, when warranted according to disease prevalence.

The strengths of this review include a systematic approach that identified relevant literature; the incorporation of many studies enabled subgroup analyses, including geographic regions and country-income levels, providing further insight into the factors influencing GBS colonization rates. This review also included GBS serotyping and AMR rates that will inform GBS treatment and vaccine strategies.

The first limitation of our study is that we excluded gray literature, such as theses and dissertations, committee reports, conference abstracts, and government reports, as well as non-English publications.

Therefore, our findings might not fully represent the global body of evidence, especially data from non-English or nontraditional publication sources. Second, a single reviewer conducted the data extraction and risk of bias assessments, which might have introduced potential bias in the findings. Third, sampling sites and laboratory testing methods varied by country income status; thus, the independent effects of sampling site and testing method could not be distinguished from effects of country income level or geographic region. Finally, we did not perform subgroup analyses for regions within countries having the highest invasive GBS–mediated death rates in children <5 years of age because of limited data availability and heterogeneity in reporting across studies.

In conclusion, this study identified a pooled estimate of 18.0% GBS colonization among pregnant women in the Asia-Pacific region. Limited data are available for the Asia-Pacific region, particularly for countries within the Pacific region and parts of Southeast Asia, where neonatal mortality rates remain high. Current estimates of invasive GBS disease derived from maternal GBS colonization might be underestimated, especially in regions with limited data. Epidemiologic studies are urgently needed in potentially high-prevalence settings to elucidate the prevalence of maternal GBS colonization, circulating serotypes, and neonatal invasive GBS disease. Strengthening diagnostic capacity, evaluating key determinants of disease (including IAP implementation and antimicrobial drug use during pregnancy), and surveillance of circulating GBS serotypes and antimicrobial resistance patterns will be needed to guide prevention strategies and maternal GBS vaccine implementation.

Acknowledgments

We thank Poh Chua for help in developing the literature search strategy and Eleanor Neal for help with the meta-analysis.

F.M.R. is supported by an Australian National Health and Medical Research Council Investigator Grant. The Murdoch Children's Research Institute is supported by the Government of Victoria Operational Infrastructure Support Program.

About the Author

Dr. Toh is a senior research officer at the Murdoch Children's Research Institute, Parkville, Victoria, Australia, and an honorary research fellow at the University of Melbourne, Melbourne, Victoria, Australia. His primary research interests include infectious diseases, immunology, and vaccinology.

References

1. Liu L, Oza S, Hogan D, Chu Y, Perin J, Zhu J, et al. Global, regional, and national causes of under-5 mortality in 2000–15: an updated systematic analysis with implications for the Sustainable Development Goals. Lancet. 2016;388:3027–35. https://doi.org/10.1016/S0140-6736(16)31593-8
2. Gonçalves BP, Procter SR, Paul P, Chandna J, Lewin A, Seedat F, et al.; GBS Danish and Dutch collaborative group for long term outcomes; GBS Low and Middle Income Countries collaborative group for long term outcomes; GBS Scientific Advisory Group, epidemiological sub-group; CHAMPS team. Group B streptococcus infection during pregnancy and infancy: estimates of regional and global burden. Lancet Glob Health. 2022;10:e807–19. https://doi.org/10.1016/S2214-109X(22)00093-6
3. Seale AC, Bianchi-Jassir F, Russell NJ, Kohli-Lynch M, Tann CJ, Hall J, et al. Estimates of the burden of group B streptococcal disease worldwide for pregnant women, stillbirths, and children. Clin Infect Dis. 2017;65:S200–19. https://doi.org/10.1093/cid/cix664
4. Paul P, Gonçalves BP, Le Doare K, Lawn JE. 20 million pregnant women with group B Streptococcus carriage: consequences, challenges, and opportunities for prevention. Curr Opin Pediatr. 2023;35:223–30. https://doi.org/10.1097/MOP.0000000000001223
5. Schuchat A. Group B *Streptococcus*. Lancet. 1999;353:51–6. https://doi.org/10.1016/S0140-6736(98)07128-1
6. Panneflek TJR, Hasperhoven GF, Chimwaza Y, Allen C, Lavin T, Te Pas AB, et al. Intrapartum antibiotic prophylaxis to prevent Group B streptococcal infections in newborn infants: a systematic review and meta-analysis comparing various strategies. EClinicalMedicine. 2024;74:102748. https://doi.org/10.1016/j.eclinm.2024.102748
7. Snider JB, Mithal LB, Kwah JH, Rhodes NJ, Son M. Antibiotic choice for group B *Streptococcus* prophylaxis in mothers with reported penicillin allergy and associated newborn outcomes. BMC Pregnancy Childbirth. 2023;23:400. https://doi.org/10.1186/s12884-023-05697-0
8. Le Doare K, O'Driscoll M, Turner K, Seedat F, Russell NJ, Seale AC, et al.; GBS Intrapartum Antibiotic Investigator Group. Intrapartum antibiotic chemoprophylaxis policies for the prevention of group B streptococcal disease worldwide: systematic review. Clin Infect Dis. 2017;65:S143–51. https://doi.org/10.1093/cid/cix654
9. HogenEsch E, De Mucio B, Haddad LB, Vilajeliu A, Ropero AM, Yildirim I, et al. Differences in maternal group B *Streptococcus* screening rates in Latin American countries. Vaccine. 2021;39:B3–11. https://doi.org/10.1016/j.vaccine.2020.10.082
10. Llor C, Bjerrum L. Antimicrobial resistance: risk associated with antibiotic overuse and initiatives to reduce the problem. Ther Adv Drug Saf. 2014;5:229–41. https://doi.org/10.1177/2042098614554919
11. Russell NJ, Seale AC, O'Driscoll M, O'Sullivan C, Bianchi-Jassir F, Gonzalez-Guarin J, et al.; GBS Maternal Colonization Investigator Group. Maternal colonization with group B *Streptococcus* and serotype distribution worldwide: systematic review and meta-analyses. Clin Infect Dis. 2017;65:S100–11. https://doi.org/10.1093/cid/cix658
12. Kwatra G, Cunnington MC, Merrall E, Adrian PV, Ip M, Klugman KP, et al. Prevalence of maternal colonisation with group B *Streptococcus*: a systematic review and meta-analysis. Lancet Infect Dis. 2016;16:1076–84. https://doi.org/10.1016/S1473-3099(16)30055-X

13. Bianchi-Jassir F, Paul P, To KN, Carreras-Abad C, Seale AC, Jauneikaite E, et al. Systematic review of group B streptococcal capsular types, sequence types and surface proteins as potential vaccine candidates. Vaccine. 2020;38:6682–94. https://doi.org/10.1016/j.vaccine.2020.08.052
14. Li L, Wang X, Li D, Liu Z. Serum inflammatory and coagulation markers in GBS infection and adverse pregnancy outcomes. Biomark Med. 2026;20:17–25. https://doi.org/10.1080/17520363.2025.2538429
15. Lai X, Chen M, Wang J, Wang J, Lv H, Xie H, et al. CAMP-negative *Streptococcus agalactiae* strains exhibited complete or partial chromosomal deletions of the CAMP-factor encoding gene *cfb*. Microbiol Spectr. 2025;13:e0325724. https://doi.org/10.1128/spectrum.03257-24
16. Chen Y, Liu L, Liu J, Ji T, Gao Y, Yang D, et al. Serotype distribution, antimicrobial resistance, and molecular characterization of group B *Streptococcus* isolates from Chinese pregnant woman. J Matern Fetal Neonatal Med. 2024;37:2295805. https://doi.org/10.1080/14767058.2023.2295805
17. Li X, Gao W, Jia Z, Yao K, Yang J, Tong J, et al. Characterization of group B Streptococcus recovered from pregnant women and newborns attending in a hospital in Beijing, China. Infect Drug Resist. 2023;16:2549–59. https://doi.org/10.2147/IDR.S395942
18. Wang X, Cao X, Li S, Ou Q, Lin D, Yao Z, et al. Phenotypic and molecular characterization of *Streptococcus agalactiae* colonized in Chinese pregnant women: predominance of ST19/III and ST17/III. Res Microbiol. 2018;169:101–7. https://doi.org/10.1016/j.resmic.2017.12.004
19. Ji W, Zhang L, Guo Z, Xie S, Yang W, Chen J, et al. Colonization prevalence and antibiotic susceptibility of group B *Streptococcus* in pregnant women over a 6-year period in Dongguan, China. PLoS One. 2017;12:e0183083. https://doi.org/10.1371/journal.pone.0183083
20. Wang P, Tong JJ, Ma XH, Song FL, Fan L, Guo CM, et al. Serotypes, antibiotic susceptibilities, and multi-locus sequence type profiles of *Streptococcus agalactiae* isolates circulating in Beijing, China. PLoS One. 2015;10:e0120035. https://doi.org/10.1371/journal.pone.0120035
21. Lu B, Li D, Cui Y, Sui W, Huang L, Lu X. Epidemiology of group B *Streptococcus* isolated from pregnant women in Beijing, China. Clin Microbiol Infect. 2014;20:O370–3. https://doi.org/10.1111/1469-0691.12416
22. Nakano S, Hasegawa Y, Koide S, Hosaka Y, Ishida-Kuroki K, Kawakami S, et al. Increased recovery of *Streptococcus agalactiae* from vaginal-rectal swabs using a selective enrichment broth medium. J Obstet Gynaecol Res. 2025;51:e70084. https://doi.org/10.1111/jog.70084
23. Kawaguchiya M, Urushibara N, Aung MS, Shimada S, Nakamura M, Ito M, et al. Molecular characterization and antimicrobial resistance of *Streptococcus agalactiae* isolated from pregnant women in Japan, 2017–2021. IJID Reg. 2022;4:143–5. https://doi.org/10.1016/j.ijregi.2022.07.002
24. Shibata M, Morozumi M, Maeda N, Komiyama O, Shiro H, Iwata S, et al. Relationship between intrapartum antibiotic prophylaxis and group B streptococcal colonization dynamics in Japanese mother–neonate pairs. J Infect Chemother. 2021;27:977–83. https://doi.org/10.1016/j.jiac.2021.02.006
25. Takayama Y, Matsui H, Adachi Y, Nihonyanagi S, Wada T, Mochizuki J, et al. Detection of *Streptococcus agalactiae* by immunochromatography with group B *Streptococcus*–specific surface immunogenic protein in pregnant women. J Infect Chemother. 2017;23:678–82. https://doi.org/10.1016/j.jiac.2017.07.001
26. Choi SJ, Kang J, Uh Y. Recent epidemiological changes in group B *Streptococcus* among pregnant Korean women. Ann Lab Med. 2021;41:380–5. https://doi.org/10.3343/alm.2021.41.4.380
27. Lee HT, Kim SY, Park PW, Ahn JY, Kim KH, Seo JY, et al. Detection and genomic analysis of genital group B *Streptococcus* in pregnant Korean women. J Obstet Gynaecol Res. 2019;45:69–77. https://doi.org/10.1111/jog.13810
28. Nguyen VL, Dao HN, Le VTH, Nguyen AV, Ha VTT, Nguyen QTN, et al. Prevalence, risk factors, and serotypes of group B *Streptococcus* rectovaginal colonization among pregnant women: a cross-sectional study at three hospitals in Hanoi, Vietnam. Ther Adv Infect Dis. 2025;12:20499361251365028. https://doi.org/10.1177/20499361251365028
29. Hanh TQ, Van Du V, Hien PT, Chinh DD, Loi CB, Dung NM, et al. Prevalence and capsular type distribution of group B *Streptococcus* isolated from vagina of pregnant women in Nghe An province, Vietnam. Iran J Microbiol. 2020;12:11–7.
30. Kwatra G, Izu A, Cutland C, Akaba G, Ali MM, Ahmed Z, et al. Prevalence of group B *Streptococcus* colonisation in mother–newborn dyads in low-income and middle-income south Asian and African countries: a prospective, observational study. Lancet Microbe. 2024;5:100897. https://doi.org/10.1016/S2666-5247(24)00129-0
31. Gogoi M, Das MK, Das JK, Barman N, Das P, Devi U, et al. Group B *Streptococcus* colonising the genital tract of pregnant women from Dibrugarh, Assam: circulating serotypes, susceptibility pattern and phylogenetic analysis. J Clin Diagn Res. 2021;15:DC13–8. https://doi.org/10.7860/JCDR/2021/47750.14824
32. Saha SK, Ahmed ZB, Modak JK, Naziat H, Saha S, Uddin MA, et al. Group B *Streptococcus* among pregnant women and newborns in Mirzapur, Bangladesh: colonization, vertical transmission, and serotype distribution. J Clin Microbiol. 2017;55:2406–12. https://doi.org/10.1128/JCM.00380-17
33. Mumtaz M, Saleem S, Sattar A, Waheed A, Jahan S, Gill M. Identification of serotypes of non-typeable group b streptococci by polymerase chain reaction. [cited 2026 Mar 5]. https://pjmhsonline.com/2020/jan_march/pdf/338.pdf
34. Sapugahawatte DN, Li C, Liyanapathirana V, Kandauda C, Gihan C, Zhu C, et al. Colonization of group B *Streptococcus* in pregnant women and their neonates from a Sri Lankan hospital. Pathogens. 2022;11:386. https://doi.org/10.3390/pathogens11040386
35. Safari D, Gultom SM, Tafroji W, Azzahidah A, Soesanti F, Khoeri MM, et al. Prevalence, serotype and antibiotic susceptibility of group B *Streptococcus* isolated from pregnant women in Jakarta, Indonesia. PLoS One. 2021;16:e0252328. https://doi.org/10.1371/journal.pone.0252328
36. Furfaro LL, Nathan EA, Chang BJ, Payne MS. Group B *Streptococcus* prevalence, serotype distribution and colonization dynamics in Western Australian pregnant women. J Med Microbiol. 2019;68:728–40. https://doi.org/10.1099/jmm.0.000980
37. Organisation for Economic Co-operation and Development. Health at a glance: Asia/Pacific 2024. [cited 2026 Mar 5]. https://www.oecd.org/en/publications/health-at-a-glance-asia-pacific-2024_51fed7e9-en/full-report/neonatal-mortality_7e9a9a5f.html
38. Orwa SA, Gudnadottir U, Boven A, Pauwels I, Versporten A, Vlieghe E, et al. Global prevalence of antibiotic consumption during pregnancy: a systematic review and meta-analysis. J Infect. 2024;89:106189. https://doi.org/10.1016/j.jinf.2024.106189

39. Megli CJ, DePuyt AE, Goff JP, Munyoki SK, Hooven TA, Jašarević E. Diet influences community dynamics following vaginal group B *Streptococcus* colonization. Microbiol Spectr. 2024;12:e0362323. https://doi.org/10.1128/spectrum.03623-23
40. Esmaon R, Lim BK, Gan F, Hamdan M, Tan PC. Sexual activity, vaginal symptoms, maternal perineal hygiene behavior, and constipation on ano-vaginal colonization of group B *Streptococcus* in near term pregnancy. BMC Pregnancy Childbirth. 2024;24:461. https://doi.org/10.1186/s12884-024-06616-7
41. Madrid L, Seale AC, Kohli-Lynch M, Edmond KM, Lawn JE, Heath PT, et al.; Infant GBS Disease Investigator Group. Infant group B streptococcal disease incidence and serotypes worldwide: systematic review and meta-analyses. Clin Infect Dis. 2017;65:S160–72. https://doi.org/10.1093/cid/cix656
42. Wong HK, Lam KL, Tsang AK, Hung DL, Ng T, Au AK, et al. A large outbreak of invasive group B *Streptococcus* sequence type 283 infection linked to physical contact of freshwater fish. Epidemiol Infect. 2025;153:e76. https://doi.org/10.1017/S0950268825100186
43. Madhi SA, Anderson AS, Absalon J, Radley D, Simon R, Jongihlati B, et al. Potential for maternally administered vaccine for infant group B *Streptococcus*. N Engl J Med. 2023;389:215–27. https://doi.org/10.1056/NEJMoa2116045
44. Madhi SA, Cutland CL, Jose L, Koen A, Govender N, Wittke F, et al. Safety and immunogenicity of an investigational maternal trivalent group B *Streptococcus* vaccine in healthy women and their infants: a randomised phase 1b/2 trial. Lancet Infect Dis. 2016;16:923–34. https://doi.org/10.1016/S1473-3099(16)00152-3
45. Antimicrobial Resistance Collaborators. Global burden of bacterial antimicrobial resistance in 2019: a systematic analysis. Lancet. 2022;399:629–55. https://doi.org/10.1016/S0140-6736(21)02724-0
46. Winteler C, Ardabili S, Hodel M, Stocker M. A systematic review of perinatal antibiotic stewardship—where we are, where to go? J Perinatol. 2025;45:1411–22. https://doi.org/10.1038/s41372-025-02209-0
47. Da Cunha V, Davies MR, Douarre PE, Rosinski-Chupin I, Margarit I, Spinali S, et al.; DEVANI Consortium. *Streptococcus agalactiae* clones infecting humans were selected and fixed through the extensive use of tetracycline. Nat Commun. 2014;5:4544. https://doi.org/10.1038/ncomms5544
48. Ding Y, Wang Y, Hsia Y, Russell N, Heath PT. Systematic review and meta-analyses of incidence for group B *Streptococcus* disease in infants and antimicrobial resistance, China. Emerg Infect Dis. 2020;26:2651–9. https://doi.org/10.3201/eid2611.181414
49. Navarro-Torné A, Curcio D, Moïsi JC, Jodar L. Burden of invasive group B *Streptococcus* disease in nonpregnant adults: a systematic review and meta-analysis. PLoS One. 2021;16:e0258030. https://doi.org/10.1371/journal.pone.0258030
50. Sabroske EM, Iglesias MAS, Rench M, Moore T, Harvey H, Edwards M, et al. Evolving antibiotic resistance in group B streptococci causing invasive infant disease: 1970–2021. Pediatr Res. 2023;93:2067–71. https://doi.org/10.1038/s41390-022-02375-3

Address for correspondence: Zheng Quan Toh, Department of Paediatrics, The University of Melbourne; Infection, Immunity and Global Health, Murdoch Children's Research Institute, Parkville, VIC 3052, Australia; email: zheng.quantoh@mcri.edu.au

Human Myiasis Resulting from Reemergence of *Cochliomyia hominivorax* Screwworm, Mexico, 2025–2026

Oscar Manuel Delgado-Cuellar, Clemente Mosso-González, Jorge Castañeda-Gómez, Farah Zamira Vera-Maloof, Karla Reyna Navarro-Fuentes, Edgar Sebastián Mejía-Navarro, Héctor Armando Rincón-León

After its elimination from Mexico in 2003, myiasis caused by New World screwworm (NWS), *Cochliomyia hominivorax*, has recently reemerged as a public and animal health concern. We conducted a retrospective study of human New World screwworm myiasis cases reported through Mexico's national surveillance system during April 13, 2025–March 14, 2026. Of 204 cases in official surveillance summaries, 202 had sufficient information for case-level clinical and epidemiologic analysis. Cases were concentrated in southern Mexico, particularly Chiapas, followed by Yucatán, Oaxaca, and Quintana Roo. Most (71.8%) cases occurred in men; mean patient age was 61.1 years. Lower limbs (55.0%) were the most frequently reported anatomic location, and 76.7% of patients had ≥1 concurrent condition. Six deaths were reported among patients with NWS myiasis; at the time of reporting, 1 death was attributed directly to NWS myiasis. Our findings support proactive clinical detection and integrated One Health surveillance along the expected northward spread of NWS.

Cochliomyia hominivorax, the New World screwworm (NWS) fly, is an obligate parasite during its larval stage. Adult female flies are attracted to blood, wounds, inflamed tissue, mucous membranes, and natural body orifices, where they deposit eggs that hatch within 12–24 hours. The larvae invade and feed on living tissue for 5–7 days before dropping to the soil to continue development (*1*–*3*). Because female NWS flies usually mate only once, mass release of irradiated sterile flies can interrupt reproduction. That sterile insect technique, combined with quarantine and treatment of infested animals, supported eradications of NWS from North America southward to the Darién Gap in Panama (*4*). After eradication north of the Darién Gap, continued releases of sterile flies were used to maintain a biologic barrier intended to prevent reinvasion from NWS-endemic areas of South America. Environmental conditions, including moderate-to-heavy rainfall and temperatures ≈35°C, can favor NWS fly development (*5*).

Human infestation by *C. hominivorax* causes rapidly progressive and potentially severe myiasis. Clinical manifestations are usually classified according to the involved site as cutaneous, cavitary, or intestinal myiasis (*6*,*7*). Diagnosis relies on identification of larvae, and treatment includes larval removal, wound or lesion care, management of bacterial complications, analgesia, and, in selected cases, antiparasitic drugs such as ivermectin (*8*,*9*).

Mexico was declared free of NWS in 2003; Chiapas was the last state to achieve elimination (*10*,*11*). However, animal cases have been reported in Mexico since 2024 and human cases since 2025, raising concern about reemergence of NWS as a public and animal

Author affiliations: Instituto Mexicano del Seguro Social, Unidad de Medicina Familiar No. 1, Tapachula, Mexico (O.M. Delgado-Cuellar); SECIHTI–Instituto Nacional de Salud Pública, Centro Regional de Investigación en Salud Pública, Tapachula (C. Mosso-González, F.Z. Vera-Maloof); Unidad de Investigación en Enfermedades Infecciosas, Cancun, Mexico (J. Castañeda-Gómez); Instituto Mexicano del Seguro Social, Unidad de Medicina Familiar No. 11, Tapachula (K.R. Navarro-Fuentes); Hospital General "Dra. Matilde Petra Montoya Lafragua," Instituto de Seguridad y Servicios Sociales de los Trabajadores del Estado, Mexico City, Mexico (E.S. Mejía-Navarro); Instituto Mexicano del Seguro Social, OOAD Estatal en Chiapas, Jefatura de Servicios de Prestaciones Médicas, Coordinación Auxiliar Médica de Investigación, Tapachula (H.A. Rincón-León).

DOI: https://doi.org/10.3201/eid3210.261235

health problem. Because the same obligate parasite affects livestock, wildlife, companion animals, and humans, animal cases can indicate local circulation of the fly and potential risk for human infestation. In this context, a One Health approach entails coordinated surveillance, diagnosis, reporting, animal movement controls, and fly suppression across human and animal health sectors. Areas along the southern coast of Mexico, including Chiapas, Campeche, Tabasco, and Veracruz, have been considered at increased risk (*12*). A modeling study estimated that the reemerging NWS outbreak was moving northward from Central America at 1.2–1.9 km/day (*13*). We characterized confirmed human NWS myiasis cases in Mexico to provide information for epidemiologic surveillance, prevention, and control.

Methods

We conducted an observational, descriptive, retrospective study. The study population comprised confirmed human NWS myiasis cases reported in Mexico through the National Epidemiologic Surveillance System from epidemiologic week 16 of 2025 through epidemiologic week 10 of 2026, corresponding to April 13, 2025–March 14, 2026. Those dates represent the epidemiologic reporting period and do not necessarily indicate the dates of infestation onset.

To construct the temporal series, we reviewed official epidemiologic bulletins published by the Directorate General of Epidemiology, Ministry of Health, Mexico, which enabled us to identify the number of confirmed cases reported by epidemiologic week (*14*–*16*). To characterize clinical and epidemiologic features, we used nonidentifiable information available from the official monthly situation reports on human NWS myiasis in Mexico, published by the Directorate General of Epidemiology, Ministry of Health (*17*). We also used cumulative state-level counts from those reports to describe geographic spread at selected epidemiologic reporting weeks; those state-level summaries comprised all 204 confirmed cases.

The unit of analysis for case-level clinical and epidemiologic characterization was each confirmed human NWS myiasis case recorded during the study period, defined as a probable case with taxonomic identification of *C. hominivorax* from a laboratory in the National Network of Public Health Laboratories. We included records with available information on the state and municipality of notification, sex, age, reported anatomic location, concurrent conditions, and discharge or death status. We excluded records with insufficient information for case-level clinical or epidemiologic characterization. Of the 204 confirmed cases included in the official state-level summaries, 2 lacked sufficient case-level information; therefore, we included 202 cases in the clinical and epidemiologic analyses.

We analyzed variables including epidemiologic week of notification, state, municipality, sex, age, reported anatomic location or locations, presence and type of concurrent conditions, number of concurrent conditions, recorded death, and attributed cause of death. The monthly situation reports listed multiple anatomic terms for some patients but did not provide a data dictionary describing how those terms were assigned. When multiple anatomic locations were listed for a patient, we counted each recorded term in the descriptive frequency analysis. We did not interpret multiple listed locations as separate infestations because the reports did not indicate whether they represented distinct infestations, contiguous extension of a single infestation, or different levels of anatomic description. We therefore analyzed reported anatomic locations and concurrent conditions as non–mutually exclusive categories.

We performed descriptive statistical analysis. We summarized categorical variables as absolute frequencies and percentages and age as mean ±SD. We did not conduct confirmatory hypothesis testing because of the descriptive design and the absence of a population comparison group. We performed analyses in Microsoft Excel (https://www.microsoft.com) and Stata 17 (StataCorp LLC, https://www.stata.com) software.

This study used nonidentifiable secondary information from public official epidemiologic surveillance sources. The authors did not have access to names, personal identifiers, medical record numbers, addresses, or any information that would permit individual identification. The Local Ethics and Research Committee 703 of the Instituto Mexicano del Seguro Social in Chiapas determined that the study was exempt from formal ethics board review because it was a retrospective secondary analysis of public, nonidentifiable data, involved no intervention, and included no contact with patients. Therefore, informed consent was not required.

Results

Official state-level surveillance summaries included 204 confirmed human NWS myiasis cases; we used those data to describe cumulative geographic spread during the reporting period. Two records lacked sufficient case-level information for clinical and epidemiologic characterization; therefore, the analyses included 202 cases.

The temporal series derived from the official epidemiologic bulletins included 202 confirmed human NWS myiasis cases. During the 2025 reporting period, 111 cases were recorded, corresponding to a mean of 3 confirmed cases per epidemiologic week. During the first 10 epidemiologic weeks of 2026, a total of 91 confirmed cases were recorded, averaging 9.1 cases per epidemiologic week (Figure 1).

The first confirmed cases were reported in Chiapas during epidemiologic week 16 of 2025. Cases were subsequently identified in Campeche in week 20, in Yucatán and Tabasco in week 33, and in Oaxaca in week 47 of the same year. By epidemiologic week 10 of 2026, a total of 12 of Mexico's 32 states had reported confirmed human NWS myiasis cases.

We mapped the cumulative geographic spread of confirmed cases by state at selected epidemiologic reporting weeks (Figure 2). In the official state-level summaries, Chiapas accounted for 119 (58.3%) of 204 confirmed cases. The next most affected states were Yucatán with 23 (11.3%) cases, Oaxaca with 16 (7.8%) cases, Quintana Roo with 12 (5.9%) cases, Veracruz with 8 (3.9%) cases, Guerrero and Tabasco with 7 (3.4%) cases each, Campeche with 6 (2.9%) cases, Puebla and San Luis Potosí with 2 (1.0%) cases each, and the states of Mexico and Michoacán with 1 (0.5%) case each. The remaining municipality-level, demographic, clinical, and concurrent-condition analyses were based on the 202 records with sufficient case-level information.

The municipalities with the highest number of cases were Tapachula, Chiapas, with 35 (17.3%) cases; Huixtla, Chiapas, with 14 (6.9%) cases; and Mérida, Yucatán, with 14 (6.9%) cases. Together, those 3 municipalities accounted for 63 cases, representing 31.2% of all cases analyzed.

We summarized the clinical and epidemiologic characteristics of confirmed cases (Table 1). Of the 202 confirmed cases, 145 (71.8%) occurred in male patients and 57 (28.2%) in female patients. Mean age was 61.1 years (SD 19.2, range 12–93 years); for male patients, mean age was 59.2 (SD 19.0) years, and for female patients, 65.9 (SD 18.9) years.

The most frequent anatomic location for myiasis was the lower limbs, listed in 111 (55.0%) cases, followed by the neck in 41 (20.3%) cases, nose in 22 (10.9%) cases, mouth in 21 (10.4%) cases, eyes and head in 16 (7.9%) cases each, upper limbs in 14 (6.9%) cases, trunk in 12 (5.9%) cases, ear in 5 (2.5%) cases, genitalia in 2 (1.0%) cases, and abdominal cavity in 2 (1.0%) cases. More than 1 anatomic location could be recorded for the same patient. The source reports did not provide sufficient information to determine whether multiple locations represented separate infestations, contiguous involvement from a single infestation, or different levels of anatomic description.

A total of 155 (76.7%) cases had ≥1 concurrent condition. One concurrent condition was identified in 107 (53.0%) cases, 2 in 32 (15.8%) cases, 3 in 9 (4.5%) cases, and ≥4 in 7 (3.5%) cases. Overall, 48 (23.8%) cases had ≥2 concurrent conditions. The most frequently reported concurrent conditions were diabetes mellitus in 41 (20.3%) cases, alcoholism in 27 (13.4%) cases, hypertension in 26 (12.9%) cases, neoplasia in 22 (10.9%) cases, and conditions associated with cutaneous ulcers in 15 (7.4%) cases. The source reports did not consistently provide the type, location, or stage of reported neoplasms.

During the reporting period, 6 deaths were recorded among patients with confirmed human NWS myiasis (Table 2). At the time of reporting, 1 death was attributed to NWS myiasis. The recorded causes of death for the other 5 patients were basal cell carcinoma, squamous cell carcinoma, encephalitis, respiratory failure, and septic shock. The reports did not

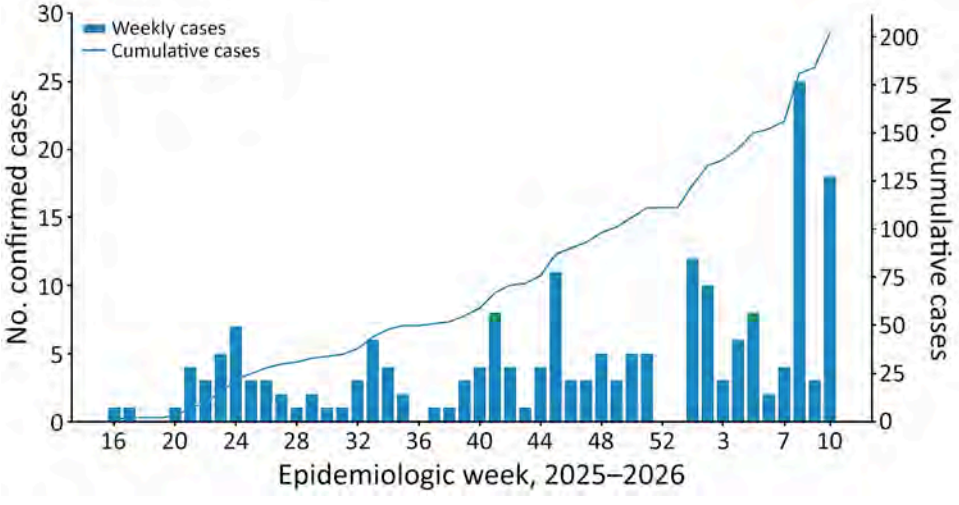

Figure 1. Confirmed human New World screwworm myiasis cases resulting from reemergence of *Cochliomyia hominivorax* screwworm, by epidemiologic week and cumulative, Mexico, April 13, 2025–March 14, 2026. Data were obtained from official epidemiologic bulletins of the Directorate General of Epidemiology, Ministry of Health (*14–16*).

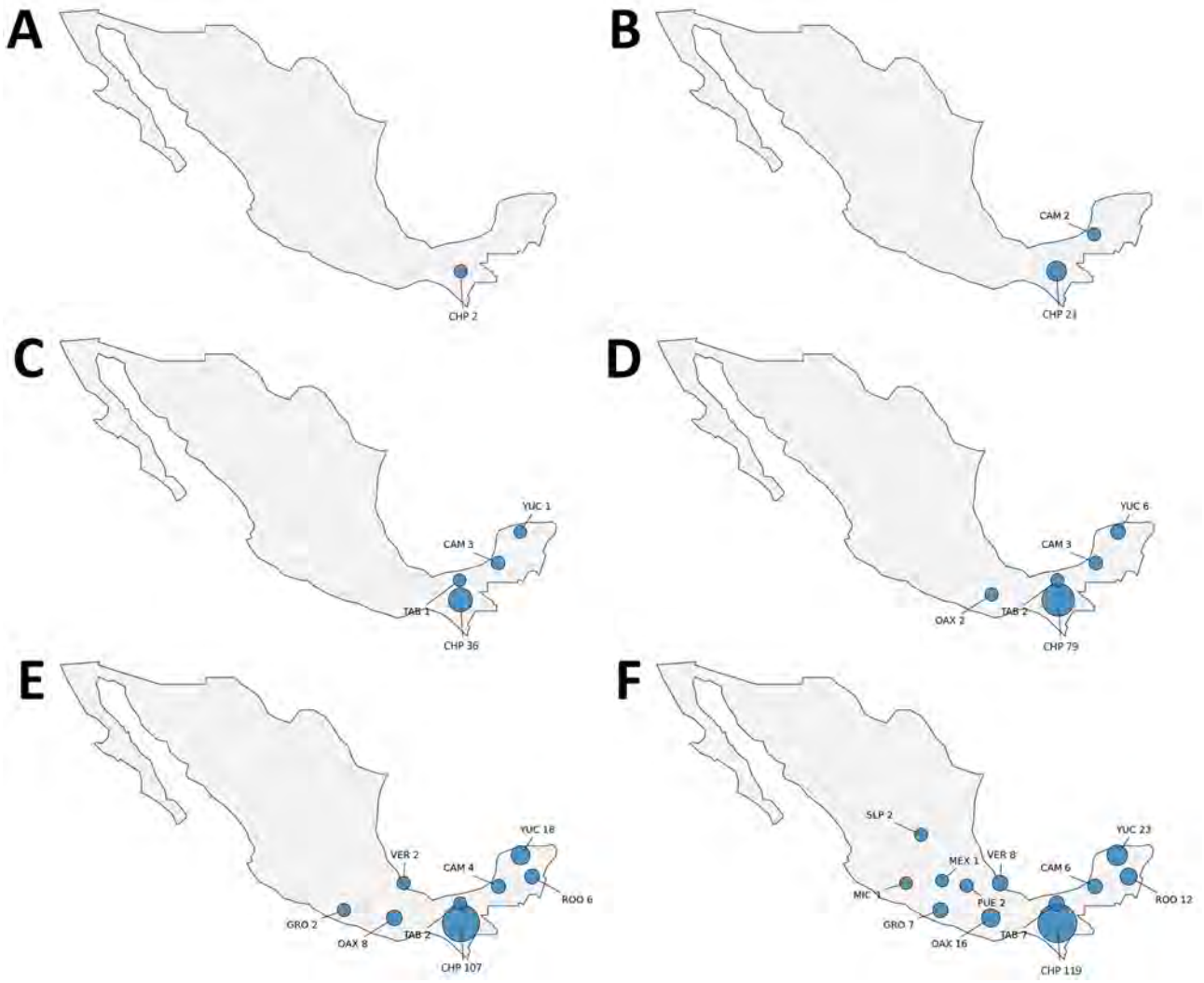

Figure 2. Cumulative geographic spread of confirmed human New World screwworm myiasis cases from reemergence of *Cochliomyia hominivorax* screwworm by state at selected epidemiologic reporting weeks, Mexico, 2025–2026. Panels show cumulative cases reported through each indicated epidemiologic week (EW): A) EW17 of 2025 (n = 2 cases); B) EW24 of 2025 (n = 23 cases); C) EW33 of 2025 (n = 41 cases); D) EW47 of 2025 (n = 92 cases); E) EW5 of 2026 (n = 149 cases); and F) EW10 of 2026 (n = 204 cases). Circle sizes are proportional to the cumulative number of confirmed cases; labels indicate state abbreviation and case count. Counts in this figure reflect all 204 confirmed cases included in official state-level surveillance summaries; 2 records lacking sufficient information were excluded from the individual-level analysis. Data were obtained from official monthly situation reports on human myiasis caused by *Cochliomyia hominivorax* in Mexico, Directorate General of Epidemiology, Ministry of Health (*17*). CAM, Campeche; CHP, Chiapas; GRO, Guerrero; MEX, state of Mexico; MIC, Michoacán; OAX, Oaxaca; PUE, Puebla; ROO, Quintana Roo; SLP, San Luis Potosí; TAB, Tabasco; VER, Veracruz; YUC, Yucatán.

provide the interval between diagnosis of NWS myiasis and death, whether the infestation had resolved before death, or sufficient clinical information to assess infestation severity or its potential contribution to the other deaths. The mean age of patients who died was 79.5 (SD ±9.6) years. Four (66.7%) deaths occurred in female patients and 2 (33.3%) in male patients. Four (66.7%) deaths were reported in Chiapas, 1 (16.7%) in Yucatán, and 1 (16.7%) in Campeche. The most frequently reported concurrent conditions among patients who died were neoplasia and hypertension, each present in 3 (50.0%) cases, followed by diabetes mellitus and social abandonment/neglect, each present in 2 (33.3%) cases.

Discussion

In this national series of confirmed human NWS myiasis cases in Mexico, the main findings were concentration of reported cases in southern Mexico, particularly Chiapas, as well as a higher mean number of weekly confirmed cases during the first 10 epidemiologic weeks of 2026 than during the 2025 reporting

period, predominance among adult men, frequent reporting of lower-limb involvement, and a high proportion of patients with concurrent clinical or social conditions. Six deaths were reported among patients with NWS myiasis, and at the time of reporting, 1 death was attributed to NWS myiasis. Those findings provide early information about the clinical and epidemiologic characteristics of human infestation during the reemergence of NWS in Mexico.

The concentration of cases in Chiapas, particularly in municipalities such as Tapachula and Huixtla, is consistent with the initial distribution observed in southern Mexico. That distribution overlaps geographically with areas reporting high numbers of NWS myiasis cases in animals, according to reports from the National Service for Agrifood Health, Safety, and Quality (*18*). However, that overlap should be interpreted with caution because our study did not assess the individual-level or ecologic relationships between animal and human cases. Even so, the geographic overlap highlights the need to strengthen integrated surveillance among human health, animal health, and animal movement control systems, particularly in border, livestock-producing, and environmentally suitable areas where NWS could become established or disperse (*19*,*20*).

The higher mean number of weekly confirmed cases during the first epidemiologic weeks of 2026, compared with the 2025 reporting period, could reflect a combination of territorial spread, increased clinical detection, strengthened reporting, or a true increase in transmission. Because this study was descriptive and based on secondary surveillance

Table 1. Clinical and epidemiologic characteristics of confirmed cases of human myiasis resulting from reemergence of *Cochliomyia hominivorax* screwworm, Mexico, April 13, 2025–March 14, 2026*

Characteristic	Male patients, n = 145	Female patients, n = 57	Total, n = 202
Confirmed cases	145 (100.0)	57 (100.0)	202 (100.0)
Age, y			
Mean (SD)	59.2 (19.0)	65.9 (18.9)	61.1 (19.2)
Range	13–90	12–93	12–93
Reported anatomic location			
Lower limbs	66 (45.5)	45 (78.9)	111 (55.0)
Neck	27 (18.6)	14 (24.6)	41 (20.3)
Nose	13 (9.0)	9 (15.8)	22 (10.9)
Mouth	15 (10.3)	6 (10.5)	21 (10.4)
Eyes	10 (6.9)	6 (10.5)	16 (7.9)
Head	10 (6.9)	6 (10.5)	16 (7.9)
Upper limbs	10 (6.9)	4 (7.0)	14 (6.9)
Trunk	9 (6.2)	3 (5.3)	12 (5.9)
Ear	2 (1.4)	3 (5.3)	5 (2.5)
Genitalia	1 (0.7)	1 (1.8)	2 (1.0)
Abdominal cavity	0	2 (3.5)	2 (1.0)
No. concurrent conditions			
0	34 (23.4)	13 (22.8)	47 (23.3)
1	80 (55.2)	27 (47.4)	107 (53.0)
2	20 (13.8)	12 (21.1)	32 (15.8)
3	8 (5.5)	1 (1.8)	9 (4.5)
≥4	3 (2.1)	4 (7.0)	7 (3.5)
Concurrent condition			
Diabetes mellitus	29 (20.0)	12 (21.1)	41 (20.3)
Alcoholism	27 (18.6)	0	27 (13.4)
Hypertension	12 (8.3)	14 (24.6)	26 (12.9)
Neoplasia	20 (13.8)	2 (3.5)	22 (10.9)
Conditions associated with cutaneous ulcers	10 (6.9)	5 (8.8)	15 (7.4)
Obesity	5 (3.4)	5 (8.8)	10 (5.0)
Social abandonment/neglect	6 (4.1)	2 (3.5)	8 (4.0)
Altered consciousness	3 (2.1)	4 (7.0)	7 (3.5)
Recent surgery	6 (4.1)	1 (1.8)	7 (3.5)
Venous insufficiency	4 (2.8)	2 (3.5)	6 (3.0)
Other intoxications	4 (2.8)	0	4 (2.0)
Psoriasis	2 (1.4)	1 (1.8)	3 (1.5)
Sensory disorder	1 (0.7)	2 (3.5)	3 (1.5)
Schizophrenia	2 (1.4)	1 (1.8)	3 (1.5)

*Values are no. (%) except as indicated. Percentages for male and female patients were calculated by using sex-specific denominators. Reported anatomic locations and concurrent conditions were not mutually exclusive categories; therefore, percentages may sum to >100%. The source reports did not provide a data dictionary for anatomic location terms or sufficient information to determine whether multiple listed locations represented separate infestations, contiguous extension of a single infestation, or different levels of anatomic description. Concurrent conditions reported in ≤2 cases are not shown individually. Data source: official monthly situation reports on human myiasis caused by *Cochliomyia hominivorax* in Mexico, Directorate General of Epidemiology, Ministry of Health (*17*).

Table 2. Characteristics of patients with recorded death among confirmed human New World screwworm myiasis cases resulting from reemergence of *Cochliomyia hominivorax* screwworm, Mexico, April 13, 2025–March 14, 2026*

Characteristic	Male patients, n = 2	Female patients, n = 4	Total, n = 6
Cases with recorded death	2	4	6 (100.0)
Age, y			
Mean (SD)	70.5 (13.4)	84.0 (3.6)	79.5 (9.6)
Range	61–80	79–87	61–87
State			
Chiapas	2	2	4 (66.7)
Yucatán	0	1	1 (16.7)
Campeche	0	1	1 (16.7)
Recorded cause of death			
New World screwworm myiasis	0	1	1 (16.7)
Basal cell carcinoma	0	1	1 (16.7)
Squamous cell carcinoma	0	1	1 (16.7)
Encephalitis	1	0	1 (16.7)
Respiratory failure	0	1	1 (16.7)
Septic shock	1	0	1 (16.7)
No. concurrent conditions			
1	1	0	1 (16.7)
2	1	2	3 (50.0)
4	0	1	1 (16.7)
5	0	1	1 (16.7)
Concurrent condition			
Neoplasia	1	2	3 (50.0)
Hypertension	1	2	3 (50.0)
Diabetes mellitus	1	1	2 (33.3)
Social abandonment/neglect	0	2	2 (33.3)
Altered consciousness	0	1	1 (16.7)
Conditions associated with cutaneous ulcers	0	1	1 (16.7)
Sensory disorders	0	1	1 (16.7)
Immobility	0	1	1 (16.7)
Wasting syndrome	0	1	1 (16.7)
Chronic kidney disease	0	1	1 (16.7)

*Values are absolute no. or no. (%) except as indicated. Recorded causes of death reflect the classifications provided in the official source reports. The reports did not provide the interval between diagnosis of New World screwworm myiasis and death, whether the infestation had resolved before death, or sufficient information to assess infestation severity or its contribution to deaths attributed to other causes. Concurrent conditions were not mutually exclusive categories; therefore, percentages may sum to >100%. Data source: official monthly situation reports on human myiasis caused by *Cochliomyia hominivorax* in Mexico, Directorate General of Epidemiology, Ministry of Health (*17*).

information, we could not distinguish among those mechanisms. Nevertheless, the observed temporal pattern underscores the need to maintain active epidemiologic surveillance, improve clinical diagnostic capacity, and ensure timely notification of suspected and confirmed cases.

The predominance of cases among adult men is consistent with findings from other series of human myiasis, in which higher frequencies have been reported among male patients (*21*,*22*). That pattern could be related to differences in occupational exposure, outdoor activities, contact with animals, unattended wounds, or delayed healthcare seeking. However, those variables were not available in the data sources we used, and therefore, we could not assess them directly. The older mean age of patients also suggests that adults and older persons with concurrent clinical conditions might represent a particularly vulnerable group.

The lower limbs were the most frequently reported anatomic location, consistent with previous studies reporting frequent involvement of the legs and feet (*23*–*25*). Wounds, chronic ulcers, trauma, and other cutaneous lesions in those anatomic regions might increase the risk for infestation, particularly among persons with diabetes mellitus, venous insufficiency, sensory disorders, or other conditions that can delay recognition of skin lesions. However, the surveillance reports did not provide sufficient information for us to determine whether multiple recorded anatomic terms represented separate infestations or contiguous extension of a single infestation. In that context, wound and lesion care, periodic examination of feet and lower limbs, and intentional examination for larvae in patients with exposed lesions remain clinically relevant.

The high proportion of cases with concurrent conditions highlights that NWS myiasis should be considered not only as an acute parasitic infestation but also as a condition favored by clinical and social vulnerability (*26*–*29*). In this series, the most frequent concurrent conditions were diabetes mellitus, alcoholism, hypertension, neoplasia, and conditions associated with cutaneous ulcers. Those findings suggest that chronic diseases, persistent skin lesions, sensory disorders, immobility, social abandonment or

neglect, and other conditions that impair self care could contribute to the clinical manifestation of infestation. However, because this study was a case series without a comparison group, we could not estimate the magnitude of risk associated with each concurrent condition.

Six deaths were recorded among patients with confirmed human NWS myiasis; however, only 1 was attributed to NWS myiasis at the time of reporting. The official reports did not provide the interval between diagnosis of infestation and death, whether the NWS infestation had resolved before death, or detailed information about the number of larvae, extent of tissue involvement, treatment, secondary infection, or other indicators of infestation severity. Consequently, we could not assess the contribution of NWS myiasis to the other reported deaths. Nevertheless, the occurrence of deaths among older patients with substantial concurrent clinical and social vulnerability underscores the importance of timely detection, larval removal, lesion care, management of secondary bacterial infection, and comprehensive treatment of underlying conditions.

The first limitation of our study is that it was based on epidemiologic surveillance information and, therefore, depends on the quality, timeliness, consistency, and completeness of reporting. Second, underreporting of human NWS myiasis is possible, particularly for cases that were not clinically recognized, taxonomically confirmed, or reported through the national surveillance system. The available information did not permit classification of cases by severity or number of larvae. Third, population denominators were unavailable, so we could not estimate incidence, population-based rates, or individual risk. Fourth, the source reports did not provide a data dictionary for anatomic location terms, so we could not determine whether multiple recorded locations represented separate infestations, contiguous extension of a single infestation, or different levels of anatomic description. Head and neck designations and combinations of adjacent structures, such as the nose, mouth, and eye, were particularly difficult to interpret. Fifth, available clinical information did not permit analysis of occupation, animal contact, wound or lesion type, time from symptom onset, treatment received, duration of infestation, resolution, or subsequent clinical course. The type, location, and stage of neoplasia were not consistently reported. For patients with recorded death, the reports did not provide the interval from NWS infestation to death, whether the infestation had resolved, or sufficient information to determine infestation severity or contribution to death. Finally, because of the descriptive design and absence of a comparison group, our findings cannot establish causal associations between concurrent conditions, animal exposure, environmental conditions, and the occurrence of human NWS myiasis.

The reemergence of NWS in Mexico and the resulting human NWS myiasis cases represent an event of public and animal health importance. The initial concentration of reported human cases in southern Mexico, predominance among adult men, frequent reporting of lower limb involvement, and high proportion of patients with concurrent conditions support strengthened clinical detection, timely reporting, and integrated One Health surveillance. Earlier diagnosis and treatment could help prevent progressive tissue destruction, secondary bacterial infection, and functional impairment.

Because animal and human cases reflect northward spread of the NWS fly and that spread is expected to continue, surveillance, diagnostic preparedness, animal movement controls, and fly-suppression activities should be implemented proactively at the leading edge of expansion, rather than only after human cases are detected. Coordination between human health, animal health, wildlife, and agricultural sectors will be essential to guide prevention and control measures.

Derived datasets generated and analyzed for this study are available from the corresponding author upon reasonable request.

Part of the data analyzed in this study came from official epidemiologic bulletins and monthly situation reports on human myiasis caused by *Cochliomyia hominivorax* in Mexico, published by the Directorate General of Epidemiology of the Ministry of Health. Data extraction, restructuring, and analysis were the sole responsibility of the authors and do not represent an official position, endorsement, or sponsorship by the Ministry of Health. The source institution is not responsible for possible numeric variations resulting from data extraction, restructuring, rounding, or tabulation by the authors.

O.M.D.-C. conceived and designed the study and conducted the investigation. O.M.D.-C., C.M.-G., J.C.-G., F.Z.V.-M., K.R.N.-F., E.S.M.-N., and H.A.R.-L. contributed to conceptualization and manuscript preparation for submission. O.M.D.-C., K.R.N.-F., E.S.M.-N., and H.A.R.-L. contributed to data cleaning and visualization. O.M.D.-C., C.M.-G., J.C.-G., F.Z.V.-M., K.R.N.-F., E.S.M.-N., and H.A.R.-L. contributed to the formal analysis and drafting of the original and final manuscript. All authors contributed to manuscript review and editing and approved the final version.

Artificial intelligence tools were used solely for editorial support to improve clarity, grammar, and style. All conceptual, methodological, analytical, and interpretive decisions were made and verified by the authors. Artificial intelligence was not used for statistical analysis or for autonomous generation of results.

About the Author

Dr. Delgado-Cuellar is a clinician-researcher at Unidad de Medicina Familiar No. 1, Instituto Mexicano del Seguro Social, Chiapas, Mexico. His research interests include the clinical epidemiology of infectious diseases, particularly vectorborne and emerging infections.

References

1. Venegas-Montero DP, Alfaro-Vellanero MJ, Rojas-Araya D, Calderón-Arguedas Ó, Vargas-Castro CM, Baldioceda-Villarreal A, et al. Case report: re-emergence of *Cochliomyia hominivorax* in Costa Rica: report of a human myiasis case 23 years after elimination. Am J Trop Med Hyg. 2024;111:1020–3. https://doi.org/10.4269/ajtmh.24-0342
2. Organización Mundial de Sanidad Animal. 3.1.14. Miasis por *Cochliomyia hominivorax* y miasis por *Chrysomya bezziana*. In: Manual Terrestre de la OIE 2019. Paris: OMSA (Organización Mundial de Sanidad Animal); 2019. p. 1–11 [cited 2026 Mar 8]. https://www.woah.org/fileadmin/Home/esp/Health_standards/tahm/3.01.14_SCREWW.pdf
3. Thomas DB, Chen AC. Age distribution of adult female screwworms (Diptera: Calliphoridae) captured on sentinel animals in the coastal lowlands of Guatemala. J Econ Entomol. 1990;83:1422–9. https://doi.org/10.1093/jee/83.4.1422
4. Gutierrez AP, Ponti L, Arias PA. Deconstructing the eradication of New World screwworm in North America: retrospective analysis and climate warming effects. Med Vet Entomol. 2019;33:282–95. https://doi.org/10.1111/mve.12362
5. Rahn JJ, Barger GL. Weather conditions and screwworm activity. 1973 [cited 2026 Jun 19]. https://agris.fao.org/search/en/providers/122535/records/65ddecfa0f3e94b9e5c771c8
6. de Barros GP, Bricarello PA. Myiasis by *Cochliomyia hominivorax* (Coquerel, 1858): a neglected zoonosis in Brazil. Open J Vet Med. 2020;10:80–91. https://doi.org/10.4236/ojvm.2020.106007
7. Francesconi F, Lupi O. Myiasis. Clin Microbiol Rev. 2012;25:79–105. https://doi.org/10.1128/CMR.00010-11
8. Akhoundi M, Mathieu A, Hannachi W, Nasrallah J, Quezel G, Blaizot R, et al. Morphological and molecular characterizations of *Cochliomyia hominivorax* (Diptera: Calliphoridae) larvae responsible for wound myiasis in French Guiana. Diagnostics (Basel). 2023;13:2575. https://doi.org/10.3390/diagnostics13152575
9. Licona LA, Laud PM, Argueta RF. Anorectal myiasis caused by *Cochliomyia hominivorax* in a septic tank worker. Cureus. 2025;17:e90842. https://doi.org/10.7759/cureus.90842
10. Servicio Nacional de Sanidad, Inocuidad y Calidad Agroalimentaria. Miasis por Gusano Barrenador [cited 2026 Jun 19]. http://www.gob.mx/senasica/documentos/miasis-por-gusano-barrenador?state=published
11. Secretaría de Salud. Aviso Epidemiológico por Caso humano confirmado de miasis por *Cochliomyia hominivorax*. Sistema Nacional de Vigilancia Epidemiológica [cited 2026 Jun 19]. http://www.gob.mx/salud/documentos/aviso-epidemiologico-por-caso-humano-confirmado-de-miasis-por-cochliomyia-hominivorax
12. Valdez-Espinoza UM, Fadda LA, Marques R, Osorio-Olvera L, Jiménez-García D, Lira-Noriega A. The reemergence of the New World screwworm and its potential distribution in North America. Sci Rep. 2025;15:23819. https://doi.org/10.1038/s41598-025-04804-9
13. Zaldivar-Gomez A, Gomez-Vazquez JP, Iniesta-Valencia AJ, Figueroa-Martínez LG, Rico-Chávez O. Estimation the reinvasion of New World screwworm (*Cochliomyia hominivorax*) in Central America: the role of animal movement in disease dispersal and control measures. Vet Parasitol Reg Stud Reports. 2025;59:101220. https://doi.org/10.1016/j.vprsr.2025.101220
14. Secretaría de Salud. Boletín Epidemiológico Sistema Nacional de Vigilancia Epidemiológica Sistema Único de Información. Edición del 12 de enero de 2026. México: Dirección General de Epidemiología; 2026 [cited 2026 Jun 4]. https://www.gob.mx/salud/documentos/boletinepidemiologico-sistema-nacional-de-vigilancia-epidemiologica-sistema-unico-de-informacion-387843
15. Secretaría de Salud. Boletín Epidemiológico Sistema Nacional de Vigilancia Epidemiológica Sistema Único de Información. Semana Epidemiológica 21 (Edición del 2 de junio de 2026). México: Dirección General de Epidemiología; 2026 [cited 2026 Jun 4]. https://www.gob.mx/salud/documentos/boletinepidemiologico-sistema-nacional-de-vigilancia-epidemiologica-sistema-unico-de-informacion-417103
16. Secretaría de Salud. Boletín Epidemiológico. Sistema Nacional de Vigilancia Epidemiológica, Sistema Único de Información. Número 10, volumen 43, Semana 10 (Del 8 al 14 de marzo de 2026). México: Dirección General de Epidemiología; 2026 [cited 2026 Jun 4]. https://www.gob.mx/cms/uploads/attachment/file/1068893/Boletin-1026.pdf
17. Secretaría de Salud. Gobierno de México. Ciudad de México, México, 2026. Situación actual de miasis (*Cochliomyia hominivorax*) en el humano: México; 2026 [cited 2026 Jun 1]. https://www.gob.mx/salud/documentos/situacion-actual-de-miasis-cochliomyia-hominivorax-en-el-humano-mexico-2026
18. Servicio Nacional de Sanidad, Inocuidad y Calidad Agroalimentaria. Informe de casos acumulados de Gusano Barrenador del Ganado en México del 20/11/2024 al 06/06/2026. Edición del 6 de junio de 2026 [Internet]. México: Comisión México-Estados Unidos para la Prevención de la Fiebre Aftosa y otras Enfermedades Exóticas de los Animales (CPA); 2026 [cited 2026 Jun 9]. https://app.powerbi.com/view?r=eyJrIjoiMjkzMzAzMz-UtZmRlNi00ZTMzLTk1NDEtNjkzZTEwNzZjZGFlIiwidCI6ImM1OWRjNTZhLTkzZWMtNGIwNy1iNzFkLTQzYzg0ND-kyNTcxOCIsImMiOjR9
19. Secretaría de Agricultura y Desarrollo Rural. Gobierno de México. 2015. Ganadería bovina y sus derivados [cited 2026 Jun 9]. https://www.gob.mx/agricultura/articulos/ganaderia-bovina-y-sus-derivados
20. Comité Estatal de Información Estadística y Geográfica. CEIEG Chiapas. 2021. Datos geográficos del Estado de Chiapas [cited 2026 Jun 9]. https://www.ceieg.chiapas.gob.mx/info-geografica
21. Kuria SK, Oyedeji AO. Human myiasis cases originating and reported in Africa for the last two decades (1998–2018): a

review. Acta Trop. 2020;210:105590. https://doi.org/10.1016/j.actatropica.2020.105590
22. Rivera JIR, Rivera MER, Figueroa JMM, Plaza JPB, Sagbay ZVP, Aspiazu DAT. Caracterización clínica de los pacientes ingresados por miasis en el Hospital del Niño Dr. Francisco de Icaza Bustamante, Guayaquil, Ecuador. Rev Cubana Med Trop. 2020;72:1–11.
23. Batista-da-Silva JA, Moya-Borja GE, Queiroz MMC. Factors of susceptibility of human myiasis caused by the New World screw-worm, *Cochliomyia hominivorax* in São Gonçalo, Rio de Janeiro, Brazil. J Insect Sci. 2011;11:14. https://doi.org/10.1673/031.011.0114
24. do Nascimento EMF, de Oliveira JB, Paes MJ, Lobo AP, da Silva ALA, dos Santos Júnior ER, et al. Miíases humanas por *Cochliomyia hominivorax* (Coquerel, 1858) (Diptera, Calliphoridae) em hospitais públicos na cidade do Recife, Pernambuco, Brasil. Entomol Vectores. 2005;12:37–51. https://doi.org/10.1590/S0328-03812005000100003
25. Hernández-Molina O, Peña-Fernández PG. Miasis por gusano barrenador en Humanos. In: III JC UCCM (Jornada Científica de la Universidad de Ciencias Médicas de Camagüey). 2025 [cited 2026 Jun 19]. https://jcuccm.sld.cu/index.php/jcuccm/2025/paper/view/587/0
26. Ye X, Wang Y, Zou Y, Tu J, Tang W, Yu R, et al. Associations of socioeconomic status with infectious diseases mediated by lifestyle, environmental pollution and chronic comorbidities: a comprehensive evaluation based on UK Biobank. Infect Dis Poverty. 2023;12:5. https://doi.org/10.1186/s40249-023-01056-5
27. Rodrigues FT, Aguiar VM, Lessa CS. Diabetic foot ulcers with myiasis: a potential route for resistance gene dissemination for enterococci? Rev Soc Bras Med Trop. 2018;51:879–879. https://doi.org/10.1590/0037-8682-0335-2017
28. Olea MS, Centeno N, Aybar CAV, Ortega ES, Galante GB, Olea L, et al. First report of myiasis caused by *Cochliomyia hominivorax* (Diptera: Calliphoridae) in a diabetic foot ulcer patient in Argentina. Korean J Parasitol. 2014;52:89–92. https://doi.org/10.3347/kjp.2014.52.1.89
29. Calvopiña M, Jordan-Guarnizo E, Galeas C, Rodriguez-Hidalgo R. Severe oral myiasis in an elderly man with epilepsy caused by the New World screwworm (*Cochliomyia hominivorax*) in subtropical Ecuador. Am J Trop Med Hyg. 2026;114:1180–3. https://doi.org/10.4269/ajtmh.25-0779

Address for correspondence: Héctor Armando Rincón-León, Coordinación Auxiliar Médica de Investigación, Jefatura de Servicios de Prestaciones Médicas, OOAD Estatal en Chiapas, Instituto Mexicano del Seguro Social, Calle 11 Poniente No 8, Tercer Piso, Colonia Centro, Tapachula, México; email: hrincon@hotmail.com

etymologia revisited

Mycobacterium chimaera

[mi'ko-bak-tēr'e-əm ki-mēr'ə]

Formerly an unnamed *Mycobacterium* sequevar within the *M. avium–M. intracellulare–M. scrofulaceum* group (MAIS), *M. chimaera* is an emerging opportunistic pathogen that can cause infections of heart valve prostheses, vascular grafts, and disseminated infections after open-heart surgery. Heater–cooler units used to regulate blood temperature during cardiopulmonary bypass have been implicated, although most isolates are respiratory. In 2004, Tortoli et al. proposed the name *M. chimaera* for strains that a reverse hybridization–based line probe assay suggested belonged to MAIS but were different from *M. avium, M. intracellulare*, or *M. scrofulaceum*. The new species name comes from the chimera, a mythological being made up of parts of 3 different animals.

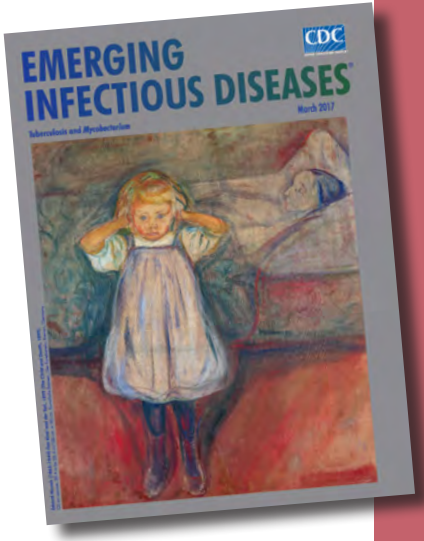

Originally published in March 2017

References:

1. Schreiber PW, Kuster SP, Hasse B, Bayard C, Rüegg C, Kohler P, et al. Reemergence of *Mycobacterium chimaera* in heater–cooler units despite intensified cleaning and disinfection protocol. Emerg Infect Dis. 2016;22:1830–3.
2. Struelens MJ, Plachouras D. *Mycobacterium chimaer*a infections associated with heater-cooler units (HCU): closing another loophole in patient safety. Euro Surveill. 2016;21:1–3.
3. Tortoli E, Rindi L, Garcia MJ, Chiaradonna P, Dei R, Garzelli C, et al. Proposal to elevate the genetic variant MAC-A, included in the *Mycobacterium avium* complex, to species rank as *Mycobacterium chimaera* sp. nov. Int J Syst Evol Microbiol. 2004;54:1277–85.

https://wwwnc.cdc.gov/eid/article/23/3/et-2303_article

Meta-analysis of Asymptomatic Monkeypox Virus Prevalence in Nonendemic Regions, 2022–2024

Kelsey J. MacCuish, Robert Snyder, Kelly A. Johnson, Edwin Chojolan, Awa Keinde, Kathleen Jacobson, Kayla Saadeh

In this meta-analysis, we performed a literature search for articles relating to asymptomatic monkeypox virus (MPXV) detections published worldwide during May 12, 2022–September 13, 2024. The primary outcome was to determine the pooled prevalence of asymptomatic MPXV detections. We conducted a random-effects analysis that yielded a final pooled prevalence of 1.0% (95% prediction interval 0.1%–11.2%). Results did not substantially differ by geographic region or study design. Although those findings are reassuring, we did not evaluate infectivity or transmission potential among asymptomatic persons. MPXV continues to circulate globally; the viral dynamics that enable its persistence remain poorly understood and merit further study.

Clade IIb of human monkeypox virus (MPXV), which causes mpox, an infectious disease in the same family as smallpox, began spreading globally in 2022 and prompted international public health concern (*1*). MPXV can be transmitted through close or intimate contact between humans, through infected animals, or through fomites (*1*). In the United States, most MPXV infections are spread person-to-person through sexual contact, primarily among gay, bisexual, and other men who have sex with men (GBMSM) (*1*). The emergence of the disease in the United States and Europe, where clinical and epidemiologic resources are more abundant than sub-Saharan Africa, has improved our understanding of the clinical manifestations and epidemiologic characteristics of MPXV. It is now understood that MPXV can be transmitted in 1–4 days before a person has onset of symptoms of infection (*1*). However, whether persons who remain asymptomatic throughout the course of infection can transmit MPXV to others is much less clear. This uncertainty arises partly because persons need to have lesions to be clinically tested for MPXV in the United States. The prevalence of asymptomatic MPXV infection in the ongoing global outbreak also is unknown and could have important implications for public health efforts.

A previous systematic review and meta-analysis of the prevalence of asymptomatic MPXV detections estimated a pooled prevalence of 10.2% (95% CI 2.5%–17.9%) but only included reports available through September 2022 (*2*). Because most studies in that meta-analysis preceded the 2022 global MPXV outbreak and the analysis also included a report from an outbreak that began in a primate sanctuary in Cameroon, the results may not be generalizable to the ongoing outbreak that primarily affects GBMSM (*2*).

The absence of asymptomatic MPXV detections in study populations has been noted in numerous reports (*3*–*8*). For example, a retrospective study noted that only 0.2% of patients tested through PCR were asymptomatic. However, that study was conducted in the summer and fall of 2022, the peak of the global outbreak, when transmission was more widespread in the GBMSM community (*9*). In contrast, 2 studies that assessed the prevalence of asymptomatic MPXV detections among GBMSM in France and Belgium retrospectively screened anorectal, urine, and oropharyngeal samples and found higher prevalences of asymptomatic detections (5.5% in France and 1.3% in Belgium), although a notable methodologic limitation of those studies is that detection of viral genetic material does not necessarily mean that a person is infectious, whereas a negative test result indicates that infectiousness is highly unlikely (*10*,*11*). Because overlooking asymptomatic viral infections, if highly prevalent, could hinder disease control and

Author affiliations: California Department of Public Health Office of Sexually Transmitted Infections and Hepatitis C Virus, Richmond, California, USA (K.J. MacCuish, R. Snyder, K.A. Johnson, E. Chojolan, A. Keinde, K. Jacobson, K. Saadeh); University of California, San Francisco School of Medicine, San Francisco, California, USA (K.A. Johnson)

DOI: https://doi.org/10.3201/eid3210.260305

prevention, we assessed the prevalence of asymptomatic MPXV detections worldwide through a meta-analysis of peer-reviewed articles published during May 12, 2022–September 13, 2024.

Methods

Search Strategy and Selection Criteria

We searched PubMed for relevant articles by using the search terms (asymptomatic OR non-lesion OR no lesion* OR without lesion* OR without cutaneous lesion* OR undetected OR unrecognized OR proctitis OR undiagnosed OR no symptom*) AND (monkeypox OR mpox OR MPXV OR MPX OR monkey pox OR monkeypox virus OR MPV). Because PubMed contains relevant biomedical literature related to MPXV and because of resource constraints and the substantial overlap between PubMed, Web of Science, and Embase, we opted for using PubMed as our primary database. We found additional relevant articles through citations from screened studies. We limited results to publication dates during May 12, 2022–September 13, 2024, to yield results relevant to the ongoing outbreak.

Data Extraction and Management

The primary outcome was determination of the pooled prevalence of asymptomatic MPXV detections among persons tested for MPXV. We used the Preferred Reporting Standard of Systematic Reviews and Meta-Analysis (PRISMA) checklist to evaluate the searched articles (Figure 1). We did not prospectively register the review protocol. The first author began by screening and removing studies whose titles did not indicate asymptomatic MPXV detections; she also briefly reviewed abstracts of excluded articles. She then screened the abstracts for inclusion and exclusion criteria, after which 2 other authors independently reviewed the remaining full-text articles for inclusion. If discordance about whether to include an article occurred, we consulted a third co-author to determine whether the article met eligibility criteria.

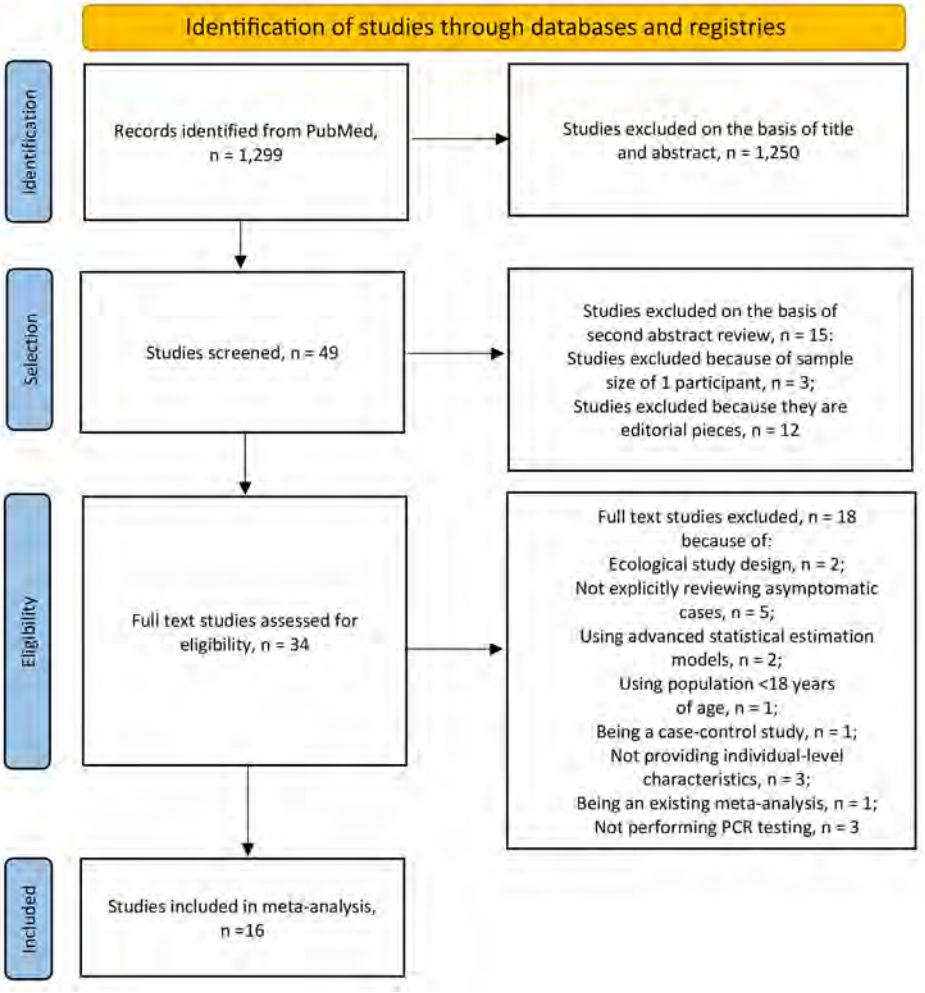

Figure 1. Preferred Reporting Standard of Systematic Reviews and Meta-Analysis flowchart for studies published during May 12, 2022–September 13, 2024, that were included in a meta-analysis of asymptomatic monkeypox virus detections in nonendemic regions.

Inclusion and Exclusion Criteria

Studies about asymptomatic MPXV detections published during May 12, 2022–September 13, 2024, were eligible for inclusion. We followed the PICO (population, intervention, comparison, outcome) framework to synthesize our research question. We searched for articles that assessed individual adults (population) who tested positive for MPXV by PCR. PCR testing for asymptomatic persons enrolled in those studies was conducted by using pharyngeal, anorectal, urethral swabs, urine, or blood. We compared those asymptomatic persons who tested positive for MPXV to those who tested negative for MPXV (comparison).

We used the following inclusion and exclusion criteria and completed the JBI (formerly Joanna Briggs Institute) critical appraisal checklist for prevalence studies to determine whether studies should be included in the meta-analysis. The study must have been conducted during May 12, 2022–September 13, 2024; taken place outside of sub-Saharan Africa (in nonendemic regions for MPXV); been primary research (not a review of already published studies); must have had a population of >1 person; been conducted on the individual patient level (e.g., not an ecologic study or a study that does not provide counts of individual characteristics); researched people ≥18 years of age (e.g., any sex, sexual orientation, or race/ethnicity); researched transmission between humans only; not selectively sampled on MPXV infection (e.g., the study did not only include persons with MPXV); performed PCR testing to determine the presence of MPXV infection; and included persons who displayed no physical symptoms of MPXV as determined by explicitly stating that persons were asymptomatic, undetected, clinically inapparent, did not experience lesions or rashes, or a combination of these descriptions. Any mention of symptomology excluded a person from being asymptomatic or (if it did not otherwise include asymptomatic MPXV) the entire article from inclusion.

We initially considered vaccination status as inclusion criteria but ultimately did not include the criteria because very few studies accounted for vaccination status. We then excerpted the following from each included article: author (or authors), study design (cross-sectional, prospective cohort, retrospective cohort, mixed cohort), publication date, study recruitment dates, country where the study participants were recruited, number of asymptomatic MPXV patients in the study population, and total number of persons who were tested for MPXV in the study population.

Data Analysis

We calculated the prevalence of asymptomatic MPXV detections as the cumulative number of asymptomatic MPXV detections divided by the total number of study participants tested for MPXV. We first constructed a funnel plot of the included research studies and statistically tested for biases and then estimated the pooled effect by using random effects estimates and their associated 95% prediction intervals (PIs) (*12*). We built logistic regression models to calculate random effects estimates, which assume that included studies estimated different interventional effects that follow an approximately normal distribution, and implemented a continuity correction of 0.5 for studies without any events. Our models used a logit transformation before pooling with the restricted maximum-likelihood estimator for between-study variance. To estimate the 95% PIs, we used the τ statistic that quantifies the variance between effect sizes, which, in this case, was the observed proportion of asymptomatic MPXV detections across studies. We used the 95% PIs to predict the underlying effect that would be seen in a hypothetical study similar to the studies included in the meta-analysis.

We conducted sensitivity analyses by using meta-regression to determine whether the prevalence of asymptomatic MPXV detections differed by geographic region or study design. We defined regions by continent and included Asia, Europe, and North America. Study designs included cross-sectional studies, mixed cohorts, prospective cohorts, and retrospective cohorts. If a study could not be grouped into a mutually exclusive category for either of those potential effect modifiers, we excluded it from that specific sensitivity analysis.

Finally, we quantitatively assessed between-study heterogeneity using the ι^2 test, which measures the percentage of variability between studies that is not attributable to chance (*13*). We classified heterogeneity as low (<25%), moderate (25%–50%), and high (>50%). We conducted all analyses by using the meta and metafor packages from R version 4.4.1 (The R Project for Statistical Computing, https://www.r-project.org) (*14*,*15*).

Results

Our search criteria yielded 1,299 articles, of which we excluded 1,250 (96.2%) based on the titles, which did not include information about asymptomatic MPXV or MPXV transmission (Figure 1). We also reviewed the abstracts of those excluded articles to ensure they did not include information about asymptomatic MPXV detections. We screened the abstracts and

introductions of the 49 remaining articles and excluded 15 (31%) that did not meet inclusion criteria; 3 (6%) of the excluded articles described individual MPXV patients, and 12 (24%) were not primary studies (i.e., they were descriptive reviews, editorials, or commentaries). We then reviewed the remaining 34 full-text articles and excluded 18 (53%) because they either were ecologic studies (n = 2), did not explicitly study asymptomatic MPXV detections (n = 5), used modeling to project the number of MPXV detections (n = 2), studied a population <18 years of age (n = 1), were a case–control study that selectively sampled on MPXV case status (n = 1), did not provide individual-level characteristics (n = 3), were an already existing meta-analysis that included studies of primate sanctuary workers with MPXV (n = 1), or did not perform PCR testing to determine MPXV infection (n = 3).

A total of 16 articles met all inclusion criteria. One author compiled the JBI checklist for all included studies and a second author validated the checklist (Appendix Table, https://wwwnc.cdc.gov/EID/article/32/10/26-0305-App1.pdf). Of the included studies, 8 were prospective cohort studies, 2 were cross-sectional studies, 5 were retrospective cohort studies, and 1 was a mixed cohort study (i.e., containing prospective and retrospective cohorts) (Table 1). Three studies were from the United States, 3 from Belgium, 2 from Germany, and 1 each from Austria, Denmark, England, France, Italy, Japan, Spain, and Switzerland. Of the 16 included studies, 14 reported the number of male participants (Table 1). The study populations ranged in size from 25 in the cross-sectional study by Brosius et al. (*17*) to 6,600 in the cross-sectional study conducted by Koppe et al. (*21*).

Cumulatively, of 14,511 persons who were tested for MPXV by PCR, 128 persons (weighted by the study's inverse variance) had asymptomatic MPXV. Results of the Egger's test to evaluate for publication bias was not statistically significant (p = 0.08), also yielding a symmetric funnel plot. Combined, those findings offered no significant evidence of publication bias having occurred and provided sufficient evidence to proceed with a random-effects analysis (Appendix Figure) (*12*). The ι^2 value was 82.6% (95% CI 72.9%–88.8%), indicating a high level of heterogeneity between studies. The random-effects analysis yielded a final pooled prevalence of 1.0% (95% PI 0.1%–11.2%) (Figure 2).

We included all 16 studies in the meta-regression analysis of geographic region and study design. We observed no statistically significant difference in the odds of asymptomatic MPXV detections in Asia (odds ratio [OR] 0.45 [95% CI 0.02–10.03]) and Europe (OR 1.70 [95% CI 0.29–10.05]) compared with the odds in North America. In our assessment of the odds of asymptomatic MPXV detections by study design, we found no significant difference in the odds of MPXV detections in mixed cohorts (OR 0.06 [95% CI 0.00–3.94]), prospective cohorts (0.17 OR [95% CI 0.02– 1.20]), and retrospective cohorts (OR 0.24 [95% CI 0.03–1.83]), all relative to the odds of MPXV detections in cross-sectional studies (Table 2).

Discussion

We assessed the prevalence of asymptomatic MPXV detections during the global outbreak of clade IIb MXV in nonendemic regions that has been ongoing since 2022. We included 16 peer-reviewed studies that encompassed 14,511 adults of both sexes (95.0% of all participants were men), sexual orientations, races, and ethnicities who were tested for MPXV. The pooled prevalence of asymptomatic MPXV detections in this population was 1%, much lower than the previously reported pooled prevalence of 10% reported in a previous meta-analysis that included a large proportion of cases from Cameroon (where MPXV is endemic). We found that asymptomatic MPXV prevalence did not differ by study design or geographic region.

Most of the 16 studies we included were conducted in countries in Europe and were either prospective or retrospective analyses. The prevalence of asymptomatic MPXV detections in all 16 studies ranged from 0% to 8%; mean prevalence was 1.55%. Studies with larger sample sizes were weighted more heavily in our analysis, which led to a lower pooled prevalence of asymptomatic MPXV detections. The prospective study conducted by Brosius et al. (*17*) found the highest prevalence of asymptomatic MPXV among tested persons, probably because they restricted their sample to persons reporting sexual or intimate contact with someone with MPXV, whereas all other studies sampled from sexually active populations (largely those attending sexual health clinics); some, but not all, reported contact with a person with MPXV.

The low prevalence of asymptomatic MPXV detections observed in our study may be, in part, attributable to the increasing number of persons who have been previously infected with or vaccinated against MPXV with modified vaccinia Ankara–Bavarian Nordic vaccine, the latter of which may reduce the risk for infection from 75% to 86% (depending on the number of doses received) and reduces the severity of MPXV disease if the patient is infected (*24*,*25*). Because studies have shown that prophylactic vaccination with

Table 1. Summary of studies included in meta-analysis of prevalence of asymptomatic MPXV detections in nonendemic regions*

Authors and year (reference)	Study design	Country	Sampling dates	Recruitment sites	Specimen type	No. (%) men	Asymptomatic MPXV detections	Sample size
Agustí et al. 2023 (*16*)	Cross-sectional	Spain	2022 Aug–2022 Oct	Community center	Pharyngeal swabs, anal swabs	89 (78.8)	7	113
De Baetselier et al. 2022 (*11*)	Retrospective cohort	Belgium	2022 Jan–2022 May	Sexual health clinic	Pharyngeal swabs, anal swabs	224 (100)	3	224
Brosius et al. 2023 (*17*)	Prospective cohort	Belgium	2022 Jun–2022 Jul	Sexual health clinic	Pharyngeal swabs, anal swabs, blood	24 (96.0)	2	25
Contag et al. 2023 (*18*)	Retrospective cohort	USA	2022 Apr–2022 Sep	Public hospital and clinic system	Pharyngeal swabs, anal swabs, urine		4	1,645
Ferre et al. 2022 (*10*)	Retrospective cohort	France	2022 Jun–2022 Jul	Sexual health clinic	Anal swabs, urine	200 (100)	11	200
Golden et al. 2024 (*19*)	Prospective cohort	USA	2022 May–2023 May	Sexual health clinic	Pharyngeal swabs, anal swabs	1,586 (93.9)	18	1,689
Grabmeier-Pfistershammer et al. 2024 (*4*)	Retrospective cohort	Austria	2023 Jan–2023 Mar	Sexual health clinic	Anal swabs	90 (100)	0	90
Hampel et al. 2023 (*20*)	Prospective cohort	Switzerland	2022 Aug–2022 Oct	SwissPrEPared program	Pharyngeal swabs, anal swabs	198 (98.5)	1	201
Koppe et al. 2024 (*21*)	Cross-sectional	Germany	2022 Apr–2023 Oct	Community center	Anal swabs, urethral swabs		75	6,600
Mizushima et al. 2023 (*22*)	Prospective cohort	Japan	2023 Jan–2023 Mar	Unknown	Anal swabs, urine	1,346 (100)	3	1,346
Ogale et al. 2023 (*23*)	Prospective cohort	USA	2022 Aug	Health clinic	Pharyngeal swabs, anal swabs, blood	359 (66.1)	2	543
Pestel et al. 2022 (*5*)	Prospective cohort	Germany	2022 Jun–2022 Jul	Infectious disease clinic	Pharyngeal swabs, anal swabs	53 (100)	0	53
Pitt-Kendall et al. 2023 (*9*)	Retrospective cohort	England	2022 Aug–2022 Oct	Sexual health clinic	Pharyngeal swabs, anal swabs, urine	1,159 (100)	2	1,159
Rossotti et al. 2023 (*6*)	Prospective cohort	Italy	2022 Sep–2022 Oct	Sexual health clinic	Pharyngeal and anal swabs	72 (100)	0	72
Thomassen et al. 2024 (*7*)	Prospective cohort	Denmark	2022 Sep–2022 Oct	Danish PrEP database	Anal swabs	224 (100)	0	224
Van Dijck et al. 2023 (*8*)	Mixed cohort	Belgium	2022 Jun–2022 Sep	Sexual health clinic	Anal swabs	327 (100)	0	327

*MPXV, monkeypox virus; PrEP, preexposure prophylaxis.

modified vaccinia Ankara–Bavarian Nordic vaccine reduces the severity of disease, vaccinated persons who become infected with MPXV may experience symptoms that are so mild that they may be classified as asymptomatic (and, especially in the United States, because of the absence of non–lesion-based testing, go undetected) (*26*,*27*). Persons who are asymptomatic or minimally symptomatic also may be less likely to seek medical attention, and the most ubiquitous assays to evaluate MPXV in clinical settings require an active lesion to swab for viral testing. However, the studies included in this analysis did not require lesions for testing; detection was assessed through PCR testing of oropharyngeal, rectal, or urethral swab samples or of urine or blood, and most of those studies evaluated high-risk groups (e.g., men at sexual health clinics).

One major strength of this meta-analysis was the inclusion of 16 different studies. We found a low pooled prevalence of asymptomatic MPXV detections among the entire pooled study population; however, that finding may be an underestimate because of

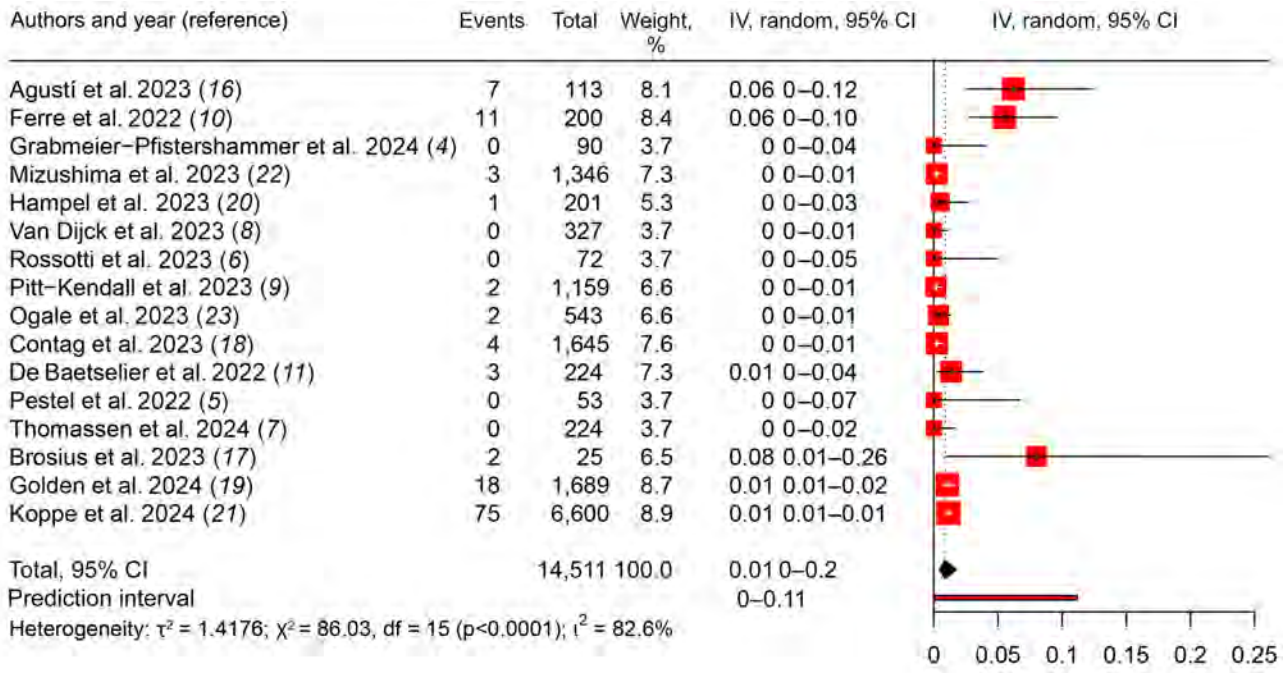

Figure 2. Forest plot of 16 studies eligible for inclusion to assess the pooled prevalence in a meta-analysis of asymptomatic monkeypox virus detections in nonendemic regions. Red blocks indicate point estimate; size of box indicates statistical weight of study. df, degrees of freedom; IV, inverse variance weighting.

underreporting of asymptomatic MPXV. Although the findings are reassuring, because we did not evaluate infectivity or transmission potential among asymptomatic persons, more accurate and widely available diagnostic MPXV testing tools (e.g., oropharyngeal swabs, as recommended by the World Health Organization) would help to better characterize the epidemiology and virology of MPXV from a surveillance standpoint, even if the use of those testing tools would be unlikely to change clinical practice (*1*,*26*,*28*).

Another strength of our meta-analysis is the inclusion of studies only relevant to the ongoing MPXV outbreak (i.e., those conducted since the outbreak began in May 2022). Because our analysis excluded studies conducted before the most recent MPXV outbreak began, we can be sure that our findings are a closer representation of the actual proportion of current asymptomatic MPXV infections than the findings from the prior meta-analysis that included studies conducted before 2022 (*2*). Finally, because antibody-based testing cannot be used to distinguish between past and current MPXV infection (or prior vaccination against MPVX), our meta-analysis includes only studies that performed PCR tests because the World Health Organization declared PCR tests the standard for diagnosing MPXV infection in humans (*26*).

One limitation of our analysis is that some persons might not have been followed long enough to have onset of symptoms or to be infected with MPXV; Rossotti et al. (*6*) only followed their study population for 21 days. Patients may have remained presymptomatic throughout the 21-day study period, experiencing symptom onset later. Because studies included in this analysis did not differentiate between presymptomatic and persistently asymptomatic infections, some persons may have been characterized as presymptomatic rather than persistently asymptomatic. In addition, we defined asymptomatic patients as persons without any physical symptoms (*29*). However, no formal definition of asymptomatic MPXV exists; asymptomatic MPXV infection in some instances could refer to a lack of lesions or rashes, a lack of classical MPXV infection symptoms, or a lack of physical symptoms entirely. A concrete definition of asymptomatic MPXV infection is needed to ensure a complete understanding. This limitation is not unique to MPXV infection and has been described among other viral infections (*30*,*31*).

Because only 5 studies in this meta-analysis included vaccination status of participants, we could

Table 2. Odds ratios and 95% CIs for meta-regression analysis of asymptomatic monkeypox virus detections in nonendemic regions, by geographic region and study design

Meta-regression variable	Odds ratio (95% CI)
Asia vs. North America	0.45 (0.02–10.03)
Europe vs. North America	1.70 (0.29–10.05)
Mixed cohort vs. cross-sectional	0.06 (0.00–3.94)
Prospective cohort vs. cross-sectional	0.17 (0.02–1.20)
Retrospective cohort vs. cross-sectional	0.24 (0.03–1.83)

not differentiate whether patients were asymptomatic or if they experienced milder nonlesion symptoms (e.g., febrile illness) because of attenuation of illness by vaccination. Future epidemiologic studies ideally will involve serologic MPXV antibody testing to more accurately assess the prevalence of previous (possibly asymptomatic) MPXV infection while also controlling for prior vaccination status. This approach is necessary because a limited number of serologic assays can differentiate antibodies specifically derived from MPXV infection from antibodies derived from other orthopox infections. In addition, because PCR testing can detect nonviable genetic material, future studies will need to assess the prevalence of replication-competent virus among asymptomatic persons who test positive for MPXV (*32*).

Most of the studies included in this analysis sampled highly selected populations, including GBMSM, sexual health clinic or vaccine clinic attendees, and contacts of persons with known MPXV infection. Such selection bias limits our interpretation of results to those populations, rather than the population of all adults in nonendemic countries.

The high level of heterogeneity among studies, indicated by the ι^2 value and large 95% CI (82.6% [95% CI 72.9%–88.8%]), indicates important variability, probably attributable to differences in study populations, recruitment settings, definitions of asymptomatic infection, specimen collection methods, and laboratory testing approaches. The high level of heterogeneity also may have distorted our results from the Egger's test of publication bias and could have resulted in an underpowered test. Given this variability and potential for an underpowered test, the pooled estimate should be interpreted with caution.

Finally, understanding the prevalence of asymptomatic MPXV detections does not help to elucidate the role of asymptomatically infected persons in MPXV transmission dynamics; in fact, MPXV detection in the absence of symptoms may not necessarily translate to infection (i.e., someone may have been recently exposed and have residual virus present but may not actually become infected). Whether persons who are asymptomatic (i.e., no symptoms whatsoever) can transmit infection, or whether persons who do not have lesions but do have respiratory or other prodromal symptoms are able to transmit infection, remains unclear. Previous studies already have demonstrated that transmission is possible when mild or atypical symptoms are present and that presymptomatic or asymptomatic transmission plays a vital role in other viral disease dynamics (*30*,*33*–*36*). We could not ascertain the prevalence of asymptomatic MPXV infections effectively in 2024 and 2025 because most of MPXV infections during the global outbreak outside of sub-Saharan Africa occurred in summer and fall of 2022. In California, 88% of MPXV cases during May 12, 2022–September 13, 2024, occurred in 2022.

Of note, we only summarize clade IIb MPXV infections in this article. Recent travel-imported cases of clade Ib MPXV underscore the complexity of MPXV clinical manifestations in relation to traditional symptoms and screening (*37*). Although clade Ib MPXV can be more pathogenic and infectious than clade IIb, whether clade Ib MPXV has the same low asymptomatic MPXV prevalence as clade IIb remains to be seen (*38*).

We found a low pooled study prevalence of asymptomatic clade IIb MPXV detections during May 12, 2022–September 13, 2024, outside of sub-Saharan Africa. Although the findings are reassuring, we did not evaluate infectivity or transmission potential among asymptomatic persons. MPXV continues to circulate in the United States overall and in California; the viral dynamics that enable its persistence remain poorly understood and merit further study. In unvaccinated persons, especially those living with HIV, mpox can cause serious disease and death, underscoring the importance of ongoing surveillance, vaccination, and vigilance for this disease.

About the Author

Ms. MacCuish is the lead data analyst and project manager for the Healthy Places Index at the Public Health Alliance of Southern California. At the time of this study, she was an informaticist in the Mpox Epidemiology Unit at the California Department of Public Health. Her primary research interests include the intersection of infectious diseases, health equity, and environmental health, with a focus on understanding how built and social environments shape health outcomes across communities.

References

1. World Health Organization. Mpox. 2024 Aug 26 [cited 2025 Jun 4]. https://www.who.int/news-room/fact-sheets/detail/mpox
2. Satapathy P, Mohanty P, Manna S, Shamim MA, Rao PP, Aggarwal AK, et al. Potentially asymptomatic infection of monkeypox virus: a systematic review and meta-analysis. Vaccines (Basel). 2022;10:2083. https://doi.org/10.3390/vaccines10122083
3. de Vries HJ, Götz HM, Bruisten S, van der Eijk AA, Prins M, Oude Munnink BB, et al. Mpox outbreak among men who have sex with men in Amsterdam and Rotterdam,

the Netherlands: no evidence for undetected transmission prior to May 2022, a retrospective study. Euro Surveill. 2023;28:2200869. https://doi.org/10.2807/1560-7917.ES.2023.28.17.2200869
4. Grabmeier-Pfistershammer K, Skorepa C, Breuer M, Masood M, Chromy D, Strassl R. No evidence of asymptomatic monkeypox infection in a highly sexually active MSM population in Austria. HIV Med. 2024;25:150–3. https://doi.org/10.1111/hiv.13535
5. Pestel J, Matthews H, Schmiedel S, Hüfner A, Jordan S, Scheiter RL, et al. Screening for monkeypox infection in asymptomatic high-risk-behaviour men having sex with men (MSM). Infect Dis Rep. 2022;14:794–7. https://doi.org/10.3390/idr14050081
6. Rossotti R, Calzavara D, Cernuschi M, D'Amico F, De Bona A, Repossi R, et al. Detection of asymptomatic mpox carriers among high-risk men who have sex with men: a prospective analysis. Pathogens. 2023;12:798. https://doi.org/10.3390/pathogens12060798
7. Thomassen SE, von Schreeb S, Kirkby NS, Pinholt M, Lebech AM, Kronborg G, et al. Prospective screening for monkeypox infection among users of HIV pre-exposure prophylaxis in Denmark. Int J STD AIDS. 2024;35:374–8. https://doi.org/10.1177/09564624231223764
8. Van Dijck C, De Baetselier I, Kenyon C, Liesenborghs L, Vercauteren K, Van Esbroeck M; ITM Monkeypox Study Group. Mpox screening in high-risk populations finds no asymptomatic cases. Lancet Microbe. 2023;4:e132–3. https://doi.org/10.1016/S2666-5247(22)00357-3
9. Pitt-Kendall R, Foster C, Rayment M, Orzechowska B, Mammadov R, Soni S, et al. Retrospective testing for mpox virus in routine STI screens from men who have sex with men in England, August-October 2022. Sex Transm Infect. 2023;99:548–51. https://doi.org/10.1136/sextrans-2023-055841
10. Ferré VM, Bachelard A, Zaidi M, Armand-Lefevre L, Descamps D, Charpentier C, et al. Detection of monkeypox virus in anorectal swabs from asymptomatic men who have sex with men in a sexually transmitted infection screening program in Paris, France. Ann Intern Med. 2022;175:1491–2. https://doi.org/10.7326/M22-2183
11. De Baetselier I, Van Dijck C, Kenyon C, Coppens J, Michiels J, de Block T, et al.; ITM Monkeypox study group. Retrospective detection of asymptomatic monkeypox virus infections among male sexual health clinic attendees in Belgium. Nat Med. 2022;28:2288–92. https://doi.org/10.1038/s41591-022-02004-w
12. Higgins JPT, Thomas J, Chandler J, Cumpston M, Li T, Page MJ, et al. Cochrane handbook for systematic reviews of interventions version 6.5. 2024 Aug [cited 2025 Jun 4]. https://www.cochrane.org/authors/handbooks-and-manuals/handbook
13. Riley RD, Higgins JP, Deeks JJ. Interpretation of random effects meta-analyses. BMJ. 2011;342(feb10 2):d549. https://doi.org/10.1136/bmj.d549
14. Balduzzi S, Rücker G, Schwarzer G. How to perform a meta-analysis with R: a practical tutorial. Evid Based Ment Health. 2019;22:153–60. https://doi.org/10.1136/ebmental-2019-300117
15. Viechtbauer W. Conducting meta-analyses in R with the metafor package. J Stat Softw. 2010;36:1–48. https://doi.org/10.18637/jss.v036.i03
16. Agustí C, Martínez-Riveros H, Hernández-Rodríguez À, Casañ C, Díaz Y, Alonso L, et al. Self-sampling monkeypox virus testing in high-risk populations, asymptomatic or with unrecognized Mpox, in Spain. Nat Commun. 2023;14:5998. https://doi.org/10.1038/s41467-023-40490-9
17. Brosius I, Van Dijck C, Coppens J, Vandenhove L, Bangwen E, Vanroye F, et al.; ITM MPOX Study Group. Presymptomatic viral shedding in high-risk mpox contacts: a prospective cohort study. J Med Virol. 2023;95:e28769. https://doi.org/10.1002/jmv.28769
18. Contag CA, Renfro ZT, Lu J, Shen S, Karan A, Solis D, et al. Prevalence of Mpox (Monkeypox) in patients undergoing STI screening in northern California, April–September 2022. J Clin Virol. 2023;164:105493. https://doi.org/10.1016/j.jcv.2023.105493
19. Golden MR, Soge OO, Mills M, Berzkalns A, Cannon C, Ramchandani M, et al. Asymptomatic and subclinical mpox: an association with modified vaccinia Ankara vaccine. Sex Transm Dis. 2024;51:342–7. https://doi.org/10.1097/OLQ.0000000000001939
20. Hampel B, Farnham A, Lamothe-Molina PJ, Capelli C, Schibler M, Ustero Alonso P, et al. Low prevalence of asymptomatic mpox in populations at high risk. Lancet Microbe. 2023;4:e856. https://doi.org/10.1016/S2666-5247(23)00248-3
21. Koppe U, Jansen K, Schmidt AJ, Weber C, Schulze H, Kulis-Horn RK, et al. Clinically inapparent mpox virus (MPXV) infections among clients of three anonymous Community Based Voluntary Counselling and Testing centres in Berlin, Germany, 2022-2023. BMC Infect Dis. 2024;24:613. https://doi.org/10.1186/s12879-024-09510-x
22. Mizushima D, Shintani Y, Takano M, Shiojiri D, Ando N, Aoki T, et al. Prevalence of asymptomatic mpox among men who have sex with men, Japan, January–March 2023. Emerg Infect Dis. 2023;29:1872–6. https://doi.org/10.3201/eid2909.230541
23. Ogale YP, Baird N, Townsend MB, Berry I, Griffin I, Lee M, et al.; DC Mpox Response Project Team. DC Mpox Response Project Team. Evidence of mpox virus infection among persons without characteristic lesions or rash presenting for first dose of JYNNEOS vaccine—District of Columbia, August 2022. Clin Infect Dis. 2023;77:298–302. https://doi.org/10.1093/cid/ciad145
24. Centers for Disease Control and Prevention. JYNNEOS vaccine effectiveness. 2024 Aug 27 [cited 2025 Jun 4]. https://www.cdc.gov/mpox/data-research/vaccines/index.html
25. Farrar JL, Lewis NM, Houck K, Canning M, Fothergill A, Payne AB, et al.; Mpox Cases in Vaccinated Persons Team. Demographic and clinical characteristics of mpox in persons who had previously received 1 dose of JYNNEOS vaccine and in unvaccinated persons—29 U.S. jurisdictions, May 22–September 3, 2022. Am J Transplant. 2023;23:298–303. https://doi.org/10.1016/j.ajt.2023.01.003
26. World Health Organization. Testing for mpox: individuals and communities. 2023 Dec 11 [cited 2025 Jun 4]. https://www.who.int/news-room/questions-and-answers/item/testing-for-mpox–individuals-and-communities
27. Granskog L, Saadeh K, Snyder R, Tang EC, Lo T, Quint J, et al. Effectiveness of JYNNEOS vaccination in preventing lesion dissemination among individuals with confirmed mpox infection. Open Forum Infect Dis. 2025;12(Suppl 1):ofae631.074. https://doi.org/10.1093/ofid/ofae631.074
28. Coppens J, Vanroye F, Brosius I, Liesenborghs L, van Henten S, Vanbaelen T, et al.; ITM MPX study group. Alternative sampling specimens for the molecular detection of mpox (formerly monkeypox) virus. J Clin Virol. 2023;159:105372. https://doi.org/10.1016/j.jcv.2022.105372
29. MedlinePlus. Asymptomatic. 2024 Oct 9 [cited 2025 Jun 4]. https://medlineplus.gov/ency/article/002217.htm

30. Shaikh N, Swali P, Houben RMGJ. Asymptomatic but infectious—the silent driver of pathogen transmission. A pragmatic review. Epidemics. 2023;44:100704. https://doi.org/10.1016/j.epidem.2023.100704
31. Espinoza B, Marathe M, Swarup S, Thakur M. Asymptomatic individuals can increase the final epidemic size under adaptive human behavior. Sci Rep. 2021;11:19744. https://doi.org/10.1038/s41598-021-98999-2
32. Sberna G, Specchiarello E, Mija C, Carletti F, Belladonna S, Girardi E, et al. Measurement of the infection and integrity of monkeypox virus: a new method using PMAxx-ddPCR. Int J Mol Sci. 2025;26:1195. https://doi.org/10.3390/ijms26031195
33. Snyder RE, Saadeh K, Tang EC, Johnson KA, Holland SN, Quint J, et al. Sexual exposures associated with mpox infection: California, November 2022 to June 2023. J Infect Dis. 2024;229(Supplement_2):S188–96. https://doi.org/10.1093/infdis/jiad447
34. Liu Y, Funk S, Flasche S; Centre for Mathematical Modelling of Infectious Diseases nCoV Working Group. The contribution of pre-symptomatic infection to the transmission dynamics of COVID-2019. Wellcome Open Res. 2020;5:58. https://doi.org/10.12688/wellcomeopenres.15788.1
35. Pollock AM, Lancaster J. Asymptomatic transmission of covid-19. BMJ. 2020;371:m4851. https://doi.org/10.1136/bmj.m4851
36. Sayampanathan AA, Heng CS, Pin PH, Pang J, Leong TY, Lee VJ. Infectivity of asymptomatic versus symptomatic COVID-19. Lancet. 2021;397:93–4. https://doi.org/10.1016/S0140-6736(20)32651-9
37. Alvi MI, Kliner M, Welfare W, Gordon NC, Thomas S, Padfield S, et al. Case series of the first five human infections with monkeypox virus clade Ib and report on the public health response, United Kingdom, October to November 2024. Euro Surveill. 2025;30:2500131. https://doi.org/10.2807/1560-7917.ES.2025.30.10.2500131
38. Centers for Disease Control and Prevention. Ongoing clade II mpox global outbreak. 2025 [cited 2025 Jun 4]. https://www.cdc.gov/mpox/outbreaks/2022/index-1.html

Address for correspondence: Kayla Saadeh, California Department of Public Health Office of STIs and HCV, 850 Marina Bay Pkwy, Richmond, California, 94804, USA; email: kayla.saadeh@cdph.ca.gov

etymologia revisited

Salmonella

[sal′′mo-nel′ə]

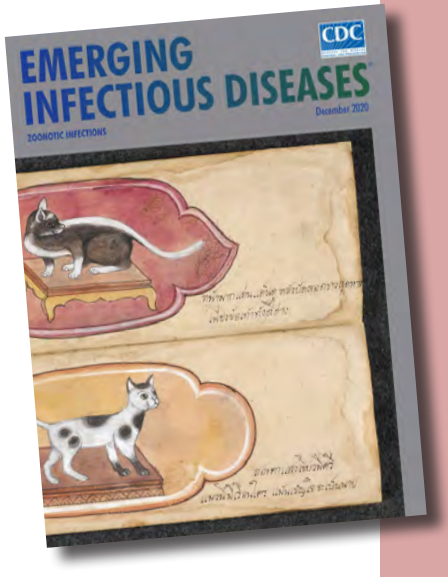

Originally published in December 2020

Named in honor of Daniel Elmer Salmon, an American veterinary pathologist, *Salmonella* is a genus of motile, gram-negative bacillus, nonspore-forming, aerobic to facultatively anaerobic bacteria of the family Enterobacteriaceae. In 1880, Karl Joseph Eberth was the first to observe *Salmonella* from specimens of patients with typhoid fever (from the Greek *typhōdes* [like smoke; delirious]), which was formerly called *Eberthella typhosa* in his tribute. In 1884, Georg Gaffky successfully isolated this bacillus (later described as *Salmonella* Typhi) from patients with typhoid fever, confirming Eberth's findings. Shortly afterward, Salmon and his assistant Theobald Smith, an American bacteriologist, isolated *Salmonella* Choleraesuis from swine, incorrectly assuming that this germ was the causative agent of hog cholera. Later, Joseph Lignières, a French bacteriologist, proposed the genus name *Salmonella* in recognition of Salmon's efforts.

References:

1. Dorland's Illustrated Medical Dictionary. 32nd ed. Philadelphia: Elsevier Saunders; 2012.
2. Gossner CM, Le Hello S, de Jong B, Rolfhamre P, Faensen D, Weill FX, et al. Around the world in 1,475 *Salmonella* geo-serotypes [Another Dimension]. Emerg Infect Dis. 2016;22:1298–302.
3. Issenhuth-Jeanjean S, Roggentin P, Mikoleit M, Guibourdenche M, de Pinna E, Nair S, et al. Supplement 2008-2010 (no. 48) to the White-Kauffmann-Le Minor scheme. Res Microbiol. 2014;165:526–30.
4. Salmon DE. The discovery of the germ of swine-plague. Science. 1884;3:155–8.
5. Su LH, Chiu CH. Salmonella: clinical importance and evolution of nomenclature. Chang Gung Med J. 2007;30:210–9.

https://wwwnc.cdc.gov/eid/article/26/12/et-2612_article

Multiple Introductions and Cross-Sector Transmission of *Salmonella enterica* Serovar Infantis Carrying *bla*$_{CTX-M-65}$ Gene, South Korea, 2022–2024

Eunkyung Shin,[1] Tae-Min La,[1] Jaeil Yoo, Sungsuck Oh, Juhee Kim, Junyoung Kim,[2] Ji-Yeon Hyeon[2]

Salmonella enterica subspecies *enterica* serovar Infantis carrying the *bla*$_{CTX-M-65}$ gene has been increasingly detected globally, including in South Korea, since 2022. We analyzed 65 *bla*$_{CTX-M-65}$–positive *Salmonella* Infantis isolates from humans, poultry, and wastewater collected during 2022–2024 by using whole-genome sequencing and phylogenomic analysis. All isolates were multidrug-resistant, commonly to aminoglycosides, β-lactams, quinolones, tetracyclines, amphenicols, and folate pathway inhibitors. Phylogenetic analysis revealed high genetic similarity among isolates from humans, poultry, and wastewater, which were intermingled within monophyletic clades with high bootstrap support, indicating close genomic relatedness across sectors. Bayesian phylogeographic reconstruction suggested multiple potential introductions during 2018–2022, including 1 lineage related to isolates from the United States (clade I) and others related to isolates from the United Kingdom (clade II). Those findings highlight the emergence and genomic diversity of *bla*$_{CTX-M-65}$–positive *Salmonella* Infantis in South Korea and support the value of continued genomic surveillance across sectors.

Salmonella enterica subspecies *enterica* serovar Infantis has emerged as a leading serovar of human salmonellosis (*1*) and is listed among the top 15 *Salmonella* serovars globally (*2*). Poultry and poultry-derived products are major reservoirs for this serovar, which has shown a steady global increase over the past decade, driven by its adaptation to poultry production systems and persistence throughout the food chain (*3*). Concurrently, multidrug-resistant (MDR) and extended-spectrum β-lactamase (ESBL)–producing *Salmonella* Infantis strains have been increasingly reported, posing a growing public health concern (*4*). Those resistant clones have emerged through acquisition of large plasmids carrying multiple resistance and virulence determinants. One of the earliest reports, from Israel in 2008, described an ≈280-kb megaplasmid, termed a plasmid of emerging *Salmonella* Infantis (pESI) (*5*). That plasmid harbored multiple resistance genes, including genes conferring resistance to tetracycline, trimethoprim, sulfamethoxazole, antiseptics, and heavy metals, as well as virulence factors, such as yersiniabactin (*ybt* operon) and fimbrial operons (*fea* and *ipf*) that enhance survival, adaptation, and colonization under antimicrobial and environmental stress, strengthening bacterial fitness (*5*). pESI-like plasmids have rapidly disseminated worldwide, evolving to carry ESBL genes such as *bla*$_{CTX-M-1}$ and *bla*$_{CTX-M-65}$. *Salmonella* Infantis carrying *bla*$_{CTX-M-65}$ was reported from fecal samples collected from children in Peru during 2012–2013 (*6*); subsequently spread across humans, food animals, and retail meat in the United States (*7*); and later was detected from human and food animal samples in Chile (*8*). Those reports indicated that *bla*$_{CTX-M-65}$–positive *Salmonella* Infantis had emerged in humans, food animals, and food products, highlighting its relevance for One Health surveillance.

In South Korea, isolates collected through the national gastrointestinal infection surveillance networks (EnterNet Korea) have shown an increase

Author affiliations: Division of Bacterial Disease, Korea Disease Control and Prevention Agency, Cheongju, South Korea (E. Shin, J. Yoo, Junyoung Kim); College of Veterinary Medicine, Konkuk University, Seoul, South Korea (T.-M. La, J.-Y. Hyeon); Division of Emerging Infectious Diseases, Incheon Metropolitan City Institute of Public Health and Environment, Incheon, South Korea (S. Oh, Juhee Kim)

DOI: https://doi.org/10.3201/eid3210.251758

[1]These first authors contributed equally to this article.

[2]These authors contributed equally to this article.

in *Salmonella* Infantis since 2022 (*9*). More recently, $bla_{CTX\text{-}M\text{-}65}$–positive *Salmonella* Infantis has been increasingly identified in the poultry sector (*10*). However, genomic characterization from human sources remains limited, with only 1 human isolate reported to date (*11*). Thus, although recent studies have documented the emergence of this lineage in South Korea, integrated genomic data spanning human, poultry, and environmental sources remain scarce. That gap has limited understanding of the origins, phylogenomic relationships, and public health implications of $bla_{CTX\text{-}M\text{-}65}$–positive *Salmonella* Infantis in South Korea. To address that gap, we conducted whole-genome sequencing (WGS) and phylogenomic analysis of $bla_{CTX\text{-}M\text{-}65}$–positive *Salmonella* Infantis isolates from humans, poultry, and wastewater in South Korea and compared those isolates with global genomes to investigate genetic relationships and phylogenomic context of this bacterium.

Materials and Methods

Bacterial Isolates

We analyzed a total of 65 $bla_{CTX\text{-}M\text{-}65}$–positive *Salmonella* Infantis isolates collected during 2022–2024, including 45 from human patients, 16 from poultry, and 4 from wastewater. Human isolates were collected through national surveillance programs (EnterNet and PulseNet Korea) maintained by the Korea Disease Control and Prevention Agency. During 2022–2024, a total of 2,817 human *Salmonella* isolates were collected, of which 258 were identified as *Salmonella* Infantis. From those, we included all 45 ESBL-producing *Salmonella* Infantis isolates in this study.

Wastewater isolates were obtained from influent samples collected at 2 public wastewater treatment facilities (Songdo 2 and Namhang) in Incheon through a wastewater-based infectious disease surveillance program. Through that surveillance program, 4 ESBL-producing *S*. Infantis isolates were identified during the study period; we included all 4 in this study.

We obtained poultry isolates collected from chicken fecal samples from poultry farms through the foodborne pathogen tracking and monitoring program. During 2023, a total of 40 poultry-derived *Salmonella* isolates were collected from 32 poultry farms, of which 20 *Salmonella* Infantis isolates were recovered from 17 farms. Among those, 16 ESBL-producing *Salmonella* Infantis isolates from 16 farms were collected, and we included all 16 in this study (Appendix Table 1, https://wwwnc.cdc.gov/EID/article/32/10/25-1758-App1.pdf).

We performed species identification by using the VITEK-II automated system (bioMérieux, https://www.biomerieux.com) and conducted serotyping according to the Kauffmann–White scheme with specific antiserum (BD Biosciences, https://www.bdbiosciences.com). We performed antimicrobial susceptibility testing by broth microdilution using customized Sensititer KRCDC2F plates (TREK Diagnostic Systems, https://www.trekds.com), according to Clinical and Laboratory Standards Institute guidelines (*12*).

WGS

We used the DNeasy Blood and Tissue Kit (QIAGEN, https://www.qiagen.com) to extract genomic DNA. We performed WGS on a MiSeq platform (Illumina Inc., https://www.illumina.com) by using the MiSeq Reagent Kit v2 (Illumina) at 500 cycles for 2 × 250-nt reads. We used Trimmomatic version 0.36 (*13*) to process reads, then SPAdes version 3.15.5 (*14*) to assemble trimmed raw reads. We confirmed serovar prediction by using sistr_cmd version 1.1.2 (https://github.com/phac-nml/sistr_cmd). We used ABRicate version 1.0.1 (https://github.com/tseemann/abricate) with the ResFinder database (*15*) to identify antimicrobial resistance (AMR) genes and with a custom database comprising 283 genes from the reference strain 119944 (GenBank accession no. CP047882) to identify pESI-like megaplasmid markers. For additional plasmid characterization, we randomly selected 1 human isolate (23SAL-3252) and 1 poultry isolate (SAL-AN014) from clade II for long-read sequencing. We used the Ligation Sequencing Kit to prepare libraries and performed sequencing on a MinION platform with R10.4.1 flow cells using MinKNOW software (all Oxford Nanopore Technologies, https://nanoporetech.com) with default settings. We used Autocycler version 0.6.1 (*16*) to assemble nanopore reads, then used Unicycler_polish (*17*) to polish with the corresponding Illumina reads under default parameters. For clade I, we assessed plasmid context by using previously reported complete genome sequences from retail chicken meat in South Korea (*18*). In addition, to illustrate broader structural variation and conserved AMR gene organization, we used Proksee (https://proksee.ca) to compare previously defined pESI-like plasmid variants from South Korea (*18*) with the clade II plasmid sequences from this study.

Phylogenetic Analysis

To investigate the genetic relationships of our 65 isolates, we constructed 2 whole-genome single-

nucleotide polymorphism (wgSNP) phylogenetic trees. One tree compared our 65 isolates with 37 $bla_{CTX-M-65}$–positive *Salmonella* Infantis isolates from South Korea; the other compared our isolates with a total of 2,305 $bla_{CTX-M-65}$–positive *Salmonella* Infantis isolates, including the 37 from South Korea used in the first tree and 2,268 global genomes from EnteroBase (https://enterobase.warwick.ac.uk).

To perform the phylogenetic analysis of South Korea isolates, we downloaded 52 additional *Salmonella* Infantis genomes collected from South Korea from GenBank in October 2024 and evaluated genomes by using sistr_cmd version 1.1.2 (Appendix Table 2). After quality filtering, we retained 16 genomes harboring $bla_{CTX-M-65}$ and pESI-like plasmids and used those for further analysis. In addition, the College of Veterinary Medicine, Konkuk University, Seoul, South Korea, provided 21 genomes of $bla_{CTX-M-65}$–positive *Salmonella* Infantis collected from poultry isolates in 2023. For the global phylogenetic analysis, we retrieved 2,723 *Salmonella* Infantis genomes carrying $bla_{CTX-M-65}$ from EnteroBase in October 2024 by using the search terms Infantis (serovar) and $bla_{CTX-M-65}$ (AMR analysis). After quality evaluation with sistr_cmd version 1.1.2 and metadata filtering, we included a total of 2,268 strains for further analysis.

We identified wgSNPs by using Snippy version 4.6.0 (https://github.com/tseemann/snippy) and used *Salmonella* Infantis N55391 (GenBank accession no. CP016410) as the reference. We used PHASTEST (*19*) to identify prophages and the Nucmer tools from the Mummer package version 3.23 (*20*) to identify repetitive regions within the reference genome. We excluded single-nucleotide polymorphisms (SNPs) located in prophage and in repetitive regions. We used Gubbins version 3.3.1 (*21*) to identify and subsequently mask recombination regions from the wgSNP alignment before phylogenetic analysis. We used IQ-TREE with a TVMe model selected by ModelFinder (*22*) and 1,000 bootstrap replicates to infer the maximum-likelihood tree for the South Korea dataset and used FastTree (*23*) to infer the maximum-likelihood tree for the global dataset.

Bayesian Phylogenetic Analysis

To reconstruct the evolutionary history, we identified a subtree consisting of 101 strains from South Korea and 116 strains from 12 other countries on the basis of a FastTree support value of ≥0.9. Of those, we included 97 domestic and 79 international strains (Appendix Table 3) with available FASTQ data in the analysis, for a total of 176 strains. We downloaded raw reads from the National Center for Biotechnology Information Sequence Read Archive (https://ncbi.nlm.nih.gov/sra) by using fasterq-dump (https://github.com/ncbi/sra-tools), then quality-trimmed and processed reads for SNP calling as described.

We used TempEst version 1.5.3 (*24*) to assess the temporal signal (R^2 >0.8561). We performed Bayesian phylogenetic analysis by using BEAST version 1.10.4 (*25*) with a TVMe substitution model selected by using ModelTest-NG (*26*). We used path and stepping-stone sampling (*27*) to evaluate marginal likelihood of 2 clock models, constant and lognormal relaxed; and 3 tree models, constant population size, exponential growth, and Gaussian Markov random field Bayesian Skyride model. The lognormal relaxed clock model with Gaussian Markov random field Bayesian Skyride model yielded the highest Bayes factor (BF), indicating the best fit.

For discrete trait phylogeographic analysis, we reconstructed ancestral locations and estimated asymmetric exchanges between regions by using a nonreversible continuous-time Markov chain model. We excluded the United States and Italy because those countries were each represented by 1 sequence. To identify well-supported transitions between discrete states, we used Bayesian stochastic search variable selection and Bayes factor (BF) testing, as implemented in SPREAD3 software version 0.9.6 (*28*). We considered transitions with posterior probability >0.5 and BF >3 significant (*28*). We used stochastic mapping (*29*) to estimate transition rate and count (Markov jumps). We ran 3 independent chains of 100 million generations in parallel with sampling every 10,000 generations. We evaluated the results in Tracer (http://beast.community/tracer) to ensure that effective sample sizes were >200 and to ensure convergence between all 3 runs. We used LogCombiner version 1.10.4 (https://beast.community/logcombiner) to combine the log and tree files from 3 runs, with 10% burn-in. We used TreeAnnotator version 1.10.4 (https://beast.community/treeannotator) to generate a maximum clade credibility tree with 10% burn-in and common ancestor node heights. We annotated the maximum clade credibility tree by using FigTree version 1.4.4 (https://tree.bio.ed.ac.uk/software/figtree).

To evaluate the potential effects of unequal sampling across discrete geographic states, we used a generalized linear model as an extension of phylogeographic inference in BEAST version 1.10.4 (*25*). Coefficients quantified the effect size, and we used Tracer version 1.7.1 to analyze indicators that deter-

mined predictor inclusion. We used the number of sequences assigned to each discrete state as predictors to inform transition rate estimates.

Results

Phenotypic and Genotypic AMR

We assessed antimicrobial susceptibility profiles for the 65 *bla*$_{CTX-M-65}$–positive *Salmonella* Infantis isolates from South Korea (Appendix Table 4). All isolates were resistant to ampicillin, cefotaxime, ceftriaxone, and tetracycline but remained susceptible to azithromycin and amikacin. We observed high resistance rates for nalidixic acid (98.5%; n = 64), chloramphenicol (93.8%; n = 61), gentamicin (81.5%; n = 53), and trimethoprim/sulfamethoxazole (80.0%; n = 52).All isolates were resistant to ≥3 antimicrobial classes and thus classified as MDR (Table). The predominant resistance profile, observed in 43 (66.2%) isolates, included resistance to aminoglycosides, β-lactams, quinolones, tetracyclines, amphenicols, and folate pathway inhibitors. Of note, 1 human isolate displayed resistance to 7 antimicrobial classes.

We evaluated AMR gene profiles of 102 *bla*$_{CTX-M-65}$–positive *Salmonella* Infantis isolates from South Korea, including the 65 isolates from this study (Figure 1). All isolates harbored >3 distinct aminoglycoside resistance genes. The most prevalent genes were *aph*(4)-Ia (100%), *aac*(3)-Iva (100%), *aac*(6′)-Iaa (99%), *ant*(3″)-Ia (98%), and *aph*(3′)-Ia (68%). All the isolates carried *tet*(*A*), whereas we detected *sul1* in 98%, *floR* in 91%, and *dfrA14* in 71% of the isolates. In addition, we identified *bla*$_{TEM-30}$ in 1 human isolate.

Phylogenetic Analysis of *bla*$_{CTX-M-65}$–Positive *Salmonella* Infantis Isolates

The final alignment of the 2 wgSNP phylogenetic trees included 687 SNP sites in the South Korea dataset and 12,616 SNP sites in the global dataset (data not shown). The South Korea genomes formed 2 distinct clades (clade I and clade II) (Figure 1). Clade I comprised 5 isolates, including 2 from humans and 3 from poultry, all collected in 2023, with a median of 5 (range 3–7) SNPs difference (Appendix Figure 1). Clade II contained 97 isolates from human, poultry, and wastewater sources interspersed throughout the clade, with a median of 28 (range 0–60) SNPs difference (Appendix Figure 1). The median pairwise distance between clades I and II was 69 (range 60–81) SNPs (Appendix Figure 1).

In the global phylogeny, all South Korea isolates were separated into 2 major clades (Figure 2), consistent with the national-level analysis. Clade II isolates from South Korea clustered with 116 isolates from 12 countries, whereas clade I isolates clustered with 15 isolates from the United States and 2 others from South Korea. Considering the broad international distribution of clade II isolates, we conducted a phylogeographic analysis to determine their potential geographic origins and transmission routes.

All South Korea and related global isolates carried 256–283 of the 283 genes in the reference genome and harbored all 6 hallmark loci (i.e., *ardA*, *pilL*, *sogS*, *trbA*, *ipf*, and *ipr2*) (*30*), confirming the presence of a pESI-like plasmid (data not shown). In addition, long-read sequencing and assembly of 2 randomly selected clade II isolates, 1 human and 1 poultry isolate, confirmed that *bla*$_{CTX-M-65}$ was located on pESI-like megaplasmids. For clade I, previously reported complete genome sequences of MDR *Salmonella* Infantis carrying *bla*$_{CTX-M-65}$ from retail chicken meat in South Korea showed similar pESI-like plasmid structures and resistance gene organization, despite structural variation among the plasmid variants (Appendix Figure 3).

Phylogeographic Analysis of *bla*$_{CTX-M-65}$–Positive *Salmonella* Infantis Isolates

Bayesian phylogenetic reconstruction of the global clade revealed 6 South Korea subclades (A–F), each strongly supported by a posterior probability of 1 (Figure 3; Appendix Figure 2). The estimated times to most recent common ancestor were 2019.29

Table. Antimicrobial resistance patterns of 65 isolates from a study of multiple introductions and cross-sector transmission of *Salmonella enterica* serovar Infantis carrying *bla*$_{CTX-M-65}$ gene, South Korea, 2022–2024

Antimicrobial resistance pattern	No. (%) isolates
β-lactams–quinolones–tetracyclines	2 (3.1)
β-lactams–tetracyclines–amphenicols	1 (1.5)
β-lactams–quinolones-tetracyclines–amphenicols	2 (3.1)
Aminoglycosides–β-lactams-quinolones–tetracyclines	1 (1.5)
β-lactams–quinolones–tetracyclines–amphenicols–folate pathway inhibitors	7 (10.8)
Aminoglycosides–β-lactams–quinolones–tetracyclines–folate pathway inhibitors	1 (1.5)
Aminoglycosides–β-lactams–quinolones–tetracyclines–amphenicols	7 (10.8)
Aminoglycosides–β-lactams–quinolones–tetracyclines–amphenicols–folate pathway inhibitors	43 (66.2)
Aminoglycosides–β-lactams–quinolones–polymyxins–tetracyclines–amphenicols–folate pathway inhibitors	1 (1.5)

(highest posterior density [HPD] 2018.58–2020.15) for clade A (n = 67), 2021.59 (HPD 2020.67–2022.51) for clade B (n = 3), 2020.07 (HPD 2019.24–2020.98) for clade C (n = 17), 2022.02 (HPD 2021.03–2022.81) for clade D (n = 2), 2020.07 (HPD 2019.24–2020.98) for clade E (n = 7, including 2 from the United Kingdom), and 2020.06 (HPD 2019.62–2021.66) for clade F (n = 2).

Bayesian phylogeographic analysis suggested that South Korea lineages were most closely related to isolates from the United Kingdom, with strong statistical support for this transition pattern (BF 983.911;

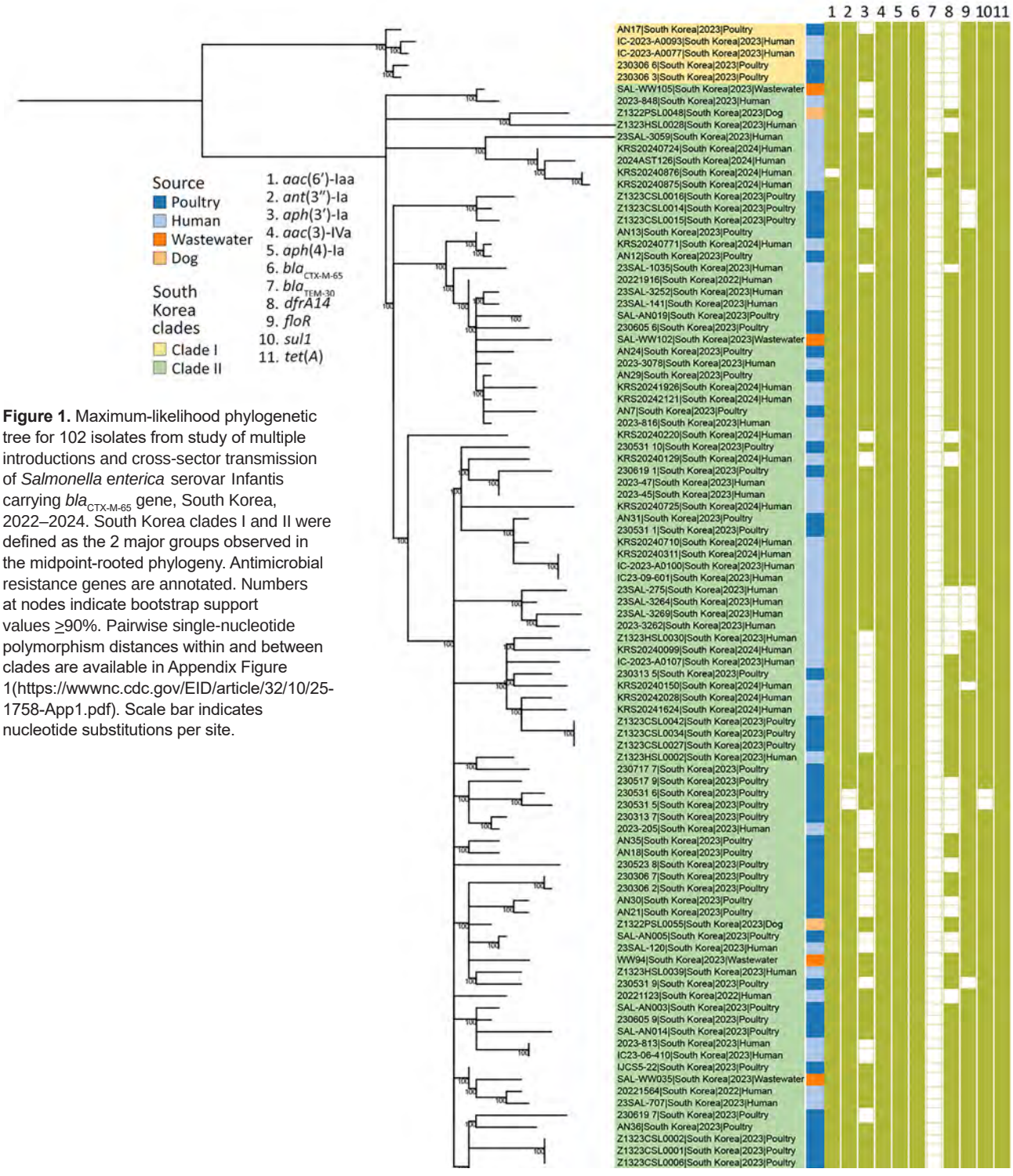

Figure 1. Maximum-likelihood phylogenetic tree for 102 isolates from study of multiple introductions and cross-sector transmission of *Salmonella enterica* serovar Infantis carrying *bla*$_{CTX-M-65}$ gene, South Korea, 2022–2024. South Korea clades I and II were defined as the 2 major groups observed in the midpoint-rooted phylogeny. Antimicrobial resistance genes are annotated. Numbers at nodes indicate bootstrap support values ≥90%. Pairwise single-nucleotide polymorphism distances within and between clades are available in Appendix Figure 1(https://wwwnc.cdc.gov/EID/article/32/10/25-1758-App1.pdf). Scale bar indicates nucleotide substitutions per site.

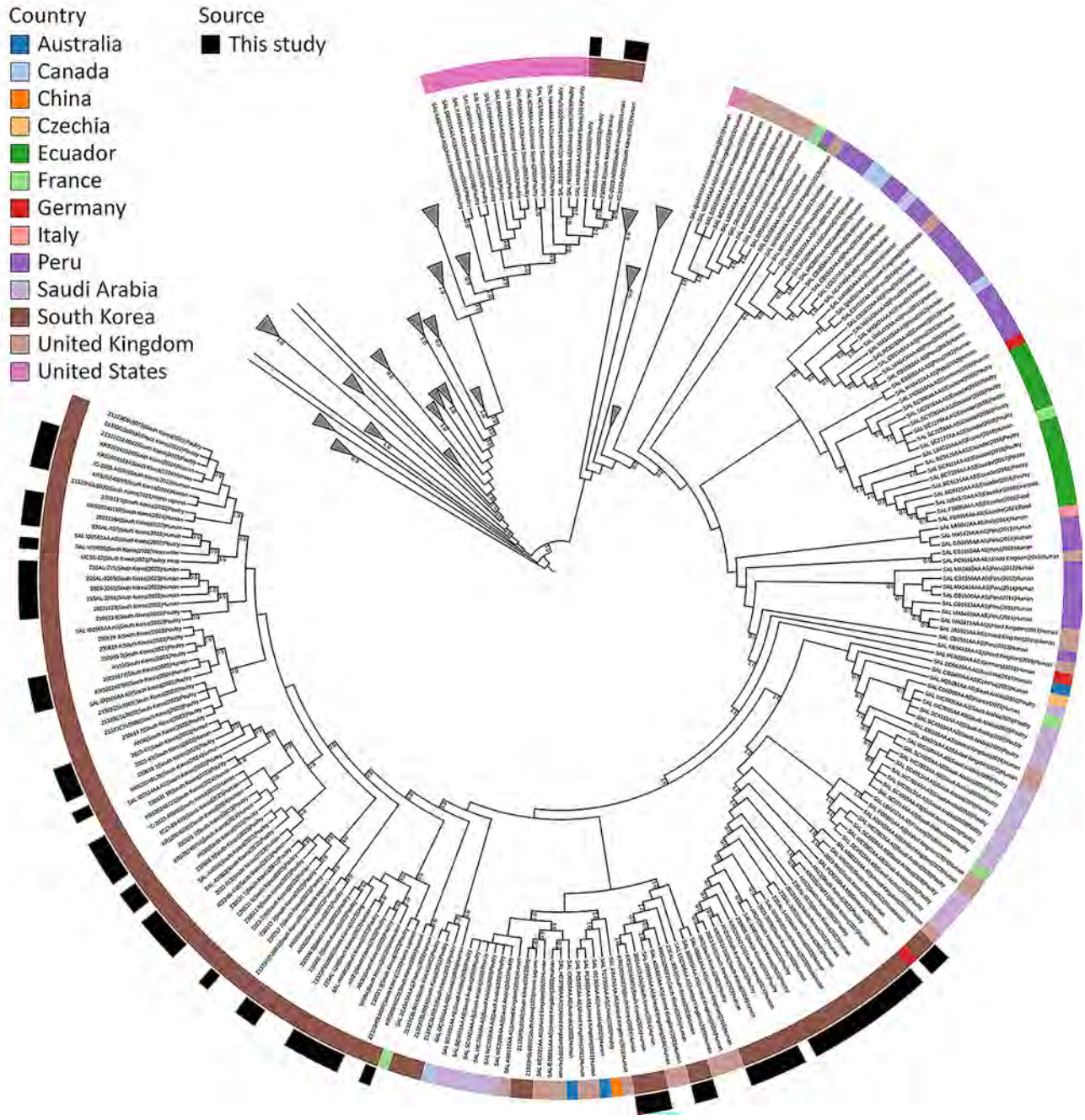

Figure 2. Global phylogenetic placement of isolates from study of multiple introductions and cross-sector transmission of *Salmonella enterica* serovar Infantis carrying $bla_{\text{CTX-M-65}}$ gene, South Korea, 2022–2024. The cladogram was inferred from the global whole-genome single-nucleotide polymorphism dataset, and branches without South Korea isolates were collapsed for clarity. The inner ring denotes country of origin, and the outer ring denotes isolates sequenced in this study. Numbers at nodes indicate FastTree (*23*) support values ≥0.9.

posterior probability 0.994; transition rate 3.853 [95% HPD 2–5]). The generalized linear model analysis indicated minimal sampling bias because effects of source and sink sample sizes were negligible (source indicator 3.185×10^{-3}; source coefficient -1.77×10^{-3}; sink indicator 1.148×10^{-3}; and sink coefficient -7.949×10^{-3}).

Discussion

This study provides a comprehensive genomic analysis of $bla_{\text{CTX-M-65}}$–positive *Salmonella* Infantis in South Korea, revealing its recent emergence, genetic characteristics, and potential transmission routes. Our findings indicate close phylogenetic relatedness among isolates from humans, poultry, and waste-

water, consistent with intersectoral circulation of closely related lineages.

Among the 65 $bla_{CTX-M-65}$–positive *Salmonella* Infantis isolates, all exhibited resistance to multiple antimicrobial classes, including β-lactams, quinolones, tetracyclines, amphenicols, and folate pathway inhibitors. National surveillance conducted during 2016–2017 reported no MDR *Salmonella* Infantis isolates (*31*). Likewise, a regional surveillance study conducted in Seoul during 2020–2022 identified no MDR *Salmonella* Infantis isolates (*32*). Together, those findings highlight the recent emergence and dissemination of MDR *Salmonella* Infantis in South Korea, consistent with detection of ESBL-producing *Salmonella* Infantis carrying pESI-like plasmids in poultry in South Korea in 2021 and 2022 (*10*). The pESI-like plasmid might enhance stress tolerance and persistence, conferring an advantage to this clone over non-MDR strains.

The $bla_{CTX-M-65}$–positive *Salmonella* Infantis isolates in this study carried a conserved resistance gene repertoire, with frequent additional determinants for aminoglycosides, tetracyclines, phenicols, sulfonamides, and trimethoprim. Similar multidrug-resistance repertoires have been reported in *Salmonella* Infantis lineages from multiple geographic settings, including lineages associated with pESI-like plasmids (*33*). Such a stable yet adaptable genetic background likely supports the long-term persistence and ecologic success of *Salmonella* Infantis across hosts.

The close genetic relatedness of wastewater isolates to human and poultry isolates suggests that closely related strains were in all sectors. However, the limited number of wastewater isolates warrants cautious interpretation regarding the role of wastewater as an environmental reservoir. Consistent with recent evidence of global cross-sector clustering (*4*,*34*), those findings underscore the interconnectedness of

Figure 3. Bayesian phylogenetic tree from study of multiple introductions and cross-sector transmission of *Salmonella enterica* serovar Infantis carrying $bla_{CTX-M-65}$ gene, South Korea, 2022–2024. The geographic origin was treated as a discrete trait in the analysis. Branches are colored according to geographic origin. Branches without South Korea isolates were collapsed for clarity. South Korea clusters supported by a posterior probability of 1 were also collapsed to improve readability. Asterisks indicate clusters with posterior probability of 1. South Korea clusters are highlighted in color, with the inferred median MRCA age for South Korea isolates along with the 95% HPD interval. The full phylogeny is available in Appendix Figure 2 (https://wwwnc.cdc.gov/EID/article/32/10/25-1758-App1.pdf). HPD, highest posterior density; MRCA, most recent common ancestor.

human, animal, and environmental reservoirs. Integrating genomic characterization into surveillance frameworks could improve tracking of $bla_{CTX\text{-}M\text{-}65}$–positive *Salmonella* Infantis across sectors.

Globally, emergent *Salmonella* Infantis carrying pESI-like plasmids has been shown to form geographically structured lineages, with different subpopulations associated with distinct ESBL-gene variants, including $bla_{CTX\text{-}M\text{-}1}$ and $bla_{CTX\text{-}M\text{-}65}$ (*35*). All isolates from South Korea in this study belonged to ST32, supporting the emergence of a $bla_{CTX\text{-}M\text{-}65}$–positive ST32 lineage in South Korea. Distinct pESI-like multidrug-resistant lineages, including ST2283, have been reported in other geographic settings, supporting the broader international diversity of pESI-like *Salmonella* Infantis (*4*). Our phylogeographic analysis suggested more recent introduction of $bla_{CTX\text{-}M\text{-}65}$–positive *Salmonella* Infantis into South Korea during 2018–2022, comprising 4 potential introduction events: 1 from the United States (clade I) and 3 from the United Kingdom (clade II, supported by Bayesian discrete trait analysis with a transition rate of 3.853). That finding raises the possibility that importation of grandparent and parent stock poultry from those countries could represent an introduction route, consistent with previous reports linking the poultry trade to the spread of $bla_{CTX\text{-}M\text{-}65}$–positive *Salmonella* in Taiwan and North America (*36*,*37*). Such introductions are consistent with a possible role for global trade in the transboundary spread of high-risk MDR clones (*38*), and parallel the recent emergence of a distinct *Salmonella* Enteritidis lineage in South Korea (*39*), which also might have been influenced by international transmission. During 2015–2023, South Korea imported ≈165,000 live chickens annually from the United States (≈$6.81 million US) and ≈93,000 from the United Kingdom (≈$3.26 million US) (*40*). Those findings support the integration of genomic characterization into existing surveillance frameworks in South Korea, including EnterNet Korea, PulseNet Korea, the wastewater-based infectious disease surveillance program, and poultry-associated foodborne pathogen monitoring programs. Such integration could enhance the early detection of emerging multidrug-resistant *Salmonella* Infantis lineages, strengthen source-attributed public health risk assessment, and support risk-based monitoring in poultry production and import settings.

The first limitation of our study is that direct epidemiologic links between human and poultry cases were not available; therefore, genomic clustering across sectors should not be interpreted as evidence of direct transmission or transmission directionality. Second, although phylogeographic analysis suggested potential international introductions, definitive source attribution and specific introduction routes could not be determined because of uneven global sampling, the availability of reference genomes in EnteroBase, and limited epidemiologic metadata. In addition, source-specific contextual information for some wastewater and poultry isolates was limited, few wastewater isolates were available, and import-lineage information was unavailable for the poultry isolates, limiting further epidemiologic interpretation. Third, long-read sequencing was performed only for selected representative isolates; consequently, plasmid structural diversity and transferability across the full collection could not be comprehensively assessed. Future studies comparing pESI-like plasmids across diverse *Salmonella* Infantis clades will be essential to clarify plasmid evolution, structural variation, and their roles in AMR, virulence, and host adaptation. Continued genomic surveillance and strengthened biosecurity could help improve early detection and risk assessment for further dissemination of multidrug-resistant *Salmonella* Infantis.

In conclusion, our genomic analysis suggests that $bla_{CTX\text{-}M\text{-}65}$–positive *Salmonella Infantis* was introduced into South Korea on multiple occasions since 2018 and that isolates from poultry, wastewater, and humans showed close phylogenetic relatedness. Those findings are consistent with the emergence and intersectoral circulation of closely related multidrug-resistant lineages in South Korea and highlight the value of continued genomic surveillance across sectors.

Paired-end reads of the *Salmonella* Infantis isolates in this study were deposited at the National Center for Biotechnology Information under BioProject accession no. PRJNA1321976.

This research was supported by the KU Research Professor Program of Konkuk University. This work was supported by a grant from the Korea Disease Control and Prevention Agency (grant no. 6331-301-210).

About the Authors

Dr. Shin is a staff scientist at the Division of Bacterial Diseases, Korea Disease Control and Prevention Agency, Cheongju, South Korea, and is a manager of PulseNet Korea System. Her research focuses on molecular epidemiology and foodborne bacterial pathogens. Dr. La is a postdoctoral researcher at the College of Veterinary Medicine, Konkuk University, Seoul, South Korea. His research focuses on molecular epidemiology and pathobiology of bacterial pathogens.

References

1. European Food Safety Authority (EFSA); European Centre for Disease Prevention and Control (ECDC). The European Union One Health 2022 zoonoses report. EFSA J. 2023;21:e8442. https://doi.org/10.2903/j.efsa.2023.8442
2. Hendriksen RS, Vieira AR, Karlsmose S, Lo Fo Wong DM, Jensen AB, Wegener HC, et al. Global monitoring of *Salmonella* serovar distribution from the World Health Organization Global Foodborne Infections Network Country Data Bank: results of quality assured laboratories from 2001 to 2007. Foodborne Pathog Dis. 2011;8:887–900. https://doi.org/10.1089/fpd.2010.0787
3. Georganas A, Graziosi G, Catelli E, Lupini C. *Salmonella enterica* serovar Infantis in broiler chickens: a systematic review and meta-analysis. Animals (Basel). 2024;14:3453. https://doi.org/10.3390/ani14233453
4. Mattock J, Chattaway MA, Hartman H, Dallman TJ, Smith AM, Keddy K, et al. A One Health perspective on *Salmonella enterica* serovar Infantis, an emerging human multidrug-resistant pathogen. Emerg Infect Dis. 2024;30:701–10. https://doi.org/10.3201/eid3004.231031
5. Aviv G, Tsyba K, Steck N, Salmon-Divon M, Cornelius A, Rahav G, et al. A unique megaplasmid contributes to stress tolerance and pathogenicity of an emergent *Salmonella enterica* serovar Infantis strain. Environ Microbiol. 2014;16:977–94. https://doi.org/10.1111/1462-2920.12351
6. Granda A, Riveros M, Martínez-Puchol S, Ocampo K, Laureano-Adame L, Corujo A, et al. Presence of extended-spectrum β-lactamase, CTX-M-65 in *Salmonella enterica* serovar Infantis isolated from children with diarrhea in Lima, Peru. J Pediatr Infect Dis. 2019;14:194–200. https://doi.org/10.1055/s-0039-1685502
7. Tate H, Folster JP, Hsu CH, Chen J, Hoffmann M, Li C, et al. Comparative analysis of extended-spectrum-β-lactamase CTX-M-65–producing *Salmonella enterica* serovar Infantis isolates from humans, food animals, and retail chickens in the United States. Antimicrob Agents Chemother. 2017;61:e00488-17. https://doi.org/10.1128/aac.00488-17
8. Piña-Iturbe A, Díaz-Gavidia C, Álvarez FP, Barron-Montenegro R, Álvarez-Espejo DM, García P, et al. Genomic characterisation of the population structure and antibiotic resistance of *Salmonella enterica* serovar Infantis in Chile, 2009–2022. Lancet Reg Health Am. 2024;32:100711. https://doi.org/10.1016/j.lana.2024.100711
9. Jeong HJ, Shin E, Kim J, Yoo J. Trends in the serotype distribution of *Salmonella enterica* isolated from patients with diarrhea in the Republic of Korea from 2022 to 2024 [in Korean]. Jugan Geongang Gwa Jilbyeong. 2025;18:1790–812. https://doi.org/10.56786/PHWR.2025.18.45.2
10. Jeong J, Chae M, Kang MS, Lee JY, Kwon YK, Lee HJ, et al. Emergence and characteristics of multidrug-resistant *Salmonella enterica* subspecies enterica serovar Infantis harboring the pESI plasmid in chicken slaughterhouses in South Korea. Microbiol Spectr. 2025;13:e0295524. https://doi.org/10.1128/spectrum.02955-24
11. Kim Y, Cho H, Lee M, Jung SH, Chung YJ, Ko KS, et al. Molecular epidemiology of pESI-carrying *Salmonella* Infantis in Korea: insights from a one health framework. Emerg Microbes Infect. 2025;14:2565389. https://doi.org/10.1080/22221751.2025.2565389
12. Clinical and Laboratory Standards Institute. Performance standards for antimicrobial susceptibility testing; twenty-ninth informational supplement (M100-S29). Wayne (PA): The Institute; 2019.
13. Bolger AM, Lohse M, Usadel B. Trimmomatic: a flexible trimmer for Illumina sequence data. Bioinformatics. 2014;30:2114–20. https://doi.org/10.1093/bioinformatics/btu170
14. Bankevich A, Nurk S, Antipov D, Gurevich AA, Dvorkin M, Kulikov AS, et al. SPAdes: a new genome assembly algorithm and its applications to single-cell sequencing. J Comput Biol. 2012;19:455–77. https://doi.org/10.1089/cmb.2012.0021
15. Zankari E, Hasman H, Cosentino S, Vestergaard M, Rasmussen S, Lund O, et al. Identification of acquired antimicrobial resistance genes. J Antimicrob Chemother. 2012;67:2640–4. https://doi.org/10.1093/jac/dks261
16. Wick RR, Howden BP, Stinear TP. Autocycler: long-read consensus assembly for bacterial genomes. Bioinformatics. 2025;41:btaf474. https://doi.org/10.1093/bioinformatics/btaf474
17. Wick RR, Judd LM, Gorrie CL, Holt KE. Unicycler: Resolving bacterial genome assemblies from short and long sequencing reads. PLoS Comput Biol. 2017;13:e1005595. https://doi.org/10.1371/journal.pcbi.1005595
18. La TM, Kim T, Lee SW, Hyeon JY. Complete genome sequences and structural variants of pESI-like plasmids in multidrug-resistant Salmonella Infantis carrying $bla_{CTX-M-65}$ from retail chicken meat in South Korea. J Glob Antimicrob Resist. 2026;47:38–40. https://doi.org/10.1016/j.jgar.2026.01.005
19. Wishart DS, Han S, Saha S, Oler E, Peters H, Grant JR, et al. PHASTEST: faster than PHASTER, better than PHAST. Nucleic Acids Res. 2023;51:W443–50. https://doi.org/10.1093/nar/gkad382
20. Marçais G, Delcher AL, Phillippy AM, Coston R, Salzberg SL, Zimin A. MUMmer4: A fast and versatile genome alignment system. PLoS Comput Biol. 2018;14:e1005944. https://doi.org/10.1371/journal.pcbi.1005944
21. Croucher NJ, Page AJ, Connor TR, Delaney AJ, Keane JA, Bentley SD, et al. Rapid phylogenetic analysis of large samples of recombinant bacterial whole genome sequences using Gubbins. Nucleic Acids Res. 2015;43:e15. https://doi.org/10.1093/nar/gku1196
22. Nguyen LT, Schmidt HA, von Haeseler A, Minh BQ. IQ-TREE: a fast and effective stochastic algorithm for estimating maximum-likelihood phylogenies. Mol Biol Evol. 2015;32:268–74. https://doi.org/10.1093/molbev/msu300
23. Price MN, Dehal PS, Arkin AP. FastTree 2—approximately maximum-likelihood trees for large alignments. PLoS One. 2010;5:e9490. https://doi.org/10.1371/journal.pone.0009490
24. Rambaut A, Lam TT, Max Carvalho L, Pybus OG. Exploring the temporal structure of heterochronous sequences using TempEst (formerly Path-O-Gen). Virus Evol. 2016;2:vew007. https://doi.org/10.1093/ve/vew007
25. Suchard MA, Lemey P, Baele G, Ayres DL, Drummond AJ, Rambaut A. Bayesian phylogenetic and phylodynamic data integration using BEAST 1.10. Virus Evol. 2018;4:vey016. https://doi.org/10.1093/ve/vey016
26. Darriba D, Posada D, Kozlov AM, Stamatakis A, Morel B, Flouri T. ModelTest-NG: a new and scalable tool for the selection of DNA and protein evolutionary models. Mol Biol Evol. 2020;37:291–4. https://doi.org/10.1093/molbev/msz189
27. Xie W, Lewis PO, Fan Y, Kuo L, Chen MH. Improving marginal likelihood estimation for Bayesian phylogenetic model selection. Syst Biol. 2011;60:150–60. https://doi.org/10.1093/sysbio/syq085

28. Bielejec F, Baele G, Vrancken B, Suchard MA, Rambaut A, Lemey P. SpreaD3: interactive visualization of spatiotemporal history and trait evolutionary processes. Mol Biol Evol. 2016;33:2167–9. https://doi.org/10.1093/molbev/msw082
29. Minin VN, Suchard MA. Fast, accurate and simulation-free stochastic mapping. Philos Trans R Soc Lond B Biol Sci. 2008;363:3985–95. https://doi.org/10.1098/rstb.2008.0176
30. García-Soto S, Abdel-Glil MY, Tomaso H, Linde J, Methner U. Emergence of multidrug-resistant *Salmonella enterica* subspecies *enterica* serovar Infantis of multilocus sequence type 2283 in German broiler farms. Front Microbiol. 2020;11:1741. https://doi.org/10.3389/fmicb.2020.01741
31. Kim SH, Sung GH, Park EH, Hwang IY, Kim GR, Song SA, et al. Serotype distribution and antimicrobial resistance of Salmonella isolates in Korea between 2016 and 2017. Ann Lab Med. 2022;42:268–73. https://doi.org/10.3343/alm.2022.42.2.268
32. Jin YH, Yu YA, Song MO, Kwon EY, Kim JK, Suh HS, et al. Serotype distribution and antimicrobial resistance of Salmonella isolates in Seoul, 2020–2022. J Bacteriol Virol. 2023;53:131–40. https://doi.org/10.4167/jbv.2023.53.2.131
33. Alvarez DM, Barrón-Montenegro R, Conejeros J, Rivera D, Undurraga EA, Moreno-Switt AI. A review of the global emergence of multidrug-resistant *Salmonella enterica* subsp. *enterica* serovar Infantis. Int J Food Microbiol. 2023;403:110297. https://doi.org/10.1016/j.ijfoodmicro. 2023.110297
34. Su B, Du G, Hou S, Chen Z, Wu X, He G, et al. Antimicrobial resistance analysis and whole-genome sequencing of *Salmonella* isolates from environmental sewage—Guangzhou City, Guangdong Province, China, 2022–2023. China CDC Wkly. 2024;6:254–60. https://doi.org/10.46234/ccdcw2024.050
35. Piña-Iturbe A, Tichy-Navarro D, Miranda-Riveros J, Navarrete MJ, Moreno-Switt AI. Emergent *Salmonella enterica* serovar Infantis forms a monophyletic lineage shaped by geographic structuring. Int J Food Microbiol. 2026;446:111536. https://doi.org/10.1016/j.ijfoodmicro. 2025.111536
36. Liao YS, Wei HL, Kuo HC, Chen BH, Wang YW, Teng RH, et al. Chromosome-borne CTX-M-65 extended-spectrum β-Lactamase–producing *Salmonella enterica* serovar Infantis, Taiwan. Emerg Infect Dis. 2023;29:1634–7. https://doi.org/10.3201/eid2908.230472
37. Monte DFM, Harrell E, Harden L, Thakur S. Clonal spread of $bla_{\text{CTX-M-65}}$ producing Salmonella enterica serovars detected in poultry retail meat in North Carolina, USA. Sci Rep. 2025;15:26520. https://doi.org/10.1038/s41598-025-02972-2
38. Li S, He Y, Mann DA, Deng X. Global spread of *Salmonella* Enteritidis via centralized sourcing and international trade of poultry breeding stocks. Nat Commun. 2021;12:5109. https://doi.org/10.1038/s41467-021-25319-7
39. Shin E, La TM, Yoo J, Kim J, Hyeon JY. Emergence of distinct *Salmonella enterica* serovar Enteritidis lineage since 2020, South Korea. Emerg Infect Dis. 2025;31:1386–93. https://doi.org/10.3201/eid3107.250043
40. Food and Agriculture Organization of the United Nations. FAOSTAT [cited 2025 May 5]. https://www.fao.org/faostat

Address for correspondence: Ji-Yeon Hyeon, College of Veterinary Medicine, Konkuk University, 120 Neungdong-ro, Gwangjin-gu, Seoul 05029, South Korea; email: sh702@konkuk.ac.kr

Molecular Epidemiology and Evolution of Swine Influenza A Viruses, Vietnam, 2020–2024

Ngoc Anh Bui,[1] Zoe Yi Song,[1] Samuel M.S. Cheng,[1] Duy Tung Dao, Lydia D.J. Chang, Gigi Y.Z. Liu, Quang Huy Nguyen, Thi Hang Dang, Quoc Hung Nguyen, Tom L.Y. Woo, Coco H.C. Chan, Tommy T.Y. Lam, Vuong N. Bui, Malik Peiris

Swine influenza A viruses (IAV-S) caused the 2009 H1N1 pandemic and pose a future zoonotic and pandemic threat. Vietnam represents a critical hotspot for IAV-S emergence within East and Southeast Asia, with dense swine and human populations and intensive livestock trade. We conducted genomic surveillance of IAV-S in Vietnam during 2020–2024, extending previous surveillance from 2013–2019. We identified multiple co-circulating H1 and H3 clades, including pandemic H1N1, Eurasian avian-like, and European lineages, by conducting phylogenetic analysis of 56 IAV-S isolates (21 H1N1, 31 H1N2, and 4 H3N2). Three H1 clades persisted exclusively in Vietnam, circulating up to 12 years. Phylogeographic analysis revealed multiple independent introduction events from North America, Europe, China, Thailand, and Cambodia. We detected extensive reassortment that frequently involved pandemic H1N1 virus internal genes. We identified several lineage-specific mutations associated with mammalian adaptation. Our findings underscore the ongoing IAV-S evolution and need for sustained surveillance in Vietnam.

Swine influenza A viruses (IAV-S) contribute to zoonotic and pandemic risk because of their genetic diversity, rapid evolution, and interspecies transmission (*1*). Swine are evolutionary intermediaries, enabling reassortment between avian, human, and endemic swine influenza viruses and generating genotypes with pandemic potential (*2*). Circulation in swine might also enable the adaptation of avian virus hemagglutinins to bind to α2,6-linked sialic acids receptors found in the mammalian upper respiratory tract. This unique role was dramatically illustrated by the 2009 H1N1 pandemic, caused by a reassortant swine virus containing gene segments from classical swine, Eurasian avian-like swine, and human seasonal virus lineages (*3*).

Globally, influenza A virus subtypes H1N1, H1N2, and H3N2 are endemic in swine populations, displaying extensive genetic and antigenic diversity across different geographic regions. A phylogenetic nomenclature system for IAV-S defines 3 lineages for IAV-S H1, the classical swine lineage (1A, including the 2009 H1N1 pandemic virus [pH1N1]), the pre-2009 human seasonal lineage (1B), and the Eurasian avian-like lineage (1C). IAV-S H3N2 are defined by the introduction from human seasonal virus and circulation decade (1970, 1990, 2000, and 2010) (*4*). The evolutionary dynamics of IAV-Ss are influenced by multiple human seasonal influenza spillovers into swine, followed by sustained within-host transmission and rapid adaptation (*5*). The diversification of IAV-Ss is amplified by the intensive global swine production and international trade, which enables the movement of live swine and viruses across continents, heightening the risk for zoonotic emergence (*6*).

East and Southeast Asia is a critical hotspot for the emergence and evolution of IAV-Ss. High, dense human and swine populations with poultry production, including live-bird markets, enabled frequent reassortment and interspecies transmission in the region (*7*). Vietnam is the second largest swine producer in Asia other than China (https://www.fas.usda.gov/data/production/0113000). Longitudinal IAV-S surveillance was initiated in 2013 at the Van Phuc slaughterhouse in Hanoi, Vietnam, which sources pigs from 23 provinces across the country (*8*). Surveillance data from 2013–2019 revealed the co-circulation of diverse H1N1, H1N2, and H3N2 subtypes and demonstrated

Author affiliations: Vietnam Institute of Animal and Veterinary Science, Hanoi, Vietnam (N.A. Bui, D.T. Dao, Quang H. Nguyen, T.H. Dang, Quoc H. Nguyen, V.N. Bui); The University of Hong Kong, Hong Kong, China (Z.Y. Song, S.M.S. Cheng, L.D.J Chang, G.Y.Z. Liu, T.L.Y. Woo, C.H.C. Chan, T.T.Y. Lam, M. Peiris).

DOI: https://doi.org/10.3201/eid3210.260593

[1]These first authors contributed equally to this article.

the persistence of swine-origin H1N2 and H3N2 viruses, likely introduced by the swine trade from other Asian countries and North America. The mix of the viruses was shaped by repeated reverse zoonotic introductions of human-origin pH1N1 viruses and extensive reassortment events, with H1N2 and H3N2 genotypes frequently incorporating pH1N1 internal gene segments (*9*). Strengthened surveillance and molecular characterization of those viruses in Vietnam are crucial for timely risk assessment and regional preparedness. We report findings from Van Phuc slaughterhouse surveillance during 2020–2024.

Methods

Sample Collection

During October 2020–April 2024, we collected nasal swab specimens monthly at Van Phuc slaughterhouse, the main centralized swine slaughterhouse in Hanoi, Vietnam. Multiple trucks transport pigs to the abattoir from farms, primarily from North Vietnam. The pigs on each truck might originate from a single farm or be consolidated from several farms within the same region. Upon arrival in the abattoir, the pigs are distributed into multiple holding pens, each assigned to a specific slaughterer. All pigs within the pens were slaughtered on the same day, but a small residual number might be carried over to the next day, potentially mixing with newly arrived pigs. Our sampling team was divided to 3–4 groups and each group collect samples randomly from pigs in ≥1 pens. We collected swabs and serum samples immediately after slaughter. Pigs sampled at the facility were 4–6 months of age. On the basis of the reported origin at slaughter, 64.3% of pigs originated from the Red River Delta, 21.3% from Northern midland and mountain provinces, 13.7% from the North Central Coast, 0.5% from the Central Highlands, and 0.2% from the South-East region of Vietnam. We inserted sterile dry swabs (Copan, https://www.copanusa.com) ≈10 cm into the nasal cavity and then placed the swabs into tubes containing 1 mL viral transport medium supplemented with antimicrobial drugs and bovine serum albumin (Thermo Fisher Scientific, https://www.thermofisher.com). We transported specimens to the National Institute of Veterinary Research (Hanoi, Vietnam) in an icebox and stored at 4°C upon arrival. We initiated virus isolation on the day of collection by inoculating viral transport medium onto MDCK cells (*9*).

Virus Isolation

We cultured MDCK cells in DMEM (Thermo Fisher Scientific) with 20 mM HEPES (Thermo Fisher Scientific) and 5% fetal bovine serum (Thermo Fisher Scientific) on 24-well cell-culture plates (TPP, https://www.tpp.ch) to confluency. We then removed all culture medium, washed the cells, and replaced the medium with DMEM with 20 mM HEPES and 2 μg/mL L-1 tosylamido-2-phenylethyl chloromethyl ketone treated trypsin. After inoculation, we incubated the cultures at 37°C; we replaced the medium with fresh culture medium the next day. We monitored the cultures for cytopathic effect at 3–4 days postinoculation and harvested supernatants for hemagglutination testing. When we detected cytopathic effect or hemagglutination, we performed a second passage. We screened putative influenza A–positive cultures by using a rapid antigen detection assay (Standard Q Influenza A&B Test; SD BIOSENSOR, https://www.sdbiosensor.com). We stored confirmed virus isolates at −80°C until shipment to the University of Hong Kong (Hong Kong, China) on dry ice.

Whole-genome Sequencing and Assembly

We extracted viral RNA from MDCK culture isolates by using the QIAamp Viral RNA Mini Kit (QIAGEN, https://www.qiagen.com), according to the manufacturer's instructions. We synthesized complementary DNA by using SuperScript IV reverse transcriptase (Invitrogen, https://www.invitrogen.com). We performed full-length amplification of all 8 influenza A virus gene segments by using an in-house universal multisegment reverse transcription PCR primer set and the TaKaRa LA Taq Hot Start Version kit (Takara Bio, https://www.takarabio.com) (*9*). We purified amplicons by using the QIAquick PCR Purification Kit (QIAGEN). We used purified PCR products for next-generation sequencing library preparation with Illumina DNA Prep (Illumina, https://www.illumina.com), and sequenced libraries on the iSeq 100 System (Illumina). We assembled sequence reads by using the US Centers for Disease Control and Prevention MIRA pipeline (https://github.com/CDCgov/MIRA-NF).

Phylogenetic Analysis

We sourced influenza A virus whole-genome sequences and associated metadata from the GISAID (http://www.gisaid.org) and National Center for Biotechnology Information databases (accessed February 1, 2025). To maintain computational feasibility for phylogenetic analysis, we randomly subsampled human seasonal influenza (H3N2 and H1N1) to 1% of the available data. We then curated the dataset by removing laboratory-derived strains, those of unknown subtype, and duplicate entries identified by strain name. We aligned individual gene segments separately by using MAFFT

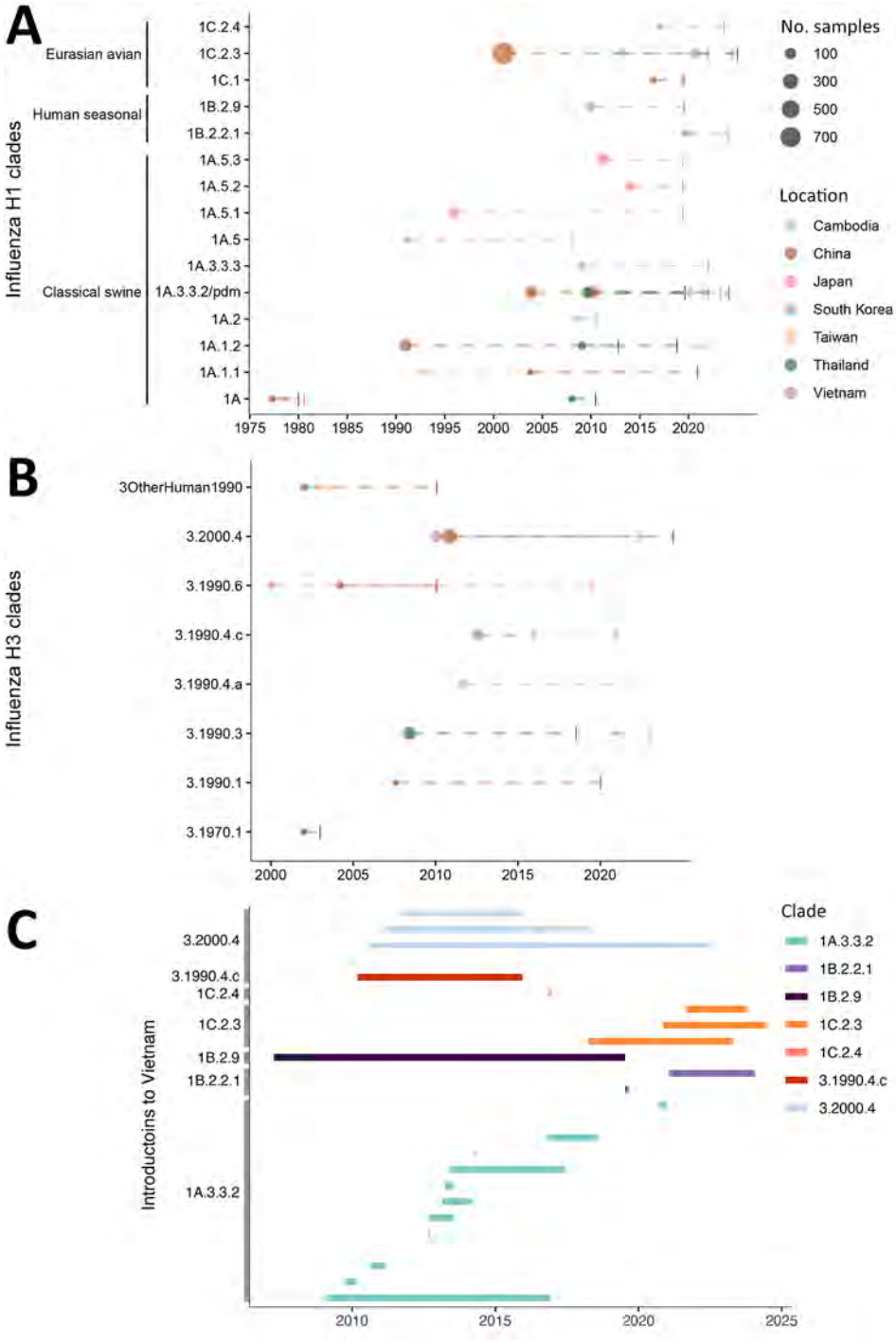

Figure 1. Duration of swine influenza clades circulated in Asia for H1 (A) and H3 (B) and clusters of each clade introduced into Vietnam (C) as part of study of molecular epidemiology and evolution of swine influenza A viruses, Vietnam, 2020–2024. In panels A and B, the dots indicate the sampling dates of the earliest viruses of each clade displayed, the vertical bars are the times of the latest samples, and the size of the dots represents the total number of samples of the clade in that location. In panel C, each bar starts from the time of the most recent common ancestor and the sampling time of the latest virus of each clade.

version 7.490 (*10*). We inferred maximum-likelihood phylogenies for each gene segment by using IQ-TREE version 2.2.2.6 (https://iqtree.github.io) under the general time reversible plus empirical frequencies plus free rate 4 model (*11*). We assessed branch support with 1,000 Shimodaira-Hasegawa–like approximate likelihood-ratio test replicates (*12*). We reconstructed a time-scaled phylogeny by using TreeTime version 0.11.2 (*13*). We identified clades for H1 and H3 according to the global IAV-S nomenclature system (*4,14*). We reconstructed ancestral states representing viral clades on the phylogeny by using PASTML version 1.9.42 with the DELTRAN (delayed transformation) algorithm (*15*). We identified reassortment events as internal nodes where the inferred clade state changed between ancestral and descendant nodes.

Results

Persistence of Clades in Vietnam

Phylogenetic analysis identified 3 H1 clades, 1B.2.2.1, 1B.2.9, and 1C.2.4, that were detected persistently only in Vietnam among all monitored Asia countries (Figure 1). In contrast, the Eurasian avian-like clade 1C.2.3 was first introduced into China before subsequently spreading to South Korea and Vietnam. For H3 viruses, the circulation of clades 3.2000.4 and 3.1990.4.c in Vietnam occurred contemporaneously with clade detection in China and South Korea, whereas the introduction of clade 3.1990.3 into Vietnam came after its initial establishment in Thailand. That pattern highlights Vietnam's role as both a recipient and a source within the regional network of IAV-S transmission.

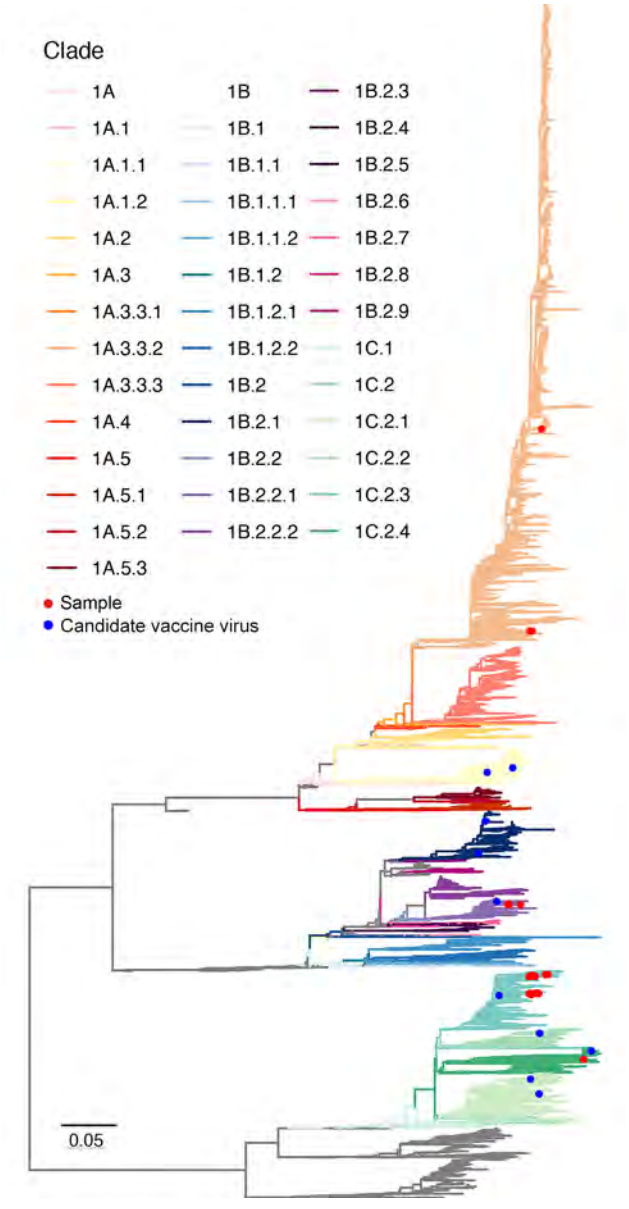

Figure 2. Maximum-likelihood tree of influenza A virus H1 gene from study of molecular epidemiology and evolution of swine influenza A viruses, Vietnam, 2020–2024. Branches are colored by clades. Scale bar represents the number of nucleotide substitutions per site.

Introduction and Reassortment of IAV-S in Vietnam

Our surveillance uncovered multiple lineages co-circulating in Vietnam during 2020–2024. We detected 21 H1N1 and 31 H1N2 isolates from clades 1A.3.3.2/pdm, 1B.2.2.1, and 1C.2.4 and 4 H3N2 isolates from clades 3.2000.4 and 3.1990.3 (Figures 2, 3).

Within the Eurasian avian-like lineage, clade 1C.2.3 sequences from Vietnam clustered phylogenetically with isolates from China; however, long branches and major gaps in sampling time indicated periods of unsampled diversity and cryptic local circulation. Two samples from 2021 and 2023 clustered closely with viruses from Vietnam from 2020, providing evidence for the sustained persistence of this specific viral cluster for ≥3 years. The 1C.2.3 viruses exchanged gene segments with co-circulating clades 1A.3.3.2/pdm, 1B.2.9, 1B.2.2.1, and 1C.2.4 (Figure 4). Clade 1C.2.4 viruses in Vietnam originated from sporadic introductions from European swine populations, having acquired internal genes from the 1A.3.3.2/pdm, 1B.2.2.1, and 3.2000.4 lineages (Figure 5).

We detected 3 monophyletic Vietnam 1B clusters. The oldest cluster, circulating during 2010–2019, was not described in the most recent global nomenclature. We therefore refer to it as a proposed new clade, 1B.2.9, pending formal nomenclature review. The other 2 clusters fell into clade 1B.2.2.1, each representing independent introduction events from the United States. The smaller one only included Vietnam viruses from 2019. The more recent cluster exhibited continuous evolutionary progression from 2021–2024, indicating sustained local transmission after initial introduction (Figure 6). We identified no reassortment in clade 1B.2.2.1 genomes. Clade 1A.3.3.2, corresponding to the pH1N1 lineage, showed evidence of constant reverse zoonotic transmissions from humans to swine populations (Figure 7).

H3 clade 3.2000.4 demonstrated sustained persistence in Vietnam, with continuous detection from its initial identification in 2010–2022 (Figure 8). Phylogenetic analysis revealed that the most recent Vietnam isolates clustered with isolates from Cambodia and China, suggesting active cross-border transmission within the East and Southeast Asian region. Clade 3.1990.3 viruses detected in Vietnam clustered most closely with viruses from Thailand and had reassorted with internal genes from clades 1A.1.2 (circulating in

Thailand) and 1A.3.3.2/pdm. The phylogenetic relationships were compatible with ≥2 introductions from Thailand or from an unsampled related source in the region, although sparse regional surveillance limits definitive source attribution (Figure 9). Clade 3.1990.4.c samples were detected during 2012–2015 but absent from recent surveillance samples, suggesting either local extinction or displacement by competing lineages.

Mutations Across Lineages

Analysis of mutation patterns across Vietnam IAV-S lineages revealed lineage-specific adaptive mutations involving polymerase activity, receptor binding, and virulence (Appendix Figure, http://wwwnc.cdc.gov/EID/article/32/10/26-0593-App1.pdf) (*16*,*17*). The K389R substitution in polymerase basic (PB) 2 gene, found in clade 1C.2.3, was acquired from reassortment with 1B.2.2.1. We detected the D701E substitution in 1 H1N2 isolate from 2022. That change affects the same PB2 residue as the well-characterized mammalian-adaptive substitution D701N, but it is a different amino-acid replacement, and its phenotypic effect requires experimental confirmation. K158N in the polymerase acidic gene emerged from the evolution within Vietnam IAV-S in 2023 and sustained in the swine population in 2024. We found H1 Q189E (H3 numbering Q192E) within the Sb antigenic site in a monophyletic IAV-S 1C.2.3 cluster in 2023, which we also found in swine samples from 1A.3.3.2/pdm in 2023. Nonstructural 1 gene mutations N127K and S189G emerged in clade 1C.2.3, resembling the 189G in other human-related swine samples.

Discussion

This analysis extended IAV-S surveillance in Vietnam and revealed evolutionary and epidemiologic patterns characterizing IAV-S in Vietnam. Lineages circulating in Vietnam arose through repeated introductions from various geographic regions, including North America, Europe, and other regions of Asia, likely enabled by international swine trade. Importation of live pigs for breeding stock from Europe and North America does occur. Illegal cross-border pig imports could potentially happen, but there are no data on such movements. Most H1 lineages and H3 clade 3.1990.3 exhibited evidence of multiple independent introduction events, whereas clades 1B.2.9 and 3.2000.4 demonstrated sustained local persistence for 9–12 years after initial introduction. Frequent reassortment occurred among co-circulating lineages, generating extensive genomic diversity through gene segment exchange. We detected frequent genetic mixing between human pH1N1 and endemic swine influenza viruses in reassortant viruses. Those findings collectively demonstrate the complex evolutionary dynamics driving IAV-S diversity in Vietnam, shaped by international virus introductions, local persistence and evolution, interlineage reassortment, and reverse zoonosis from humans.

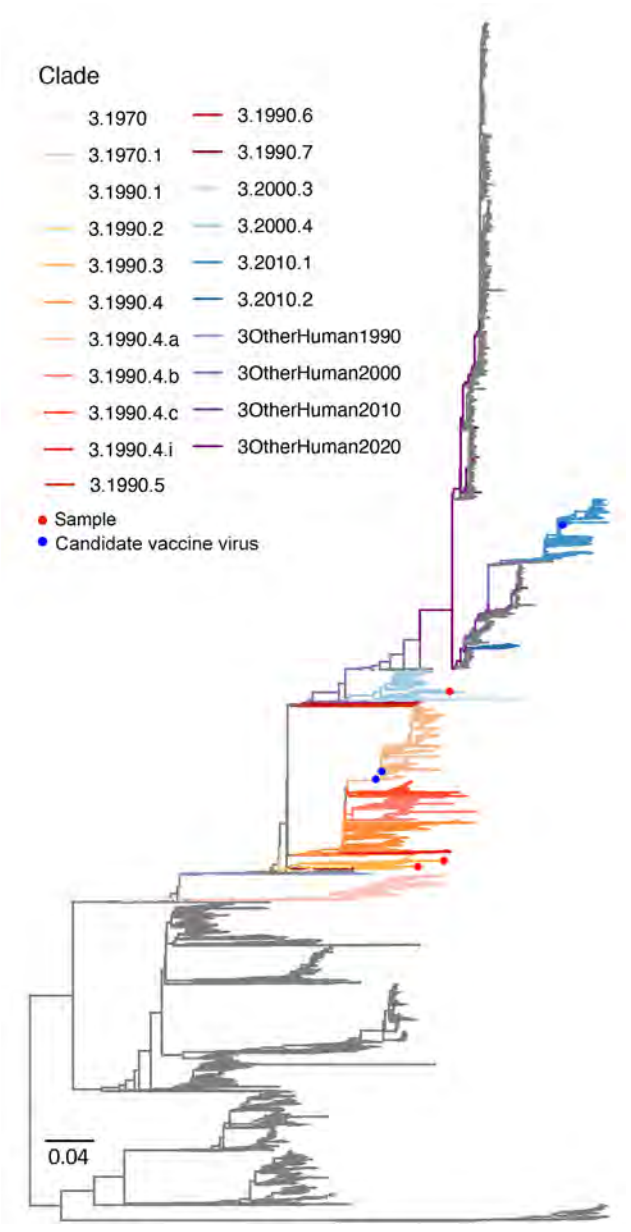

Figure 3. Maximum-likelihood tree of influenza A virus H3 gene from study of molecular epidemiology and evolution of swine influenza A viruses, Vietnam, 2020–2024. Branches are colored by clades. Scale bar represents the number of nucleotide substitutions per site.

Recent surveillance highlights region-specific IAV-S dominance. In North America, IAV-S diversity is driven mainly by clades 1A.3.3.3-c3, 1B.2,

and 3.1990.4.a. In Europe, swine populations show co-circulation of clades 1A.3.3.2/pdm, 1B.1, and 1C, with frequent 1C.2.4 detections. China has sustained prominent 1C.2.3 viruses with pH1N1-derived internal genes (*18*–*20*). Vietnam shares those global patterns through clades 1A.3.3.2/pdm, North America–like 1B.2.2.1, and Eurasian avian-like 1C.2.3 but differs by showing prolonged local persistence of proposed 1B.2.9 and H3 3.2000.4. Vietnam IAV-Ss clustered closely with viruses from China, South Korea, Thailand, and Cambodia, indicating frequent inter-regional transmission within East and Southeast Asia. Phylogeographic analyses have demonstrated that south central China serves as a dominant source of IAV-S dissemination to other regions in China and Southeast Asia, with strong migration pathways extending to northeast China and subsequently to Vietnam (*21*). That spatial diffusion pattern is driven by factors including pig production levels, trade networks, and pork consumption patterns.

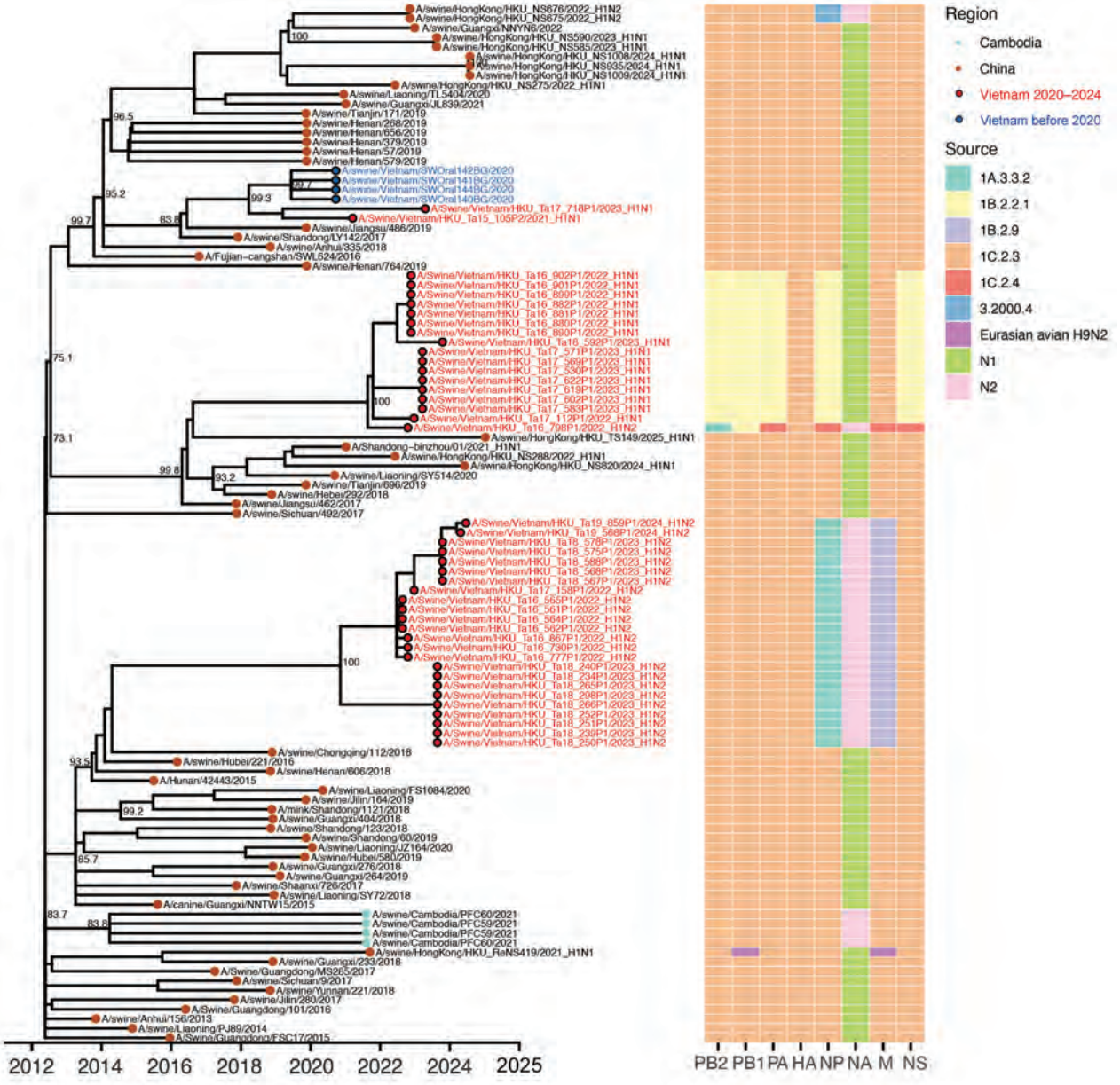

Figure 4. Time-scaled maximum likelihood phylogeny of swine influenza A virus hemagglutinin H1 clade 1C.2.3 from study of molecular epidemiology and evolution of swine influenza A viruses, Vietnam, 2020–2024. The heatmap shows the genetic source of all genes. Dots are colored by geographic regions. Red and blue circled dots and labels show the samples in Vietnam from this study and from previous studies. Shimodaira-Hasegawa–like approximate likelihood ratio test branch support values are labeled on nodes. The horizontal axis represents calendar time.

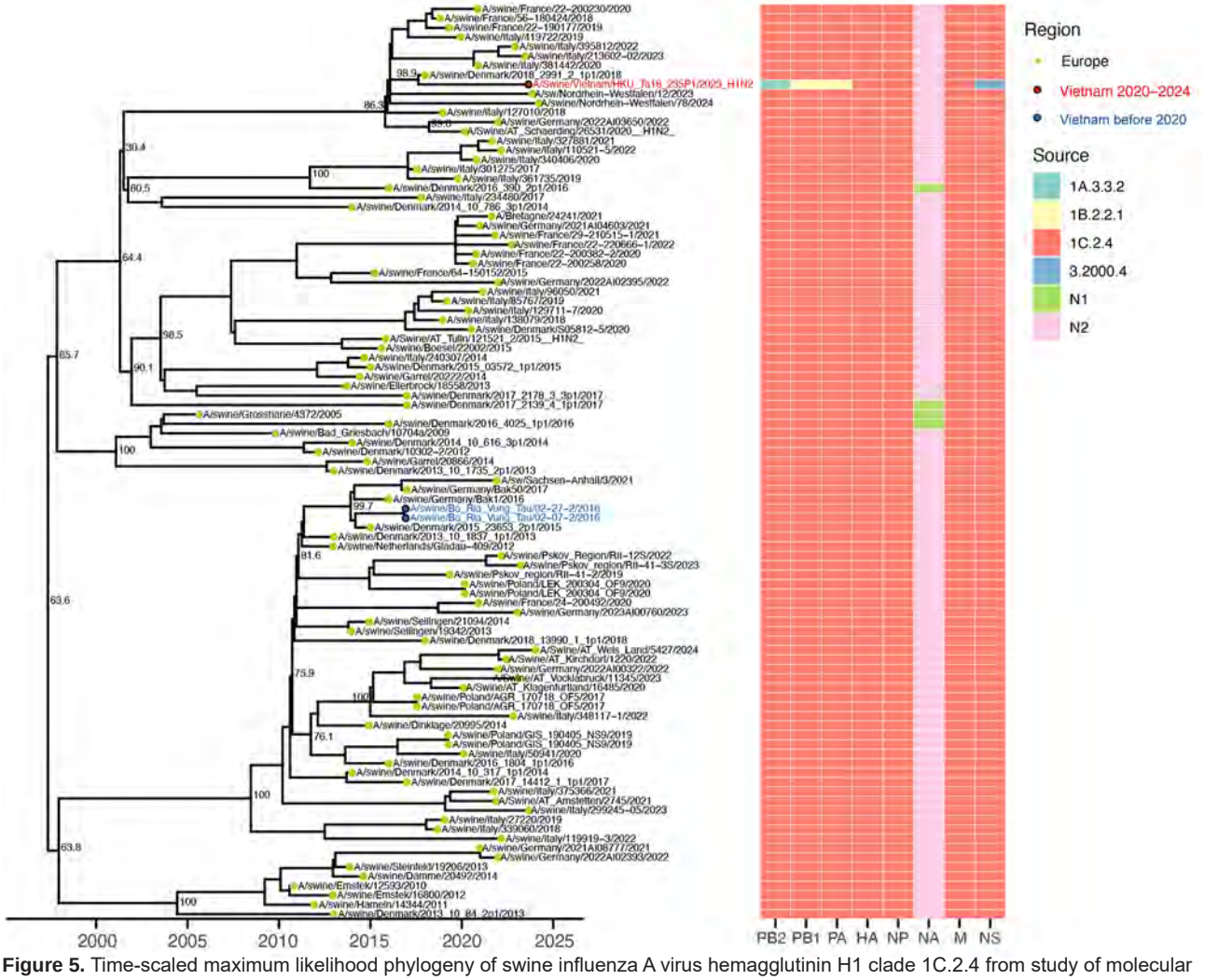

Figure 5. Time-scaled maximum likelihood phylogeny of swine influenza A virus hemagglutinin H1 clade 1C.2.4 from study of molecular epidemiology and evolution of swine influenza A viruses, Vietnam, 2020–2024. The heatmap shows the genetic source of all genes. Dots are colored by geographic regions. Red and blue circled dots and labels show the samples in Vietnam from this study and from previous studies. Shimodaira-Hasegawa–like approximate likelihood ratio test branch support values are labeled on nodes. The horizontal axis represents calendar time.

Livestock movement can act as a catalyst for viral diversification. Pigs are often transported over long distances from farms to central slaughterhouses in Vietnam, a process that involves mixing of animals from different sources. Research from Hong Kong, which imports >90% of its swine from mainland China, has demonstrated that the transport and marketing stages of the supply chain provide a high-risk environment for IAV-S transmission. The force of infection during transport was estimated to be 229%–414% higher per unit time than within farms, enabling cross-infections and potential reassortment among viruses from different geographic origins (*22*).

Reassortments occurred among co-circulating IAV-Ss in Vietnam. pH1N1-derived internal gene segments in IAV-Ss were detected in reassortant H1N2 and H3N2 viruses, reflecting a global phenomenon documented across multiple regions. In the United States, the matrix gene from pH1N1 rapidly replaced triple-reassortant matrix genes (*23*,*24*). Similarly, in Thailand and China, reverse zoonotic transmission of pH1N1 into swine populations generated genetically distinct sublineages with predominantly pH1N1-derived internal genes (*25*–*27*). Introductions of human pH1N1 viruses into swine populations from Vietnam underscored continuous reverse zoonotic transmission at the human-animal interface. This reassortment process drives rapid IAV-S evolution and expansion of genotypic diversity.

Mutations associated with polymerase activity and mammalian adaptation were detected across multiple lineages. The K389R substitution in the PB2 gene, prominently identified in clade 1C.2.3, highly

increased polymerase activity in mammalian cells through enhanced viral transcription and replication (*28*). The D701E substitution, detected exclusively in an H1N2 isolate in 2022, represents a divergent mammalian-adaptive pathway compared with the canonical D701N mutation, which is well-characterized as promoting adaptation to mammalian hosts through enhanced nuclear localization signal exposure and importin-α binding (*29*). The D701E variant suggests alternative adaptive strategies emerging within Vietnam swine populations. Q189E (H3 numbering Q192E) was detected in clade 1C.2.3 and 1A.3.3.2/pdm samples in 2023 in Vietnam. The Q189E located in the Sb antigenic epitope represents antigenic drift driven by immune selection pressures. This mutation parallels substitutions seen in the H1N1 clade 6B.1A.5a and its descendants that were prevalent in the Northern Hemisphere since the 2019–2020 influenza season (*30*). In Vietnam, the World Health Organization (WHO) reported a laboratory-confirmed human infection with

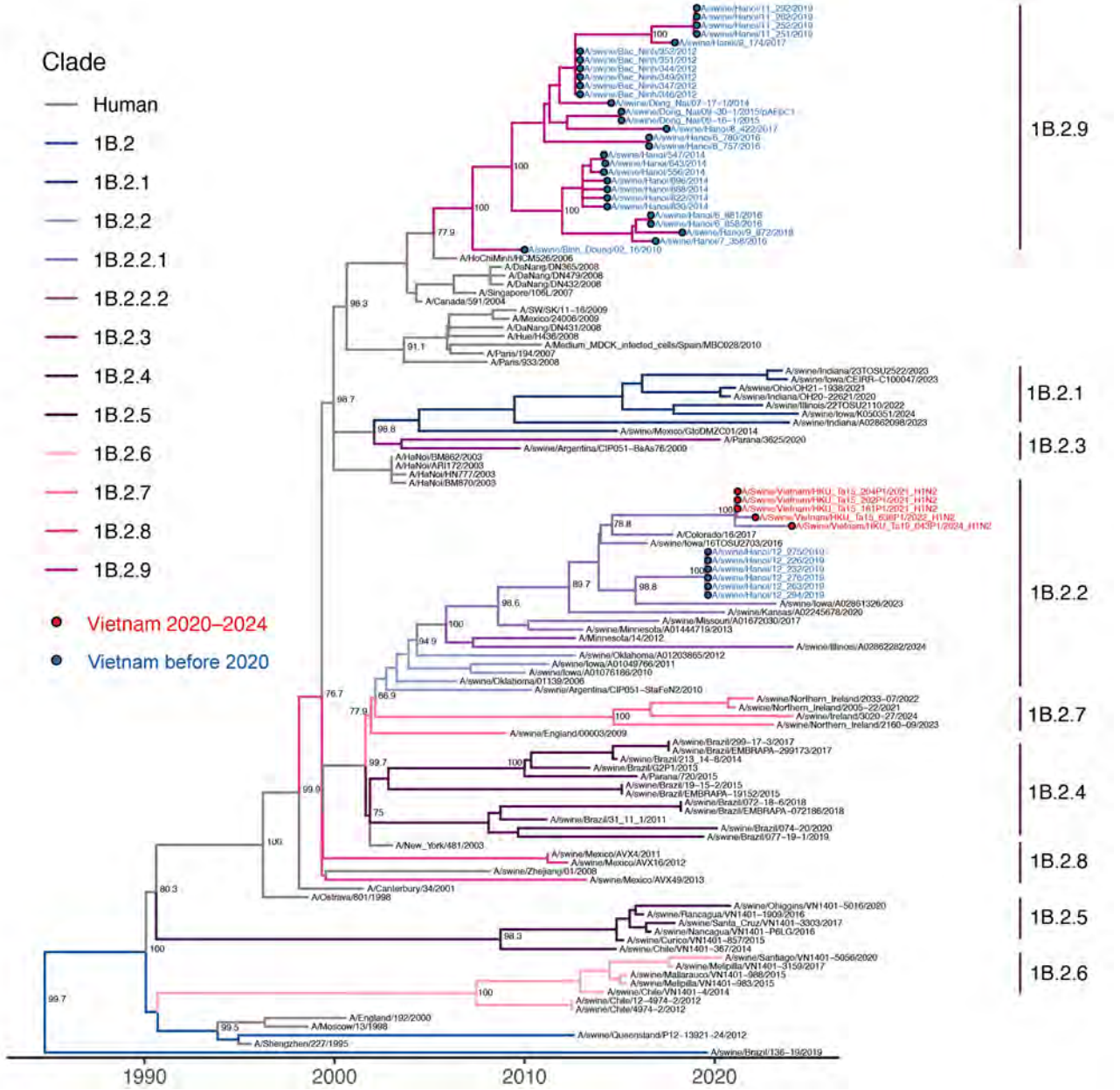

Figure 6. Time-scaled maximum likelihood phylogeny of swine influenza A virus hemagglutinin H1 lineage 1B from study of molecular epidemiology and evolution of swine influenza A viruses, Vietnam, 2020–2024. Branches colored by lineage 1B clades. Red and blue circled dots and labels show the samples in Vietnam from this study and from previous studies. Shimodaira-Hasegawa–like approximate likelihood ratio test branch support values are labeled on nodes. The horizontal axis represents calendar time.

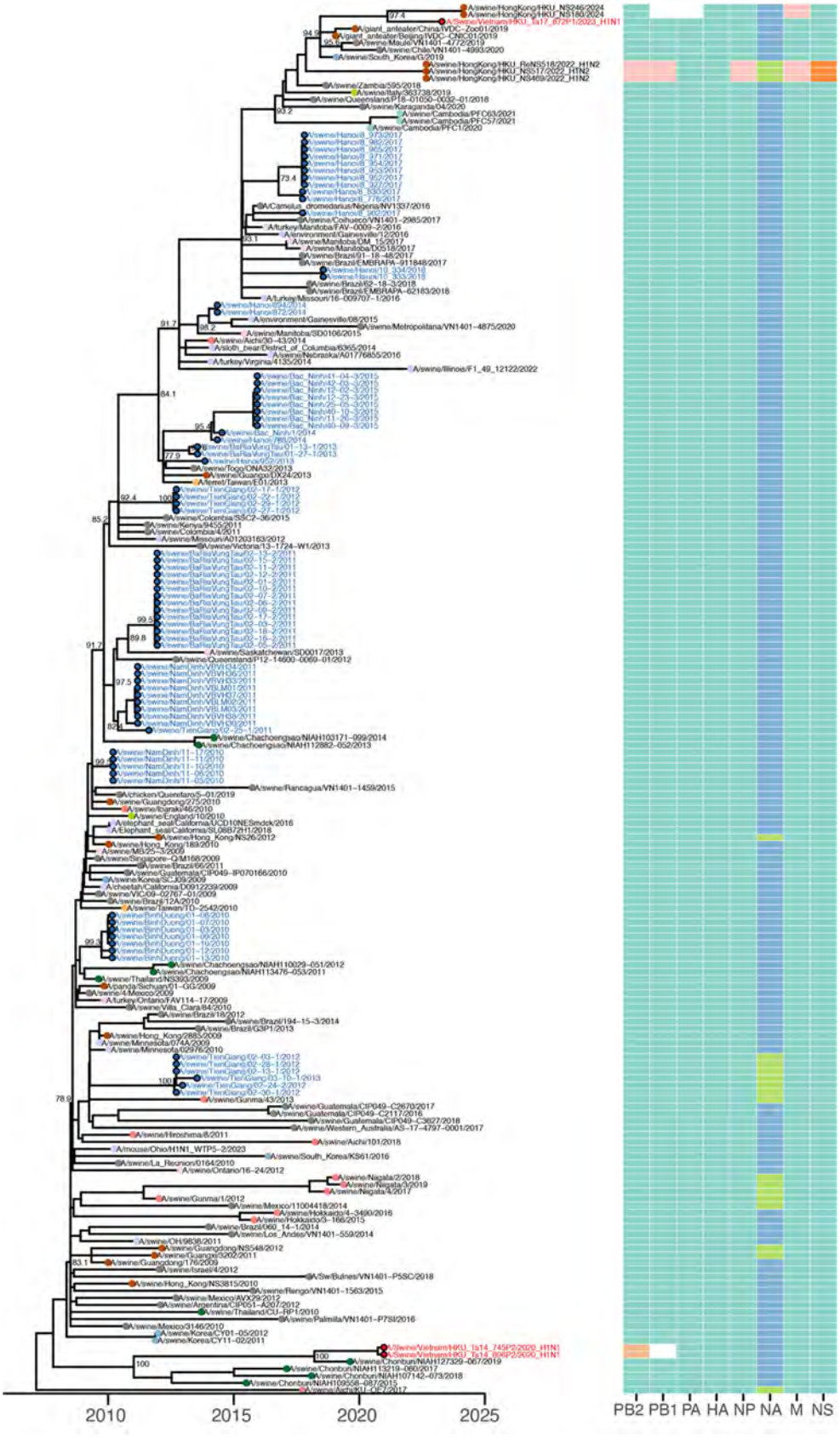

Figure 7. Time-scaled maximum likelihood phylogeny of swine influenza A virus hemagglutinin H1 clade 1A.3.3.2/pdm from study of molecular epidemiology and evolution of swine influenza A viruses, Vietnam, 2020–2024. Tips colored by geographic region. Red and blue circled dots and labels show the samples in Vietnam from this study and from previous studies. Shimodaira-Hasegawa–like approximate likelihood ratio test branch support values are labeled on nodes. The horizontal axis represents calendar time.

swine-origin influenza A(H1N1) variant virus in Son La province in 2024; no additional respiratory illness was reported among contacts, and WHO assessed the risk to the general population as low (*31*). Subsequent WHO genetic and antigenic characterization classified this virus as H1 clade 1C.2.3 and described it as closely related to swine viruses circulating in the region, with good reactivity to postinfection ferret antiserum raised against the clade 1C.2.3 candidate vaccine virus A/Hunan/42443/2015 (*32*). Clade 1C.2.3 was detected in Vietnam swine in our surveillance during 2020–2024, but public summaries of the human case do not report whether the human virus contained any specific substitutions. Human variant infections demonstrated

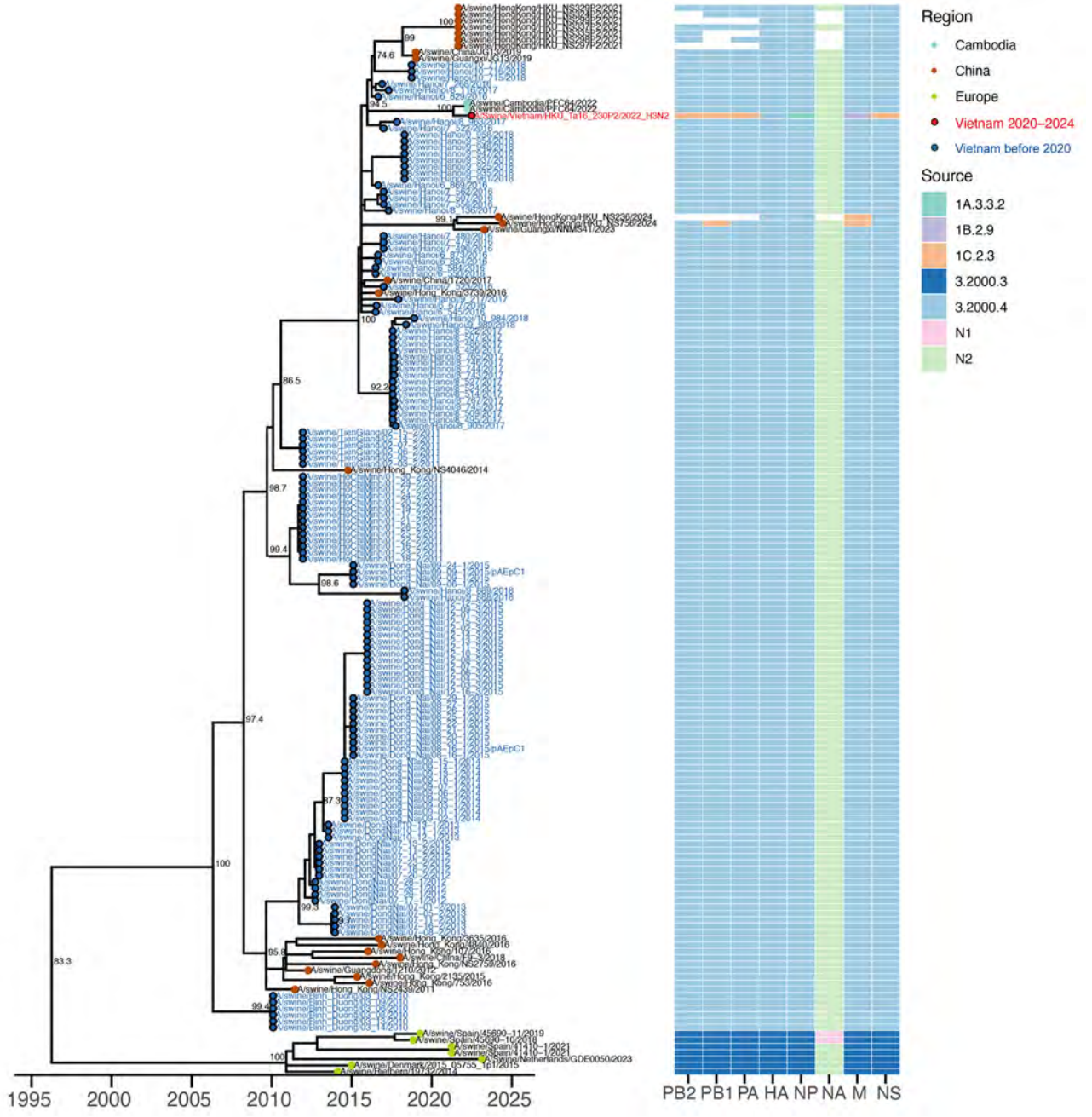

Figure 8. Time-scaled maximum likelihood phylogeny of swine influenza A virus hemagglutinin H3 clade 3.2000.4 from study of molecular epidemiology and evolution of swine influenza A viruses, Vietnam, 2020–2024. The heatmap shows the genetic source of all genes. Dots are colored by geographic regions. Red and blue circled dots and labels show the samples in Vietnam from this study and from previous studies. Shimodaira-Hasegawa–like approximate likelihood ratio test branch support values are labeled on nodes. The horizontal axis represents calendar time.

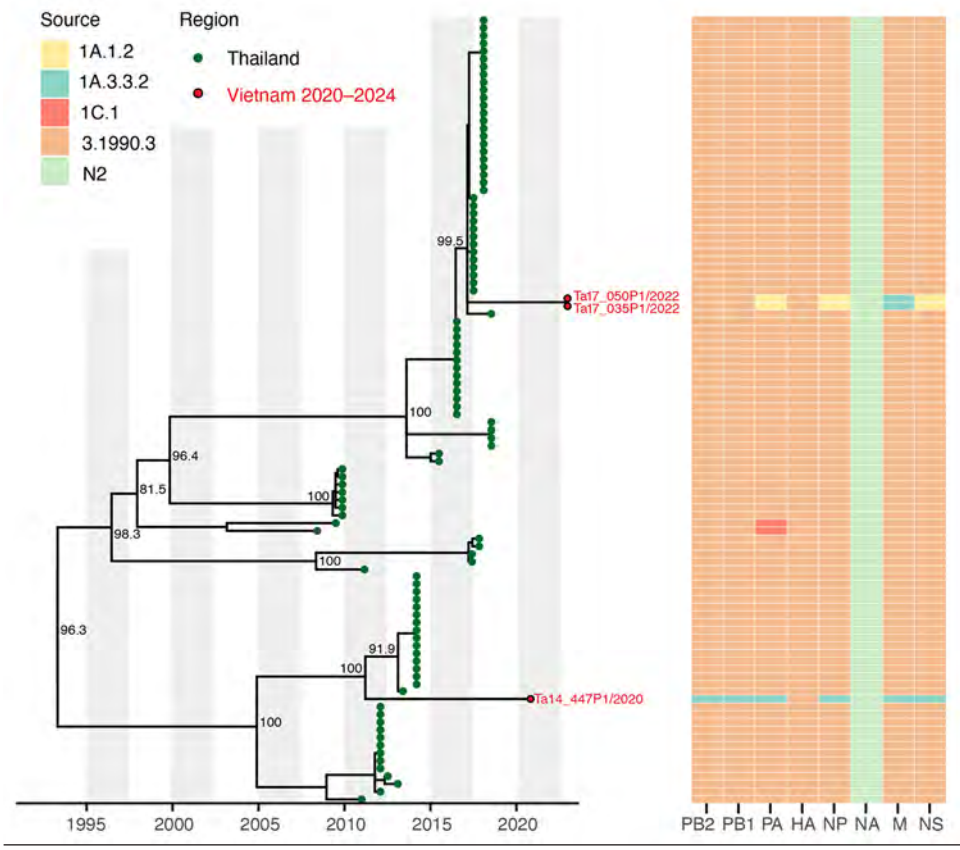

Figure 9. Time-scaled maximum likelihood phylogeny of swine influenza A virus hemagglutinin H3 clade 3.1990.3 from study of molecular epidemiology and evolution of swine influenza A viruses, Vietnam, 2020–2024. The heatmap shows the genetic source of all genes. Dots are colored by geographic regions. Red and blue circled dots and labels show the samples in Vietnam from this study and from previous studies. Shimodaira-Hasegawa–like approximate likelihood ratio test branch support values are labeled on nodes. The horizontal axis represents calendar time.

that some lineages detected in swine can cross the species barrier, although current evidence supports sporadic zoonotic transmission rather than sustained human-to-human spread.

The first limitation of this study is that molecular detection methods might yield higher detection rates of virus, but virus isolation has the advantage of providing viruses for further phenotypic characterization. Second, our study does not provide data on swine viruses that circulate in the southern part of Vietnam. Finally, because swine are transported long distances by truck in closely confined spaces, there is opportunity for cross-infection during transport, increasing the true IAV-S infection rates in swine, compared with what might be observed in farms.

The persistent circulation and repeated introductions of multiple IAV-S lineages in Vietnam underscore the region's risk for novel zoonotic influenza emergence. IAV-Ss circulating in Vietnam showed close phylogenetic relationships with isolates from other countries in Asia, although temporal and geographic surveillance gaps limit a complete characterization of regional transmission networks and the capacity for early detection and effective intervention.

This project has been funded in whole or in part with Federal funds from the National Institute of Allergy and Infectious Diseases, National Institutes of Health, Department of Health and Human Services (contract no. 75N93021C00016).

About the Author

Dr. Bui is a researcher at the Institute of Animal and Veterinary Science, Hanoi, Vietnam. Her research interests include the epidemiology and pathogenesis of animal viruses, including swine influenza viruses.

References

1. VanderWaal K, Deen J. Global trends in infectious diseases of swine. Proc Natl Acad Sci U S A. 2018;115:11495–500. https://doi.org/10.1073/pnas.1806068115
2. Nelson MI, Worobey M. Origins of the 1918 pandemic: revisiting the swine "mixing vessel" hypothesis. Am J Epidemiol. 2018;187:2498–502. https://doi.org/10.1093/aje/kwy150
3. Smith GJD, Vijaykrishna D, Bahl J, Lycett SJ, Worobey M, Pybus OG, et al. Origins and evolutionary genomics of the 2009 swine-origin H1N1 influenza A epidemic. Nature. 2009;459:1122–5. https://doi.org/10.1038/nature08182
4. Anderson TK, Chang J, Arendsee ZW, Venkatesh D, Souza CK, Kimble JB, et al. Swine influenza A viruses and the tangled relationship with humans. Cold Spring Harb Perspect Med. 2021;11:a038737. https://doi.org/10.1101/cshperspect.a038737

5. Nelson MI, Stratton J, Killian ML, Janas-Martindale A, Vincent AL. Continual reintroduction of human pandemic H1N1 influenza A viruses into swine in the United States, 2009 to 2014. J Virol. 2015;89:6218–26. https://doi.org/10.1128/JVI.00459-15
6. Nelson MI, Viboud C, Vincent AL, Culhane MR, Detmer SE, Wentworth DE, et al. Global migration of influenza A viruses in swine. Nat Commun. 2015;6:6696. https://doi.org/10.1038/ncomms7696
7. Zhu H, Webby R, Lam TTY, Smith DK, Peiris JSM, Guan Y. History of swine influenza viruses in Asia. Curr Top Microbiol Immunol. 2013;370:57–68. https://doi.org/10.1007/82_2011_179
8. Baudon E, Chu DKW, Tung DD, Thi Nga P, Vu Mai Phuong H, Le Khanh Hang N, et al. Swine influenza viruses in Northern Vietnam in 2013–2014. Emerg Microbes Infect. 2018;7:123. https://doi.org/10.1038/s41426-018-0109-y
9. Cheung J, Bui AN, Younas S, Edwards KM, Nguyen HQ, Pham NT, et al. Long-term epidemiology and evolution of swine influenza viruses, Vietnam. Emerg Infect Dis. 2023;29:1397–406. https://doi.org/10.3201/eid2907.230165
10. Katoh K, Standley DM. MAFFT multiple sequence alignment software version 7: improvements in performance and usability. Mol Biol Evol. 2013;30:772–80. https://doi.org/10.1093/molbev/mst010
11. Minh BQ, Schmidt HA, Chernomor O, Schrempf D, Woodhams MD, von Haeseler A, et al. IQ-TREE 2: new models and efficient methods for phylogenetic inference in the genomic era. Mol Biol Evol. 2020;37:1530–4. https://doi.org/10.1093/molbev/msaa015
12. Guindon S, Dufayard J-F, Lefort V, Anisimova M, Hordijk W, Gascuel O. New algorithms and methods to estimate maximum-likelihood phylogenies: assessing the performance of PhyML 3.0. Syst Biol. 2010;59:307–21. https://doi.org/10.1093/sysbio/syq010
13. Sagulenko P, Puller V, Neher RA. TreeTime: maximum-likelihood phylodynamic analysis. Virus Evol. 2018;4:vex042. https://doi.org/10.1093/ve/vex042
14. OFFLU. OFFLU swine influenza report July 2024 to December 2024, 2025 [cited 2025 Oct 28]. https://offlu.org/technical-activities/february-2025-swine-influenza
15. Ishikawa SA, Zhukova A, Iwasaki W, Gascuel O. A fast likelihood method to reconstruct and visualize ancestral scenarios. Mol Biol Evol. 2019;36:2069–85. https://doi.org/10.1093/molbev/msz131
16. Mertens E, Dugan VG, Stockwell TB, Lindsay LL, Plancarte M, Boyce WM. Evaluation of phenotypic markers in full genome sequences of avian influenza isolates from California. Comp Immunol Microbiol Infect Dis. 2013;36:521–36. https://doi.org/10.1016/j.cimid.2013.06.003
17. Suttie A, Deng Y-M, Greenhill AR, Dussart P, Horwood PF, Karlsson EA. Inventory of molecular markers affecting biological characteristics of avian influenza A viruses. Virus Genes. 2019;55:739–68. https://doi.org/10.1007/s11262-019-01700-z
18. Janzen GM, Inderski BT, Chang J, Arendsee ZW, Janas-Martindale A, Torchetti MK, et al. Sources and sinks of influenza A virus genomic diversity in swine from 2009 to 2022 in the United States. J Virol. 2025;99:e0054125. https://doi.org/10.1128/jvi.00541-25
19. Coggon A, Lopes S, Simon G, Arendsee Z, Chen KF, Chiapponi C, et al. Quantifying the zoonotic risk profile of European influenza A viruses in swine from 2010 to 2020 inclusive. J Virol. 2025;99:e0030625. https://doi.org/10.1128/jvi.00306-25
20. Sun H, Liu H, Zhang J, Qu X, Pang Z, Xu F, et al. Genome-scale evolution and phylodynamics of swine influenza A viruses in China: a genomic epidemiology study. Lancet Microbe. 2025;6:101020. https://doi.org/10.1016/j.lanmic.2024.101020
21. Zeller MA, Ma J, Wong FY, Tum S, Hidano A, Holt H, et al. The genomic landscape of swine influenza A viruses in Southeast Asia. Proc Natl Acad Sci U S A. 2023;120:e2301926120. https://doi.org/10.1073/pnas.2301926120
22. Cheung JTL, Lau EH, Jin Z, Zhu H, Guan Y, Peiris M. Influenza A virus transmission in swine farms and during transport in the swine supply chain. Transbound Emerg Dis. 2022;69:e3101–10. https://doi.org/10.1111/tbed.14667
23. Takemae N, Harada M, Nguyen PT, Nguyen T, Nguyen TN, To TL, et al. Influenza A viruses of swine (IAV-S) in Vietnam from 2010 to 2015: multiple introductions of A(H1N1)pdm09 viruses into the pig population and diversifying genetic constellations of enzootic IAV-S. J Virol. 2016;91:e01490–16.
24. Rajão DS, Walia RR, Campbell B, Gauger PC, Janas-Martindale A, Killian ML, et al. Reassortment between swine H3N2 and 2009 pandemic H1N1 in the United States resulted in influenza A viruses with diverse genetic constellations with variable virulence in pigs. J Virol. 2017;91:10–128. https://doi.org/10.1128/JVI.01763-16
25. Nasamran C, Janetanakit T, Chiyawong S, Boonyapisitsopa S, Bunpapong N, Prakairungnamthip D, et al. Persistence of pdm2009-H1N1 internal genes of swine influenza in pigs, Thailand. Sci Rep. 2020;10:19847. https://doi.org/10.1038/s41598-020-76771-2
26. Cao Z, Zeng W, Hao X, Huang J, Cai M, Zhou P, et al. Continuous evolution of influenza A viruses of swine from 2013 to 2015 in Guangdong, China. PLoS One. 2019;14:e0217607. https://doi.org/10.1371/journal.pone.0217607
27. Zhao Y, Han L, Sang H, Yang P, Hou Y, Xiao Y. Two genotypes of H3N2 swine influenza viruses identified in pigs from Shandong Province, China. Front Cell Infect Microbiol. 2024;14:1517023. https://doi.org/10.3389/fcimb.2024.1517023
28. Hu M, Yuan S, Zhang K, Singh K, Ma Q, Zhou J, et al. PB2 substitutions V598T/I increase the virulence of H7N9 influenza A virus in mammals. Virology. 2017;501:92–101. https://doi.org/10.1016/j.virol.2016.11.008
29. Czudai-Matwich V, Otte A, Matrosovich M, Gabriel G, Klenk HD. PB2 mutations D701N and S714R promote adaptation of an influenza H5N1 virus to a mammalian host. J Virol. 2014;88:8735–42. https://doi.org/10.1128/JVI.00422-14
30. Swanson NJ, Marinho P, Dziedzic A, Jedlicka A, Liu H, Fenstermacher K, et al. 2019-2020 H1N1 clade A5a.1 viruses have better in vitro fitness compared with the co-circulating A5a.2 clade. Sci Rep. 2023;13:10223. https://doi.org/10.1038/s41598-023-37122-z
31. World Health Organization. Influenza A(H1N1) variant virus—Viet Nam [cited 2026 May 27]. https://www.who.int/emergencies/disease-outbreak-news/item/2024-DON532
32. World Health Organization. Genetic and antigenic characteristics of zoonotic influenza A viruses and development of candidate vaccine viruses for pandemic preparedness [cited 2026 May 27]. https://cdn.who.int/media/docs/default-source/vcm-southern-hemisphere-recommendation-2025/202409_zoonotic_recommendations_final.pdf

Address for correspondence: Malik Peiris, University of Hong Kong School of Public Health, No. 7 Sassoon Rd, Pokfulam, Hong Kong, China; email: malik@hku.hk

Genomic Epidemiology of *Salmonella enterica* Serovar Hadar Strain Linked to Poultry-Associated Salmonellosis Outbreaks, United States

Lingzi Xiaoli, Taylor Griswold, G. Sean Stapleton, Lee S. Katz, Zachary Ellison, Kaitlin A. Tagg, Hattie E. Webb, Katharine Benedict, Jessica C. Chen

Nontyphoidal *Salmonella enterica* serovar Hadar causes poultry-associated salmonellosis outbreaks in the United States. One persisting strain of *Salmonella* Hadar caused 5 multistate outbreaks resulting in ≈2,000 human cases during 2020–2023. The Centers for Disease Control and Prevention designated the strain as reoccurring, emerging, or persisting (REP), related within 26 core-genome allele differences. That REP strain has caused human illnesses by consumption of commercial poultry food products or contact with backyard poultry. To investigate the REP strain's evolution and identify possible markers for source attribution, we performed phylogenetics and molecular clock analysis on 404 genomes subsampled from routine surveillance and outbreaks. The most recent common ancestor likely emerged in early 2018. We identified 2 clades: clade 1, associated with backyard poultry and other food sources, and clade 2, predominantly linked to commercial poultry products. We found 2 clade-specific single-nucleotide polymorphism markers; in silico screening of additional isolates supported their use for source attribution.

Nontyphoidal *Salmonella enterica* subspecies *enterica* causes >1 million human salmonellosis cases annually in the United States (*1*,*2*). Although illness is often self-limiting, with symptoms including diarrhea, fever, or abdominal pain, severe complications such as meningitis and septicemia may occur in vulnerable populations, including children <5 years of age, adults >65 years of age, immunocompromised persons, and pregnant women (*3*).

Author affiliations: Centers for Disease Control and Prevention, Atlanta, Georgia, USA (L. Xiaoli, T. Griswold, G.S. Stapleton, L.S. Katz, K.A. Tagg, H.E. Webb, K. Benedict, J.C. Chen); ASRT Inc., Smyrna, Georgia, USA (Z. Ellison)

DOI: https://doi.org/10.3201/eid3210.260501

Poultry can shed *Salmonella* in their feces even when they appear healthy and clean, contaminating their living environments or food products, such as poultry and eggs (*4*,*5*). Consumption of contaminated poultry products remains the largest contributor to the overall burden of foodborne *Salmonella* infections (*6*). Similarly, contact with backyard poultry (BYP, defined as noncommercial, privately owned chickens, ducks, turkeys, or other poultry) causes more multistate outbreak–associated salmonellosis in the United States annually than any other live animal source (*7*).

Among >2,600 identified serovars of *Salmonella*, *S. enterica* serovar Hadar has emerged as a prominent contributor to multistate poultry-associated outbreaks. Its primary transmission routes include exposure to contaminated commercial poultry (CP) food products (e.g., ground turkey) and contact with BYP and their environments (*7*,*8*). Industries supplying CP and BYP are considered distinct because of differences including scale, predominant breeds produced, husbandry, and biosecurity practices, although potential overlap of upstream stages of the supply chain, such as shared hatcheries, egg suppliers, or shared feed sources, might occur (*8*–*10*). Some BYP distribution and shipping practices might contribute to further dissemination of *Salmonella* strains across species (e.g., between turkeys and chickens) when BYP hatcheries package different species together for shipping (*11*) to meet minimum customer order sizes or when feedstores display multiple species for sale in the same facility.

In 2020, a *Salmonella* Hadar strain caused outbreak A, which included >800 human infections linked to contact with BYP, and isolates were related within 15 core-genome allele differences determined by core genome multilocus sequence typing (cgMLST). During 2020–2021, *Salmonella* Hadar also caused outbreak B,

linked to consumption of contaminated ground turkey in which isolates were related within 8 allele differences (*8*). Isolates from both outbreaks were closely related within 16 allele differences by cgMLST (*8*). After those outbreaks, the Centers for Disease Control and Prevention (CDC) classified isolates of *Salmonella* Hadar within a cgMLST range of 26 allele differences as a reoccurring, emerging, or persisting (REP) strain designated as REPTDK01 (*12*,*13*). REPTDK01 caused 3 more multistate outbreaks linked to contact with BYP alone (outbreaks C and D) or to BYP and CP concurrently (outbreak E). As of May 2023, ≈2,000 illnesses caused by REPTDK01 have been reported in the United States (*12*). Epidemiologic and pangenomic data suggest that REPTDK01 originated from extant populations circulating in CP and subsequently disseminated into BYP environments (*8*,*12*,*14*); however, when and where that persisting REP strain arose is unknown.

CDC developed its REP strain framework after the widespread implementation of whole-genome sequencing (WGS), which increased the ability to identify genetically related strains over a longer time period than was typically used to investigate outbreaks (*15*). The prolonged period can enable detection of related strains with broader allele differences than are typically considered for outbreak investigation. The definition of REP strains considers several factors, including information about the pathogen, the genetic relationship of investigated isolates, related epidemiologic information, and knowledge about potential sources and routes of transmission. The REP framework provides additional tools to investigate enteric illnesses and assess source tracking and overall genomic and epidemiologic trends.

To elucidate REPTDK01's evolutionary history and identify potential genomic markers indicative of transmission vehicles, we leveraged existing epidemiologic and genomic data. Here, we conducted a molecular clock (or time tree) analysis based on single-nucleotide polymorphism (SNP) differences to estimate the emergence of the outbreak strain and investigate clade-defining SNP differences (*16*–*18*) (Appendix 1, https://wwwnc.cdc.gov/EID/article/32/10/26-0501-App1.pdf). Coupling those molecular findings with epidemiologic data, we elucidated REPTDK01's clade association with specific transmission vehicles. We conducted our investigations consistent with applicable federal law and CDC policy: 45 C.F.R. part 46, 21 C.F.R. part 56; 42 U.S.C. §241(d); 5 U.S.C. §552a; 44 U.S.C. §3501 et seq. This work includes activities approved by the Centers for Disease Control and Prevention Institutional Review Board (approval no. 7172).

Materials and Methods

Data Collection

In the United States, when *Salmonella* is cultured from patient specimens, state or local public health laboratories perform WGS on the clinical isolates and upload data to PulseNet, the national molecular subtyping network for enteric disease surveillance coordinated by CDC (*19*). PulseNet uses cgMLST to assess genetic relatedness of isolates and identify potential outbreaks. For *Salmonella*, a potential outbreak cluster is flagged for investigation if ≥7 clinical cases (≥3 cases for more rare serovars) are detected within 60 days of each other and the cases are related within 0–10 cgMLST alleles; however, that range is not used to constrain the addition of isolates (*20*). Public health officials interview patients with salmonellosis using outbreak questionnaires to obtain exposure information (e.g., foods consumed or animal contact before patient's illness onset) to help identify transmission vehicles (*19*). During outbreak investigations, CDC or partner agencies might collect and sequence nonclinical samples from suspected foods, animals, environments at patients' households, food production facilities, or other locations to confirm transmission vehicles. PulseNet member entities compile and analyze sequenced data from resulting nonclinical isolates. In addition, nonhuman isolates collected from routine surveillance programs such as National Antimicrobial Resistance Monitoring System (NARMS) (*21*) or ad hoc sampling are also integrated into PulseNet for analysis whenever possible.

We used a bulk dataset generated for a previous pangenomic study of REPTDK01 (*14*) as the basis for this study. That study evaluated a broader serovar Hadar dataset with carefully curated metadata, including isolates beyond REPTDK01 and from sources beyond CDC; the dataset included data generated through federal partnerships with the US Department of Agriculture and Food and Drug Administration. To study the emergence, genomics, and epidemiology of REPTDK01 more clearly, we restricted our analysis to a subsampled set of isolates from multiple sources confirmed as REPTDK01 (Appendix 2 Table 1, https://wwwnc.cdc.gov/EID/article/32/10/26-0501-App2.xlsx). To analyze the overall relationships among isolates in the bulk dataset, we performed cgMLST profiling in BioNumerics version 7.6 (bioMérieux, https://www.biomerieux.com) using the EnteroBase scheme for *Salmonella* as described previously (*20*,*22*) and subsampled and analyzed REPTDK01 genomes in this study. We categorized the resulting REPTDK01 genomes into 6 groups: BYP, BYP and CP, CP, beef, pork, and unknown, using patient exposure

information (e.g., individual exposure to a specific food, animal, or both) and other available metadata for food, animal, or environmental isolates. The BYP category included clinical isolates from patients who reported BYP contact as well as animal or environmental isolates obtained from samples collected from BYP or BYP habitats. The CP category included commercial poultry food isolates or clinical isolates from patients who reported consuming any type of CP food products. The BYP and CP category represented clinical isolates obtained from patients reporting exposures to both BYP and CP food products. The beef categories encompassed food isolates from cattle and pork from swine. The unknown category contained clinical or animal isolates with no available exposure information.

For REPTDK01 isolates linked to a known outbreak, we anonymized the outbreak information as A, B, C, D, and E, consistent with the nomenclature used in CDC web postings for the *Salmonella* strain (*12*). We included isolates in instances in which the incident of detection met standard criteria for opening an outbreak investigation (*19*) and the investigation determined that illnesses were likely attributed to a common source on the basis of epidemiologic information (*23*).

Subsampling Process

We restricted our analysis to the REPTDK01 genomes within a curated collection generated for a previous pangenome study (*14*), comprising 2,021 isolates collected during 2018–2023. Most of the isolates originated during 3 consecutive years 2020–2022 (Appendix 2 Tables 1, 2). To address computational limitations and minimize oversampling of closely related isolates within the period, we stratified isolates by year of isolation and randomly subsampled ≈16% of isolates per year. In contrast, we included all available isolates for 2018, 2019, and 2023 to enhance representation. After we removed isolates not meeting our data quality criteria, the resulting subsampled dataset included 404 isolates, 78% of which were human clinical, food, animal isolates, or environmental isolates linked to 5 documented outbreaks (Appendix 1 Figure; Appendix 2 Table 2).

Data Quality Assessment

We downloaded sequence reads from National Center for Biotechnology Information Sequence Read Archive (https:// ncbi.nlm.nih.gov/sra) (Appendix 2 Table 3). In addition to routine quality checks performed by PulseNet (*20*), we verified quality scores and read coverage using CG Pipeline version 0.5 (https://github.com/lskatz/CG-Pipeline) (*24*). We included paired-end reads in the REPTDK01 subset that had an average read coverage >30× and average quality score ≥28. Average quality score of 29 required 40× coverage and a score of 28 required 50× coverage. We excluded genomes that failed to meet those quality control requirements (n = 8) from subsequent analyses (Appendix 1 Figure). We generated assemblies using shovill version 1.0.9 (https://github.com/tseemann/shovill) as previously described (*14*); that study excluded contigs with coverage of <10% of the average genome coverage.

Time Tree Analysis

To elucidate the emergence of REPTDK01 in the United States, we performed a time tree analysis. In brief, we used Lyve-SET version 1.1.4f (*25*) to construct a high-quality SNP (hqSNP)–based phylogenetic tree using default parameters for *Salmonella* and a closed chromosomal sequence of 2021K-0017 (GenBank accession no. CP093072) as the reference. We further analyzed the SNP alignment in BEAST version 2.6.3 (*26*) to generate a time tree (Appendix 1). We visualized the resulting time tree using ggtree (https://github.com/YuLab-SMU/ggtree) within R version 4.4.0 (The R Project for Statistical Computing, https://www.r-project.org).

Identification of Clade-Defining SNPs

We performed clade-defining SNP identification by comparing a centrally related representative genome from each clade to all other representatives from that clade. First, we processed assemblies using Mashtree version 1.4.6 (*27*) to determine central genomes based on the calculated Mash distances. Using the SNP matrix generated from the previous Lyve-SET analysis, we extracted SNPs that distinguish the representative genome from clade 2 in comparison to that from clade 1. After compiling a list of candidate SNPs, we assessed their presence or absence across isolates within the same clade. We conducted χ^2 test to statistically identify clade-specific SNPs ($p \leq 0.05$). Subsequently, we focused on SNPs deemed present in almost all isolates within clade 2 and investigated their associated genes and functions through assembly annotations using Bakta version 1.9.1 (*28*).

Pangenome Analysis

We annotated whole genome assemblies inclusive of all accessory elements using Bakta version 1.9.1 and conducted subsequent pangenomic analysis using Roary version 3.13.0 (*29*) and Scoary version 1.6.16 (*30*); we used default parameters to identify clade-defining variations in accessory genes among the REPTDK01 subset isolates.

Genomic Marker Screening

We extracted gene sequences of *yihS* and *pdxA* from the reference genome 2021K-0017. We then used

them as BLAT version 35 (*31*) references to screen 703 nonhuman REPTDK01 genomes with known epidemiologic linkages in the bulk dataset.

Results

Diverse Sources for *Salmonella* Hadar REPTDK01

As of May 31, 2023, the 2,021 REPTDK01 genomes from the bulk dataset were related within 26 allele differences by cgMLST (Appendix 2 Table 1). Of those, 1,544 clinical isolates (76.4%) were from patients involved in 5 multistate outbreaks (outbreaks A–E) during April 2020–May 2023; the earliest detection of the clinical isolate was in July 2019. The remaining 477 isolates were either clinical isolates not linked to a known outbreak (n = 275 [13.6%]) or isolates from other source types of food (n = 161 [8.0%]), animal (n = 35 [1.7%]), or environment (n = 6 [0.3%]).

The REPTDK01 subset included 404 isolates: 336 (83.2%) clinical, 55 (13.6%) food, and 13 (3.2%) animal isolates (Appendix 2 Table 3). Of the clinical isolates, 269 (66.6%) were associated with an outbreak. Detailed isolate metadata or exposure information was available for 163 (40.3%) of REPTDK01 subset isolates regardless of their source type (e.g., human, animal, and food), enabling categorization of the isolates into 5 exposure groups: beef (n = 1), pork (n = 1), BYP (n = 91), CP (n = 69), and BYP and CP (n = 1). We classified as unknown the remaining isolates, 173 (42.8%) outbreak-associated clinical isolates for which no exposure information was available and 68 (16.8%) not linked to outbreaks (66 clinical, 2 animal).

Time Tree Analysis Results

Time tree analysis revealed that all but 1 REPTDK01 genomes fell within 2 well-supported clades, which shared a most recent common ancestor around early 2018 (median date February 16, 2018; 95% highest posterior density (HPD) interval April 25, 2017–July 29, 2018) (Figure). Within each clade, tree tips annotated by outbreak showed the gradual temporal evolution of REPTDK01. The full subset of 404 isolates had a median of 5 (range 0–21) allele differences characterized by cgMLST. Clade 1 consisted of 308 isolates with a median of 4 allele differences (range 0–6), and clade 2 included 95 isolates with a median of 3 allele differences (range 0–14). The corresponding hqSNP ranges were a median of 9 (range 0–40) overall, a median of 8 (range 0–33) for clade 1, and a median of 6 (range 0–24) for clade 2.

The separation of 2 clades in the time tree corresponded to distinct epidemiologic linkages. Those in clade 1 exhibited greater exposure group diversity based on 104 isolates with detailed exposure information or source metadata, encompassing not only CP-associated isolates (10%, n = 11) but also those linked to BYP (88%, n = 91), beef (1%, n = 1), and pork (1%, n = 1) (Table 1). Of note, we found BYP-associated isolates only in clade 1. In contrast, isolates with detailed information in clade 2 (n = 59) were all linked to CP in some way (Table 1), including 74.5% (n = 44) from CP food, 8.5% (n = 5) from CP animals, and 17% (n = 10) from clinical isolates from case-patients exposed to CP (n = 9) or both CP and BYP (n = 1).

Salmonella Hadar REPTDK01 Clades Defined by 2 SNPs

We identified 2 clade-defining SNPs using a closed genome (GenBank accession no. CP093072) from clade 1 as the reference. The first SNP led to a synonymous mutation in *pdxA*, which encodes a dehydrogenase. The second SNP, a G→A mutation in the isomerase gene *yihS*, introduced a premature stop codon (Table 1). Nearly all clade 2 isolates (97.9%) carried *pdxA* SNP, and all of them (100%) had the *yihS* SNP. Except for a truncated *yihS* gene identified in clade 2 versus wild type *yihS* in clade 1, pangenomic analysis in this study found no accessory genes distinguishing the 2 clades (data not shown).

Discussion

Although the factors contributing to the emergence of the REPTDK01 strain of *Salmonella* Hadar remain unknown, molecular clock analysis estimated that the strain emerged in early 2018, before the earliest human case reported to PulseNet in mid-2019. Although *Salmonella* Hadar exhibits notable clonality based on previous cgMLST and pangenomic analysis (*14*), our time tree constructed on core SNPs revealed 2 clades, each harboring specific genomic variations associated with distinct epidemiologic delineations. We identified 2 clade-defining SNPs in 2 genes, *pdxA* and *yihS* (Table 2), both of which are core genes included in the cgMLST scheme used by PulseNet for outbreak detection as of July 2026 (*20*,*22*).

Although the *pdxA* mutation is synonymous, the SNP in *yihS* introduces a premature stop codon, potentially resulting in a truncated protein in clade 2 isolates. The *yihS* functions as an aldose–ketose isomerase within the conserved *yih* operon (*32*) and is implicated in sulfoquinovose metabolism, extracellular polymeric substance synthesis, and the modification of outer membrane protein antigenicity, all of which potentially influence environmental persistence under stressors such as acidity and bleach exposure (*33*–*35*). Further functional studies are needed to assess whether that *yihS* mutation contributes to clade-specific

phenotypic differences in relation to differences in management across different types of poultry production systems. A 2020 study (*36*) described the expansion of a clonal group of *Salmonella* serovar Reading in turkey production. The strain was distinguished by plasmid and prophage content, as well as 2 gene disruptions, 1 in the *cirA* gene, which encodes a catecholate siderophore receptor, and 1 in a *uidA*-like gene deletion of the adjacent peptidoglycan deacetylase, *pgdA*. Those findings, combined with ours in this study, suggest mutations that inactivate genes may be a key evolutionary mechanism by which strains expand and emerge in poultry.

We observed isolates from clade 1 to have epidemiologic exposure information and isolate metadata that indicated diverse transmission vehicles including beef, pork, CP, and BYP. Of note, isolates associated with BYP exclusively belonged to clade 1, whereas isolates associated with CP predominated clade 2. That finding suggests that screening clade-defining SNPs within REPTKD01 isolates could demonstrate their linkages to a specific transmission vehicle. Preliminary in silico screening of the 2 genomic markers in an additional 703 nonsubsampled REPTDK01 isolates that had detailed epidemiologic information from the bulk dataset revealed similar patterns: all BYP-related, beef, and pork isolates along with a few CP-related and both of the CP and BYP–related isolates were assigned to clade 1, whereas most (>80%) CP-related isolates were expected to belong to clade 2 (Appendix 2 Table 4). The pangenomic study (*14*) grouped REPTDK01 isolates in 2 subgroups, JI-A and JI-C; JI-A included both BYP and CP isolates, and JI-C contained almost entirely BYP isolates. Within JI-A, the clade-defining SNPs can help further distinguish CP and BYP isolates, thus complementing those pangenomic findings. That study found that *Salmonella* Hadar subsampled for our work that carried a specific IncI1 plasmid was more often associated with BYP. Combined with the 2 genetic markers we identified, that plasmid could provide additional resolution to disentangle transmission vehicle signals of CP and BYP isolates within clade 1. Therefore, those clade-defining genomic

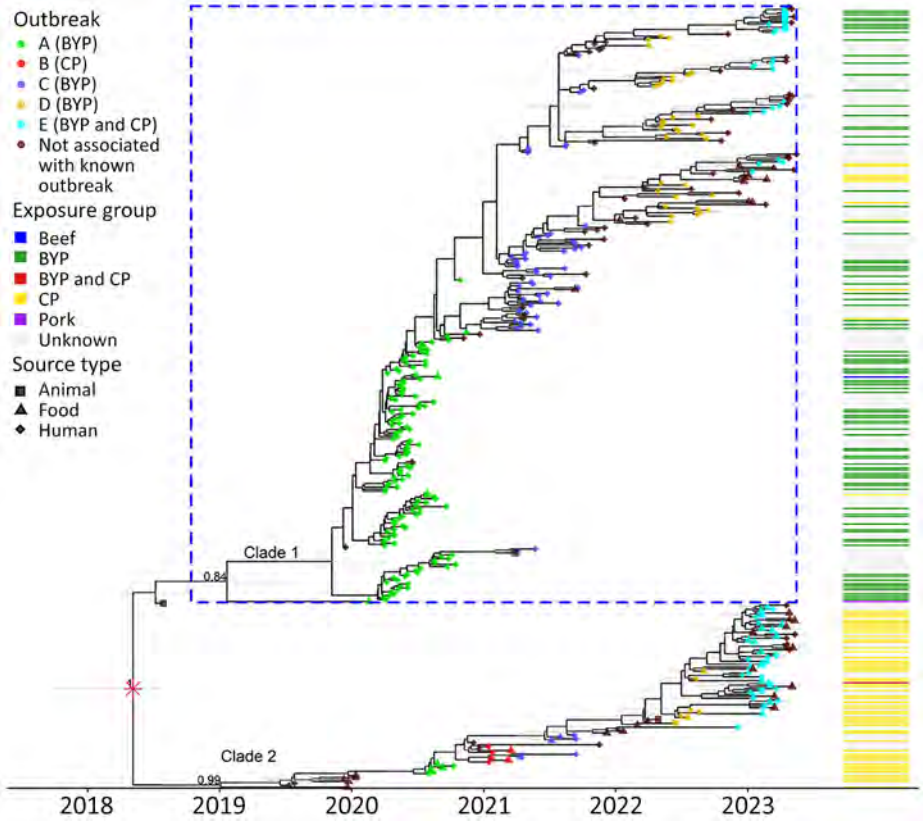

Figure. Maximum clade credibility tree of 404 persistent *Salmonella* Hadar REPTDK01 genomes from study of *Salmonella enterica* serovar Hadar strain linked to poultry-associated salmonellosis outbreaks, United States. Genomes subsampled from multistate poultry-associated outbreaks and routine surveillance revealed 2 distinct clades corresponding to separate epidemiologic linkages. The tree was generated using BEAST2 (https://www.beast2.org). Isolate tips are aligned to isolation dates and color-coded by outbreak and vehicle. Colored shape indicates source type. Red asterisk marks the most recent common ancestor, estimated to have emerged in early 2018. Posterior support values are shown for the most recent common ancestors of the 404 REPTDK01 genomes (tree root), clade 1, and clade 2. Gray horizontal bars indicate 95% highest posterior density interval for node heights. Column at right of tree indicates exposure group based on patient-related exposures and isolate metadata. Blue dashed box contains data for clade 1, comprising 308 isolates with diverse epidemiologic links to beef, pork, CP, and BYP. Isolates within clade 1 differ by a median of 8 hqSNPs (hqSNP range 0–33), and a median of 4 allele cgMLST differences (allele range 0–16). Clade 2 includes 95 isolates predominantly linked to CP; those isolates differ by a median of 6 hqSNPs (hqSNP range 0–24) or a median of 3 alleles (allele range 0–14). The full subset contains 404 isolates that differ by a median of 9 hqSNPs (hqSNP range 0–40) or 5 alleles (allele range: 0–21). BYP, backyard poultry; cgMLST, core genome multilocus sequence typing; CP, commercial poultry; hqSNP, high-quality single-nucleotide polymorphism.

Table 1. Characteristics of isolates from genomic epidemiology study of *Salmonella enterica* serovar Hadar strain linked to poultry-associated salmonellosis outbreaks, United States*

		Clade 1		Clade 2	
Outbreak (vehicle)	Total no.	No. isolates	Exposure information and isolate metadata	No. isolates	Exposure information and isolate metadata
A (BYP)	140	134	54 clinical isolates with BYP exposure 77 clinical isolates with unknown exposure 1 beef food product isolate 1 pork food product isolate 1 CP food product isolate	6	4 CP food product isolates 1 Clinical isolate with CP exposure 1 Clinical isolate with unknown exposure
B (CP)	6	0		6	2 CP food product isolates 1 clinical isolate with CP exposure 3 clinical isolates with unknown exposure
C (BYP)	58	52	17 clinical isolates with BYP exposure 35 clinical isolates with unknown exposure	6	1 CP animal isolate 1 CP food product isolate 1 clinical isolate with CP exposure 3 clinical isolates with unknown exposure
D (BYP)	42	35	9 clinical isolates with BYP exposure 26 clinical isolates with unknown exposure	7	1 CP animal isolate 2 CP food product isolates 2 clinical isolates with CP exposure 2 clinical isolates with unknown exposure
E (BYP and CP)	66	24	6 BYP animal isolates 5 clinical isolates with BYP exposure 1 clinical isolate with CP exposure 12 clinical isolates with unknown exposure	42	2 CP animal isolates 21 CP food product isolates 4 clinical isolates with CP exposure 1 clinical isolate with CP and BYP exposure 14 clinical isolates with unknown exposure
Not outbreak-associated	91	63	53 clinical isolates with unknown exposure 1 clinical isolate with CP exposure 8 CP food product isolates 1 animal isolate with unknown exposure	28	1 CP animal isolate 14 CP food product isolates 13 clinical isolates with unknown exposure
Total	403	308		95	

*BYP, backyard poultry; CP, commercial poultry food products.

markers could inform hypothesis generation regarding transmission vehicles when epidemiologic information is absent or limited, particularly during the early stages of outbreak investigations.

Moreover, the codetection of CP- and BYP-related isolates within clade 1 (Table 1; Figure) might indicate ongoing transmission between the 2 industries through common upstream suppliers in the production chain, rather than a single introduction from CP into BYP environments. Previous outbreak investigations have reported that BYP hatcheries occasionally source fertilized eggs and chickens used for egg production from CP industry (*10*,*37*). Some BYP hatcheries have reported sourcing specific poultry breeds (e.g., broiler or meat-producing breeds) from CP hatcheries; however, limited traceback information hinders our understanding of these upstream dynamics (*8*). Applying our proposed clade-based genomic markers for source attribution during outbreak investigations could improve

Table 2. Clade-defining SNP annotations for the *Salmonella enterica* serovar Hadar REPTDK01 subset used in genomic epidemiology study of *Salmonella enterica* serovar Hadar linked to poultry-associated salmonellosis outbreaks, United States†

							SNP prevalence, no. (%)		
Gene‡	Position	Ref	Alt	Type	Amino acid	Function	Clade 1	Clade 2	χ^2 test
pdxA	3818146	C	T	synonymous_variant	p.Pro271Pro	Dehydrogenase	C, 308/308 (100)	C, 2/95 (2.1) T, 93/95 (97.9)	$\chi^2 = 385.8$, $p = 6.82 \times 10^{-86}$
yihS	4534475	G	A	stop_gained	p.Trp290*	Isomerase	G, 308/308 (100)	A, 95/95 (100)	$\chi^2 = 396.8$, $p = 2.78 \times 10^{-86}$

†χ^2 performed at 1 degree of freedom. Alt, nucleotide observed in sequence with the SNP mutation; Ref, nucleotide observed in the reference sequence; SNP, single-nucleotide polymorphism.
‡The reference genome used was 2021K-0017 (GenBank accession no. CP093072) from clade 1. χ^2 test showed a significant difference in the distribution of the clade-defining SNP between 2 clades for each gene ($p<0.05$).

future communication and collaboration with industry partners. Such mutual efforts could contribute to tailored, effective prevention measures aimed at reducing *Salmonella* transmission throughout the supply and distribution chains for poultry industries.

We noted several limitations regarding the epidemiologic information available for the full REPTDK01 dataset. First, some clinical isolates lacked detailed exposure information, which is a common issue encountered in outbreak investigations, caused by limited patient consent rates for interviews. Second, during the BYP-associated outbreak in 2020, when knowledge of the REPTDK01 strain was constrained, patient questionnaires focused solely on BYP exposure and did not necessarily include questions on exposure to CP food products for all patients, leading to inadequate attribution of epidemiologic source for those isolates. That approach has since been improved to capture additional exposure history for infected patients. Third, the REPTDK01 dataset we studied here included nonhuman isolates from retail meats and CP cecal samples collected through NARMS surveillance; it is still composed predominantly of human-associated isolates. Furthermore, NARMS surveillance sampling is focused on specific foods and food animals, so it is possible that REPTDK01 also exists in unrecognized animal populations or environments. We noted no isolates from on-farm sources or hatcheries, largely because of the difficulty in obtaining such samples. Efforts to address these limitations could include enhanced epidemiologic data collection, collaboration with experts representing poultry industries, and application of the proposed genomic markers to refine the predictive source attributions.

In conclusion, our study used a genomic epidemiology approach to better understand challenges encountered during outbreak investigations. Our findings contribute to our understanding of REPTDK01 transmission dynamics across different poultry industries and could aid in identifying transmission vehicles during outbreak investigations. Genomic markers identified in this study could suggest earlier in the investigation process whether CP or BYP industry is likely involved in prospective detections of REPTDK01 outbreaks, thereby providing earlier opportunities to coordinate across sectors and collaborate on the development of effective control and prevention measures for reducing *Salmonella* transmission.

Acknowledgments

We thank the PulseNet-participating laboratories as well as federal public health and regulatory laboratories for sequencing the isolates that were used for this study. We also thank the investigators in state, local, and territorial agencies who collected exposure data for this study. We acknowledge industry partners that contributed information to outbreak investigations and partnered in reducing *Salmonella* transmission.

About the Author

Dr. Xiaoli completed this project as a molecular epidemiology fellow in the Division of Foodborne, Waterborne, and Environmental Diseases, National Center for Emerging and Zoonotic Infectious Diseases, Centers for Disease Control and Prevention. Her primary research interest is applying molecular genomics and epidemiologic approaches to investigate multistate enteric outbreaks linked to animal contact using a One Health approach.

References

1. Collier SA, Deng L, Adam EA, Benedict KM, Beshearse EM, Blackstock AJ, et al. Estimate of burden and direct healthcare cost of infectious waterborne disease in the United States. Emerg Infect Dis. 2021;27:140–9. https://doi.org/10.3201/eid2701.190676
2. Scallan Walter EJ, Cui Z, Tierney R, Griffin PM, Hoekstra RM, Payne DC, et al. Foodborne illness acquired in the United States—major pathogens, 2019. Emerg Infect Dis. 2025;31:669–77.
3. Shane AL, Mody RK, Crump JA, Tarr PI, Steiner TS, Kotloff K, et al. 2017 Infectious Diseases Society of America Clinical practice guidelines for the diagnosis and management of infectious diarrhea. Clin Infect Dis. 2017;65:e45–80. https://doi.org/10.1093/cid/cix669
4. Anderson AS, Bauer H, Nelson CB. Salmonellosis due to *Salmonella* typhimurium with Easter chicks as likely source. J Am Med Assoc. 1955;158:1153–5. https://doi.org/10.1001/jama.1955.02960130007003
5. Centers for Disease Control and Prevention. Multistate outbreaks of *Salmonella* infections associated with live poultry—United States, 2007. MMWR Morb Mortal Wkly Rep. 2009;58:25–9.
6. Centers for Disease Control and Prevention. Foodborne illness source attribution estimates—United States, 2022. 2024 [cited 2025 Mar 1]. https://www.cdc.gov/ifsac/php/data-research/annual-report-2022.html
7. Stapleton GS, Habrun C, Nemechek K, Gollarza L, Ellison Z, Tolar B, et al. Multistate outbreaks of salmonellosis linked to contact with backyard poultry—United States, 2015–2022. Zoonoses Public Health. 2024;71:708–22. https://doi.org/10.1111/zph.13134
8. Brandenburg JM, Stapleton GS, Kline KE, Khoury J, Mallory K, Machesky KD, et al. *Salmonella* Hadar linked to two distinct transmission vehicles highlights challenges to enteric disease outbreak investigations. Epidemiol Infect. 2024;152:e86. https://doi.org/10.1017/S0950268824000682
9. Gentile N, Carrasquer F, Marco-Fuertes A, Marin C. Backyard poultry: exploring non-intensive production systems. Poult Sci. 2024;103:103284. https://doi.org/10.1016/j.psj.2023.103284
10. Nichols M, Stevenson L, Whitlock L, Pabilonia K, Robyn M, Basler C, et al. Preventing human *Salmonella* infections resulting from live poultry contact through interventions at retail stores. J Agric Saf Health. 2018;24:155–66. https://doi.org/10.13031/jash.12756

11. Habing GG, Kessler SE, Mollenkopf DF, Wittum TE, Anderson TC, Barton Behravesh C, et al. Distribution and diversity of *Salmonella* strains in shipments of hatchling poultry, United States, 2013. Zoonoses Public Health. 2015;62:375–80. https://doi.org/10.1111/zph.12157
12. Centers for Disease Control and Prevention. Data summary: persistent strain of *Salmonella* Hadar (REPTDK01) 2025 [cited 2025 Apr 30]. https://www.cdc.gov/salmonella/php/data-research/reptdk01.html
13. Centers for Disease Control and Prevention. Reoccurring, emerging, and persisting enteric bacterial strains. 2024 [cited 2025 Apr 30]. https://www.cdc.gov/foodborne-outbreaks/php/rep-strains
14. Tagg KAP-CA, Peñil-Celis A, Webb HE, Stapleton GS, Ellison Z, Leeper M, et al. Pangenome dynamics and population structure of the zoonotic pathogen *Salmonella enterica* serotype Hadar. Nat Commun. 2026;17:1270. https://doi.org/10.1038/s41467-025-68026-3
15. Wise ME, Vasser M, Adams J, Beal J, Conrad A, Cote A, et al. Reoccurring, emerging, and persisting (REP) strains: a framework for surveillance and investigation of pathogens of public health importance. J Food Prot. 2026;89:100739. https://doi.org/10.1016/j.jfp.2026.100739
16. Ochieng C, Chen JC, Osita MP, Katz LS, Griswold T, Omballa V, et al. Molecular characterization of circulating *Salmonella* Typhi strains in an urban informal settlement in Kenya. PLoS Negl Trop Dis. 2022;16:e0010704. https://doi.org/10.1371/journal.pntd.0010704
17. Chen JC, Patel K, Smith PA, Vidyaprakash E, Snyder C, Tagg KA, et al. Reoccurring *Escherichia coli* O157:H7 strain linked to leafy greens–associated outbreaks, 2016–2019. Emerg Infect Dis. 2023;29:1895–9. https://doi.org/10.3201/eid2909.230069
18. Brown AC, Chen JC, Watkins LKF, Campbell D, Folster JP, Tate H, et al. CTX-M-65 extended-spectrum β-lactamase–producing *Salmonella enterica* serotype Infantis, United States. Emerg Infect Dis. 2018;24:2284–91. https://doi.org/10.3201/eid2412.180500
19. Marshall KE, Nguyen TA, Ablan M, Nichols MC, Robyn MP, Sundararaman P, et al. Investigations of possible multistate outbreaks of *Salmonella*, Shiga toxin–producing *Escherichia coli*, and *Listeria monocytogenes* infections—United States, 2016. MMWR Surveill Summ. 2020;69:1–14. https://doi.org/10.15585/mmwr.ss6906a1
20. Leeper MM, Tolar BM, Griswold T, Vidyaprakash E, Hise KB, Williams GM, et al. Evaluation of whole and core genome multilocus sequence typing allele schemes for *Salmonella enterica* outbreak detection in a national surveillance network, PulseNet USA. Front Microbiol. 2023;14:1254777. https://doi.org/10.3389/fmicb.2023.1254777
21. Centers for Disease Control and Prevention. About the National Antimicrobial Resistance Monitoring System (NARMS). 2024 [cited 2025 Apr 30]. https://www.cdc.gov/narms/about/index.html
22. Alikhan NF, Zhou Z, Sergeant MJ, Achtman M. A genomic overview of the population structure of *Salmonella.* PLoS Genet. 2018;14:e1007261. https://doi.org/10.1371/journal.pgen.1007261
23. Tolar B, Joseph LA, Schroeder MN, Stroika S, Ribot EM, Hise KB, et al. An overview of PulseNet USA databases. Foodborne Pathog Dis. 2019;16:457–62. https://doi.org/10.1089/fpd.2019.2637
24. Kislyuk AO, Katz LS, Agrawal S, Hagen MS, Conley AB, Jayaraman P, et al. A computational genomics pipeline for prokaryotic sequencing projects. Bioinformatics. 2010;26:1819–26. https://doi.org/10.1093/bioinformatics/btq284
25. Katz LS, Griswold T, Williams-Newkirk AJ, Wagner D, Petkau A, Sieffert C, et al. A comparative analysis of the Lyve-SET phylogenomics pipeline for genomic epidemiology of foodborne pathogens. Front Microbiol. 2017;8:375. https://doi.org/10.3389/fmicb.2017.00375
26. Bouckaert R, Vaughan TG, Barido-Sottani J, Duchêne S, Fourment M, Gavryushkina A, et al. BEAST 2.5: An advanced software platform for Bayesian evolutionary analysis. PLOS Comput Biol. 2019;15:e1006650. https://doi.org/10.1371/journal.pcbi.1006650
27. Katz LS, Griswold T, Morrison SS, Caravas JA, Zhang S, Bakker HC, et al. Mashtree: a rapid comparison of whole genome sequence files. J Open Source Softw. 2019;4:1762. https://doi.org/10.21105/joss.01762
28. Schwengers O, Jelonek L, Dieckmann MA, Beyvers S, Blom J, Goesmann A. Bakta: rapid and standardized annotation of bacterial genomes via alignment-free sequence identification. Microb Genom. 2021;7:000685. https://doi.org/10.1099/mgen.0.000685
29. Page AJ, Cummins CA, Hunt M, Wong VK, Reuter S, Holden MT, et al. Roary: rapid large-scale prokaryote pan genome analysis. Bioinformatics. 2015;31:3691–3. https://doi.org/10.1093/bioinformatics/btv421
30. Brynildsrud O, Bohlin J, Scheffer L, Eldholm V. Rapid scoring of genes in microbial pan-genome-wide association studies with Scoary. Genome Biol. 2016;17:238. https://doi.org/10.1186/s13059-016-1108-8
31. Kent WJ. BLAT—the BLAST-like alignment tool. Genome Res. 2002;12:656–64.
32. Itoh T, Mikami B, Hashimoto W, Murata K. Crystal structure of YihS in complex with D-mannose: structural annotation of *Escherichia coli* and *Salmonella enterica yihS*-encoded proteins to an aldose–ketose isomerase. J Mol Biol. 2008;377:1443–59. https://doi.org/10.1016/j.jmb.2008.01.090
33. Snow AJD, Burchill L, Sharma M, Davies GJ, Williams SJ. Sulfoglycolysis: catabolic pathways for metabolism of sulfoquinovose. Chem Soc Rev. 2021;50:13628–45. https://doi.org/10.1039/D1CS00846C
34. Marshall JM, Gunn JS. The O-antigen capsule of *Salmonella enterica* serovar Typhimurium facilitates serum resistance and surface expression of FliC. Infect Immun. 2015;83:3946–59. https://doi.org/10.1128/IAI.00634-15
35. Gibson DL, White AP, Snyder SD, Martin S, Heiss C, Azadi P, et al. *Salmonella* produces an O-antigen capsule regulated by AgfD and important for environmental persistence. J Bacteriol. 2006;188:7722–30. https://doi.org/10.1128/JB.00809-06
36. Miller EA, Elnekave E, Flores-Figueroa C, Johnson A, Kearney A, Munoz-Aguayo J, et al. Emergence of a novel *Salmonella enterica* serotype reading clonal group is linked to its expansion in commercial turkey production, resulting in unanticipated human illness in North America. MSphere. 2020;5:e00056-20. https://doi.org/10.1128/mSphere.00056-20
37. Behravesh CB, Brinson D, Hopkins BA, Gomez TM. Backyard poultry flocks and salmonellosis: a recurring, yet preventable public health challenge. Clin Infect Dis. 2014;58:1432–8. https://doi.org/10.1093/cid/ciu067

Address for correspondence: Jessica Chen, Centers for Disease Control and Prevention, 1600 Clifton Rd NE, Mailstop H23-7, Atlanta, GA 30329-4018, USA; email: jchen8@cdc.gov

Persistent *Bartonella quintana* Infection in Macaques at Primate Research Institute, Japan

Yoshiki Nomura, Yuka Fukudome, Akihiro Homma, Tadashi Sankai, Munehiro Okamoto, Hidenori Kabeya, Soichi Maruyama, Shingo Sato

Bartonella quintana, the causative agent of trench fever, is a louseborne bacterial pathogen. During 2016–2017, we investigated *B. quintana* infection in macaques housed at 2 primate research institutes in Japan. We isolated *B. quintana* from 3 wild-caught Japanese macaques, which had been introduced into 1 institute in 2009. The macaques had received periodic ivermectin treatment every 1–2 years to control blood-feeding arthropods. Whole-genome comparisons revealed that the 3 isolates exhibit higher homology to a Japanese macaque–derived strain than to rhesus macaque–derived or human-derived strains. In addition, in all 3 isolates, the *bepA* locus was absent; we classified the *trwL* locus as structural variant C, consistent with known Japanese macaque–derived strains. Our findings suggest that *B. quintana* bacteremia in the macaques might have persisted for 7–8 years in captivity, and that the bacterium was not accidentally transmitted to them from humans by reverse zoonosis.

The genus *Bartonella* belongs to the class Alphaproteobacteria, order Rhizobiales, and family Bartonellaceae and currently comprises 49 species and 3 subspecies (*1*). *Bartonella* bacteria are transmitted among their natural hosts by blood-feeding arthropods, including fleas, lice, keds, and sand flies, which excrete the bacteria in their feces (*2*). Mammals, such as bats, cats, deer, rabbits, and rodents serve as natural reservoirs for *Bartonella* species (*3*–*6*). Vascular endothelial cells are the initial cellular targets during *Bartonella* infection, after which the bacteria are released into the host bloodstream and adhere to erythrocytes. Adherence of *Bartonella* bacteria to erythrocytes is mediated through the Trw type IV secretion system, a key determinant of host specificity among *Bartonella* species (*7*). Once established within erythrocytes, *Bartonella* bacteria are thought to persist as long-term intraerythrocytic parasites.

B. quintana is the etiologic agent of trench fever, a human infectious disease transmitted by the human body louse. Trench fever was first documented among Allied and German troops during World War I and sporadically reemerged during World War II (*8*). In immunocompetent persons, the disease typically manifests as relapsing fever for several days accompanied by bacteremia, severe headache, dizziness, and persistent pain in the tibias. More severe manifestations, including bacillary angiomatosis and infective endocarditis, have been reported in immunocompromised patients, particularly those with human immunodeficiency virus infection (*8*). Epidemiologic studies have demonstrated that *B. quintana* infection occurs predominantly among homeless populations in urban settings in the Americas, Europe, and Asia (*9*–*13*). Consequently, *B. quintana* is regarded as a reemerging pathogen found in modern societies.

Although those symptoms are observed in trench fever patients, *B. quintana* infection typically manifests as an asymptomatic condition in which the bacteria harbor within erythrocytes (*14*). A previous study conducted in Marseille, France, showed that 10/71 ho meless persons tested positive for *B. quintana* bacteremia; 6 of those were afebrile (*10*). The remaining 4 patients exhibited prolonged bacteremia, persisting for 4–6 weeks. Asymptomatic carriers with *B. quintana* have been identified in other homeless populations in Marseille (*11*); 1 person exhibited chronic *B. quintana* bacteremia for 78 weeks, and 2 others remained bacteremic for 17 and 53 weeks. In the 1930s and 1940s, the first reports of chronic *B. quintana* bacteremia emerged among employees of laboratories

Author affiliations: Nihon University, Fujisawa, Japan (Y. Nomura, Y. Fukudome, A. Homma, H. Kabeya, S. Maruyama, S. Sato); Yokohama City University Graduate School of Medicine, Yokohama, Japan (T. Sankai); Kyoto University Primate Research Institute, Inuyama, Japan (M. Okamoto)

DOI: https://doi.org/10.3201/eid3210.260771

producing Weigl's type vaccines against typhus in Poland. As reported in the literature, *B. quintana* has been isolated from those employees for as long as 8 years (*15*). Subsequently, chronic bacteremia was demonstrated in experimental studies in the 1960s in which human volunteers were inoculated with the bacterium (*16*). From those findings, the duration of *B. quintana* bacteremia in the carriers is estimated to range from several weeks to ≈8 years.

Macaques inhabiting Asia have been identified as additional hosts for *B. quintana*. The first reported case of *B. quintana* infection in macaques was in a captive-bred cynomolgus macaque (*Macaca fascicularis*) imported into the United States from Vietnam (*17*). Subsequently, the bacterium was isolated from cynomolgus macaques and rhesus macaques (*M. mulatta*) born and reared at primate research centers in China (*18*,*19*) as well as from wild-caught Japanese macaques (*M. fuscata*) in Japan (*20*). In a previous study (*20*), no clinical signs were observed in the Japanese macaques positive for *B. quintana* infection, as seen in human patients with chronic *B. quintana* bacteremia; however, the duration of bacteremia in the macaques remains unknown.

A comparative genomic analysis of complete *B. quintana* genomes has revealed notable genomic differences among *B. quintana* strains from human, rhesus macaque, and Japanese macaque (*21*). Among those strains, the Japanese macaque–derived strains exhibit unique genomic features not observed in the others. Of note, strains MF1-1, MF3-1, MF10-1, MF11-1, MF19-1, and MF34-1 lack *bepA*, a gene known to confer anti-apoptotic effects in vascular endothelial cells. In addition, those strains harbor novel genomic structures within the *trwL* locus, which is implicated in erythrocyte adhesion. The human-derived strain Toulouse and the rhesus macaque–derived strain RM-11 share a conserved *trwL* structure, comprising *trwL1* to *trwL8*, in common. On the other hand, 3 distinct structural variants (A–C) have been identified among Japanese macaque strains; variant A consists of the gene order *trwL1–trwL5–trwL3–trwL7–trwL8*, variant B of *trwL1–trwLx–trwL5–trwL7–trwL8*, and variant C of *trwL1–trwLx–trwL5–trwL3–trwL7–trwL8*. The presence of *trwLx*, newly identified between *trwL1* and *trwL5* in variants B and C, highlights substantial genomic diversity within the *trwL* locus even among Japanese macaque strains (*21*).

Although the prevalence of *B. quintana* infection and the genomic properties of *Bartonella* in wild-caught Japanese macaques have been documented, its occurrence in experimental macaques controlled by human management in Japan remains unknown. In this study, we investigated *B. quintana* infection in macaque populations maintained at 2 primate research institutes in Japan. Furthermore, we performed whole-genome sequencing of *B. quintana* strains from the infected macaques to genetically characterize the *bepA* and *trwL* loci.

Materials and Methods

Blood Sampling

During 2016–2017, blood samples were aseptically collected from 92 wild-caught Japanese macaques and from 336 captive-bred macaques including 235 Japanese macaques and 101 rhesus macaques at the Primate Research Institute (PRI), Kyoto University (Inuyama, Japan). In 2017, additional blood samples were aseptically collected from 90 captive-bred cynomolgus macaques at the Tsukuba Primate Research Center (TPRC), National Institutes of Biomedical Innovation, Health, and Nutrition (Tsukuba, Japan) (Table 1). All blood samples were immediately stored at −70°C until further analysis.

The wild-caught Japanese macaques originated from several geographic locations and were transferred to PRI as follows: 8 macaques from Aichi Prefecture, in August 2003; 15 from Shizuoka Prefecture, in June 2008; 22 from Wakayama Prefecture in February 2009; and 47 from Osaka Prefecture during March 2008–June 2009. Upon arrival at the facility, all wild-caught macaques underwent deworming treatments with ivermectin. The ivermectin solution Ivermec Inj (Fujita Pharmaceutical Co., http://www3.fujita-pharm.co.jp) was administered subcutaneously at a dose of 0.1 mL/kg. In addition, both wild-caught and captive-bred macaques received periodic ivermectin treatments during routine physical examinations conducted at intervals of 1–2 years. At PRI, macaques were kept outdoors in social groups according to their geographic origin. In contrast, macaques at the TPRC were housed indoors in individual cages and received medicated baths with the organophosphorus ectoparasiticide Neguvon (Bayer, https://www.bayer.com) at 2-year intervals.

All animal procedures were conducted in accordance with applicable animal welfare regulations. Blood sampling at the PRI was performed under approved animal experimentation protocols (approval nos. 2016-158 and 2017-089). Blood samples from the TPRC were provided through the Nonhuman Primate Reagent and Resource Program under an institutional agreement for the distribution of research materials.

Table 1. Blood sample collection of macaques in study of persistent *Bartonella quintana* infection in macaques at primate research institute, Japan*

Institute	Year	No. samples			
		Japanese macaques, wild-caught	Japanese macaques, captive-bred	Rhesus macaques, captive-bred	Cynomolgus macaques, captive-bred
PRI	2016	22	151	NA	NA
	2017	70	84	101	NA
TPRC	2017	NA	NA	NA	90
Total		92	235	101†	90‡

*NA, not applicable; PRI, Primate Research Institute, Kyoto University, Kyoto, Japan; TPRC, Tsukuba Primate Research Center, National Institutes of Biomedical Innovation, Health and Nutrition.
†The macaques originated from China (n = 56) and India (n = 45).
‡The macaques originated from Indonesia (n = 30), the Philippines (n = 30), and Malaysia (n = 30).

Detection of *Bartonella* DNA from Macaque Blood Samples

To screen for *B. quintana* infection in the macaque populations, we performed nested PCR targeting the RNA polymerase β-subunit gene (*rpoB*) of the genus *Bartonella*. We designed the first PCR primers in this study, 1913f and 2357r, based on the *rpoB* sequences from *B. quintana* strains MF1-1 and RM-11. We designed the second PCR primers, 600f-m and 800r-m, with some modification based on original primers (*22*) (Table 2). The positive control was genomic DNA extracted from *B. quintana* strain MF1-1, whereas the negative control was genomic DNA extracted from a blood of a cynomolgus macaque classified as SPF grade. Conditions for the nested PCR were as follows: 2 minutes at 94°C followed by 35 cycles of 30 seconds at 94°C, 30 seconds at 54°C, and 1 minutes at 72°C, and a final extension of 2 minutes at 72°C. We purified the second PCR amplicon using a Wizard SV Gel and PCR Clean-Up System (Promega Corporation, https://www.promega.com), followed by direct DNA sequencing with the Genetic Analyzer models 3730xl (Thermo Fisher Scientific, https://www.thermofisher.com). We compared the obtained *rpoB* sequences with those in the International Nucleotide Sequence Database using the BLAST (https://blast.ncbi.nlm.nih.gov/Blast.cgi).

Isolation and Identification of *Bartonella* Bacteria from Macaque Bloods

We isolated *Bartonella* bacteria as described previously (*20*). In brief, we spread a 100 μL of freeze-thawed blood samples onto 5% rabbit blood chocolate agar plates and incubated them at 35°C under 5% CO_2 for up to 4 weeks. We tentatively identified colonies as *Bartonella* species on the basis of characteristic morphology (small, round, gray to cream-yellow colonies) and the requirement for a long culture period (>1 week). We calculated colony-forming units (CFUs) per milliliter of blood. We recovered 5 colonies from each culture-positive sample and subcultured them on fresh chocolate agar plates under the same conditions as the primary culture.

We extracted genomic DNA from each isolate using InstaGene Matrix (Bio-Rad Laboratories, https://www.bio-rad.com). We performed species identification by *Bartonella*-specific PCR targeting the *rpoB* (*23*), citrate synthase (*gltA*) (*24*), and 16S–23S rDNA intergenic transcribed spacer (ITS) regions (*25*). We used genomic DNA from *B. alsatica* strain IBS382^T as the positive control and nuclease-free distilled water as the negative control. We purified and sequenced PCR amplicons and compared them with the corresponding sequences derived from *B. quintana* strain MF1-1 (RefSeq [https://www.ncbi.nlm.nih.gov/refseq] accession no. NZ_AP019773).

Whole-Genome Sequencing Analysis

We extracted genomic DNAs from representative strains using DNeasy Blood and Tissue Kit (QIAGEN, https://www.qiagen.com). We prepared sequencing DNA libraries from the extracted genomic DNAs by using Illumina DNA Prep and IDT for Illumina DNA-RNA UD Indexes Set A, Tagmentation (Illumina, https://www.illumina.com). We sequenced the DNA libraries on a MiSeq platform using the MiSeq Reagent Nanokit version 2 (500 cycle) (Illumina). We quality-checked raw reads and assembled them using a de novo assembler program, the strategic K-mer extension for scrupulous assemblies (*26*), to generate contigs. We assessed de novo assembly qualities using Benchmarking Universal Single-Copy Orthologs (BUSCO) version 5.4.3 (*27*).

Table 2. Primer information for nested PCR targeting the *rpoB* gene used for study of persistent *Bartonella quintana* infection in macaques at primate research institute, Japan

Use application	Primer	Nucleotide sequences, 5′ → 3′	Amplicon size, bp	Reference
1st PCR	1913f	ACGCTGAGGGACGTTTTACAG	445	This study
	2357r	ACATGCACGAGAGGACGCTG		
2nd PCR	600f-m	GAAAATGATGATGCRAATCG	211	22
	800r-m	GATCTAAATCTTCTGTRGCACG		

We assessed nucleotide sequence identities at whole-genome levels by pairwise average nucleotide identity (ANI) (*28*) and digital DNA-DNA hybridization (dDDH) (*29*). We compared the assemblies of representative strains with strains MF1-1, RM-11, and Toulouse.

We confirmed the presence or absence of the *bepA* locus comprising *bepA1* and *bepA2* by *bepA*-specific PCR and subsequently validated by whole-genome sequencing data. We identified structural variants within the *trwL* locus by comparison with previously reported data (*21*).

Data Availability

We deposited raw reads of all the sequenced *B. quintana* strains in this study in the Sequence Read Archive of the DNA Data Bank of Japan. All are available under BioProject accession no. PRJDB40655.

Results

Prevalence of *B. quintana* in Macaque Populations at PRI and TPRC

We confirmed *Bartonella* infection by the *rpoB*-targeting PCR in 3 (3.3%) (sample IDs TB1, MN51, and MN57) of the 92 wild-caught Japanese macaques housed at PRI. All PCR amplicons showed an identical sequence to the *rpoB* of strain MF1-1. In contrast, we detected no *Bartonella* DNA in the captive-bred macaques at either the PRI or the TPRC.

We isolated *Bartonella* bacteria from the 3 PCR-positive Japanese macaques but not from any of the captive-bred macaques we examined. Bacteremia levels were 2.9×10^3 CFU/mL for TB1, 4.0×10^2 CFU/mL for MN51, and 3.0×10^3 CFU/mL for MN57. We recovered a total of 15 *Bartonella* isolates, 5 isolates per *Bartonella*-positive macaque. All the isolates showed 100% sequence identity for the *gltA* and *rpoB* and 99.9%–100% sequence identity for the ITS, compared with those of strain MF1-1.

According to management records at PRI, macaque TB1 was captured in Wakayama Prefecture and transferred to the PRI in February 2009. Similarly, macaques MN51 and MN57 were captured in Osaka Prefecture and transferred to PRI in June 2009. Blood samples for this study were collected in November 2016 from TB1 and in November 2017 from MN51 and MN57.

De Novo Assemblies Using Whole-Genome Sequences

We randomly selected 1 representative strain from each culture-positive macaque, yielding strains TB1-1, MN51-1, and MN57-1 for whole-genome sequencing analysis. The number of sequencing reads generated by the MiSeq platform ranged from 303,794 for strain MN51-1 to 1,065,204 for strain MN57-1 (Table 3). De novo assembly produced 43 contigs for strain TB1-1, 52 contigs for strain MN51-1, and 47 contigs for strain MN57-1; average genome coverage exceeded 46×. We estimated genome sizes of the 3 strains on the basis of the assembled contigs as ≈1.6 Mbp with guanine-cytosine contents of 38.8% for all strains. BUSCO scores of the 3 assembled contigs were 97.8–97.9.

We compared whole-genome sequences by ANI and dDDH. We compared the 3 representative strains with strain MF1-1 from a Japanese macaque, strain RM-11 from a rhesus macaque, and strain Toulouse from a human (Table 4). The ANI values obtained from the comparison of the representative 3 strains with strain MF1-1 were 99.8%, higher than those against strain RM-11 (99.4%) and strain Toulouse (98.3%). Similarly, the dDDH values obtained from comparing the representative strains with strain MF1-1 were 98.9%–99.0%, which exceeded those against strain RM-11 (95.3%–95.4%) and strain Toulouse (85.2%–85.3%).

Genomic Characterization of the *bepA* and *trwL* Loci

The *bepA* locus (1,612bp) was absent from all 3 representative strains (Figure 1), which we confirmed by the whole-genome sequencing data. Gene synteny analysis revealed that the *trwL* locus in the representative strains corresponded to structural variant C, characterized by the gene order of *trwL1*, *trwLx*, *trwL5*, *trwL3*, *trwL7*, and *trwL8* (Figure 2).

Discussion

In this study, we isolated *B. quintana* in a research colony of 3 Japanese macaques housed at the PRI, all

Table 3. Whole-genome sequencing data of 3 *Bartonella quintana* strains from wild-caught Japanese macaques kept in primate research institute in study of persistent *B. quintana* infection in macaques at primate research institute, Japan*

Strain	No. short reads	Total bases calculated from all reads	No. contigs	Coverage†	Estimated genome size, mbp	GC, %	BUSCO score, %
TB1-1	700,410	166,315,725	43	106-fold	1.6	38.8	97.8
MN51-1	303,794	73,058,573	52	46-fold	1.6	38.8	97.9
MN57-1	1,065,204	258,705,960	47	165-fold	1.6	38.8	97.9

*BUSCO, benchmarking universal single-copy orthologs; GC, guanine–cytosine contents.
†Indicates increase over average coverage.

Table 4. Whole-genome comparisons based on ANI and dDDH values in study of persistent *Bartonella quintana* infection at primate research institute, Japan*

Strain	Host	% ANI value/dDDH value		
		TB1-1	MN51-1	M
MF1-1	Japanese macaque	99.8/99.0	99.8/98.9	9
RM-11	Rhesus macaque	99.4/95.4	99.4/95.3	9
Toulouse	Human	98.3/85.2	98.3/85.3	9

*ANI, pairwise average nucleotide identity; dDDH, digital DNA-DNA hybridization.

of which originated from wild-caught populations. The bacteremia levels (400–3,000 CFU/mL) were comparable to those previously reported in Japanese macaques (*20*). In contrast, no *Bartonella* infection was detected in any of the captive-bred Japanese, cynomolgus, or rhesus macaques housed at either of the 2 primate facilities. Although both wild-caught and captive-bred macaques at the 2 facilities received periodic antiparasitic treatments, the *B. quintana*–positive Japanese macaques might have been infested with some kind of blood-feeding arthropods, such as monkey lice (*Pedicinus* sp.) (*30*), before they were captured in their habitats. We found monkey lice on wild-caught Japanese macaques in Kanagawa Prefecture, Japan, during 2018–2022 and successfully detected *B. quintana* DNA from the lice (data not shown). Because the *B. quintana*–positive Japanese macaques were introduced into the PRI in 2009 and tested positive for *B. quintana* infection in 2016–2017, we presumed that they maintained persistent *B. quintana* infection for up to 8 years. Similarly, in 1949, *B. quintana* bacteremia was documented as persisting for up to 8 years in trench fever patients (*15*). On the basis of all those findings, we concluded that *B. quintana* can establish long-term persistent infections in both humans and nonhuman primates. Such long-term, asymptomatic *B. quintana* bacteremia demonstrates that infected individuals can act as chronic carriers of the pathogen without manifesting distinct clinical symptoms. However, we noted that chronic bacteremic states in humans might eventually progress to severe complications, such as endocarditis (*31*).

We performed subsequent whole-genome sequencing to genetically characterize the 3 representative strains TB1-1, MN51-1, and MN57-1 from the *B. quintana*–positive Japanese macaques. We evaluated genome assembly quality using BUSCO analysis, which yielded completeness scores >95% for all strains (*27*), supporting the reliability of the de novo assemblies. In addition, the estimated genome sizes and guanine-cytosine contents were highly consistent with those reported for other known *B. quintana* strains (*21*,*32*), indicating that the assembled genomes were suitable for downstream comparative analyses. Comparisons at the whole-genome level using ANI and dDDH revealed that the 3 strains exhibit higher homology to strain MF1-1 from a Japanese macaque (*21*) than to strain RM-11 from a rhesus macaque and strain Toulouse from a human. Of note, in all 3 strains, the

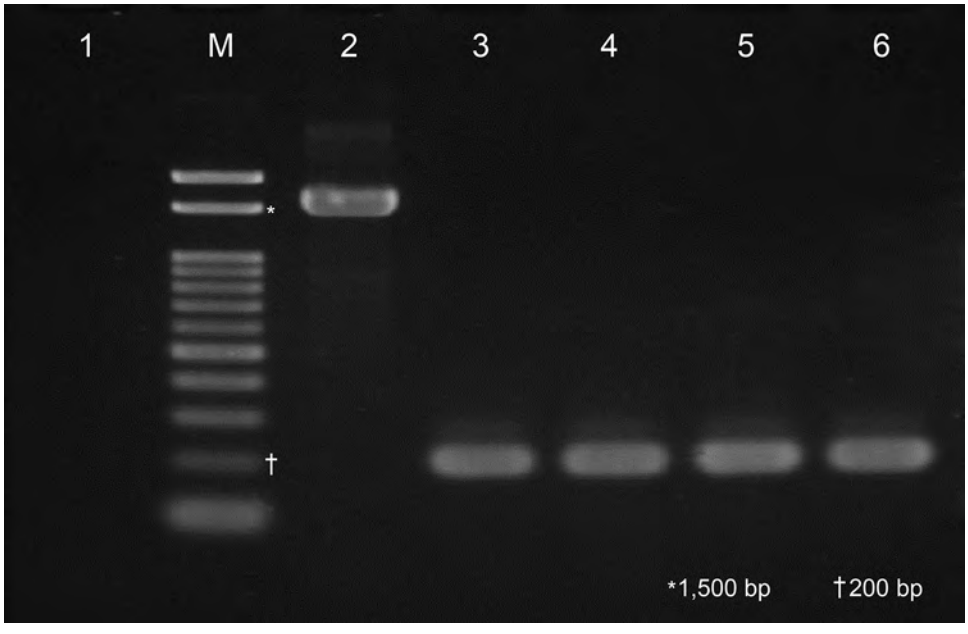

Figure 1. Electrophoretic analysis of *bepA*-specific PCR amplicons in study of persistent *Bartonella quintana* infection in macaques at primate research institute, Japan. Lane M, 0.1–2 kb DNA size marker; lane 1, nuclease-free water (negative control); lane 2, *Bartonella quintana* strain Fuller^T (positive control); lane 3, strain MF1-1; lane 4, strain TB1-1; lane 5, strain MN51-1; lane 6, strain MN57-1. The expected amplicon size for the *bepA* locus is 1,612 bp, as observed in the positive control (lane 2). As with strain MF1-1 (lane 3), amplicon size of strains TB1-1, MN51-1, and MN57-1 (lanes 4–6) was ≈200 bp, indicating the absence of the *bepA* locus in the chromosome.

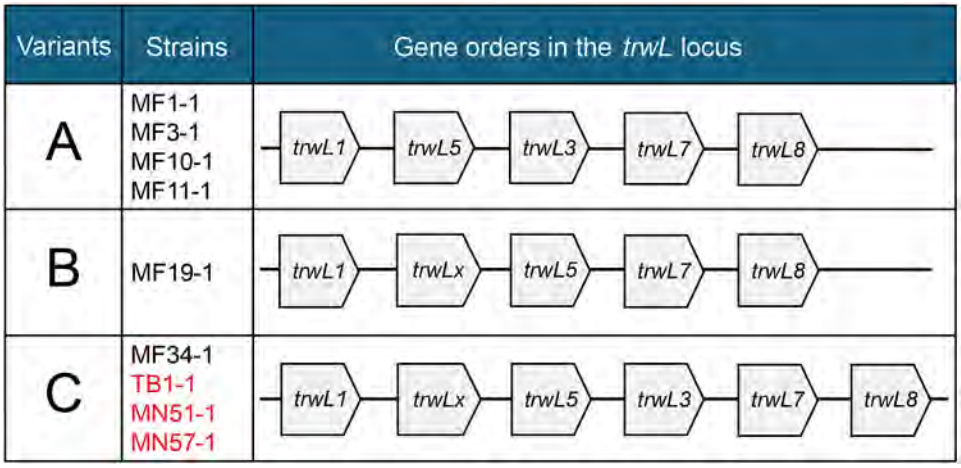

Figure 2. Structural variants of the *trwL* locus among *Bartonella quintana* strains from Japanese macaques in study at primate research institute, Japan. We reviewed 3 structural variants (A–C) of the *trwL* locus as previously described (*21*). Red text indicates representative strains analyzed in this study, which were classified as variant C.

bepA locus was absent, and the *trwL* locus was classified as structural variant C; we had demonstrated previously that both loci seem to be unique to Japanese macaque–derived strains (*21*). Those findings suggest that the *B. quintana*–positive Japanese macaques did not accidentally acquire the bacterium from humans within this facility, ruling out the likelihood that reverse zoonosis caused the infections. Future surveillance of *B. quintana* infection in other nonhuman primates, such as apes and New World monkeys, will increase understanding of the host range of the bacterium in nature.

Studying infection state in the same animals over time would be helpful to further confirm long-term persistent infection. However, the PRI ethics guidelines restrict blood sampling from the same macaques to once every 2 years. Furthermore, the macaque TB1 died in June 2018 from an accident within the PRI enclosure, which prevented the collection of consecutive blood samples. Although we attempted to collect additional blood samples from macaques MN51 and MN57 since November 2019, experiments at PRI were suspended for several years during the COVID-19 pandemic, making subsequent medical research applications exceedingly challenging. To address those issues, we would need to conduct infection experiments for *Macaca* spp. monkeys with Japanese macaque–derived strains in another primate research facility.

In conclusion, we identified *B. quintana* bacteremia in 3 wild-caught Japanese macaques housed at PRI and noted evidence suggesting persistent infection for up to 8 years after capture. Given that the *trw* operon, particularly the *trwL* and *trwJ* loci, plays a crucial role in erythrocyte adhesion (*7*), further investigation is warranted to determine whether structural variations in *trwL* influence the ability of macaque-derived *B. quintana* strains to infect human erythrocytes. Such studies would be particularly relevant from One Health perspective. Our findings highlight the capacity of *B. quintana* bacteria to establish long-term infection in Japanese macaques and support previous documentation of prolonged bacteremia in humans.

This work was supported in part by the Japan Society for the Promotion of Science Grant-in-Aid for Young Scientists (B) (grant no. 17K15373) and the Cooperative Research Program of Primate Research Institute, Kyoto University (2016 to 2018).

About the Author

Mr. Nomura is a PhD candidate graduate student in the Department of Veterinary Medicine, College of Bioresource Sciences, Nihon University, Japan. His primary research interests are the epidemiology, elucidation of the virulence mechanisms, and prevention of bacterial zoonoses.

References

1. List of prokaryotic names with standing in nomenclature. Genus *Bartonella* [cited 2026 Jan 11]. https://lpsn.dsmz.de/genus/Bartonella
2. Tsai YL, Chang CC, Chuang ST, Chomel BB. *Bartonella* species and their ectoparasites: selective host adaptation or strain selection between the vector and the mammalian host? Comp Immunol Microbiol Infect Dis. 2011;34:299–314. https://doi.org/10.1016/j.cimid.2011.04.005
3. Qiu Y, Kajihara M, Nakao R, Mulenga E, Harima H, Hang'ombe BM, et al. Isolation of Candidatus *Bartonella rousetti* and other bat-associated *Bartonellae* from bats and their flies in Zambia. Pathogens. 2020;9:469. https://doi.org/10.3390/pathogens9060469
4. Ciceroni L, Fabbi M, Ciarrocchi S, Pinto A, Ciervo A, Kasten RW, et al. Characterization of the first *Bartonella henselae* strain isolated from a cat in Italy. Comp Immunol Microbiol Infect Dis. 2002;25:217–28. https://doi.org/10.1016/S0147-9571(02)00013-9
5. Sato S, Kabeya H, Yamazaki M, Takeno S, Suzuki K, Kobayashi S, et al. Prevalence and genetic diversity of *Bartonella* species in sika deer (*Cervus nippon*) in Japan. Comp Immunol Microbiol Infect Dis. 2012;35:575–81.

https://doi.org/10.1016/j.cimid.2012.07.001
6. Gonçalves-Oliveira J, Gutierrez R, Schlesener CL, Jaffe DA, Aguilar-Setién A, Boulouis HJ, et al. Genomic characterization of three novel *Bartonella* strains in a rodent and two bat species from Mexico. Microorganisms. 2023; 11:340. https://doi.org/10.3390/microorganisms11020340
7. Deng H, Pang Q, Zhao B, Vayssier-Taussat M. Molecular mechanisms of *Bartonella* and mammalian erythrocyte interactions: a review. Front Cell Infect Microbiol. 2018;8:431. https://doi.org/10.3389/fcimb.2018.00431
8. Maurin M, Raoult D. *Bartonella* (*Rochalimaea*) *quintana* infections. Clin Microbiol Rev. 1996;9:273–92. https://doi.org/10.1128/CMR.9.3.273
9. Spach DH, Kanter AS, Dougherty MJ, Larson AM, Coyle MB, Brenner DJ, et al. *Bartonella* (*Rochalimaea*) *quintana* bacteremia in inner-city patients with chronic alcoholism. N Engl J Med. 1995;332:424–8. https://doi.org/10.1056/NEJM199502163320703
10. Brouqui P, Lascola B, Roux V, Raoult D. Chronic *Bartonella quintana* bacteremia in homeless patients. N Engl J Med. 1999;340:184–9. https://doi.org/10.1056/NEJM199901213400303
11. Foucault C, Barrau K, Brouqui P, Raoult D. *Bartonella quintana* bacteremia among homeless people. Clin Infect Dis. 2002;35:684–9. https://doi.org/10.1086/342065
12. Capo C, Amirayan-Chevillard N, Brouqui P, Raoult D, Mege JL. *Bartonella quintana* bacteremia and overproduction of interleukin-10: model of bacterial persistence in homeless people. J Infect Dis. 2003;187:837–44. https://doi.org/10.1086/368384
13. Sasaki T, Adachi T, Itoh K, Matsuoka M, Yamagishi T, Hirao M, et al. Detection of *Bartonella quintana* infection among the homeless population in Tokyo, Japan, from 2013–2015. Jpn J Infect Dis. 2021;74:411–5. https://doi.org/10.7883/yoken.JJID.2020.505
14. Rolain JM, Foucault C, Guieu R, La Scola B, Brouqui P, Raoult D. *Bartonella quintana* in human erythrocytes. Lancet. 2002;360:226–8. https://doi.org/10.1016/S0140-6736(02)09462-X
15. Kostrzewski J. The epidemiology of trench fever [in Polish]. Bull Int Acad Pol Sci Let Cl Med. 1949;7:233–63.
16. Vinson JW, Varela G, Molina-Pasquel C. Trench fever. Am J Trop Med Hyg. 1969;18:713–22. https://doi.org/10.4269/ajtmh.1969.18.713
17. O'Rourke LG, Pitulle C, Hegarty BC, Kraycirik S, Killary KA, Grosenstein P, et al. *Bartonella quintana* in cynomolgus monkey (*Macaca fascicularis*). Emerg Infect Dis. 2005;11:1931–4. https://doi.org/10.3201/eid1112.030045
18. Huang R, Liu Q, Li G, Li D, Song X, Birtles RJ, et al. *Bartonella quintana* infections in captive monkeys, China. Emerg Infect Dis. 2011;17:1707–9. https://doi.org/10.3201/eid1709.110133
19. Li H, Bai JY, Wang LY, Zeng L, Shi YS, Qiu ZL, et al. Genetic diversity of *Bartonella quintana* in macaques suggests zoonotic origin of trench fever. Mol Ecol. 2013;22:2118–27. https://doi.org/10.1111/mec.12261
20. Sato S, Kabeya H, Yoshino A, Sekine W, Suzuki K, Tamate HB, et al. Japanese macaques (*Macaca fuscata*) as natural reservoir of *Bartonella quintana.* Emerg Infect Dis. 2015;21:2168–70. https://doi.org/10.3201/eid2112.150632
21. Sato S, Nishioka E, Kabeya H, Maruyama S. Genomic properties of a *Bartonella quintana* strain from Japanese macaque (*Macaca fuscata*) revealed by genome comparison with human and rhesus macaque strains. Sci Rep. 2024;14:10941. https://doi.org/10.1038/s41598-024-61782-0
22. Gutiérrez R, Morick D, Gross I, Winkler R, Abdeen Z, Harrus S. Bartonellae in domestic and stray cats from Israel: comparison of bacterial cultures and high-resolution melt real-time PCR as diagnostic methods. Vector Borne Zoonotic Dis. 2013;13:857–64. https://doi.org/10.1089/vbz.2013.1308
23. Kabeya H, Inoue K, Izumi Y, Morita T, Imai S, Maruyama S. *Bartonella* species in wild rodents and fleas from them in Japan. J Vet Med Sci. 2011;73:1561–7. https://doi.org/10.1292/jvms.11-0134
24. Norman AF, Regnery R, Jameson P, Greene C, Krause DC. Differentiation of *Bartonella*-like isolates at the species level by PCR-restriction fragment length polymorphism in the citrate synthase gene. J Clin Microbiol. 1995;33:1797–803. https://doi.org/10.1128/jcm.33.7.1797-1803.1995
25. Roux V, Raoult D. The 16S-23S rRNA intergenic spacer region of *Bartonella* (Rochalimaea) species is longer than usually described in other bacteria. Gene. 1995;156:107–11. https://doi.org/10.1016/0378-1119(94)00919-J
26. Souvorov A, Agarwala R, Lipman DJ. SKESA: strategic k-mer extension for scrupulous assemblies. Genome Biol. 2018;19:153. https://doi.org/10.1186/s13059-018-1540-z
27. Simão FA, Waterhouse RM, Ioannidis P, Kriventseva EV, Zdobnov EM; M Simão FA. BUSCO: assessing genome assembly and annotation completeness with single-copy orthologs. Bioinformatics. 2015;31:3210–2. https://doi.org/10.1093/bioinformatics/btv351
28. Richter M, Rosselló-Móra R, Oliver Glöckner F, Peplies J. JSpeciesWS: a web server for prokaryotic species circumscription based on pairwise genome comparison. Bioinformatics. 2016;32:929–31. https://doi.org/10.1093/bioinformatics/btv681
29. Meier-Kolthoff JP, Carbasse JS, Peinado-Olarte RL, Göker M. TYGS and LPSN: a database tandem for fast and reliable genome-based classification and nomenclature of prokaryotes. Nucleic Acids Res. 2022;50(D1):D801–7. https://doi.org/10.1093/nar/gkab902
30. Li H, Liu W, Zhang GZ, Sun ZZ, Bai JY, Jiang BG, et al. Transmission and maintenance cycle of *Bartonella quintana* among rhesus macaques, China. Emerg Infect Dis. 2013;19:297–300. https://doi.org/10.3201/eid1902.120816
31. Okaro U, Addisu A, Casanas B, Anderson B. *Bartonella* species, an emerging cause of blood-culture-negative endocarditis. Clin Microbiol Rev. 2017;30:709–46. https://doi.org/10.1128/CMR.00013-17
32. Alsmark CM, Frank AC, Karlberg EO, Legault BA, Ardell DH, Canbäck B, et al. The louse-borne human pathogen *Bartonella quintana* is a genomic derivative of the zoonotic agent *Bartonella henselae.* Proc Natl Acad Sci U S A. 2004;101:9716–21. https://doi.org/10.1073/pnas.0305659101

Address for correspondence: Shingo Sato, Nihon University—Veterinary Medicine,1866 Kameino, Fujisawa Kanagawa 252-0880, Japan; email: sato.shingo@nihon-u.ac.jp

Detection of Influenza D Virus using Reverse Transcription Loop-Mediated Isothermal Amplification

Carlos Abelardo dos Santos, Jialu Li, Pauline M. van Diemen, Andrew McMahon, Benjamin C. Mollett, Andrew M. Ramsay, Meshach M. Maina, Joe James, Helen E. Everett, Janet M. Daly, Nicole C. Robb

The *Orthomyxoviridae* family includes influenza D virus (IDV), an emerging pathogen primarily affecting cattle and swine; there is evidence of cross-species transmission and potential zoonotic risk. Although active human infections have yet to be confirmed, high seroprevalence in cattle-exposed populations highlights the need for continued surveillance. We developed and validated a rapid, field-deployable reverse transcription loop-mediated isothermal amplification assay for IDV detection; specificity was 99.2% and sensitivity ranged from 95.6% (cycle quantification <30) to 81.8% (cycle quantification <40). This method offers a cost-effective, accessible alternative to quantitative reverse transcription PCR, enabling improved monitoring of IDV and reinforcing preparedness for emerging influenza threats.

The family *Orthomyxoviridae* consists of 9 genera, 4 of which are influenza viruses. Influenza A virus (IAV) and influenza B virus (IBV) are the main viruses responsible for human seasonal influenza epidemics; IAV poses a pandemic threat linked to bidirectional transmission between animals and humans. Both IAV and IBV can cause severe illness in humans, whereas influenza C virus (ICV) infection is associated with milder upper respiratory tract symptoms, most commonly in children < 2 years of age. Influenza D virus (IDV) was first discovered in 2011 in pigs in Oklahoma, USA, and was subsequently found in cattle, which are now considered the main livestock reservoir. In cattle, IDV infection is associated with bovine respiratory disease as the primary viral infection, which might predispose cattle to opportunistic secondary bacterial infections (*1*).

Although most IDV occurrences have been in swine and cattle, IDV antibodies have also been found in other domesticated animals, such as sheep (*2*), goats (*3*), horses (*3*), wild boars (*4*), and camelids (*5*), suggesting that cross-species transmission might occur. Mice, ferrets, and guinea pigs have also been found to be susceptible to experimental viral infection (*6*). Similarly to ICV, IDV has been shown to bind to sialic acid receptors on the cell surface of the host, specifically 9-O-acetylated sialic acid receptors (*7*). Those receptors are found throughout the respiratory tract in cattle, as well as in the nasal and pharyngeal epithelium of pigs, sheep, goats, and horses, suggestive of a potentially wide host range (*8*).

IDV has been shown to propagate effectively in various human cell types (*9*), but no active infection in humans has been reported to date; although IDV was detected in a nasal wash sample from a swine farm worker in Malaysia, no infectious virions were retrieved (*10*). The presence of IDV antibodies has been the primary method of inferring past exposure to IDV in humans. A 2011 study (*11*) found a 1.3% seroprevalence of IDV antibodies in the general human population in the United States and Canada. Another study in Italy discovered that the seroprevalence of IDV in the general human population increased from 5% in 2005 to 46% in 2014 (*12*). In human cohorts occupationally exposed to cattle, the prevalence of IDV antibodies reached as high as 97% (*13*), reflecting a similar prevalence of antibodies in cattle (*14*).

Although IDV infection has not been observed to induce severe disease in humans, monitoring its

Author affiliations: Warwick Medical School, University of Warwick, Coventry, UK (C.A. dos Santos, J. Li, N.C. Robb); Animal and Plant Health Agency Weybridge, Addlestone, UK (P.M. van Diemen, B.C. Mollett, A.M. Ramsay, J. James, H.E. Everett); School of Life Sciences, University of Warwick, Coventry (A. McMahon); One Virology, Wolfson Centre for Global Virus Research, University of Nottingham, Nottingham, UK (M.M. Maina, J.M. Daly)

DOI: https://doi.org/10.3201/eid3210.260499

prevalence remains crucial because of the ability of influenza viruses to evolve and transmit across species barriers. Antibody detection serves as a robust epidemiologic tool on a population scale (*15*), but quantitative reverse transcription PCR (qRT-PCR) is the standard for detecting viral RNA (and thus active infection) at an individual level. However, the need for specialized laboratories and trained personnel to process and analyze samples, coupled with high costs and limited utility for field-based testing, poses a substantial challenge to high throughput. Reverse transcription loop-mediated isothermal amplification (RT-LAMP) is a rapid, highly sensitive, and cost-effective molecular diagnostic tool that has emerged as a potential alternative to PCR-based methods (*16*). RT-LAMP can be performed at a constant temperature and return a result in <1 hour, making it well suited for point-of-sample testing. The success of RT-LAMP during the COVID-19 pandemic underscores its potential as a valuable tool in our ongoing efforts to combat infectious diseases (*17*). We report an RT-LAMP assay specifically designed to detect IDV with particular application for field-setting diagnostic assays in resource-poor settings.

Materials and Methods

Study Samples

We tested a total of 28 experimentally spiked samples and 46 isolated RNA samples from swine and cattle using the RT-LAMP assay. The animal samples consisted of nasal swab and respiratory tissue samples (lung, viscera) from pigs and cattle with signs of respiratory disease (cough and/or dyspnea) submitted through the passive Animal and Plant Health Agency surveillance networks and contained a mixture of samples positive or negative for IAV or IDV.

Virus Isolates

We propagated the isolates D/swine/Oklahoma/1334/2011 (*11*) in embryonated chicken eggs and D/bovine/France/5920/2014 (*18*,*19*) on hRT18G cells. Both strains are well characterized and produced with a minimum number of passages to avoid loss of strain fidelity. D/swine/England/126471/2023 is a more recent isolate and was propagated on ST cells (*20*).

RNA Extraction

We carried out preisolation steps depending on the nature of the sample. For viral isolates, we lysed 20 µL of the cell supernatant with 350 µL of Monarch StabiLyse DNA/RNA Buffer (New England Biolabs, https://www.neb.com) and carried out the extraction according to the manufacturer's protocol. We also extracted RNA from a swine lung fragment by excising a 10 mg tissue fragment and lysing it in 200 µL of StabiLyse DNA/RNA Buffer and 200 µL of nuclease-free water (IDT, https://eu.idtdna.com) in a FastPrep-24 bead beater homogenizer (MP Biomedicals, https://www.mpbio.com) for ≈10 minutes. We extracted total RNA from each preparation using the Monarch Spin RNA Isolation Kit (New England Biolabs), according to the manufacturer's instructions. We extracted positive (IDV cultures) and negative (with nuclease-free water) controls with every batch and tested them by qRT-PCR to guarantee extraction efficiency and the absence of cross-contamination during extraction.

qRT-PCR for IDV

The qRT-PCR primers and probes for IDV detection used in this study were originally published by Faccini et al. (*21*). We performed the reactions in a 384-well Quant Studio 5 Real-Time PCR System (Thermo Fisher Scientific, https://www.thermofisher.com) using the Luna Universal Probe One-Step RT-qPCR Kit (New England Biolabs), according to the manufacturer's instructions. The primers and probe target the polymerase basic (PB) 1 gene (from position 1215 to 1323; GenBank accession no. JQ922306); we designed a PB1 gBlock to use as control containing the nucleotides from position 500 to 1,500. The gBlock was synthesized by Integrated DNA Technologies (https://www.idtdna.com). We eluted the gBlock according to the manufacturer's protocol and confirmed the concentration by UV absorbance using a NanoDrop spectrophotometer (Thermo Fisher Scientific). We used serial dilutions ranging from 10^6 to 10 copies of the IDV gBlock to generate a standard curve, which we used to quantify the RNA material from isolates, mock samples, and samples.

RT-LAMP Primer Design

We designed primers targeting the 2 most conserved genes in IDV, PB1 and PB2 (*18*,*22*) (Appendix Table 1). We downloaded all available sequences from the National Center for Biotechnology Information (NCBI) Nucleotide database (https://www.ncbi.nlm.nih.gov/nucleotide) and generated alignments using the MAFFT multiple sequence alignment tool (https://mafft.cbrc.jp/alignment/software). We designed the primers for RT-LAMP against PB1 and PB2 using the PrimerExplorer version 5 software (https://primerexplorer.eiken.co.jp/lampv5e/index.html). To improve coverage and guarantee amplification of the maximum number of sequences, we set the consensus threshold to 90%. We marked all

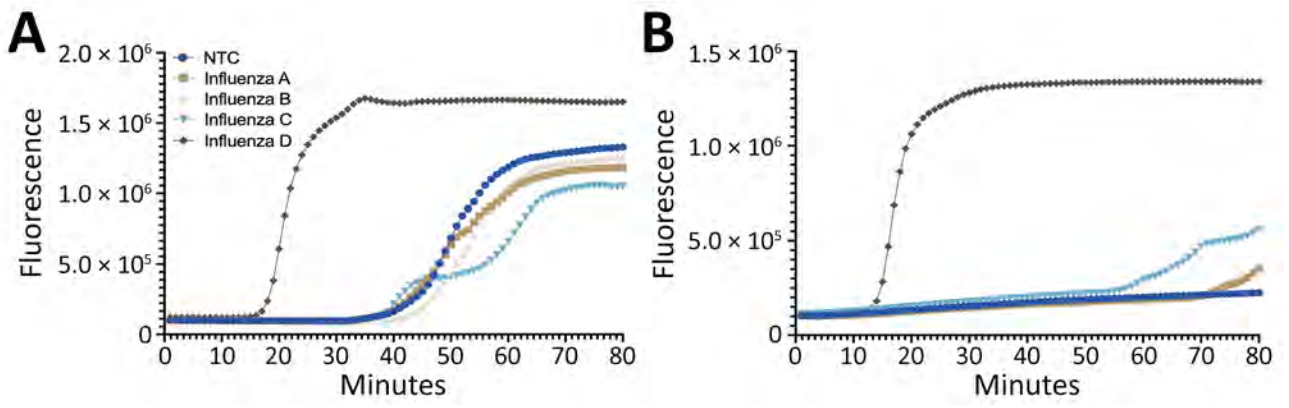

Figure 1. Mean amplification curves from reverse transcription loop-mediated isothermal amplification (RT-LAMP) reaction triplicates showing the onset of specific and nonspecific signal over time in study of isothermal detection of influenza D virus (IDV) using RT-LAMP. Graphs indicate results of RT-LAMP on gBlocks containing the influenza A, B, C, and D virus polymer basic protein 2 gene sequences. All gBlocks were tested at a concentration of 10^6 copies per µL of input. A) Reactions using the primers in IDV_set1. The amplification of the IDV gBlock positive control started within the first 20 minutes, whereas influenza A, influenza B, and influenza C gBlocks and the NTC (water) produced false-positive signals after only 35 minutes of incubation. B) Reactions using the primers in IDV_set2. The amplification of the IDV gBlock positive control started within the first 15 minutes, whereas influenza A, influenza B, and influenza C gBlocks and the NTC produced delayed false-positive signals after 65 minutes of incubation. NTC, nontemplate control.

mutated positions in the primer design software and created the primers using the common design option, which enables primers to be designed targeting mutated regions if the position of the variable nucleotide within the primer is unlikely to affect amplification efficiency. We filtered primers by end stability and set the maximum ΔG for the 3′ end of F3/B3, F2/B2, LF/LB and the maximum ΔG for the 5′ end of F1c/B1c to be ≤–4.00 kcal/mol. We also checked primers for the presence of stable hairpins, self-dimers, and homodimers using IDT's Oligo Analyzer tool (https://eu.idtdna.com/pages/tools/oligoanalyzer). We did not synthesize sets containing primers with stable hairpins or dimers. The primers FIP and BIP consist of 2 different regions (F1c/F2 for FIP and B1c/B2 for BIP), which mediate the creation of the loops characteristic of LAMP. Target recognition by LAMP primers creates an ever-growing concatemer containing single-stranded loops that also serves as a target for continuous amplification. To decrease local Tm in the loops and lower

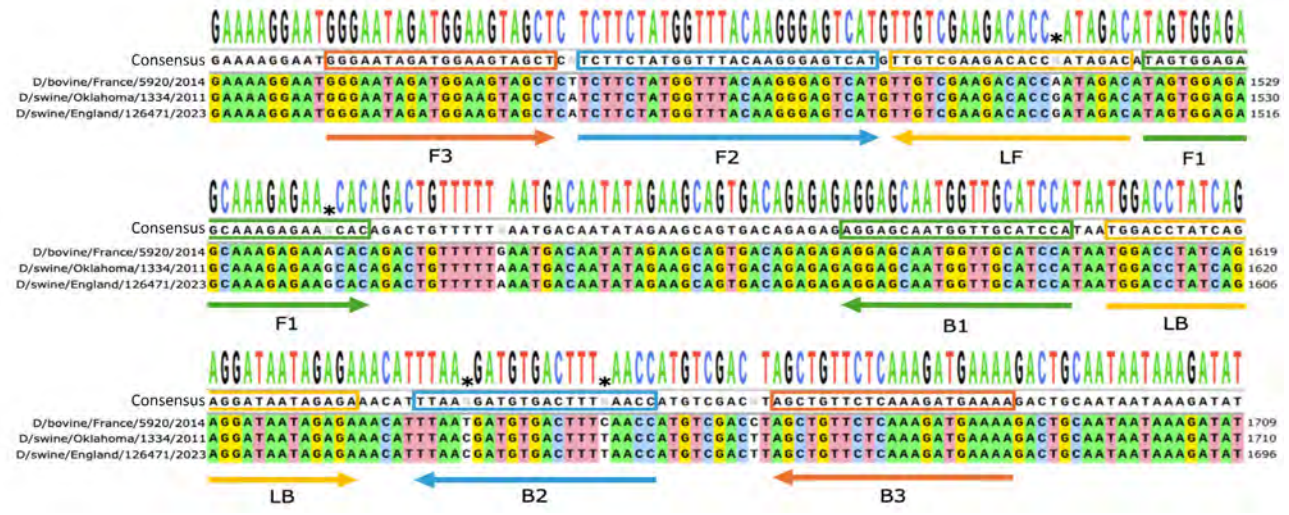

Figure 2. Reverse transcription loop-mediated isothermal amplification (RT-LAMP) primers targeting the influenza D virus polymer basic protein 2 gene in study of isothermal detection of influenza D virus. All available influenza D virus polymer basic protein 2 gene sequences in the National Center for Biotechnology Information Nucleotide database (https://www.ncbi.nlm.nih.gov/nucleotide) were aligned and mutations were annotated. To improve coverage, primers were synthesized with degenerate nucleotides in positions with heterogeneity in the sequences. The consensus sequence and sequences of the 3 isolates (D/bovine/France/5920/2014, D/swine/Oklahoma/1334/2011, and D/swine/England/126471/2023) are shown for comparison. Primer target sequences are presented within the boxes, and the direction of binding is represented by the arrows.

the chances of undesired secondary structures that could hinder amplification, we inserted T linkers (23) between the F1c/F2 and B1c/B2 regions in the FIP/BIP primers. We also aligned primers against other influenza viruses to guarantee specificity for influenza D and followed that with a BLAST analysis (https://blast.ncbi.nlm.nih.gov).

Colorimetric One-Step RT-LAMP Assay for IDV

We prepared all reactions as a total volume of 20 µL, each containing a final concentration of 1X WarmStart Colorimetric LAMP Master Mix with UDG (Uracil DNA Glycosylate) (New England Biolabs), 1× primer mix (containing 0.2 µM F3/B3, 1.6 µM FIP/BIP and 0.8 µM LF/LB primers), 10% (vol/vol) of target, and nuclease-free water (Integrated DNA Technologies). For real-time analysis, we added 1 µM of SYTO9 (Thermo Fisher Scientific) to the reaction mixture. To optimize the assay, we incubated the reactions in a QuantStudio 3 real-time thermocycler (Thermo Fisher Scientific) at 65°C for 80 cycles, each cycle consisting of 45 seconds of incubation followed by fluorescence read in the FAM channel for 15 seconds. We incubated subsequent reactions in a conventional T-100 PCR instrument (Bio-Rad Laboratories, https://www.bio-rad.com) at 65°C for 60 minutes. Unless otherwise specified, we performed all reactions in triplicate.

Sensitivity and Specificity of IDV Assay

To assess whether we could differentiate IDV from closely related viruses, we tested the RT-LAMP assay for IDV against gBlocks containing the PB2 target gene segment of all other influenza strains. We used the gBlock containing the complete PB2 gene for IDV (D/swine/Oklahoma/1334/2011) as a positive control in our reactions and used gBlocks containing the complete PB2 gene for IAV (A/Puerto Rico/8/1934), IBV (B/Lee/1940), and ICV (C/Ann Arbor/1/50) as negative controls. We carried out reactions using either 2 µL of the respective gBlock controls or the equivalent amount of nuclease-free water as a nontemplate control (NTC). All gBlocks were tested at a concentration of 10^6 copies per µL for 1 hour. We analyzed results in triplicate on the basis of the colorimetric change in the reaction from pink (negative) to yellow (positive).

To determine the sensitivity of the assay, we mixed equimolar amounts of extracted RNA from each of the 3 viral isolates (D/bovine/France/5920/2014, D/swine/Oklahoma/1334/2011, and D/swine/England/126471/2023), which had been quantified by qRT-PCR using the assay described previously. We serially-diluted the RNA mix and verified the concentrations by qRT-PCR. We tested the serially diluted RNA mix by RT-LAMP in octuplicate and fitted a Probit regression curve (dose-response plot) using SPSS Statistics 29.0.2.0 (IBM, https://www.ibm.com). We defined the limit of detection to be equal to the minimum number of copies detected in ≥95% of the reactions.

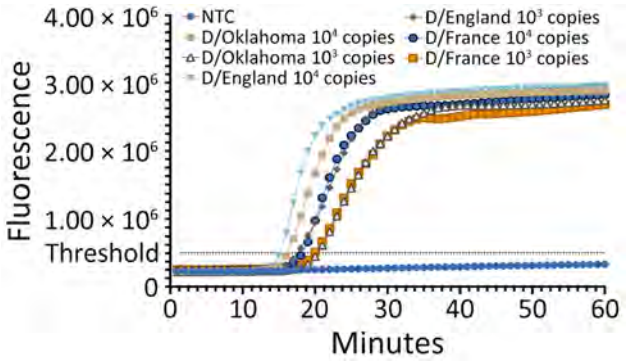

Figure 3. Mean amplification curves from reverse transcription loop-mediated isothermal amplification reaction triplicates showing the onset of amplification in study of isothermal detection of influenza D virus. All influenza D virus isolate RNAs at 10^4 and 10^3 copies per µL amplified within the first 20 minutes regardless of the lineage. NTC, nontemplate control.

We analyzed the amplification products on a 2% agarose gel in 1X TBE (Tris-Borate-EDTA) Buffer using SYBR Safe DNA Gel Stain (Thermo Fisher Scientific) and the Quick-Load 100 bp DNA Ladder (New England Biolabs). We ran the gel at 100V for 60 minutes and acquired images with a ChemiDoc Imaging System (BioRad).

Evaluation Using Spiked and Field-Collected Animal Samples

To assess the performance of the test in a more complex sample matrix, we prepared 28 spiked samples by mixing total purified RNA extracted from swine lung tissue with variable amounts of viral RNA from the 3 virus isolates used in this study. We quantified samples by qRT-PCR and tested by RT-LAMP. We analyzed results by the color change from pink (negative) to yellow (positive) in the reaction after 60 minutes of incubation. We assessed the specificity and sensitivity of the RT-LAMP assay for detecting IDV by comparing its results with those of the qRT-PCR using the free online tool Medcalc (https://www.medcalc.org/calc/diagnostic_test.php).

Results

Optimization of RT-LAMP Assay for IDV

We evaluated the primer sets generated for the PB1 and PB2 gene sequences of IDV in silico for their end stabilities, formation of hairpins, self-dimers, and

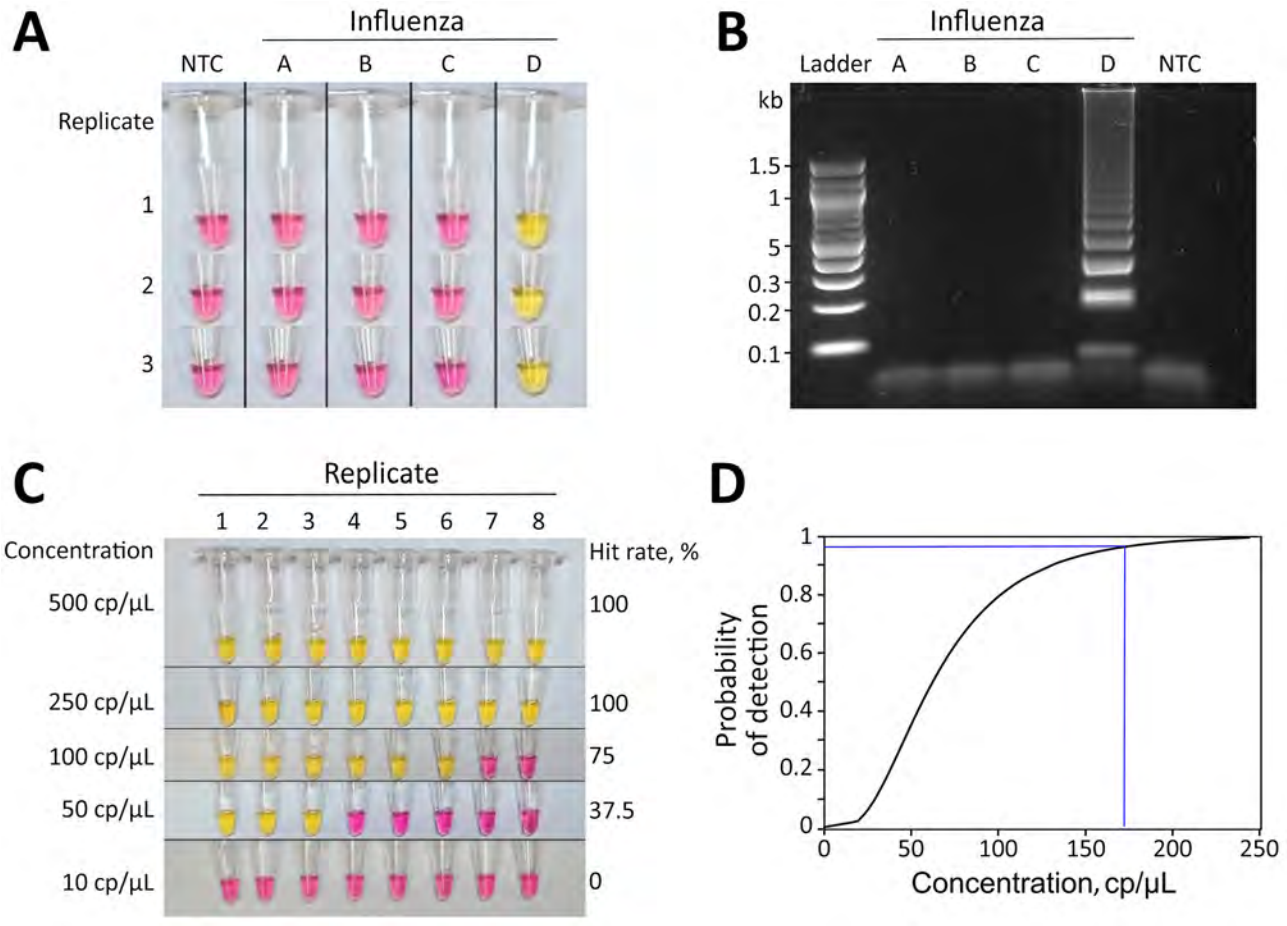

Figure 4. Specificity and sensitivity assays for influenza D virus (IDV) detection in study of isothermal detection of IDV using reverse transcription loop-mediated isothermal amplification (RT-LAMP). A) The total of 10^6 copies/µL of gBlocks containing the influenza A, B, C and D virus polymer basic protein 2 gene sequences were tested. Only the gBlocks containing the target sequences were amplified, as demonstrated by color change in reactions. B) Two percent gel electrophoresis of 1 representative of each amplification products of the RT-LAMP reactions shown in panel A, showing the typical lamp ladder-like pattern in IDV virus samples and no visible nonspecific bands in the other target samples. C) Dilutions of target RNA in 8 replicates for sensitivity analysis at different concentrations, varying from 500 copies per µL (cp/µL) of target (top row) to 10 cp/µL of target (bottom row). D) Probit-analysis curve of probability of detection in relation to the number of copies. The limit of detection is defined as the minimum number of copies detected >95% of the time. NTC, nontemplate control.

heterodimers. We found that none of the sets targeting the PB1 gene passed our filters, whereas 2 primer sets targeting the PB2 gene met our criteria and were synthetized (Appendix Table 2).

We initially trialed both primer sets by performing the RT-LAMP reaction in a real-time thermocycler targeting gBlocks containing the complete PB2 sequence of IDV, as well as IAV, IBV, and ICV as negative controls, using SYTO9 DNA dye to track the accumulation of amplification products over time (Figure 1). Each gBlock was incubated at a concentration of 10^6 copies per µL of input. Because nonspecific amplification is a well-known problem with RT-LAMP reactions, we incubated the reactions for ≤80 minutes to assess the maximum incubation time for each primer set, defined as the longest time in which reactions could proceed without producing false-positive signals in the negative samples or nontemplate controls. Although both primer sets amplified the IDV target gBlock before the 20-minute mark, the IDV_set1 showed early onset of nonspecific amplification at ≈40 minutes (Figure 1, panel A), compared with 65 minutes with the IDV_set2 (Figure 1, panel B). Because of the increased specificity, we chose IDV_set2 for all subsequent analysis and defined the maximum incubation time as 60 minutes. We defined the threshold at the start of the exponential phase of amplification.

To ensure complete coverage of ≥90% of the published IDV lineages, including the 3 viral isolates we had access to (D/bovine/France/5920/2014, D/swine/Oklahoma/1334/2011, and D/swine/England/

126471/2023), we incorporated degenerate nucleotides into the primers from IDV_set2 where necessary (Figure 2; Appendix Table 2). To test whether the primer set containing degenerate nucleotides enabled detection of all 3 available isolates of IDV, we incubated dilutions of extracted RNA at 10^4 and 10^3 copies/μL for each of the isolates. All concentrations of the 3 isolates were efficiently amplified after ≈15 minutes (Figure 3).

High Sensitivity and Specificity in Colorimetric RT-LAMP Assay

Having demonstrated that the RT-LAMP primers efficiently detected IDV RNA using a real-time thermocycler, we incubated subsequent reactions in a conventional thermocycler and analyzed the results visually on the basis of a colorimetric change in the reaction from pink (negative) to yellow (positive). To demonstrate that the addition of the degenerate nucleotides did not affect primer specificity, we incubated a high number of gBlock copies (10^6 copies/μL) of the PB2 gene of influenza A, B, C, and D with the RT-LAMP mixture for 60 minutes at 65°C. Only the IDV target was amplified (Figure 4, panel A), suggesting that our assay is specific to IDV. This result was confirmed through gel electrophoresis of the amplicons (Figure 4, panel B).

Next, we estimated the sensitivity of the assay from the amplification results of 8 replicates at low target concentrations (500, 250, 100, 50, and 10 copies per μL of input) using an equimolar mix containing the RNA from the 3 IDV isolates used in this study. We plotted the calculated probit regression curve; the minimum number of copies detected 95% of the time was estimated to be 167 copies/μL (95% CI 103–3115 copies/μL) (Figure 4, panels C and D).

Evaluation of RT-LAMP Assay on Spiked and Diagnostic Samples

To assess the efficiency of the RT-LAMP test in a more complex matrix, we spiked varying concentrations of IDV RNA into total RNA extracted from swine lung tissue. Before the addition of the IDV RNA, the swine lung tissue was confirmed to be free of IDV RNA by qRT-PCR. We tested 27 spiked samples in duplicate in different amounts of swine lung RNA to mimic different target/background ratios, using 4 nonspiked samples as negative controls (a total of 58 individual RT-LAMP reactions). We also quantified the IDV RNA in all spiked samples by qRT-PCR. The RT-LAMP assay successfully detected all 30 reactions that had a sample Cq ≤29. It failed to amplify 2 out of 6 reactions using samples with a Cq >29 to ≤30, 4 out of 14 reactions using samples with Cq >30 to ≤32, and 3 out of 4 reactions using samples with a Cq >32 (Figure 5, panel A). All 4 uninfected swine lung RNA samples were negative.

Finally, we tested the performance of the RT-LAMP assay in detecting IDV viral RNA in total RNA extracted from samples collected from animals in the field. We analyzed a total of 46 RNA samples extracted from cattle and swine. The samples were composed of negative samples, samples containing IDV, and samples containing IAV RNA. We tested the samples in triplicate and compared the results with qRT-PCR results (Table). The RT-LAMP assay successfully detected IDV RNA in 3 of the 4 animal samples that were positive for IDV RNA by qRT-PCR.

Altogether, we tested a total of 196 individual RT-LAMP reactions, consisting of 58 spiked RNA and 138 animal RNA samples. We compared the RT-LAMP results to the results of the standard qRT-PCR and calculated the sensitivity, specificity, positive and negative likelihood ratios, and positive and

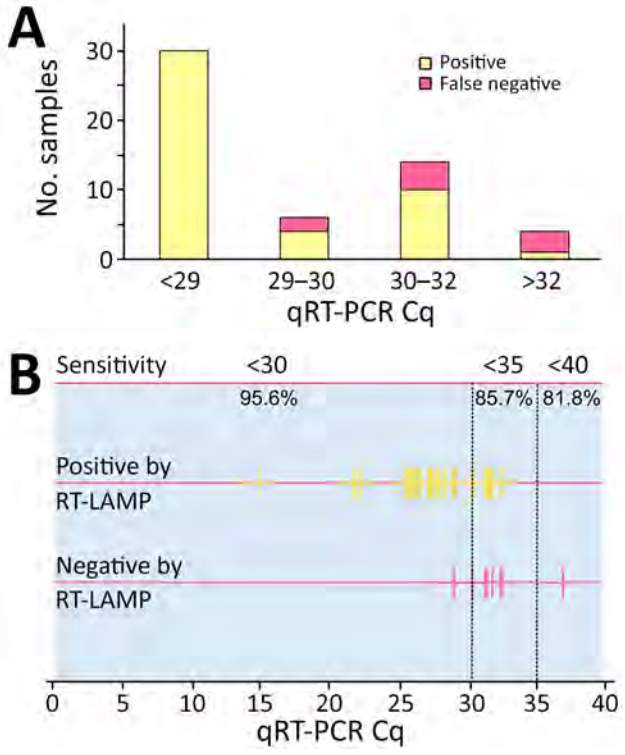

Figure 5. Sensitivity of RT-LAMP assay in relation to qRT-PCR Cq in study of isothermal detection of influenza D virus using RT-LAMP. A) Detection of spiked samples detected by RT-LAMP in relation to the Cq value. B) Each true positive sample was sorted according to its Cq value and RT-LAMP result. Yellow lines along the top line were positive by both RT-LAMP and qRT-PCR, pink lines on the lower line were positive by qRT-PCR but negative by RT-LAMP. The sensitivity of each range is presented as percentages at the top of the graph. Cq, cycle quantification; RT-LAMP, reverse transcription loop-mediated isothermal amplification; qRT-PCR, quantitative reverse transcription PCR.

Table. Comparison between qRT-PCR and RT-LAMP results for animal RNA samples in study of isothermal detection of influenza D virus using RT-LAMP*

Sample	IDV RT-LAMP	IDV qRT-PCR	IAV qRT-PCR
1	Negative	Negative	Negative
2	Negative	Negative	Positive, Cq 36.45
3	Negative	Negative	Negative
4	Negative	Negative	Negative
5	Negative	Negative	Negative
6	Negative	Negative	Negative
7	Negative	Negative	Negative
8	Negative	Negative	Positive, Cq 39.24
9	Negative	Negative	Negative
10	Negative	Negative	Negative
11	Negative	Negative	Negative
12	Negative	Negative	Negative
13	Negative	Negative	Negative
14	Negative	Negative	Positive, Cq 32.19
15	Negative	Negative	Negative
16	Positive	Positive, Cq 22.29	Negative
17	Negative	Negative	Negative
18	Negative	Negative	Negative
19	Negative	Negative	Negative
20	Negative	Negative	Positive, Cq 27.88
21	Negative	Negative	Negative
22	Negative	Negative	Negative
23	Negative	Negative	Negative
24	Negative	Positive, Cq 37.09	Negative
25	Negative	Negative	Negative
26	Negative	Negative	Negative
27	Negative	Negative	Negative
28	Negative	Negative	Negative
29	Negative	Negative	Negative
30	Negative	Negative	Negative
31	Negative	Negative	Negative
32	Negative	Negative	Negative
33	Negative	Negative	Negative
34	Negative	Negative	Negative
35	Positive	Positive, Cq 14.84	Negative
36	Negative	Negative	Negative
37	Negative	Negative	Negative
38	Positive	Positive, Cq 21.81	Negative
39	Negative	Negative	Negative
40	Negative†	Negative	Negative
41	Negative	Negative	Negative
42	Negative	Negative	Negative
43	Negative	Negative	Negative
44	Negative	Negative	Negative
45	Negative	Negative	Negative
46	Negative	Negative	Negative

*Cq, cycle quantification; IAV, influenza A virus; IDV, influenza D virus; qRT-PCR, quantitative reverse transcription PCR; RT-LAMP, reverse transcription loop-mediated isothermal amplification.
†Sample number 40 showed a change in color in 1 replicate that did not fully convert into yellow, but for statistical calculations, it was considered a false positive.

negative predictive values. Given that amplification of low abundance targets close to the limit of detection are probabilistic events, multiple replicates are required to estimate the detection probability (or hit rate) at a given concentration. To account for that, we treated every replicate of a spiked and diagnostic sample as an independent observation for statistical analysis, and we compared each result individually with qRT-PCR. A total of 54 of reactions were positive both by qRT-PCR and RT-LAMP (true positive), 129 were negative by both qRT-PCR and RT-LAMP (true negative), 12 were positive by qRT-PCR and negative by RT-LAMP (false negative), and 1 was positive by RT-LAMP but negative by qRT-PCR (false positive) (Appendix Table 3). The calculated specificity of the test was 99.23%, the sensitivity of the test was 81.82%, and the overall accuracy was 93.37%. The sensitivity of the test for samples with a Cq <35 was 85.7%; sensitivity for samples with a Cq <30 was 95.6% (Figure 5, panel B; Appendix Table 4).

Discussion

We developed a colorimetric RT-LAMP assay capable of detecting IDV RNA in both experimentally

spiked and field-collected samples. The assay demonstrated a high analytical specificity of 99.23%, as well as analytical sensitivity of 167 viral RNA copies/μL of target input within a 60-minute reaction time, using a 1-step assay and a simple colorimetric detection system for result interpretation. The single-tube format enables simpler handling because fewer manipulations are required, decreasing time from collection to final result. Active viral infections typically produce millions of viral copies; therefore, the detection limit in the hundreds of copies range (equivalent to Cq values >30 in qRT-PCR) will enable infections to be identified during early-stage viral replication and throughout extended viral shedding periods. Although sensitivity remains lower than qRT-PCR methodologies, the assay exceeds the analytical performance of most rapid antigen tests and could provide direct evidence of active infection compared with serologic approaches.

Primer design incorporated strategically positioned degenerate nucleotides to ensure comprehensive viral lineage coverage, achieving detection capability for ≥90% of published IDV sequences, including the recently identified D/swine/England/126471/2023 lineage from UK swine populations (*20*). The degenerate nucleotides were specifically integrated avoiding the ends of the primers to minimize potential amplification interference while maximizing lineage inclusivity.

Current IDV detection relies mainly on qRT-PCR and antibody detection, which both present distinct analytical trade-offs that affect surveillance implementation strategies. qRT-PCR is the standard method and offers superior analytical sensitivity with viral load quantification, enabling precise molecular characterization essential for genetic surveillance and outbreak investigation. However, that approach requires sophisticated laboratory infrastructure, specialized personnel, and complex sample preparation protocols. Those requirements limit point-of-care applications and increase costs per sample. Conversely, antibody sampling provides simplified collection protocols with enhanced sample stability and cost-effective population seroprevalence assessment, enabling large-scale epidemiologic studies. Nevertheless, serologic methods exhibit inherent limitations because of seroconversion kinetics, cannot distinguish active from historical infections, and might demonstrate cross-reactivity with related viruses, precluding their utility for acute infection diagnosis and real-time outbreak response. Those complementary yet functionally distinct methodological constraints necessitate the development of alternative diagnostic platforms that bridge the gap between laboratory-based precision and field-deployable practicality.

RT-LAMP offers a promising point-of-care alternative to qRT-PCR, because its simplified equipment requirements and minimal reaction components enable field-deployable testing with reduced sample processing demands. The colorimetric RT-LAMP approach provides qualitative detection results, enabling rapid screening of larger sample volumes at lower per-reaction costs than conventional qRT-PCR methodologies. Even though RT-LAMP might be used to differentiate between known lineages, RT-LAMP cannot fully replace qRT-PCR or sequencing for comprehensive genetic surveillance applications, because its amplification products are difficult to sequence. That issue is particularly problematic when detecting novel or uncharacterized viral lineages that have not been sequenced and deposited in public databases. Despite those genetic surveillance limitations, RT-LAMP offers potential for cost-effective sample triage protocols, enabling preliminary screening before confirmatory molecular characterization through more sophisticated diagnostic platforms.

In summary, our RT-LAMP assay for detecting IDV demonstrated high specificity and sensitivity, indicating its utility as a rapid and accessible diagnostic tool. To further enhance its applicability, future optimizations could focus on integrating the assay into lab-on-a-chip microfluidic platforms or coupling the reaction with a compact detector, enabling fully automated, portable testing. Further field validation across varied sample types and conditions will be essential; however, embedding this RT-LAMP assay into existing surveillance infrastructures can bolster real-time IDV detection and strengthen One Health strategies for pandemic preparedness.

The isolate D/bovine/France/5920/2014 was kindly provided by Mariette Ducatez.

This work was supported by a Royal Society Dorothy Hodgkin Research Fellowship (to N.R.; DKR00620) and an Institute for Global Pandemic Planning–funded PhD at the University of Warwick, UK (to C.A.dS). Influenza research at the Animal and Plant Health Agency (APHA) is supported by Defra and the devolved Scottish and Welsh Governments previously through FluFutures2 (SE2213) and currently through FluFocus (SE2227). Surveillance sample submissions to APHA were obtained under the National Defra-funded surveillance programs SV3041 (swine influenza) and ED1000 and ED200 (bovine respiratory virus). The authors and their affiliated institutions declare they have no ownership, patent, royalty, or other financial interest in the technique or reagents.

Mr. dos Santos is a molecular biologist and a PhD student at the Institute for Global Pandemic Planning at the University of Warwick, Coventry, UK. His primary research interest is the development of new molecular assays, with a special emphasis on increasing access to accurate diagnostics in resource-limited settings

References

1. Ng TFF, Kondov NO, Deng X, Van Eenennaam A, Neibergs HL, Delwart E. A metagenomics and case-control study to identify viruses associated with bovine respiratory disease. J Virol. 2015;89:5340–9. https://doi.org/10.1128/JVI.00064-15
2. Robinson E, Schulein C, Jacobson BT, Jones K, Sago J, Huber V, et al. Pathophysiology of influenza D virus infection in specific-pathogen-free lambs with or without prior *Mycoplasma ovipneumoniae* exposure. Viruses. 2022;14:1422. https://doi.org/10.3390/v14071422
3. Nedland H, Wollman J, Sreenivasan C, Quast M, Singrey A, Fawcett L, et al. Serological evidence for the co-circulation of two lineages of influenza D viruses in equine populations of the Midwest United States. Zoonoses Public Health. 2018;65:e148–54. https://doi.org/10.1111/zph.12423
4. Gorin S, Fablet C, Quéguiner S, Barbier N, Paboeuf F, Hervé S, et al. Assessment of influenza D virus in domestic pigs and wild boars in France: apparent limited spread within swine populations despite serological evidence of breeding sow exposure. Viruses. 2019;12:25. https://doi.org/10.3390/v12010025
5. Salem E, Cook EAJ, Lbacha HA, Oliva J, Awoume F, Aplogan GL, et al. Serologic evidence for influenza C and D virus among ruminants and Camelids, Africa, 1991–2015. Emerg Infect Dis. 2017;23:1556–9. https://doi.org/10.3201/eid2309.170342
6. Sreenivasan C, Thomas M, Sheng Z, Hause BM, Collin EA, Knudsen DEB, et al. Replication and transmission of the novel bovine influenza D virus in a guinea pig model. J Virol. 2015;89:11990–2001. https://doi.org/10.1128/JVI.01630-15
7. Song H, Qi J, Khedri Z, Diaz S, Yu H, Chen X, et al. An open receptor-binding cavity of hemagglutinin-esterase-fusion glycoprotein from newly-identified influenza D virus: basis for its broad cell tropism. PLoS Pathog. 2016;12.
8. Nemanichvili N, Berends AJ, Wubbolts RW, Gröne A, Rijks JM, de Vries RP, et al. Tissue microarrays to visualize influenza d attachment to host receptors in the respiratory tract of farm animals. Viruses. 2021;13:586. https://doi.org/10.3390/v13040586
9. Holwerda M, Kelly J, Laloli L, Stürmer I, Portmann J, Stalder H, et al. Determining the replication kinetics and cellular tropism of influenza D virus on primary well-differentiated human airway epithelial cells. Viruses. 2019;11:377. https://doi.org/10.3390/v11040377
10. Borkenhagen LK, Mallinson KA, Tsao RW, Ha SJ, Lim WH, Toh TH, et al. Surveillance for respiratory and diarrheal pathogens at the human-pig interface in Sarawak, Malaysia. PLoS One. 2018;13:e0201295. https://doi.org/10.1371/journal.pone.0201295
11. Hause BM, Ducatez M, Collin EA, Ran Z, Liu R, Sheng Z, et al. Isolation of a novel swine influenza virus from Oklahoma in 2011 which is distantly related to human influenza C viruses. PLoS Pathog. 2013;9:e1003176. https://doi.org/10.1371/journal.ppat.1003176
12. Trombetta CM, Marchi S, Manini I, Kistner O, Li F, Piu P, et al. Influenza D virus: serological evidence in the Italian population from 2005 to 2017. Viruses. 2019;12:30. https://doi.org/10.3390/v12010030
13. White SK, Ma W, McDaniel CJ, Gray GC, Lednicky JA. Serologic evidence of exposure to influenza D virus among persons with occupational contact with cattle. J Clin Virol. 2016;81:31–3. https://doi.org/10.1016/j.jcv.2016.05.017
14. Ferguson L, Eckard L, Epperson WB, Long LP, Smith D, Huston C, et al. Influenza D virus infection in Mississippi beef cattle. Virology. 2015;486:28–34. https://doi.org/10.1016/j.virol.2015.08.030
15. Alvarez I, Carrera M, Chiapponi C, Ducatez M, El Agrebi N, Faccini S, et al. Developing an integrated approach to assess the emergence threat associated with influenza D viruses' circulating in Europe. EFSA Support Publ. 2024;21. https://doi.org/10.2903/sp.efsa.2024.EN-8641
16. Baba MM, Bitew M, Fokam J, Lelo EA, Ahidjo A, Asmamaw K, et al. Diagnostic performance of a colorimetric RT -LAMP for the identification of SARS-CoV-2: A multicenter prospective clinical evaluation in sub-Saharan Africa. EClinicalMedicine. 2021;40:101101. https://doi.org/10.1016/j.eclinm.2021.101101
17. Choi G, Moehling TJ, Meagher RJ. Advances in RT-LAMP for COVID-19 testing and diagnosis. Expert Rev Mol Diagn. 2023;23:9–28.
18. 18. Ducatez MF, Pelletier C, Meyer G. Influenza D virus in cattle, France, 2011–2014. Emerg Infect Dis. 2015;21:368–71. https://doi.org/10.3201/eid2102.141449
19. Salem E, Hägglund S, Cassard H, Corre T, Näslund K, Foret C, et al. Pathogenesis, host innate immune response, and aerosol transmission of influenza D virus in cattle. J Virol. 2019;93:e01853-18. https://doi.org/10.1128/JVI.01853-18
20. van Diemen PM, Ramsay AR, Bernard M, Floyd T, Byrne AMP, Khatri M, et al. Influenza D virus in Great Britain [cited 2026 Jan 8]. https://www.researchgate.net/publication/388946074_Pig_Influenza_D_virus_in_Great_Britain
21. Faccini S, De Mattia A, Chiapponi C, Barbieri I, Boniotti MB, Rosignoli C, et al. Development and evaluation of a new real-time RT-PCR assay for detection of proposed influenza D virus. J Virol Methods. 2017;243:31–4. https://doi.org/10.1016/j.jviromet.2017.01.019
22. Collin EA, Sheng Z, Lang Y, Ma W, Hause BM, Li F. Cocirculation of two distinct genetic and antigenic lineages of proposed influenza D virus in cattle. J Virol. 2015;89:1036–42. https://doi.org/10.1128/JVI.02718-14
23. Lamas A, Azinheiro S, Roumani F, Prado M, Garrido-Maestu A. Evaluation of the effect of outer primer structure, and inner primer linker sequences, in the performance of loop-mediated isothermal amplification. Talanta. 2023;260:124642. https://doi.org/10.1016/j.talanta.2023.124642

Address for correspondence: Nicole Robb, Warwick Medical School, University of Warwick, Gibbet Hill Road, Coventry CV4 7AL, UK; email: nicole.robb@warwick.ac.uk

Multisectoral Emergence of Multidrug-Resistant *Campylobacter coli* Sequence Type 10042 Lineage, Europe, 2018–2025

Mónica Azevedo,[1] Alexandra Nunes,[1] Maria-Leonor Lemos, Paulo Martins Costa, Ana Amaro, Lurdes Clemente, Célia Leão, Sónia Ramos, Isabel Santos, Katrine Grimstrup Joensen, Catherine Ragimbeau, Lena de Baets, Joël Mossong, Sangeeta Banerji, Antje Flieger, Diana Espadinha, William Byrne, Oda van den Berg, Andries Augustus Kampfraath, Quentin Jehanne, Philippe Lehours, João Paulo Gomes, Mónica Oleastro

Campylobacter spp. remain the leading bacterial cause of foodborne gastroenteritis in Western countries. We report sustained, previously unrecognized circulation of a multidrug-resistant *Campylobacter coli* sequence type 10042 lineage across Europe during 2018–2025. Whole-genome sequencing of 217 isolates from 9 countries spanning human, animal, food, and environmental sources identified cross-border clusters, including a large lineage linking primarily Portugal and Luxembourg, as well as Germany, Ireland, Spain, and the United Kingdom. Genomic data indicates ongoing clonal expansion with increasing diversification over time. Isolates exhibited a conserved multidrug-resistant phenotype, including resistance to fluoroquinolones, tetracyclines, and β-lactams; reduced susceptibility to carbapenems was observed. Resistance was associated with GyrA Thr86Ile, *tet*(O/32/O)/*tet*(O) genes, and bla_{OXA-61} promoter variants; variation in *porA* was linked to variable amoxicillin/clavulanic acid and ertapenem susceptibility. Those findings demonstrate that *C. coli* infections can involve sustained international transmission rather than sporadic cases and highlight the need for coordinated, cross-sector genomic surveillance to detect emerging antimicrobial-resistant lineages.

Since 2005, campylobacteriosis has been the most frequently reported foodborne zoonosis in the European Union (EU); 168,396 human cases were reported in 2024 (*1*). Infections affect all age groups but are most severe in young children, the elderly, and immunocompromised persons (*2*). Campylobacteriosis typically manifests as bloody or watery diarrhea, abdominal cramping, fever, vomiting, and

Author affiliations: National Institute of Health Doutor Ricardo Jorge (INSA), Lisbon, Portugal (M. Azevedo, A. Nunes, M.-L. Lemos, J.P. Gomes, M. Oleastro); Research in Veterinary Medicine (I-MVET)/Animal and Veterinary Research Center (CECAV), Faculty of Veterinary Medicine, Lusófona University—Lisbon University Centre, Lisbon (A. Nunes, S. Ramos, I. Santos, J.P. Gomes); ICBAS-Institute of Biomedical Sciences Abel Salazar, University of Porto, Porto, Portugal (M.-L. Lemos, P.M. Costa); Laboratory of Bacteriology and Mycology, National Institute of Agrarian and Veterinary Research, Oeiras, Portugal (A. Amaro, L. Clemente, C. Leão); Statens Serum Institut, Copenhagen, Denmark (K.G. Joensen); Laboratoire National de Santé, Dudelange, Luxembourg (C. Ragimbeau); Laboratoire Vétérinaire et Alimentaire, Division of the Luxembourg Veterinary and Food Administration, Dudelange (L. de Baets); Ministère de la Santé et de la Sécurité Sociale, Direction de la Santé, Luxembourg, Luxembourg (J. Mossong); Robert Koch-Institute, Wernigerode, Germany (S. Banerji, A. Flieger); Public Health Laboratory Dublin, Health Service Executive, Dublin, Ireland (D. Espadinha); Backweston Complex, Celbridge, Ireland (W. Byrne); National Institute of Public Health and the Environment (RIVM), Bilthoven, the Netherlands (O. van den Berg); European Centre for Disease Prevention and Control, Stockholm, Sweden (O. van den Berg); Wageningen Bioveterinary Research, Wageningen UR, Lelystad, the Netherlands (A.A. Kampfraath); French National Reference Centre for Campylobacters and Helicobacters, Bordeaux Hospital University Centre, Bordeaux, France (Q. Jehanne, P. Lehours); University of Bordeaux, INSERM, Bordeaux Institute of Oncology, Bordeaux (P. Lehours)

DOI: https://doi.org/10.3201/eid3210.260512

[1]These authors contributed equally to this work and share first authorship.

nausea (*3*,*4*). Severe or prolonged infections can lead to complications, such as bacteremia, that occasionally require hospitalization or result in death (*3*,*4*). Antimicrobial therapy is warranted in those cases, highlighting growing concerns regarding *Campylobacter* antimicrobial resistance (AMR), particularly to fluoroquinolones, macrolides, and carbapenems (*4*,*5*).

Campylobacteriosis cases are primarily caused by *Campylobacter jejuni* (≈90%) and *C. coli* (≈10%) (*2*). Poultry is the main reservoir, although livestock commodities, domestic and wild animals, humans, and contaminated water or soil also contribute to transmission (*2*,*6*). Although most *Campylobacter* infections have historically been considered sporadic (*7*), recent whole-genome sequencing (WGS)–based surveillance has demonstrated that many cases occur as genetically related clusters (*8*–*12*).

Genomic surveillance leveraging WGS-based approaches, including whole-genome and core-genome multilocus sequence typing (MLST), has markedly enhanced identification of outbreaks, investigation of transmission pathways, and detection of emerging epidemic lineages, providing high-resolution insights into genetic diversity, AMR determinants, and source attribution (*8*–*12*). WGS data also expand knowledge on novel AMR determinants, such as *porA* gene, which encodes the major *Campylobacter* outer-membrane porin and whose allelic variants might reduce β-lactam and carbapenem influx through altered membrane permeability (*5*,*13*). *C. coli* is less frequently associated with outbreaks, despite its broad ecologic niche, which includes broilers, pigs, and wild birds, emphasizing the risk for zoonotic transmission and environmental contamination (*1*,*14*,*15*).

Taking advantage of ongoing WGS-based surveillance in Portugal, we aimed to characterize the multidrug-resistant *C. coli* sequence type (ST) 10042 strain, which is associated with a peak of *C. coli* infections in Portugal and has been detected in other countries (Germany, Luxembourg, France, Ireland, Denmark, the Netherlands, the United Kingdom, and Spain) and diverse sectors (human, animal, food, and environment). The objectives were to elucidate its transmission dynamics and AMR determinants, assess its potential public health significance as an emerging *C. coli* lineage, and provide a more refined perspective on *Campylobacter* surveillance and the pathogen's overall burden.

Materials and Methods

Campylobacter Surveillance in Portugal

Since 2013, the Portuguese National Reference Laboratory for Gastrointestinal Infections (NRL-GI) at the National Institute of Health Doutor Ricardo Jorge has coordinated sentinel laboratory-based surveillance of human campylobacteriosis, involving hospital laboratories from the 3 (of 5 total) most populated geographic areas in mainland Portugal (the North, Centre, and Metropolitan Lisbon Area regions) and from 2 private laboratory networks covering the entire mainland. The network routinely submits *Campylobacter* isolates on a monthly basis, covering the entire year (*16*). Since 2022, WGS has been systematically implemented, achieving ≈90% coverage for *C. coli* WGS and antimicrobial susceptibility testing (AST).

Animal and food-chain surveillance programs are conducted by the National Institute for Agricultural and Veterinary Research. Livestock isolates are recovered from cattle, broiler, and turkey cecal contents at slaughter under the Europe monitoring framework established by Commission Decision 2020/1729 (*17*). We obtained environmental isolates and additional isolates from animals and meat products from collaborative research projects, including screening in poultry meat in retail (2022–2025) (A. Nunes et al., unpub. data) and targeted studies on dogs (2022–2023) (M.-L. Lemos et al., unpub. data).

C. coli ST10042 Study Sample

This study included *C. coli* ST10042 isolates identified since the start of WGS-based surveillance in Portugal in 2022. To ensure temporal completeness, we retrospectively sequenced all *C. coli* isolates received at the NRL-GI during 2016–2021 exhibiting the conserved ST10042 AMR phenotype. ST10042 had been previously underrecognized in public databases; WGS surveillance in Portugal revealed it as a predominant and relevant ST.

Collaborating partners in Germany, Luxembourg, France, Ireland, Denmark, and the Netherlands provided additional *C. coli* ST10042 isolates, generated through national WGS surveillance or research monitoring. Sampling, WGS coverage, and methodologies varied across countries and sectors (Table 1). The dataset was complemented with a limited number of genomes from the United Kingdom and Spain, retrieved from the PubMLST database (http://pubmlst.org), last accessed in January 2026. In total, we integrated 217 *C. coli* ST10042 isolates into the study (Appendix Table, https://wwwnc.cdc.gov/EID/article/32/10/26-0512-App1.pdf).

Antimicrobial Susceptibility Testing

As part of the surveillance system in Portugal, AST was performed for 4 priority antimicrobial drugs (ciprofloxacin, erythromycin, tetracycline, and gentamicin) by disk diffusion (Bio-Rad Laboratories,

https://www.bio-rad.com), using the breakpoints established by European Committee on Antimicrobial Susceptibility Testing (*18*). AST was also performed for 3 optional antibiotics (ampicillin, amoxicillin/clavulanic acid, and ertapenem) by MIC determination using E-test strips (bioMérieux, https://www.biomerieux.com), using the interpretive criteria established by the Comité de l'antibiogramme de la Société Française de Microbiologie (*19*), as previously described (*16*).

Whole-Genome Sequencing

For the *C. coli* ST10042 isolates from the NRL-GI in Portugal, we extracted total DNA using the Viral NA SV Kit on a MagNA Pure 96 System (Roche, https://www.roche.com) and quantified it using Qubit (Thermo Fisher Scientific, https://www.thermofisher.com), followed by Nextera XT library preparation (Illumina, https://www.illumina.com). We performed paired-end sequencing (2 × 250 bp or 2 × 150 bp) on MiSeq, NextSeq 550, or NextSeq 2000 platforms at National Institute of Health Doutor Ricardo Jorge, according to manufacturer instructions. Isolates from collaborators were provided as raw sequencing (Table 1).

All isolates underwent read quality assessment, species confirmation, and de novo assembly using the INNUca version 4.2.2 pipeline (https://github.com/B-UMMI/INNUca), as previously described (*5*). We annotated draft genome sequences with RAST server version 2.05 (*20*).

Genomic Characterization of *Campylobacter coli* ST10042

We determined in silico MLST using mlst version 2.18.1 (https://github.com/tseemann/mlst) and performed *porA* typing using the PubMLST scheme based on Dingle et al. (*21*). We identified AMR-related genes and mutations by querying genome assemblies against ResFinder version 4.7.2 (https://github.com/genomicepidemiology/resfinder), CARD 3.3.0/RGI 6.0.3 (https://card.mcmaster.ca/analyze/rgi), and AMRFinderPlus version 4.0.3 (https://github.com/ncbi/amr). We defined positive matches using minimum thresholds of 70% coverage and 80% nucleotide identity. We identified additional mutations in promoter regions of the *cmeRABC* efflux pump operon and bla_{OXA-61}, assemblies by mapping assemblies against CIT382 (GenBank accession no. AY598796.4) and CCUG11283 (VZOM01000001.1) strains using Snippy version 4.6.0 (https://github.com/tseemann/snippy) with default parameters.

Comparative Genomic Analysis

We performed a comparative genomic analysis for the complete *C. coli* ST10042 dataset (N = 217) and the subset of isolates from Portugal (n = 104) using the PubMLST *Campylobacter* core-genome MLST version 1 scheme (1,343 loci) (*22*). We conducted allele calling with chewBBACA version 3.1.2 (https://github.com/B-UMMI/chewBBACA) using default parameters (bsr_theshold: 0.6, size_threshold: 0.2). Only exact and inferred allele assignments were retained for the construct of allelic profile matrices; we treated other allelic classification categories (https://chewbbaca.readthedocs.io/en/latest/index.html) as missing loci.

We performed genetic clustering and epidemiologic associations (country, year, source, AMR profile) using ReporTree version 2.5.4 (https://github.com/insapathogenomics/ReporTree) (*23*). We generated minimum-spanning trees with the MSTreeV2 algorithm implemented in GrapeTree. We excluded assemblies with <95% loci called in the core-genome MLST scheme. We defined clusters using a maximum threshold of 5 allelic distances (ADs).

Results

Emergence and Temporal Dynamics of *C. coli* ST10042 in Portugal

Under the scope of campylobacteriosis surveillance, an increase in *C. coli* infections was observed in 2022; *C. coli* infections accounted for 19% (83/441) of isolates processed at the NRL-GI in Portugal, compared with 14% (47/334) in 2021. *C. coli* ST10042 was predominant in Portugal in 2022, representing 30% (25/83) of *C. coli* cases, detected in the metropolitan Lisbon area (44% [11/25]), the northern (36% [9/25]) and central (20% [5/25]) regions. Circulating at much lower frequencies that year, ST832 (10% [8/83]) was most common, followed by ST827 and ST1595 (6% each [5/83]), and ST825, ST855, ST3017, and ST5659 (5% each [4/83]). All those STs belong to ST828 clonal complex.

After a 2022 peak, ST10042 declined to 14% (11/79) in 2023 and stayed at 15% (14/95) in 2024, before rising to 24% (29/120) of *C. coli* infections in 2025. Retrospectively, it was lower in preceding years: 15% (7/47) in 2021 and 1 case in September 2020 (1/42). Overall, ST10042 was Portugal's most frequent *C. coli* ST during 2021–2025 and its 2022 and 2025 prevalence coincided with and drove overall infection peaks (Figure 1). Consistent with previous data (*16*), cases lacked a clear seasonal pattern and occurred year-round.

Table 1. *Campylobacter* spp. whole-genome sequencing–based surveillance by country and source in study of multisectoral emergence of multidrug-resistant *Campylobacter coli* sequence type 10042 lineage, Europe, 2018–2025*

Country (sector)	*Campylobacter* WGS surveillance and coverage
Ireland (human)	WGS-based surveillance since February 2019. Approximately 10% of national *Campylobacter* cases sequenced annually; ≈10% of sequenced isolates are *C. coli*.
Luxembourg (human, animal, food)	WGS-based surveillance since 2013. 100% of isolates are sequenced.
Netherlands (human)	WGS-based surveillance since May 2021. ≈400–500 isolates selected annually; ≈90% of sequenced isolates are *C. jejuni* and ≈10% are *C. coli*.
Netherlands (animal, food)	No routine WGS. Sequencing performed on subsets since 2000. During 2021–2022 monitoring, 549 *C. jejuni* and 960 *C. coli* isolates were recovered, 540 were sequenced.
Germany (human)	WGS-based surveillance since 2019. 100% of isolates are sequenced.
France (human)	WGS-based surveillance since 2024. ≈50% of received *C. coli* are sequenced.
Portugal (human)	WGS-based surveillance since 2022. 90% of *C. coli* isolates are sequenced.
Portugal (animal, food)	No routine WGS. Sequencing performed on subsets.

*WGS, whole-genome sequencing.

Epidemiology of *C. coli* ST10042 in Europe

Given the increase in *C. coli* infections in Portugal in 2022 driven by the emergence of ST10042, we conducted an extended investigation of Europe. In total, we included 217 *C. coli* ST10042 isolates collected during August 2018–December 2025 in the study. The isolates originated from 9 countries in Europe, and most were human isolates (n = 184 cases); of those, Portugal contributed the largest number (n = 85), followed by Germany (n = 30), Luxembourg (n = 21), France (n = 12), Ireland (n = 11), Denmark (n = 9), the Netherlands (n = 8), the United Kingdom (n = 7), and Spain (n = 1). Portugal, Luxembourg, the Netherlands, and Ireland also contributed animal/food isolates (n = 30); environmental isolates were detected only in Portugal and Luxembourg (n = 3) (Table 2). Within the study sample, the earliest detections (2018–2019) were reported in Luxembourg, Germany, and Ireland (Table 2; Figure 2). During 2020–2025, other countries reported ST10042 sporadically and at low frequency, whereas Portugal experienced a marked increase in 2022 and 2025, corresponding to the highest annual totals of reported cases during the overall period (Table 2; Figure 2).

Animal, Food, and Environmental Isolates

Food-derived isolates (n = 16) and animal-derived isolates (n = 14) collected during 2019–2024 were identified from Portugal (n = 17), Luxembourg (n = 7), the Netherlands (n = 4), and Ireland (n = 2); of those, 83% (25/30) originated from poultry. The food isolates included 11 recovered from raw poultry meat in Portugal (chicken [n = 9] and turkey [n = 2]) in 2021, 2023 and 2024 and 5 recovered from chicken-based prepared dishes in Luxembourg in 2019, 2020, and 2022. A total of 13 animal isolates (93% [13/14]) originated from livestock; those consisted of 5 from Portugal (chicken [n = 2], turkey [n = 2], and cattle [n = 1] in 2021–2023), 4 from the Netherlands (poultry [n = 2], cattle [n = 2] in 2021–2022), 2 from Luxembourg (poultry [n = 1] and cattle [n = 1] in 2019 and 2022) and 2 from Ireland (poultry [n = 2] in 2022 and 2024). One isolate (7% [1/13]) was recovered from a dog in Portugal (2023). In addition, 3 environmental isolates were recovered from surface waters, 2 from Portugal (2020 and 2022) and 1 from Luxembourg (2021).

AMR Phenotype and Genotype of *C. coli* ST10042

We performed AST on the *C. coli* isolates from the NRL-GI in Portugal (85 human, 10 food, 2 environmental, and 1 companion animal). All were resistant to ciprofloxacin, tetracycline, and ampicillin (MIC

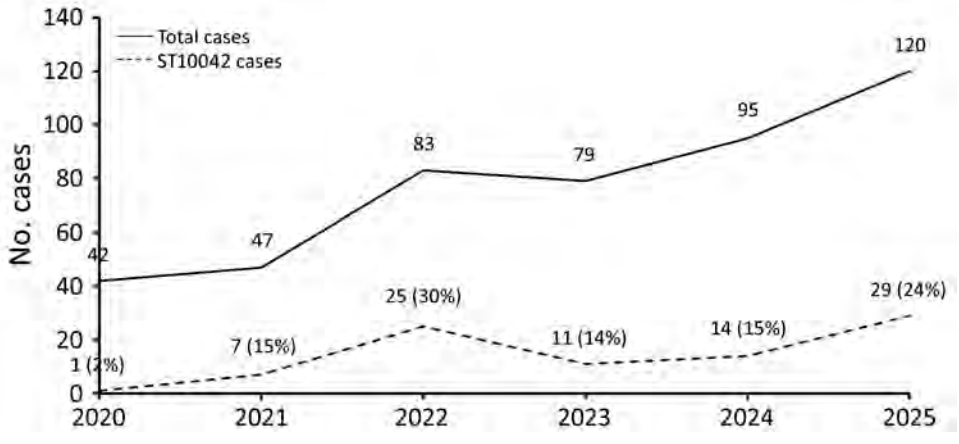

Figure 1. Temporal trend of *Campylobacter coli* human isolates (n = 466) and ST10042 isolates (n = 87), Portugal, 2020–2025, in study of multisectoral emergence of multidrug-resistant *C. coli* ST10042 lineage, Europe, 2018–2025. ST, sequence type.

>256 mg/L) (Table 3). All but 2 isolates were also resistant to amoxicillin/clavulanic acid (MIC = 12–64 mg/L); 1 isolate exhibited a higher MIC (>256 mg/L). Regarding ertapenem, all but 2 isolates exhibited increased MIC values (MIC = 0.38–1.0 mg/L) compared with those typically observed among susceptible *C. coli* isolates (MIC = 0.016–0.125 mg/L) according to previously published data (*16*), which we defined as decreased susceptibility (Table 3). The 2 exceptions had lower MICs for amoxicillin/clavulanic acid and ertapenem: 8 and 0.125 mg/L for PT-85 and 0.094 and 0.032 mg/L for PT-93 (Table 3). We detected resistance to erythromycin (MIC >256 mg/L) in 2 isolates (PT-7 and PT-28) (Table 3).

In silico analysis of the 217 *C. coli* ST10042 isolates revealed an overall conserved resistance profile, harboring known genetic determinants of resistance to ciprofloxacin (GyrA Thr86Ile), tetracycline [*tet*(O/32/O)/*tet*(O)], and ampicillin (bla_{OXA-61} promoter: −57G>T) (Table 3). The single isolate from Portugal exhibiting MIC >256 mg/L for amoxicillin/clavulanic acid (PT-86) harbored an additional deletion (−69delA) in the bla_{OXA-61} promoter (Table 3). We identified erythromycin resistance–associated mutations in *23S rRNA* in 8 isolates (Table 3; Appendix Table). All but 6 isolates carried the *porA* allele 35 (Table 3; Appendix Table). Of note, the 2 Portugal isolates with lower MICs to amoxicillin/clavulanic acid and

Table 2. Distribution of isolates (n = 217) by year, country and source in study of multisectoral emergence of multidrug-resistant *Campylobacter coli* sequence type 10042 lineage, Europe, 2018–2025*

Year of isolation	Country of isolation	No. isolates by source				Total no. isolates
		Human	Animal	Food	Environmental	
2018	Luxembourg	1	0	0	0	1
2019	Germany	1	0	0	0	1
	Luxembourg	1	1	1	0	3
	Ireland	1	0	0	0	1
2020	Portugal	1	0	0	1	2
	Germany	9	0	0	0	9
	Luxembourg	3	0	3	0	6
	France	2	0	0	0	2
	Denmark	3	0	0	0	3
2021	Portugal	5	1	1	0	7
	Germany	7	0	0	0	7
	Luxembourg	3	0	0	1 (*24*)	4
	France	1	0	0	0	1
	Ireland	1	0	0	0	1
	Denmark	2	0	0	0	2
	The Netherlands	0	3	0	0	3
2022	Portugal	25	4	0	1	30
	Germany	2	0	0	0	2
	Luxembourg	4	1	1	0	6
	France	1	0	0	0	1
	Ireland	8	1	0	0	9
	The Netherlands	1	1	0	0	2
	United Kingdom	3	–	–	–	3
2023	Portugal	11	1	4	0	16
	Germany	6	0	0	0	6
	Luxembourg	2	0	0	0	2
	France	1	0	0	0	1
	Denmark	3	0	0	0	3
	The Netherlands	2	0	0	0	2
	United Kingdom	4	–	–	–	4
	Spain	1	–	–	–	1
2024	Portugal	14	0	6	0	20
	Germany	3	0	0	0	3
	Luxembourg	4	0	0	0	4
	France	3	0	0	0	3
	Ireland	1	1	0	0	2
	The Netherlands	4	0	0	0	4
2025	Portugal	29	0	0	0	29
	Germany	2	0	0	0	2
	Luxembourg	3	0	0	0	3
	France	4	0	0	0	4
	Denmark	1	0	0	0	1
	The Netherlands	1	0	0	0	1
Total		184	14	16	3	217

*Dash indicates no available data because correspondent countries' data were retrieved from PubMLST.

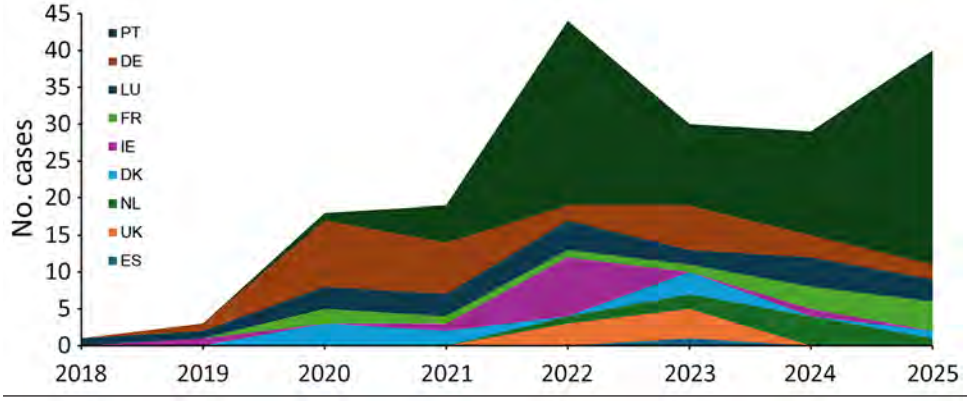

Figure 2. Annual distribution of *Campylobacter coli* ST10042 human isolates (n = 184) by country in study of multisectoral emergence of multidrug-resistant *C. coli* ST10042 lineage, Europe, 2018–2025. DE, Germany; DK, Denmark; ES, Spain; FR, France; IE, Ireland; LU, Luxembourg; NL, the Netherlands; PT, Portugal; ST, sequence type; UK, United Kingdom.

ertapenem harbored the *porA* allele 1512 instead. All isolates carried the *cmeRABC* efflux pump operon, for which no previously described resistance-associated point mutations or the resistance-enhancing *cmeB* variant (GenBank accession no. KT778508.1) were identified (*25*,*26*).

Genetic Diversity of *C. coli* ST10042

Cluster analysis of the 217 *C. coli* ST10042 isolates assessed genomic diversity and relatedness. We generated 2 minimum-spanning trees, 1 including all 104 Portugal isolates (Figure 3) and another including 211 filtered isolates from the full study sample (Figure 4). The 104 Portugul isolates (2020–2025) exhibited high genetic diversity, and consisted of 1 main cluster of 28 isolates, 15 smaller clusters of 2–4 isolates (totalizing 35 isolates), and 41 singletons (Figure 3).

Among the 85 human isolates, 57% (4/7) from 2021 and 43% (13/30) from 2022 grouped in the main cluster (Figure 3, panel A). Conversely, from 2023 onward, the population structure became more dispersed and genetically heterogeneous; human isolates primarily formed small clusters or singletons (81% in 2023, 95% in 2024, and 100% in 2025) (Figure 3, panel A). The main cluster consisted of 20 human isolates (2021–2024), mostly from 2021–2022 (85% [17/20]), and 8 nonhuman isolates: 5 livestock (chicken, turkey, or cattle collected in 2021–2022) and 3 poultry meat isolates from 2021, 2023, and 2024 (Figure 3, panels A, B). We observed no clear geographic aggregation.

Considering the complete dataset of 211 isolates, we observed a high level of genetic diversity. We identified a total of 28 clusters (defined as ≥2 isolates) that accounted for 129 isolates, whereas 82 isolates were singletons. Three clusters were predominant: cluster 21 (44 isolates), cluster 20 (15 isolates), and cluster 15 (10 isolates) (Figure 4).

Cluster 21 (Figure 4) was the largest cluster, embedding the main Portugal cluster (Figure 3) within a broader lineage within Europe. The human isolates were predominantly from Portugal (n = 19 [2021–2023]) and Luxembourg (n = 7 [2018–2022]), with sporadic isolates from Germany (n = 2 [2021]), Ireland (n = 1 [2019]), the United Kingdom (n = 1 [2023]), and Spain (n = 1 [2023]) (Figure 4, panels A, B). That cluster also included 13 source isolates: 7 livestock from Portugal (chicken, n = 2; turkey, n = 2; cattle, n = 1 [2021–2022]), Luxembourg (cattle, n = 1 [2019]), and the Netherlands (cattle, n = 1 [2021]), and 6 food samples from Portugal (poultry meat, n = 3 [2021, 2023, and 2024]) and Luxembourg (chicken-based dishes, n = 3 [2019–2020]) (Figure 4, panel C). The second largest cluster, cluster 20, consisted of 15 human isolates from Germany (n = 9 [2019–2021]), Denmark (n = 5 [2020–2021]), and France (n = 1 [2020]); the isolate from France came from a patient residing in Strasbourg, which borders Germany (Figure 4, panels A–C). Finally, cluster 15 consisted of 9 human isolates and 1 chicken isolate, all from Ireland and collected during 2021–2022 (Figure 4, panels A–C).

Overall, both minimum-spanning trees (Figure 3, panel A; Figure 4, panel B) revealed increasing genetic diversification over time; isolates progressively dispersed toward the periphery as singletons or smaller clusters. Although the core multidrug-resistance profile remained conserved across the sample, specific AMR phenotypes and genotypes, including the *porA* allele variants and the −69A deletion in $bla_{\text{OXA-61}}$ promoter (associated with high-level resistance to amoxicillin-clavulanic), occurred mainly among peripheral isolates (Figure 4, panel D).

Discussion

Since *Campylobacter* WGS surveillance was implemented in Portugal, key achievements have been reached, such as the detection of relevant STs, transmission events, AMR profiles, genomic clusters, and attribution of sources (*16*,*27*). Leveraging the high resolution of this surveillance, we identified previously

unrecognized clusters of an emerging ST and assembled a study sample consisting of 217 *C. coli* ST10042, from human (n = 184) and nonhuman (animal, food, and environmental) (n = 33) isolates, encompassing 9 countries in Europe over 7 years (2018–2025).

ST10042, belonging to the globally disseminated ST828 clonal complex, first drew attention in Portugal in 2022, in which it accounted for 30% of human *C. coli* infections and demonstrated consistency with a poultry-related outbreak. Despite low international reports, collaboration revealed its presence across databases from collaborators across Europe, forming distinct genetic clusters across countries and sectors. The detection of ST10042 in poultry, cattle, dog, surface water, and human sources reinforces its ecologic plasticity and adaptability, underscoring the challenge of implementing control measures across diverse sources (*28*). Cluster 21, the largest cluster, consisted mainly of isolates from Portugal and Luxembourg, along with sporadic cases from Germany, Ireland, the United Kingdom, and Spain. Other larger clusters included cluster 15 (Ireland) and cluster 20 (Germany–Denmark). Although *C. coli* is typically associated with sporadic, unrelated infections (*7*), our WGS-based surveillance we demonstrated that major *C. coli* lineages form genetically related clusters with transnational and cross-sectoral dissemination, challenging previous population structure assumptions. Of note, cross-country cluster detection and comparison depend on national surveillance variations, such as sampling strategies and sequencing coverage. Although all 6 participating nations have longstanding public health WGS surveillance, coverage spans from 10% in Ireland to 100% in Germany (Table 1), differences that likely bias cluster resolution, sensitivity, and the apparent geographic distribution of ST10042.

In Portugal, *C. coli* ST10042 emerged in September 2020 and persisted through 2025, peaking in 2022 and 2025 (Figure 1). Most 2021–2022 isolates belonged to a large genetic cluster (Figure 3) integrated within

Table 3. *Campylobacter coli* ST10042 isolates phenotypic and genotypic (antimicrobial resistance profiles in study of multisectoral emergence of multidrug-resistant *C. coli* ST10042 lineage, Europe, 2018–2025*

		Phenotype, n = 98, NRL-GI Portugal isolates			Genotype, N = 217, all isolates	
Class	Antibiotic	Disk, mm, or MIC, mg/L	Susceptibility	No. tested/ no. positive	Resistance determinants	No. tested/ no. positive
Fluoroquinolones	Ciprofloxacin	6 mm	R	98/98	GyrA Thr86Ile	217/217
Tetracyclines	Tetracycline	6 mm	R	98/98	*tet*(32/O/32)	213/217
					tet(O)	4/217
β-lactams	Ampicillin	≥256 mg/L	R	98/98	bla_{OXA-61}	216/217
					bla_{OXA-61} promoter: −57G>T	
	Amoxicillin/clavulanic acid	≥256 mg/L	R	1/98	bla_{OXA-61}	1/217
					bla_{OXA-61} promoter: −57G>T	
					−69delA *porA* 35	
		12–64 mg/L	R	95/98	bla_{OXA-61}	211/217
					bla_{OXA-61} promoter: −57G>T	
					porA 35/1006/4736	
		8/0.094 mg/L	S	2/98	bla_{OXA-61}	4/217
					bla_{OXA-61} promoter: −57G>T	
		–			bla_{OXA-61} *porA* 35	1/217
Carbapenems	Ertapenem	0.30–1.0 mg/L	DS	96/98	*porA* 35/1006/4736†	213/217
		0.032/0.125 mg/L	S	2/98	x	4/217
Macrolides	Erythromycin	6 mm/>256 mg/L	R	2/98	*23S rRNA* (A2075G)	6/217
					23S rRNA (A2074G)	1/217
					23S rRNA (A2074C)	1/217
		≥24 mm	S	96/98	x	209/217

*Dash indicates no antimicrobial susceptibility testing was performed. X indicates absence of resistance determinants. DS, decreased susceptibility; NRL-GI, National Reference Laboratory for Gastrointestinal Infections; R, resistant; S, susceptible; ST, sequence type.
†*porA* 1006 and *porA* 4736 differ from allele 35 by a single synonymous substitution. Other genetic determinants included: *aadE* (n = 1/217), *aad9* (n = 1/217), *aph(3')-IIIa* (n = 1/217) and *ant (6)-Ia* (n = 3/217). Gentamicin was tested and found to be susceptible for NRL-GI Portuguese isolates (≥17 mm). Zone diameter breakpoints for ciprofloxacin (S ≥26 mm), tetracycline (S ≥30) and erythromycin (S ≥24 mm), and MIC breakpoint for erythromycin (S ≤8 mg/L) established by EUCAST v16.1 were used; interpretive criteria for ampicillin (S ≤8 mg/L), amoxicillin/clavulanic acid (S ≤8 mg/L) and ertapenem (S ≤1 mg/L), established by the CA-SFM V.1.1 were used.

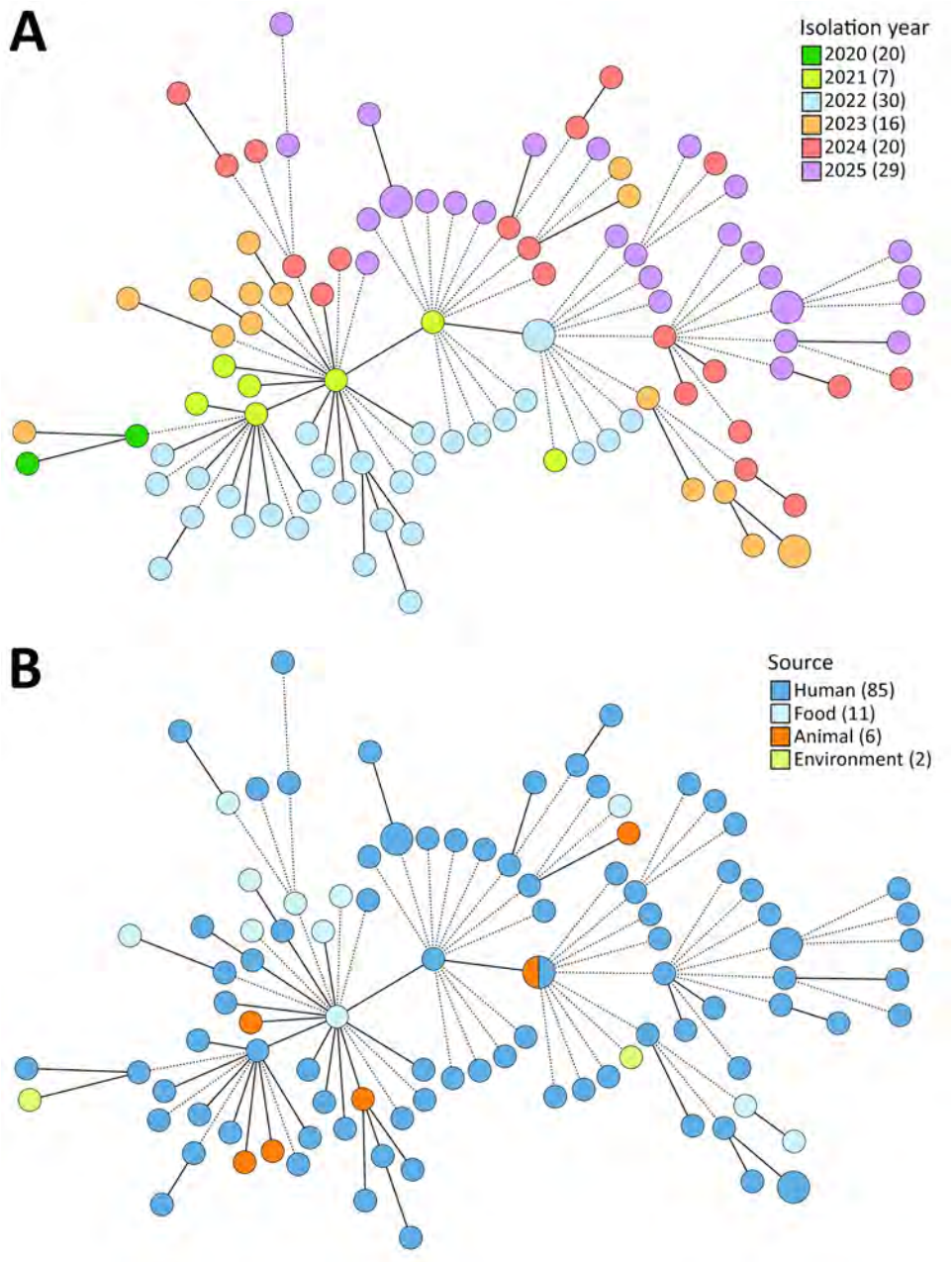

Figure 3. Diversity of the *Campylobacter coli* sequence type 10042 isolates from Portugal in study of multisectoral emergence of multidrug-resistant *C. coli* sequence type 10042 lineage, Europe, 2018–2025. Minimum-spanning tree of 104 Portugal isolates shows genetic diversity assessed using a gene-by-gene approach based on the PubMLST core-genome MLST v1 scheme (1,343 loci). Minimum-spanning tree was generated using the MSTreeV2 algorithm in GrapeTree (https://github.com/achtman-lab/grapetree) and based on allelic differences. Filled circles (sizes proportional to the number of isolates) represent unique allelic profiles. Nodes are colored by year of isolation (A) and source (B). Solid lines indicate genetic clusters defined by an allelic distance ≤5, whereas dashed lines indicate an allelic distance >5.

cluster 21 from Europe, whereas 2023–2025 isolates formed smaller clusters or singletons (Figure 3, panel A), which was also observed at the Europe-wide level (Figure 4, panel B). Those patterns support ongoing circulation and diversification of ST10042 lineage, highlighting its outbreak potential, without excluding unsampled reservoirs.

Cluster 21 (2018–2024) (Figure 4, panel C) evidences interconnected transmission across animal, food, and human compartments, potentially through food production or animal trade. The predominance of poultry-derived isolates within the cluster (77% [10/13]), together with the fact that 83% (25/30) of animal and food-related cases in the overall study were traced to poultry, underscores the central role of this reservoir in *C. coli* transmission and the importance of strengthened surveillance and targeted control measures in the poultry production chain (*2*,*9*,*12*,*28*). The early detection of isolates from Luxembourg (2018–2020) might reflect differences in surveillance coverage and sampling intensity rather than a primary point of introduction. At the same time, the presence of a substantial Portuguese community in Luxembourg (on average 15% of residents)

(https://statistiques.public.lu/en.html) that contributes to the availability of Portuguese food products through import and retail networks potentially provides a cross-border contamination pathway. However, without detailed epidemiologic and supply-chain data, that possibility remains speculative (*23*,*27*).

Cluster 15 from Ireland, which clustered chicken and human isolates and showed temporal concentration (2021–2022) (Figure 4, panels A and B), was consistent with an outbreak, possibly linked to chicken-born contamination in the food-chain. The Germany–Denmark cluster 20 emphasized the cross-broader circulation of ST10042 lineage (Figure 4, panel A), which was potentially sustained by an unsampled contamination source, such as a food item.

Overall, *C. coli* ST10042 lineage exhibits stable multidrug resistance, including decreased ertapenem susceptibility; genotype-phenotype concordance is strong. It exhibited resistance to both ciprofloxacin and tetracycline, consistent with the widespread occurrence of resistance to these antibiotics across the EU (*29*). In contrast, macrolide resistance was uncommon in this lineage, in agreement with the overall situation in Europe, where erythromycin resistance in *C. coli* remains substantially lower than for ciprofloxacin and tetracycline, although moderate levels are still reported in some countries, including Portugal and Spain (*29*). Resistance to amoxicillin/clavulanic acid and carbapenems remains rare (*5*,*30*); therefore, ST10042 stands out from other *C. coli* populations, raising concern given the critical role of β-lactams and carbapenems in treating invasive or complicated *Campylobacter* infections (*5*,*31*,*32*). That concern is amplified by ST10042 becoming the predominant *C. coli* ST in Portugal (2021–2025) and by its capacity for sustained, transnational, cross-sectoral circulation and dissemination. Those factors might reflect a well-established, stable lineage

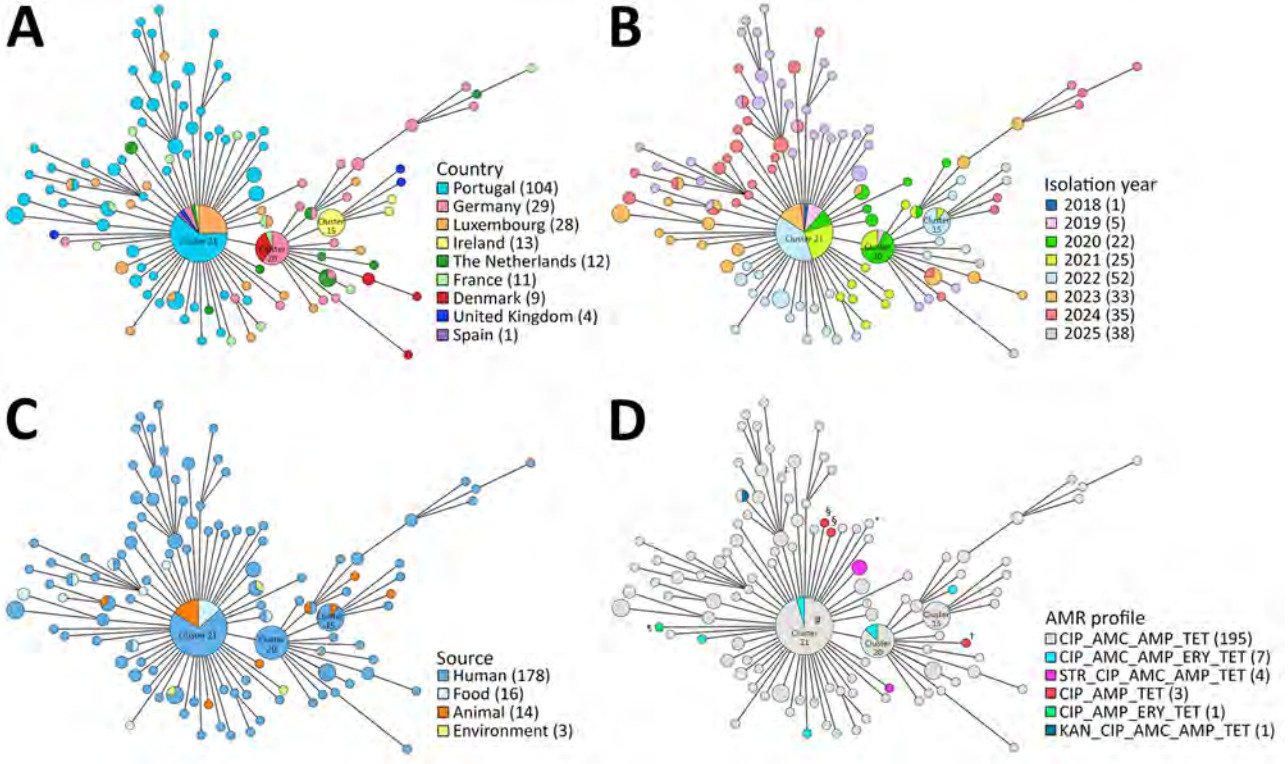

Figure 4. Diversity of *Campylobacter coli* sequence type 10042 isolates in study of multisectoral emergence of multidrug-resistant *C. coli* sequence type 10042 lineage, Europe, 2018–2025. Minimum-spanning tree of 211 isolates from 9 countries in Europe (Portugal, Germany, Luxembourg, France, Ireland, Denmark, the Netherlands, the United Kingdom, and Spain). Genetic diversity was assessed using a gene-by-gene approach based on the PubMLST cgMLST v1 scheme (1,343 *loci*). Minimum-spanning tree was generated using the MSTreeV2 algorithm in GrapeTree and based on allelic differences. Filled circles (sizes proportional to the number of isolates) indicate unique allelic profiles. Nodes are collapsed at an allelic distance ≤5 and colored according to country (A), year (B), source (C), and antimicrobial resistance profile (D). For clarity, only the 3 main clusters (*15*,*21*,*20*) are labeled. In panel D, all isolates harbor bla_{OXA-61} and the −57G>T promoter mutation. Isolates marked with a symbol additionally carry the promoter deletion or a different *porA*. *bla_{OXA-61} + promoter(–57G>T; *delA*-69)_*porA*(35) (n = 1); †bla_{OXA-61} + promoter(–57G>T)_*porA*(4736) (n = 1); ‡bla_{OXA-61} + promoter(–57G>T)_*porA*(914) (n = 1); §bla_{OXA-61} + promoter(–57G>T)_ *porA*(1512) (n = 2); ¶bla_{OXA-61} + promoter(–57G>T)_ *porA*(4735) (n = 1); #bla_{OXA-61} + promoter(–57G>T)_*porA*(1006) (n = 1).

that confers selective advantage under antimicrobial pressure from human medicine and food or animal production systems (*33*), highlighting the need for strengthened antimicrobial stewardship.

Resistance to amoxicillin/clavulanic acid had only been previously linked to the −69A deletion in bla_{OXA-61} promoter (*30*). Although most *C. coli* ST10042 isolates in Portugal were resistant, only 1 carried that deletion, conferring high-level resistance (MIC ≥256 mg/L). Our data suggest that *porA* allele 35 influences susceptibility to amoxicillin/clavulanic acid and ertapenem. The cumulative presence of determinants, specifically the *porA* 35 allele, the –57 G→T transversion, and the −69A deletion in the bla_{OXA-61} promoter, appears to contribute to elevated amoxicillin/clavulanic acid resistance, whereas isolates lacking the deletion show lower resistance MICs.

The main limitations of this study relate to both epidemiologic and surveillance-related constraints. The lack of detailed epidemiologic metadata precludes confirmation of transmission routes or outbreak causality. Outbreak definition also requires validated genomic cutoffs. Overrepresentation of Portugal and differences in WGS surveillance coverage between countries resulted in sampling bias. Finally, a deeper understanding of the link between AMR genotypes and observed phenotypes is also needed. Regarding ertapenem, the absence of established clinical breakpoints and corresponding clinical outcome data jeopardizes definitive interpretation of decreased susceptibility and its clinical and public health implications. Further studies correlating MIC distributions with clinical outcomes are needed to clarify those associations.

This study highlights coordinated One Health WGS surveillance for detecting epidemiologically relevant *C. coli* lineages and monitoring AMR across human, animal, food, and environmental sectors. Multicountry genomic data revealed prolonged, transnational, and multisectoral circulation of the multidrug-resistant *C. coli* ST10042 lineage driven by poultry. Because single-sector surveillance is insufficient to capture transmission dynamics, those findings emphasize the need for harmonized, standardized WGS surveillance frameworks across Europe, including consistent sampling strategies, harmonized analytical pipelines, and shared genomic databases to enable real-time cross-border comparison of high-risk clones. Future work should integrate longitudinal WGS with detailed epidemiologic metadata and systematic production-chain sampling, while advancing higher-resolution species-specific typing schemes. Our findings support EU-level One Health WGS surveillance aligned with the recent Commission Implementing Regulation (EU) 2025/179, which mandates cross-sector genomic surveillance of key foodborne pathogens, including *C. coli* (http://data.europa.eu/eli/reg_impl/2025/179/oj).

Acknowledgments

We thank all the clinical pathology laboratories that provided clinical isolates for campylobacteriosis surveillance in Portugal.

Raw sequence reads *C. coli* isolates are deposited in the European Nucleotide Archive in the following Bioproject nos.: ERR16782028, PRJEB109289, PRJEB46733, PRJEB58624, PRJEB62515, PRJEB75211, PRJEB77053, PRJNA1011226, PRJNA1088320, PRJNA1363081, and PRJNA1427394.

M.A. and M.-L.L. are recipients of PhD fellowships from Fundação para a Ciência e Tecnologia (M.A.: 2024.05639.BDANA; M.-L.L.: 2022.10133.BD). This work was also supported by the European Union project "Sustainable use and integration of enhanced infrastructure into routine genome-based surveillance and outbreak investigation activities in Portugal" (GENEO 101113460 to J.P.G. on behalf of the EU4H program [EU4H-2022-DGA-MS-IBA-01-02]). We also acknowledge the ResisCampyOH project, funded by Research in Veterinary Medicine (I-MVET), Faculty of Veterinary Medicine, Lusófona University—Lisbon University Centre, Lisbon, Portugal.

About the Author

Ms. Azevedo is a PhD student at the National Institute of Health Doutor Ricardo Jorge, Lisbon. Her main interests include infectious diseases, microbial genomics, and antibiotic stewardship, particularly in the context of surveillance and epidemiology. Dr. Nunes is a researcher at the National Institute of Health Doutor Ricardo Jorge, Lisbon. She co-leads the whole-genome sequencing–based surveillance of several bacterial pathogens, including antimicrobial resistance monitoring.

References

1. European Food Safety Authority; European Centre for Disease Prevention and Control. The European Union One Health 2024 zoonoses report. EFSA J. 2025;23:e9759.
2. European Food Safety Authority; European Centre for Disease Prevention and Control. The European Union One Health 2022 zoonoses report. EFSA J. 2023;21:e8442.
3. Man SM. The clinical importance of emerging *Campylobacter* species. Nat Rev Gastroenterol Hepatol. 2011;8:669–85. https://doi.org/10.1038/nrgastro.2011.191
4. Tinévez C, Velardo F, Ranc AG, Dubois D, Pailhoriès H, Codde C, et al.; Campylobacteremia study group. Retrospective multicentric study on *Campylobacter* spp.

bacteremia in France: the Campylobacteremia Study. Clin Infect Dis. 2022;75:702–9. https://doi.org/10.1093/cid/ciab983
5. Nunes A, Oleastro M, Alves F, Liassine N, Lowe DM, Benejat L, et al. Recurrent *Campylobacter jejuni* infections with *In Vivo* selection of resistance to macrolides and carbapenems: molecular characterization of resistance determinants. Microbiol Spectr. 2023;11:e0107023. https://doi.org/10.1128/spectrum.01070-23
6. Cody AJ, Maiden MCJ, Strachan NJC, McCarthy ND. A systematic review of source attribution of human campylobacteriosis using multilocus sequence typing. Euro Surveill. 2019;24:1800696. https://doi.org/10.2807/1560-7917.ES.2019.24.43.1800696
7. Strachan NJC, Forbes K. Extensive spatial and temporal clustering of *Campylobacter* infections evident in high-resolution genotypes. In: Sheppard SK, editor. *Campylobacter* ecology and evolution. Norfolk (UK): Caister Academic Press; 2014. p. 253–63.
8. Benedetti G, Sørensen G, Canabarro APF, White ED, Larsen TG, Schjørring S, et al. Increased severity of two concurrent *Campylobacter jejuni* clones causing large outbreaks, Denmark, July to October 2025. Euro Surveill. 2025;30:2500856. https://doi.org/10.2807/1560-7917.ES.2025.30.47.2500856
9. Joensen KG, Schjørring S, Gantzhorn MR, Vester CT, Nielsen HL, Engberg JH, et al. Whole genome sequencing data used for surveillance of *Campylobacter* infections: detection of a large continuous outbreak, Denmark, 2019. Euro Surveill. 2021;26:2001396. https://doi.org/10.2807/1560-7917.ES.2021.26.22.2001396
10. Joensen KG, Kiil K, Gantzhorn MR, Nauerby B, Engberg J, Holt HM, et al. Whole-genome sequencing to detect numerous *Campylobacter jejuni* outbreaks and match patient isolates to sources, Denmark, 2015–2017. Emerg Infect Dis. 2020;26:523–32. https://doi.org/10.3201/eid2603.190947
11. Nennig M, Llarena AK, Herold M, Mossong J, Penny C, Losch S, et al. Investigating major recurring *Campylobacter jejuni* lineages in Luxembourg using four core or whole genome sequencing typing schemes. Front Cell Infect Microbiol. 2021;10:608020. https://doi.org/10.3389/fcimb.2020.608020
12. García-Fernández A, Artuso I, Marotta F, Di Romualdo R, Arena S, De Marchis ML, et al. WGS-based surveillance for *Campylobacter* spp. in human infections and chicken meat production in Italy (2023). BMC Microbiol. 2025;25:696. https://doi.org/10.1186/s12866-025-04272-1
13. Maurille C, Guérin F, Jehanne Q, Audemard-Verger A, Isnard C, Verdon R, et al. Occurrence of in vivo carbapenem-resistant *Campylobacter coli* mediated by porA point mutation and overexpression of $bla_{OXA-489}$ under meropenem treatment. Clin Microbiol Infect. 2024;30:1478–80. https://doi.org/10.1016/j.cmi.2024.06.027
14. Kempf I, Kerouanton A, Bougeard S, Nagard B, Rose V, Mourand G, et al. *Campylobacter coli* in organic and conventional pig production in France and Sweden: prevalence and antimicrobial resistance. Front Microbiol. 2017;8:955. https://doi.org/10.3389/fmicb.2017.00955
15. Mughini-Gras L, Pijnacker R, Coipan C, Mulder AC, Fernandes Veludo A, de Rijk S, et al. Sources and transmission routes of campylobacteriosis: a combined analysis of genome and exposure data. J Infect. 2021;82:216–26. https://doi.org/10.1016/j.jinf.2020.09.039
16. Duarte A, Pereira L, Lemos ML, Pinto M, Rodrigues JC, Matias R, et al. Epidemiological data and antimicrobial resistance of *Campylobacter* spp. in Portugal from 13 years of surveillance. Pathogens. 2024;13:147. https://doi.org/10.3390/pathogens13020147
17. European Commission. Commission Implementing Decision (EU) 2020/1729 of 17 November 2020 on the monitoring and reporting of antimicrobial resistance in zoonotic and commensal bacteria and repealing Implementing Decision 2013/652/EU. Off J. Eur Union. 2020;L387:8–21.
18. The European Committee on Antimicrobial Susceptibility Testing (EUCAST). Breakpoint tables for interpretation of MICs and zone diameters. Version 16.1 [cited 2026 Mar 19]. https://www.eucast.org/bacteria/clinical-breakpoints-and-interpretation/clinical-breakpoint-tables
19. Société Française de Microbiologie, Comité de l' antibiogramme de la Société Française de Microbiologie (CA-SFM): recommendations 2025 [in French]. Version 1.1. Paris: Société Française de Microbiologie; 2025.
20. Aziz RK, Bartels D, Best AA, DeJongh M, Disz T, Edwards RA, et al. The RAST Server: rapid annotations using subsystems technology. BMC Genomics. 2008;9:75. https://doi.org/10.1186/1471-2164-9-75
21. Dingle KE, McCarthy ND, Cody AJ, Peto TEA, Maiden MCJ. Extended sequence typing of *Campylobacter* spp., United Kingdom. Emerg Infect Dis. 2008;14:1620–2. https://doi.org/10.3201/eid1410.071109
22. Cody AJ, Bray JE, Jolley KA, McCarthy ND, Maiden MCJ. Core genome multilocus sequence typing scheme for stable, comparative analyses of *Campylobacter jejuni* and *C. coli* human disease isolates. J Clin Microbiol. 2017;55:2086–97. https://doi.org/10.1128/JCM.00080-17
23. Mixão V, Pinto M, Sobral D, Di Pasquale A, Gomes JP, Borges V. ReporTree: a surveillance-oriented tool to strengthen the linkage between pathogen genetic clusters and epidemiological data. Genome Med. 2023;15:43. https://doi.org/10.1186/s13073-023-01196-1
24. Hock L, Walczak C, Mosser J, Ragimbeau C, Cauchie HM. Exploring the role of the environment as a reservoir of antimicrobial-resistant *Campylobacter*: insights from wild birds and surface waters. Microorganisms. 2024;12:1621. https://doi.org/10.3390/microorganisms12081621
25. Yao H, Shen Z, Wang Y, Deng F, Liu D, Naren G, et al. Emergence of a potent multidrug efflux pump variant that enhances *Campylobacter* resistance to multiple antibiotics. MBio. 2016;7:e01543–16. https://doi.org/10.1128/mBio.01543-16
26. Dai L, Wu Z, Sahin O, Zhao S, Yu EW, Zhang Q. Mutation-based mechanism and evolution of the potent multidrug efflux pump RE-CmeABC in *Campylobacter*. Proc Natl Acad Sci U S A. 2024;121:e2415823121. https://doi.org/10.1073/pnas.2415823121
27. Thystrup C, Brinch ML, Henri C, Mughini-Gras L, Franz E, Wieczorek K, et al. Source attribution of human *Campylobacter* infection: a multi-country model in the European Union. Front Microbiol. 2025;16:1519189. https://doi.org/10.3389/fmicb.2025.1519189
28. Alter T, Reich F. Management strategies for prevention of *Campylobacter* infections through the poultry food chain: a European perspective. Curr Top Microbiol Immunol. 2021;431:79–102. https://doi.org/10.1007/978-3-030-65481-8_4
29. European Food Safety Authority, European Centre for Disease Prevention and Control. The European Union Summary Report on Antimicrobial Resistance in zoonotic and indicator bacteria from humans, animals and food in 2023–2024. EFSA J. 2026;24:e9887.
30. Deforet F, Jehanne Q, Bénéjat L, Aptel J, Prat R, Desbiolles C, et al. Combined genomic-proteomic approach

in the identification of *Campylobacter coli* amoxicillin-clavulanic acid resistance mechanism in clinical isolates. Front Microbiol. 2023;14:1285236. https://doi.org/10.3389/fmicb.2023.1285236
31. Monselise A, Blickstein D, Ostfeld I, Segal R, Weinberger M. A case of cellulitis complicating *Campylobacter jejuni* subspecies *jejuni* bacteremia and review of the literature. Eur J Clin Microbiol Infect Dis. 2004;23:718–21. https://doi.org/10.1007/s10096-004-1201-x
32. Pereira L, Sampaio S, Tavares I, Bustorff M, Pestana M. Bacteremia due to *Campylobacter* in renal transplantation: a case report and review of literature. Transpl Infect Dis. 2014;16:1007–11. https://doi.org/10.1111/tid.12302
33. Luber P, Wagner J, Hahn H, Bartelt E. Antimicrobial resistance in *Campylobacter jejuni* and *Campylobacter coli* strains isolated in 1991 and 2001–2002 from poultry and humans in Berlin, Germany. Antimicrob Agents Chemother. 2003;47:3825–30. https://doi.org/10.1128/AAC.47.12.3825-3830.2003

Address for correspondence: Mónica Oleastro, National Reference Laboratory for Gastrointestinal Infections, Department of Infectious Diseases, National Institute of Health Doutor Ricardo Jorge, Avenida Padre Cruz, 1649-016 Lisbon, Portugal; email: monica.oleastro@insa.min-saude.pt

Experimental Highly Pathogenic Avian Influenza A(H5N1) Clade 2.3.4.4b Virus Infection in Alpacas, 2026

Jacob Schön, Angele Breithaupt, Nico Joel Halwe, Maxi Hertel, Ann Kathrin Ahrens, Andrea Aebischer, Donata Hoffmann, Martin Beer

Highly pathogenic avian influenza (HPAI) A(H5N1) clade 2.3.4.4b virus continues to spread globally and sporadically transmits from avian reservoirs to mammalian hosts. In May 2024, H5N1 infections in young goats and alpacas in the United States were reported. Nevertheless, the overall susceptibility of camelids to clade 2.3.4.4b virus remains unclear. We conducted a controlled experimental infection study in 6 alpacas, assessing clinical signs, viral shedding, tissue distribution, and serologic responses after intranasal inoculation with HPAI H5N1 genotype B3.13 virus. Observed illness was generally mild; body temperature increased slightly and food intake reduced for up to 3 days postinfection. We detected viral RNA in nasal swab samples and confirmed infectious HPAI H5N1 virus. Immunohistochemistry and RNA in situ hybridization detected virus only in the nasopharyngeal tonsil and nasal conchae at 4 days postinfection. Our findings suggest alpacas are susceptible to productive H5N1 infection, highlighting implications for livestock surveillance and biosecurity in regions with ongoing circulation.

In 1996, highly pathogenic avian influenza (HPAI) H5N1 virus (goose/Guangdong/96) appeared in southern China, causing outbreaks in poultry and infecting 18 humans, 6 of whom died (*1*–*3*). Descendants of that lineage subsequently triggered major outbreaks in poultry in Southeast Asia and Europe, including H5N1 clades 2.2 (2005–2006) and 2.3.2.1c (2010) and H5N8 clade 2.3.4.4a (2014), reflecting a global rise in HPAI virus (HPAIV) outbreaks (*4*–*7*). In 2016, Europe experienced major HPAI H5 clade 2.3.4.4b outbreaks in wild birds and domestic poultry (*4*), followed by major outbreaks during 2020–2021 (*7*–*9*); the clade then became endemic (*10*). Nevertheless, during that period, clade 2.3.4.4b virus continuously evolved; serotype H5N8 predominated in 2016, transitioning to H5N6 by 2018, and shifting to H5N1 by 2020 (*9*,*11*,*12*). Although the virus remained in the same clade as classified by homologies of the hemagglutinin (HA) segment, the genotypes changed through continuous reassortment events (*7*,*13*).

In December 2021, HPAI H5N1 clade 2.3.4.4b virus spread from Europe to Canada and the United States via wild birds (*14*,*15*). Subsequently, several Eurasian H5N1 clade 2.3.4.4b virus genotypes entered North America, and lineages A1 and A3 reassorted with local low pathogenicity avian influenza viruses in migratory birds, giving rise to new H5N1 clade 2.3.4.4b genotypes like B3.13 (late 2023–early 2024) and D1.1 (September 2024) (*15*,*16*). Those viruses spread rapidly in US wild bird populations, including waterfowl, birds of prey, seabirds, shorebirds, and a wide range of common land birds; during December 2021–December 2025, a total of 17,718 wild birds tested positive (*17*). In addition, clade 2.3.4.4b virus spread to domestic livestock birds, affecting 186.18 million birds in 2,029 flocks during February 2022–January 2026 (*18*).

Besides avian species, a wide range of mammals have been infected, including 683 wild mammals tested during April 2022–December 2025, mostly terrestrial carnivores feeding on H5-infected birds, including 148 red fox (*Vulpus vulpus*), 81 skunks (various species), 34 raccoons (*Procyon lotor*), 28 mountain lions (*Puma concolor*), and 18 bobcats (*Lynx rufus*) (*19*). In addition, 148 domestic cats (*Felis catus*), 110 house

Author affiliations: Institute of Diagnostic Virology, Friedrich-Loeffler-Institut, Greifswald, Germany (J. Schön, N.J. Halwe, A.K. Ahrens, A. Aebischer, D. Hoffman, M. Beer); Department of Experimental Animal Facilities and Biorisk Management, Friedrich-Loeffler-Institut, Greifswald (A. Breithaupt, M. Hertel)

DOI: https://doi.org/10.3201/eid3210.260491

mice (*Mus musculus*), and 26 deer mice (*Peromyscus* spp.) also were infected, mostly in the context of affected farms (*19*).

In March 2024, H5N1 clade 2.3.4.4b genotype B3.13 virus was detected in US dairy cattle, representing the first well-documented instance of widespread HPAIV infection in bovines (*20*). That detection was accompanied by evidence of high infectious virus shedding in milk, making milk-mediated cow-to-cow transmission highly likely (*20*–*23*). Concurrently, young goat kids co-located with infected poultry on a Minnesota farm exhibited neurologic signs and tested positive for H5N1 genotype B3.6 virus (*24*,*25*). During March 2024–May 2025, a total of 70 cases of human H5N1 infection were reported in the United States (*26*); most were associated with exposure to infected dairy cattle (41 cases) or commercial poultry (24 cases) (*15*). Among human cases, the most common reported symptoms were conjunctivitis (89%), fever (46%), and respiratory symptoms (41%) (*26*). All sequenced viruses from human cases belonged to clade 2.3.4.4b, predominantly B3.13 and D1.1 genotypes, but 1 D1.3 genotype virus also was identified (*15*).

In May 2024, the US National Veterinary Services Laboratories confirmed detection of HPAI H5N1 virus from alpacas at a premises where poultry had previously tested positive (*27*). The viral genome matched the B3.13 genotype circulating in US dairy cattle and the depopulated poultry, strongly implicating environmental contamination and cross-species exposure (*27*). The alpacas shared pasture and water sources with infected poultry and ducks but initially showed no clinical signs (*27*–*29*). However, on May 10, the day H5N1 virus infection was confirmed in poultry, 1 alpaca experienced spontaneous late-term abortion; 2 more aborted on May 14 and 15, and another spontaneous abortion occurred before September 2024 (*29*). By May 15, 2024, four of 18 alpacas showed clinical signs, including depression, weakness, and mild respiratory symptoms (*29*). An additional alpaca died acutely, without prior reported signs, 10 days after the first reports of influenza-like illness in poultry; a nasal swab sample collected on the day of death tested H5N1-positive, but no postmortem examination was conducted (*29*). Of the 18 adult alpacas (14 female, 4 male), only the female animals were affected (*29*). One aborted fetus was later examined, and H5N1 was confirmed in brain tissue (*29*). Ten surviving female alpacas seroconverted (*29*). Of note, alpaca milk samples tested positive for viral genome, indicating acute infection of the udder, but also later tested positive for influenza virus A–specific antibodies (*29*). On the same farm, milk from 1 llama tested positive for specific antibodies 4 months after the outbreak, and 2 of 13 yaks (both female) also seroconverted (*29*). That detection expanded the known host range of HPAI H5N1 virus and raised questions regarding its susceptibility, pathogenesis, and transmission dynamics in camelids.

HPAIV H5N1 continues to pose a threat to birds and, under certain conditions, to mammalian species. Although spillover into mammals is generally rare, the recent detections in nonavian hosts have heightened concerns about cross-species transmission, adaptation, and the emergence of novel mammalian hosts (*11*,*20*). Given that precedent, controlled experimental infection studies can address key knowledge gaps, including the incubation period, clinical spectrum, transmission routes, duration of viral shedding, tissue tropism, and the potential for adaptation in nonavian hosts. We report an experimental challenge study in alpacas using HPAIV H5N1 genotype B3.13, the same genotype identified in the US field case in camelids, to characterize virus kinetics, pathology, and shedding. Our aim was to clarify risk for H5N1 infection among camelid populations, elucidate cross-species transmission dynamics, and better define the potential for additional mammalian adaptation.

Methods

The experiment and all subsequent sample analyses were conducted at the Friedrich-Loeffler-Institut (Greifswald, Germany) in the licensed high containment Biosafety Level 3 laboratories and Biosafety Level 3 large animal facilities by using required personal protective measures in accordance with the respective permits. We obtained 6 healthy male alpacas (*Vicugna pacos*), 12–24 months of age, from a local breeder. We housed animals in 2 groups of 3 (stable 1 and stable 2) and allowed them to acclimatize to housing conditions for >2 weeks before infection. We provided loose hay in hay bags and specialized camelid feed in troughs; water was available ad libitum throughout the study period.

Experimental Setup and Sampling

We obtained baseline jugular venous blood samples and nasal and rectal swab samples 1 day before inoculation. Then, we intranasally inoculated each of the 6 alpacas by using a nasal nebulizer device on a 1-mL syringe. Animals received $10^{5.9}$ 50% tissue culture infectious dose ($TCID_{50}$), $10^{5.6}$ $TCID_{50}$/mL per nostril, of HPAI H5N1 genotype B3.13 virus isolate A/Cattle/Texas/063224-24-1/2024 (GISAID accession no. EPI_ISL_19155861). We confirmed inoculum titer by back-titration.

Staff monitored animals daily for wellbeing and collected nasal and rectal swab samples on days 1–9 and 11 after inoculation. At 4 days postinoculation (dpi), the 3 animals from stable 1 were euthanized to collect serum and organ samples, including nasal conchae (respiratory and olfactory regions), trachea (cranial and caudal), lungs (all lobes), liver, kidney, and spleen. The 3 animals from stable 2 were euthanized at 20 dpi for collection of the same sample panel.

Sample Preparation

We collected blood samples by using KABEVETTE G systems with disposable needles (KABE Labortechnik, https://kabe-labortechnik.de). We suspended swabs in 2 mL of Dulbecco Modified Eagle Medium supplemented with 1 mg/mL enrofloxacin, 1 mg/mL lincomycin, 0.05 mg/mL gentamycin, and 0.05 mg/mL amphotericin. We transferred organ samples (≈2 mm^3) into tubes containing medium with penicillin (10 U/mL) and streptomycin (10 µg/mL) and a stainless-steel bead. We homogenized organ samples for 2 minutes at 300 Hz by using TissueLyser II (QIAGEN, https://www.qiagen.com). We extracted viral RNA from 100 µL of swab medium and organ homogenates by using the NucleoMag Vet kit (Macherey-Nagel, https://www.mn-net.com) on a BioSprint 96 platform (QIAGEN).

ELISAs

We evaluated serum samples by using 2 different ELISAs. First, we used an in-house clade 2.3.4.4b–adapted H5 nanoluciferase–based ELISA (*30*). In brief, we coated high-binding ELISA plates overnight at 4°C with 0.2 µg/well H5 HA1 and blocked with 5% skim milk. We preincubated 1:10 serum samples with 2×10^5 luciferase light units (LU) H5-nanoluciferase for 1 hour at room temperature, then added to ELISA plates for and incubated another hour. We measured bioluminescence in LU by using the Nano-Glo Luciferase Assay System (Promega, https://www.promega.com). Second, we used an updated version of the ID Screen Influenza H5 Antibody Competition 3.0 Multi-species ELISA (Innovative Diagnostics, https://innovative-diagnostics.com), following the manufacturer's protocol. We diluted heat-inactivated serum 1:10 and incubated on H5-coated plates with controls. After washing, we sequentially added conjugate and substrate and measured absorbance at 450 nm. We interpreted results by using bovine thresholds, considering signal-to-noise ratio ≤40% as positive and 40%–50% as doubtful.

Virus Neutralization Test

We determined virus-neutralizing antibodies by using a 100% virus neutralization assay on MDCKII cells. We serially diluted serum samples by $\log_2$ steps, mixed with 100 $TCID_{50}$ of virus, and incubated for 1 hour at 37°C. We then added MDCKII cells and incubated at 37°C for 72 hours. We defined neutralization titers as the highest dilution without visible cytopathic effect.

Viral RNA Detection

We used quantitative reverse transcription PCR (qRT-PCR) to detect matrix (M) gene segment 7 of the H5N1 virus genome (*31*), according to European Union Reference Laboratory recommendations (*32*). We performed relative quantification in CFX Maestro software (Bio-Rad Laboratories, https://www.bio-rad.com).

Infectious Titer Determination

We determined virus titers in nasal swab samples and PCR-positive organ samples by $TCID_{50}$ endpoint dilution assays on MDCKII cells. We applied serial 10-fold dilutions to cell monolayers and incubated at 37°C for 72 hours, then calculated titers by using the Spearman–Kärber method on the basis of cytopathic effect.

Pathology

During necropsies, we recorded lesions and fixed tissue samples in 4% buffered formaldehyde. On the basis of virologic data, we paraffin-embedded nasal conchae from the respiratory and olfactory regions, nasopharyngeal tonsil, mandibular lymph node, trachea (cranial, caudal), lung (left cranial, caudal lobe; right cranial, middle, caudal, accessory lobe), and brain. We sectioned 2–4 µm of tissue and stained with hematoxylin and eosin, following routine protocols (*33*). We prepared consecutive sections for viral antigen detection by using a primary antibody against influenza A virus (IAV) nucleoprotein (ATCC clone HB-64), as previously described (*21*). As a negative control, we tested 20 dpi PCR-negative conchae with the primary antibody and labeled consecutive sections of PCR-positive samples with a 1:45 dilution of irrelevant SARS antibody clone 4F3C4 (*21*). We processed consecutive slides of the nasal conchae and tonsil for RNA in situ hybridization (ISH). To visualize RNA, we used a custom-designed probe and the RNAScope 2-5 HD Reagent Kit Red (Advanced Cell Diagnostics, https://info.acdbio.com), according to the manufacturer's instructions. We used

probes against peptidylprolyl isomerase B and dihydrodipicolinate reductase genes as technical controls. We used archived tissues from HPAIV-infected chickens as positive controls for immunohistochemistry (IHC) and ISH.

To clarify histologic findings, we used IHC and ISH to test the olfactory bulb of animal 6 for virus antigen and RNA, as described. We performed immune cell labeling by using a 1:500 dilution of Anti Iba-1, Rabbit (FUJIFILM Wako Chemicals Europe, https://labchem-wako.fujifilm.com) antibodies against ionized calcium binding adaptor molecule 1 (Iba-1) targeting microglia and macrophages. To detect Iba-1 antibodies, we used biotinylated goat anti-rabbit IgG secondary antibody and incubated slides with Vectastain Elite ABC-HRP Kit (both Vector Laboratories, https://vectorlabs.com). We also targeted T cells by using a 1:100 dilution of Polyclonal Rabbit Anti-Human CD3 (DAKO Agilent, https://www.agilent.com) and ImmPRESS HRP Goat Anti-Rabbit IgG Polymer Detection Kit (Vector Laboratories) for detection. We used sections of the nasal tonsil as positive controls for Iba-1 and CD3. As a negative control, we tested consecutive sections with an irrelevant antibody targeting rustrela virus clone 2H11B1. We produced bright red intracytoplasmic chromogen labeling by using the AEC Substrate Kit (abcam, https://www.abcam.com). We counter-stained sections with Mayer hematoxylin.

A pathologist certified through the European College of Veterinary Pathologists digitally evaluated and interpreted IHC and ISH by using NDP.view2 software (Hamamatsu Photonics, https://www.hamamatsu.com). We also processed brain paraffin sections for viral genome detection by PCR following the same protocol as other tissues.

Results

Clinical Signs

We observed no major reduction in alpaca wellbeing after H5N1 infection. Overall mean body temperature remained constant (38.3°C) and within physiologic range (37.5°C–38.9°C) (*34*), but animals 3 and 5 had temperature peaks of 39.6°C at 1 dpi, and animal 2's temperature peaked at 39.1°C at 2 dpi, indicating early antiviral immune response (Figure 1, panel A).

We retrospectively estimated the semiquantitative feed intake at the stable level. At 2 dpi, feed intake in stable 2 decreased to ≈40% of typical intake; at 3 dpi, both stables had feed intake of ≈30% of the typical intake (Figure 1, panel B). Feed intake in both stables returned to 100% at 4 dpi.

Transient Respiratory Virus Shedding

Cycle threshold (Ct) values <45 reflect detection of viral RNA; we considered Ct values <30 to indicate high viral shedding. Nasal swab samples began yielding positive results at 1 dpi with a mean Ct value of 32.95 (Figure 1, panel C). Samples from animals 1 and 3 became negative at 3 dpi, 1 day before planned euthanasia, but other animals constantly shed viral RNA for several days. At 9 dpi, animal 6 was the last to shed traces of viral genome (Ct value 40.17). Two animals demonstrated high viral genome loads on various days: animal 6 at 1 dpi (Ct value 29.98) and 4 dpi (Ct value 27.56) and animal 4 at 2 dpi (Ct value 24.30), 5 dpi (23.47), and 6 dpi (27.90). At 11 dpi, all nasal swab samples tested negative.

Nasal swab sample virus titers showed high individual variation: at 1 dpi, titers ranged from negative (below limit of detection [LOD], $10^{1.5}$ $TCID_{50}$/mL) to $10^{3.3}$ $TCID_{50}$/mL; at 4 dpi, titers were 10^{3} to $10^{3.8}$ $TCID_{50}$/mL; and at 6 dpi, titers ranged from negative to $10^{3.8}$ $TCID_{50}$/mL (Figure 1, panel D). Rectal swab samples did not demonstrate continuous viral shedding by qRT-PCR (Figure 1, panel E).

Among organ samples collected at 4 dpi from stable 1 animals, individual nose and trachea samples revealed slightly positive Ct values of 36.4–42 (LOD 45), all remaining organ samples tested negative (Figure 1, panel F); we observed the same for samples collected at 20 dpi (data not shown). Of note, the back right nose sample of animal 2 and the cranial trachea sample and back left nose sample of animal 1 tested positive for virus genome by PCR and by endpoint dilution at $10^{1.88}$, $10^{1.82}$, and $10^{1.62}$ $TCID_{50}$/mL (Figure 1, panel F).

We used MinION (Oxford Nanopore Technologies, https://nanoporetech.com) to conduct next-generation sequencing on washing samples collected at 6 dpi (Appendix, https://wwwnc.cdc.gov/EID/article/32/9/26-0491-App1.pdf). Those results did not indicate any mutations. We deposited sequences in GISAID (accession no. EPI_ISL_20453888).

Humoral Immune Response

All 20 dpi serum samples tested positive for H5 binding antibodies by the in-house ELISA, but samples from animals euthanized at 4 dpi were nonreactive (Figure 1, panel G). The H5-specific commercial ELISA confirmed those results for all but 1 animal (Appendix Figure 2). Of note, microneutralization confirmed the ELISA positivity in 2 of 3 animals at 20 dpi; the weakly ELISA-positive animal was negative by microneutralization (Figure 1, panel H).

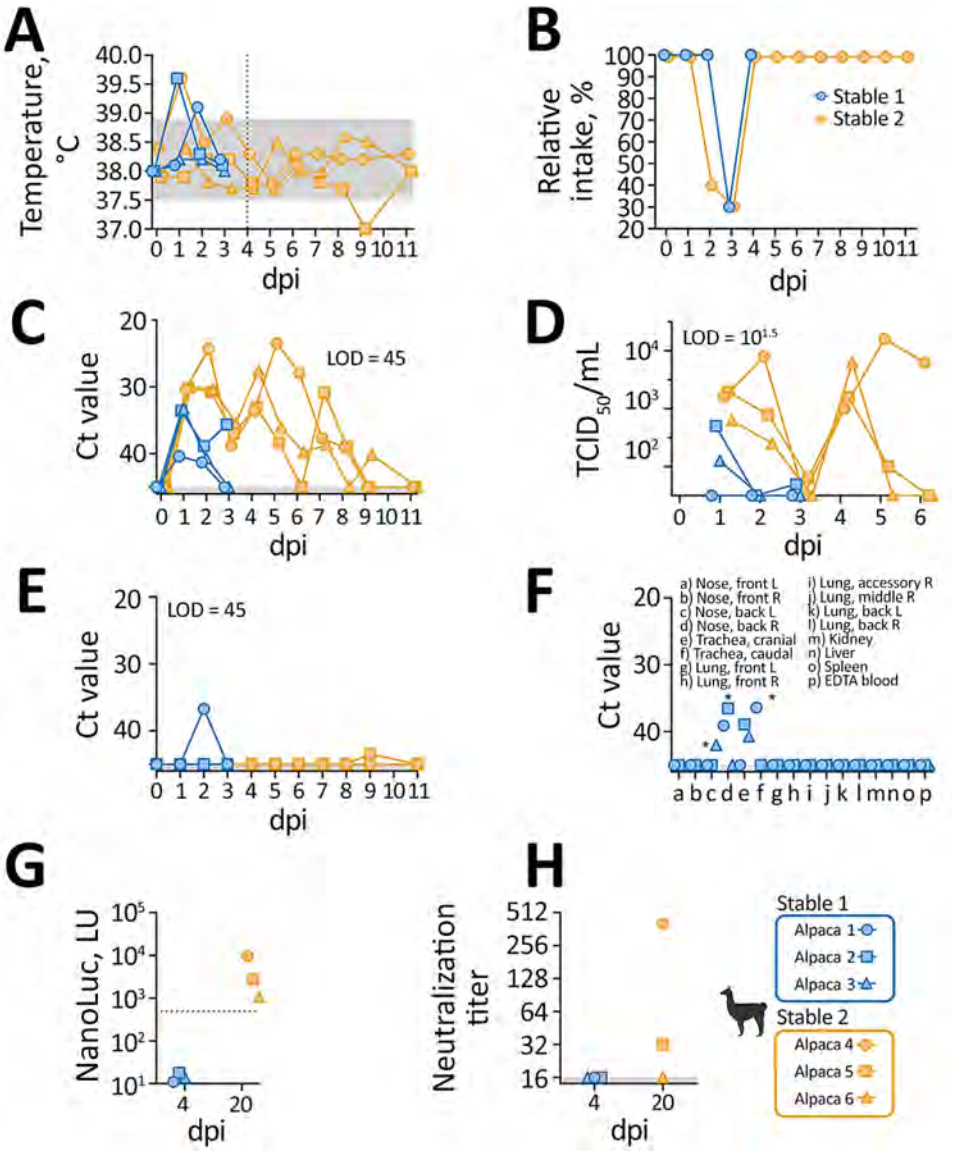

Figure 1. Clinical and laboratory findings from experimental highly pathogenic avian influenza A(H5N1) clade 2.3.4.4b virus infection in alpacas, 2026. Stable 1 alpacas were sampled before euthanasia at 4 dpi; stable 2 alpacas were sampled for 20 dpi before euthanasia. A, B) Clinical signs; C–H) laboratory findings. A) Body temperature; shading indicates physiologic range; dotted vertical line indicates dpi that stable 1 alpacas were euthanized. B) Percentage of typical feed intake. C) Quantitative reverse transcription PCR (qRT-PCR) results on nasal swab samples showing H5N1 viral genome was detected until 9 dpi. Shading indicates LOD. D) Nasal swab sample infectious titers. E) qRT-PCR results on rectal swab samples. Shading indicates LOD. F) qRT-PCR results on tissue samples. Of note, only nose and trachea samples were qRT-PCR–positive as evaluated by endpoint dilution assays for quantification of infectious virus. Asterisks indicate samples that tested positive for infectivity by endpoint dilution at $10^{1.88}$, $10^{1.82}$, and $10^{1.62}$ $TCID_{50}$/mL. G) ELISA specific for H5 antibodies, confirming positivity of samples collected at 20 dpi. H) Neutralization titers determined by using a live virus neutralization test against 100 $TCID_{50}$, with the endpoint defined as complete protection from cytopathic effect. Titers are expressed as reciprocal serum dilution, confirming measurable neutralizing capacity for 2 of the samples that tested positive by ELISA. dpi, days postinfection; L, left; LOD, limit of detection; LU, light unit; NanoLuc, nanoluciferase; R, right; $TCID_{50}$, 50% tissue infective dose.

IHC and ISH

IHC and ISH identified viral RNA and antigen in the nasopharyngeal tonsil from all 3 animals euthanized at 4 dpi. ISH showed marked labeling, but antigen detection was less prominent. In animals 1 and 3, virus detection was limited to cytoplasmic signals in macrophages or dendritic cells, indicating phagocytosis of virus RNA and protein (Figure 2, panels A–C). In alpaca 2, we detected virus RNA and minimal virus protein in the nucleus and cytoplasm in cells of the follicle-associated epithelium, indicating infection and potential replication (Figure 2, panels D–F). Only alpaca 1 exhibited viral RNA within the lumen of the left cranial nasal cavity, associated with cellular detritus (Figure 2, panel G).

Whether the minimal viral RNA detected in the ciliated respiratory nasal epithelium in animals 1 and 4 (Figure 2, panels H, I) is attributable to infection remains speculative. Histopathology revealed minor lesions consistent with rhinitis (animals 1, 2, 4–6), tracheitis (animals 5, 6), and 1 instance each of chronic interstitial pneumonia (animal 1), pleuritis (animal 3), and even encephalitis affecting the olfactory bulb (animal 6). However, none of the findings can be reliably associated with IAV infection because we did not detect viral RNA nor viral antigen associated with those lesions by IHC and

ISH (Appendix Table 1, Figure 1). In addition, brain paraffin sections of animal 6 tested PCR-negative for viral genome.

Discussion

In May 2024, HPAI H5N1 clade 2.3.4.4b virus infection was confirmed in alpacas, the first documented

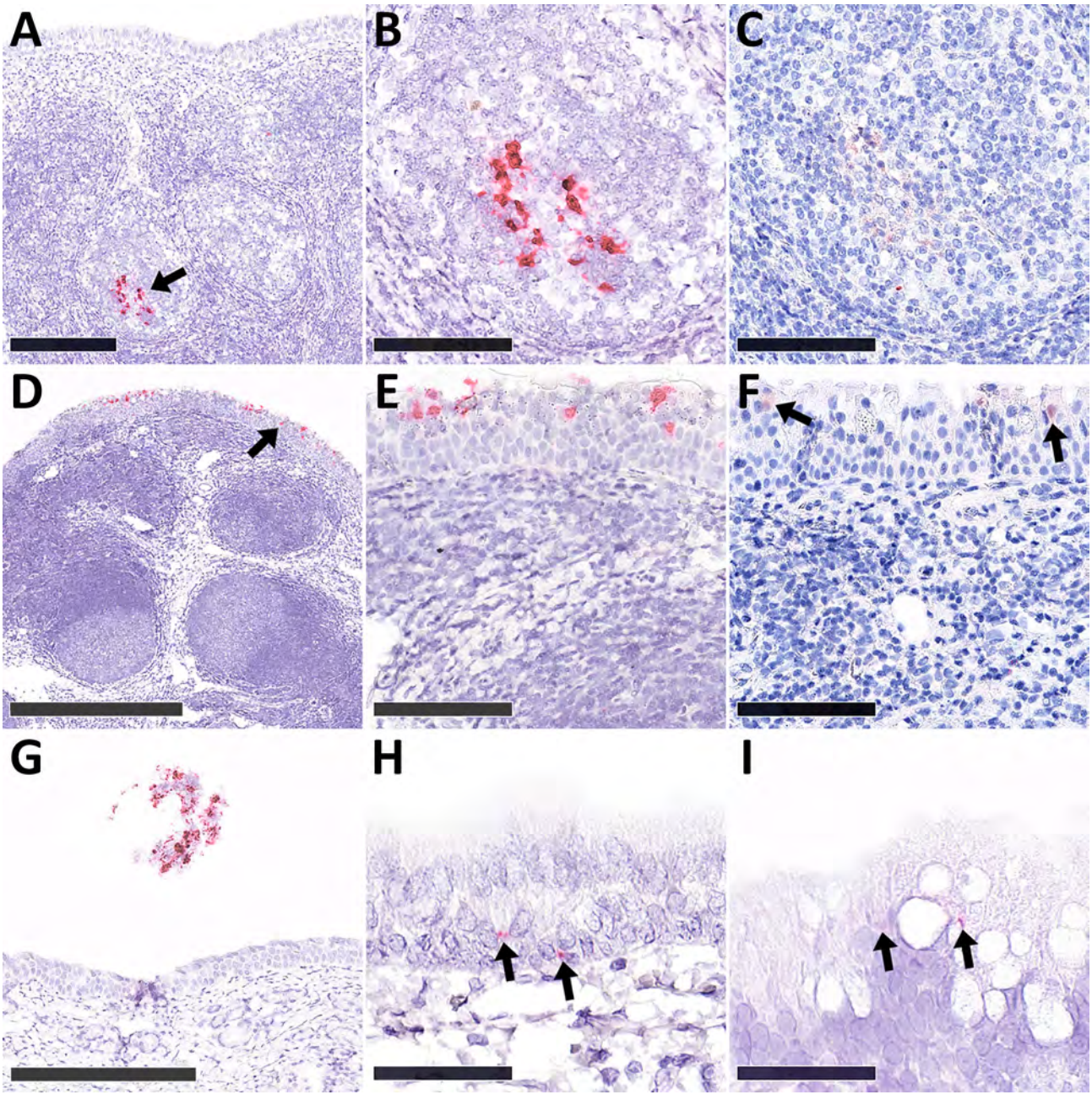

Figure 2. Histopathologic detection in nasopharyngeal tonsil and nasal conchae from experimental highly pathogenic avian influenza A(H5N1) clade 2.3.4.4b virus infection in alpacas, 2026. In situ hybridization (ISH) performed by using Fast Red chromogen; immunohistochemistry (IHC) performed by using 3-amino-9-ethylcarbazole substrate for red-brown chromogen; Mayer's hematoxylin counterstain used for both ISH and IHC. A, B) ISH showing strong cytoplasmic RNA labeling (arrow in A [scale bar indicates 250 μm], detail in B [scale bar indicates 100 μm]) from nasopharyngeal tonsil of alpaca 3. C) IHC of nasopharyngeal tonsil from alpaca 3 showing weak antigen signals within follicular macrophages and dendritic cells; scale bar indicates 100 μm. D–F) Tonsillar epithelium from alpaca 2. D, E) ISH showing viral RNA (arrow in D [scale bar indicates 250 μm], detail in E [scale bar indicates 100 μm]); F) IHC showing antigen (arrows) in the nucleus and cytoplasm. Scale bar indicates 100 μm. G–I) ISH showing abundant detection of viral RNA within cellular debris on left cranial nasal cavity tissue from alpaca 1 (G; scale bar indicates 250 μm), nasal epithelium of alpaca 1 at 4 days postinfection (H), and alpaca 4 at 20 days postinfection (I) (arrows). Scale bars indicate 50 μm.

natural infection of this virus type in camelids (*27*). The detection occurred on premises where poultry had been culled because of HPAIV H5N1, and genomic analysis revealed that the viral sequence was identical to the B3.13 genotype circulating in US dairy cattle and consistent with the depopulated poultry on site (*27*).

Camelid IAV infections have previously been reported. For instance, after the 1977 influenza epidemic in Russian, an epizootic was reported among camels in Mongolia (*35*). A reassorted virus was identified as the cause but was shown to be antigenically highly related to A/USSR/90/77 (H1N1), the strain from the epidemic in Russia (*35*). In the same region, camel infections with low pathogenicity avian influenza H7N9 and equine H3N8 viruses also have been reported (*36*,*37*). IAV exposure and infection, including H1 and H3 subtypes, have been detected in camels in Africa (*38*). However, H5 infection had not been reported in camelids until HPAIV H5N1 was confirmed in US alpacas in 2024 (*27*). Although transmission was not unexpected considering high viral load in the environment and co-mingling of livestock species (*27*), identification of alpacas as susceptible hosts expands the known mammalian host range of HPAIV H5N1. The experimentally generated data from this study, including the detailed pathologic characterization, will enable meaningful comparisons in the future.

Roughly 262,000 alpacas are housed in the United States (*39*). In South America, the total camelid population is much larger, ≈12 million (*40*). Although no H5N1 infections have been reported among camelid species in South America, the large camelid population, comprising ≈4.0 million llamas and ≈7.5 million alpacas in domestic herds, and ≈350,000 vicuñas and ≈600,000 guanacos in wild herds, represents a substantial interface with humans and a huge potential reservoir (*40*). Among domesticated species, 85% are raised by small producers, often women, with herds of <100 animals playing a fundamental role in milk, meat, and fiber production (*40*). That demographic and livestock structure underscores why surveillance in a diverse set of mammalian hosts is vital for public health, especially considering H5N1 clade 2.3.4.4b virus has caused mass die-offs in sea lions and elephant seals in South America since late 2022 (*41*). That marine mammal–adapted virus clade has shown mutations consistent with mammal-to-mammal transmission, raising concern for further mammalian adaptation (*41*).

H5N1 clade 2.3.4.4b viruses in North America comprise multiple genotypes and efficiently replicate and spread in wild bird populations (*42*). Those factors increase risk for clade 2.3.4.4b virus spillover to a range of mammals, including ruminants, carnivores, and camelids, potentially enhancing the virus' capacity for adaptation to mammalian hosts. Most bird-to-mammal transmissions appear to be dead-end infections mostly affecting terrestrial carnivores feeding on infected prey (*19*). Mammal-to-mammal transmissions rarely become established because large mammal groups and frequent contact are needed to maintain transmission chains; however, H5N1 receptor specificity remains avian α2-3–like (*43*). That observation matches the observed clinical picture for bovine and zoonotic infections because α2-3 linked sialic acids are abundant not only in avian species but also in bovine mammary glands and human conjunctiva (*11*). Nevertheless, efficient mammal-to-mammal H5 virus transmission has been confirmed in mink farms (*44*), among aquatic mammals in South America (*41*,*45*), and from cattle to cats and humans via milk (*20*). Those transmission events correlated with accumulation of further mammal-adaptive mutations (*11*,*46*), and a shift toward mammal-adapted variants was evident in some cases, reflected in accumulation of multiple mammalian-adaptive mutations (*11*). Data of intramammary and oronasal experimental H5N1 B3.13 virus infection of goats show efficient virus replication in the mammary glands, comparable to that in cows, but only limited virus replication and necrotizing interstitial pneumonia at early (3 dpi) timepoints (*47*).

We experimentally confirmed that alpacas can be intranasally infected with a bovine HPAIV H5N1 B3.13 isolate, leading to subsequent nasal shedding of infectious virus. IHC and ISH confirmed H5N1 virus replication in the nasopharyngeal tonsil and the nasal conchae. Productive infection was corroborated by seroconversion at 20 dpi. We detected individual variation of neutralizing antibody levels, but the small number of animals does not enable general conclusions. The infection did not cause fever, but alpacas reduced feed intake. Whether the viral load shed by the alpacas would be sufficient to cause transmission to contact animals remains undetermined. Intermittent viral RNA detection and low viral titer at 3 dpi might reflect technical variability of the sampling procedure rather than reduced shedding.

Our data did not suggest that alpacas replicate H5N1 clade 2.3.4.4b genotype B3.13 virus with exceptionally high efficiency. However, nasal replication occurred, and infectious virus was detectable in nasal swab samples for up to 6 dpi, but sequencing did not indicate accumulation of mutation to that timepoint. Nevertheless, viral adaptation after

infection or shedding to naive contact animals or humans cannot be excluded. A follow-up study should include direct-contact animals to assess the biologic relevance of low-level shedding and to clarify the potential role of alpacas in H5N1 transmission. In addition, future studies should include experimental intramammary inoculation of female alpacas to evaluate susceptibility via that route.

In conclusion, H5N1 clade 2.3.4.4b virus will likely continue to drive substantial mortality rates in wild birds and marine mammals across North and South America. Risk for virus spillover into domestic animals, including poultry and potentially camelids, will continue considering their large populations on the continents. The demonstrated capacity of H5N1 clade 2.3.4.4b virus to acquire mammalian-adaptive mutations heightens concern about cross-species transmission and possible establishment in new mammalian hosts, which could intensify wildlife losses, disrupt livestock production, and generate new zoonotic risks. Sustained surveillance, strengthened biosecurity, and rapid response measures will be essential to limit those impacts.

Acknowledgments

We thank Diego Diel and his team from the Cornell University College of Veterinary Medicine for providing the B3.13 virus isolate. We gratefully acknowledge Anne Pohlmann for her valuable assistance with sequence analysis. We thank the laboratory staff Mareen Grawe and Robin Brandt for their excellent technical assistance. We also thank the animal care staff, Felix Zimak, Frank Klipp, Steffen Kiepert, and Christian Lipinski, for their dedicated husbandry support and commitment to animal welfare throughout this study.

The ethics committee of the State Office of Agriculture, Food, Safety, and Fishery in Mecklenburg–Western Pomerania (LALLF M-V) evaluated the experiment and governmental approval was granted under the registration number 7221.3-2-010/23. The experiment followed the relevant requirements of the German Infection Protection Act, the Biologic Agents Ordinance and the Animal Pathogens Ordinance.

This work was funded by the DURABLE project, cofunded by the European Union, under the EU4Health Programme (EU4H project no. 101102733).

Selected sections of this manuscript were reviewed and edited with assistance from ChatGPT (OpenAI, https://chatgpt.com) to improve readability and English language quality. All such content was reviewed and approved by the authors, who take full responsibility for the final content.

Author contributions: M.B. and D.H. conceptualized the study. M.H., A.B., J.S., N.H., A.A., A.K.A., and D.H. performed the experiments. J.S. wrote the original draft. All authors reviewed and approved the final manuscript. M.B. supervised the project and acquired funding.

About the Author

Dr. Schön is a postdoctoral researcher at the Friedrich-Loeffler-Institute, Germany's Federal Research Institute for Animal Health. His work focuses on zoonotic respiratory viral infections such as SARS-CoV-2 and Influenza A.

References

1. Xu X, Subbarao K, Cox NJ, Guo Y. Genetic characterization of the pathogenic influenza A/Goose/Guangdong/1/96 (H5N1) virus: similarity of its hemagglutinin gene to those of H5N1 viruses from the 1997 outbreaks in Hong Kong. Virology. 1999;261:15–9. https://doi.org/10.1006/viro.1999.9820
2. Bender C, Hall H, Huang J, Klimov A, Cox N, Hay A, et al. Characterization of the surface proteins of influenza A (H5N1) viruses isolated from humans in 1997–1998. Virology. 1999;254:115–23. https://doi.org/10.1006/viro.1998.9529
3. Chan PK. Outbreak of avian influenza A(H5N1) virus infection in Hong Kong in 1997. Clin Infect Dis. 2002;34(Suppl 2):S58–64. https://doi.org/10.1086/338820
4. Globig A, Staubach C, Sauter-Louis C, Dietze K, Homeier-Bachmann T, Probst C, et al. Highly pathogenic avian influenza H5N8 clade 2.3.4.4b in Germany in 2016/2017. Front Vet Sci. 2018;4:240. https://doi.org/10.3389/fvets.2017.00240
5. Guan Y, Smith GJ. The emergence and diversification of panzootic H5N1 influenza viruses. Virus Res. 2013;178:35–43. https://doi.org/10.1016/j.virusres.2013.05.012
6. Lee D-H, Bertran K, Kwon J-H, Swayne DE. Evolution, global spread, and pathogenicity of highly pathogenic avian influenza H5Nx clade 2.3.4.4. J Vet Sci. 2017;18:269–80. https://doi.org/10.4142/jvs.2017.18.S1.269
7. Xie R, Edwards KM, Wille M, Wei X, Wong S-S, Zanin M, et al. The episodic resurgence of highly pathogenic avian influenza H5 virus. Nature. 2023;622:810–7. https://doi.org/10.1038/s41586-023-06631-2
8. King J, Staubach C, Lüder C, Koethe S, Günther A, Stacker L, et al. Connect to protect: dynamics and genetic connections of highly pathogenic avian influenza outbreaks in poultry from 2016 to 2021 in Germany. Viruses. 2022;14:1849. https://doi.org/10.3390/v14091849
9. Zeng J, Du F, Xiao L, Sun H, Lu L, Lei W, et al. Spatiotemporal genotype replacement of H5N8 avian influenza viruses contributed to H5N1 emergence in 2021/2022 panzootic. J Virol. 2024;98:e0140123. https://doi.org/10.1128/jvi.01401-23
10. Ahrens AK, Pohlmann A, Grund C, Harder T, Beer M. Novel genotypes of highly pathogenic avian influenza H5N1 clade 2.3.4.4b viruses, Germany, November 2023. Emerg Infect Dis. 2024;30:1737–9. https://doi.org/10.3201/eid3008.240103
11. Peacock TP, Moncla L, Dudas G, VanInsberghe D, Sukhova K, Lloyd-Smith JO, et al. The global H5N1 influenza panzootic in mammals. Nature. 2025;637:304–13. https://doi.org/10.1038/s41586-024-08054-z

12. Kandeil A, Patton C, Jones JC, Jeevan T, Harrington WN, Trifkovic S, et al. Rapid evolution of A(H5N1) influenza viruses after intercontinental spread to North America. Nat Commun. 2023;14:3082. https://doi.org/10.1038/s41467-023-38415-7
13. Huang P, Sun L, Li J, Wu Q, Rezaei N, Jiang S, et al. Potential cross-species transmission of highly pathogenic avian influenza H5 subtype (HPAI H5) viruses to humans calls for the development of H5-specific and universal influenza vaccines. Cell Discov. 2023;9:58. https://doi.org/10.1038/s41421-023-00571-x
14. Caliendo V, Lewis NS, Pohlmann A, Baillie SR, Banyard AC, Beer M, et al. Transatlantic spread of highly pathogenic avian influenza H5N1 by wild birds from Europe to North America in 2021. Sci Rep. 2022;12:11729. https://doi.org/10.1038/s41598-022-13447-z
15. Mostafa A, Nogales A, Martinez-Sobrido L. Highly pathogenic avian influenza H5N1 in the United States: recent incursions and spillover to cattle. Npj Viruses. 2025;3:54. https://doi.org/10.1038/s44298-025-00138-5
16. Youk S, Torchetti MK, Lantz K, Lenoch JB, Killian ML, Leyson C, et al. H5N1 highly pathogenic avian influenza clade 2.3.4.4b in wild and domestic birds: introductions into the United States and reassortments, December 2021–April 2022. Virology. 2023;587:109860. https://doi.org/10.1016/j.virol.2023.109860
17. US Department of Agriculture Animal and Plant Health Inspection Service. Detections of highly pathogenic avian influenza in wild birds [cited 2026 Jan 19]. https://www.aphis.usda.gov/livestock-poultry-disease/avian/avian-influenza/hpai-detections/wild-birds
18. US Department of Agriculture Animal and Plant Health Inspection Service. Confirmations of highly pathogenic avian influenza in commercial and backyard flocks [cited 2026 Jan 19]. https://www.aphis.usda.gov/livestock-poultry-disease/avian/avian-influenza/hpai-detections/commercial-backyard-flocks
19. US Department of Agriculture Animal and Plant Health Inspection Service. Detections of highly pathogenic avian influenza in mammals [cited 2026 Jan 19]. https://www.aphis.usda.gov/livestock-poultry-disease/avian/avian-influenza/hpai-detections/mammals
20. Caserta LC, Frye EA, Butt SL, Laverack M, Nooruzzaman M, Covaleda LM, et al. Spillover of highly pathogenic avian influenza H5N1 virus to dairy cattle. Nature. 2024;634:669–76. https://doi.org/10.1038/s41586-024-07849-4
21. Halwe NJ, Cool K, Breithaupt A, Schön J, Trujillo JD, Nooruzzaman M, et al. H5N1 clade 2.3.4.4b dynamics in experimentally infected calves and cows. Nature. 2025;637:903–12. https://doi.org/10.1038/s41586-024-08063-y
22. Hu S, Cui J. Cattle H5N1 outbreak in US driven by cow's "cross-nursing" behaviour: elucidating a novel transmission mechanism. Emerg Microbes Infect. 2025;14:2547736. https://doi.org/10.1080/22221751.2025.2547736
23. Shi J, Kong H, Cui P, Deng G, Zeng X, Jiang Y, et al. H5N1 virus invades the mammary glands of dairy cattle through 'mouth-to-teat' transmission. Natl Sci Rev. 2025;12:nwaf262. https://doi.org/10.1093/nsr/nwaf262
24. Sah R, Srivastava S, Kumar S, Mehta R, Donovan S, Sierra-Carrero L, et al. Concerns on H5N1 avian influenza given the outbreak in U.S. dairy cattle. Lancet Reg Health Am. 2024;35:100785. https://doi.org/10.1016/j.lana.2024.100785
25. Callahan D. Stevens County goat tests positive for same influenza virus affecting poultry. Minnesota Board of Animal Health. March 20, 2024 [cited 2026 Mar 17]. https://www.bah.state.mn.us/news_release/stevens-county-goat-tests-positive-for-same-influenza-virus-affecting-poultry
26. Rolfes MA, Kniss K, Kirby MK, Garg S, Reinhart K, Davis CT, et al. Human infections with highly pathogenic avian influenza A(H5N1) viruses in the United States from March 2024 to May 2025. Nat Med. 2025;31:3889–98. https://doi.org/10.1038/s41591-025-03905-2
27. US Department of Agriculture National Veterinary Servies Laboratories. Highly pathogenic avian influenza (HPAI) H5N1 detections in alpacas [cited 2026 Mar 17]. https://www.aphis.usda.gov/livestock-poultry-disease/avian/avian-influenza/hpai-detections/mammals/highly-pathogenic-avian
28. Alexakis L, Fusaro A, Kuiken T, Mirinavičiūtė G, Ståhl K, Staubach C, et al.; European Food Safety Authority; European Centre for Disease Prevention and Control; European Union Reference Laboratory for Avian Influenza. Avian influenza overview March–June 2024. EFSA J. 2024;22:e8930. https://doi.org/10.2903/j.efsa.2024.8930
29. Lehman KA, Leibsle SR, Detwiler L, Gaborick C, McCoy-Harrison L, Snekvik K, et al. Detection of highly pathogenic avian influenza A(H5N1) virus 2.3.4.4b in alpacas. J Vet Diagn Invest. 2026;12:10406387251414557. https://doi.org/10.1177/10406387251414557
30. Aebischer A, Günther A, Piesche R, Wernike K, Murr M, Harder T, et al. Development of a multi-species luciferase-based double-antigen ELISA for the detection of antibodies against influenza A virus H5 clade 2.3.4.4b. J Clin Microbiol. 2026 Aug 13 [Epub ahead of print]. https://doi.org/10.1128/jcm.01907-25
31. Laconi A, Fortin A, Bedendo G, Shibata A, Sakoda Y, Awuni JA, et al. Detection of avian influenza virus: a comparative study of the in silico and in vitro performances of current RT-qPCR assays. Sci Rep. 2020;10:8441. https://doi.org/10.1038/s41598-020-64003-6
32. Experimental Zooprophylactic Institute of the Veneto, European Union Reference Laboratory for Avian Influenza and Newcastle Disease. Detection of type A avian influenza virus by real-time RT-PCR [cited 2026 Mar 17]. https://www.izsvenezie.com/documents/reference-laboratories/avian-influenza/diagnostic-protocols/sop-vir-018.pdf
33. Wick MR. The hematoxylin and eosin stain in anatomic pathology—an often-neglected focus of quality assurance in the laboratory. Semin Diagn Pathol. 2019;36:303–11. https://doi.org/10.1053/j.semdp.2019.06.003
34. Animal and Plant Health Agency. Veterinary information sheet: South American camelids 2025 Jan 27 [cited 2026 Jan 29]. https://assets.publishing.service.gov.uk/media/678792c73f1182a1e258a235/APHA_Veterinary_Information_Sheet_-_South_American_Camelids.pdf
35. Yamnikova SS, Mandler J, Bekh-Ochir ZH, Dachtzeren P, Ludwig S, Lvov DK, et al. A reassortant H1N1 influenza A virus caused fatal epizootics among camels in Mongolia. Virology. 1993;197:558–63. https://doi.org/10.1006/viro.1993.1629
36. Yondon M, Heil GL, Burks JP, Zayat B, Waltzek TB, Jamiyan BO, et al. Isolation and characterization of H3N8 equine influenza A virus associated with the 2011 epizootic in Mongolia. Influenza Other Respir Viruses. 2013;7:659–65. https://doi.org/10.1111/irv.12069
37. Yin Y, Liu Y, Fen J, Liu K, Qin T, Chen S, et al. Characterization of an H7N9 influenza virus isolated from

camels in Inner Mongolia, China. Microbiol Spectr. 2023; 11:e0179822. https://doi.org/10.1128/spectrum.01798-22
38. Chu DKW, Perera RAPM, Ali A, Oladipo JO, Mamo G, So RTY, et al. Influenza A virus infections in dromedary camels, Nigeria and Ethiopia, 2015–2017. Emerg Infect Dis. 2020;26:173–6. https://doi.org/10.3201/eid2601.191165
39. Alpaca Owners Association Inc. Alpacas in the US [cited 2026 Mar 17]. https://www.alpacainfo.com/about/statistics/alpacas-us
40. Food and Agriculture Organization of the United Nations. FOA: camelids are a livelihood for 200,000 families in the Andean highlands of South America [cited 2026 Mar 17]. https://www.fao.org/americas/news/news-detail/camelidos-medio-subsistencia-altiplanos-andinos/en?com
41. Uhart MM, Vanstreels RET, Nelson MI, Olivera V, Campagna J, Zavattieri V, et al. Epidemiological data of an influenza A/H5N1 outbreak in elephant seals in Argentina indicates mammal-to-mammal transmission. Nat Commun. 2024;15:9516. https://doi.org/10.1038/s41467-024-53766-5
42. Fang K, Li J, Zhao H, Bahati J, Zhao Z, Song W, et al. Assessing HPAI-H5 transmission risk across wild bird migratory flyways in the United States. Nat Commun. 2026;17:2524. https://doi.org/10.1038/s41467-026-69344-w
43. Pulit-Penaloza JA, Belser JA, Brock N, Kieran TJ, Sun X, Pappas C, et al. Transmission of a human isolate of clade 2.3.4.4b A(H5N1) virus in ferrets. Nature. 2024;636:705–10. https://doi.org/10.1038/s41586-024-08246-7
44. Agüero M, Monne I, Sánchez A, Zecchin B, Fusaro A, Ruano MJ, et al. Highly pathogenic avian influenza A(H5N1) virus infection in farmed minks, Spain, October 2022. Euro Surveill. 2023;28:2300001. https://doi.org/10.2807/1560-7917.ES.2023.28.3.2300001
45. Leguia M, Garcia-Glaessner A, Muñoz-Saavedra B, Juarez D, Barrera P, Calvo-Mac C, et al. Highly pathogenic avian influenza A (H5N1) in marine mammals and seabirds in Peru. Nat Commun. 2023;14:5489. https://doi.org/10.1038/s41467-023-41182-0
46. Man W, Du L, Liu Y, Pang Z, Zhu H, Hong B, et al. Evolution of H5N1 cross-species transmission: adaptive mutations driving avian-to-human infection. Adv Genet (Hoboken). 2026;7:e00051. https://doi.org/10.1002/ggn2.202500051
47. Alkie TN, Embury-Hyatt C, Signore AV, Ramos D, Moffat E, Raj S, et al. Dairy cow- and avian-origin clade 2.3.4.4b H5N1 induce severe mastitis in lactating goats and transmission to suckling goats. Cell Rep. 2025;44:116346. https://doi.org/10.1016/j.celrep.2025.116346

Address for correspondence: Jacob Schön, Friedrich-Loeffler-Institut, Bundesforschungsinstitut für Tiergesundheit, Federal Research Institute for Animal Health Südufer 10, 17493 Greifswald–Insel Riems, Germany; email: jacob.schoen@fli.de

etymologia revisited

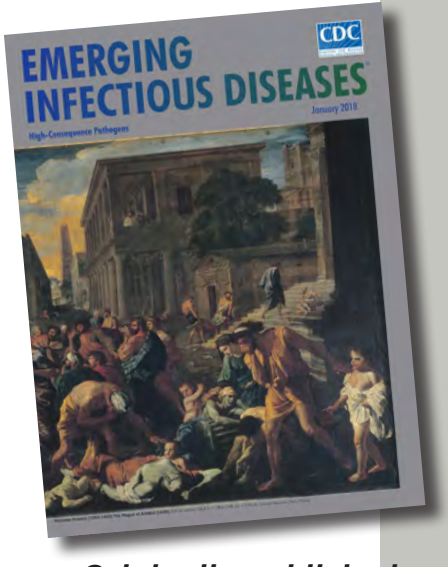

Originally published in January 2018

Plague

[plāg]

Plague (from the Latin *plaga*, "stroke" or "wound") infections are believed to have been common since at least 3000 BCE. Plague is caused by the ancestor of current *Yersinia* (named for Swiss bacteriologist Alexandre Yersin, who first isolated the bacterium) *pestis* strains. However, this ancestral *Y. pestis* lacked the critical *Yersinia* murine toxin (*ymt*) gene that enables vectorborne transmission. After acquiring this gene (sometime during 1600–950 BCE), which encodes a phospholipase D that protects the bacterium inside the flea gut, *Y. pestis* evolved the ability to cause pandemics of bubonic plague. The first recorded of these, the Justinian Plague, began in 541 ACE and eventually killed more than 25 million persons.

References:

1. Alexandre Yersin BW. Etymologia: yersinia. Emerg Infect Dis. 2010;16:496.
2. Centers for Disease Control and Prevention. History of plague [cited 2017 Oct 19]. https://www.cdc.gov/plague/history/index.html.
3. Rasmussen S, Allentoft ME, Nielsen K, Orlando L, Sikora M, Sjögren K-G, et al. Early divergent strains of Yersinia pestis in Eurasia 5,000 years ago. Cell. 2015;163:571–82.

https://wwwnc.cdc.gov/eid/article/24/1/et-2401_article

Wastewater Surveillance to Track Resurgent Measles Outbreak, Ontario, Canada, 2025

Ryland Corchis-Scott, Élisabeth Mercier, Edgard M. Mejia, Qiudi Geng, Ethan Harrop, Ana Podadera, Jackie Fong, Natalie Lewoc, Kenneth K.S. Ng, Nataliya Santiago, Natalie Knox, Lawrence Goodridge, Chand S. Mangat, Chrystal Landgraff, Karen B. Riddell, Mehdi Aloosh, Robert Delatolla, R. Michael McKay

The province of Ontario, Canada, experienced a major resurgent outbreak of measles in 2025. We conducted wastewater surveillance concurrently with clinical-based surveillance to track measles incidence in southwestern Ontario, adjacent to the United States. Measles virus (MeV) signal in wastewater was positively associated with clinical cases but did not provide early alert of changes in measles incidence when resolved by epidemiologic week. Assessment of virus partitioning showed MeV RNA was broadly distributed in the liquid phase but is most concentrated in the solids. We adapted an assay for differentiation of vaccine and wild-type MeV and used it to detect vaccine genotype measles after a vaccination campaign targeting underserved groups. We estimated MeV shedding in wastewater through sampling of sewer laterals serving a hospital treating measles infections. This outbreak is a case study in which we highlighted the use of wastewater surveillance for measles while supporting method development in real time.

Wastewater surveillance (WS) gained traction during the COVID-19 pandemic as an effective and unbiased means to track community infection complementary to clinical testing. Sampling a wastewater treatment plant (WWTP) or locations within a sewershed revealed infection hotspots and tracked genetic variants (*1*). Wastewater yielded high-quality whole-genome SARS-CoV-2 sequence data (*2*); it is a resource for tracking disease spread and a complement to clinical data to identify disease burden and routes of pathogen transmission (*3*,*4*). WS has extended to additional targets, including respiratory diseases (*5*), foodborne illness (*6*), and diseases of emerging concern, such as mpox and highly pathogenic avian influenza (*7*–*9*). Public health officials warned of the increased potential for outbreaks of vaccine-preventable diseases (*10*). COVID-19 pandemic–associated disruptions and vaccine misinformation affected immunization campaigns, including measles vaccination programs (*11*).

In 2025, Ontario experienced a large outbreak of measles; ≈2,400 confirmed cases were reported. Total cases nationwide reached 5,461 in 2025, positioning Canada as a hotspot for measles in North America (*12*). In November 2025, after 12 months of sustained transmission, Canada lost measles elimination status (*13*), a designation attained in 1998 (*14*). The 2025 outbreak of measles in Canada likely resulted from reduced vaccination coverage (*15*) and was the largest outbreak in 3 decades, overwhelming public health services, especially in southwestern Ontario, which experienced the highest caseload (*16*). Concurrent outbreaks in the US Southwest (*17*) and in Alberta, Canada (*18*), have raised interest in WS to complement clinical testing (*19*).

WS accounts for community members who might be hesitant to seek medical care (*20*); that characteristic is relevant to measles, considering most cases in North America have been linked to close-knit undervaccinated communities (*21*,*22*). Studies since 2025 have highlighted the application of WS to track measles at a community level (*23*–*26*) and assays that differentiate between wild-type virus and vaccine genotypes (*20*,*27*). Despite early successes, many challenges persist to broader and

Author affiliations: University of Windsor, Windsor, Ontario, Canada (R. Corchis-Scott, Q. Geng, E. Harrop, A. Podadera, J. Fong, K.K.S. Ng, R.M. McKay); University of Ottawa, Ottawa, Ontario, Canada (É. Mercier, R. Delatolla); National Microbiology Laboratory, Winnipeg, Manitoba, Canada (E.M. Mejia, N. Santiago, N. Knox, C.S. Mangat, C. Landgraff); Windsor Essex County Health Unit, Windsor (N. Lewoc, M. Aloosh); University of Guelph, Guelph, Ontario, Canada (L. Goodridge); Windsor Regional Hospital, Windsor (K.B. Riddell); McMaster University, Hamilton, Ontario, Canada (M. Aloosh)

DOI: https://doi.org/10.3201/eid3210.260092

more actionable adoption, including the clinical dynamics of viral shedding, viral partitioning within wastewater, and detection sensitivity (*21*), as well as the proximity of cases to monitored sewersheds. Here, we present a case study from a rural border municipality in southwestern Ontario demonstrating the application of WS for MeV during a measles outbreak. The outbreak persisted for >9 months, affording an opportunity for WS method development and enabling investigation to produce insights on MeV partitioning and on rates of viral shedding in wastewater. Our investigation used the outbreak as an opportunity to determine the feasibility of WS for MeV in a semirural setting and to help address challenges to its implementation.

Methods

Sample Collection

As part of an ongoing WS program, we collected composite wastewater samples over 24-hour periods, 3 per week, from the Leamington Pollution Control Centre (LPCC) in the Windsor-Essex region of Ontario, Canada, during February–November 2025. The LPCC serves the urban center of Leamington and accepts septage from residential septic tanks and frequently emptied storage tanks serving congregate living facilities in the rural area (≈30,000 total population served). We monitored sewer laterals draining Windsor Regional Hospital (WRH) using passive samplers (tampons) deployed 1–2 times/week. Passive samplers were submerged in the hospital effluent stream for 17–24 hours; at collection, they were transported to the laboratory for immediate processing (*28*).

Sample Processing for MeV Monitoring

We concentrated wastewater influent samples by filtration or affinity capture methods, and hospital effluent samples by centrifugation. After concentration, we extracted total nucleic acids and measured viral concentrations with quantitative reverse transcription PCR (qRT-PCR). We used an assay targeting the MeV nucleoprotein (N) gene for measles quantification (Appendix Table 1, https://wwwnc.cdc.gov/EID/article/32/10/26-0092-App1.pdf). We used a separate assay to measure pepper mild mottle virus in samples (*28*). We conducted sequencing to validate the identity of the amplicons obtained from the N gene of MeV (Appendix).

Partitioning of Endogenous MeV in Wastewater

To determine the partitioning of endogenous MeV in wastewater, we processed a 4-L postgrit wastewater

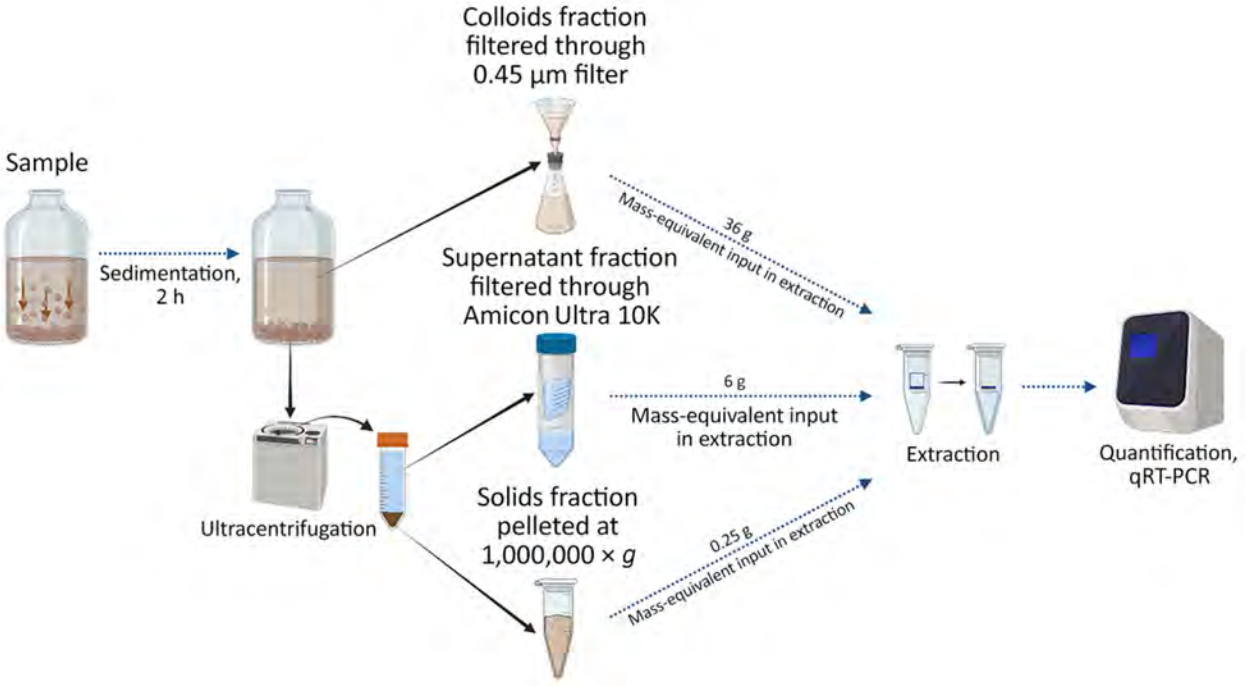

Figure 1. Schematic overview of wastewater processing in study of the utility of wastewater surveillance to track a resurgent outbreak of measles, Ontario, Canada, 2025. Sample processing and fractionation protocol were used to partition endogenous measles virus into solids, colloids, and supernatant fractions using Amicon Ultra 10K filters (Sigma Aldrich, https://www.sigmaaldrich.com) in wastewater collected from Leamington, Ontario, Canada.

sample collected from LPCC to derive fractions of solids, colloids, and supernatant (Figure 1). We performed partitioning calculations using 3 different assumptions: whole-sample basis, which considered wastewater composition; equal-mass basis; and operational volume basis, which reflects processing volumes commonly used in laboratory workflows (Appendix).

Detection of Vaccine Genotype MeV

We shipped raw influent samples weekly to the National Microbiology Laboratory (Winnipeg, MB, Canada) for additional analysis. Samples were processed as described previously (*29*), with minor modifications. To measure MeV wild-type and vaccine genotypes in wastewater, we used a multiplex assay developed for clinical detection (*30*). That triplex assay targets the large (L) gene for pan-MeV detection and the hemagglutinin (H) gene for wild-type and vaccine differentiation using a locked nucleic acid (LNA) probe for each target (Appendix).

Additional Data Sources

The WRH provided deidentified hospital admission and discharge dates for patients admitted with measles along with hospital water usage data. We obtained weekly measles case data from the Windsor-Essex County Health Unit (WECHU). We deemed symptomatic persons who sought care for fever; maculopapular rash for ≥3 days; and cough, coryza, or conjunctivitis, along with laboratory confirmation of infection, as having confirmed cases of measles. We also considered clinically compatible signs and symptoms in a person with an epidemiologic link to a laboratory-confirmed measles cases(*31*). The WECHU provided weekly vaccination data consisting of the number of measles, mumps, and rubella (MMR) vaccines administered in a targeted vaccination campaign. LPCC provided metadata (pH, temperature, flow) for each sample and the septage volume deposited at LPCC by private companies. The Windsor Regional Hospital Research Ethics Board (REB no. 25-529) and the University of Windsor Research Ethics Board (REB no. 25-127) provided research ethics approval.

Estimation of Viral Shedding

We estimated viral shedding rates for MeV using passive samplers deployed at WRH as described previously (*28*), with slight modifications. Because it is challenging to measure viral gene concentration in sampled flows using passive samplers, we calculated the concentration of MeV in hospital effluent using a previously reported mean suspended solids value for hospital effluent (*32*) and accounting for MeV partitioning. We reported shedding rates in $\log_{10}$ gene copies per day per person. We used admission and discharge times for MeV hospitalizations to determine both the number of hospitalized patients and the temporal overlap value. We reported shedding rates in $\log_{10}$ gene copies per day per person. We used median estimated shedding rate, average weekly flow, and MeV concentration to create an estimated weekly case count for LPCC sewershed (Appendix).

Statistical Methods

We performed statistical analyses using R version 4.5.1 (The R Project for Statistical Computing, https://www.r-project.org). We analyzed data collected during February–July 2025, ending with the last reported measles case in Leamington (Appendix).

Results

Partitioning of MeV in Wastewater

We determined the distribution of endogenous MeV across settled solids, colloids, and supernatant fractions of wastewater. We calculated MeV distribution using 3 different approaches (Figure 2). When accounting for typical wastewater composition (99.96% liquid and 0.04% solids), we detected most of the MeV signal (±SD) in the supernatant (91.20% ±7.22%), followed by the colloids (8.58% ±1.24%) and settled solids (0.22% ±0.06%) (Figure 2, panel A). That approach was influenced by the disproportionate volume of the liquid phase and might not reflect the concentration potential of each matrix. On an equivalent-mass basis (1 g each of solids and liquids), we found the highest concentration of MeV in the solids (85.43% ±15.24%), with lower proportions in supernatant (13.31% ±1.05%) and colloids (1.25% ±0.18%) (Figure 2, panel B). However, routine enrichment methods do not process equivalent masses, which limited the relevance of our comparison. We used weight and volume units typically processed in laboratory workflows (0.25 g for solids, 150 mL for colloids, and 37 mL for supernatant) for the final calculation. Under operational conditions, we recovered most of the MeV signal from the supernatant (70.18% ±5.55%), followed by colloids (26.77 ±3.87%), and solids (3.04% ±0.79%) (Figure 2, panel C). Those findings demonstrated that MeV RNA was broadly distributed in the liquid phase but was most concentrated in the solids. However, when considering viral recovery in accordance with standard enrichment protocol, the supernatant yields the highest amount of MeV RNA because it

contains the largest volume, supporting its use for optimal detection.

Wastewater Surveillance of MeV at Outbreak Location

WS of MeV began in March 2025, after reports of cases in Windsor-Essex. We conducted retrospective analysis of archived samples from February onward.

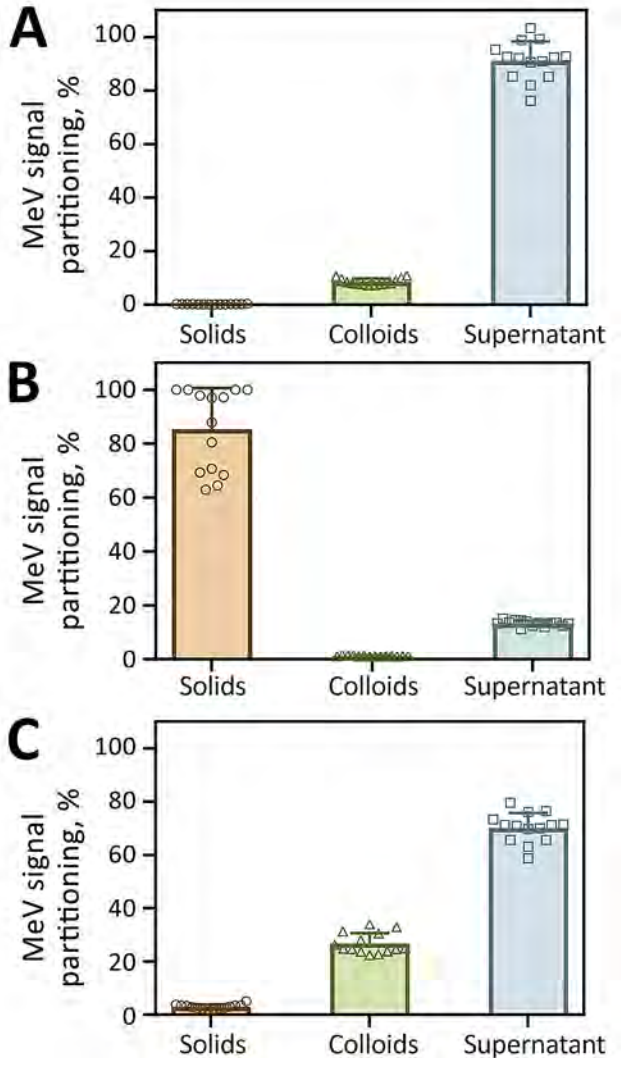

Figure 2. Partitioning of MeV signal across wastewater fractions in a study of wastewater surveillance conducted in Leamington, Ontario, Canada, during the 2025 outbreak. Partitioning of measles virus is shown for 3 calculation bases. Each point represents 1 technical triplicate for each of the biologic replicates (n = 14). For each bar, the upper border of each bar indicates the mean; whiskers indicate standard error. Where the standard deviation is too small, the error bars are not displayed. A) Signal partitioned assuming the composition of a typical wastewater sample (99.96% liquid, 0.04% solids). B) Signal partitioned on an equivalent mass basis, assuming 1 g of each fraction. C) Signal partitioned based on typical laboratory processing volumes: 0.25 g for settled solids, 150 mL for the colloids fraction, and 37 mL for the supernatant. MeV, measles virus.

The first wastewater samples that tested positive for MeV were collected on March 7, 2025 (Figure 3); samples tested positive through mid-August 2025. MeV wastewater signal showed a strong positive correlation with cases during February–July 2025 for normalized (Spearman correlation coefficient [ρ] = 0.77 [95% CI 0.51–0.87]; p<0.001) and raw (ρ = 0.77 [95% CI 0.49–0.90]; p<0.001) signal. Correlations between wastewater signal derived from a subset of samples concentrated with affinity capture techniques corroborated that result for normalized (ρ = 0.84 [95% CI 0.60–0.94]; p<0.001) and raw (ρ = 0.87 [95% CI 0.68–0.95]; p<0.001) signal. The increased correlation for that sample set could result from the truncated dataset or the use of affinity capture methods, which are more effective than filtration in concentrating MeV. We observed the correlation even where populations might underutilize health services, which likely contributed to underreporting of measles cases (*33*). We confirmed the identity of amplicons obtained by qRT-PCR by sequencing. Sequence alignments determined using BLAST (http://blast.ncbi.nlm.nih.gov/Blast.cgi) confirmed that the reads we obtained shared ≥99% identity with MeV N gene.

Previous research has shown WS to be a leading indicator of disease incidence (*34*–*38*). We used time-lagged cross-correlation (TLCC) to determine if WS for measles is a leading indicator of clinical reporting. We found the highest association when MeV wastewater signal lagged clinical cases by 1 week for pepper mild mottle virus normalized and raw signal (Appendix Figures 1, 2). However, correlations at a lag of 1 week were not different from the correlations of aligned time series (ρ = 0.79 for raw and ρ = 0.78 for normalized signal). TLCC suggested that wastewater was not a leading indicator of measles cases for data aggregated by epidemiologic week. Weekly averaging or potential delays in the detection of MeV signals at LPCC associated with septic hauling could have obscured lead time. The WS approach failed to warn of outbreak onset, potentially because of RNA degradation in archived samples (*39*), 3 times weekly sampling frequency, method sensitivity, or the rural nature of the sewershed where the outbreak occurred.

Modeling Determinants of MeV RNA Concentration in Wastewater Samples

The gamma generalized linear model (GLM) explained 75% of the variation in normalized MeV (pseudo R^2 = 0.75). Clinical cases were the only statistically significant predictor. Cases had a positive influence on MeV signal (β = 2.05 ±0.77; z = 2.67; p = 0.008); an increase in cases by 1 SD resulted in ≈8-fold

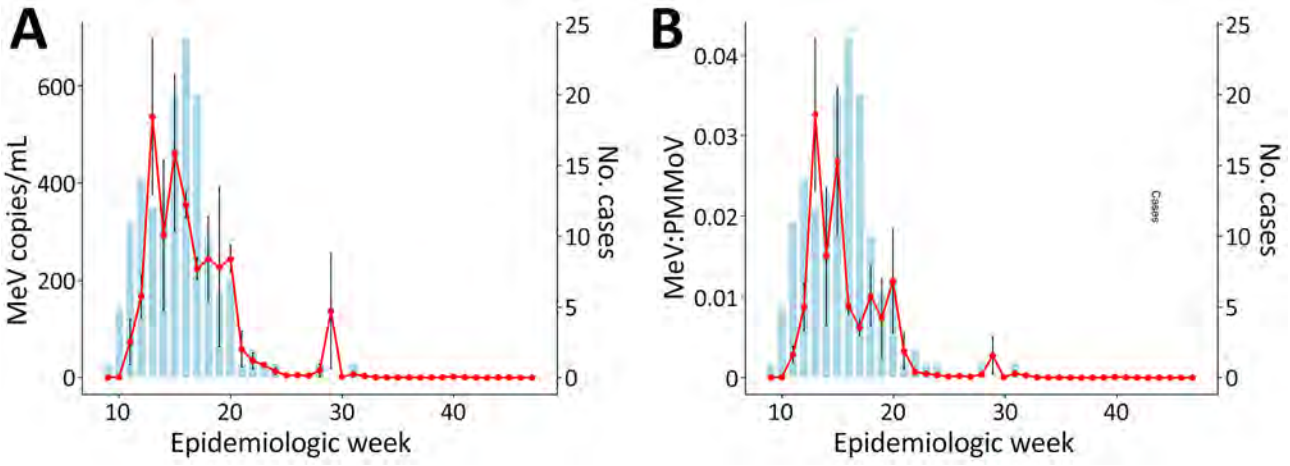

Figure 3. MeV wastewater surveillance signal and clinical case counts in Leamington, Ontario, outbreak, 2025. Clinical cases (blue bars) are compared against (A) raw MeV RNA concentrations (copies/mL; red points/line) and (B) MeV RNA concentrations normalized to PMMoV (red points/line). Data are aggregated by epidemiologic week; wastewater values represent weekly mean (points) ± SE. MeV, measles virus; PMMoV, pepper mild mottle virus.

increase in normalized MeV. Other fixed effects (flow, pH, epidemiologic week, and vaccination rates) were not statistically significant (Appendix Table 2).

We fitted a separate gamma GLM to a truncated dataset (n = 14), including cases and total sewage volume as predictors of normalized measles concentration (Appendix Table 3). The model explained 72% of variability in normalized MeV concentration (pseudo $R^2 = 0.72$). Residuals simulated in DHARMa (https://CRAN.R-project.org/package=DHARMa) showed evidence of mild heteroskedasticity (Appendix Table 3). Analysis of the truncated dataset corroborated that cases are the most significant factor explaining variability in normalized MeV concentration at the WWTP; that finding reinforced the use of WS as an independent measure of disease within a community. The total volume of sewage deposited at the WWTP was a significant predictor of MeV signal. Septic sewage could contain MeV RNA, contributing to MeV signal at the WWTP when tanks are emptied frequently. Delivery delays the arrival of viral material to the WWTP and likely contributes to the observed lag at epidemiologic week temporal granularity (Appendix Figure 3). We ran Spearman correlations between physicochemical parameters of wastewater, MeV signal, and the total volume deposited by septic sewage hauling companies each week; those analyses showed that the volumes deposited by select companies and MeV signal were correlated (Appendix Figure 4). Total volume for company 3 was correlated with both normalized ($\rho = 0.83$; $p<0.001$) and raw ($\rho = 0.78$; $p = 0.002$) MeV signal in wastewater. We also observed a correlation between the total volume of all septage deposited and both raw ($\rho = 0.78$; $p = 0.002$) and normalized ($\rho = 0.81$; $p<0.001$) MeV signal. Those correlations indicated that septic hauling might contribute to the MeV signal at LPCC. We tested the association on a dataset that included only days when septage deliveries coincided with wastewater sample

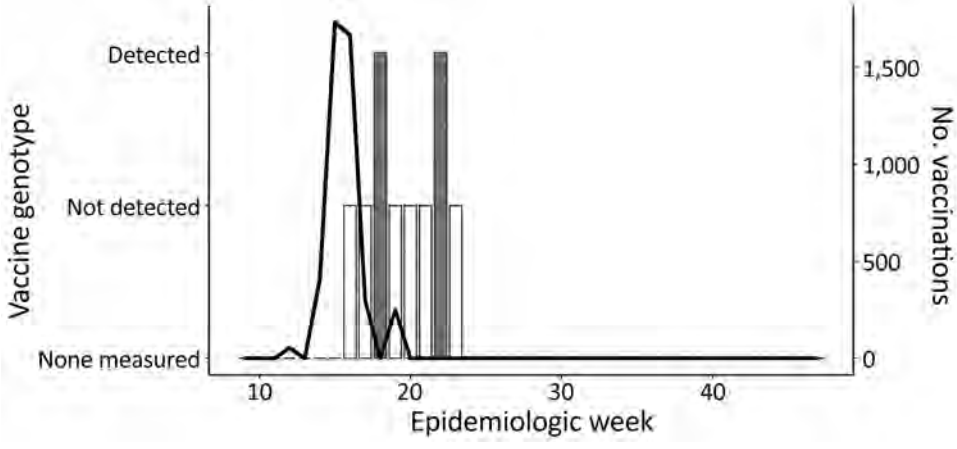

Figure 4. Wastewater surveillance for vaccine genotype measles and vaccination data for measles virus in Leamington, Ontario, 2025. Black line indicates weekly vaccine administrations and trend; dark bars indicate wastewater detections of MeV hemagglutinin gene single-nucleotide polymorphism unique to the vaccine genotype. White bars indicate weeks in which vaccine genotype measles virus was not detected.

collection (Appendix Figure 5). Correlations were weaker and nonsignificant when restricted to days with coincident sampling, (Appendix Figure 6). Thus, septic deliveries play a more minor role in explaining wastewater signal than the first correlation analysis suggested.

Vaccine Genotype Detection

We performed an assay that targets a single-nucleotide polymorphism (SNP) in the MeV H gene to distinguish vaccine genotype MeV RNA from wild-type MeV RNA (*30*). We treated the assay as a binary indicator of the presence of vaccine genotype MeV RNA. We detected vaccine genotype MeV in Leamington wastewater ≈6 weeks after the start of vaccination campaigns and ≈4 weeks after the intensification of the vaccination campaign (Figure 4). Research in MeV shedding dynamics after vaccination indicates that shedding can start >1 day after inoculation and can persist for up to 14 days in urine and 29 days in nasopharyngeal swabs (*40*,*41*). Those values partially explain the delay between the start of the vaccination campaign and the first detections in wastewater but are unlikely to account for the full lag. In this outbreak, the vaccination campaign focused on agri-food workers in bunkhouses served by frequently emptied septic tanks; thus, the delayed delivery of MeV RNA to the WWTP could explain the delay. The frequency of septic hauling could contribute to the temporal dynamics of WS for rural sewersheds.

MeV Shedding and Case Estimation

The city of Windsor was less affected by the measles outbreak, consistent with higher vaccination rates in urban centers (*42*,*43*). Data from cases and wastewater signal were sporadic; each supported lower incidence in Windsor (data not shown). Simultaneous detections in hospital effluent at a campus of WRH and hospitalizations enabled us to estimate viral shedding rates on 6 dates (Table). Shedding rates ranged over 4 orders of magnitude; median shedding rate was 1.41×10^{11} gene copies/person/day. For 1 hospitalized patient, we estimated shedding on consecutive days. Shedding nominally decreased between measurements, but that decrease could be measurement error. Studies have shown that shedding rates of measles vary over the course of infection and between patients, generally declining in titers over time (*44*,*45*). The declining trend was not consistently supported; another study found no difference in MeV RNA concentration between early or intermediate oral fluid or serum samples (*46*). Shedding rates varied between patients and excreta type (*47*); urine displayed relatively high MeV concentrations (*21*). MeV RNA levels did not differ by vaccination status or age (*46*,*48*).

Table. Daily measles virus shedding estimates based on samples collected from hospital effluent in Windsor, Ontario, Canada, March–May 2025*

Date	No. patients hospitalized	Shedding estimate, gc/d/person, ±SD
Mar 25	2	$1.53 \times 10^{12} \pm 2.64 \times 10^{11}$
Mar 26	2	$6.60 \times 10^{12} \pm 4.13 \times 10^{11}$
Apr 8	1	$3.73 \times 10^{8} \pm 1.47 \times 10^{8}$
Apr 9	1	$3.32 \times 10^{8} \pm 1.59 \times 10^{8}$
Apr 22	2	$7.61 \times 10^{8} \pm 7.02 \times 10^{8}$
May 6	1	$4.17 \times 10^{11} \pm 9.73 \times 10^{10}$

*gc, gene copies.

Our estimates of MeV shedding rates were higher than previous estimates (*21*). However, given multiple sources of excreta contribute to the wastewater signal and high variability in MeV RNA measurements previously reported (*44*), the shedding estimates we derived seem reasonable. In addition, when we used the calculated median of shedding rate to extrapolate the number of measles cases in Leamington on the basis of the wastewater signal, we observed general agreement (Figure 5). Public health officials estimated the true incidence of measles in the Leamington outbreak to be 5–10 times higher than reported cases (M. Aloosh, pers. comm., email, 2025 Oct 3). That estimate is consistent with MeV outbreaks in undervaccinated communities in the Netherlands (*49*).

Discussion

WS has the potential to become an important complementary public health tool, particularly for identifying MeV transmission in populations that are undervaccinated or less likely to access healthcare. Case-based surveillance alone might underestimate transmission (*49*). WS also provides more timely situation awareness during outbreaks, particularly when delays in reporting or low healthcare utilization might hamper clinical surveillance. WS could provide advanced warnings for changes in disease incidence during a respiratory season, outbreak, or epidemic, and can also warn of the onset of an outbreak or respiratory season (*6*,*38*). WS could be useful for early detection of MeV outbreaks because infected persons shed RNA during the prodromal period, before rash onset, whereas clinical surveillance generally identifies cases after symptom onset and laboratory confirmation (*24*). Studies have also shown that WS can provide early warning for MeV outbreaks (*25*,*26*). Early outbreak detection enables rapid mobilization of public health resources, including expedited testing, contact tracing, isolation of suspected cases, and targeted vaccinations; such actions can reduce

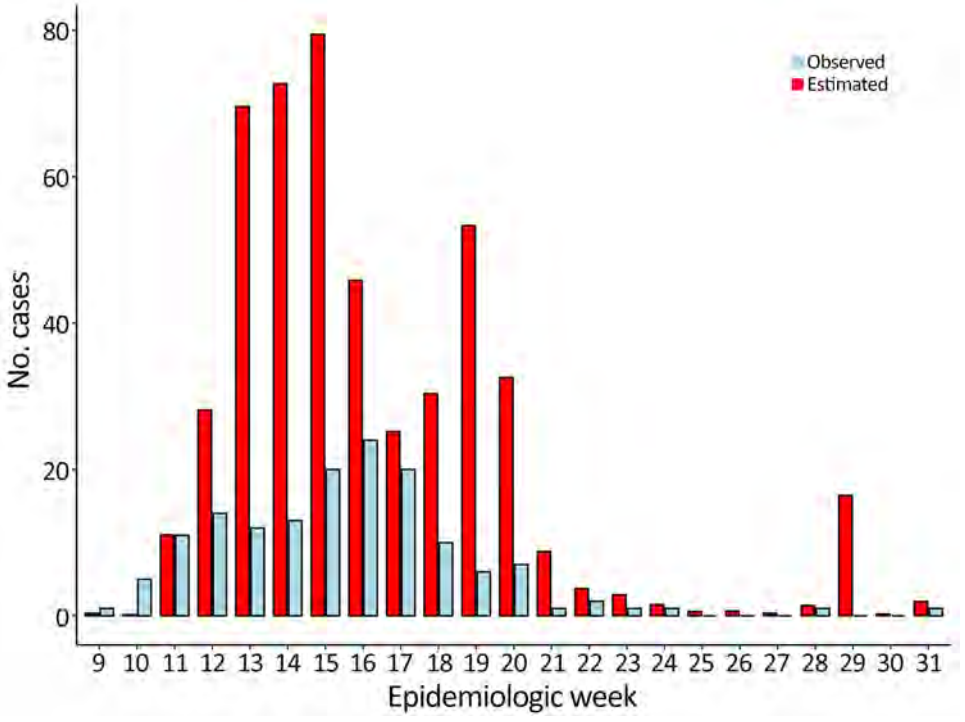

Figure 5. Measles case estimates for the municipality of Leamington, Ontario, Canada, based on wastewater signal and measles virus shedding approximations generated in Windsor, Ontario. Case estimations are based on median shedding rate approximations. Blue bars represent observed cases; red bars represent estimated cases.

transmission and infections, which is especially important for highly contagious pathogens such as MeV.

In our investigation, WS did not provide warning of MeV circulation or outbreak onset before routine case-based surveillance; we implemented surveillance reactively in response to a clinical case of measles. Retrospective analysis of archival samples showed MeV RNA was not detected in wastewater samples before the first case was identified; possible reasons were RNA degradation in archived samples caused by handling and freeze–thaw cycles (*39*), sampling frequency, method sensitivity, or the rural nature of the sewershed where the outbreak occurred.

In our study, WS for measles was robust, even though it was conducted in a community where a substantial portion of the population is served by septic systems. Septic systems and sewage hauling can influence the dynamics of measles signal in wastewater; weekly averaging or potential delays in the detection of MeV signals associated with septic hauling could obscure lead time. Our findings could likely be extrapolated to other viruses in different rural systems with similar sewage systems. Despite the possible influence of septic hauling on the temporal dynamics of wastewater signal, WS retained the ability to track disease at the community level, independent of traditional surveillance. We applied shedding rates calculated from a sewer lateral of a hospital with confirmed measles admissions to wastewater data to produce plausible estimates of measles cases. Investigation of MeV fractionation in wastewater indicates that most virus was found within the liquid phase of the wastewater matrix, consistent with MeV shedding primarily in urine and with previous work (*27*). Concentration of the supernatant may be most efficient for the purpose of WS for MeV. Our findings suggest that WS can act as an independent weekly measure of MeV at LPCC. We did not find that WS was a leading indicator of cases when data were aggregated by epidemiologic week.

Despite its promise, WS for MeV has limitations. Early warning requires ongoing WS with sufficiently frequent sampling. Establishing and operating WS programs requires investment in infrastructure, personnel, and reagents. WS is less feasible in rural or remote communities lacking centralized wastewater infrastructure or relying on septic systems. WS for MeV is more effective in communities with undervaccinated populations and centralized WWTPs, where high transmission risk and actionable surveillance data align. Of importance, WS is not a replacement for clinical surveillance; it cannot identify infected persons, confirm diagnosis, or establish transmission chain. Assessing the accuracy of WS through comparison with reported clinical cases is flawed when clinical cases are likely underreported. Our study does not draw conclusions about the ability of WS to provide early warning of outbreak onset; retrospective analysis of archived samples is likely to miss early signals close to the assay limit of detection because of sample degradation.

We indirectly estimated shedding rates on the basis of mean suspended solids values for hospital effluent and MeV partitioning in wastewater, so those estimates must be cautiously interpreted. Additional uncertainty in shedding rate estimates arises from the use of facility water for flow-rate estimation. The LPCC receives waste from residences served by septic systems. However, outside of the agrifood industry, most septic tanks are emptied infrequently. It is unlikely that households emptied septic tanks during the measles outbreak in a manner that contributed meaningfully to the MeV signal at the treatment facility. In addition, diapering of infected children reduces the MeV load at the WWTP and potentially influences the signal.

This investigation supports the continued use of WS for MeV; it complements routine case-based surveillance for measles. Despite the cost of establishing WS for MeV, it can provide a net positive investment for the healthcare system; the high cost of measles outbreaks means that preventing even a few cases through informed or early action could offset WS expenses (*21*). Once established, a WS system can be adapted to survey multiple pathogens for little additional cost with judicious selection of target pathogens and informed variation in sampling frequency. WS remains viable in circumstances in which clinical metrics may underrepresent actual cases and can inform public health services of changes in disease trajectory.

Acknowledgments

We extend appreciation to the operators and laboratory team with the Leamington Pollution Control Centre, Shannon Belleau, and Kevin Douglas who provided logistical support.

This work was supported by INSPIRE (Integrated Network for the Surveillance of Pathogens: Increasing REsilience and capacity in Canada's pandemic response), a program funded through the Canada Biomedical Research Fund Stage 2 (grant no. CBRF2-2023-00008), the Biosciences Research Infrastructure Fund Stage 2, and the Ontario Research Fund. Additional support was provided by the CIHR Applied Public Health Research Chair in Environment, Climate Change and One Health (to R.D.).

About the Author

Mr. Corchis-Scott is a PhD candidate at the University of Windsor's Great Lakes Institute for Environmental Research. His doctoral research focuses on wastewater-based surveillance of pathogens and antimicrobial resistance genes, utilizing a One Health framework to improve public health outcomes.

References

1. D'Aoust PM, Hegazy N, Ramsay NT, Yang MI, Dhiyebi HA, Edwards E, et al.; WSI Consortium. SARS-CoV-2 viral titer measurements in Ontario, Canada wastewaters throughout the COVID-19 pandemic. Sci Data. 2024;11:656. https://doi.org/10.1038/s41597-024-03414-w
2. Kirby AE, Welsh RM, Marsh ZA, Yu AT, Vugia DJ, Boehm AB, et al.; New York City Department of Environmental Protection. Notes from the field: early evidence of the SARS-CoV-2 B.1.1.529 (Omicron) variant in community wastewater—United States, November–December 2021. MMWR Morb Mortal Wkly Rep. 2022;71:103–5. https://doi.org/10.15585/mmwr.mm7103a5
3. Martin MA, VanInsberghe D, Koelle K. Insights from SARS-CoV-2 sequences. Science. 2021;371:466–7. https://doi.org/10.1126/science.abf3995
4. du Plessis L, McCrone JT, Zarebski AE, Hill V, Ruis C, Gutierrez B, et al.; COVID-19 Genomics UK (COG-UK) Consortium. Establishment and lineage dynamics of the SARS-CoV-2 epidemic in the UK. Science. 2021;371:708–12. https://doi.org/10.1126/science.abf2946
5. Ahmed W, Bivins A, Stephens M, Metcalfe S, Smith WJM, Sirikanchana K, et al. Occurrence of multiple respiratory viruses in wastewater in Queensland, Australia: potential for community disease surveillance. Sci Total Environ. 2023;864:161023. https://doi.org/10.1016/j.scitotenv.2022.161023
6. Hellmér M, Paxéus N, Magnius L, Enache L, Arnholm B, Johansson A, et al. Detection of pathogenic viruses in sewage provided early warnings of hepatitis A virus and norovirus outbreaks. Appl Environ Microbiol. 2014;80:6771–81. https://doi.org/10.1128/AEM.01981-14
7. Adams C, Kirby AE, Bias M, Riser A, Wong KK, Mercante JW, et al. Detecting mpox cases through wastewater surveillance—United States, August 2022–May 2023. MMWR Morb Mortal Wkly Rep. 2024;73:37–43. https://doi.org/10.15585/mmwr.mm7302a3
8. Louis S, Mark-Carew M, Biggerstaff M, Yoder J, Boehm AB, Wolfe MK, et al. Wastewater surveillance for influenza A virus and H5 subtype concurrent with the highly pathogenic avian influenza A(H5N1) virus outbreak in cattle and poultry and associated human cases—United States, May 12–July 13, 2024. MMWR Morb Mortal Wkly Rep. 2024;73:804–9. https://doi.org/10.15585/mmwr.mm7337a1
9. Mejia EM, Hizon NA, Dueck CE, Lidder R, Daigle J, Wonitowy Q, et al. Detection of mpox virus in wastewater provides forewarning of clinical cases in Canadian cities. Sci Total Environ. 2024;933:173108. https://doi.org/10.1016/j.scitotenv.2024.173108
10. Kaur G, Danovaro-Holliday MC, Mwinnyaa G, Gacic-Dobo M, Francis L, Grevendonk J, et al. Routine vaccination coverage—worldwide, 2022. MMWR Morb Mortal Wkly Rep. 2023;72:1155–61. https://doi.org/10.15585/mmwr.mm7243a1
11. Delgado C. Measles: millions of children missed routine vaccination last year, WHO and CDC warn. BMJ. 2024;387:q2541. https://doi.org/10.1136/bmj.q2541
12. Public Health Agency of Canada. Measles and rubella weekly monitoring report (2025). 2026 [cited 2026 May 22]. https://health-infobase.canada.ca
13. Webster P. Canada's loss of measles-free status highlights public health gaps. Lancet. 2025;406:2407–8. https://doi.org/10.1016/S0140-6736(25)02361-X
14. King A, Varughese P, De Serres G, Tipples GA, Waters J; Working Group on Measles Elimination. Measles elimination

in Canada. J Infect Dis. 2004;189(Suppl 1):S236–42. https://doi.org/10.1086/378499
15. Osman S, Crowcroft N, McLachlan E, Hatchette T, Perez-Iratxeta C, Joh E, et al. Population immunity to measles in Canada using Canadian Health Measures survey data—a Canadian Immunization Research Network (CIRN) study. Vaccine. 2022;40:3228–35. https://doi.org/10.1016/j.vaccine.2022.04.011
16. Public Health Ontario. Measles in Ontario: enhanced epidemiological summaries. Toronto: Public Health Ontario; 2025 Nov [cited 2025 Dec 8]. https://www.publichealthontario.ca/en/Diseases-and-Conditions/Infectious-Diseases/Vaccine-Preventable-Diseases/Measles/EPI
17. Mathis AD, Raines K, Filardo TD, Wiley N, Leung J, Rota PA, et al. Measles update—United States, January 1–April 17, 2025. MMWR Morb Mortal Wkly Rep. 2025;74:232–8. https://doi.org/10.15585/mmwr.mm7414a1
18. Taylor L. Canada sees surge in measles as cases rise across North America. BMJ. 2025;390:r1653. https://doi.org/10.1136/bmj.r1653
19. Gan C, Pitton M, de Korne-Elenbaas J, Cobuccio L, Cassini A, Ort C, et al. Retrospective wastewater tracking of measles outbreak in western Switzerland in winter 2024. Environ Sci Technol Lett. 2025;12:689–94. https://doi.org/10.1021/acs.estlett.5c00244
20. Chen W, Bibby K. Temporal, spatial, and methodological considerations in evaluating the viability of measles wastewater surveillance. Sci Total Environ. 2025;959:178141. https://doi.org/10.1016/j.scitotenv.2024.178141
21. Sundaram ME, Guterman LB, Omer SB. The true cost of measles outbreaks during the postelimination era. JAMA. 2019;321:1155–6.
22. Kuppalli K, Perl TM. Measles in Texas: waning vaccination and a stark warning for public health. Lancet Infect Dis. 2025;25:485–7. https://doi.org/10.1016/S1473-3099(25)00162-8
23. Rector A, Bloemen M, Hoorelbeke B, Van Ranst M, Wollants E. Detection of measles virus genotype D8 in wastewater of the Brussels capital region, Belgium. J Med Virol. 2025;97:e70251. https://doi.org/10.1002/jmv.70251
24. Tomalty E, Mercier É, Pisharody L, Nguyen T, Tian X, Kabir MP, et al. Detection of measles virus genotype A in a non-endemic wastewater setting: insights from measles wastewater and environmental monitoring in Canada's capital region. Environ Sci Technol Lett. 2025;12:124–9. https://doi.org/10.1021/acs.estlett.4c00945
25. Plymesser K, Wu J, West RM, Stadler LB. Measles wild-type virus detection through wastewater surveillance in Sandoval County, New Mexico. JAMA Netw Open. 2026;9:e2611124. https://doi.org/10.1001/jamanetworkopen.2026.11124
26. Jensen GM, Gidfar C, Weisbeck K, Barnes M, Minnerath E, Matzinger S, et al. Notes from the field: wastewater surveillance for measles virus during a measles outbreak—Colorado, August 2025. MMWR Morb Mortal Wkly Rep. 2026;75:20–2. https://doi.org/10.15585/mmwr.mm7502a2
27. Wu J, Wang MX, Kalvapalle P, Nute M, Treangen TJ, Ensor K, et al. Multiplexed detection, partitioning, and persistence of wild-type and vaccine strains of measles, mumps, and rubella viruses in wastewater. Environ Sci Technol. 2024;58:21930–41. https://doi.org/10.1021/acs.est.4c05344
28. Corchis-Scott R, Geng Q, Al Riahi AM, Labak A, Podadera A, Ng KKS, et al. Actionable wastewater surveillance: application to a university residence hall during the transition between Delta and Omicron resurgences of COVID-19. Front Public Health. 2023;11:1139423. https://doi.org/10.3389/fpubh.2023.1139423
29. Peterson SW, Lidder R, Daigle J, Wonitowy Q, Dueck C, Nagasawa A, et al. RT-qPCR detection of SARS-CoV-2 mutations S 69-70 del, S N501Y and N D3L associated with variants of concern in Canadian wastewater samples. Sci Total Environ. 2022;810:151283. https://doi.org/10.1016/j.scitotenv.2021.151283
30. Pabbaraju K, Gill K, Wong AA, Tipples GA, Hiebert J, Severini A, et al. Simultaneous detection and differentiation between wild-type and vaccine measles viruses by a multiplex real-time reverse transcription-PCR assay. J Clin Microbiol. 2019;57:e01828-18. https://doi.org/10.1128/JCM.01828-18
31. Ontario Ministry of Health. Appendix 1: case definitions and disease-specific information—disease: measles. Toronto: The Ministry; 2022. p. 1–13 [cited 2026 May 11]. https://www.ontario.ca/files/2024-03/moh-measles-appendix-en-2024-03-19.pdf
32. Verlicchi P, Galletti A, Petrovic M, Barceló D. Hospital effluents as a source of emerging pollutants: an overview of micropollutants and sustainable treatment options. J Hydrol (Amst). 2010;389:416–28. https://doi.org/10.1016/j.jhydrol.2010.06.005
33. Sibley LM, Weiner JP. An evaluation of access to health care services along the rural-urban continuum in Canada. BMC Health Serv Res. 2011;11:20. https://doi.org/10.1186/1472-6963-11-20
34. D'Aoust PM, Graber TE, Mercier E, Montpetit D, Alexandrov I, Neault N, et al. Catching a resurgence: increase in SARS-CoV-2 viral RNA identified in wastewater 48 h before COVID-19 clinical tests and 96 h before hospitalizations. Sci Total Environ. 2021;770:145319. https://doi.org/10.1016/j.scitotenv.2021.145319
35. Hill DT, Alazawi MA, Moran EJ, Bennett LJ, Bradley I, Collins MB, et al. Wastewater surveillance provides 10-days forecasting of COVID-19 hospitalizations superior to cases and test positivity: A prediction study. Infect Dis Model. 2023;8:1138–50. https://doi.org/10.1016/j.idm.2023.10.004
36. Olesen SW, Imakaev M, Duvallet C. Making waves: defining the lead time of wastewater-based epidemiology for COVID-19. Water Res. 2021;202:117433. https://doi.org/10.1016/j.watres.2021.117433
37. Mercier E, D'Aoust PM, Thakali O, Hegazy N, Jia JJ, Zhang Z, et al. Municipal and neighbourhood level wastewater surveillance and subtyping of an influenza virus outbreak. Sci Rep. 2022;12:15777. https://doi.org/10.1038/s41598-022-20076-z
38. Mercier E, Pisharody L, Guy F, Wan S, Hegazy N, D'Aoust PM, et al. Wastewater-based surveillance identifies start to the pediatric respiratory syncytial virus season in two cities in Ontario, Canada. Front Public Health. 2023;11:1261165. https://doi.org/10.3389/fpubh.2023.1261165
39. Williams RC, Perry WB, Lambert-Slosarska K, Futcher B, Pellett C, Richardson-O'Neill I, et al. Examining the stability of viral RNA and DNA in wastewater: effects of storage time, temperature, and freeze-thaw cycles. Water Res. 2024;259:121879. https://doi.org/10.1016/j.watres.2024.121879
40. Rota PA, Khan AS, Durigon E, Yuran T, Villamarzo YS, Bellini WJ. Detection of measles virus RNA in urine specimens from vaccine recipients. J Clin Microbiol. 1995;33:2485–8. https://doi.org/10.1128/jcm.33.9.2485-2488.1995
41. Washam MC, Leber AL, Oyeniran SJ, Everhart K, Wang H. Shedding of measles vaccine RNA in children after receiving measles, mumps, and rubella vaccination. J Clin Virol. 2024;173:105696. https://doi.org/10.1016/j.jcv.2024.105696

42. Newcomer SR, Michels SY, Albers AN, Freeman RE, Clarke CL, Glanz JM, et al. Early childhood vaccination coverage and patterns by rural–urban commuting area. Am J Prev Med. 2025;68:773–83. https://doi.org/10.1016/j.amepre.2025.01.006
43. Olusanya OA, Masters NB, Zhang F, Sugerman DE, Carter RJ, Weiss D, et al. Sociodemographic trends and correlation between parental hesitancy towards pediatric COVID-19 vaccines and routine childhood immunizations in the United States: 2021–2022 National Immunization Survey—child COVID module. Vaccines (Basel). 2024;12:495. https://doi.org/10.3390/vaccines12050495
44. Bankamp B, Sein C, Pukuta Simbu E, Anderson R, Abernathy E, Chen MH, et al. Use of FTA cards to transport throat swabs and oral fluid samples for molecular detection and genotyping of measles and rubella viruses. J Clin Microbiol. 2019;57:e00048-19. https://doi.org/10.1128/JCM.00048-19
45. Lin WHW, Kouyos RD, Adams RJ, Grenfell BT, Griffin DE. Prolonged persistence of measles virus RNA is characteristic of primary infection dynamics. Proc Natl Acad Sci U S A. 2012;109:14989–94. https://doi.org/10.1073/pnas.1211138109
46. Michel Y, Saloum K, Tournier C, Quinet B, Lassel L, Pérignon A, et al. Rapid molecular diagnosis of measles virus infection in an epidemic setting. J Med Virol. 2013;85:723–30. https://doi.org/10.1002/jmv.23515
47. Takao S, Shigemoto N, Shimazu Y, Tanizawa Y, Fukuda S, Matsuo T. Detection of exanthematic viruses using a TaqMan real-time PCR assay panel in patients with clinically diagnosed or suspected measles. Jpn J Infect Dis. 2012;65:444–8. https://doi.org/10.7883/yoken.65.444
48. Kurata T, Yamamoto SP, Nishimura H, Yumisashi T, Motomura K, Kinoshita M. A measles outbreak in Kansai International Airport, Japan, 2016: analysis of the quantitative difference and infectivity of measles virus between patients who are immunologically naive versus those with secondary vaccine failure. J Med Virol. 2021;93:3446–54. https://doi.org/10.1002/jmv.26733
49. Woudenberg T, Woonink F, Kerkhof J, Cox K, Ruijs WLM, van Binnendijk R, et al. The tip of the iceberg: incompleteness of measles reporting during a large outbreak in the Netherlands in 2013–2014. Epidemiol Infect. 2018;147:e23. https://doi.org/10.1017/S0950268818002698

Address for correspondence: Ryland Corchis-Scott, Great Lakes Institute for Environmental Research, University of Windsor, 401 Sunset Ave, Windsor, ON N9B 3P4, Canada; email: corchisr@uwindsor.ca

etymologia revisited

Scrapie

[skra'pe]

Originally published in June 2020

Scrapie is a fatal neurodegenerative disease of sheep and goats that was the first of a group of spongiform encephalopathies to be reported (1732 in England) and the first whose transmissibility was demonstrated by Cuille and Chelle in 1936. The name resulted because most affected sheep develop pruritis and compulsively scratch their hides against fixed objects. Like other transmissible spongiform encephalopathies, scrapie is associated with an alteration in conformation of a normal neural cell glycoprotein, the prion protein. The scrapie agent was first described as a prion (and the term coined) by Stanley Prusiner in 1982, work for which he received the Nobel Prize in 1997.

References

1. Brown P, Bradley R. 1755 and all that: a historical primer of transmissible spongiform encephalopathy. BMJ. 1998;317:1688–92.
2. Cuillé J, Chelle PL. The so-called "trembling" disease of sheep: is it inoculable? [in French]. Comptes Rendus de l'Académie Sciences. 1936;203:1552.
3. Laplanche J-L, Hunter N, Shinagawa M, Williams E. Scrapie, chronic wasting disease, and transmissible mink encephalopathy. In: Prusiner SB, editor. Prion biology and diseases. Cold Spring Harbor (NY): Cold Spring Harbor Laboratory Press; 1999. p. 393–429.
4. Prusiner SB. Novel proteinaceous infectious particles cause scrapie. Science. 1982;216:136–44.

https://wwwnc.cdc.gov/eid/article/26/6/et-2606_article

Variolation Techniques, Medical Explanations, and Dissemination in Late Imperial China

Linyu Guan,[1] Shenjia Gu,[1] Yunhai Pan, Lance E. Rodewald, Chuanxi Fu

Variolation in China has a long history, yet the method remains underrepresented internationally, having limited recognition of medical rationale and indigenous development. We reviewed medical texts and records from late Imperial China and compared variolation chronology, techniques, and explanatory frameworks used in China versus India. Variolation in China was already in practice no later than the Chenghua–Longqing period of the Ming dynasty (1465–1572 CE), earlier than that reported in other countries. Sources from China described garment/blanket, lymph, and scab-derived inoculum methods for smallpox prevention. Scab-derived inocula, intranasal administration, and repeated passage techniques reflected empirical efforts to improve variolation reliability and reduce risk. Concepts of fetal toxin and seasonal pathogenic qi made variolation intelligible within contemporaneous medicine in China. Records from China predated sources from India and contained more detailed descriptions of variolation practices, supporting indigenous development and highlighting China's central place in the early history of prophylactic inoculation.

Smallpox caused substantial illness and death worldwide until its eradication was certified by the World Health Organization in 1980 after sustained vaccination, surveillance, and containment efforts (*1*). Natural infection generally conferred long-lasting protection among survivors; however, case-fatality rates averaged ≈30% for variola major and, typically, <1% for variola minor viruses (*2*,*3*). Before the advent of vaccinia virus–based vaccination, communities used measures such as isolation and quarantine to limit transmission. In several regions, communities also practiced variolation, which is the intentional introduction of material from smallpox lesions to induce an infection expected to be milder than naturally acquired smallpox, conferring subsequent protection. Surviving records document variolation traditions in China, South Asia, the Ottoman Empire, and the Caucasus (*4*,*5*). Among those regional traditions, variolation in China is distinguished by an early and extensive textual record.

Variolation in China was interpreted within contemporaneous medical thought that included concepts such as fetal toxin (胎毒) and seasonal pathogenic qi (时气); the correlation between those concepts and documented practice supports the view that variolation methods developed indigenously within China. Three successive inoculation methods evolved historically during variolation development, followed by a trajectory of progressive technical refinement. Together, the evidence provides insight into early human immunologic thought.

Scholars from China have long engaged in research on the origins, transference, evolution, and historical effects of variolation. Later accounts retrospectively trace variolation in China to the Tang (618–907 CE) or Song (960–1279 CE) dynasties. Qing dynasty texts recorded nasal inoculation of smallpox in the Jiangnan (江南) region during the Tang Kaiyuan (开元) era (713–741 CE) (*6*) and variolation by a Mount Emei physician for the son of a Song prime minister (*7*). Those early origin claims lack independent corroboration, whereas the transference of variolation during the mid-to-late Ming dynasty (mid-1400s to mid-1600s CE) is well substantiated. Records describe variolation practitioners in Taiping (太平) County, Anhui (安徽) Province, during the Ming Longqing (隆庆) reign (1567–1572 CE) (*8*); practitioners in Jiangxi (江西) dated to the same period (*9*,*10*). Collectively, evidence indicates that variolation was established in Jiangxi between the Chenghua (成化; 1465–1487 CE) and Longqing eras and later spread across provinces of the Yangtze Basin, including

Author affiliations: Zhejiang Chinese Medical University, Hangzhou, China (L. Guan, S. Gu, Y. Pan, C. Fu); Chinese Center for Disease Control and Prevention, Beijing, China (L.E. Rodewald)

DOI: https://doi.org/10.3201/eid3210.260729

[1]These first authors contributed equally to this article.

Anhui, Zhejiang (浙江), Jiangsu (江苏), and Hunan (湖南). The practice became more widespread during the Qing dynasty and received imperial support; the Kangxi (康熙) Emperor recruited skilled physicians from Jiangxi Province to deliver inoculation at court and in Mongolia (*7*,*11*).

During the 17th and 18th Centuries, variolation practices circulated beyond East Asia through multiple pathways, and accounts noted precedents from China. Late 17th-Century envoys from Russia reported variolation practices derived from China; variolation was also documented in Circassia, Ottoman territories, North Africa, and the Americas (*12*). India is often cited as an early center for variolation, although definitive written records date mainly from the 18th century. In the early 1700s, variolation was practiced in Ottoman Turkey; transfer of methods through Silk Road routes or via Russia has been proposed, although direct documentary evidence remains limited (*13*). Lady Mary Wortley Montagu helped introduce Ottoman variolation to Britain in the 1720s, contributing to wider adoption of this practice in Europe (*14*). Edward Jenner's familiarity with variolation formed part of the practical context for his cowpox research (https://www.jenner.ac.uk/about/edward-jenner).

The early history of variolation in Asia has received sustained scholarly attention. Although the precise date and place of its initial development remain uncertain, surviving evidence identifies both China and India as early centers of variolation (*15*), whereas the earliest detailed records currently known are from China. Much international scholarship has focused on variolation in South Asia, particularly practices in British India during the 18th and 19th Centuries. Scholars from China have long been engaged in research on the origins, transference, development, and historical effects of variolation within their country. However, that body of work has not been fully integrated into international scholarship, which has devoted comparatively less attention to the technical development and medical explanatory framework of variolation. Therefore, we examined the documented chronology, technical development, and explanatory framework of variolation in China and assessed its significance within the global history of prophylactic inoculation.

Methods

We collected evidence from historical sources in China on inoculation methods, chronology, and regional conveyance of variolation. We also compared documentation chronology, inoculation methods, and medical explanatory frameworks for variolation in China versus India. Ethical approval and informed consent were not required for this study because it was performed exclusively by using published literature, historical texts, and archival materials and did not involve human participants, identifiable personal data, or animal experiments.

Analysis of Historical Medical Literature

We retrieved bibliographic records of ancient traditional Chinese medicine (TCM) on variolation (种痘) or human variolation (人痘) during the Ming and Qing dynasties from the General Catalogue of Ancient Traditional Chinese Medical Classics (中国中医古籍总目) (Duxiu database, https://www.duxiu.com). We obtained full texts from the Zhonghua Yidian (中华医典) compendium of TCM classics database (https://github.com/wanghaisheng/zhognhuayidian), the Shidian Ancient Classics (识典古籍) database (https://www.shidianguji.com), and collections from several libraries. We selected the earliest available works that had sufficiently detailed descriptions of inoculation techniques, inoculum selection, and theoretical principles of variolation; 8 works met those criteria. We conducted an in-depth reading of those works and precisely elucidated the meanings of characters, phrases, and sentences therein. We then extracted and organized information on inoculation approaches, inoculum selection, cultivation protocols for a mature inoculum, preservation conditions for variolation vaccines, inoculation timing, eligible populations for inoculation, contraindications, and postinoculation care and regimen.

We searched records from medical texts spanning the Han (202 BCE–220 CE) to the Qing (1644–1912 CE) dynasty to explore the pivotal theories proposed by physicians of successive dynasties regarding the etiology, pathogenesis, prevention, and treatment of smallpox. We conducted searches in the Encyclopedia of TCM and Shidian Ancient Classics databases by using historical terms for smallpox in China, including douchuang (痘疮), luchuang (虏疮), wandouchuang (豌豆疮), dengdouchuang (登痘疮), tianchuang (天疮), and tiandou (天痘). We selected texts recording innovative theories from each historical period or marking paradigm shifts in the understanding of smallpox for inclusion; 12 works met those criteria. We arranged the works chronologically and analyzed to trace changes in medical explanations of smallpox in China. We evaluated evidence for indigenous originality of variolation in China from 2 perspectives: the completeness of its technical system and the traceability of theoretical interpretation.

Comparative Analysis of Variolation in China and India

The relative chronology of variolation in China and India remains uncertain. We compared available historical sources from both countries to assess the earliest documented evidence of variolation.

We developed a search strategy for variolation in India (Table 1). We identified additional sources through manual screening of the reference lists of all retrieved documents. In total, we included 35 historical review articles. Access to early indigenous medical texts in India addressing smallpox prevention and treatment is highly limited. Among the accessible sources, only 1 classic Ayurvedic work, the Bhāvaprakāśa, met the inclusion criteria. We used an English translation of the original Sanskrit.

We compared historical medical texts from China with the Bhāvaprakāśa to evaluate explanations of smallpox etiology and pathogenesis and approaches to prevention and treatment. We assessed evidence relevant to the indigenous development of variolation in China and the possibility of its transfer from India.

Results

Variolation Techniques

The reviewed medical texts from China described 3 principal variolation methods, the smallpox garment/blanket method (dou yi fa, 痘衣法/dou bei fa, 痘被法), lymph method (dou jiang fa, 痘浆法), and scab method (dou jia fa, 痘痂法). Scab-based methods used aqueous inocula (wet, shui miao fa, 水苗法) or dry (han miao fa, 旱苗法) preparations (*8*,*16*). Healthy children <3 years of age were generally selected, although older children were sometimes inoculated.

The garment/blanket method was described as the earliest form of variolation. Healthy children were exposed to clothing or bedding used by patients with smallpox; the aim was to induce an infection that was expected to be milder and to confer subsequent protection (Figure 1, panel A). In the lymph method, a cotton plug soaked with fluid from fully mature pustules was inserted into one nostril of the recipient (Figure 1, panel B). The scab method used scabs from smallpox skin lesions as the inoculum. For the aqueous inoculum method, the scabs were ground into powder and mixed with clean cotton and a small amount of water to form oval-shaped pellets, which were inserted into 1 nostril. For the dry inoculum method, powdered scabs were blown into the nostrils through a specially designed silver or bamboo tube (Figure 1, panel C) (*17*). Regardless of the inoculation method used, pediatric smallpox donors were required to have a stable clinical disease course, mild fever, and mild pustular eruption and be free of any critical or life-threatening symptoms, as a foundational safeguard for inoculum safety. Among the approaches, the aqueous inoculum method was recommended in official medical texts and regarded as the safest technique, followed by the dry inoculum method. The lymph method was criticized because collecting the inoculum required puncturing pustules, causing substantial pain to the child from whom the material was obtained. The garment/blanket method was considered less reliable and was not recommended. Although variolation remained hazardous, historical estimates indicated that the mortality rate from that method was substantially lower than that for naturally acquired smallpox. Reported mortality rates following variolation ranged from 0.5%–2% compared with ≈30% for naturally acquired smallpox; variolation typically produced a far milder generalized rash than that seen in regular smallpox (*1*).

For analytical clarity, we described the documented practices using 3 modern categories without attributing modern virologic or immunologic concepts to historical practitioners. We described scab-derived inoculum, intranasal (mucosal) delivery, and serial human passage in the mature inoculum tradition.

Scab-Derived Inoculum

Variola virus can be detected in scabs shed by convalescents; however, scabs appear to have played a limited role in virus transmission compared with respiratory spread, which was predominant in community settings (*15*). For variolation, human-derived scabs were used as the inoculum and could elicit protection by provoking a modified course of disease. After a successful infection via variolation, fever, pustulation, and scabbing typically followed; survivors generally had long-term protection. For scientific clarity, we compared variolation with vaccinia-based

Table 1. Search strategy for variolation in India in study of variolation techniques, medical explanations, and dissemination in late Imperial China*

Database	Search string
PubMed	(Smallpox inoculation[Title/Abstract] OR Variolation[Title/Abstract] OR Smallpox vaccination[Title/Abstract]) AND (India[Title] OR Bengal[Title] OR South Asia[Title] OR Punjab[Title] OR Madras[Title] OR "East Indies"[Title])
Internet archive	Mediatype:texts AND date:[1700–01–01 TO 1900–12–31] AND ((Inoculation OR Inoculating OR Variolation) AND (India OR "East Indies" OR Bengal OR Bengall OR Hindostan OR Hindoostan OR Calcutta OR Madras OR Punjab))

*PubMed, https://www.ncbi.nlm.nih.gov/pubmed; Internet archive, https://archive.org

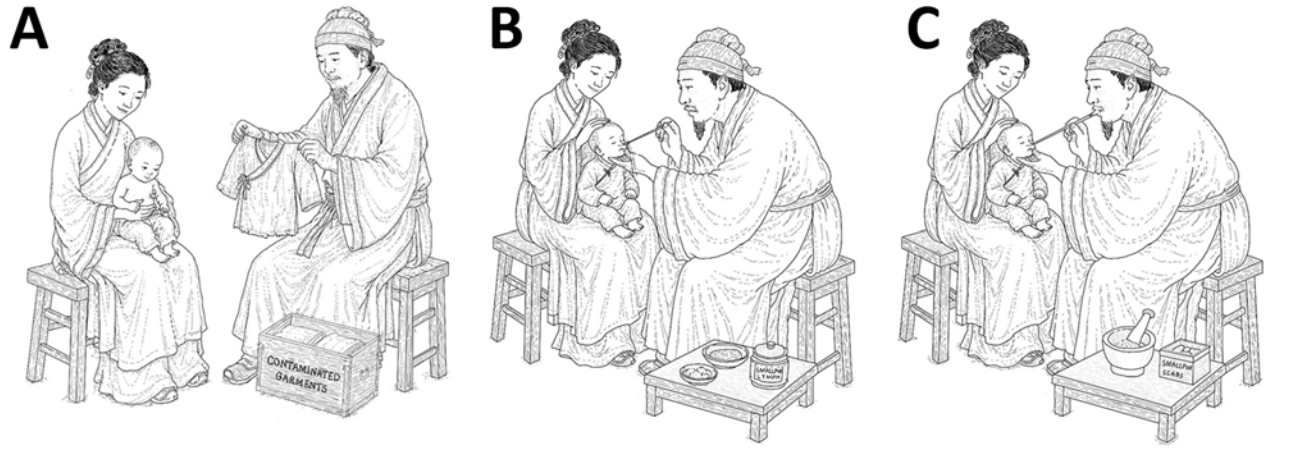

Figure 1. Principal variolation methods described in historical medical texts in study of variolation techniques, medical explanations, and dissemination in late Imperial China. A) Smallpox garment/blanket method, in which a healthy child was exposed to clothing or bedding used by a patient with smallpox. The aim was to induce infection that was expected to be milder and to confer subsequent protection. B) Smallpox lymph method, in which a cotton plug soaked with fluid from fully mature pustules was inserted into one nostril of the recipient. A silk thread was tied to the cotton plug to ensure that it could be safely removed. C) Smallpox scab method (dry inoculum method), in which powdered smallpox scabs were insufflated into the child's nostril through a slender tube while the mother stabilized the child. Illustrations were hand-drawn reconstructions by an author (S.G.) according to descriptions in historical medical texts from China.

smallpox vaccination, the platform used in eradication campaigns, which followed standardized procedures and, in practice, often involved revaccination. Overall, scab-based variolation could confer protection but still carried risks of severe disease and secondary transmission.

Intranasal (Mucosal) Administration

Modern evidence indicates that variola infection is initiated at the respiratory mucosa and spreads predominantly via aerosols and droplets (*18*,*19*). The nasal insufflation route of variolation in China aligned with this virus entry portal. Practitioners recognized that donors could not be screened for other infections. By avoiding percutaneous scarification, intranasal delivery might have reduced certain iatrogenic exposure pathways, although it did not eliminate infectious risks.

Serial Human Passage in the Mature Inoculum Tradition

The reviewed texts distinguished 2 scab-based variolation traditions in China according to the inoculum source. The Huzhou (湖州; in Zhejiang Province) tradition used mild and stable scabs from naturally infected persons, known as the natural inoculum method (shi miao fa, 时苗法). The Songjiang (松江; a district previously part of the Jiangsu Province and currently a part of Shanghai) tradition used scabs derived from successive human variolations, known as the mature inoculum method (shu miao fa, 熟苗法). Variolation practitioners discovered that reactogenicity was reduced and safety increased through successive human-to-human passages. Serial passage of scab material through variolated recipients was considered to produce milder postinoculation illness and greater safety; inocula obtained after ≥7 passages were preferred (*20*). The mature inoculum tradition in China is best understood as an empirical approach to risk reduction through inoculum selection and repeated passage. Viewed retrospectively, the procedure resembles serial passages used in attenuation. However, historical sources neither show that practitioners understood attenuation in modern virologic terms nor document measured changes in virulence. Therefore, the mature inoculum method should not be equated with laboratory attenuation or regarded as a validated precursor of live-attenuated vaccine development.

Indigenous Development of Variolation in China

In China, smallpox was generally regarded as an imported infectious disease, first introduced from Vietnam during the Jianwu (建武; 25–56 CE) period of Emperor Guangwu (光武; 25–56 CE) of the Eastern Han dynasty (*21*). Over subsequent centuries, physicians gradually deepened their understanding of the disease by adapting traditional medical theories to explain its etiology and pathogenesis, a process that ultimately culminated in the development of variolation. Within this intellectual environment, variolation emerged as a practice that corresponded to local theory while also corresponding to observed patterns of contagion. We emphasized compatibility between

practice and explanatory framework rather than a claim of linear theory-to-practice causation. We summarized the historical development of medical knowledge of smallpox and variolation in China (Table 2) (*7*,*21*–*23*) and show a logical progression from recognition of contagion and susceptibility to preventive intervention (Figure 2). Those summaries are analytic aids generated according to historical sources and do not imply complete unanimity across texts or regions. Ancient China had a progressive theoretical logic for understanding smallpox and variolation as well as an academic context that could foster the emergence of variolation. Variolation practices in China originated from the country's theoretical system of ancient medicine and preventive practices.

Comparative Analysis of Variolation in China Versus India

Debate over the geographic origin of variolation persists. Some authors have proposed that variolation in China was introduced from India. One account attributed to missionary physician Daniel Jerome MacGowan indicated an 11th-Century Buddhist nun in China learned the practice through a monk who had acquired it in India (*24*). However, no clear description of prophylactic variolation was identified in the Sanskrit medical material available in our study. Variolation practices were well established in India by at least the 17th–18th Centuries. The earliest written record of variolation in India dates to 1731, when Robert Coult wrote to Dr. Oliver Coult in Great Britain, describing variolation practices in the Bengal region of India (*1*). A later, detailed description of variolation in India was found in a correspondence by John Zephaniah Holwell in 1767 that was addressed to the Royal College of Physicians in London, titled An Account of the Manner of Inoculating for the Smallpox in the East Indies (*25*). Variolation procedures were performed exclusively by a dedicated cohort of Brahmin practitioners. The method involved

Table 2. Development of smallpox and variolation in study of variolation techniques, medical explanations, and dissemination in late Imperial China*

Period; key works	Development of smallpox studies in TCM	Contribution to the invention of variolation
The Wei, Jin, and Northern and Southern dynasties (3rd–6th centuries); Ge Hong's handbook of prescriptions for emergencies (Zhouhou Beiji Fang) (*21*)	Recognized the contagiousness of smallpox (shi xing bing). Texts inferred that lesion material might participate in transmission.	Early recognition of contagion generated the idea that material from patients could induce disease in others, which was a conceptual precursor to deliberate inoculation.
Song dynasty (≈12th century); Qian Yi's Key to Therapeutics of Children's Diseases (Xiao'er Yao Zheng Zhi Jue) (*22*)	Proposed congenital susceptibility (pathogenic qi contracted in utero) as part of smallpox etiology. This pathogenic qi originates from the mother's behaviors during pregnancy, such as indulging in greasy and sweet foods, being frequently depressed or angry, indulging in sexual desires, or having malignant diseases, including syphilis. The toxic fire generated from those factors is stored in the essence and blood. The fetus is affected by this toxin from the mother during fetal development, leading to diseases after birth.	Laid the foundation for the etiologic theory of fetal toxin (tai du). Fetal toxin is an etiologic term in TCM.
Ming dynasty (≈15th–16th centuries); Wang Quan's jade fragments on smallpox (Pian Yu Dou Zhen) and essential principles of smallpox (Dou Zhen Xin Fa) (*23*)	Consolidated the belief that 1 attack implied durable protection. Elucidating the etiology and pathogenesis of smallpox according to the theories of fetal toxin and external pathogens. Seasonal pathogenic qi (Shi Qi) was considered contagious, and smallpox pustules were believed to spread through interpersonal transmission. Because fetal toxin was viewed as an intrinsic bodily factor, it was believed that everyone carried the risk of developing smallpox.	Mapped historical categories to prevention, if disease confers durable protection; a milder, induced course might preempt severe natural disease, a rationale later invoked for variolation. It was also believed that a single infection could eliminate fetal toxin, rendering the person immune to future attacks. This led to the idea of inducing a mild, controlled infection through artificial means, thus, guiding the excretion of fetal toxin from the body and removing internal susceptibility and building immunity, rather than waiting for natural exposure.
Ming dynasty (≈15th–16th century); Wang Quan's essential principles of smallpox (Dou Zhen Xin Fa) (*23*)	Identified lifelong immunity after a single smallpox infection, frequently cited later to justify deliberate, milder smallpox induction.	
Middle to late Ming to early Qing dynasties (15th–17th century); Zhu Chungu's Conclusive theories on smallpox and rashes (Dou Zhen Ding Lun) (*7*)	Articulated "While the external factor—the pathogenic qi—was beyond human control, the internal factor, fetal toxin, could be controlled through human intervention. Before exposure to the external virus, individuals could deliberately introduce inoculum into the body to expel fetal toxin." With its relatively low virulence, this inoculum caused only a mild smallpox infection, safely and effectively expelling fetal toxin and thus preventing life-threatening disease.	The synthesis of theory and practice provided internal coherence to variolation within TCM, enabling acceptance and widespread implementation.

*TCM, traditional Chinese medicine.

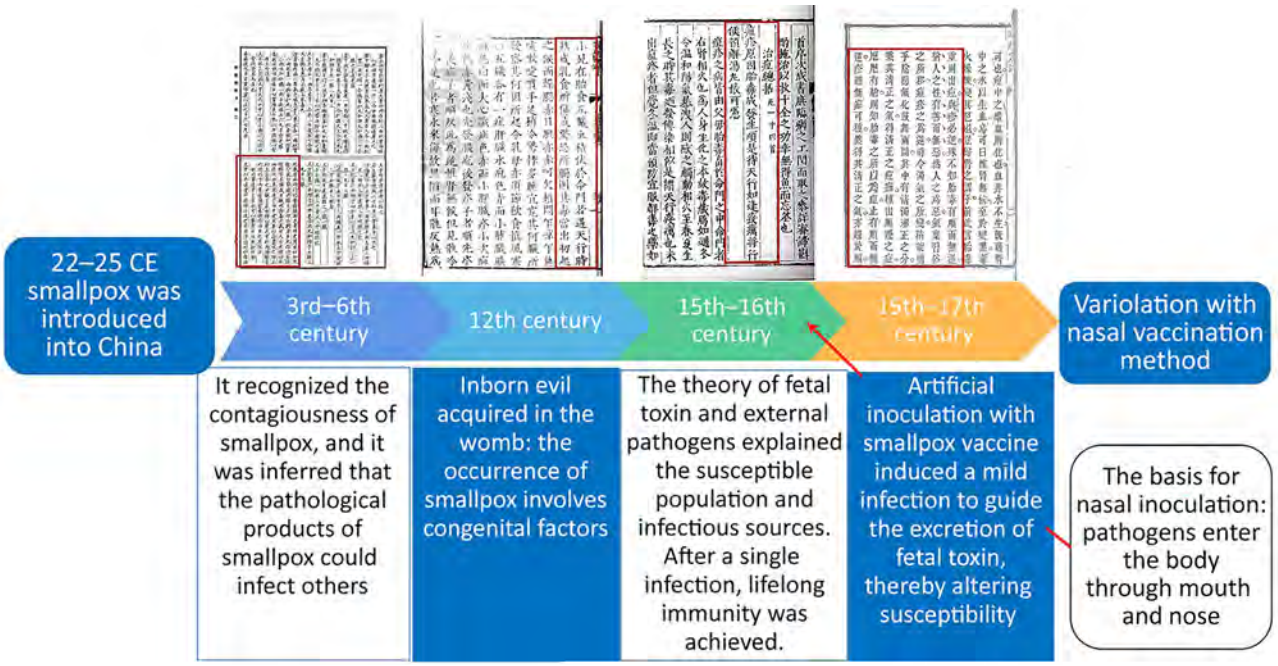

Figure 2. Logical progression underlying intranasal variolation in study of variolation techniques, medical explanations, and dissemination in late Imperial China. Schematic outlines the cognitive evolution of smallpox in traditional Chinese medicine that gave rise to variolation, spanning from the introduction of smallpox (25–55 CE) to recognition of its transmissibility, formulation of fetal toxin etiology, and eventual formalization of intranasal variolation. Developmental trajectory underpins the indigenous originality of variolation in China. Screenshots of ancient medical texts from China are shown at the top, sequentially sourced from references (*21*), (*22*), (*23*), and (*7*). Direct excerpts from original ancient medical text are outlined in red, serving as the primary source supporting the summary descriptions at the bottom. Schematic is only an analytical simplification and does not imply a unidirectional or deterministic progression.

soaking sharp needles in smallpox pus, making several punctures in the depression below the deltoid muscle or on the forehead or on the fingers and wrists, and then covering the area with a small paste made from cooked rice; alternatively, the inoculation site was dressed with gauze (*26*–*29*).

We compared medical accounts from China and Ayurvedic accounts of smallpox etiology, pathogenesis, prevention, and treatment (Table 3). Ayurvedic theories on smallpox were derived from chapter 58, titled Diagnosis and Treatment of Smallpox, obtained from the English translation of Bhāvaprakāśa (*30*), one of the 3 minor classic treatises of Ayurveda. Written by Brahmin Bhāramisra of India in the 16th Century, that book records the basic theories of Ayurvedic medicine, traditional pharmaceutical knowledge in India, and the diagnosis and treatment of diseases in various disciplines.

Reviewed medical texts from China explained that smallpox occurred when external pathogenic factors activated a latent fetal toxin within the child's body. According to TCM, fetal toxin is a latent pathogenic factor acquired in the womb. Within this framework, variolation was understood to induce a milder episode that expelled the toxin, thereby reducing susceptibility to subsequent smallpox. The mechanism of variolation is consistent with TCM theories on the etiology, pathogenesis, and treatment of smallpox.

As reflected in the English translation of the Bhāvaprakāśa, the Ayurvedic conceptualization of smallpox does not address intrinsic bodily factors or demonstrate recognition of the body's susceptibility. External pathogenic factors are framed as accidental exposures, including dietary disturbances, sun exposure, and climatic aberrations, which constitute a theoretical framework that offers no clear rationale for proactively modifying such factors to achieve long-term preventive effects. Within that documented medical context, the endogenous emergence of variolation within the Ayurvedic tradition appears unlikely on the basis of currently available evidence.

Taken together, we believe that it is unlikely that variolation in China was introduced from India. Instead, variolation more likely emerged within the cognitive framework of ancient TCM and has its origins in China.

Discussion

We reconstructed the technical system and evolution of variolation in late Imperial China and identified

efforts used to improve reliability and reduce health risk. The mature inoculum (shu miao) tradition might be interpreted as empirical risk reduction through inoculum selection and repeated passage. The distinctive intranasal route, aligned with variola virus's natural respiratory entry site, raises testable questions for modern vaccinology regarding mucosal immunogenicity, reactogenicity, and the potential of dry scab-based formulations for thermostable vaccine development. The predominance of nasal insufflation over cutaneous puncture in China is plausibly linked to the Confucian tradition of filial piety, which prohibits intentional bodily injury according to classical precepts.

We evaluated and clarified the relationship between variolation and its indigenous explanatory framework or rationale in China. The TCM concept of fetal toxins provided a rationale for intentional inoculation as a preventive intervention rather than merely inducing infection. Because of the absence of a similar preventive framework in contemporary Ayurvedic medicine, indigenous emergence of variolation in China is likely, although we remain cautious about single-origin claims and acknowledge possible parallel developments elsewhere. Nevertheless, according to the earliest surviving detailed documentation, China is the country with the earliest known development and practice of variolation; variolation practitioners in China also contributed substantially to technical refinement and health risk reduction.

The transregional circulation of variolation reshapes the understanding of prevaccine medical history. As a critical node in the global network of prophylactic practices, our findings challenge Western-centric narratives by demonstrating that preventive medicine evolved via multidirectional exchange rather than a unilinear trajectory. Furthermore, Edward Jenner's cowpox research later arose in a medical world already familiar with variolation.

The first limitation of our study is that the earliest origins of variolation in China remain uncertain because corroborating pre–Ming dynasty evidence is scarce. Second, regional variations in techniques and interpretations are not fully addressed. Translational parallels drawn here require further validation through interdisciplinary historical and experimental research. Finally, the Ayurvedic comparison relied mainly on an English translation of the Bhāvaprakāśa. Untranslated Sanskrit manuscripts,

Table 3. Comparison of cognitive theories on smallpox between TCM and Ayurveda in study of variolation techniques, medical explanations, and dissemination in late Imperial China*

Category	Country tradition	
	TCM, China	Ayurveda, India
Etiology	Fetal toxin and external pathogenic factors: fetal toxin is congenital and latent in the body; Shi Qi refers to pathogenic qi generated by abnormal climate, originating from nature.	Dietary disorders, including consumption of spicy, sour, penetrating, heating, burning (during digestion), dry, and alkaline foods and beverages; indigestion; overeating; sun exposure; abnormal climate. In 1767, Holwell recorded that direct cause was the mortal part of each human and animal form; indirect cause was multitudes of imperceptible animalculae floating in the atmosphere (*25*).
Pathogenesis	Shi Qi invades the body, triggers the inherent fetal toxin within, causes the fetal toxin to be expelled from inside to outside, and eventually manifests as pox eruptions on the skin.	Dietary disorders, sun exposure, and abnormal climate cause an imbalance in ≥1 of the 3 vital life energies—Vata (wind), Pitta (bile), and Kapha (phlegm)—which in turn leads to damage to the blood, muscles, and bones, as well as the formation of blisters (smallpox) on the skin, accompanied by fever.
Prevention and treatment	Treatment is divided into 6 stages: febrile, eruption, swelling, pustulation, crusting, and desquamation stages, with syndrome differentiation and treatment applied respectively. For each stage, the main focus is on differentiating the conditions of qi and blood (deficiency or excess), cold, heat, and toxic fire; corresponding prescriptions are used for replenishing qi and blood, warming the middle and dispelling cold, clearing heat and detoxifying, supporting the interior, and expelling toxins. TCM treatment of smallpox emphasizes protecting and replenishing qi and blood, believing that fetal toxin relies on qi and blood for expulsion. Prevention is variolation.	Treatment involves first fasting and inducing emesis with appropriate use of purgation. Then, according to the type of smallpox (i.e., which one or more of the vital energies are imbalanced), corresponding herbal decoctions are administered, and topical medications are applied to the skin to relieve blisters, burning sensations, and pain. The medications used are traditional natural medicines used in India. Prevention is variolation.
Inoculum	Smallpox scab (serial passaging, mature inoculum)	Smallpox pus
Inoculation site	Intranasal (mucosal)	Skin on the forearms, fingers, or forehead
Inoculation procedure	The technique evolved sequentially from the smallpox garment/blanket method to the lymph method, and the scab method was ultimately recognized as the optimal protocol.	The core operation consisted of skin puncture followed by inoculation with smallpox pus.

*Shi Qi, seasonal pathogenic qi; TCM, traditional Chinese medicine.

regional-language texts, and local records were not included, limiting generalization to the wider Ayurvedic variolation tradition.

In conclusion, variolation in late Imperial China developed as a coherent preventive tradition and as an empirical practice for treating smallpox. Historical medical writings from China document a progressively elaborated knowledge of smallpox pathogenesis and rationale for variolation. Together, the surviving evidence supports the view that China was the earliest country known to have developed and practiced variolation and to have documented corresponding medical explanations. The core technical features of variolation in China, including scab-derived inoculum, intranasal administration, and repeated passage in the mature inoculum tradition, reflect sustained empirical efforts to improve reliability and reduce risk. Although those practices arose in a very different historical and scientific context, they offer informed ideas for vaccine development and inoculation, particularly regarding inoculum selection, mucosal delivery, serial-passage strategies, preservation of biologic materials, and vaccination practices in public health.

Acknowledgments

We thank colleagues who provided informal feedback during the development of this manuscript.

All data supporting this review were derived from published historical sources cited in the reference list. No new individual-level or unpublished data were generated or analyzed. The extracted source information and comparative materials are available from the corresponding author upon reasonable request.

This work was supported by the Philosophy and Social Sciences Foundation of Zhejiang Province (grant no. 25NDJC096YBMS).

About the Author

Ms. Guan is a teacher and researcher at the School of Public Health, Zhejiang Chinese Medical University, Hangzhou. Her research areas include the history of vaccines, historical documents of traditional Chinese medicine, and traditional Chinese medicine literature on epidemic diseases.

References

1 World Health Organization. Smallpox and its eradication. 1988 [cited 2026 Apr 21]. https://iris.who.int/items/ba4ab312-1c43-4304-8235-969979499717
2. Shchelkunova GA, Shchelkunov SN. Smallpox, monkeypox, and other human orthopoxvirus infections. Viruses. 2022;15:103. https://doi.org/10.3390/v15010103
3. Parrino J, Graham BS. Smallpox vaccines: past, present, and future. J Allergy Clin Immunol. 2006;118:1320–6. https://doi.org/10.1016/j.jaci.2006.09.037
4. Dinc G, Ulman YI. The introduction of variolation "à la Turca" to the West by Lady Mary Montagu and Turkey's contribution to this. Vaccine. 2007;25:4261–5. https://doi.org/10.1016/j.vaccine.2007.02.076
5. Theves G. Smallpox: an historical review [in German]. Bull Soc Sci Med Grand Duche Luxemb. 1997;134:31–51.
6. Ma BY. History of Chinese medical culture, vol. 1 [in Chinese; Zhongguo Yixue Wenhua Shi (中国医学文化史)]. Shanghai: Shanghai People's Publishing House; 2010. p. 423–533.
7. Zhu CG. Conclusive theories on smallpox and rashes [in Chinese; Dou Zhen Ding Lun (痘疹定论)]. Block-printed edition; 1852 [cited 2026 Apr 21]. https://dpul.princeton.edu/eastasian/catalog/m613n1179
8. Yu MK. Annotations on the golden mirror ode to smallpox, vol 2 [in Chinese; Dou Ke Jin Jing Fu Ji Jie (痘科金镜赋集解)]. Guangxu Emperor reign, block-printed edition; p 25 [cited 2026 Apr 21]. https://www.shidianguji.com/book/CADAL02035678/chapter/1l7lgzw1rdvl2
9. Zhang Y. New treatise on variolation, vol 3 [in Chinese; Zhong Dou Xin Shu (种痘新书)]. Block-printed edition, 1741 [cited 2026 Apr 21]. https://dpul.princeton.edu/eastasian/catalog/td96k515v
10. Fan XZ. History of Chinese preventive medical thought [in Chinese; Zhongguo Yufang Yixue Sixiang Shi (中国预防医学思想史)]. Shanghai: East China Medical Life Press; 1953. p. 81–144.
11. Leung AKC. "Variolation" and vaccination in late Imperial China, ca 1570–1911. In: Plotkin SA, editor. History of vaccine development. New York: Springer; 2011. p. 5–12.
12. Ma BY, Gao X, Hong ZL. History of Sino-foreign medical cultural exchange [in Chinese; Zhongwai Yixue Wenhua Jiaoliu Shi (中外医学文化交流史)]. Shanghai: Wenhui Press; 1993. p. 613.
13. Needham J. China and the origins of immunology. East Horiz. 1980;19:6–12. PubMed
14. Sugandi R. Knowledge Ottoman Turkish medicine: from methods immunization traditional to pioneer world vaccine [cited 2026 Apr 21]. https://pdfs.semanticscholar.org/2543/f626141eda58a870e47e6152d4e5bc1f0057.pdf
15. Plotkin SA, Orenstein WA, Offit PA, Edwards KM. Plotkin's vaccines, 7th edition. Luo FJ, Li CG, Yang XM, translators. Beijing: People's Medical Publishing House; 2023.
16. Zhang L. Zhang's Comprehensive Medicine [in Chinese; Zhang Shi Yi Tong (张氏医通)]. Li JF, Jian Y, annotators. Beijing: China Traditional Chinese Medicine Press; 1995. p. 329–30.
17. Wu Q. The Golden Mirror of Medicine [in Chinese; Yi Zong Jin Jian (医宗金鉴)]. An YZ, Yuan H, editors. Beijing: China Traditional Chinese Medicine Press; 1994. p. 691–92.
18. Fu CX. Vaccines and immunization. Beijing: People's Medical Publishing House; 2020.
19. Noble J Jr, Rich JA. Transmission of smallpox by contact and by aerosol routes in Macaca virus. Bull World Health Organ. 1969;40:279–86.
20. Zhu YL. Essentials of variolation [in Chinese; Zhong Dou Xin Fa (种痘心法)]. In: Wang YW, editor. Cong Shu Ji Cheng Chu Bian. Shanghai: Commercial Press; 1936. p. 5–6.
21. Ge H. Transcendent Master Ge's emergency-preparedness recipes to keep close at hand, vol 2 [in Chinese; Ge Xian Weng Zhou Hou Bei Ji Fang (葛仙翁肘后备急方)]. Li Shi block-printed edition. Beijing: National Library of China collection; 1574. p. 18.

22. Qian Y. Key to the therapeutics of children's diseases [in Chinese; Xiao Er Yao Zheng Zhi Jue (小儿药证直诀). Yan XZ, compiler; Guo JS, collator. Beijing: People's Medical Publishing House; 2017.
23. Wan Q. Complete medical works of Wan Mizhai [in Chinese; Wan Mi Zhai Yi Xue Quan Shu (万密斋医学全书)]. Fu PF, Yao CS, Wang XP, editors. Beijing: China Traditional Chinese Medicine Press; 1999.
24. Hopkins DR. The great killer: smallpox in history. Shen YM, Jiang GN, translators. Shanghai: Shanghai People's Publishing House; 2005.
25. Naraindas H. Preparing for the pox: a theory of smallpox in Bengal and Britain. Asian J Soc Sci. 2003;31:304–39. https://doi.org/10.1163/156853103322318252
26. Nicholas RW. The goddess Sitala and epidemic smallpox in Bengal. J Asian Stud. 1981;41:21–45.
27. Fitchett JR, Heymann DL. Smallpox vaccination and opposition by anti-vaccination societies in 19th century Britain [cited 2026 Apr 21]. https://www.healthchoicevt.com/wp-content/uploads/2016/01/E17.pdf
28. Maty M. XVII. A short account of the manner of inoculating the small pox, on the Coast of Barbary, and at Bengal, in the East Indies, extracted from a memoir written in Dutch, by the Reverend Mr. Chais, at the Hague. Philos Trans. 1768;58:128–31. https://doi.org/10.1098/rstl.1768.0017
29. Ainslie W III. Observations respecting the small-pox and inoculation in eastern countries; with some account of the introduction of vaccination into India. Transactions of the Royal Asiatic Society of Great Britain and Ireland. 1830;2:52–73. https://doi.org/10.1017/S0950473700001294
30. Bhāramiśra. Bhāvaprakāśa. Murthy KRS, translator. Varanasi: Chowkhamba Krishnadas Academy; 2008. p. 632–35.

Address for correspondence: Chuanxi Fu, Department of Vaccinology, School of Public Health, Zhejiang Chinese Medical University, Hangzhou 310053, China; email: fuchuanxi@zcmu.edu.cn

etymologia revisited

The Color Puce

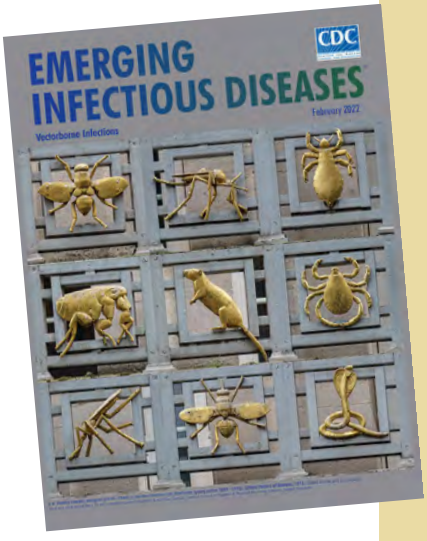

Originally published in February 2022

For those with synesthesia, in whom stimulating 1 sensory pathway gives rise to a subjective sensation of a different character, the word plague may chromatically resonate with puce. In pre-revolutionary France, an era of "evocative color nomenclature," Marie Antoinette's reign was precipitating intense criticism. Her countrymen were experiencing severe socioeconomic stress, thus her sartorial self-indulgence was much resented.

After discovering the Queen wearing a new gown, her husband, Louis XVI, the King of France, chided her, describing the dress's unflattering purple–brown hue as "*couleur de puce*" (color of fleas). This admonishment had the unintended consequence of promoting puce as the exclusive color worn by the French court. Puce, the French word for flea, descends from *pulex* (Latin). Flea droppings leave puce colored "bloodstains" on bedsheets. The role of fleas, however, as a vector for bubonic plague was not proven until about 1895.

References:

1. Stedman's Medical Dictionary. 23rd ed. Baltimore: The Williams & Wilkins Company; 1976. p. 1392.
2. St. Clair K. The secret lives of color. New York: Penguin Books; 2017. p. 122–3.
3. Zietz BP, Dunkelberg H. The history of the plague and the research on the causative agent *Yersinia pestis*. Int J Hyg Environ Health. 2004;207:165–78. https://doi.org/10.1078/1438-4639-00259
4. Plague bacteria found in Arizona fleas, by Rachael Rettner, August 14, 2017 [cited 2021 Nov 4]. https://www.livescience.com/60130-plague-fleas-arizona.html.)

https//wwwnc.cdc.gov/eid/article/28/2/et-2802_article

Emergence of Rabies in Cape Fur Seals, South Africa

Chuene Ernest Ngoepe,[1] Lesley van Helden,[1] Wonderful Shumba, Laura C. Roberts, Deon Kriel, Munangatire Mparamoto, Claude Taurai Sabeta

Rabies was diagnosed in Cape fur seals by using direct fluorescent antibody testing in South Africa, 2024. We investigated the origin of rabies virus in this species. Phylogenetic analysis revealed virus introduction from jackals into seals, followed by sustained viral transmission within the seal population and spillover into a domestic dog.

Rabies is a viral encephalitis caused by members of the *Lyssavirus* genus within the Rhabdoviridae family (*1*). Rabies virus (RABV) is a prototype species of the *Lyssavirus* genus and has a wide host range, including various Chiroptera and terrestrial Carnivora species (*2*). In southern Africa, RABV is maintained by domestic dogs and wildlife species such as black-backed jackals (*Lupulella mesomelas*), bat-eared foxes (*Otocyon megalotis*), aardwolves (*Proteles cristatus*), and yellow mongooses (*Cynictis penicillata*) (*3*).

In 2021, reports of unusually aggressive Cape fur seals (*Arctocephalus pusillus pusillus*) surfaced in South Africa; the behavior was attributed to domoic acid toxicity (*4*,*5*). On May 20, 2024, an unvaccinated domestic dog, henceforth referred to by its sample reference number, 170/24WC, from a walled suburban home in Cape Town was diagnosed with rabies using direct fluorescent antibody test (dFAT) on a brain tissue sample at the Agricultural Research Council–Onderstepoort Veterinary Research (Pretoria, South Africa). The owner suspected that a Cape fur seal had bitten the dog because the dog had a habit of approaching seals and sustained a bite wound while out of sight during an off-leash beach walk with the owner 2 weeks before the onset of clinical signs.

As part of the ensuing investigation, stakeholders in Cape Town were contacted to determine if any seals showing aggression or abnormal behavior had been observed or removed from beaches in the preceding month. A report stated that a Cape fur seal had been in a fight with dogs on Big Bay Beach in Cape Town on May 22, 2024, and suffered several injuries. The seal was captured by authorities and died in transit to a veterinary facility. A brain sample from this seal (sample reference 186/24WC) was obtained and tested positive for rabies by dFAT.

The Cape fur seal is the only resident pinniped species in southern Africa; an estimated 2 million animals are distributed from Baía dos Tigres in Angola to Algoa Bay, South Africa. The seals breed in colonies on land, where they frequently encounter people and face predation from terrestrial hunters such as the brown hyena (*Hyaena brunnea*) and the black-backed jackal (*6*). To our knowledge, the only previous confirmed case of rabies in a pinniped occurred in a ringed seal (*Pusa hispida*) in Svalbard, Norway in 1980 (*7*). We investigated to determine the origin and geographic spread of rabies virus infection in Cape fur seals in South Africa.

The Study

Rabies is a notifiable disease in South Africa, and all suspected animal cases must be reported to government veterinary services. Beginning in June 2024, after RABV was confirmed in a Cape fur seal (186/24WC), all marine mammals showing neurologic signs were suspected to be rabid, and brain samples were collected from those that either died or could be captured and euthanized via lethal dose of pentobarbital or gunshot (Figure 1). In addition, opportunistic sampling of Cape fur seal or other marine mammal carcasses in remote

Author affiliations: Agricultural Research Council–Onderstepoort Veterinary Research, Pretoria, South Africa (C.E. Ngoepe, M. Mparamoto, C.T. Sabeta); Western Cape Department of Agriculture, Elsenburg, South Africa (L. van Helden, L.C Roberts); Northern Cape Department of Agriculture, Environmental Affairs, Rural Development and Land Reform, Kimberley, South Africa (W. Shumba, D. Kriel); University of Pretoria, Pretoria (C.T. Sabeta)

DOI: https://doi.org/10.3201/eid3210.260179

[1]These authors contributed equally to this article.

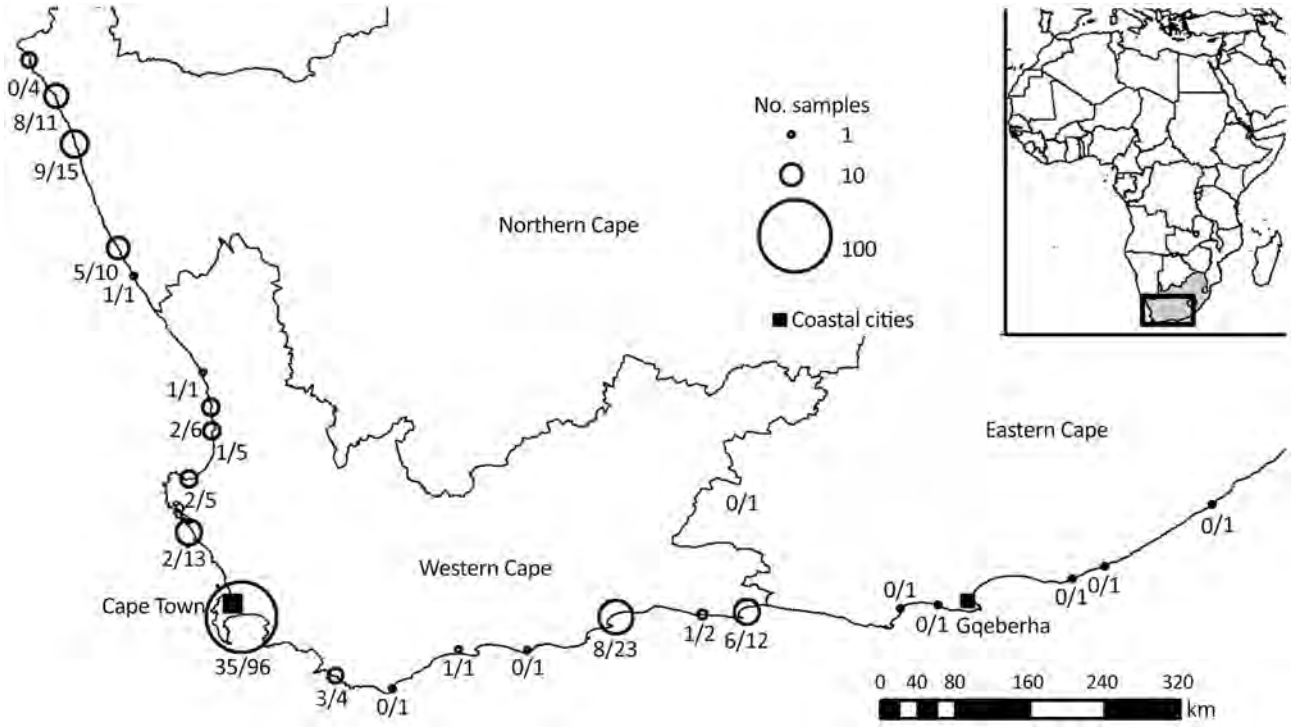

Figure 1. Sampling locations for study of emergence of rabies in Cape fur seals, South Africa. Numbers next to circles indicate no. positive/otal no. samples. Inset map shows location of study area in Africa.

areas of the coast was undertaken. We also sourced Cape fur seal brain samples collected during March 2023–May 2024 stored frozen and retrospectively tested for the RABV antigen, as previously described (*8*), and undertook RNA extractions, reverse transcription PCR, partial genome sequencing, and phylogenetic analyses of RABVs (Appendix, https://wwwnc.cdc.gov/EID/article/32/10/26-0179-App1.pdf).

A total of 216 Cape fur seal brain tissue samples were collected along the South Africa coast during March 2023–November 2025, including 6 retrospective samples (Figure 1). Of those, 85 (39%) tested positive for lyssavirus antigen by dFAT; the remaining 131 (61%) tested negative. Positive samples were obtained from multiple locations along the coasts of the Northern and Western Cape provinces of South Africa. Of the 85 confirmed positive cases, 45 were found dead, and the other 40 were euthanized or shot. The earliest confirmed positive sample originated from Cape Town in September 2023 from a retrospective sample. The only other marine animal tested for rabies was an orca (*Orcinus orca*) found dead in St. Helena Bay in October 2024; results were negative.

A total of 51 RABVs detected in Cape fur seals and 1 from dog 170/24WC were available for sequencing. We deposited the generated nucleotide sequences in GenBank (Appendix Table). Phylogenetic analysis revealed 4 distinct clusters (A–D) of closely related viral sequences with posterior probability values of 1 (Figure 2). Cluster A comprised RABVs from 51 Cape fur seals and dog 170/24WC. The pairwise distance comparisons of RABVs in cluster A showed 99.79% nucleotide sequence identity. Furthermore, cluster A contained a subcluster (A1) with a posterior probability of 0.99. Cluster B consisted of RABVs from black-backed jackals and a bat-eared fox. Phylogenetic analysis showed that the RABVs in clusters A and B had a 98% nucleotide sequence identity and shared a common ancestor. Cluster C consisted of RABVs from bat-eared foxes and aardwolves, whereas cluster D contained RABVs from domestic dogs.

BEAST evolutionary analysis (https://beast.community) showed that the mean rate of nucleotide substitutions for the RABVs included in the analysis was 3.7838×10^{-4} substitutions/site/year (95% highest posterior density $2.0322–5.6575 \times 10^{-4}$ substitutions/site/year). The estimated time to the most recent common ancestor (tMRCA) of clusters A and B was 1998. The tMRCA of cluster A was estimated at 2015 and subcluster A1 at 2020 (Figure 2).

RABV typically spreads among animals of the same species, but direct interaction of a susceptible mammal with a reservoir host could result in cross-

species transmission. In rare cases, such events have historically enabled RABV to evolve and adapt to new hosts (*3*), as observed in Cape fur seals in this study. All RABVs analyzed from seals had 99.79% sequence identity, indicating a single source of infection and subsequent viral transmissions within the seal population. RABVs introduced from multiple sources would show a lower degree of similarity (*3*,*9*). On the basis of available nucleotide sequence data, the black-backed jackal is the most likely source of introduction of RABV into the Cape fur seal population, given that tMRCA was closest for RABVs from the seals and the jackals. The RABVs in cluster A are estimated to have diverged from a common ancestor in 2015; thus, RABV was probably introduced into the seal population some years before it was laboratory confirmed. The large number of rabies-positive cases (n = 85) detected in this study that occurred during March 2023–November 2025 provides further evidence for a long period of seal-to-seal transmission, across almost the entire range of this species in South Africa. That spread was presumably aided by the ability of Cape fur seals to travel extensively in the ocean, resulting in a high degree of interaction across geographic areas (*10*). The RABV from dog 170/24WC clustered with the Cape fur seal RABVs, confirming the seal as its likely source of infection.

Conclusions

Our findings demonstrate the ability of RABV to emerge in new host species and subsequently maintain

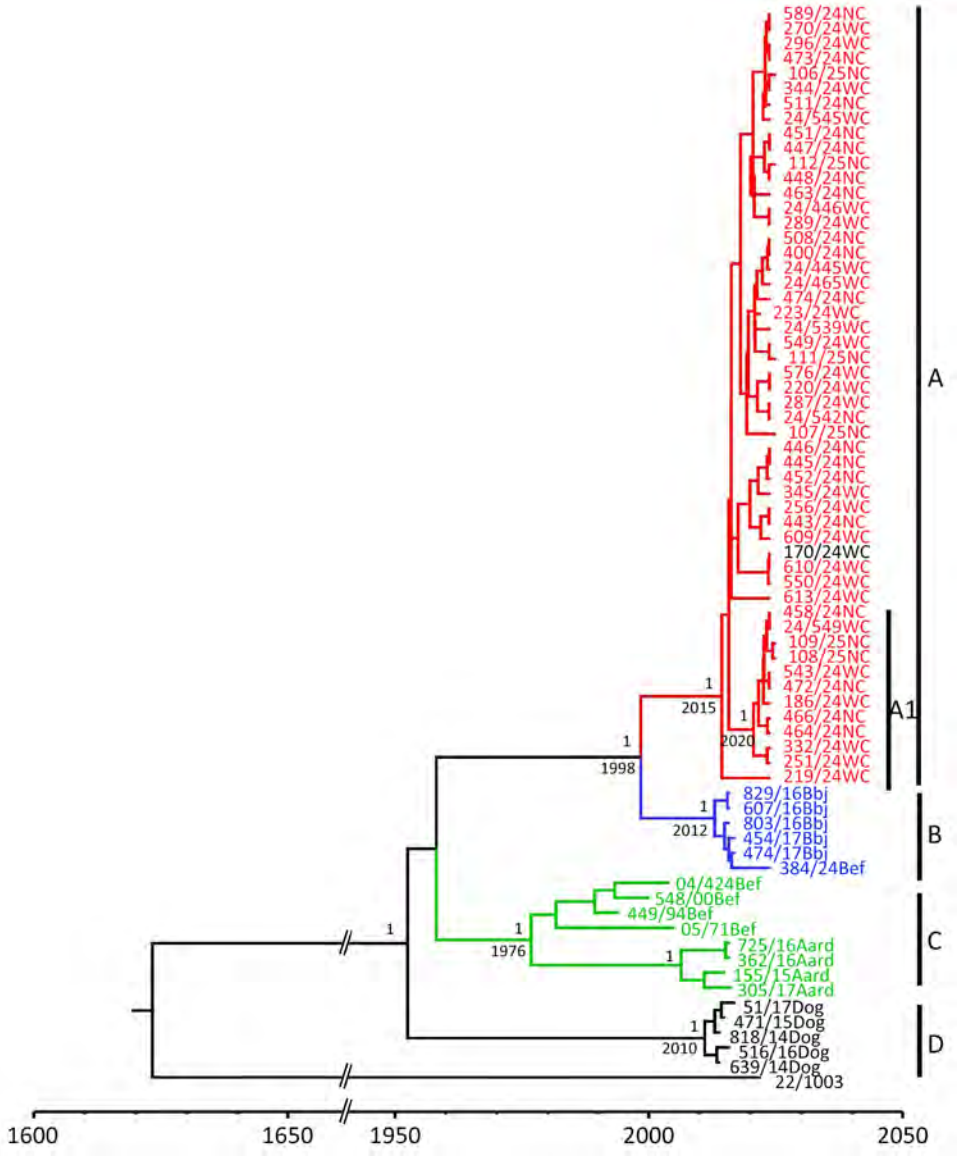

Figure 2. Timescale phylogenetic analysis for study of emergence of rabies in Cape fur seals, South Africa. Red font indicates sequences from Cape fur seals from this study, including retrospective samples; black text among seal samples indicates sample from a domestic dog (170/24WC) likely infected by contact with a seal. Green text indicates sequences from bat eared foxes (Bef) and aardwolves (Aard); blue text indicates sequences from black-backed jackals (Bbj) and one from bat eared fox; black text at bottom of tree indicates sequences from domestic dogs retrieved from GenBank.

transmission cycles in such hosts. However, this study is limited in its ability to estimate the prevalence of RABV within the Cape fur seal population because it relied on passive surveillance. Rabies virus remained undetected in Cape fur seal for years, highlighting the need for continuous surveillance in mammals displaying unusual behavior and neurologic signs to detect emerging lyssavirus variants. In addition, interventions that prevent cross-species transmission of RABV, such as large-scale parenteral vaccination of domestic dogs, should be continued and strengthened.

Acknowledgments

We thank Christine Lotter and Debrah Mohale for their technical and administrative support and the Department of Forestry, Fisheries and the Environment and Sea Search Research & Conservation for assisting in the collection of samples.

The study was approved by the Animal Ethics Committee of the Agricultural Research Council Onderstepoort Veterinary Research (AEC 23.21), and section 20 approval was granted by the Director of Animal Health of the Department of Agriculture (certificate no. 12/11/1/1(a)()/6658(HP)).

This study was supported by the Agricultural Research Council Onderstepoort Veterinary Research, Rabies Diagnostic Project (OVI01240300024) and the Department of Agriculture, project number A162 (OVI01240300038). The funders had no role in the design of the study; in the collection, analyses, or interpretation of data; in the writing of the manuscript; or in the decision to publish the results.

About the Author

Mr. Ngoepe is a researcher at World Organization for Animal Health Reference Laboratory for Rabies in Agricultural Research Council, South Africa. His research interests include studies on *Lyssavirus* genus phylogeny, rabies surveillance and control, production of biologics for lyssaviruses, pathogenicity studies, and developing and improving diagnostic methods primarily for lyssaviruses of African origin.

References

1. Walker PJ, Freitas-Astúa J, Bejerman N, Blasdell KR, Breyta R, Dietzgen RG, et al.; ICTV Report Consortium. ICTV virus taxonomy profile: Rhabdoviridae. J Gen Virol. 2022;103:001689.
2. Badrane H, Tordo N. Host switching in *Lyssavirus* history from the Chiroptera to the Carnivora orders. J Virol. 2001;75:8096–104. https://doi.org/10.1128/JVI.75.17.8096-8104.2001
3. Viljoen N, Sabeta C, Markotter W, Weyer J. Temporal and spatial analysis of rabies virus lineages in South Africa. Viruses. 2025;17:340. https://doi.org/10.3390/v17030340
4. Gridley T, Elwen SH, Childerhouse S, Constantine R, Frouin H, Galatius A, et al. ToxMap: a global network to monitor contaminants in marine mammals. Presented at: Scientific Committee on Oceanic Research Annual Meeting; Busan, South Korea; 2022 October 4–6 [cited 2026 Feb 9]. https://scor-int.org/wp-content/uploads/2022/05/ToxMAP-SCOR-WG-2022-Proposal_Gridley-et-al_Final.pdf
5. Glasby B. Why are we seeing an increase in aggressive behaviour by seals? Daily Maverick. 2023 Jan 5 [cited 2026 Feb 9]. https://www.dailymaverick.co.za/article/2023-01-05-why-are-we-seeing-an-increase-in-aggressive-behaviour-by-seals
6. Kirkman SP, Hofmeyr GJG, Seakamela SM, Pistorius PA. A conservation assessment of *Arctocephalus pusillus pusillus*. In: Child MF, Roxburgh L, Do Linh San E, Davies-Mostert HT, editors. The red list of mammals of South Africa, Swaziland and Lesotho. Pretoria: South African National Biodiversity Institute and Endangered Wildlife Trust; 2016. p. 1–9.
7. Odegaard OA, Krogsrud J. Rabies in Svalbard: infection diagnosed in arctic fox, reindeer and seal. Vet Rec. 1981;109:141–2. https://doi.org/10.1136/vr.109.7.141
8. Dean DJ, Albelseth MK, Atanasiu P. The fluorescent antibody test. In: Meslin FX, Kaplan MM, Koprowski H, editors. Laboratory techniques in rabies, 4th edition. Geneva: World Health Organization; 1996. p. 88–95.
9. Sabeta CT, Mansfield KL, McElhinney LM, Fooks AR, Nel LH. Molecular epidemiology of rabies in bat-eared foxes (*Otocyon megalotis*) in South Africa. Virus Res. 2007;129:1–10. https://doi.org/10.1016/j.virusres.2007.04.024
10. Robbertse M, Hofmeyr GJG, de Bruyn PJN, Dalton D, Mwale M. Mitochondrial DNA diversity and phylogeographic patterns among South African Cape fur seals, *Arctocephalus pusillus pusillus.* Aquat Conserv. 2025;35:e70210. https://doi.org/10.1002/aqc.70210

Address for correspondence: Chuene Ernest Ngoepe, World Organization for Animal Health Rabies Reference Laboratory, Agricultural Research Council-Onderstepoort Veterinary Research, Onderstepoort, 0110, Pretoria, South Africa; email: ngoepee@arc.agric.za

Fatal Infection with Dengue Virus and Avian Orthoavulavirus 1 in Traveler Returning from Saudi Arabia to France, 2025

Maud Salmona, Salomé Schlupmann, Morgane Mailhe, Dorothée Chopin, Quentin Richier, Karine Lacombe, Lila Bouadma, Jean-Francois Timsit, Vincent Bondet, Quentin Le Hingrat, Jérôme Le Goff, Jamie Sugrue, Darragh Duffy, Olivier Schwartz, Michael White, Valérie Paradis, Franck Verdonk, François-Xavier Lescure, Marie Jaspard

A previously healthy 26-year-old man died of hemorrhagic fever with fulminant hepatitis and shock 36 hours after returning to France from Mecca, Saudi Arabia. Postmortem analyses detected low-level dengue virus RNA and positive NS1 antigen along with unexpected extremely high-titer disseminated velogenic avian orthoavulavirus 1 infection with elevated systemic cytokine responses.

A previously healthy 26-year-old man sought care in Paris, France, immediately after returning from Mecca, Saudi Arabia, in January 2025. He was experiencing fever, myalgia, headache, abdominal pain, and diarrhea that began 4 days earlier. He reported no specific exposure during his trip, including no contact with animals, contaminated food or water, or insect bites. He had no history of immunosuppression or repeated infection. No family members traveling with him experienced similar symptoms. We report the patient's clinical course and laboratory findings.

The Study

At admission to the intensive care unit in Saint-Antoine hospital (Paris, France), the patient had fever (40°C), tachypnoea (45 breaths/min, SpO_2 95% on room air), poor tissue perfusion, and oliguria. Results of cardiopulmonary, abdominal, and neurologic examination were unremarkable. Conjunctival hemorrhage and hematuria were present at hospital admission. Despite early fluid resuscitation and empirical antimicrobial treatment, his condition rapidly deteriorated. He experienced multiple organ dysfunction syndrome including hypotension, purpuric livedo, anuria, and acute kidney failure (creatinine 600 µmol/L), elevated level of lactate (4.4 mmol/L), major hepatic dysfunction (alanine aminotransferase and aspartate aminotransferase levels were >100 times the upper limit of normal and factor V was at 51%), thrombocythemia (29×10^9/L), decreased hematocrit (39%), decreased prothrombin time (52%), and disseminated intravascular coagulation. Inflammatory markers were elevated (C-reactive protein 320 mg/L; procalcitonine 136 µg/L). We could not perform bacterial analysis because the patient was isolated for initial suspicion of highly infectious pathogens. Body computed tomography results were unremarkable. We applied resuscitation measures and escalated antimicrobial therapy.

Etiologic assessment included PCR testing for malaria, SARS-CoV-2, influenza, cytomegalovirus, Ebola virus, Zika virus, chikungunya virus, and serology for HIV and for hepatitis A, B, C, and E; all results were negative. At that time, the patient's blood tested negative by PCR and IgM and IgG serology for dengue virus (DENV). The patient's condition continued to deteriorate; he experienced refractory shock, fulminant hepatitis, and disseminated intravascular coagulation. He died 36 hours after hospital admission.

Author affiliations: Hôpital Saint-Louis, Paris, France (M. Salmona, J. Le Goff); Hôpital Saint-Antoine, Paris (S. Schlupmann, D. Chopin, Q. Richier, K. Lacombe, M. Jaspard); Hôpital Bichat Claude-Bernard, Paris (M. Mailhe, F.-X. Lescure); Sorbonne Université, Paris (Q. Richier, K. Lacombe, F. Verdonk); Assistance Publique—Hôpitaux de Paris, Paris (L. Bouadma, J.-F. Timsit, Q. Le Hingrat, V. Paradis, F.-X. Lescure); IAME, INSERM, Université Paris Cité, Paris (L. Bouadma, J.-F. Timsit, F.-X. Lescure); Université Paris Diderot, Paris (J.-F. Timsit, F.-X. Lescure); Institut Pasteur, Paris (V. Bondet, J. Sugrue, D. Duffy, O. Schwartz, M. White)

DOI: https://doi.org/10.3201/eid3210.260736

Postmortem laboratory results revealed a low dengue viral load in urine with quantitative reverse transcription PCR results at a cycle threshold (Ct) of 39 from a pan-dengue duo test and Ct of 40 from a dengue-1–specific test; both had a robust fluorescence curve. Serum was positive for nonstructural 1 glycoprotein antigen (positivity ratio 2.5) by VIDAS Dengue NS1 (bioMérieux, https://www.biomerieux.com). Postmortem liver biopsy demonstrated normal architecture and extensive parenchymal necrosis without any viral inclusions (Figure 1).

We further analyzed plasma and liver biopsy samples using metagenomic shotgun next-generation sequencing (mNGS). mNGS detected avian orthoavulavirus 1 (AOAV-1), the virus historically associated with Newcastle disease, at extremely high levels; 191,718 reads per million in liver tissue, and 244,781 reads per million in plasma. We obtained complete coverage of all AOAV-1 coding sequences (GenBank accession no. PX575854). Phylogenetic analysis classified the strain as AOAV-1 clade II, genotype VI, subgenotype VI.2.1.2 (Figure 2), a pigeon-adapted lineage historically termed pigeon paramyxovirus type 1, with a velogenic fusion protein cleavage site motif (RRRKRF) (*1*). Velogenic strains are highly virulent AOAV-1 variants defined by a polybasic fusion-protein cleavage site, which enables ubiquitous protease activation and systemic multiorgan tissue tropism, in contrast to low-virulence strains, which carry a monobasic cleavage site and remain confined to the respiratory and enteric tract (*1*).

We confirmed AOAV-1 infection by specific real-time PCR detection on postmortem liver biopsy (Ct 17.23) and plasma (Ct 15.74) samples, as well as on premortem urine (Ct 18.23), cerebrospinal fluid (Ct 35.9), and sputum (Ct 18.5) specimens, confirming a disseminated infection. In addition, analysis of the plasma type I interferon (IFN) response by single molecule array digital-ELISA using an in-house Simoa bead-based assay on the HD-X platform (Quanterix, https://www.quanterix.com) showed extremely high levels of IFN-α (>10^4 pg/mL) (Figure 3, panel A) and IFN-β (>10^4 pg/mL, data not shown), as well as extremely high levels of IFN-γ, C-X-C motif chemokine ligand 10 and 11, interleukin 6, and tumor necrosis factor-α measured by Luminex (R&D Systems, Inc., https://www.rndsystems.com) (Figure 3, panels B–F).

Conclusions

We describe a fulminant febrile illness associated with 2 unusual virologic findings: low-level evidence of DENV infection and high-titer disseminated AOAV-1. We could not establish the relative contribution of

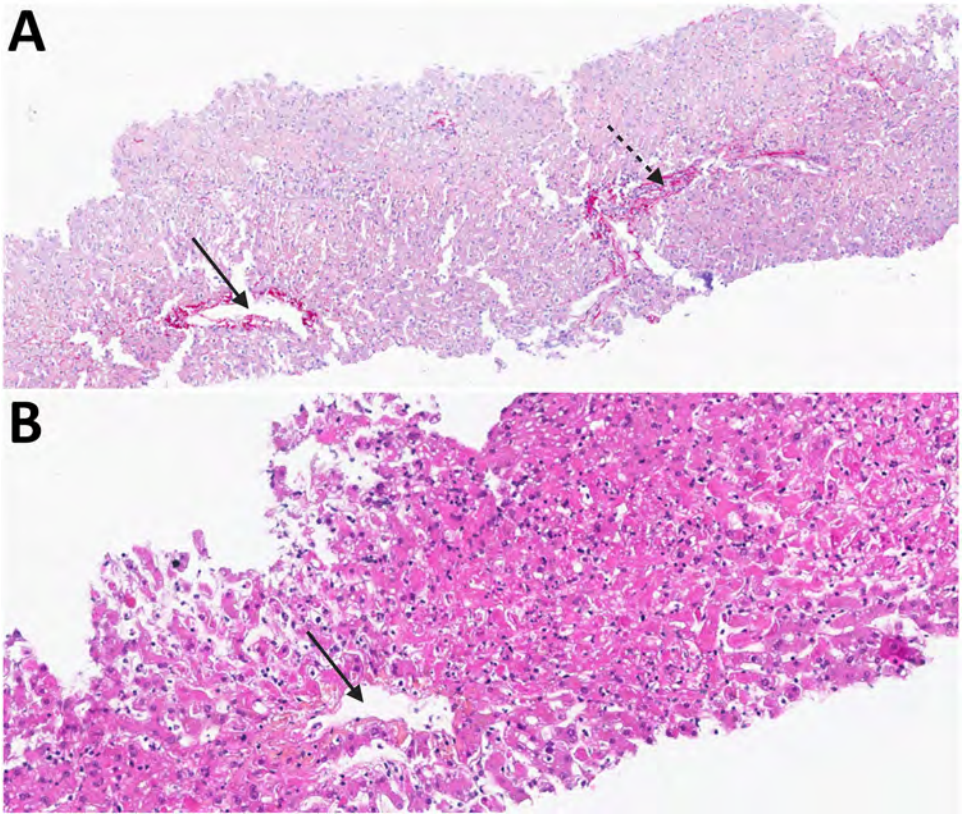

Figure 1. Liver biopsy images from study of a fatal infection with dengue virus and avian orthoavulavirus 1 in traveler from Saudi Arabia, 2025. A) Sirius red stain showing normal architecture without any fibrosis. Solid arrow indicates centrilobular vein; dashed arrow indicates portal tract. Original magnification ×100. B) Hematoxylin and eosin stain showing extensive parenchymal necrosis; all hepatocytes of the lobule are necrotic. Lobules contain few inflammatory cells. Solid arrow indicates centrilobular vein. Original magnification ×200.

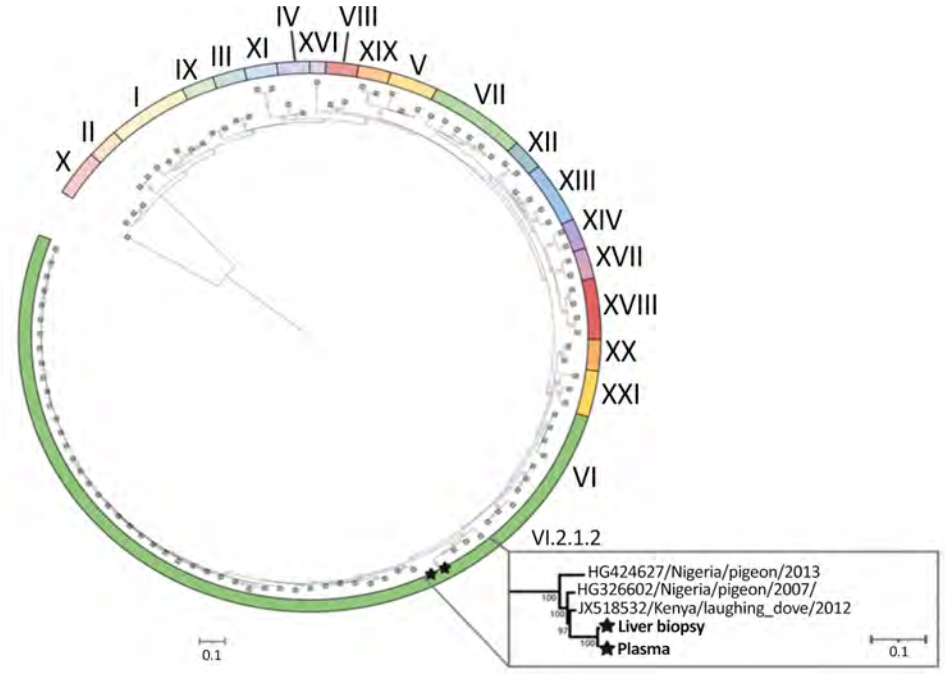

Figure 2. Maximum-likelihood phylogenetic tree of APMV-1 from study of a fatal infection with dengue virus and avian orthoavulavirus 1 in traveler from Saudi Arabia, 2025. The tree was inferred from 120 complete APMV-1 clade II genomes retrieved from GenBank. Black stars indicate sequences obtained from the patient's liver biopsy and plasma samples, which cluster within subgenotype VI.2.1.2 (inset). Scale bar indicates nucleotide substitutions per site. APMV-1, avian paramyxovirus type-1.

each virus to the fatal syndrome with certainty. However, the high AOAV-1 loads detected in plasma and multiple tissues and body fluids provide strong evidence of disseminated infection and a major role for AOAV-1 in the clinical manifestation of the infection.

Severe forms of dengue occur in ≈5% of cases (*2*). Because this patient had no history of dengue infection and no detected DENV IgG, his illness was consistent with primary dengue fever, which although typically milder than subsequent infections, can also lead to severe disease (*2*). Initial blood PCR and serology were negative for DENV, as was the mNGS performed in the liver biopsy. We diagnosed dengue on the basis of DENV-1–specific and pan-dengue PCR assay on urine and the detection of NS1 antigen in blood.

AOAV-1 infection was detected after patient's death and was completely unexpected. The AOAV-1 strain genotype VI.2 is a lineage maintained primarily in a pigeon/columbiform reservoir (*3*–*5*). Genotype VI.2.1 has been reported circulating in backyard pigeons in eastern Saudi Arabia (*6*); pigeons are numerous around the Grand Mosque in Mecca, where the patient stayed for 2 weeks. In immunocompetent hosts, human AOAV-1 infection is typically an uncomplicated, self-limited, localized illness, most often manifesting as conjunctivitis with or without mild systemic symptoms; it occurs predominantly in poultry workers exposed to infected flocks (*7*). Infection is more severe in immunosuppressed patients, in whom it causes pulmonary disease with symptoms ranging from upper respiratory tract disorder to fatal respiratory failure with large infiltrative lesion of the lung, and neurologic disorders such as seizure and encephalitis (*8*–*10*). No cases of hepatitis have been reported in humans, although AOAV-1 has been detected in liver biopsy samples (*10*). However, hepatitis caused by AOAV-1 remains plausible; velogenic strains have a broad tropism in birds (*11*).

Since the advent of mNGS, the number of severe human cases reported in the literature has increased, suggesting that human AOAV-1 infections have previously been underestimated. As of March 2026, a total of 7 severe human AOAV-1 cases had been reported globally: 4 pneumonia and 3 encephalitis cases (*8*–*10*,*12*–*15*). Four patients were immunosuppressed (*8*–*10*,*13*). Disseminated infection was confirmed in 3 cases. Proximity to pigeons was documented in 2 cases (*12*,*14*). Six cases resulted in death. Our case-patient, like 3 others (*12*,*14*,*15*), showed no evidence of immunosuppression related to a known disease or treatment. However, we cannot exclude potential inborn genetic errors affecting immune response. Indeed, we observed a cytokine storm suggestive of an inadequate immune response, which raised questions about possible genetic immune deficiencies. As in our case, all patients experiencing severe infection harbored a velogenic AOAV-1 strain, which is characterized by a multibasic cleavage site in the fusion protein enabling extensive tissue tropism and widespread dissemination.

In summary, the fatal combination of DENV and AOAV-1 infections most likely reflected a multifactorial process. The extremely high, disseminated AOAV-1 loads and the associated extreme type I/III interferon and pro-inflammatory cytokine response are the best-documented and most plausible contributors to the fulminant clinical course. A causal contribution from DENV, despite its low viral load, cannot be excluded. However, our case, together with previous reports, highlights the potential for severe disseminated disease after infection with velogenic AOAV-1 strains. Our findings underscore the value of considering AOAV-1 infection and of applying mNGS in unexplained severe febrile illness after travel.

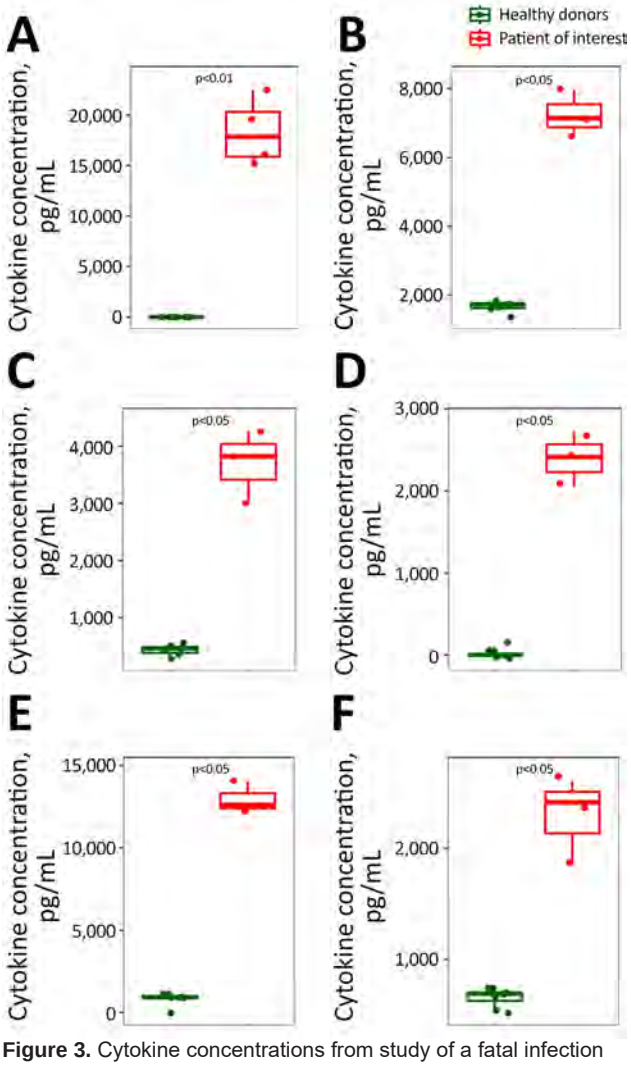

Figure 3. Cytokine concentrations from study of a fatal infection with dengue virus and avian orthoavulavirus 1 in traveler from Saudi Arabia, 2025. A) IFN-α. B) IFN-γ. C) IFN-induced CXCL10. D) IFN-induced CXCL11. E) Pro-inflammatory IL-6. F) Pro-inflammatory TNF-α. We measured concentrations in blood samples from the study patient compared with those from healthy donors. Boxes indicate 95% CI; horizontal bars within boxes indicate median; whiskers indicate ranges; dots indicate individual patient samples. We measured concentrations for interferon-α using single molecule array digital-ELISA using an in-house Simoa bead-based assay on the HD-X platform (Quanterix, https://www.quanterix.com) and multiplexed Luminex assay (R&D Systems, Inc., https://www.rndsystems.com) for other cytokines. We determined p values by Mann-Whitney test. CXCL, C-X-C motif chemokine ligand; IFN, interferon; IL, interleukin; TNF, tumor necrosis factor-α.

Acknowledgments

We thank Sylvain Baize and team and Xavier de Lamballerie and team for their support in the viral management of this patient.

Author contributions: M.J. wrote the first draft of the manuscript. All authors reviewed and revised the manuscript. M.J., S.S., F.V., D.C., L.B., and J.-F.T. provided medical care to the patient. M.M., F.-X.L., K.L., F.V., and M.J. managed the biological risk of the patient. M.S., V.B., Q.R., V.P., Q.L.H., J.L.G., D.D., O.S., M.W., and J.S. analyzed the biological samples.

About the Author

Dr. Salmona is an associate professor and hospital practitioner in virology at Hôpital Saint-Louis (AP-HP), Université Paris Cité, Inserm UMR 1342, Paris, France. Her primary research interests include clinical metagenomics, viral genomics, and viral infections in immunocompromised patients, with a particular focus on adenoviruses and emerging or unexpected viral infections.

Reference

1. Dimitrov KM, Ramey AM, Qiu X, Bahl J, Afonso CL. Temporal, geographic, and host distribution of avian paramyxovirus 1 (Newcastle disease virus). Infect Genet Evol. 2016;39:22–34. https://doi.org/10.1016/j.meegid.2016.01.008
2. Paz-Bailey G, Adams LE, Deen J, Anderson KB, Katzelnick LC. Dengue. Lancet. 2024;403:667–82. https://doi.org/10.1016/S0140-6736(23)02576-X
3. Thomazelli LM, Sinhorini JA, Oliveira DBL, Knöbl T, Bosqueiro TCM, Sano E, et al. An outbreak in pigeons caused by the subgenotype VI.2.1.2 of Newcastle disease virus in Brazil. Viruses. 2021;13:2446. https://doi.org/10.3390/v13122446
4. Yu X, Luo Y, Wang J, Shu B, Jiang W, Liu S, et al. A molecular, epidemiological, and pathogenicity analysis of pigeon paramyxovirus type 1 viruses isolated from live bird markets in China in 2014–2021. Virus Res. 2022;318:198846. https://doi.org/10.1016/j.virusres.2022.198846
5. Ross CS, Sutton D, Skinner P, Mahmood S, Wynne F, Londt B, et al. Comparative pathogenesis of two genotype VI.2 avian paramyxovirus type-1 viruses (APMV-1) in pheasants, partridges and chickens. Avian Pathol. 2023;52:36–50. https://doi.org/10.1080/03079457.2022.2133680
6. Al-Mubarak AIA, Al-Kubati AAG, Sheikh A, Abdelaziz AM, Hussen J, Kandeel M, et al. Detection of avian orthoavulavirus-1 genotypes VI.2.1 and VII.1.1 with

neuro-viscerotropic tropism in some backyard pigeons (Columbidae) in eastern Saudi Arabia. Front Vet Sci. 2024;11:1352636. https://doi.org/10.3389/fvets.2024.1352636
7. Capua I, Alexander DJ. Human health implications of avian influenza viruses and paramyxoviruses. Eur J Clin Microbiol Infect Dis. 2004;23:1–6. https://doi.org/10.1007/s10096-003-1059-3
8. Hurley S, Eden JS, Bingham J, Rodriguez M, Neave MJ, Johnson A, et al. Fatal human neurologic infection caused by pigeon avian paramyxovirus-1, Australia. Emerg Infect Dis. 2023;29:2482–7. https://doi.org/10.3201/eid2912.230250
9. Winter S, Lechapt E, Gricourt G, N'debi M, Boddaert N, Moshous D, et al. Fatal encephalitis caused by Newcastle disease virus in a child. Acta Neuropathol. 2021;142:605–8. https://doi.org/10.1007/s00401-021-02344-w
10. Kuiken T, Breitbart M, Beer M, Grund C, Höper D, van den Hoogen B, et al. Zoonotic infection with pigeon paramyxovirus type 1 linked to fatal pneumonia. J Infect Dis. 2018;218:1037–44. https://doi.org/10.1093/infdis/jiy036
11. Kim SH, Subbiah M, Samuel AS, Collins PL, Samal SK. Roles of the fusion and hemagglutinin-neuraminidase proteins in replication, tropism, and pathogenicity of avian paramyxoviruses. J Virol. 2011;85:8582–96. https://doi.org/10.1128/JVI.00652-11
12. Zou X, Suo L, Wang Y, Cao H, Mu S, Wu C, et al. Concurrent pigeon paramyxovirus-1 and *Acinetobacter baumannii* infection in a fatal case of pneumonia. Emerg Microbes Infect. 2022;11:968–77. https://doi.org/10.1080/22221751.2022.2054366
13. Goebel SJ, Taylor J, Barr BC, Kiehn TE, Castro-Malaspina HR, Hedvat CV, et al. Isolation of avian paramyxovirus 1 from a patient with a lethal case of pneumonia. J Virol. 2007;81:12709–14. https://doi.org/10.1128/JVI.01406-07
14. Cui S, Xiong H, Feng Z, Chu Y, Que C, Qin J, et al. Severe pigeon paramyxovirus 1 infection in a human case with probable post–COVID-19 condition. Emerg Microbes Infect. 2023;12:2251600. https://doi.org/10.1080/22221751.2023.2251600
15. Veyrenche N, Boluda S, Pérot P, Malissin I, Leruez-Ville M, Jamet A, et al. One Health investigation into fatal encephalitis caused by pigeon paramyxovirus type 1, France. Emerg Infect Dis. 2026;32:753. https://doi.org/10.3201/eid3205.251576

Address for correspondence: Marie Jaspard, Infectious Disease Department, Hôpital Saint-Antoine, APHP, 184 rue du Faubourg Saint-Antoine 75012, Paris, France; email: Marie.jaspard@aphp.fr

Characteristics and Superspreading Potential of Andes Virus Person-to-Person Transmission

Zihao Guo,[1] Kailun Pan,[1] Yu Zhao, Sheikh Taslim Ali, Kai Wang, Lirong Cao, Zhuang Cui, Shengqiang Liu, Ka Chun Chong, Daihai He, Shi Zhao, Yuantao Hao[2]

By using historical contact tracing data, we estimated that 23.4% of case-patients caused 80% of Andes virus (ANDV) person-to-person transmission. We demonstrated a low but nonnegligible probability of observing a large-scale ANDV infection outbreak in a rodent-free setting consisting of close contacts, despite the historically self-limited person-to-person transmission of ANDV.

Hantaviruses are rodentborne zoonotic enveloped RNA viruses belonging to the family Hantaviridae (*1*). The genus *Orthohantavirus*, which belongs to the subfamily Mammantavirinae, is the only genus in Hantaviridae that can cause disease in humans (*1*). Infections in humans occur mainly through inhalation of aerosolized excreta from infected rodents, which can lead to hantavirus pulmonary syndrome, a severe respiratory disease with a case-fatality rate of up to 50% in the Americas, depending on the infecting hantavirus type (*2*). Although uncommon, person-to-person transmission of Andes virus (ANDV), a member of the genus *Orthohantavirus*, has been documented in South America in recent decades, typically in high-intensity close-contact settings, such as households and social gatherings (*3*–*9*).

On May 2, 2026, an ANDV outbreak aboard the MV Hondius cruise ship was reported to the World Health Organization (WHO), with the first case illness onset on April 3 (*10*). Subsequent epidemiologic investigations proposed a working hypothesis that person-to-person transmission originated from a seed case in a person who probably acquired infection through environmental exposure during travel in Argentina before boarding the ship on April 1 (*10*). By July 2, a total of 13 ANDV cases had been identified, including 12 laboratory-confirmed and 1 probable case; 3 of those cases were fatal (*10*). According to the initial WHO notification for the outbreak on May 2, public health and control measures, including contact tracing, case isolation, clinical care, and medical evacuation of symptomatic passengers, had been implemented onboard the ship (*11*). By using historical contact tracing data, we aimed to estimate key epidemiologic characteristics of person-to-person transmission of ANDV, including the serial interval (SI) distribution and transmission heterogeneity, given that those traits strongly shape outbreak size.

The Study

We conducted a literature review of historical ANDV outbreak investigations and extracted contact tracing data from ANDV case clusters that involved person-to-person transmission events. We only included studies conducted in Argentina, given that the seed case-patient of the 2026 outbreak was most likely infected there, according to the WHO report (*10*). We identified 5 eligible studies that provided detailed contact histories and viral genetic evidence strongly supporting person-to-person transmission and linking

Author affiliations: Tianjin Medical University School of Public Health, Tianjin, China (Z. Guo, K. Pan, Z. Cui, S. Zhao); The Chinese University of Hong Kong JC School of Public Health and Primary Care, Hong Kong, China (Z. Guo, L. Cao, K.C. Chong); Ningxia Medical University School of Public Health, Yinchuan, China (Y. Zhao); The University of Hong Kong, Hong Kong (S.T. Ali); Xinjiang Medical University Department of Medical Engineering and Technology, Urumqi, China (K. Wang); Tiangong University School of Mathematical Sciences, Tianjin (S. Liu); The Hong Kong Polytechnic University Department of Applied Mathematics, Hong Kong (D. He); Peking University Center for Public Health and Epidemic Preparedness and Response, Beijing, China (Y. Hao); Peking University School of Public Health, Beijing (Y. Hao); Peking University Ministry of Education Key Laboratory of Epidemiology of Major Diseases, Beijing (Y. Hao)

DOI: https://doi.org/10.3201/eid3210.260908

[1]These authors contributed equally to this article.

[2]Senior author.

infections to specific viral lineages or strains (*3*–*7*). We extracted symptom onset dates to calculate the SI and compiled case-cluster sizes to estimate the effective reproduction number (R_t) and transmission heterogeneity measured by a dispersion parameter (k) (*12*). In case-clusters, we considered terminal cases and sporadic cases attributed to environmental exposure but with no documented human contact as generating no secondary infections.

We used a Bayesian hierarchical model to estimate the epidemiologic parameters while accounting for random effects attributable to epidemiologic differences among ANDV lineages or strains during different epidemic periods. We further conducted a branching process simulation study to assess the transmission potential of the current outbreak on the MV Hondius cruise ship on the basis of the pooled estimates of epidemiologic parameters, considering a plausible range of the initial R_t for ANDV (Appendix, https://wwwnc.cdc.gov/EID/article/32/10/26-0908-App1.pdf).

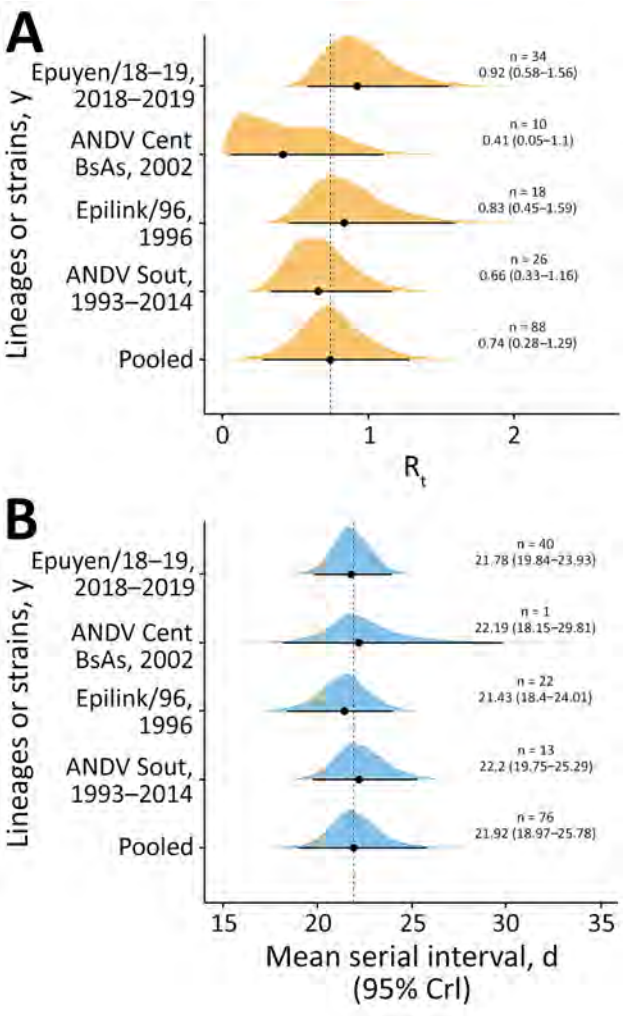

Figure 1. Transmission characteristics from a study of superspreading potential of ANDV person-to-person transmission. A) Pooled R_t estimated from historical interhuman transmission events, incorporating random effects from different ANDV lineages or strains reported in outbreaks that occurred in previous years. B) Pooled mean serial intervals across different ANDV lineages or strains. Values indicate mean (95% CrI). Dots represent mean estimates; whiskers indicate 95% CrIs. ANDV, Andes virus; CrI, credible interval; R_t, effective reproduction number.

We identified a total of 88 case-clusters from the included studies, among which 50 (56.8%) were not associated with any secondary person-to-person transmission events. After accounting for variations across lineages or strains, the pooled estimate of R_t was 0.74 (95% credible interval [CrI] 0.28–1.29) and the estimate of k was 0.64 (95% CrI 0.36–1.16). Apart from inherent differences among ANDV lineages or strains, the substantial variation in R_t across lineages or strains could also be attributed to differences in study settings and individual-level heterogeneity in reproduction numbers (*5*). We estimated that 23.4% (95% CrI 15.1%–30.3%) of the cases generated 80% of the transmission events, suggesting the person-to-person spread of ANDV exhibited relatively high heterogeneity, although it appeared lower than that observed for other pathogens known for superspreading events, including SARS-CoV, SARS-CoV-2, Middle East respiratory syndrome coronavirus, and Ebola virus (*13*,*14*).

Among 38 case-clusters that involved secondary transmissions, we identified 76 primary–secondary transmission pairs with available symptom onset dates, which enabled us to calculate the SI. We estimated a pooled mean SI of 21.92 (95% CrI 18.97–25.78) days and an SD of 6.98 (95% CrI 5.80–8.66) days. Although we observed little variation in the SI distributions across lineages or strains, our estimates are conditional on reported case-clusters and might not represent the full population-level distribution of ANDV infections. That condition is particularly relevant given that only 1 transmission pair was identified for the ANDV Cent BsAs lineage (Figure 1).

Assuming the initial reproduction number of the current ANDV outbreak lies within the 0.4–2.5 range (*3*) (Appendix Figure 1), together with the pooled SI and k estimates from historical data, we simulated plausible outbreak trajectories under a stochastic branching process framework. On the basis of the assumption that effective control measures were implemented after the WHO notification dated May 2, 2026 (*11*), we assumed the R_t decreased from that date onward (Appendix). Within 10 weeks after symptom onset of the seed case, 95% of the simulation results

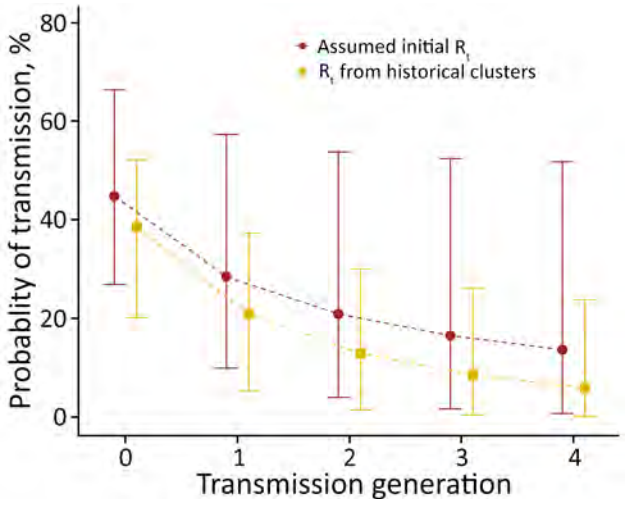

Figure 3. Probability of onward transmission from a study of characteristics and superspreading potential of Andes virus person-to-person transmission. Graph shows probability of onward transmission after a given number of transmission generations, estimated by using the assumed plausible initial R_t for the cruise ship cluster, the pooled R_t, and the pooled dispersion parameter (k) estimates from historical clusters. Dots and squares represent mean estimates; whiskers indicate 95% credible intervals. R_t, effective reproduction number.

produced <15 cumulative cases of ANDV infection (Figure 2). We estimated the probability of sustained transmission after 1 generation of spread to be 20.9% (95% CrI 5.3%–37.4%) for historical ANDV infection clusters and 28.6% (95% CrI 10.0%–57.4%) using the assumed initial reproduction numbers of the ANDV infection outbreak on the cruise ship (Figure 3). In sensitivity analyses, excluding sporadic cases from historical clusters yielded results similar to those of the main analysis (Appendix Figure 2). The absence or delayed implementation of control measures would increase the likelihood of a large-scale outbreak, under the assumption that such measures effectively reduce the reproduction number (Appendix Figure 3).

Because only 8 cases occurred within approximately 1 mean SI after the putative seed case-patient's symptom onset (18–25 days) before the initial WHO notification on May 2, 2026, conventional methods cannot reliably estimate the initial reproduction number without support of contact tracing data. Nonetheless, we used a branching process simulation model with transparent assumptions to illustrate plausible epidemic trajectories for the ANDV outbreak. We noted that person-to-person transmission of ANDV in the general community might be close to the situations of historical ANDV outbreaks, where we observed mostly self-limited risks. Timely and accurate identification of ANDV infection is critical yet challenging because of the nonspecific nature of early symptoms, which necessitates systematic risk assessment for symptomatic persons and their contacts.

A key limitation of this study was its reliance on self-reported contact histories and symptom onset dates derived from publicly available data sources. Potential misclassification of epidemiologic links attributable to unreported co-exposures to rodents, underdetection of subclinical or asymptomatic infections caused by terminal cases, and recall bias in symptom onset might have affected the parameter estimates (*15*). Of note, no clear evidence supporting transmission from asymptomatic or presymptomatic case-patients currently exists. In the simulation study, we anchored control measures to the symptom onset date of the seed case-patient, thereby overlooking the biological delay imposed by the incubation period.

Conclusions

In summary, our results provide insights into the person-to-person transmission potential of ANDV, which exhibited substantial heterogeneity. We found a low but significant chance of observing a relatively large-scale ANDV outbreak in a rodent-

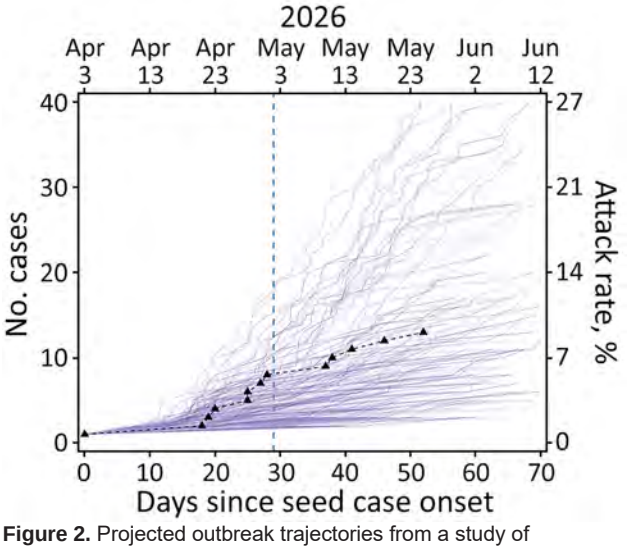

Figure 2. Projected outbreak trajectories from a study of characteristics and superspreading potential of Andes virus person-to-person transmission. Graph shows 1,000 branching process simulations within 10 weeks after symptom onset of the seed case (April 3, 2026), using a plausible range of the initial reproduction number (0.4–2.5) of the MV Hondius cruise ship cluster and pooled dispersion parameter (k) estimates from historical data. Symptom onset dates for secondary cases were randomly sampled from the pooled serial interval distribution. Black triangles indicate the cumulative number of cases observed in the cruise ship outbreak as of May 27, 2026. The blue dashed vertical line marks the initial World Health Organization notification date of the outbreak (May 2, 2026), after which effective control measures were assumed to have been implemented (i.e., the reproduction number was assumed to decrease). The right y-axis shows the corresponding attack rate based on a ship population of 147.

free setting consisting of close contacts, which might be eradicated across a few generations of person-to-person transmission. Because no vaccine or antiviral treatment for ANDV infection is currently available, continuous surveillance of person-to-person transmission risk of ANDV is essential for preparedness against future outbreaks.

Acknowledgments

The authors thank the KC Wong Education Foundation for its support.

This study was supported by the Prevention and Control of Emerging and Major Infectious Diseases National Science and Technology Major Project (grant no. 2025ZD01900802), the Health and Medical Research Fund from the Government of Hong Kong, China (grant no. 22210672), the National Natural Science Foundation of China (grant nos. 12461101 and 12401648), the China Association for Science and Technology's Young Elite Scientists Sponsorship Program (grant no. 2024QNRC001), and the start-up funding of Tianjin Medical University.

S.Z., Z.G., and K.C.C. conceived the study. Z.G., S.Z., and K.P. collected the data, conducted the analysis, and wrote the original draft. All authors critically reviewed and revised the manuscript and approved the final manuscript.

About the Author

Dr. Guo is an associate professor in the School of Public Health, Tianjin Medical University, Tianjin, China. His primary research interests include epidemiology and transmission dynamics of emerging infectious diseases.

References

1. International Committee on Taxonomy of Viruses. Genus: Orthohantavirus. 2026 [cited 2026 Jul 8]. https://ictv.global/report/chapter/hantaviridae/hantaviridae/mammantavirinae/orthohantavirus
2. Jonsson CB, Figueiredo LTM, Vapalahti O. A global perspective on hantavirus ecology, epidemiology, and disease. Clin Microbiol Rev. 2010;23:412–41. https://doi.org/10.1128/CMR.00062-09
3. Martinez VP, Bellomo C, San Juan J, Pinna D, Forlenza R, Elder M, et al. Person-to-person transmission of Andes virus. Emerg Infect Dis. 2005;11:1848–53. https://doi.org/10.3201/eid1112.050501
4. Lázaro ME, Cantoni GE, Calanni LM, Resa AJ, Herrero ER, Iacono MA, et al. Clusters of hantavirus infection, southern Argentina. Emerg Infect Dis. 2007;13:104–10. https://doi.org/10.3201/eid1301.060404
5. Martínez VP, Di Paola N, Alonso DO, Pérez-Sautu U, Bellomo CM, Iglesias AA, et al. "Super-spreaders" and person-to-person transmission of Andes virus in Argentina. N Engl J Med. 2020;383:2230–41. https://doi.org/10.1056/NEJMoa2009040
6. Alonso DO, Pérez-Sautu U, Bellomo CM, Prieto K, Iglesias A, Coelho R, et al. Person-to-person transmission of Andes virus in hantavirus pulmonary syndrome, Argentina, 2014. Emerg Infect Dis. 2020;26:756–9. https://doi.org/10.3201/eid2604.190799
7. Wells RM, Sosa Estani S, Yadon ZE, Enria D, Padula P, Pini N, et al.; Hantavirus Pulmonary Syndrome Study Group for Patagonia. An unusual hantavirus outbreak in southern Argentina: person-to-person transmission? Emerg Infect Dis. 1997;3:171–4. https://doi.org/10.3201/eid0302.970210
8. Martinez-Valdebenito C, Calvo M, Vial C, Mansilla R, Marco C, Palma RE, et al. Person-to-person household and nosocomial transmission of Andes hantavirus, southern Chile, 2011. Emerg Infect Dis. 2014;20:1629–36. https://doi.org/10.3201/eid2010.140353
9. Ferres M, Vial P, Marco C, Yanez L, Godoy P, Castillo C, et al.; Andes Virus Household Contacts Study Group. Prospective evaluation of household contacts of persons with hantavirus cardiopulmonary syndrome in Chile. J Infect Dis. 2007;195:1563–71. https://doi.org/10.1086/516786
10. World Health Organization. Hantavirus outbreak linked to cruise ship travel, multi-locations. 2026 Jul 2 [cited 2026 Jul 8]. https://www.who.int/emergencies/disease-outbreak-news/item/2026-DON611
11. World Health Organization. Hantavirus cluster linked to cruise ship travel, multi-country. 2026 May 4 [cited 2026 Jul 8]. https://www.who.int/emergencies/disease-outbreak-news/item/2026-DON599
12. Lloyd-Smith JO, Schreiber SJ, Kopp PE, Getz WM. Superspreading and the effect of individual variation on disease emergence. Nature. 2005;438:355–9. https://doi.org/10.1038/nature04153
13. Wang J, Chen X, Guo Z, Zhao S, Huang Z, Zhuang Z, et al. Superspreading and heterogeneity in transmission of SARS, MERS, and COVID-19: a systematic review. Comput Struct Biotechnol J. 2021;19:5039–46. https://doi.org/10.1016/j.csbj.2021.08.045
14. Althaus CL. Ebola superspreading. Lancet Infect Dis. 2015;15:507–8. https://doi.org/10.1016/S1473-3099(15)70135-0
15. Toledo J, Haby MM, Reveiz L, Sosa Leon L, Angerami R, Aldighieri S. Evidence for human-to-human transmission of hantavirus: a systematic review. J Infect Dis. 2022;226:1362–71. https://doi.org/10.1093/infdis/jiab461

Address for correspondence: Shi Zhao or Zihao Guo, School of Public Health, Tianjin Medical University, No. 22 Qi Xiang Tai Rd, He Ping District, Tianjin, 300070, China; email: zhaoshi.cmsa@gmail.com or zihaoguo@tmu.edu.cn

Monkeypox Virus in Healthcare Settings, Sierra Leone, June 2025

Michaella Jaba, Emmanuel Saidu, Emmanuel S. Kamanda, Christina Frederick, Laurens Liesenborghs, Megan Halbrook, Nicole A. Hoff, Placide Mbala-Kingebeni, Isaac I. Bogoch, Souradet Y. Shaw, Anne W. Rimoin,[1] Jia B. Kangbai,[1] Jason Kindrachuk[1]

During the 2025 mpox outbreak in Sierra Leone, we assessed environmental contamination in 2 hospitals. Of 89 surfaces sampled, 6 (6.7%) surface samples, primarily from doors, were PCR-positive for monkeypox virus. Our findings highlight monkeypox virus surface contamination in healthcare settings and help prioritize infection prevention and control targets in resource-limited settings.

Mpox, caused by monkeypox virus (MPXV), is a zoonotic disease historically endemic to Central and West Africa (*1*). Since 2022, the global spread of MPXV clade IIb has altered transmission dynamics, and reports of sustained human-to-human transmission have increased (*2*,*3*). Environmental contamination by MPXV has been identified, including recovery of infectious virus particles in healthcare facilities where infection prevention and control (IPC) resources might be limited (*4*,*5*). Beginning in January 2025, Sierra Leone experienced a substantial mpox outbreak, representing one of the country's largest recorded clusters, which strained public health resources. Data on environmental contamination in healthcare settings in Africa during active mpox outbreaks remain scarce. We conducted surface sampling in 2 major urban hospitals in Sierra Leone to assess the presence of MPXV and identify high-risk contamination sites to inform local IPC strategies.

Author Affiliations: University of Manitoba, Winnipeg, Manitoba, Canada (M. Jaba, C. Frederick, S.Y. Shaw, J. Kindrachuk); Njala University, Bo, Sierra Leone (E. Saidu, E.S. Kamanda, J.B. Kangbai); Institute of Tropical Medicine, Antwerp, Belgium (L. Liesenborghs); KU Leuven, Leuven, Belgium (L. Liesenborghs); University of California, Los Angeles, California, USA (M. Halbrook, N.A. Hoff, A.W. Rimoin); National Institute for Biomedical Research, Kinshasa, Democratic Republic of the Congo (P. Mbala-Kingebeni); Toronto General Hospital, University Health Network, Toronto, Ontario, Canada (I.I. Bogoch); Public Health Agency of Canada, Ottawa, Ontario, Canada (J. Kindrachuk)

DOI: https://doi.org/10.3201/eid3210.251697

The Study

The study was conducted in June 2025 at Connaught Hospital in Freetown, the capital and largest city of Sierra Leone, and Bo Government Hospital in Bo, Sierra Leone. Both facilities are referral centers currently managing suspected and confirmed mpox cases during the national mpox outbreak. We sampled 89 high-touch surfaces in clinical and nonclinical areas, including patient beds, door handles, bathroom fixtures such as toilet seats and faucet taps, and nonsingle-use medical equipment such as medical instrument trays and blood pressure cuffs that are supposed to be sterilized after every use. We swabbed each surface for ≈3 minutes by using a polyester-tipped applicator premoistened with viral transport media, by following a standardized protocol (*6*). We standardized surface area swabbing by using a template. Our sampling did not target specific rooms with known mpox patients and was conducted without interfering with routine cleaning schedules, to reflect typical environmental conditions. The study was approved by the Sierra Leone Ethics and Scientific Review Committee (protocol no. 010/05/2025) and the University of Manitoba Health Research Ethics Board.

We extracted DNA by using KingFisher Flex (Thermo Fisher Scientific, https://www.thermofisher.com), a robotic magnetic bead–based system. We performed real-time PCR targeting the MPXV B6R gene by using published primers and probe sequences (*7*). The 40-cycle assay included negative and positive controls. We set thermal cycling conditions to 95°C for 2 minutes, followed by 40 cycles of 95°C for 15 seconds, and 60°C for 1 minute. We established a positive cycle threshold (Ct)

[1]These senior authors contributed equally to this article.

cutoff of <38 on the basis of other environmental MPXV studies (*8*).

Of the 89 surfaces sampled, 6 (6.7%) surface samples were PCR-positive for MPXV. Positivity was 4.0% in Freetown (2 positive of 50 tested) and 10.3% in Bo (4 positive of 39 tested); this difference might reflect variation in IPC practices or frequency of mpox patient contact with sampled surfaces. Ct values for positive samples ranged from 32.34–37.91 (Appendix Table, https://wwwnc.cdc.gov/EID/article/32/10/25-1697-App.pdf), indicating a range of viral load. A total of 28 doors were sampled and accounted for 2 (33.3%) of the 6 positive surfaces. Other positive surfaces included a delivery bed and weighing scale, a medical ward instrument tray, a laboratory, an office bathroom, and an eye clinic table (Appendix Table). The concentration of MPXV DNA on doors and other high-touch points aligns with fomite transmission risks identified in similar investigations (*9*).

Although Ct values are not a direct proxy for infectivity, lower Ct values (<30) might indicate a higher likelihood of viable virus (*8*). The positive Ct values we observed suggest moderate viral DNA load on those surfaces, likely below the threshold for recovering infectious viruses. Other studies report similar findings, in which Ct values ranged from 22–38 on high-touch objects in healthcare and residential settings (*10*,*11*).

Conclusions

We detected MPXV DNA on 6.7% of sampled high-touch surfaces in 2 hospitals in Sierra Leone during the 2025 national mpox outbreak. Doors were the most contaminated surface type, consistent with studies from other settings and highlighting their role as critical fomites requiring targeted disinfection (*10*,*12*). The Ct values observed from positive samples (mostly >32) indicate the presence of MPXV DNA, but do not suggest infectivity. However, we did not perform viability studies. Although culture-based studies suggest a viable virus is less likely at Ct values >30, the detection of the MPXV DNA on high-contact surfaces underscores their potential as a reservoir for transmission in the absence of consistent, low, or proper IPC practices (*13*). Our study suggests that doors and other high-touch surfaces within healthcare clinics assessed are highly susceptible surfaces for MPXV contamination. This could reflect the large number of patients entering and leaving various rooms within the healthcare facility and the low frequency or improper practice of IPC within the hospital.

Limitations of our study include the cross-sectional design and purposive sampling of specific high-touch surfaces, which limits generalizability, and a lack of data on cleaning frequency or direct links to nosocomial transmission events. Furthermore, the epidemiologic context of the 2025 mpox outbreak in Sierra Leone, with high community transmission, likely influenced the background level of environmental contamination within healthcare facilities.

Despite those limitations, detection of MPXV DNA on high-touch surfaces in a resource-constrained setting reinforces the necessity of robust IPC measures and considerations. The 2025 mpox outbreak in Sierra Leone underscores the ongoing threat of mpox in West Africa and the strain on health systems. Strengthened environmental hygiene, focused and frequent disinfection of high-touch surfaces such as doors and bed rails, and adherence to hand hygiene, are necessary to reduce surface contaminations in healthcare settings (*14*). Integrating simple, periodic environmental surveillance into outbreak response might help identify IPC gaps, guide resource allocation, and tailor staff training in similar low-resource settings (*15*).

This manuscript was preprinted at https://doi.org/10.1101/2025.09.16.25335757.

Acknowledgments

The authors acknowledge the staff at the Bo Government and Connaught hospitals for providing access for sample collection in various locations around the hospitals during these challenging times. The authors also acknowledge the support provided by the Molecular Pathogenesis laboratory at the Department of Biological Sciences, Njala University, Njala Campus in Makonde, for all sample processing and analysis.

This work was supported by the Canadian Institutes of Health Research, the International Mpox Research Consortium, and the Department of Defense Threat Reduction Agency.

I.I.B. consults to the Weapons Threat Reduction Program at Global Affairs Canada.

About the Author

Ms. Jaba is an MSc student in the Department of Medical Microbiology & Infectious Diseases, Rady Faculty of Health Sciences, University of Manitoba, Winnipeg, MB, Canada, and is originally from Sierra Leone. Her research interests focus on virologic and epidemiologic characteristics of emerging zoonotic viruses.

References

1. Bunge EM, Hoet B, Chen L, Lienert F, Weidenthaler H, Baer LR, et al. The changing epidemiology of human monkeypox—a potential threat? A systematic review. PLoS Negl Trop Dis. 2022;16:e0010141. https://doi.org/10.1371/journal.pntd.0010141
2. Isidro J, Borges V, Pinto M, Sobral D, Santos JD, Nunes A, et al. Phylogenomic characterization and signs of microevolution in the 2022 multi-country outbreak of monkeypox virus. Nat Med. 2022;28:1569–72. https://doi.org/10.1038/s41591-022-01907-y
3. World Health Organization. WHO Director-General declares the ongoing monkeypox outbreak a public health emergency of international concern [cited 2024 Aug 14]. https://www.who.int/news/item/14-08-2024-who-director-general-declares-mpox-outbreak-a-public-health-emergency-of-international-concern
4. Gould S, Atkinson B, Onianwa O, Spencer A, Furneaux J, Grieves J, et al.; NHS England Airborne High Consequence Infectious Diseases Network. Air and surface sampling for monkeypox virus in a UK hospital: an observational study. Lancet Microbe. 2022;3:e904–11. https://doi.org/10.1016/S2666-5247(22)00257-9
5. Morgan CN, Whitehill F, Doty JB, Schulte J, Matheny A, Stringer J, et al. Environmental persistence of monkeypox virus on surfaces in household of person with travel-associated infection, Dallas, Texas, USA, 2021. Emerg Infect Dis. 2022;28:1982–9. https://doi.org/10.3201/eid2810.221047
6. Centers for Disease Control and Prevention. Surface sampling procedures for *Bacillus anthracis* spores from smooth, non-porous surfaces, 2012 [cited 2025 Jun 25]. https://www.cdc.gov/niosh/topics/emres/surface-sampling-bacillus-anthracis
7. Li Y, Zhao H, Wilkins K, Hughes C, Damon IK. Real-time PCR assays for the specific detection of monkeypox virus West African and Congo Basin strain DNA. J Virol Methods. 2010;169:223–7. https://doi.org/10.1016/j.jviromet.2010.07.012
8. Sukhdeo S, Muller M, McGeer A, Leis JA, Chan A, Gubbay JB, et al. Environmental surface contamination with monkeypox virus in the ambulatory setting in Toronto, Canada. Open Forum Infect Dis. 2022;10:ofac648. https://doi.org/10.1093/ofid/ofac648
9. Pfeiffer JA, Collingwood A, Ryder AM, Kling CE, Grijalva CG, Fitzpatrick NA, et al. High-contact object and surface contamination in a household with monkeypox virus—Utah, USA, June 2022. MMWR Morb Mortal Wkly Rep. 2022;71:1092–4. https://doi.org/10.15585/mmwr.mm7134e1
10. Atkinson B, Burton C, Pottage T, Thompson KA, Ngabo D, Crook A, et al. Infection-competent monkeypox virus contamination identified in domestic settings following an imported case of monkeypox into the UK. Environ Microbiol. 2022;24:4561–9. https://doi.org/10.1111/1462-2920.16129
11. Muller MP, Mishra S, McGeer A, Patel S, Gubbay J, Hasso M, et al. Environmental testing of surfaces in the room of a patient with mpox. Clin Infect Dis. 2023;76:179–81. https://doi.org/10.1093/cid/ciac654
12. Kuehn R, Fox T, Guyatt G, Lutje V, Gould S. Infection prevention and control measures to reduce the transmission of mpox: a systematic review. PLOS Glob Public Health. 2024;4:e0002731. https://doi.org/10.1371/journal.pgph.0002731
13. Peiró-Mestres A, Fuertes I, Camprubí-Ferrer D, Marcos MÁ, Vilella A, Navarro M, et al.; Hospital Clinic de Barcelona Monkeypox Study Group. Frequent detection of monkeypox virus DNA in saliva, semen, and other clinical samples from 12 patients, Barcelona, Spain, May to June 2022. Euro Surveill. 2022;27:2200503. https://doi.org/10.2807/1560-7917.ES.2022.27.28.2200503
14. World Health Organization. Infection prevention and control for monkeypox in health care settings, 2022 [cited 2025 Jun 25]. https://www.who.int/publications/i/item/WHO-MPX-IPC-2022.1
15. Ministry of Health and Sanitation Sierra Leone. Sierra Leone national infection prevention and control guidelines, 2022 [cited 2025 Jun 25]. https://www.afro.who.int/sites/default/files/2022-08/Sierra%20Leone%20National%20Infection%20Prevention%20and%20Control%20Guidelines_2022.pdf

Address for correspondence: Jason Kindrachuk, University of Manitoba, Department of Medical Microbiology and Infectious Diseases, 523-745 Bannatyne Ave, Winnipeg, MB R3E 0J9, Canada; email: jason.kindrachuk@umanitoba.ca

Emergence of Macrolide-Resistant *Bordetella pertussis*, Peru, 2025

Eduardo Juscamayta-López, Faviola Valdivia, Carmen Rodríguez-Cueva, Helen Horna, Yaneth Quispe, María Pía Soto, Segundo Torres, Victor Fiestas Solórzano, Martin Yagui, Vlademir Vicente Cantarelli, Efrain Montilla-Escudero, Víctor Silva, Ana Raquel Da Costa

We report the emergence of macrolide-resistant *Bordetella pertussis* during a pertussis outbreak in Peru. Among 68 cases, 31% carried the A2047G gene mutation, conferring resistance to macrolides. Whole-genome sequencing revealed 2 genetically distinct groups, indicating multiple introductions into Peru. Our findings support strengthening surveillance for macrolide-resistant pertussis to inform control strategies.

The bacterium *Bordetella pertussis* is the causative agent of pertussis, a highly contagious respiratory infection, which poses the greatest risk for severe illness and death in infants (*1*). Despite widespread vaccination, there is a global resurgence of pertussis and a large increase in cases reported after the COVID-19 pandemic (*2*). The pertussis resurgence is likely multifactorial, including declining vaccination coverage, improved diagnostic capacity, waning immunity, and the evolutionary adaptation of *B. pertussis* bacteria (*3*).

Macrolide antimicrobial drugs are the first-line pertussis treatment because of their effectiveness in reducing bacterial carriage and transmission, curtailing the duration of symptoms, and lowering the risk for infant death (*4*). However, macrolide-resistant *B. pertussis* (MRBP), primarily associated with the A2047G mutation in 23S rRNA genes, has emerged globally (*5*). The highest prevalence of MRBP has been reported in China (*6*), whereas reports of MRBP from Latin America remain scarce (*7*).

In 2025, the Peruvian Ministry of Health reported the largest pertussis outbreak in decades in the country. Although precisely defining the onset of the outbreak is challenging, surveillance data suggest that transmission intensified in 2024. National incidence increased from 3.9 cases/1 million inhabitants in 2023 to 7.4 cases/1 million inhabitants in 2024 and reached 57.5 cases/1 million inhabitants by August 2025 (*8*). A cumulative total of 4,976 cases (Appendix Figure, http://wwwnc.cdc.gov/EID/article/32/10/25-1477-App1.pdf) and 76 deaths were recorded by the end of 2025. The effects were concentrated in the Loreto region, which accounted for 3,922 cases and 57 deaths, disproportionately affecting Indigenous communities in Datem del Marañón, where pertussis vaccine coverage remains suboptimal (*9*,*10*).

Peru's national immunization schedule includes 3 primary doses of the pentavalent diphtheria–tetanus–whole cell pertussis–hepatitis B–*Hemophilus influenzae* type b vaccine (DTwP-HepB-Hib) at 2, 4, and 6 months of age, followed by DTwP boosters at 18 months and 4 years of age, and tetanus–diphtheria–acellular pertussis vaccination during pregnancy, recommended at 20–36 weeks of gestation. To determine *B. pertussis* transmission dynamics in Peru, we detected and characterized MRBP from *B. pertussis*–positive swab samples.

The Study

In early 2025, we screened for MRBP in *B. pertussis*–positive nasopharyngeal swab samples from 68 patients (*11*) (median 3 months of age; range 1 month–39 years of age) by using direct PCR (Appendix Table 1) targeting the A2047G mutation in the 23S rRNA genes. We detected the A2047G mutation in 21 (31%) of 68 samples. Patients infected with MRBP were significantly younger (median 3.6 vs 36.1 months of age; p = 0.007) than patients infected with macrolide-susceptible *B. pertussis* strains. However, we observed no significant differences in patient sex or vaccination status between the 2 groups (Appendix Table 2). Most MRBP infections were in infants <6 months of age (62%). Among the 16 patients with available treatment information, 14 (88%) received azithromycin.

Author affiliations: Instituto Nacional de Salud, Lima, Peru (E. Juscamayta-López, F. Valdivia, C. Rodríguez-Cueva, H. Horna, Y. Quispe, M. Pía Soto, S. Torres, V. Fiestas Solórzano, M. Yagui); American Society for Microbiology, Washington DC, USA (V. Vicente Cantarelli, E. Montilla-Escudero, V. Silva, A. Raquel Da Costa).

DOI: https://doi.org/10.3201/eid3210.251477

Table. Characteristics of patients with culture-confirmed *Bordetella pertussis* carrying the macrolide-resistant A2047G mutation in the 23S rRNA gene, Peru, 2025

Sample no.	Year of collection	Age/sex	Region, Province	Vaccine status†	Maternal Tdap‡	Antimicrobial drug treatment	Hospitalized
tf518-24*	2024	9 mo/F	Loreto, Datem del Marañón	2 doses	Unknown	No	Unknown
tf048-25	2025	1.6 y/M	Puno, Melgar	Unknown	No	No	Yes
tf098-25	2025	3 mo/F	Lima, Callao	0	No	Azithromycin	Yes
tf120-25	2025	39.5 y/F	Lima, Callao	Unknown	No	Unknown	Unknown
tf232-25	2025	16 y/M	Cusco, Cusco	1 dose	No	Azithromycin	Unknown
tf303-25	2025	1 mo/F	Arequipa, Arequipa	0	Unknown	Azithromycin, ampicillin, and amikacin	Yes
tf353-25	2025	7 mo/M	Cusco, Cusco	3 doses	Yes	Azithromycin	Unknown

*This isolate, collected in late 2024, was considered part of the early phase of the 2025 outbreak.
†Number of diphtheria–tetanus–whole cell pertussis–hepatitis B–*Hemophilus influenzae* type b vaccine doses received before illness onset.
‡Tdap (tetanus–diphtheria–acellular pertussis) vaccination during pregnancy in the patient's mother.

MRBP cases were distributed across multiple regions, including Lima (n = 11), Cusco (n = 4), Arequipa (n = 3), Ancash (n = 1), Loreto (n = 1), and Puno (n = 1) (Table; Figure 1; Appendix Table 2).

From the 68 *B. pertussis*–positive samples, we obtained 7 culture-positive *B. pertussis* isolates, all of which were MRBP: 6 collected in 2025 and 1 in late 2024 (isolate no. tf518-24). We performed phenotypic susceptibility testing by using established methods (*12*). All 7 isolates were resistant to all antimicrobial drugs tested, with no zones of inhibition for erythromycin or azithromycin.

We performed whole-genome sequencing on all 7 MRBP strains (Appendix). All sequenced isolates were assigned to sequence type 2 (ST2) and clonal complex ST2. Six isolates shared the virulence-associated allelic profile *ptxP3/ptxA1/ptxB1/ptxC4/fhaB1/fim2-1/fim3-1*, whereas 1 isolate (tf098–25) carried the closely related *ptxP29* promoter allele but retained the remaining alleles of this profile. We identified the *prn150* allele in

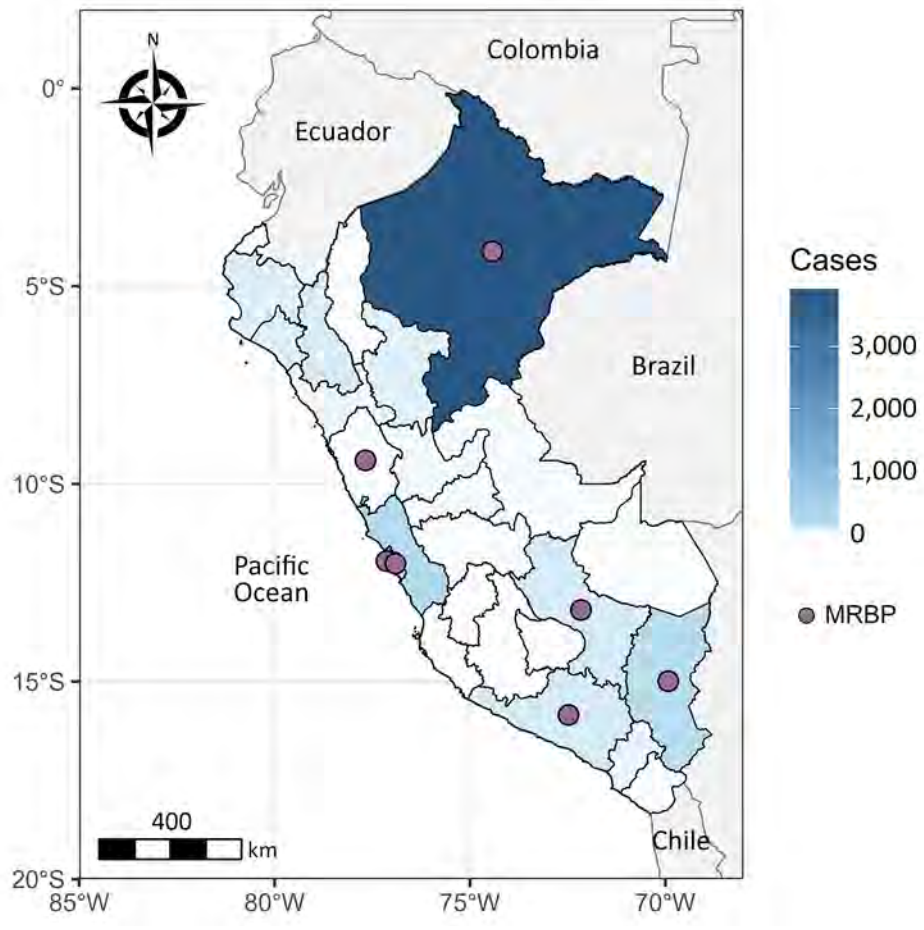

Figure 1. Geographic distribution of confirmed pertussis cases and MRBP cases in Peru, 2025. Regional shading shows cumulative confirmed pertussis cases since epidemiologic week 53 of 2025; darker blue indicates higher case counts. Purple circles indicate regions where patients carrying *B. pertussis* strains with the macrolide resistance–associated A2047G mutation were detected. MRBP, macrolide-resistant *Bordetella pertussis*.

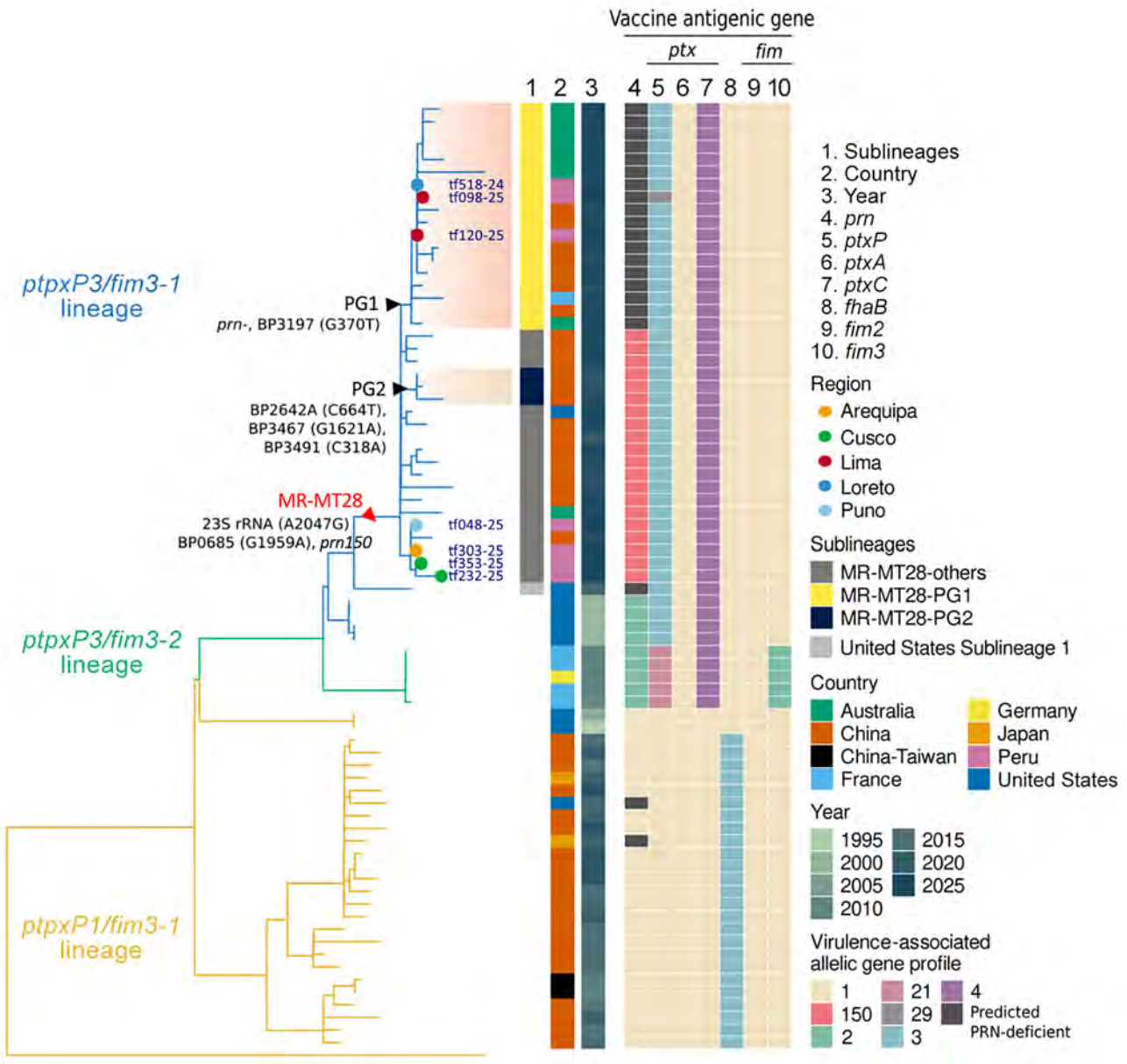

Figure 2. Maximum-likelihood phylogenetic tree of *Bordetella pertussis* isolates on the basis of genome-wide single-nucleotide polymorphism analysis, showing macrolide-resistant isolates from Peru within the emerging MR-MT28 lineage (red text) among globally distributed strains. Tohama I (NC_002929) was used as the reference genome. PRN, pertactin.

all sequenced isolates (Appendix), which is a genetic marker of the emerging MR-MT28 lineage (*8*). We did not identify any inactivating mutations in the *ptx* operon or *fhaB*, but 3 isolates (tf518-24, tf120-25, and tf098-25) had IS481-mediated *prn* disruption, consistent with a pertactin-deficient genotype (Appendix).

Expanded whole-genome single-nucleotide polymorphism phylogenetic analysis incorporating globally representative MRBP genomes placed all isolates from Peru within the recently emerged MR-MT28 lineage. That expanded analysis also detected previously identified genetic markers, including the A2047G mutation, the *prn150* allele, and the *BP0685* G1959A substitution (*8*). The 7 MRBP isolates from Peru did not form a single monophyletic cluster. Three isolates (tf518-24, tf120-25, and tf098-25) clustered within the phylogenetic group 1 (PG1) sublineage and had IS481-mediated *prn* disruption, whereas the remaining 4 isolates clustered with the MR-MT28-other group and retained an intact *prn* coding sequence despite carrying the *prn150* allele (Figure 2; Appendix).

Conclusions

We described the emergence of MRBP during the ongoing 2025 pertussis outbreak in Peru and documented circulation of the emerging MR-MT28 lineage in Latin America. Genomic analyses identified ≥2 genetically distinct MR-MT28 sublineages, including PG1-associated pertactin-deficient isolates, consistent with the ongoing international diversification and dissemination of this lineage.

Consistent with recent global genomic analyses, the close phylogenetic relationship between the 7 isolates from Peru and contemporary MR-MT28 strains is consistent with the ongoing international dissemination and diversification of this lineage (*5*,*13*). The presence of 2 genetically distinct MR-MT28 groups circulating in Peru suggests multiple international introductions of MRBP into Peru, rather than a single transmission event.

Pertactin-deficient isolates have predominantly been reported in countries using acellular pertussis vaccines, where loss of pertactin is considered an adaptive response to vaccine-induced immune pressure (*5*,*13*). Although Peru continues to use a whole-cell pertussis vaccine, 3 PG1 sublineage isolates had IS481-mediated *prn* disruption, suggesting introduction of an established pertactin-deficient MR-MT28 sublineage, rather than independent emergence under local vaccine-driven selection. Of note, 1 of those isolates (tf518-24) was recovered from an infant who received 2 doses of the pentavalent vaccine, indicating that a pertactin-deficient MR-MT28 strain was identified in a partially vaccinated infant.

We found that most patients with MRBP received azithromycin for treatment, which raises concerns about the effectiveness of macrolides as first-line therapy in Peru. Although *B. pertussis* has remained susceptible to sulfamethoxazole/trimethoprim in vitro (*14*) and possibly to other antimicrobial drugs (*15*), clinical evidence supporting alternative regimens is limited, underscoring the need for urgent clinical and epidemiologic studies.

A key limitation of our study is the lack of systematically collected clinical data linked to genomic findings within the current surveillance system, which precludes assessment of differences in disease severity and outcomes between macrolide-resistant and macrolide-susceptible *B. pertussis* infections during this outbreak. Addressing that gap will be critical to define the clinical impact of macrolide resistance and to inform evidence-based treatment strategies in high-prevalence settings.

Our findings underscore the urgent need to strengthen genomic surveillance and diagnostic capacity for *B. pertussis* to enable early detection of resistant strains and inform timely prevention and control strategies. In addition, reassessing empiric treatment recommendations and prioritizing prospective studies to evaluate the clinical effect of macrolide antimicrobial drug resistance will be critical to guide evidence-based public health responses.

Acknowledgments

We thank the American Society for Microbiology for supporting the strengthening of *Bordetella pertussis* antimicrobial resistance surveillance at the Instituto Nacional de Salud, Peru.

The assembled genome sequences generated in this study have been deposited into GenBank (BioProject accession PRJNA1332808; genome accession nos. JBRFKX000000000–JBRFLD000000000 [tf048-25–tf518-24].)

This study was supported in part by the US Centers for Disease Control and Prevention's Antimicrobial Resistance Solutions Initiative through the Global Antimicrobial Resistance Laboratory and Response Network (cooperative agreement no. 6 NU3HCK000011-03-01).

About the Author

Dr. Juscamayta-López is a molecular epidemiologist at the Instituto Nacional de Salud, Peru. His research integrates whole-genome sequencing with phenotypic data to investigate the evolution, transmission, and antimicrobial resistance of respiratory bacterial pathogens.

References

1. World Health Organization. Pertussis vaccines: WHO position paper—September 2015. Wkly Epidemiol Rec. 2015;90:433–58.
2. World Health Organization. Pertussis reported cases and incidence. Geneva: The Organization; 2025 [cited 2025 Sep 21]. https://immunizationdata.who.int/global/wiise-detail-page/pertussis-reported-cases-and-incidence
3. Sheng Y, Ma S, Zhou Q, Xu J. Pertussis resurgence: epidemiological trends, pathogenic mechanisms, and preventive strategies. Front Immunol. 2025;16:1618883. https://doi.org/10.3389/fimmu.2025.1618883
4. Ivaska L, Barkoff AM, Mertsola J, He Q. Macrolide resistance in *Bordetella pertussis*: current situation and future challenges. Antibiotics (Basel). 2022;11:1570. https://doi.org/10.3390/antibiotics11111570
5. Zhang H, Kang Z, Zhang Y, Yang Y, Li H, Wang N, et al. Evolutionary dynamics and global spread of macrolide-resistant *Bordetella pertussis* during the post-pandemic pertussis resurgence. J Infect. 2026;92:106718. https://doi.org/10.1016/j.jinf.2026.106718
6. Feng Y, Chiu CH, Heininger U, Hozbor DF, Tan TQ, von König CW. Emerging macrolide resistance in *Bordetella pertussis* in mainland China: findings and warning from the global pertussis initiative. Lancet Reg Health West Pac. 2021;8:100098. https://doi.org/10.1016/j.lanwpc.2021.100098

7. Bolstering pertussis surveillance in Latin America. Washington: American Society for Microbiology; 2024 [cited 2025 Sep 21]. https://asm.org/articles/2024/november/bolstering-pertussis-surveillance-in-latin-america
8. Celis-Salinas JC, Ramírez-García EA, Fiestas Solórzano VE, Casapía-Morales M. Twenty-five years of pertussis outbreaks in the Peruvian Amazon: a call to strengthen equity in vaccination and control. Lancet Reg Health Am. 2025;51:101255. https://doi.org/10.1016/j.lana.2025.101255
9. Health Situation Room of Peru. EW 37—2025. Lima: CDC MINSA; 2025 [cited 2025 Jul 3]. https://www.dge.gob.pe/portalnuevo/sala-de-situacion.
10. Immunization Information Dashboard. Peru 2018–2025. Lima: MINSA [cited 2025 Jul 3]. https://www.minsa.gob.pe/reunis
11. Tatti KM, Sparks KN, Boney KO, Tondella ML. Novel multitarget real-time PCR assay for rapid detection of *Bordetella* species in clinical specimens. J Clin Microbiol. 2011;49:4059–66. https://doi.org/10.1128/JCM.00601-11
12. Hill BC, Baker CN, Tenover FC. A simplified method for testing *Bordetella pertussis* for resistance to erythromycin and other antimicrobial agents. J Clin Microbiol. 2000;38:1151–5. https://doi.org/10.1128/JCM.38.3.1151-1155.2000
13. Fu P, Yan G, Li Y, Xie L, Ke Y, Qiu S, et al. Pertussis upsurge, age shift and vaccine escape post-COVID-19 caused by ptxP3 macrolide-resistant *Bordetella pertussis* MT28 clone in China. Clin Microbiol Infect. 2024;30:1439–46. https://doi.org/10.1016/j.cmi.2024.08.016
14. Hu Y, Zhai X, Yuan L, Du Q, Yao K. Phenotypic diversity of *Bordetella pertussis* against trimethoprim/sulphamethoxazole in vitro tests. Diagn Microbiol Infect Dis. 2025;111:116597. https://doi.org/10.1016/j.diagmicrobio.2024.116597
15. Hua CZ, Wang HJ, Zhang Z, Tao XF, Li JP, Mi YM, et al. In vitro activity and clinical efficacy of macrolides, cefoperazone-sulbactam and piperacillin/piperacillin-tazobactam against *Bordetella pertussis* and the clinical manifestations in pertussis patients due to these isolates: a single-centre study in Zhejiang Province, China. J Glob Antimicrob Resist. 2019;18:47–51. https://doi.org/10.1016/j.jgar.2019.01.029

Address for correspondence: Eduardo Juscamayta-López, Instituto Nacional de Salud, Jiron Capac Yupanqui 1400, Jesus Maria, Lima, Lima 11, Peru; email: jjuscamamayta@ins.gob.pe

Detection of Divergent Highly Pathogenic Avian Influenza A(H5N1) Clade 2.3.4.4b Virus, São Paulo, Brazil, 2025

Jansen de Araujo, Luciano M. Thomazelli, Thomas P. Fabrizio, Gustavo O. Fenner, Erick G. Dorlass, Ana K.A. Eisen, Viviane F. Botosso, Marcello S. Nardi, Caroline C. Aires, Sergio M.N. Teixeira, Roberta M. de Azevedo, Mayra H. Frediani, Tatiana Ometto, Mário G.L. Barboza, Edmarcia E. de Souza, Carsten Wrenger, Richard J. Webby, Edison L. Durigon

In 2025, we detected highly pathogenic avian influenza H5N1 virus in dead waterfowl at Ibirapuera Park, São Paulo, Brazil. Genomic characterization indicated a reassortant virus that emerged from locally circulating low pathogenicity avian influenza viruses and highly pathogenic North American lineages. Our results highlight cross-species transmission risk and underscore the need for enhanced surveillance.

Avian influenza virus (AIV) surveillance in South America has been limited compared with other regions. Until 2022, only 1 highly pathogenic avian influenza (HPAI) virus outbreak was reported in South America, a 2002 H7N3 event in Chile, which emerged locally (*1*). Most viruses detected before 2022 were low pathogenicity avian influenza viruses (LPAIVs) that were phylogenetically distant from North American and Eurasian strains. The emergence of influenza A(H5N1) clade 2.3.4.4b virus in Eurasia marked a major evolutionary shift. The introduction of the HPAI H5N1 virus into the Americas in 2021 by migratory birds led to extensive reassortment with locally circulating LPAIVs (*2*), generating new genotypes that spread across the continent. By late 2022, the H5N1 virus reached South America, causing high mortality rates among seabirds and marine mammals (*3*,*4*). In 2023, H5N1 viruses were detected in wild birds and backyard chickens in Brazil (*3*). By 2025, new reassortant H5N1 variants had been reported in South America, including in Brazil (*5*).

Beyond the emergence of novel genotypes, the continued expansion of HPAI viruses has been driven by broad host-range expansion and frequent interactions at the human–animal-environment interface. Those ecologic dynamics make mitigating the effects of HPAI viruses on wildlife, ecosystems, domestic animals, food security, and humans difficult (*6*). We report detection of a divergent HPAI H5N1 strain in 2 white-faced whistling ducks (*Dendrocygna viduata*) after reports of unusual avian deaths in Ibirapuera Central Park, São Paulo, Brazil.

The Study

In June 2025, we collected cloacal and tracheal swab samples from 2 dead white-faced whistling ducks (Appendix Figure 1, http://wwwnc.cdc.gov/EID/article/32/10/26-0723-App1.pdf) near the lake in Ibirapuera Park, São Paulo, Brazil (Figure 1). We detected AIV and H5N1 from the swab samples by using reverse transcription real-time PCR. We generated complete genome sequences (GenBank accession nos. PX062323–PX062330) (Appendix Table 1) directly from the original swab samples by using the Ion Torrent S5 Platform (Thermo Fisher Scientific,

Author affiliations: University of São Paulo, São Paulo, Brazil (J. de Araujo, L.M. Thomazelli, G.O. Fenner, E.G. Dorlass, A.K.A. Eisen, M.G.L. Barboza, E.E. de Souza, C. Wrenger, E.L. Durigon); St. Jude Children's Research Hospital, Memphis, Tennessee, USA (T.P. Fabrizio, R.J. Webby); Hospital Israelita Albert Einstein, São Paulo (E.G. Dorlass); Instituto Butantan, São Paulo (V.F. Botosso); Centro de Manejo e Conservação de Animais Silvestres, São Paulo (M.S. Nardi, C.C. Aires, S.M.N. Teixeira, R.M. de Azevedo, M.H. Frediani); Centro Nacional de Pesquisa em Energia e Materiais, Campinas, Brazil (T. Ometto); Institut Pasteur de São Paulo, São Paulo (C. Wrenger, E.L. Durigon).

DOI: https://doi.org/10.3201/eid3210.260723

Figure 1. Location of Ibirapuera Central Park where waterfowl were found dead from divergent highly pathogenic avian influenza A(H5N1) clade 2.3.4.4b virus, São Paulo, Brazil, 2025. Map shows location in South America. Satellite image of park shows red outline of Ibirapuera Central Park, São Paulo, Brazil; red dots indicate the location where the 2 birds were found dead. Satellite image is from the catalog of images of the National Institute for Space Research (http://www.dgi.inpe.br/catalogo).

https://www.thermofisher.com). We classified genotypes by using GenoFlu (https://github.com/USDA-VS/GenoFLU). The hemagglutinin (HA), neuraminidase, polymerase acidic, and matrix protein (MP) segments were classified as Eurasian lineages, whereas the nonstructural protein segment was classified as a North American lineage. The remaining internal genes (polymerase basic 1, polymerase basic 2, and nucleoprotein) were unassigned (Appendix Tables 2, 3). We resolved the origins of the unassigned

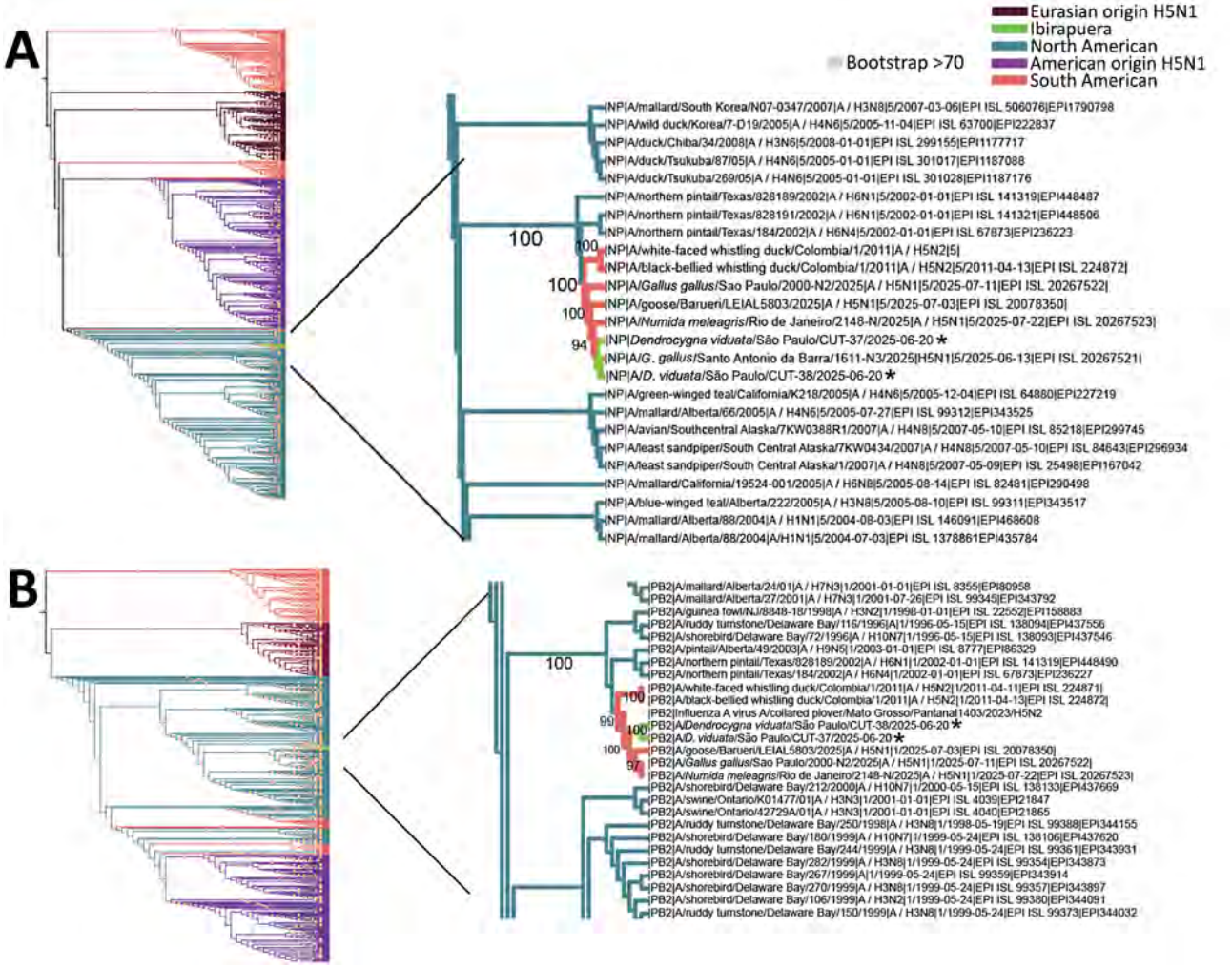

Figure 2. Maximum-likelihood phylogenies of NP and PB2 internal genes from divergent highly pathogenic avian influenza A(H5N1) clade 2.3.4.4b virus, São Paulo, Brazil, 2025. A) Alignment of NP internal gene sequences. B) Alignment of PB2 internal gene sequences. Asterisks (*) indicate sequences generated in this study. Numbers at major nodes indicate percent bootstrap values based on 1,000 replications. NP, nucleoprotein; PB2, polymerase basic 2.

segments by using BLASTn and maximum likelihood (ML) analysis. The polymerase basic 2 and nucleoprotein sequences shared >94% nucleotide identity and clustered tightly with lineages from Colombia and the Brazilian Pantanal (*7*,*8*) (Figure 2). That topologic incongruence demonstrates reassortment with regional LPAIV gene pools.

Our phylogenetic analysis showed that the polymerase acidic and MP segments remain conserved within the Eurasian lineage, clustering with the clade 2.3.4.4b backbone, characteristic of the current panzootic (Appendix Figure 2). However, the nonstructural gene (North America lineage) clustered with AIVs established during the initial introduction of H5N1 viruses into the Americas (*2*) (Appendix Figure 3). Our genetic analyses of the HA gene sequences showed 97.9% nucleotide identity with the 2023 reference isolate from Brazil (GenBank accession no. OR269887.1) (*6*), and >98.6% nucleotide identity with recent North American strains (Appendix Table 3), suggesting a divergence from the original lineage established in Brazil. The maximum likelihood phylogenies we generated of the HA and neuraminidase genes also showed the sequence divergence (Figure 3; Appendix Figure 4). The isolates we sequenced form a monophyletic cluster among North American lineages (2022–2025) (*9*), suggesting a second introduction of the HPAI H5N1 virus in South America (*10*,*11*).

We defined the timeline for the second introduction of the HPAI H5N1 virus into South America by using Bayesian temporal analysis. The estimated time to the most recent common ancestor (tMRCA) with North American H5 virus lineages was ≈mid-2023 (mean tMRCA May 2023; 95% highest posterior density March 2023–July 2023) (Figure 4). Our tMRCA estimates provide temporal support for the second H5N1 virus introduction from North America and subsequent circulation until it was detected in Ibirapuera Central Park.

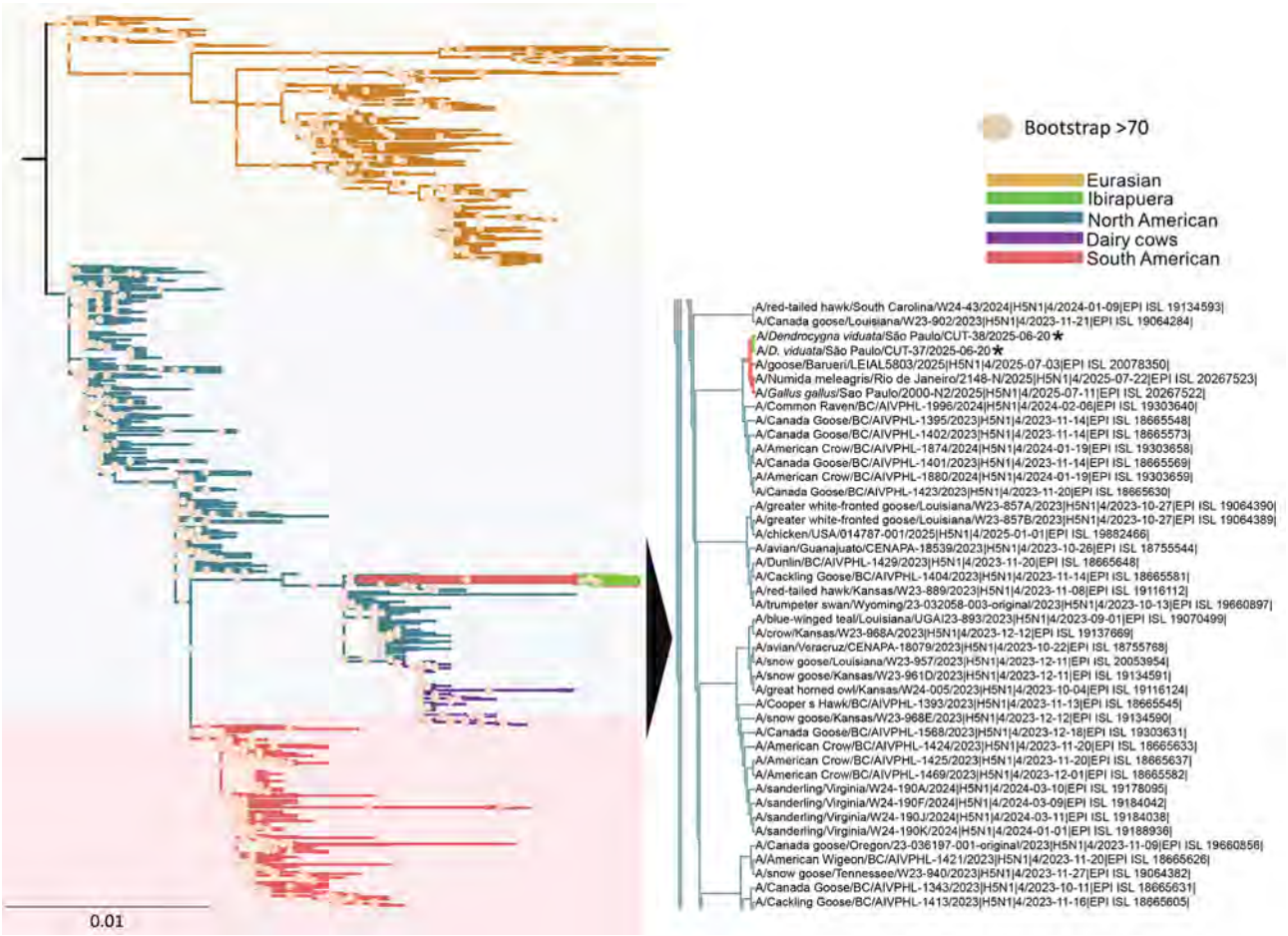

Figure 3. Phylogenetic tree of hemagglutinin gene from divergent highly pathogenic avian influenza A(H5N1) clade 2.3.4.4b virus, São Paulo, Brazil, 2025. Maximum-likelihood phylogenetic tree (left) showing alignment of global hemagglutinin gene sequences. Inset (right) shows closest related hemagglutinin gene sequences to those from this study denoted by asterisks (*). Scale bar indicates nucleotide substitutions per site.

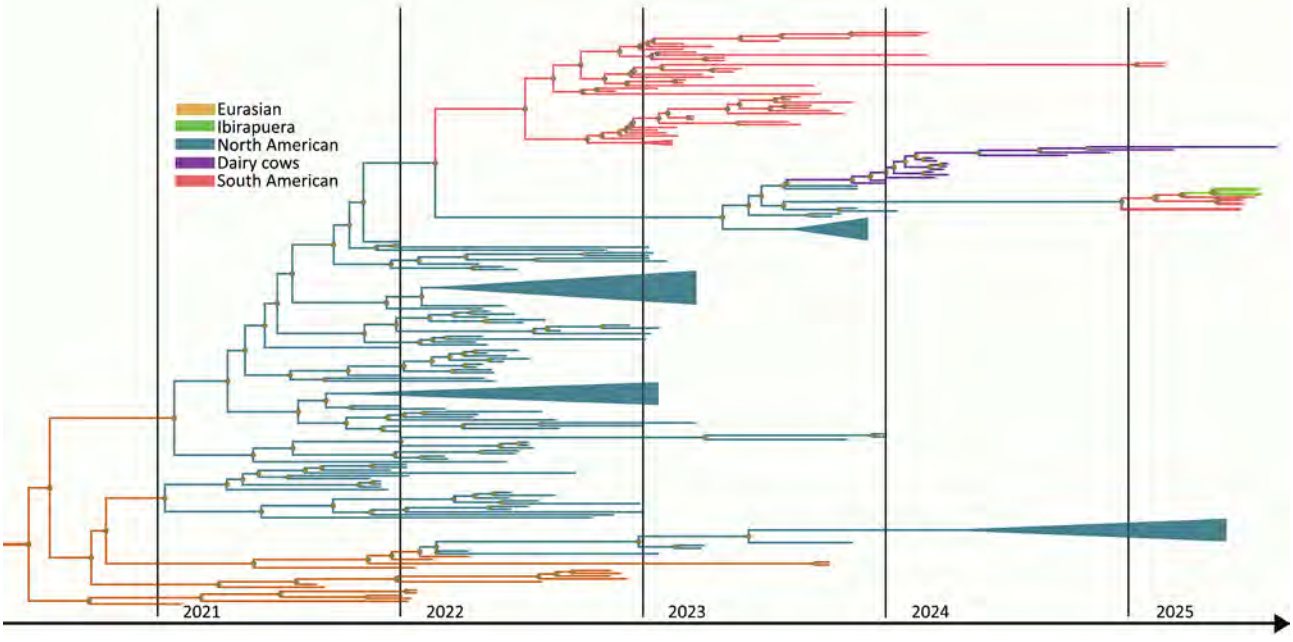

Figure 4. Time-scaled Bayesian maximum clade credibility tree of divergent highly pathogenic avian influenza A(H5N1) clade 2.3.4.4b virus, São Paulo, Brazil, 2025. The tree was inferred by using the Gaussian Markov Random Field Skyride prior model and includes 206 representative H5 clade 2.3.4.4b virus sequences from Eurasia and the Americas. Tan circle nodes indicate bootstrap >70.

Conclusions

We identified a divergent reassortant HPAI H5N1 virus strain in white-faced whistling ducks from Ibirapuera Central Park, São Paulo, Brazil. As one of the city's largest green, cultural, and recreational areas, attracting thousands of visitors each day (*12*), the park is a notable human–animal-environment interface. Following laboratory confirmation of H5N1, park authorities immediately implemented prevention, management, and isolation measures to reduce the risk for transmission.

Our phylogenetic and temporal analyses support a second introduction of HPAI H5N1virus into South America from North America, after reassortment with locally circulating LPAIVs in South America. Our findings suggest that reassortment likely occurred before the viruses dispersed through the interior regions of Brazil by regional migratory birds (*5*), although the precise movement dynamics of those waterfowl require further investigation. Similar exchanges have been described in other H5N1 genomes from South America (*5*,*11*), indicating ongoing genetic exchange between introduced HPAI viruses and regional AIV viruses, contributing to the increasing genomic diversity of H5N1 viruses circulating in South America. Together, those reassortment events position South America as a critical region for AIV surveillance.

Our results highlight that HPAIV can be detected in a major urban park that harbors multiple animal species. The coexistence of resident waterfowl, migratory birds, synanthropic mammals, domestic animals, and abundant human activity creates an opportunity for cross-species transmission events. Our observations underscore the necessity of integrating systematic monitoring of urban wildlife into One Health surveillance frameworks to improve early detection and mitigate AIV risks.

Acknowledgments

The authors thank the Parque Ibirapuera Conservação staff, the São Paulo City Hall logistical support for field surveillance by Centro de Manejo e Conservação de Animais Silvestres, and the Brazilian Ministry of Science, Technology, and Innovation for maintaining the National Network for Virus Surveillance in Wild Animals (PREVIR Network) for logistical and surveillance support.

This work was funded by Ministry of Science, Technology and Innovation, National Council for Scientific and Technological Development (grant nos. 403761/2020-4, 400172/2022-4), Fundação de Amparo a Pesquisa de São Paulo (grants nos. 2023/03041-1, 2023-07746-0, 2024/01882-1, 2025/09636-2), and Coordenação de Aperfeiçoamento de Pessoal de Nível Superior (finance code 001).

All sampling activities were conducted in compliance with Brazilian regulations (SISBIO permit nos. 87511–1/2023, 87511–2/2024, 97861–1/2025), and approved by the Institutional Animal Ethics Committee (CEUA/ICB-USP)

(permit no. 864117012 and 1716171225). Carcass sampling was performed on naturally dead birds without any experimental manipulation.

About the Author

Dr. Jansen is a researcher and coordinator of the Laboratory of Research on Emerging Viruses, Institute of Biomedical Sciences–University of São Paulo. His research focuses on the eco-epidemiology and genomic surveillance of avian influenza viruses and other zoonotic pathogens.

References

1. Suarez DL, Senne DA, Banks J, Brown IH, Essen SC, Lee CW, et al. Recombination resulting in virulence shift in avian influenza outbreak, Chile. Emerg Infect Dis. 2004;10:693–9. https://doi.org/10.3201/eid1004.030396
2. Youk S, Torchetti MK, Lantz K, Lenoch JB, Killian ML, Leyson C, et al. H5N1 highly pathogenic avian influenza clade 2.3.4.4b in wild and domestic birds: introductions into the United States and reassortments, December 2021–April 2022. Virology. 2023;587:109860. https://doi.org/10.1016/j.virol.2023.109860
3. Rivetti AV Jr, Reischak D, de Oliveira CHS, Otaka JNP, Domingues CS, Freitas TL, et al. Phylodynamics of avian influenza A(H5N1) viruses from outbreaks in Brazil. Virus Res. 2024;347:199415. https://doi.org/10.1016/j.virusres.2024.199415
4. Gamarra-Toledo V, Plaza PI, Angulo F, Gutiérrez R, García-Tello O, Saravia-Guevara P, et al. Highly pathogenic avian influenza (HPAI) strongly impacts wild birds in Peru. Biol Conserv. 2023;286:110272. https://doi.org/10.1016/j.biocon.2023.110272
5. Rivetti AV Jr, Reischak D, Carnegie L, Otaka JNP, Domingues CS, Cardoso FG, et al. Genomic diversity and reassortment of highly pathogenic avian influenza A/H5N1 virus (clade 2.3.4.4b) in Brazil: evidence of multiple introductions and intra-epidemic reassortment in 2025. Virology. 2026; 615:110751. https://doi.org/10.1016/j.virol.2025.110751
6. Koopmans MPG, Barton Behravesh C, Cunningham AA, Adisasmito WB, Almuhairi S, Bilivogui P, et al.; One Health High-Level Expert Panel. The panzootic spread of highly pathogenic avian influenza H5N1 sublineage 2.3.4.4b: a critical appraisal of One Health preparedness and prevention. Lancet Infect Dis. 2024;24:e774–81. https://doi.org/10.1016/S1473-3099(24)00438-9
7. Karlsson EA, Ciuoderis K, Freiden PJ, Seufzer B, Jones JC, Johnson J, et al. Prevalence and characterization of influenza viruses in diverse species in Los Llanos, Colombia. Emerg Microbes Infect. 2013;2:e20. https://doi.org/10.1038/emi.2013.20
8. Magalhães TBS, da Rosa Bueno E, de Assis Pereira N, Lima HAS, de Souza Pereira Gomes S, Mizuuti PJSG, et al. First detection of an H5N2 subtype of influenza A virus detected in *Charadrius collaris* from the Brazilian Pantanal. Sci Rep. 2026;16:14496. https://doi.org/10.1038/s41598-026-42819-y
9. Reischak D, Rivetti AV Jr, Otaka JNP, Domingues CS, Freitas TL, Cardoso FG, et al. First report and genetic characterization of the highly pathogenic avian influenza A(H5N1) virus in Cabot's tern (*Thalasseus acuflavidus*), Brazil. Vet Anim Sci. 2023;22:100319. https://doi.org/10.1016/j.vas.2023.100319
10. Martins-Filho PR, Quintans-Júnior LJ. Brazil's first H5N1 outbreak in commercial poultry: a sentinel event for cross-border preparedness. J Travel Med. 2025;32:taaf050. https://doi.org/10.1093/jtm/taaf050
11. Vanstreels RET, Nelson MI, Artuso MC, Marchione VD, Piccini LE, Benedetti E, et al. Novel highly pathogenic avian influenza A(H5N1) virus, Argentina, 2025. Emerg Infect Dis. 2025;31:2279–83. https://doi.org/10.3201/eid3112.250783
12. Secretaria Municipal do Verde e do Meio Ambiente. Waters of the Sapateiro Stream and Ibirapuera Park [cited 2025 Dec 4]. https://prefeitura.sp.gov.br/web/meio_ambiente/w/%C3%A1guas-do-c%C3%B3rrego-do-sapateiro-e-o-parque-ibirapuera-1

Address for correspondence: Jansen de Araujo, Laboratório de Pesquisa em Vírus Emergentes. Microbiology Department, Institute of Biomedical Science at the University of São Paulo. 1374, Prof. Lineu Prestes Avenue, 05508-000, São Paulo, Brazil; email: jansentequila@usp.br

Clinical Characterization of Invasive Meningococcal Disease Epidemic, Uzbekistan, 2026

Bakhodir B. Rakhimov, Laziz N. Tuychiev, Nilufar T. Khamzayeva, Nigora U. Tadjiyeva, Nargiza S. Saidkasimova, Nargiza X. Otamuratova, Xolmamat N. Norboev

Tashkent, Uzbekistan, registered 290 invasive meningococcal disease cases during January–April 2026; the case fatality rate was 8.3%. Meningeal signs appeared in only 3.1% of patients and were the sole signs associated with death. *Neisseria meningitidis* serogroup surveillance and conjugate vaccine introduction will be needed to prevent invasive meningococcal disease in Uzbekistan.

Invasive meningococcal disease (IMD), caused by *Neisseria meningitidis*, can kill a healthy child within hours of symptom onset (*1*). Before the COVID-19 pandemic, IMD incidence had declined across most high-income countries owing to conjugate vaccination programs (*2*). After pandemic restrictions were lifted, IMD incidence rebounded. During 2023–2024, the United States recorded its highest annual total IMD cases since 2014 (*3*); Spain's Aragon region reported a 27-fold case excess in early 2025 (*4*), and an outbreak struck Canterbury, England, in early 2026 (*5*). Uzbekistan is a lower-middle–income country within Central Asia (population ≈36 million). Uzbekistan has no published IMD epidemiology, and meningococcal conjugate vaccines are absent from the country's national immunization schedule. During 2026, a total of 290 IMD cases were registered in Tashkent, Uzbekistan. We describe the clinical profile, laboratory findings, predictors of fatal outcome, and public health response to this IMD epidemic.

The Study

We conducted a prospective epidemic investigation of all IMD cases registered at the Tashkent City Center for Sanitary-Epidemiologic Welfare and Public Health and applied 2018 World Health Organization case definitions (*6*). Confirmed cases required laboratory identification of *N. meningitidis* from a sterile site (blood culture or cerebrospinal fluid [CSF]). Probable cases met clinical criteria and had an epidemiologic link to a confirmed case, defined as household membership or attendance at the same institution within 10 days of primary IMD onset. Nasopharyngeal (NP) swab samples were collected from all patients during routine carriage screening according to the national protocol and were reported descriptively; they were not used to define case status. The ethics committee of Tashkent State Medical University approved this study (approval no. 20; June 12, 2026). Analysis of deidentified surveillance data did not require individual informed consent.

The 5 clinical signs, recorded as present or absent, were meningeal signs (nuchal rigidity, Kernig sign, or Brudzinski sign, documented by the admitting physician), loss of consciousness, hemorrhagic rash, fever, and vomiting. Clinical IMD severity was graded by the admitting physician as moderate, severe, fulminant, or extremely severe, following Uzbekistan's national meningococcal disease management protocol. Cases with unknown outcomes at the data cutoff timepoint (April 14, 2026) were excluded from case-fatality calculations.

We performed statistical analyses by using SPSS Statistics 26 (IBM Corp., https://www.ibm.com). We compared continuous variables by using Welch's *t*-tests. We tested binary associations between clinical signs and fatal outcomes by using a Pearson χ^2 or Fisher exact test and calculated odds ratios (ORs) with 95% CIs. We used multivariable binary logistic regression with simultaneous entry of all covariates to model fatal outcomes. We assessed model calibration by using the Hosmer–Lemeshow test and discrimination by using area under the receiver operating characteristic curve.

Author affiliations: Tashkent State Medical University, Tashkent, Uzbekistan (B.B. Rakhimov, L.N. Tuychiev, N.T. Khamzayeva, N.U. Tadjiyeva, N.S. Saidkasimova, N.X. Otamuratova, X.N. Norboev); Republican Specialized Scientific-Practical Medical Center for Epidemiology, Microbiology, Infectious and Parasitic Diseases, Tashkent (N.U. Tadjiyeva, N.X. Otamuratova)

DOI: https://doi.org/10.3201/eid3210.261144

A total of 290 IMD cases were registered in Tashkent during January 1–April 14, 2026 (Figure). Case numbers increased sharply through late January and February, peaked during February 12–18, and then declined through April, a pattern consistent with community-wide epidemic spread rather than a point-source outbreak.

Among 290 case-patients, 171 (59.0%) were male and 119 (41%) female (Table 1). Median patient age was 36 (interquartile range [IQR] 18–72) months. Children 2 to <5 years of age constituted the largest (41.0%) group, followed by 5 to <10 years (17.6%), 1 to <2 years (14.5%), and <1 year of age (5.9%). Cases were distributed across all 12 Tashkent administrative districts (Appendix Table 1, https://wwwnc.cdc.gov/EID/article/32/10/26-1144-App1.pdf). The highest incidence was observed in Olmazor (37 cases). Fifteen cases were reported from other regions of Uzbekistan.

Outcome data were available for 261 (90.0%) patients; 29 (10.0%) cases remained unresolved at the cutoff timepoint. Among those 261 patients, 237 (90.8%) were discharged alive and 24 (9.2%) died, yielding an overall case-fatality rate (CFR) of 8.3% (24/290). The median age was 48.0 (IQR 24–120) months for patients who died versus 33.0 (IQR 16–60) months for survivors (Welch's *t*-test p<0.001).

Fever and hemorrhagic rash were each documented in 165 (63.2%) cases, loss of consciousness in 162 (62.1%) cases, and vomiting in 161 (61.7%) cases. Meningeal signs were observed in 8/261 (3.1%) cases having known outcomes. Univariable analysis showed meningeal signs were the sole clinical sign significantly associated with death. CFR was 50.0% among case-patients with meningeal signs versus 7.9% in those without (OR 11.65 [95% CI 2.71–50.13]; Fisher exact test p = 0.003) (Table 2). The 4 high-prevalence signs showed no significant association with fatal outcome (all p>0.50) (Table 2).

Multivariable logistic regression identified older age at onset as an independent predictor of death (adjusted OR per 12 months of age 1.06 [95% CI 1.02–1.11]; p = 0.005) (Table 2). The model displayed acceptable discrimination (area under the curve 0.712 [95% CI 0.595–0.828]; p = 0.001), calibration (Hosmer–Lemeshow test p = 0.98), and performance (Nagelkerke R^2 = 0.193). Binary clinical signs did not yield stable multivariable estimates because of few meningeal signs (n = 8).

In Tashkent, all persons with suspected IMD are admitted to City Children's Infectious Disease Hospital No. 1; specimen collection is differentiated according to clinical disease form. Patients manifesting meningeal signs undergo lumbar puncture within the admissions area; those with meningococcemia without meningeal signs have blood drawn for culture; and those with mixed-form disease have CSF, blood culture, and NP swab samples collected. CSF was not obtained in 234 (80.7%) cases, reflecting predominance of meningococcemia and mixed-form disease rather than deviation from established protocol.

Among 56 patients who had lumbar punctures, 28 (50.0% of specimens; 9.7% of all cases) had confirmed *N. meningitidis* in CSF. Blood culture confirmed *N. meningitidis* in 176 (60.7%) patients. Sterile-site laboratory confirmation (blood culture or CSF) was achieved in 187/290 (64.5%) cases. NP carriage screening results were positive for *N. meningitidis* in

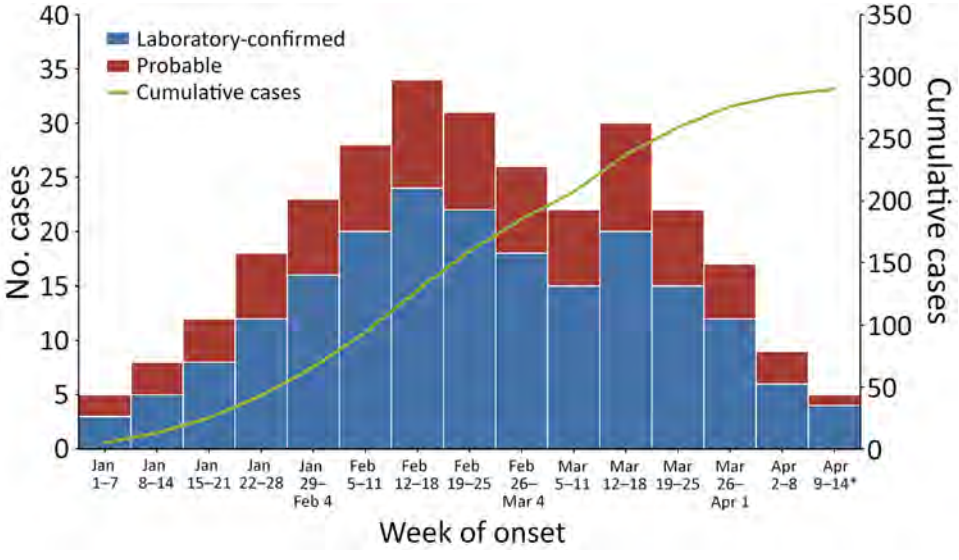

Figure. Weekly number of cases of invasive meningococcal disease in study of epidemic in Tashkent, Uzbekistan, January 1–April 14, 2026. Disease cases (n = 290) were registered in the invasive meningococcal disease case registry at the Tashkent City Center for Sanitary-Epidemiologic Welfare and Public Health. Cases were evaluated according to laboratory confirmation status and cumulative case counts. For laboratory-confirmed cases, *Neisseria meningitidis* was isolated from a sterile site (blood culture or cerebrospinal fluid). Probable cases met clinical criteria and had an epidemiologic link to a confirmed case. Asterisk indicates a partial week (April 9–14; 6 days).

Table 1. Demographic and clinical characteristics of patients in study of invasive meningococcal disease epidemic in Tashkent, Uzbekistan, January 1–April 14, 2026*

Characteristic	Patients
Total	290 (100)
Sex	
M	171 (59.0)
F	119 (41.0)
Age at onset, mo., median (IQR)	36 (18–72)
Age group, y	
<1	17 (5.9)
1 to <2	42 (14.5)
2 to <5	119 (41.0)
5 to <10	51 (17.6)
10 to <18	13 (4.5)
≥18	6 (2.1)
Missing	42 (14.5)
Outcome, n = 261 with known outcome†	
Discharged alive	237 (90.8)
Death, CFR 8.3%‡	24 (9.2)
Clinical sign at admission, n = 261†	
Fever ≥38°C	165 (63.2)
Hemorrhagic rash	165 (63.2)
Loss of consciousness	162 (62.1)
Vomiting	161 (61.7)
Meningeal signs§	8 (3.1)
Laboratory test results for sterile site	
Blood culture positive	176 (60.7)
CSF culture positive, 56 LPs performed	28 (9.7)
Sterile site confirmed, blood or CSF	187 (64.5)
Nasopharyngeal carriage screening positive¶	164 (56.6)
CSF not obtained	234 (80.7)

*Values are no. (%) except as indicated. CFR, case fatality rate; CSF, cerebrospinal fluid; IQR, interquartile range; LP, lumbar puncture.
†Twenty-nine cases were excluded because outcome was unknown at the data cutoff timepoint. Data for subgroups are no. (%) of 261 cases with known outcome.
‡CFR = deaths/all 290 cases × 100.
§Meningeal signs were defined as the presence of nuchal rigidity, Kernig sign, or Brudzinski sign (any one of which was sufficient as a clinical sign).
¶Nasopharyngeal swab samples taken from all patients as routine carriage screening; not used to define case status.

164 (56.6%) patients; other organisms were identified in 8 (2.8%) NP swab samples. Sterile-site laboratory confirmation was not associated with fatal outcome (CFR 8.4% in confirmed vs. 8.1% in unconfirmed cases; p = 0.94) (Appendix Table 2).

Postexposure ring vaccination was documented for contacts of 103 (35.5%) index patients; chemoprophylaxis was reported for contacts of 20 (6.9%) index patients. Approximately 8,024 vaccine doses were deployed citywide, and 4,862 index patient contacts were vaccinated under emergency authorization.

Conclusions

Tashkent's 2026 IMD epidemic occurred during a global post-COVID-19–pandemic meningococcal resurgence, as immunologic debt accumulated during years of restricted social mixing (*7*,*8*). A CFR of 8.3% in Tashkent falls within the globally reported range for settings without optimized intensive-care protocols (*9*,*10*). The clinical profile was markedly atypical; meningeal signs, documented in 40%–70% of patients in case series from Europe (*11*,*12*), were observed in 3.1% of cases in Tashkent, reflecting dominance of

Table 2. Clinical predictors of fatal outcome determined by univariable and multivariable analyses in study of invasive meningococcal disease epidemic in Tashkent, Uzbekistan, 2026*

Variable	CFR present, %	CFR absent, %	Crude OR (95% CI)	Adjusted OR (95% CI)	p value
Clinical signs, univariable					
Meningeal signs	50.0	7.9	11.65 (2.71–50.13)	NA	0.003†
Loss of consciousness	8.8	9.8	0.89 (0.38–2.08)	NA	0.785
Hemorrhagic rash	9.3	9.1	1.02 (0.43–2.43)	NA	0.964
Fever ≥38°C	9.3	9.1	1.02 (0.43–2.43)	NA	0.964
Vomiting	8.2	10.7	0.75 (0.32–1.75)	NA	0.503
Multivariable logistic regression‡					
Age at onset, 12 mo.				1.06 (1.02–1.11)	0.005
Sterile site confirmed				1.61 (0.50–5.15)	0.424

*N = 261 case-patients. CFR, case fatality rate; NA, not applicable; OR, odds ratio.
†Fisher exact test; all other p values determined by Pearson χ^2 test.
‡Model included age at onset, sterile-site laboratory confirmation, and all 5 clinical signs. Binary signs did not converge owing to quasi-complete separation caused by the extreme rarity of meningeal signs (n = 8; 3.1%) and are not shown as adjusted OR estimates.

meningococcemia and mixed-form disease. The low number of patients with meningeal signs is phenotypically consistent with serogroup C or W strains, which characteristically produce fulminant bacteremia and minimal meningeal inflammation (*13*). However, serogroup confirmation was not achieved during the epidemic.

The near absence of meningeal signs carries direct clinical implications. Caregivers and clinicians are trained to identify IMD primarily by neck stiffness and photophobia; thus, they might not recognize IMD when it manifests as hemorrhagic septicemia alongside altered consciousness (*14*).

The first limitation of our study is that serogroup and antimicrobial drug susceptibility data were unavailable for the entire cohort. Second, outcome data were missing for 10% of cases, and disease severity grading was inconsistently recorded. Finally, ring vaccination reached documented contacts of only 35.5% of index patients and chemoprophylaxis reached <7% of contacts, both well below World Health Organization postexposure recommendations (*15*).

In summary, Tashkent's 2026 surge in IMD cases indicates a substantial, underrecognized public health burden. Serogroup surveillance and conjugate vaccine introduction will be needed to prevent IMD in Uzbekistan.

Acknowledgments

We thank the staff at the City Children's Infectious Disease Hospital No. 1, the Tashkent City Center for Sanitary-Epidemiological Welfare and Public Health, and the district sanitary-epidemiologic stations for providing access to surveillance data during the epidemic response.

About the Author

Dr. Rakhimov is an associate professor in the Department of Environmental Hygiene, Tashkent State Medical University, Tashkent, Uzbekistan, and a doctoral candidate at Korea University in Seoul, South Korea. His primary research interests are environmental and infectious disease epidemiology in Central Asia.

References

1. Pace D, Pollard AJ. Meningococcal disease: clinical presentation and sequelae. Vaccine. 2012;30:B3–9. https://doi.org/10.1016/j.vaccine.2011.12.062
2. Nuttens C, Findlow J, Balmer P, Swerdlow DL, Tin Tin Htar M. Evolution of invasive meningococcal disease epidemiology in Europe, 2008 to 2017. Euro Surveill. 2022;27:2002075. https://doi.org/10.2807/1560-7917.ES.2022.27.3.2002075
3. Centers for Disease Control and Prevention. Increase in invasive serogroup Y meningococcal disease in the United States. Health Alert Network, CDCHAN-00505. 2024 [cited 2026 Aug 11]. https://www.cdc.gov/han/2024/han00505.html
4. Nicolau Cano C, Gallego-Royo A, Estupiñan Valido E, Perez Perez A, Gimenez Julvez T, Vela Iglesia BMP, et al. Outbreak of *Neisseria meningitidis* serogroup B in Aragón, Spain, January to February 2025. Euro Surveill. 2025;30: 2500206. https://doi.org/10.2807/1560-7917.ES.2025.30.14.2500206
5. Mahase E. Meningitis: MenB strain may have evolved to be more transmissible, say experts. BMJ. 2026;392:s549. https://doi.org/10.1136/bmj.s549
6. World Health Organization. Surveillance standards for vaccine-preventable diseases, 2nd edition. 2018 [cited 2026 Jun 18]. https://www.who.int/publications/i/item/surveillance-standards-for-vaccine-preventable-diseases-2nd-edition
7. Cohen R, Pettoello-Mantovani M, Somekh E, Levy C. European pediatric societies call for an implementation of regular vaccination programs to contrast the immunity debt associated to coronavirus disease-2019 pandemic in children. J Pediatr. 2022;242:260–261.e3. https://doi.org/10.1016/j.jpeds.2021.11.061
8. Shaw D, Abad R, Amin-Chowdhury Z, Bautista A, Bennett D, Broughton K, et al. Trends in invasive bacterial diseases during the first 2 years of the COVID-19 pandemic: analyses of prospective surveillance data from 30 countries and territories in the IRIS Consortium. Lancet Digit Health. 2023;5:e582–93. https://doi.org/10.1016/S2589-7500(23)00108-5
9. Wang B, Santoreneos R, Giles L, Haji Ali Afzali H, Marshall H. Case fatality rates of invasive meningococcal disease by serogroup and age: a systematic review and meta-analysis. Vaccine. 2019;37:2768–82. https://doi.org/10.1016/j.vaccine.2019.04.020
10. Baloche A, Dussart C, Bedouch P, Carrouel F, Mick G. Epidemiology and clinical burden of meningococcal disease in France: scoping review. J Clin Med. 2023;12:849. https://doi.org/10.3390/jcm12030849
11. van de Beek D, de Gans J, Spanjaard L, Weisfelt M, Reitsma JB, Vermeulen M. Clinical features and prognostic factors in adults with bacterial meningitis. N Engl J Med. 2004;351:1849–59. https://doi.org/10.1056/NEJMoa040845
12. Brouwer MC, Tunkel AR, van de Beek D. Epidemiology, diagnosis, and antimicrobial treatment of acute bacterial meningitis. Clin Microbiol Rev. 2010;23:467–92. https://doi.org/10.1128/CMR.00070-09
13. Ladhani SN, Beebeejaun K, Lucidarme J, Campbell H, Gray S, Kaczmarski E, et al. Increase in endemic *Neisseria meningitidis* capsular group W sequence type 11 complex associated with severe invasive disease in England and Wales. Clin Infect Dis. 2015;60:578–85. https://doi.org/10.1093/cid/ciu881
14. Thompson MJ, Ninis N, Perera R, Mayon-White R, Phillips C, Bailey L, et al. Clinical recognition of meningococcal disease in children and adolescents. Lancet. 2006;367:397–403. https://doi.org/10.1016/S0140-6736(06)67932-4
15. World Health Organization. Defeating meningitis by 2030: a global road map. 2021 [cited 2026 Jun 18]. https://www.who.int/publications/i/item/9789240026407

Address for correspondence: Bakhodir B. Rakhimov, Department of Environmental Hygiene, Tashkent State Medical University, 2 Farobiy St., Tashkent 100109, Uzbekistan; email: b.b.raximov@tashmeduni.uz

Whole-Genome Sequencing of Measles Virus from 2025 Outbreak, Texas, USA

Piyada Juntawong, Bonnie Oh, Richard Bovio, Jie Lu, Sydney Stanley, Robert F. Potter, Yan Sun, Casey Schroeder, Olivia A. Smith, Elise Huebner, Stephen L. White, Saroj Rai, Varun Shetty, Grace Kubin

We sequenced measles-positive samples from the 2025 outbreak in Texas, USA, and identified the expansion of a closely related genotype D8 lineage within broader strain diversity from North America. F:H419R was used as a lineage-associated genomic surveillance marker. Our findings demonstrate that whole-genome sequencing can strengthen measles surveillance and enhance outbreak investigations.

Measles virus importations continue to cause outbreaks in undervaccinated communities in the United States despite elimination since 2000 (*1*). In early 2025, the Texas Department of State Health Services reported the state's largest measles outbreak after elimination, centered in Gaines County and neighboring West Texas communities (*2*). Epidemiologic reports indicated 762 confirmed measles cases; more than half occurred in Gaines County, and most cases were among children, adolescents, and persons who were unvaccinated or had unknown vaccination status (*3*). The outbreak occurred during expanded measles activity in North America, raising questions about local expansion, interstate relatedness, and the utility of whole-genome sequencing (WGS) to resolve transmission patterns beyond routine genotyping.

Routine measles molecular surveillance commonly relies on the 450-nucleotide region of the nucleoprotein gene (N-450), which supports genotype and distinct sequence identifier (DSId) assignment. However, N-450 provides limited resolution of transmission chains during large outbreaks involving closely related viruses (*4*). We used WGS to characterize the measles outbreak in Texas and assessed genomic diversity and genomic relatedness to other measles virus genomes from North America.

Author affiliations: Texas Department of State Health Services, Austin, Texas, USA (P. Juntawong, B. Oh, R. Bovio, J. Lu, Y. Sun, C. Schroeder, O.A. Smith, E. Huebner, S.L. White, S. Rai, V. Shetty, G. Kubin); Children's Hospital of Philadelphia, Philadelphia, Pennsylvania, USA (S. Stanley, R.F. Potter); Perelman School of Medicine at the University of Pennsylvania, Philadelphia (S. Stanley, R.F. Potter).

DOI: https://doi.org/10.3201/eid3210.260494

The Study

We performed tiled amplicon-based sequencing on 491 reverse transcription PCR–positive measles samples (Appendix, http://wwwnc.cdc.gov/EID/article/32/10/26-0494-App1.pdf). After quality assessment, 368 measles virus genomes from 359 persons met the predefined coverage threshold for phylogenetic analysis; 9 persons each had 2 samples sequenced (Appendix Table 1). Among the 359 persons with sequenced samples and epidemiologic metadata, 204 (56.8%) were unvaccinated, 139 (38.7%) had unknown vaccination status, 7 (2.0%) had received 1 measles vaccine dose, and 9 (2.5%) had received 2 measles vaccine doses (Appendix Table 2). We determined vaccination status by using patient records. Patients without confirmed vaccination status were classified as unknown. We performed an exploratory genome-wide association study to evaluate if measles variants were associated with vaccination status, but we did not detect any variants significantly associated with vaccination status; however, our analysis was underpowered.

We performed a maximum-likelihood phylogenic analysis by using the 368 sequenced measles virus genomes. N-450 DSIds were available for 240 measles virus genomes, of which 220 (92%) were DSId 9171, a specific measles virus lineage belonging to the D8 genotype. We assigned epidemiologic weeks to measles virus genomes by using Morbidity and Mortality Weekly Report numbering (*5*). Maximum-likelihood phylogenetic analysis revealed that measles virus genomes from Texas formed a closely related genotype D8 lineage (Figure 1, panel A). Pairwise single-nucleotide

polymorphism (SNP) distances ranged from 0–15 SNPs (median 3 SNPs), supporting close genetic relatedness among outbreak genomes (Figure 1, panel B).

To estimate the time to most recent common ancestor (tMRCA) for the measles virus genomes associated with the outbreak in Texas, we performed a molecular clock analysis. We did not use tMRCA estimates from the Texas measles virus genomes alone to infer introduction timing because our molecular clock analysis revealed weak temporal signal after we excluded the temporally distant D8 reference genome (Appendix Figure 1). Early measles virus genomes from epidemiologic weeks 5–8 were concentrated in Gaines County, Texas, the outbreak epicenter. We later observed closely related genomes in nearby and more distant Texas counties (Appendix Figure 2). Those results support early localized amplification followed by wider spread, although multiple closely related introductions cannot be ruled out (*6*).

To provide genomic surveillance context, we conducted a targeted evaluation of the Fusion gene H419R substitution (F:H419R), fixed in all measles viral genomes from Texas, rather than a comprehensive genome-wide screen for recurrent, homoplasic substitution, or substitutions of functional effect. To place F:H419R in broader context, we screened publicly available genotype D8 whole genomes with adequate Fusion gene coverage (>12,500 bp of total genome coverage with an unambiguous call for the Fusion gene codon encoding residue 419). We detected F:H419R among recent publicly available D8 measles virus genomes (Figure 2, panel A; Appendix Table 3). The proportion of D8 genomes with the F:H419R substitution increased from 2% (1/49) in 2023 to 8.5% (10/118) in 2024 and 65.4% (34/52) in 2025 (Appendix Figure 3). Although residue 419 has prior residue-level annotation (*7*), this study did not evaluate functional, immunologic, vaccine-effectiveness, transmission, or clinical consequences. Selection analysis identified 2 polymerase-gene codons, which we interpreted as subclade markers rather than evidence of immune escape or functional adaptation (Appendix Figure 4).

We placed the measles genomes from Texas in the global context by using the Nextstrain measles workflow (https://github.com/nextstrain/measles). To reduce geographic and temporal sampling imbalance, we subsampled genomes to ≤30 per country–year group. Consequently, the phylogeny includes only a representative subset of 2025 measles genomes from the United States (Figure 2, panel B). Measles virus genomes from Texas clustered with contemporaneous genomes from Utah, USA, and the Netherlands (Figure 2, panel B).

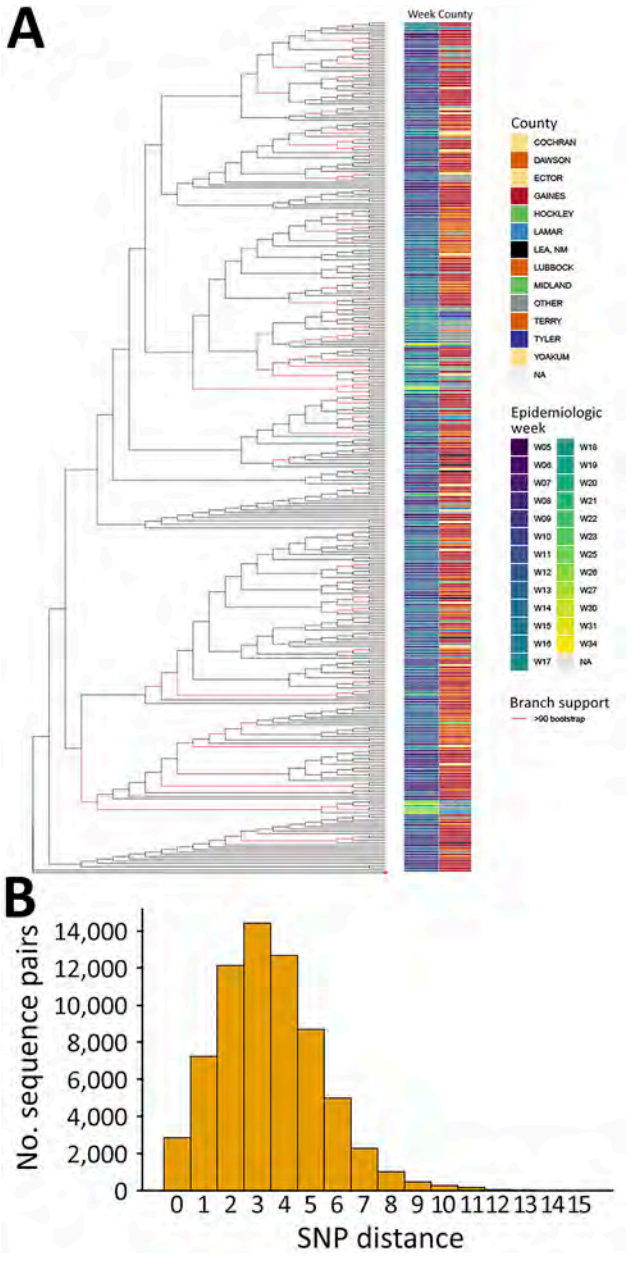

Figure 1. Genomic diversity of measles virus genomes from study of whole-genome sequencing of measles virus from 2025 outbreak, Texas, USA. A) Maximum-likelihood phylogenetic tree of 368 Texas measles genomes (January–August 2025). Color strip annotations denote epidemiologic week of specimen collection and county. Red branches indicate clusters with an ultrafast bootstrap value >90. Red asterisk indicates reference D8 strain (GenBank accession no. KJ018971.2). B) Distribution of pairwise SNP distances among Texas measles genomes. SNP, single-nucleotide polymorphism.

We analyzed a comparative dataset including genomes from Texas, Arizona, Utah, South Carolina, and other jurisdictions in North America. We observed high callable coverage across most coding regions including N-450 and the Fusion gene but

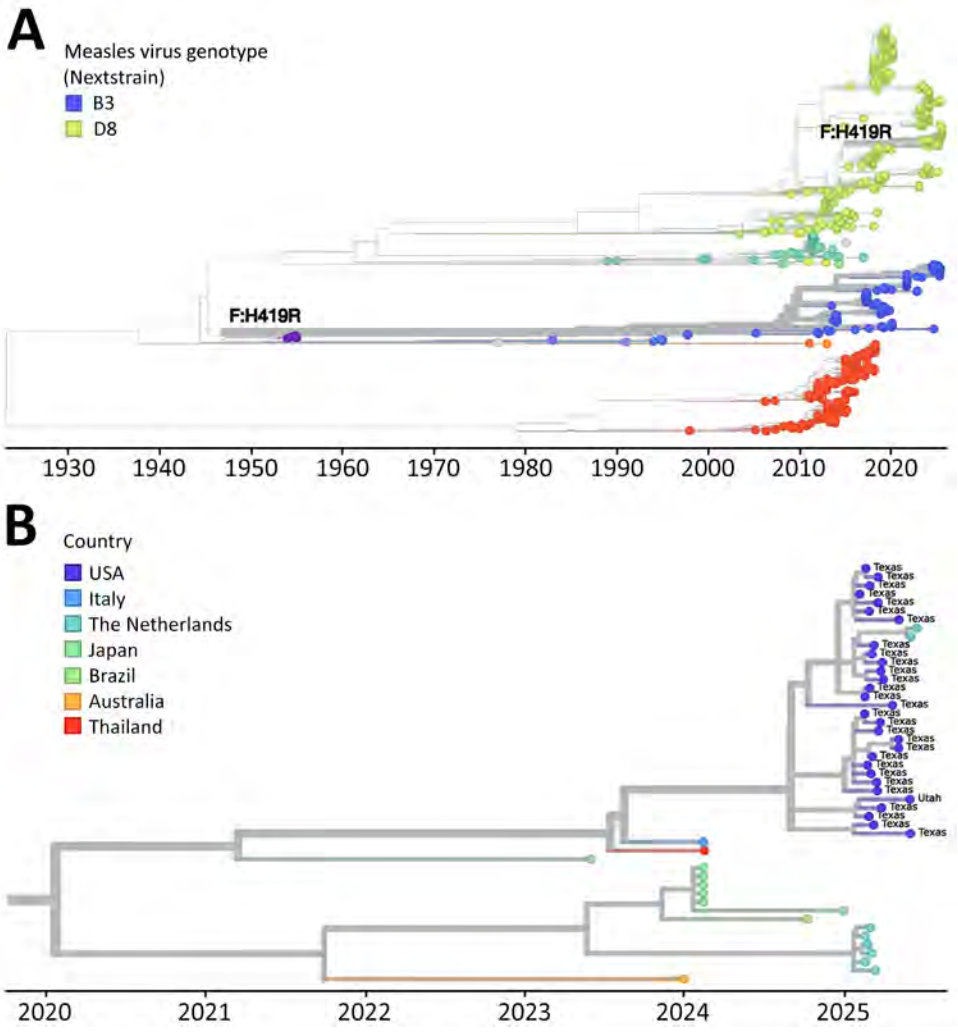

Figure 2. Genomic surveillance context of F:H419R among publicly available measles virus genomes from study of whole-genome sequencing of measles virus from 2025 outbreak, Texas, USA. A) Nextstrain time-scaled global phylogeny of measles viruses showing genotype B3 and D8 measles virus genomes with the F:H419R substitution highlighted (https://nextstrain.org/measles/genome@2025-09-24?gt=F.419R&treeZoom=selected). B) Global genotype D8 context of representative measles genomes associated with the outbreak in Texas and representative publicly available F:H419R-positive D8 genomes. F:H419R, Fusion gene H419R substitution.

more variable coverage in the matrix–fusion noncoding region (MF-NCR) (Appendix Figure 5). Masking MF-NCR positions did not alter major phylogenetic clustering, indicating that uneven coverage did not account for the broad phylogenetic structure (Appendix Figure 6). The focal measles virus genomes from North America were interspersed with other related D8 measles virus genotypes (Figure 3). Root-to-tip regression indicated limited temporal signal in state-specific datasets and moderate temporal structure in the focal North American lineage (Appendix Table 4). TreeTime (https://github.com/neherlab/treetime) estimated a tMRCA of June 14, 2024 (90% CI December 24, 2023–December 12, 2024) for the expanding North American D8 measles virus lineage, supporting recent shared ancestry and expansion of a sublineage in Texas within broader North American D8 measles virus diversity.

We observed lower pairwise SNP distances within Texas than between Texas and Utah or Arizona, indicating a more compact genetic cluster among measles virus genomes associated with the outbreak in Texas (Figure 4; Appendix Table 5). Measles virus genomes from Arizona and Utah were related to genomes from Texas but demonstrated heterogeneous phylogenetic placement. In contrast, measles virus genomes from South Carolina formed a distinct sublineage within broader North American D8 diversity. Those findings support local expansion of a closely related Texas lineage within wider North American D8 diversity, with distinguishable but related sublineages circulating concurrently in other jurisdictions.

Conclusion

Our genomic investigation of the largest after elimination measles outbreak in Texas demonstrated expansion of a closely related genotype D8 lineage and demonstrated the added resolution of WGS beyond routine N-450 genotyping. Measles virus genomes from Texas clustered closely with other D8 measles

genotypes from North America, including those from Arizona, Utah, and South Carolina. However, incomplete regional sampling, limited WGS availability from contemporaneous outbreaks, variable MF-NCR coverage, low sequence diversity, and molecular-clock outliers prevented definitive inference of geographic origin or transmission direction. We therefore interpreted molecular clock estimates as temporal context rather than evidence of jurisdictional source or directionality.

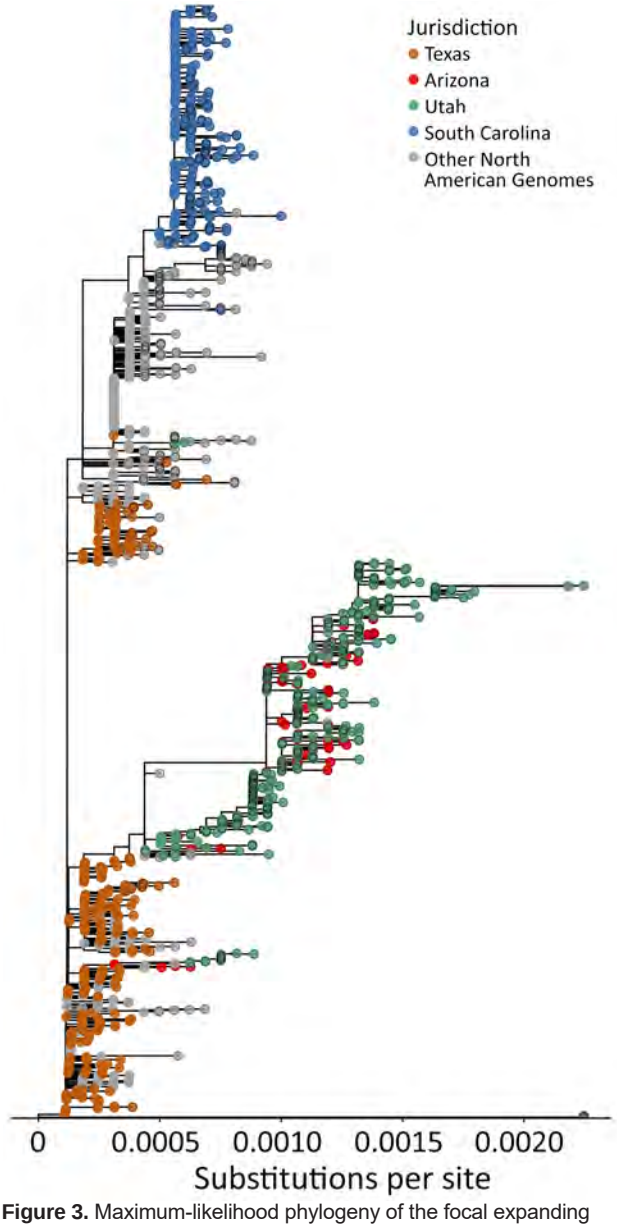

Figure 3. Maximum-likelihood phylogeny of the focal expanding North American genotype D8 measles virus lineage from study of whole-genome sequencing of measles virus from 2025 outbreak, Texas, USA. Phylogeny shows 1,760 genomes from Texas, Utah, Arizona, South Carolina, and other jurisdictions in North America included in the focal expanding North American genotype D8 lineage. We excluded 11 contextual genomes outside the focal lineage from this display. Tips are colored by jurisdiction; Canada genomes and US genomes outside Texas, Arizona, Utah, and South Carolina are grouped as other North American genomes. Tips identified by TreeTime (https://github.com/neherlab/treetime) as molecular-clock outliers are shown with black open circles. Branch lengths represent substitutions per site. The tree was rooted for visualization only; root placement should not be interpreted as evidence of ancestry, source, or transmission direction.

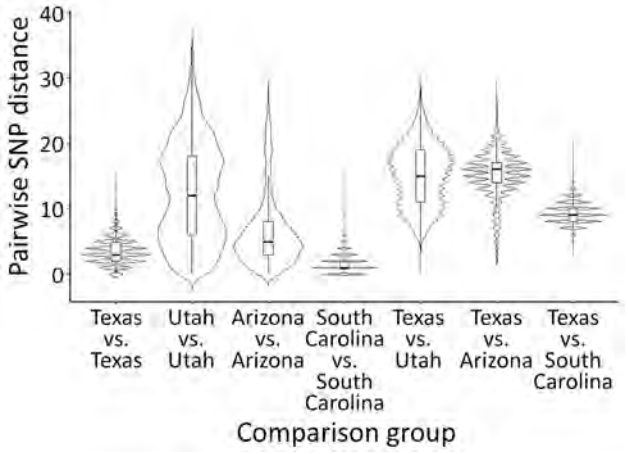

Figure 4. Pairwise SNP-distance distributions among genomes in the focal expanding North American genotype D8 lineage from study of whole-genome sequencing of measles virus from 2025 outbreak, Texas, USA. Violin plots show distributions of pairwise SNP distances within Texas, Utah, Arizona, and South Carolina and between Texas and each comparison jurisdiction. Embedded boxplots show medians (horizonal lines) and interquartile ranges (box tops and bottoms); whiskers indicate the most extreme values within 1.5x the interquartile range below the first quartile or above the third quartile. Wider sections of violins indicate greater density of pairwise comparisons. SNP, single-nucleotide polymorphism.

The F:H419R mutation was fixed among measles genomes from Texas and was detected among recent publicly available D8 whole genomes, supporting its use as a lineage-associated genomic surveillance marker. Because publicly available data are enriched for WGS whereas routine measles surveillance commonly relies on N-450 sequencing, our analysis cannot estimate the prevalence or geographic distribution of this mutation.

Our findings demonstrate how WGS can distinguish closely related measles virus lineages that routine N-450 genotyping cannot resolve and complement epidemiologic investigation during large outbreaks. Expanding timely, geographically representative WGS and integrating genomic and epidemiologic data could strengthen measles surveillance.

Acknowledgments

We thank the Microbial Genomics Team, Astrid Romero, Michael Jost, Shivangi Vayla, and Mayela Pedrueza; Genetic Sequencing Branch members Jessica Paul, Joel Wadleigh, and Sydney Zacharias; and Carolyn Crisp

for technical assistance and suggestions. We thank Erin Young, Kelly Oakeson, and the Utah Public Health Laboratory for assistance with Cecret pipeline setup and for providing genome sequences.

Canada measles whole-genome sequences were provided by the Public Health Agency of Canada (Joanne Hiebert), Alberta Precision Laboratories Public Health Laboratory (Kevin Fonseca and Tarah Lynch), and the British Columbia Centre for Disease Control Public Health Laboratory program (Agatha Jassem, Branco Cheung, and John Tyson).

Texas outbreak genome sequences are publicly available in the National Center for Biotechnology Information database (BioProject accession no. PRJNA1435643).

About the Author

Dr. Juntawong leads genomic epidemiology analyses of viral pathogen outbreaks at the Texas Department of State Health Services. Her work focuses on next-generation sequencing, pathogen genomics, and molecular surveillance to support public health decision-making.

References

1. Mathis AD, Raines K, Filardo TD, Wiley N, Leung J, Rota PA, et al. Measles update—United States, January 1–April 17, 2025. MMWR Morb Mortal Wkly Rep. 2025;74:232–8. https://doi.org/10.15585/mmwr.mm7414a1
2. Texas Department of State Health Services. Measles outbreak in Gaines County [cited 2025 Sep 24]. https://www.dshs.texas.gov/news-alerts/measles-outbreak-gaines-county-texas.
3. Texas Department of State Health Services. Measles outbreak—August 12, 2025 [cited 2025 Sep 24]. https://www.dshs.texas.gov/news-alerts/measles-outbreak-2025.
4. Penedos AR, Myers R, Hadef B, Aladin F, Brown KE. Assessment of the utility of whole genome sequencing of measles virus in the characterisation of outbreaks. PLoS One. 2015;10:e0143081. https://doi.org/10.1371/journal.pone.0143081
5. Centers for Disease Control and Prevention. National Notifiable Diseases Surveillance System. MMWR week log 2025–2026 [cited 2025 Sep 24]. https://ndc.services.cdc.gov/wp-content/uploads/MMWR-Week-Log-2025-2026.pdf
6. Masters NB, Beck AS, Mathis AD, Leung J, Raines K, Paul P, et al. Measles virus transmission patterns and public health responses during Operation Allies Welcome: a descriptive epidemiological study. Lancet Public Health. 2023;8:e618–28. https://doi.org/10.1016/S2468-2667(23)00130-5
7. Emmelot ME, Bodewes R, Maissan C, Vos M, de Swart RL, van Els CACM, et al. Impact of genotypic variability of measles virus T-cell epitopes on vaccine-induced T-cell immunity. NPJ Vaccines. 2025;10:36. https://doi.org/10.1038/s41541-025-01088-y

Address for correspondence: Piyada Juntawong, Texas Department of State Health Services, 1100 W 49 St, Austin, TX 78756, USA; email: piyada.juntawong@dshs.texas.gov

Detection of Highly Pathogenic Avian Influenza A(H5N1) Virus in Cat and Rats during Outbreak in Backyard Poultry, United States, 2025

Suzanna M. Storms, Jade Rathmann, Lynette Hemker, Miranda Vieson, Leyi Wang

In 2025, highly pathogenic avian influenza A(H5N1) virus was detected in a poultry flock in Illinois, USA. Quantitative reverse transcription PCR, sequencing, and histopathology on cat and rat samples from the farm showed multiple positive tissues and high sequence identity to an avian isolate. Small mammals might contribute to H5N1 transmission.

The current panzootic of highly pathogenic avian influenza (HPAI) A(H5N1) clade 2.3.4.4b virus emerged in Europe in 2020 and by 2022 had spread throughout Europe, Africa, and North America (*1*–*4*). Trans-Atlantic introduction into North America was first documented in December 2021 and has since persisted in wild and domestic birds, has been detected in dairy cattle, and has been reported sporadically in other mammals (*5*). Waterfowl have played an equal role to seabirds in virus spread, which is concerning given their higher likelihood of overlapping ranges with poultry farms (*2*,*6*). We describe an HPAI H5N1 outbreak in a backyard poultry flock in Illinois, USA, with subsequent spillover into domestic and wild mammals on the premises.

The Study

On March 12, 2025, a farmer in southern Illinois with a small backyard poultry flock brought remains of 6 animals to their primary veterinarian for a necropsy workup after acute illness and near-complete mortality (100/105 birds) of the flock. The farm, ≈2 miles from a 25,000-acre reservoir lake within the Mississippi Flyway, housed 4 turkeys (*Meleagris gallopavo*), 1 goose (*Anser* sp.), 20 Guinea fowl (*Numida* spp.), 80 chickens (*Gallus gallus domesticus*), 17 cattle, 15 cats, and 2 dogs. Because HPAI virus (HPAIV) was suspected, the 6 animals, a chicken, a turkey, a goose, 2 Guinea fowl, and a rat (*Rattus norvegicus*), were sent to the University of Missouri Veterinary Medical Diagnostic Laboratory (VMDL; Columbia, MO, USA) for postmortem examination. VMDL collected and evaluated fresh and formalin-fixed tissues and performed influenza A virus (IAV) quantitative reverse transcription PCR (qRT-PCR) on 1 chicken sample, according to guidelines from the US Department of Agriculture (USDA) National Animal Health Laboratory Network (NAHLN; https://www.aphis.usda.gov/labs/nahln). The sample tested presumptive positive per NAHLN guidelines, and VMDL subtyped it as H5 influenza. VMDL then forwarded the sample to the National Veterinary Services Laboratories (NVSL; Ames, IA, USA) for confirmatory testing, which verified HPAIV H5N1 clade 2.3.4.4b virus.

Further PCR testing of the avian species for *Mycoplasma gallisepticum*, *M. synoviae*, and avian paramyxovirus were all negative. The necropsy findings reported hepatitis, pulmonary hemorrhage, and pulmonary edema in the poultry species and bronchopneumonia and meningoencephalitis in the rat. No additional testing was performed on the rat or other bird species. Upon report of HPAIV on the farm, state and federal agencies were notified. The Illinois Department of Agriculture and USDA quarantined the farm and monitored it for 4 months.

Author affiliations: Texas A&M Veterinary Medical Diagnostic Laboratory, College Station, Texas, USA (S.M. Storms); University of Illinois College of Veterinary Medicine, Urbana, Illinois, USA (S.M. Storms, M. Vieson, L. Wang); Greenville Veterinary Clinic, Ltd, Greenville, Illinois, USA (J. Rathmann, L. Hemker)

DOI: https://doi.org/10.3201/eid3210.260418

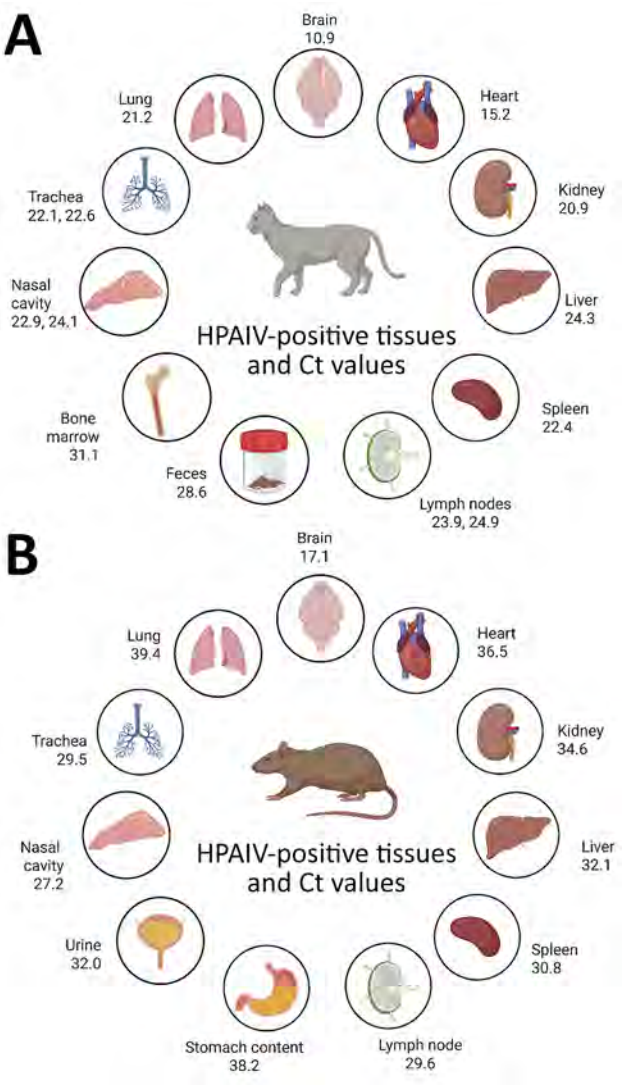

Figure 1. Quantitative reverse transcription PCR results from HPAIV A(H5N1) in cat and rats during outbreak in backyard poultry, United States, 2025. Specimens obtained from a cat (A) and a rat (B) found dead on farm where the outbreak occurred were confirmed to be positive for H5N1 clade 2.3.4.4b, genotype D1.1 virus. Graphic shows HPAIV-positive tissues and corresponding Ct values. A) For the cat, Ct values are shown for mesenteric and peripheral lymph nodes; urine, stomach content, and small intestine were not tested. B) For the rat, Ct values for peripheral lymph node only are shown; no mesenteric lymph node was tested. Also, rat feces, bone marrow, small intestine, and testis were tested, but HPAIV was not detected in those organs. Figure created with BioRender (https://www.biorender.com). Ct, cycle threshold; HPAIV, highly pathogenic avian influenza virus.

On March 16, 2025, the primary veterinarian collected the remains of a 13-year-old domestic shorthaired cat and a second feral rat from the farm. In conjunction with Illinois Department of Agriculture and USDA, the cat and rat specimens were sent to the University of Illinois Veterinary Diagnostic Laboratory (VDL; Urbana, IL, USA) on March 19. VDL performed gross necropsy and collected fresh and formalin-fixed tissues. VDL screened lung tissues from the cat and rat for IAV by qRT-PCR, following NAHLN guidelines. The cat lung tested presumptive positive (cycle threshold [Ct] value 21.2), subtyped as H5; NVSL confirmed H5N1 clade 2.3.4.4b virus. The rat lung tissue was negative upon initial screening, but NVSL conducted follow-up testing on tracheal swab samples, which were H5N1-positive.

In addition, we performed follow-up IAV qRT-PCR testing on 12 tissue samples from the cat and 15 tissue samples from the rat and considered Ct values ≤45 IAV-positive. All 12 cat tissue samples were IAV-positive (Ct values 10.9–31.1), and 11/15 rat tissues were IAV-positive (Ct 17.1–39.4) (Figure 1). Brain tissues of both animals had the highest viral loads (cat Ct 10.9; rat Ct 17.1). Of note, tracheal and nasal swab samples from both animals were IAV-positive (Ct range 22.1–29.5). A second lung sample from the rat returned a Ct of 39.4. Kidney tissues from both species were IAV-positive (cat Ct 20.9; rat Ct 34.6), and urine from the rat also tested IAV-positive (Ct 32.0). Nucleic acid in feces from the cat had a Ct value of 28.6, but no nucleic acid was detected in rat feces.

We performed whole-genome sequencing on 3 samples from the cat (brain, heart, and nasal swab) and 1 brain sample from the rat by using an amplicon-based enrichment protocol and sequencing on a MiSeq platform (Illumina, https://www.illumina.com). We used the Galaxy platform (*7*) for sequence assembly. All samples returned complete sequences for 8 segments (GenBank accession nos. PX687012–27) (Appendix Table). In addition, we included sequence data of the HPAIV H5N1 strain 25-009367-001 (GenBank accession nos. PV616546–53) from the chicken sample submitted by VMDL to NVSL in the analysis. Phylogenetic tree analysis revealed that the chicken, rat, and cat strains clustered together with other avian and mammal HPAIV (Figure 2; Appendix Figures 1–8). All 3 animal species from the outbreak contained the polymerase basic 2 E627K mutation that is associated with mammalian adaptation (*8*). All cat samples shared identical consensus sequences. We found 2 amino acid mutations, neuraminidase G392D and nucleoprotein K372E, in the cat and rat samples but not in the IAV strain from the chicken. In addition, we noted 1 synonymous polymerase basic 2 C1552T mutation in the rat strain that we did not see in cat and chicken strains. The genotype of the outbreak virus was D1.1 (*9*) (Appendix).

Gross examination during necropsy showed multifocal red mottling of the cat and rat lungs and additional right cranioventral lung consolidation in the rat. Histopathology findings in the cat included multifocal bronchointerstitial pneumonia, mild multifocal nonsuppurative meningoencephalitis, and acute adrenocortical necrosis (Figure 3, panels A–C). We noted severe cranioventral bronchopneumonia (not shown) amongst a background of diffuse alveolitis in the rat lung tissue (Figure 3, panel D), likely related to a bacterial infection. Additional lesions in the rat possibly related to viral infection included mild nonsuppurative periventricular encephalitis in brain tissue (Figure 3, panel E) and myocarditis. Immunohistochemistry for IAV in the cat lung showed apical airway epithelial immunoreactivity (Figure 3, panel A, inset), and brain tissue showed multifocal glial and neuronal immunoreactivity (Figure 3, panel C). We also noted mild periventricular immunoreactivity in neurons in the rat brain (Figure 3, panel F).

Conclusions

We describe a strain of H5N1 that resulted in high mortality in a poultry flock and fatal illness in small mammals on a backyard farm in Illinois, USA. Our results show that extensive systemic H5N1 virus spread occurred in both cat and rat tissues after natural infection. Rat nasal turbinates and trachea preferentially expressed α2,3-linked sialic acid receptors relative to lung, likely explaining the lower Ct values in upper respiratory tissues and presence of bacterial bronchopneumonia, potentially leading to increased viral shedding (*10*).

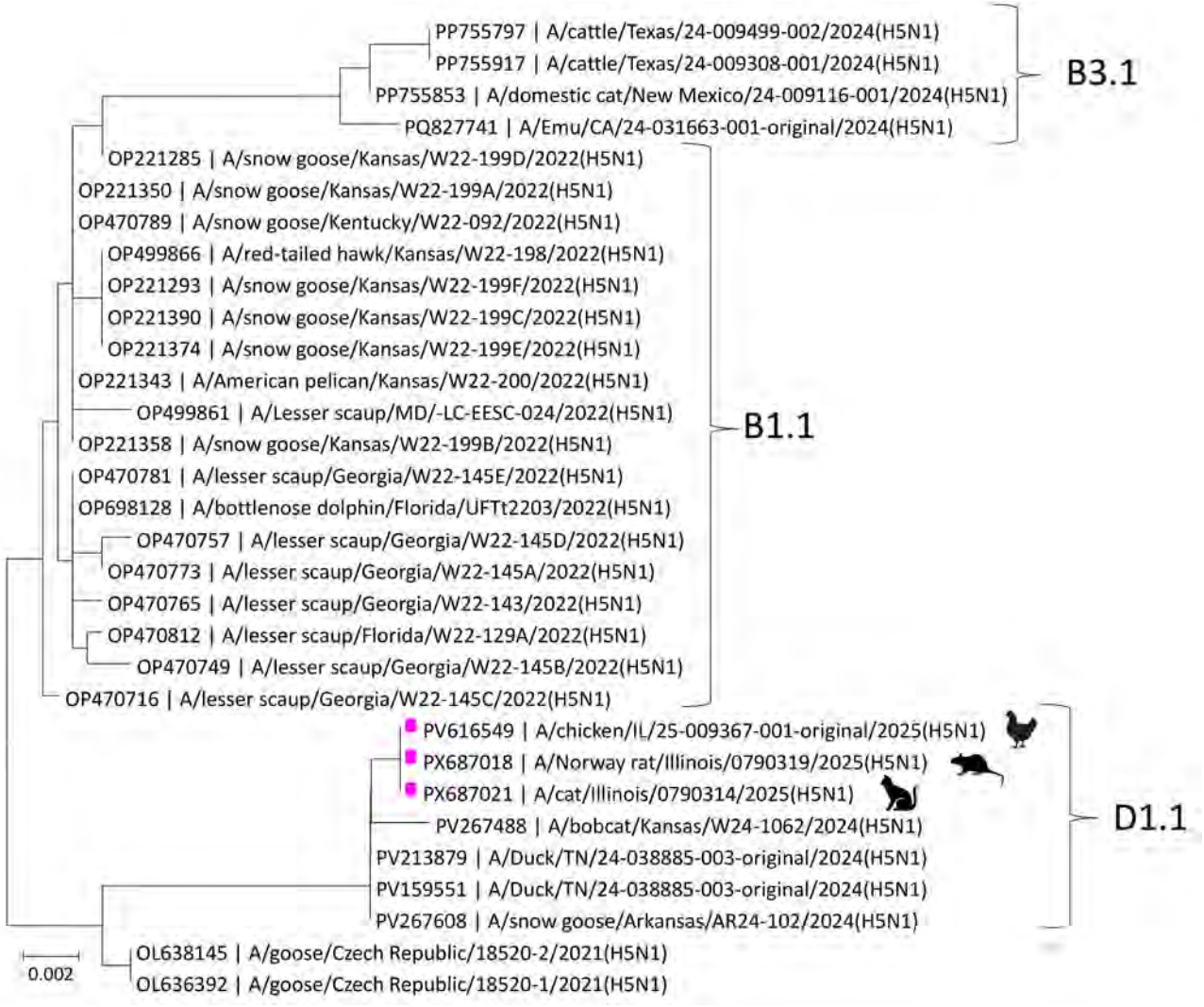

Figure 2. Phylogenetic tree of hemagglutinin gene sequences from highly pathogenic avian influenza A(H5N1) virus in cat and rats during outbreak in backyard poultry, United States, 2025. The cat, rat, and chicken from this study (pink squares) are closely related to other avian strains, as well as an isolate from a bobcat (GenBank accession no. PV267488). GenBank accession numbers are provided. Scale bar indicates nucleotide substitutions per site.

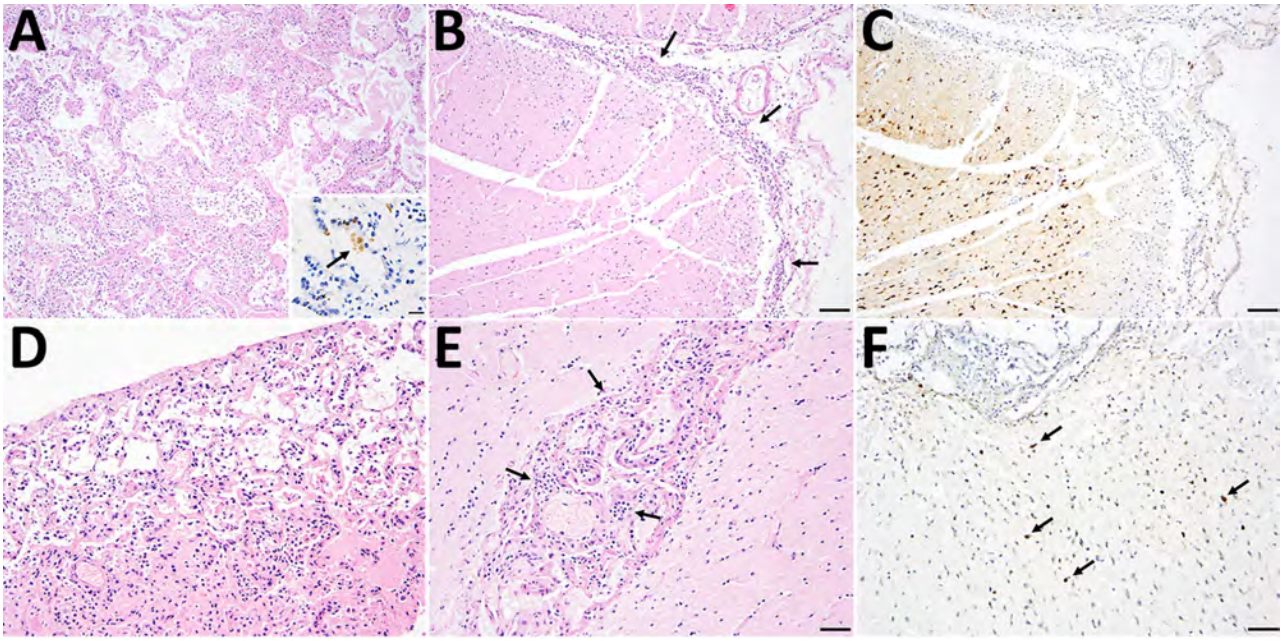

Figure 3. Histopathology and immunohistochemistry of lesions in a cat and rat found dead during outbreak of highly pathogenic avian influenza A(H5N1) virus in backyard poultry, United States, 2025. A–C) Cat samples; D–F) rat samples. A) Hematoxylin and eosin (H&E) stain of feline lung tissue showing bronchointerstitial pneumonia; original magnification ×10. Inset (immunohistochemical [IHC] stain) shows positive immunoreactivity (arrow) of the cytoplasm of apical epithelial cells within distal airways. Scale bar indicates 20 μm. B) H&E stain of feline brain tissue showing nonsuppurative meningoencephalitis (arrows). Scale bar indicates 100 μm. C) IHC stain of feline brain showing strong immunoreactivity in cerebrocortical glial cells and neurons. Scale bar indicates 100 μm. D) H&E stain of rat lung tissue showing background alveolitis. Original magnification ×20. E) H&E stain of rat brain tissue showing nonsuppurative periventricular encephalitis (arrows). Scale bar indicates 50 μm. F) IHC of rat brain tissue showing influenza immunoreactivity in few periventricular neurons (arrows). Scale bar indicates 50 μm.

Cat feces and urine have previously been shown to harbor H5N1 virus (*11*,*12*), which our results corroborate. Rats have previously been reported to harbor HPAIV in agricultural settings and have been detected in the current epizootic (*13*,*14*). Detection of HPAIV in rat urine and kidney tissue suggests that rodent urine could be a potential transmission medium and warrants further investigation. Rats reside on many farms, can predate birds, and might serve as an intermediate step between infected avian species and susceptible mammalian hosts (*15*). That coexistence is particularly threatening for commercial poultry and swine confinement farms, which frequently harbor rodent populations despite strict biosecurity efforts. A limitation of our study was that no virus isolation was performed on tissues or urine due to biosafety constraints.

Although cats have been shown to participate in HPAIV transmission, our findings indicate that further investigation is needed to clarify the role of rodents. This study raises awareness of small mammals at the wildlife–livestock interface and highlights the potential role of rats in influenza transmission to commercial livestock production.

Acknowledgments

We thank Megan Sherman for her contributions regarding immunohistochemical staining and materials information. We also thank the animal owners who allowed further investigation of their animals for this study. We thank NVSL for their confirmatory support for this outbreak.

S.M.S. was partially supported by the Veterinary Services Grant Program from the USDA's National Institute of Food and Agriculture (project award no. 2021-70024-35413).

About the Author

Dr. Storms is a veterinarian-scientist at Texas A&M Veterinary Medical Diagnostic Laboratory, College Station, Texas, USA. Her research interests center around influenza virus transmission and diagnostic development.

References

1. Abolnik C, Phiri T, Peyrot B, de Beer R, Snyman A, Roberts D, et al. The molecular epidemiology of clade 2.3.4.4B H5N1 high pathogenicity avian influenza in Southern Africa, 2021–2022. Viruses. 2023;15:6. https://doi.org/10.3390/v15061383
2. Adlhoch C, Fusaro A, Gonzales JL, Kuiken T, Marangon S, Niqueux É, et al.; European Food Safety Authority, European Centre for Disease Prevention and Control, European Union

Reference Laboratory for Avian Influenza. Avian influenza overview September–December 2022. EFSA J. 2023;21:e07786. https://doi.org/10.2903/j.efsa.2023.7786
3. Lane JV, Jeglinski JWE, Avery-Gomm S, Ballstaedt E, Banyard AC, Barychka T, et al. High pathogenicity avian influenza (H5N1) in northern gannets (Morus bassanus): global spread, clinical signs and demographic consequences. Ibis. 2024;166:633–50. https://doi.org/10.1111/ibi.13275
4. Pohlmann A, King J, Fusaro A, Zecchin B, Banyard AC, Brown IH, et al. Has epizootic become enzootic? Evidence for a fundamental change in the infection dynamics of highly pathogenic avian influenza in Europe, 2021. mBio. 2022;13:e0060922. https://doi.org/10.1128/mbio.00609-22
5. Brüssow H. The arrival of highly pathogenic avian influenza viruses in North America, ensuing epizootics in poultry and dairy farms and difficulties in scientific naming. Microb Biotechnol. 2024;17:e70062. https://doi.org/10.1111/1751-7915.70062
6. Centers for Disease Control and Prevention. A(H5) bird flu: current situation [cited 2026 Apr 27]. https://www.cdc.gov/bird-flu/situation-summary/index.html
7. Hiltemann S, Rasche H, Gladman S, Hotz HR, Larivière D, Blankenberg D, et al.; Galaxy Training Network. Galaxy training: a powerful framework for teaching! PLoS Comput Biol. 2023;19:e1010752. https://doi.org/10.1371/journal.pcbi.1010752
8. Steel J, Lowen AC, Mubareka S, Palese P. Transmission of influenza virus in a mammalian host is increased by PB2 amino acids 627K or 627E/701N. PLoS Pathog. 2009;5:e1000252. https://doi.org/10.1371/journal.ppat.1000252
9. Youk S, Torchetti MK, Lantz K, Lenoch JB, Killian ML, Leyson C, et al. H5N1 highly pathogenic avian influenza clade 2.3.4.4b in wild and domestic birds: introductions into the United States and reassortments, December 2021–April 2022. Virology. 2023;587:109860. https://doi.org/10.1016/j.virol.2023.109860
10. Li L, Chen R, Yan Z, Cai Q, Guan Y, Zhu H. Experimental infection of rats with influenza A viruses: implications for murine rodents in influenza A virus ecology. Viruses. 2025;17:4. https://doi.org/10.3390/v17040495
11. Rimmelzwaan GF, van Riel D, Baars M, Bestebroer TM, van Amerongen G, Fouchier RAM, et al. Influenza A virus (H5N1) infection in cats causes systemic disease with potential novel routes of virus spread within and between hosts. Am J Pathol. 2006;168:176–83, quiz 364. https://doi.org/10.2353/ajpath.2006.050466
12. Frye EA, Nooruzzaman M, Cronk B, Laverack M, de Oliveira PSB, Caserta LC, et al. Isolation of highly pathogenic avian influenza A(H5N1) virus from cat urine after raw milk ingestion, United States. Emerg Infect Dis. 2025;31:1636–9. https://doi.org/10.3201/eid3108.250309
13. Kutkat O, Gomaa M, Moatasim Y, El Taweel A, Kamel MN, El Sayes M, et al. Highly pathogenic avian influenza virus H5N1 clade 2.3.4.4b in wild rats in Egypt during 2023. Emerg Microbes Infect. 2024;13:2396874. https://doi.org/10.1080/22221751.2024.2396874
14. US Department of Agriculture Animal and Plant Inspection Service. HPAI detections in mammals [cited 2026 Apr 27]. https://www.aphis.usda.gov/livestock-poultry-disease/avian/avian-influenza/hpai-detections/mammals
15. Quillfeldt P, Schenk I, McGill RAR, Strange IJ, Masello JF, Gladbach A, et al. Introduced mammals coexist with seabirds at New Island, Falkland Islands: abundance, habitat preferences, and stable isotope analysis of diet. Polar Biol. 2007;31:333–49. https://doi.org/10.1007/s00300-007-0363-2

Address for correspondence: Leyi Wang, University of Illinois, Department of Veterinary Clinical Medicine, 1222A VMBSB, 2001 S Lincoln Ave, Urbana, IL 61802, USA; email: leyiwang@illinois.edu

Chlamydia psittaci Meningitis, Chile, 2023

Yazmin Ivana Pinos Garcia, Cristian Rosas, Josefa Estefania Elmohrez, Jose Vicente Gonzalez, Teresa Tapia, Juan Carlos Hormazabal

We report a confirmed case of *Chlamydia psittaci* meningitis in Latin America, diagnosed in a 50-year-old farm worker from Chile. Diagnosis was established via cerebrospinal fluid quantitative real-time PCR and serology. The patient recovered after antimicrobial treatment. This case highlights the need to consider zoonotic pathogens in atypical meningitis.

Chlamydia psittaci is an obligate intracellular bacterium that causes psittacosis, a zoonotic infection typically transmitted through contact with infected birds, particularly Psittaciformes and poultry (*1*,*2*). In humans, psittacosis typically exhibits constitutional symptoms, including fever, chills, headache, and myalgia (*3*). Although widely associated with respiratory illness, the infection also can affect other organs, including the central nervous system (CNS), resulting in rare but serious manifestations, such as encephalitis and meningitis (*4*). We report a confirmed case of *C. psittaci*–associated meningitis in Latin America supported by molecular testing and serology.

The Case

A 50-year-old male farm worker from Puerto Octay, southern Chile, sought treatment at a rural health center on August 14, 2023, with fever >38°C, myalgia, chills, headache, and painful swallowing. Health center clinicians established a diagnosis of tonsillitis and treated the patient with intramuscular benzathine penicillin. Ten days later, the patient returned with persistent fever and headache and was referred to San José Hospital in Osorno with suspected meningitis. The patient worked as a tractor operator on a dairy farm, where he had occasional direct contact with cattle through participation in calving assistance and milking activities. He reported an increased number of bovine abortions on the farm during the months preceding illness onset. Although he denied direct contact with birds, he reported the presence of wild parrots and domestic chickens on the farm.

At admission, we noted an erythematous pharynx but found the patient to be alert and oriented. Neurologic examination revealed normal cranial nerves, preserved motor function and tone, and no signs of meningeal irritation. Laboratory results revealed leukocytosis (11,400/mm^3, 65% neutrophils), elevated C-reactive protein of 16.8 mg/L (reference value <5 mg/L), and mildly elevated liver enzymes. Cerebrospinal fluid (CSF) was clear and colorless, with 1,033 leukocytes/mm^3 (56% mononuclear, 44% polymorphonuclear), protein 1.21 g/L, and glucose 50.1 mg/dL. We performed Gram stain and multiplex meningitis/encephalitis PCR panel of the CSF that included human parechovirus, adenovirus, cytomegalovirus, human enterovirus, parvovirus B19, Epstein-Barr virus, herpes simplex virus (HSV) 1 and 2, human herpesvirus 6 and 7, mumps virus, varicella-zoster virus, *Escherichia coli* K1, *Streptococcus pneumoniae*, *Hemophilus influenzae*, *Neisseria meningitidis*, *Streptococcus agalactiae*, and *Cryptococcus neoformans*; all tests were negative. HIV serology, cryptococcal antigen testing, and *Toxoplasma gondii* PCR also produced negative results. Cranial computed tomography revealed no abnormalities; magnetic resonance imaging detected white matter hyperintensities in both hemispheres at T2W, FLAIR, and DWI sequences (Figure), which have been described in meningitis caused by other pathogens, such as cytomegalovirus and *S. pneumoniae* (*5*).

We treated the patient empirically with intravenous ceftriaxone, ampicillin, dexamethasone, and

Author affiliations: Universidad Austral de Chile, Facultad de Medicina, Osorno, Chile (Y.I. Pinos Garcia, J.E. Elmohrez); Hospital Base San Jose Osorno, Osorno (Y.I. Pinos Garcia, J.V. Gonzalez); SEREMI de Salud de Los Lagos, Osorno, (C. Rosas); Unidad de Infectología - Unidad de Investigación, Osorno, Chile (J.V. Gonzalez); Institute of Public Health of Chile, Santiago, Chile (T. Tapia, J.C. Hormazabal)

DOI: http://doi.org/10.3201/eid3210.251985

acyclovir. We discontinued acyclovir after CSF PCR testing for HSV-1 and HSV-2 yielded negative results. We tested CSF samples by quantitative real-time PCR for parvovirus B19, *Brucella spp*., *Leptospira spp*., and *C. psittaci*. We tested serum samples serologically for *Coxiella burnetii*, *Brucella spp*., *Leptospira spp*., and *C. psittaci* (Table). We performed all analyses at the national reference laboratory of the Institute of Public Health of Chile (Santiago, Chile).

Quantitative real-time PCR of CSF returned a positive result for *C. psittaci*, as did serologic testing by indirect immunofluorescence assay, with an IgG titer of 1:128 (positive cutoff ≥1:64) and an IgM titer of 1:10 (positive cutoff ≥1:10) (Table). The patient remained stable, without neurologic deficits. Follow-up brain magnetic resonance imaging on August 26, 2023, showed no pathologic findings. The patient completed a 7-day course of intravenous antibiotics followed by 7 days of oral levofloxacin. Outpatient follow-up confirmed full recovery.

Although human psittacosis has been previously reported in Chile, including a confirmed case in 1956, a family cluster in 1984, and a 15-case outbreak in 2021 in southern regions (*6*), none of those cases involved CNS manifestations. Our case expands the geographic recognition of *C. psittaci* meningitis and highlights the need to consider zoonotic pathogens in patients with atypical CNS infections in Latin America.

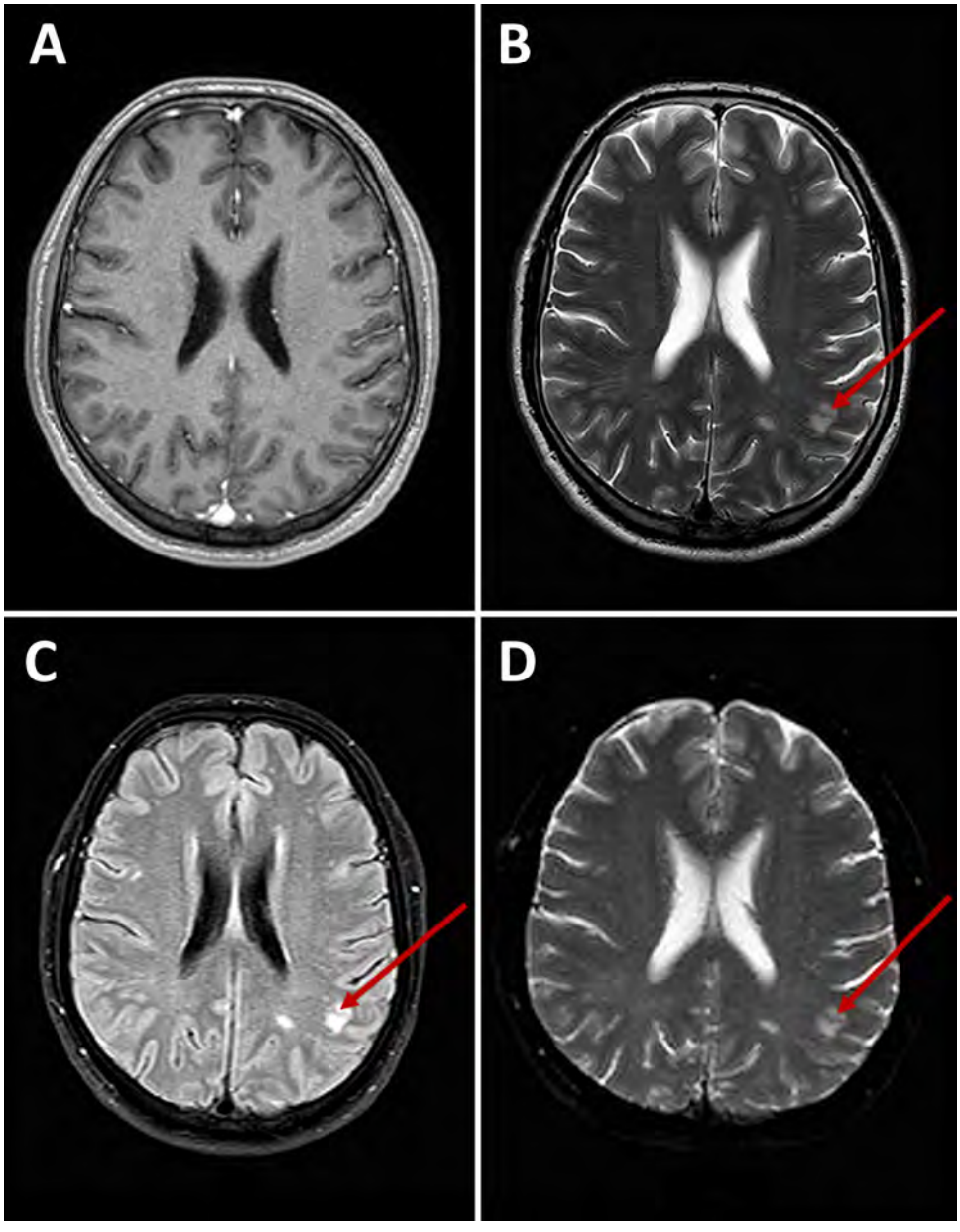

Figure. Axial brain magnetic resonance imaging of a patient with *Chlamydia psittaci* meningitis, Chile, 2023. A) T1-weighted image shows unremarkable appearance. B) T2-weighted image; C) fluid-attenuated inversion recovery image; and D) diffusion-weighted image show bilateral white matter hyperintensities (arrows).

Table. Molecular and serologic diagnostic testing results for a study of *Chlamydia psittaci* meningitis, Chile, 2023*

Pathogen	Specimen	Method	Target or antibody	Result
Parvovirus B19	CSF	qPCR	NS1, VP1	Negative
Multiplex meningitis/encephalitis panel†	CSF	Real-time multiplex PCR assay	Pathogen-specific nucleic acid targets	Negative
Brucella spp.	CSF	qPCR	*bcsp31*, *IS711*	Negative
Leptospira spp.	CSF	qPCR	*lipL32* or 16S; specify	Negative
Chlamydia psittaci	CSF	qPCR	*IncA* and *CPSIT_0607*	Positive
Toxoplasma gondii	CSF	qPCR	*B1*, REP-529	Negative
Coxiella burnetii	Serum	Serology IFA	Phase I and II for IgG, IgM	Negative
Brucella spp.	Serum	Serology ELISA	Rose Bengal, SAT, ELISA; specify	Negative
Leptospira spp.	Serum	Serology ELISA	IgM	Negative
C. psittaci	Serum	Serology IFA	IgG, IgM	Positive IgM and IgG

*Testing performed on CSF and serum samples for routine and zoonotic pathogens. *B1*, 35-fold repetitive B1 gene of *Toxoplasma gondii*; *bcsp31*, 31 kDa *Brucella* immunogenic protein gene; *CPSIT_0607*, DNA sequence gene to *C. psittaci* hypothetical protein; CSF, cerebral spinal fluid; IFA, indirect immunofluorescence assay; *IncA*, inclusion membrane protein A; *IS711*, insertion sequence 711 of *Brucella* genus; *lipL32*, recombinant leptospiral outer membrane protein gene; NS1, nonstructural protein 1; qPCR, quantitative PCR; REP-529, noncoding 529-bp DNA fragment that is repeated 200–300 times; SAT, standard agglutination test; VP1, viral protein 1.
†Allplex Meningitis-V1 and Meningitis-V2 Assays (Seegene Inc., https://www.seegene.com).

Meningitis caused by *C. psittaci* is exceedingly rare. To clarify the spectrum and rarity of CNS infection caused by *C. psittaci*, we conducted a PRISMA 2020 (*7*)–guided systematic review of published cases (Appendix, https://wwwnc.cdc.gov/EID/article/32/10/26-1985-App1.pdf). We identified only 6 previously published cases of molecularly confirmed *C. psittaci* CNS infection worldwide. Because we applied stringent eligibility criteria, requiring molecular confirmation in cerebrospinal fluid or CNS tissue, we excluded most historical reports that were diagnosed solely on the basis of serology or clinical findings (Appendix Table 1), leaving only a small number of well-characterized cases for comparison. According to those reports, clinical manifestations ranged from isolated meningitis to severe encephalitis with status epilepticus or cerebral vasculitis, whereas definitive diagnosis relied almost exclusively on molecular detection in cerebrospinal fluid (Appendix Table 2). Our findings emphasize both the exceptional rarity of confirmed CNS infection and the pivotal role of molecular diagnostics in recognizing this uncommon manifestation. We identified 6 reported cases diagnosed using molecular methods, 1 from the United States (*8*), 4 from China (*9*–*12*), and 1 from Austria (*13*), and compared those with our case from Chile.

Diagnosis of psittacosis is challenging because *C. psittaci* cannot be detected by routine bacterial cultures. Serologic testing is more widely available but often requires paired samples, which might delay confirmation and can have cross-reactivity with other *Chlamydia* species. In contrast, PCR performed on specimens collected early in the course of illness provides the highest sensitivity and specificity (*14*,*15*). Metagenomic sequencing could be a complementary diagnostic tool for characterizing *C. psittaci* CNS infections, although its availability remains limited in many clinical settings. Diagnosis in this case was difficult because of nonspecific clinical findings and the absence of classic meningeal signs. Standard CSF panels and cultures were negative, highlighting the need for molecular testing and serologic investigation in patients with a compatible exposure history and negative routine workups.

Conclusion

Our case reinforces the need to consider zoonotic pathogens in rural and agricultural populations, particularly in Latin America, where psittacosis is underdiagnosed and potentially underreported. The favorable outcome also suggests that early empirical treatment with broad-spectrum antimicrobials, followed by targeted therapy, can be an effective approach. Doxycycline is the preferred antimicrobial agent for treating psittacosis (*3*,*4*), and 21-day duration is preferred in CNS involvement (*9*). Our case also highlights the diagnostic value of integrating epidemiologic history with molecular testing in evaluating atypical meningitis and emphasizes the importance of considering *C. psittaci* as a cause of CNS infection.

Acknowledgments

We thank the clinical and laboratory teams at San Jose Hospital in Osorno and the Institute of Public Health of Chile for their contributions.

This publication was approved by the ethics committee of the Los Ríos Health Service of Chile. Written informed consent for publication was obtained from the patient. All authors have read and provided consent to publish the current version of the manuscript.

About the Author

Dr. Pinos Garcia is an infectious diseases specialist at San Jose Hospital in Osorno, southern Chile. Her areas of interest include zoonoses, emerging infections, and One Health.

References

1. Beeckman DS, Vanrompay DC. Zoonotic *Chlamydophila psittaci* infections from a clinical perspective. Clin Microbiol Infect. 2009;15:11–7. https://doi.org/10.1111/j.1469-0691.2008.02669.x
2. Ravichandran K, Anbazhagan S, Karthik K, Angappan M, Dhayananth B. A comprehensive review on avian chlamydiosis: a neglected zoonotic disease. Trop Anim Health Prod. 2021;53:414. https://doi.org/10.1007/s11250-021-02859-0
3. Ni Y, Zhong H, Gu Y, Liu L, Zhang Q, Wang L, et al. Clinical features, treatment, and outcome of psittacosis pneumonia: a multicenter study. Open Forum Infect Dis. 2023;10:ofac518. https://doi.org/10.1093/ofid/ofac518
4. Centers for Disease Control and Prevention. Psittacosis: clinical guidance [cited 2025 Nov 15]. https://www.cdc.gov/pneumonia/atypical/psittacosis.html
5. Perillo T, Capasso R, Pinto A. Neuroimaging of the most common meningitis and encephalitis of adults: a narrative review. Diagnostics (Basel). 2024;14:1064. https://doi.org/10.3390/diagnostics14111064
6. Ministerio de Salud de Chile. Psitacosis: epidemiological situation [in Spanish] [cited 2025 Nov 15]. https://epi.minsal.cl/psitacosis-situacion-epidemiologica
7. Page MJ, McKenzie JE, Bossuyt PM, Boutron I, Hoffmann TC, Mulrow CD, et al. The PRISMA 2020 statement: an updated guideline for reporting systematic reviews. BMJ. 2021;372:n71. https://doi.org/10.1136/bmj.n71
8. Davar K, Wilson MR, Miller S, Chiu CY, Vijayan T. A rare bird: diagnosis of psittacosis meningitis by clinical metagenomic next-generation sequencing. Open Forum Infect Dis. 2021;8:ofab555. https://doi.org/10.1093/ofid/ofab555
9. Shi Y, Chen J, Shi X, Hu J, Li H, Li X, et al. A case of *Chlamydia psittaci* caused severe pneumonia and meningitis diagnosed by metagenome next-generation sequencing and clinical analysis: a case report and literature review. BMC Infect Dis. 2021;21:621. https://doi.org/10.1186/s12879-021-06205-5
10. Yin XW, Mao ZD, Zhang Q, Ou QX, Liu J, Shao Y, et al. Clinical metagenomic sequencing for rapid diagnosis of pneumonia and meningitis caused by *Chlamydia psittaci*. World J Clin Cases. 2021;9:7693–703. https://doi.org/10.12998/wjcc.v9.i26.7693
11. Zhao C, Liu Y, Li J. Radiological features of encephalitis of chlamydia psittaci. Neurol India. 2026;74:378–9. https://doi.org/10.4103/neurol-india.Neurol-India-D-25-00440
12. Zhang W, Zhang S, Huang X, Dai L, Gao Y, Cao H, et al. A case of *Chlamydophila psittaci* caused pneumonia and encephalitis diagnosed by metagenome next-generation sequencing and clinical analysis. Jundishapur J Microbiol. 2024;17:e144399. https://doi.org/10.5812/jjm-144399
13. Walder G, Schönherr H, Hotzel H, Speth C, Oehme A, Dierich MP, et al. Presence of *Chlamydophila psittaci* DNA in the central nervous system of a patient with status epilepticus. Scand J Infect Dis. 2003;35:71–3. https://doi.org/10.1080/0036554021000026984
14. Xu L, Zhang C, Shi W, Ma J, Wang G. Current status and challenges in the diagnosis and treatment of psittacosis. Infect Dis Immun. 2025. https://doi.org/10.1097/ID9.0000000000000199
15. Nieuwenhuizen AA, Dijkstra F, Notermans DW, van der Hoek W. Laboratory methods for case finding in human psittacosis outbreaks: a systematic review. BMC Infect Dis. 2018;18:442. https://doi.org/10.1186/s12879-018-3317-0

Address for correspondence: Yazmin Pinos Garcia, Hospital Base San Jose Osorno - Internal Medicine - Infectious Diseases, Guillermo Bühler 1765, Osorno 5290000, Chile; email: yazmin.pinos@gmail.com

Baloxavir-Based Combination Therapy for Protection against Influenza A(H5N1) Clade 2.3.4.4b Virus Infection in Mice

Seong Cheol Min, Ju Ryeong Lee, Beom Kyu Kim, Ji-Hyun Park, Dong Gyu Lee, Gi Chan Lee, Se Hee An, Santosh Chokkakula, Aman Jain, Young Ki Choi, Yun Hee Baek, Min-Suk Song

Highly pathogenic avian influenza A(H5N1) clade 2.3.4.4b virus continues to cause animal outbreaks and sporadic zoonotic infections. In a mouse model of lethal influenza disease, we compared oseltamivir, baloxavir, and molnupiravir monotherapies with 2-drug combinations. Baloxavir-based combinations improved survival, reduced lung viral loads, and prevented extrapulmonary dissemination, supporting H5N1 preparedness strategies.

Highly pathogenic avian influenza A(H5N1) clade 2.3.4.4b virus continues to cause widespread outbreaks and sporadic zoonotic infections, underscoring the need to optimize antiviral strategies (*1*–*3*). Licensed influenza antiviral drugs can reduce disease severity but might be compromised in severe infections by high viral burdens, treatment delays, and treatment-emergent resistance, motivating evaluation of combination regimens (*4*–*7*). Recent H5N1 treatment studies using mouse models suggest antiviral performance can vary by exposure route and disease progression (*8*–*11*). To inform preparedness-oriented selection, we compared direct-acting antiviral drugs from distinct classes in a lethal mouse model. We tested monotherapies and 2-drug combinations of 2 licensed influenza antiviral agents, oseltamivir phosphate (OSP; neuraminidase inhibitor) and baloxavir acid (BXA; cap-dependent endonuclease inhibitor), and molnupiravir (MPV; nucleoside analog) to assess whether combinations provided synergistic benefit.

Author affiliations: Chungbuk National University College of Medicine, Chungbuk, South Korea (S.C. Min, J.R. Lee, B.K. Kim, J.-H. Park, D.G. Lee, G.C. Lee, S.H. An, S. Chokkakula, A. Jain, Y.H. Baek, M.-S. Song); Korea Virus Research Institute Yuseong-gu, Daejeon, South Korea (Y.K. Choi)

DOI: http://doi.org/10.3201/eid3210.260186

The Study

We challenged 6- to 8-week-old female BALB/c mice intranasally with A/mink/Spain/3691-8_22VIR10586-10/2022 (5 LD_{50} [50% median lethal dose]) in a 50-μL inoculum (90 $TCID_{50}$ [50% tissue culture infectious dose]) (Appendix, https://wwwnc.cdc.gov/EID/article/32/10/26-0186-App1.pdf). We treated mice at 6 hours postinfection (hpi). We administered OSP and MPV orally twice daily for 5 days and administered BXA once subcutaneously. For the low-dose comparison, mice received OSP 25 mg/kg, MPV 25 mg/kg, or BXA 20 mg/kg, and corresponding 2-drug pairs at the same dosages: OSP/MPV, BXA/OSP, BXA/MPV. We monitored body weight and survival through 18 days postinfection (dpi) (n = 7) and quantified infectious virus titers in lung, brain, and heart by $TCID_{50}$ assay at 4 and 6 dpi (n = 3/time point) (Figure 1; Appendix Tables 1–5).

Vehicle-treated mice exhibited rapid weight loss and uniform death. In monotherapy low-dose treatments, OSP or MPV conferred partial protection (2/7 survival each), whereas BXA administered as a single dose was more protective (4/7 survival) and more consistently limited weight loss (Figure 1, panels A–F). Dose-escalation to 50 mg/kg monotherapies also improved outcomes but did not provide 100% protection (Appendix Figures 2, 3), consistent with prior reports showing therapeutic benefit of antiviral drugs in H5N1 mouse infection models (*8*–*11*). Accordingly, we evaluated 2-drug regimens in which BXA was maintained at 20 mg/kg and partnered with OSP or MPV at either 25 or 50 mg/kg. Across

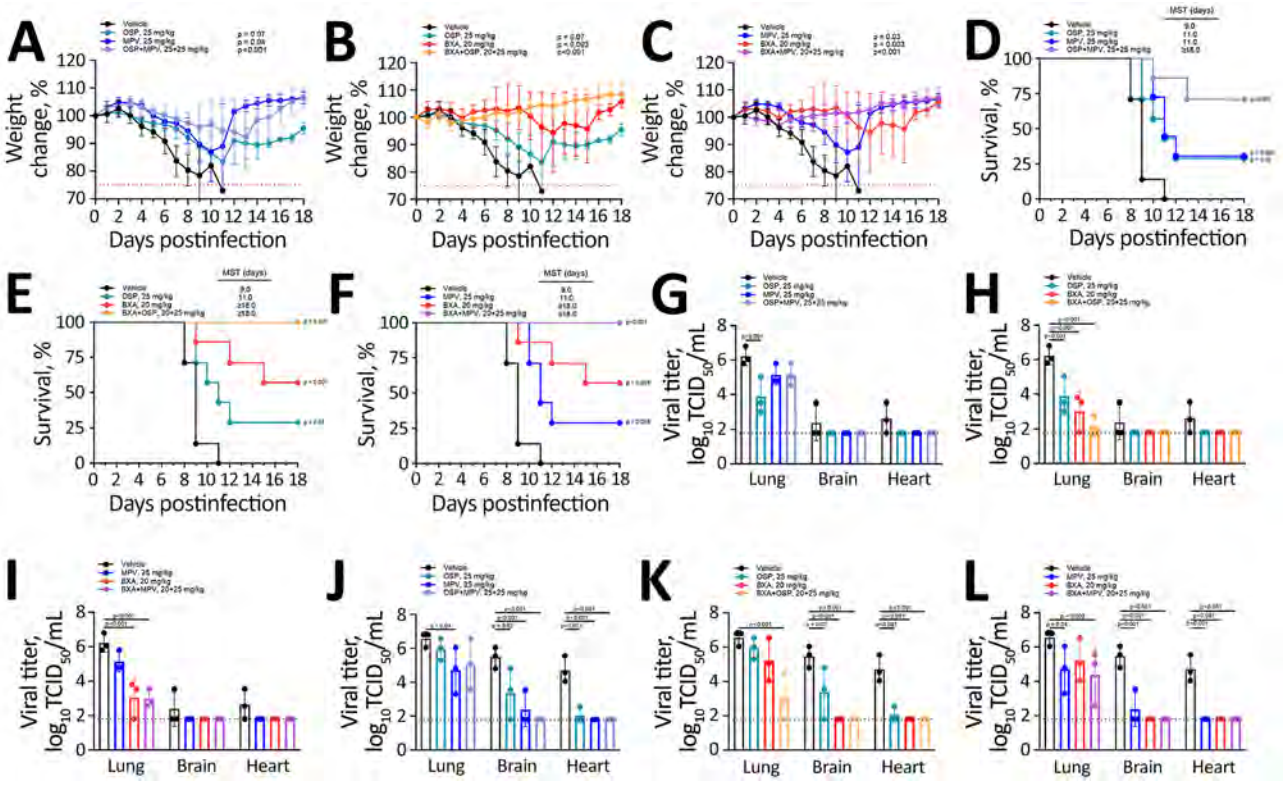

Figure 1. Therapeutic efficacy of baloxavir-based combinations and monotherapies for treating influenza A(H5N1) clade 2.3.4.4b virus infection in mice. Drug names and doses are provided in the keys (e.g., BXA+MPV 20+25 mg/kg indicates BXA/MPV at a dose of 20/25 mg/kg). A–C) Body weight change (mean ±SD; n = 7/group) through 18 days postinfection: vehicle, MPV 25 mg/kg, OSP 25 mg/kg, and OSP/MPV 25/25 mg/kg (A); vehicle, OSP 25 mg/kg, BXA 20 mg/kg, and BXA/OSP 20/25 mg/kg (B); vehicle, MPV 25 mg/kg, BXA 20 mg/kg, and BXA/MPV 20/25 mg/kg (C). Symbols represent group means; error bars indicate SDs. Red dotted horizontal line indicates the humane endpoint threshold. D–F) Kaplan–Meier survival (n = 7/group) corresponding to panels A–C; MST values shown in each panel. G–I) Viral titers in lung, brain, and heart at 4 days postinfection (n = 3/group). J–L) Viral titers at 6 dpi (n = 3/group). Bars show group means with individual animals overlaid; dashed line denotes assay limit of detection (1.801 $\log_{10}$ $TCID_{50}$/mL). BXA, baloxavir acid; MPV, molnupiravir; MST, median survival time; OSP, oseltamivir phosphate; SD, standard deviation; $TCID_{50}$, 50% tissue culture infectious dose.

all three 2-drug regimens—OSP/MPV (25/25 mg/kg and 50/50 mg/kg), BXA/OSP (20/25 mg/kg and 20/50 mg/kg), and BXA/MPV (20/25 mg/kg and 20/50 mg/kg)—combination treatment stabilized body weight and markedly improved survival relative to the corresponding monotherapies (Figure 1, panels A–F; Appendix Figure 3). BXA-containing combinations showed the greatest protection, and no deaths (7/7 survival) occurred through 18 dpi at both dose pairs, whereas OSP/MPV did not show complete protection (Figure 1, panels A–F; Appendix Figure 3). Bliss-independence analysis (*12*) of end-of-study survival (18 dpi; n = 7/group) showed positive ΔBliss estimates for BXA-containing combinations, most clearly at the 20/25 mg/kg dose pairs. At the 20/50 mg/kg dose pairs, ΔBliss values remained positive but were smaller, consistent with an attenuated interaction at higher antiviral exposure. OSP/MPV showed a weaker, dose-dependent interaction (Appendix Table 6).

We observed that clinical benefit paralleled tissue-level virologic control and prevention of extrapulmonary dissemination (Figure 1, panels G–L). At 4 dpi, monotherapy with BXA and OSP, but not MPV, reduced lung titers; brain and heart titers were near or below the limit of detection (LOD), consistent with limited dissemination at that timepoint. By 6 dpi, vehicle-treated mice showed high lung viral loads accompanied by detectable virus in brain and heart. In treated animals, BXA provided the most consistent tissue-level control, keeping viral titers in brain and heart at the LOD; 25 mg/kg OSP or MPV permitted occasional instances of replication in the brain.

Combination therapy further inhibited residual dissemination. At 4 dpi, lung titers in combination groups frequently approached the LOD, most prominently for BXA-containing pairs, whereas brain and heart remained at or near the LOD. By 6 dpi, low lung titers were sustained, and systemic spread was largely abolished in BXA-containing

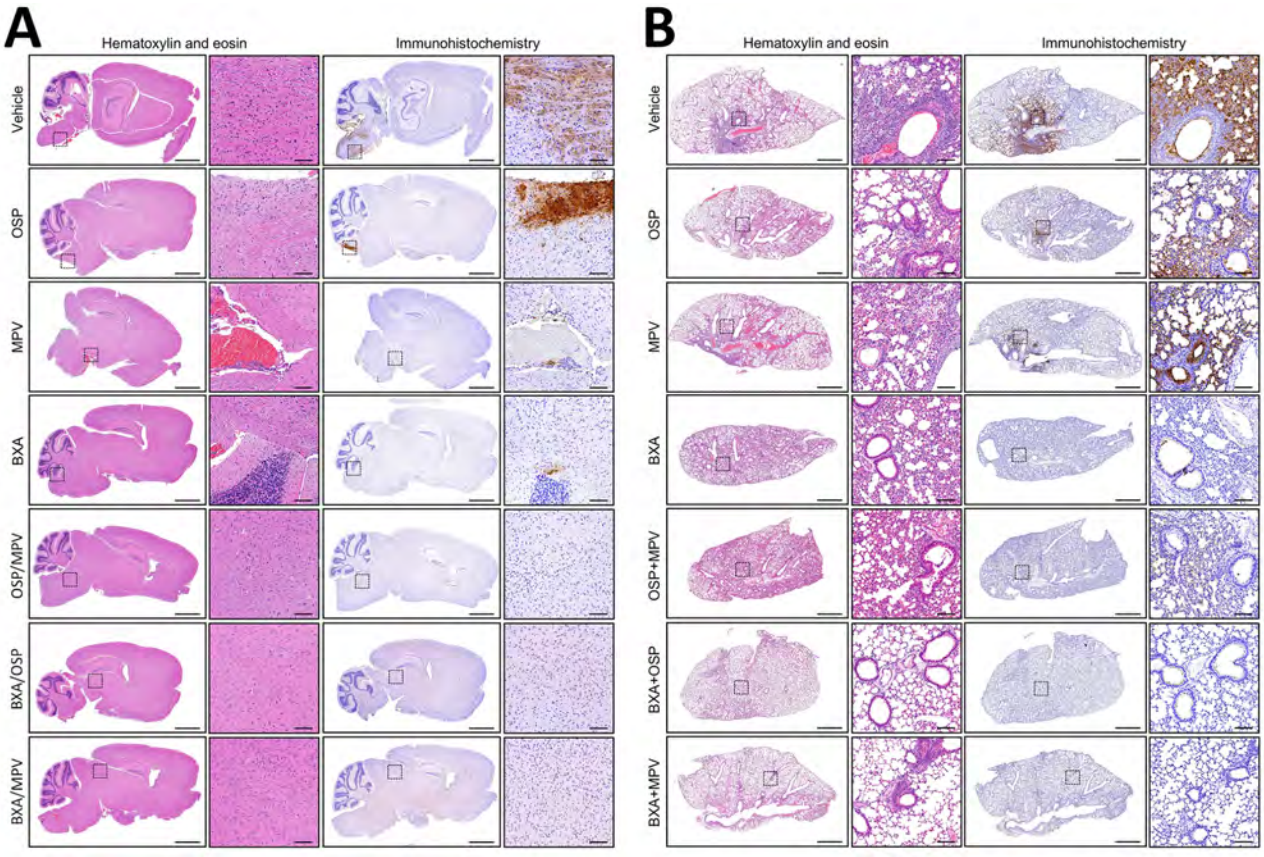

Figure 2. Lung and brain histopathology and influenza A nucleoprotein immunoreactivity at 6 dpi after monotherapy or combination therapy in a study of treating influenza A(H5N1) clade 2.3.4.4b virus infection in mice. A) Brain sections; B) lung sections. Sections from vehicle, OSP, MPV, BXA, OSP/MPV, BXA/OSP, and BXA/MPV groups. For each group, representative hematoxylin and eosin images (left) and immunohistochemistry for influenza A nucleoprotein (right; 3,3′-diaminobenzidine with hematoxylin counterstain) are shown as whole-section views with corresponding higher-magnification insets (boxed regions). Scale bars indicate 1.25 mm for whole-section views; and 100 μm for higher-magnification insets. BXA, baloxavir acid; MPV, molnupiravir; OSP, oseltamivir phosphate.

groups. In contrast, OSP/MPV combinations showed comparatively weaker lung viral clearance and survival benefit. Nevertheless, those combinations converted partial clinical protection into near-complete or complete survival, reduced pulmonary titers, and prevented neuroinvasion and detectable heart virus that were still observed under some monotherapy conditions.

We conducted histopathology and immunohistochemistry and transcriptomic profiling of lung and brain at 6 dpi (n = 3/group) (Figures 2–4). In representative sections, vehicle-treated mice showed prominent influenza nucleoprotein immunoreactivity in both lung and brain (Figure 2), consistent with extensive tissue antigen burden during lethal infection (Figure 1). Across monotherapy groups, nucleoprotein staining and associated tissue involvement appeared reduced but remained detectable. However, combination therapy showed markedly diminished to near-absent nucleoprotein signal in both organs, most consistently the BXA-containing pairs, supporting a tissue-level correlate for the observed improved survival and restricted dissemination. Concordantly, RNA sequencing at 6 dpi demonstrated treatment-associated clustering of transcriptomic profiles by principal component analysis, showing separation between vehicle-treated and antiviral-treated groups. BXA-containing combinations showed tighter clustering than monotherapies in both lung and brain, consistent with a more uniform host transcriptional response under the most protective regimens (Figure 3, panel A; Figure 4, panel A). Pathway analysis identified differential enrichment of host innate immune, inflammatory, and neuronal/synaptic pathways within both tissues. Combination therapies, particularly BXA-containing regimens, showed reduced enrichment of pathways relevant to type II interferon, innate immune response, and inflammatory response compared with monotherapies. Of note,

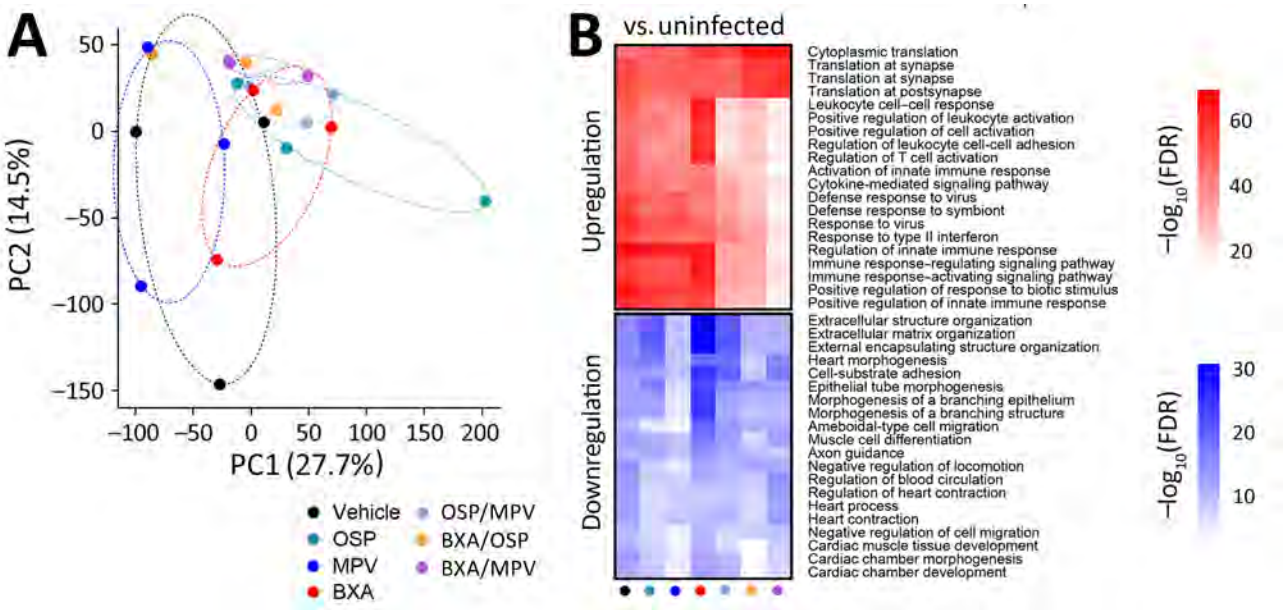

Figure 3. Lung transcriptomic responses at 6 days postinfection in comparison of baloxavir-based combinations and monotherapies for treating influenza A(H5N1) clade 2.3.4.4b virus infection in mice. Responses show treatment-associated separation and attenuation of infection-associated pathway perturbations under combination therapy. RNA sequencing performed on lung harvested at 6 days postinfection from the same experimental groups as Figure 1 (n = 3/group). A) Principal component analysis of transcriptomic profiles for lung; each point represents an individual mouse, and ellipses denote within-group dispersion. Percent variance explained by PC1 and PC2 indicated on axes. B) Pathway enrichment results comparing each infected treatment group versus uninfected controls for lung, displayed as heatmaps for representative upregulated and downregulated biologic pathways. Color intensity represents $-\log_{10}$ (false discovery rate) for enriched terms. BXA, baloxavir acid; FDR, false discovery rate; MPV, molnupiravir; OSP, oseltamivir phosphate.

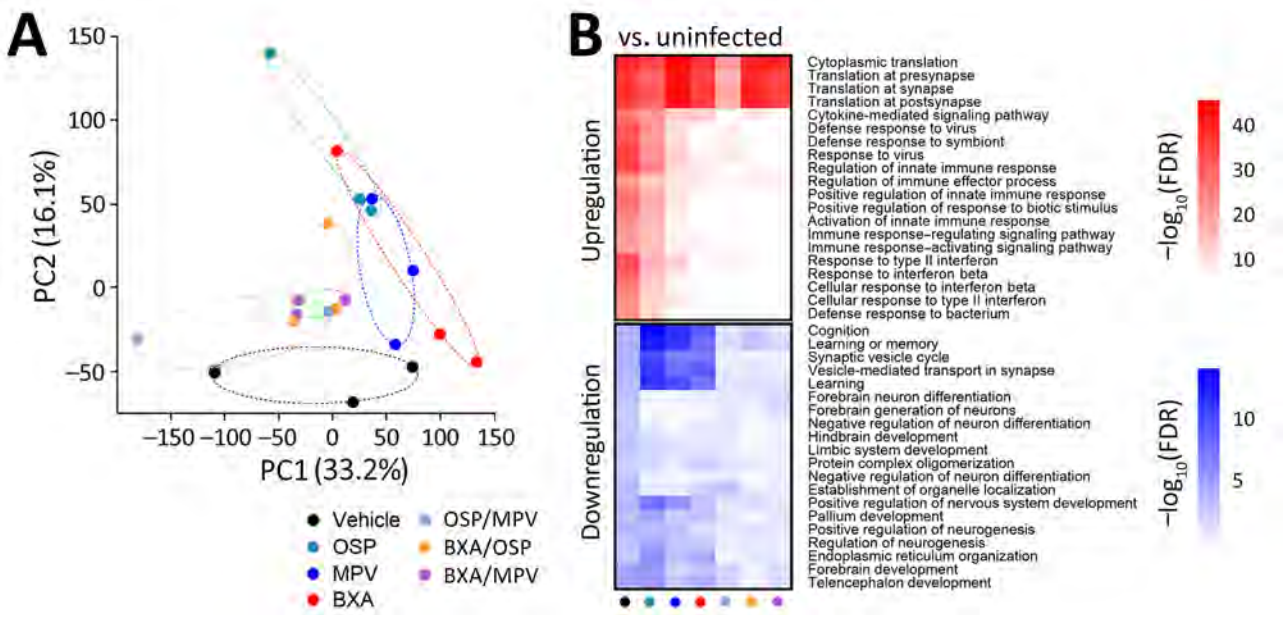

Figure 4. Brain transcriptomic responses in comparison of baloxavir-based combinations and monotherapies for treating influenza A(H5N1) clade 2.3.4.4b virus infection in mice. Response at 6 days postinfection show treatment-associated separation and attenuation of infection-associated pathway perturbations under combination therapy. RNA sequencing performed on brain harvested at 6 days postinfection from same experimental groups as Figure 1 (n = 3/group). A) Principal component analysis of transcriptomic profiles for brain; each point represents an individual mouse, and ellipses denote within-group dispersion. Percent variance explained by PC1 and PC2 indicated on axes. B) Pathway enrichment results comparing each infected treatment group versus uninfected controls for brain, displayed as heatmaps for representative upregulated and downregulated biologic pathways. Color intensity represents $-\log_{10}$ (false discovery rate) for enriched terms. BXA, baloxavir acid; FDR, false discovery rate; MPV, molnupiravir; OSP, oseltamivir phosphate.

those combinations showed relative preservation of neuronal and synaptic pathways, such as cognition, memory, and vesicle-mediated transport, and profiles shifted closer to uninfected controls (Figure 3, panel B; Figure 4, panel B).

Limitations of our investigation included early treatment initiation (6 hpi), modest sample sizes for tissue titration, and the use of MPV, which is not licensed for influenza (*13*). Exploratory single nucleotide polymorphism analysis of 6-dpi lung viral RNA did not identify canonical PA-I38 or NA-H275Y substitutions in antiviral-treated groups; however, we did not perform targeted deep sequencing and phenotypic susceptibility testing. Because we did not evaluate delayed treatment at 24 or 48 hpi, further studies are needed to determine whether BXA-based combinations retain efficacy when initiated later after infection. Nonetheless, the consistency of BXA-containing combination benefit across dosing regimens (Figure 1; Appendix Figure 3) and across endpoints (clinical course, survival, and tissue infectious virus) supports further evaluation in settings closer to clinical use, including delayed initiation, additional clade 2.3.4.4b isolates, and transmission-relevant models.

Conclusions

In a lethal clade 2.3.4.4b H5N1 mouse model, monotherapies with OSP, MPV, or BXA improved outcomes in a dose-dependent manner but did not consistently prevent death or extrapulmonary spread. In contrast, 2-drug combinations, particularly those containing BXA, achieved complete survival at both dosing regimens and suppressed pulmonary replication to near LOD while preventing neuroinvasion and cardiac dissemination. Those findings are consistent with recent clade 2.3.4.4b A(H5N1) studies showing strong in vivo activity of BXA and BXA-containing regimens and extend those observations by directly comparing BXA/OSP and BXA/MPV with OSP/MPV in a lethal mouse model (*8*,*10*,*11*,*14*). Our findings extend recent antiviral-combination studies in less virulent influenza models by showing that BXA-containing combinations provided the strongest protection in a lethal clade 2.3.4.4b H5N1 model (*14*,*15*). Together, our findings provide an experimentally grounded rationale to prioritize BXA-based 2-drug regimens as a preparedness-oriented option for emergent H5N1 infections when antiviral treatment is initiated early after infection, particularly where severe disease or resistance risk can compromise single-agent performance.

Acknowledgments

We gratefully acknowledge all data contributors, including the authors and their originating and submitting laboratories who generated and shared the sequence data for A/mink/Spain/3691-8_22VIR10586-10/2022 through GISAID, on which part of this study was based.

This work was supported by the National Research Foundation of Korea grant funded by the Korea government (Ministry of Science and Information and Communication Technology [MSIT]) (RS-2021-NR059195 to M.-S.S., RS-2020-NR049557 to M.-S.S., and RS-2025-16072074 to Y.H.B.) and Institute for Basic Science (IBS-R801-D1) funded by the National Research Foundation of Korea grant.

We used ChatGPT (OpenAI, https://chatgpt.com) to assist with language editing and clarity. All content was reviewed and approved by the authors, who take full responsibility for the accuracy and originality of the manuscript.

About the Author

Mr. Min is a PhD candidate in the Chungbuk National University College of Medicine, CheongJu, South Korea. His research focuses on virology, antiviral therapeutics, and vaccine development for emerging infectious diseases.

References

1. Webby RJ, Uyeki TM. An update on highly pathogenic avian influenza A(H5N1) virus, clade 2.3.4.4b. J Infect Dis. 2024;230:533–42. https://doi.org/10.1093/infdis/jiae379
2. Elsmo EJ, Wünschmann A, Beckmen KB, Broughton-Neiswanger LE, Buckles EL, Ellis J, et al. Highly pathogenic avian influenza A(H5N1) virus clade 2.3.4.4b infections in wild terrestrial mammals, United States, 2022. Emerg Infect Dis. 2023;29:2451–60. https://doi.org/10.3201/eid2912.230464
3. Agüero M, Monne I, Sánchez A, Zecchin B, Fusaro A, Ruano MJ, et al. Highly pathogenic avian influenza A(H5N1) virus infection in farmed minks, Spain, October 2022. Euro Surveill. 2023;28:2300001. https://doi.org/10.2807/1560-7917.ES.2023.28.3.2300001
4. Belser JA. A pandemic toolbox for clade 2.3.4.4b A(H5N1) influenza virus risk assessment. Lancet Microbe. 2026;7:101240. https://doi.org/10.1016/j.lanmic.2025.101240
5. Samson M, Pizzorno A, Abed Y, Boivin G. Influenza virus resistance to neuraminidase inhibitors. Antiviral Res. 2013;98:174–85. https://doi.org/10.1016/j.antiviral.2013.03.014
6. Omoto S, Speranzini V, Hashimoto T, Noshi T, Yamaguchi H, Kawai M, et al. Characterization of influenza virus variants induced by treatment with the endonuclease inhibitor baloxavir marboxil. Sci Rep. 2018;8:9633. https://doi.org/10.1038/s41598-018-27890-4
7. Gubareva LV, Fry AM. Baloxavir and treatment-emergent resistance: public health insights and next steps. J Infect Dis. 2020;221:337–9.
8. Jones JC, Andreev K, Fabrizio TP, Bowman AS, Govorkova EA, Webby RJ. Baloxavir improves disease

outcomes in mice after intranasal or ocular infection with influenza A virus H5N1-contaminated cow's milk. Nat Microbiol. 2025;10:836–40. https://doi.org/10.1038/s41564-025-01961-5
9. Pascua PNQ, Chesnokov AP, Nguyen HT, Champion C, Gao R, De La Cruz JA, et al. Antiviral susceptibility of clade 2.3.4.4b highly pathogenic avian influenza A(H5N1) viruses from humans in the United States, October 2024 to February 2025. Emerg Microbes Infect. 2026;15:2601372. https://doi.org/10.1080/22221751.2025.2601372
10. Gu C, Maemura T, Guan L, Eisfeld AJ, Biswas A, Kiso M, et al. A human isolate of bovine H5N1 is transmissible and lethal in animal models. Nature. 2024;636:711–8. https://doi.org/10.1038/s41586-024-08254-7
11. Andreev K, Jones JC, Kandeil A, Vogel P, Webby RJ, Govorkova EA. Baloxavir outperforms oseltamivir, favipiravir, and amantadine in treating lethal influenza A(H5N1) HA clade 2.3.4.4b infection in mice. Nat Commun. 2026;17:2937. https://doi.org/10.1038/s41467-026-69721-5
12. Bliss CI. The toxicity of poisons applied jointly. Ann Appl Biol. 1939;26:585–615. https://doi.org/10.1111/j.1744-7348.1939.tb06990.x
13. US Food and Drug Administration. Fact sheet for healthcare providers: Emergency Use Authorization for Lagevrio™ (molnupiravir) capsules. Revised 2024 Jun [cited 2026 Jan 25]. https://www.fda.gov
14. Liu D, Fan Y, Leung K-Y, Zhang R, Lam H-Y, Xie X, et al. Antiviral activities of multiple antivirals against highly pathogenic avian influenza A H5N1 in vitro and in mice. Emerg Microbes Infect. 2026;15:2645843. https://doi.org/10.1080/22221751.2026.2645843
15. Feng X, Yang X, Hu X, Liu Q, Ding Y, Cao X, et al. The combinatorial activities of oseltamivir and molnupiravir against influenza virus infections in vitro and in vivo. Virology. 2025;611:110642. https://doi.org/10.1016/j.virol.2025.110642

Address for correspondence: Min-Suk Song, Department of Microbiology, Chungbuk National University College of Medicine, 1 Chungdae-ro, Seowon-gu, Cheongju-si, Chungcheongbuk-do, 28644, South Korea; email: songminsuk@chungbuk.ac.kr

Emergence of Genotype 2.3.1 Multidrug-Resistant *Salmonella enterica* Serovar Typhi Strain, West Africa, 2021–2025

Elisabeth Njamkepo, Maria Pardos de la Gandara, Carolina Silva Nodari, Alexandra Moura, François-Xavier Weill

Since 2021, a genotype 2.3.1, ciprofloxacin-resistant, multidrug-resistant (MDR) *Salmonella enterica* serovar Typhi strain increasingly has been detected in persons returning from West Africa. This strain locally acquired 2 different MDR plasmids over a ≈25-year period, underwent chromosomal integration of the IncHI1 plasmid MDR region, and finally acquired a *gyrA* mutation.

Salmonella enterica serovar Typhi is a human-restricted pathogen causing typhoid fever through fecally contaminated food or water (*1*). In 2021, an estimated 7.1 million typhoid fever cases caused 93,300 deaths worldwide (*2*). Sporadic antimicrobial resistance (AMR) was first detected in *Salmonella* Typhi in the 1950s, followed by epidemic multidrug-resistant (MDR) populations in the Americas and South/Southeast Asia during the 1970s–1980s. Those populations initially displayed resistance to chloramphenicol, streptomycin, tetracycline, and sulfonamides and then became resistant to ampicillin and cotrimoxazole, after the acquisition of large IncHI1 plasmids (*3*–*7*). One such MDR population, H58 (*3*), now genotype 4.3.1 (*8*), emerged in South Asia in the late 1980s and spread across Southeast Asia, Oceania, and East Africa (*9*,*10*). This H58 lineage first acquired an IncHI1 MDR plasmid (belonging to plasmid multilocus sequence type [pST] 6), followed by, during the 1990s, a point mutation in the chromosomal DNA gyrase gene, *gyrA* (often *gyrA*_S83F), which confers resistance to nalidixic acid (NAL^R) and has decreased susceptibility to ciprofloxacin (now categorized as resistant to ciprofloxacin [CIP^R] according to established guidelines (Appendix 1, https://wwwnc.cdc.gov/EID/article/32/10/26-0813-App1.pdf). The MDR region initially located on the IncHI1 plasmid became stably integrated into the bacterial chromosome over time in lineage H58, and the IncHI1 plasmid was lost (*9*). This lineage subsequently became extensively drug-resistant after the acquisition of a new IncY plasmid carrying the extended-spectrum β-lactamase $bla_{CTX\text{-}M\text{-}15}$ gene in Pakistan in 2016 (*11*).

In the 2000s, MDR *Salmonella* Typhi strains of non–4.3.1 genotypes emerged in West and Central Africa. In West Africa and neighboring Cameroon, the MDR genotypes were 3.1.1 (corresponding to haplotypes H56 and H42 [*3*] or cluster A [*12*]) and 2.3.1 (corresponding to H77 [*3*] or cluster C [*12*]). Both genotypes had predominantly acquired MDR plasmids of incompatibility group IncHI1 (pST2 with *dfrA15* as the class 1 integron gene cassette for 3.1.1 isolates and pST2 with *dfrA1-aadA1* for 2.3.1 isolates) (*12*,*13*). IncY plasmids in genotype 3.1.1 isolates and IncN (pST3) plasmids in 2.3.1 isolates were less frequent (*13*,*14*). Quinolone resistance was initially rare in these MDR genotypes; only 6 (4.7%) NAL^R isolates (all genotype 3.1.1) were found among 128 *Salmonella* Typhi isolates that were collected in Nigeria during 2008–2013 (*13*). However, a recent study showed that the proportion of genotype 3.1.1 NAL^R isolates reached >75% in Nigeria after 2015 (*15*). A similar trend has not been documented for genotype 2.3.1.

In France, enteric fevers have been notifiable diseases since 1903. In addition to mandatory reporting, clinical laboratories forward the isolates to the National Reference Center for *Escherichia coli*, *Shigella*, and *Salmonella* at the Institut Pasteur (Paris, France) on a voluntary basis. Most *Salmonella* Typhi isolates are obtained from travelers or immigrants, most of whom were infected in Asia and Africa. During 2016–2025, the center received 1,603 *Salmonella* Typhi isolates (1 per patient) for expert analysis (Appendix 1),

Author affiliation: Institut Pasteur, Université Paris Cité, Paris, France

DOI: https://doi.org/10.3201/eid3210.260813

including 167 of genotype 2.3.1. The median age for those 167 patients was 28 years (range 2–85 years); 64.7% were women and girls and 35.3% men and boys, and 135 (80.8%) had reported traveling to Africa.

We used conventional microbiologic examination and whole-genome sequencing to characterize an emerging MDR-CIP^R *S.* Typhi strain of genotype 2.3.1 isolated from travelers returning to France from West Africa. We also reconstructed its evolutionary history.

The Study

In 2022, we obtained 35 MDR-CIP^R *Salmonella* Typhi isolates from persons returning from Senegal (Figure 1). All isolates belonged to genotype 2.3.1 and contained AMR genes bla_{TEM-1}, *strA*, *strB*, *aadA1*, *sul1*, *sul2*, *dfrA1*, and *tet(B)* (this particular combination of AMR genes was thereafter named MDR profile A [MDRA]) and the point mutation *gyrA*_S83F, thus explaining their AMR phenotype (resistance to ampicillin, streptomycin, sulfonamides, trimethoprim, cotrimoxazole, tetracycline, nalidixic acid and ciprofloxacin [MIC range 0.125–0.25 mg/L]) (Appendix 2, https://wwwnc.cdc.gov/EID/article/32/10/26-0813-App2.xlsx). Only 1 similar isolate had previously been documented in the Institut Pasteur registry, obtained from a case linked to Senegal in 2021 (Figure 1). The number of genotype 2.3.1 isolates linked to Senegal decreased from 21 in 2023 to 8 in 2024 but then peaked at 50 in 2025 (Figure 1). All 79 isolates recovered since 2023 were CIP^R; 71 also displayed the MDRA profile (Appendix 2). We also identified in our database 52 additional genotype 2.3.1 genomes, obtained since 2022; of those, 39 carry the MDRA-CIP^R profile (37 also carry the *gyrA*_S83F mutation), and 11 originated from persons who had traveled to countries in West Africa (Guinea, Guinea-Bissau, Niger, Nigeria, Mauritania, The Gambia, and Benin) (Appendix 2).

We constructed a maximum-likelihood phylogeny of 207 genomes of genotype 2.3.1 (167 from our

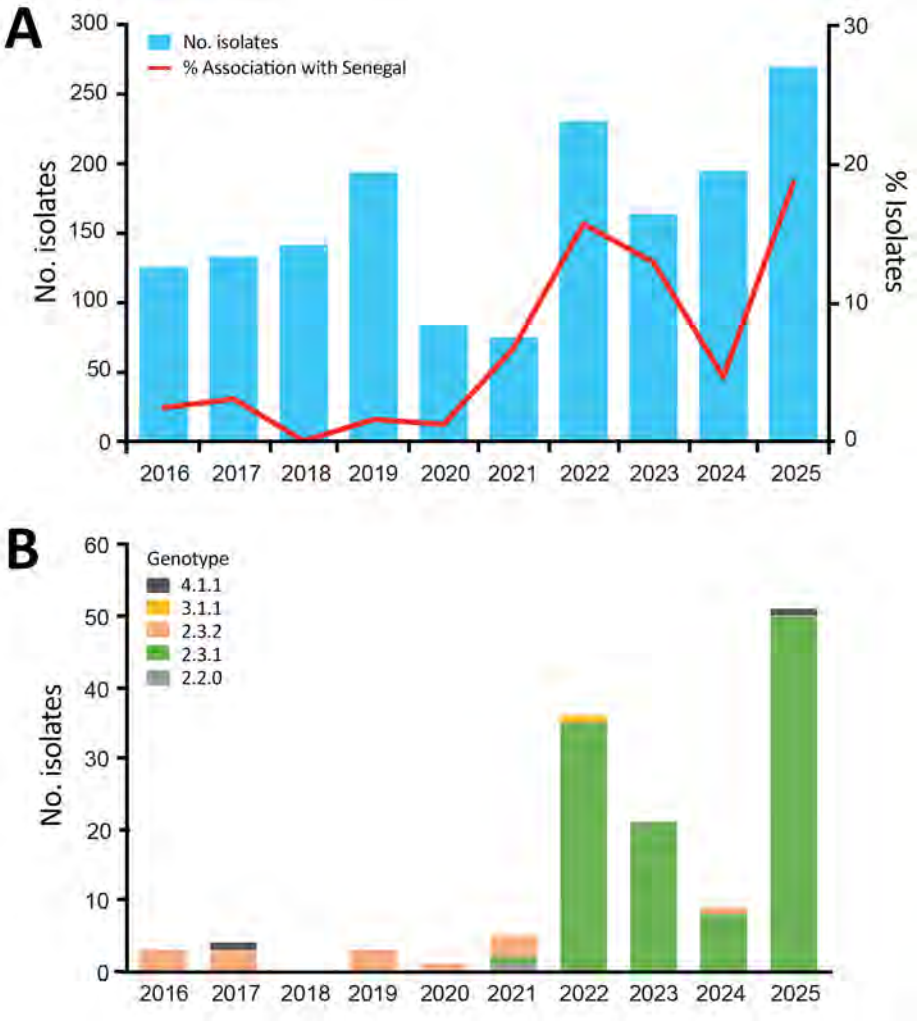

Figure 1. Distribution and genotype of *Salmonella enterica* serovar Typhi isolates in persons returning to France from Senegal in study of emergence of genotype 2.3.1 multidrug-resistant *Salmonella* Typhi strain, West Africa, 2016–2025. A) Total number of nonredundant *Salmonella* Typhi isolates received each year by France's National Reference Center for *Escherichia coli*, *Shigella*, and *Salmonella* at the Institut Pasteur and percentage of those associated with Senegal. The unusually small number of *Salmonella* Typhi isolates received in 2020 and 2021 (<100 isolates) occurred in the context of COVID-19–related travel restrictions. B) Annual distribution of genotypes for *Salmonella* Typhi isolates obtained from persons returning from Senegal.

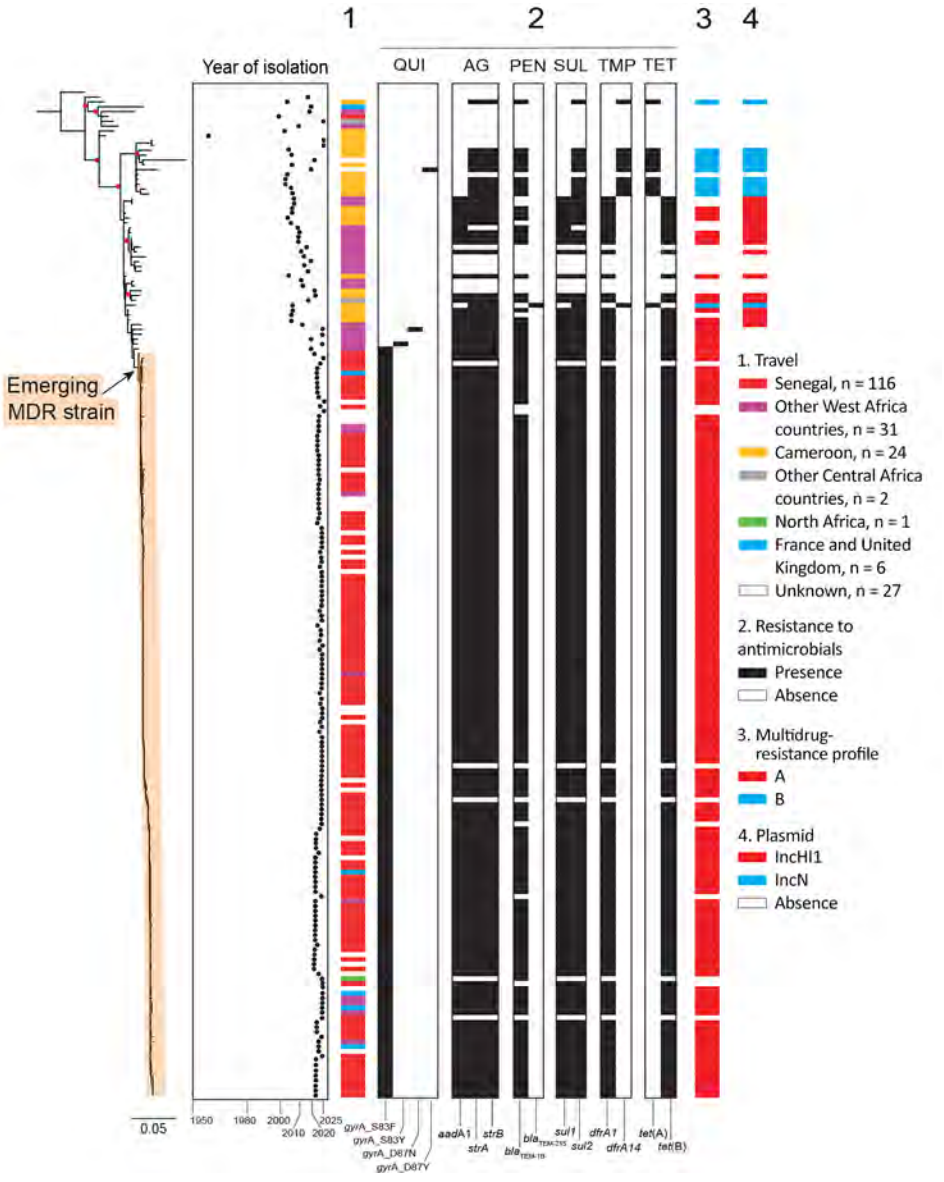

Figure 2. Maximum-likelihood phylogeny of 208 *Salmonella enterica* serovar Typhi isolates in study of emergence of genotype 2.3.1 MDR *Salmonella* Typhi strain, West Africa, 2021–2025. Included are 207 genotype 2.3.1 isolates (167 from France's National Reference Center for *Escherichia coli*, *Shigella*, and *Salmonella* and 40 published genomes) and the reference genome CT18. CT18 (genotype 3.2.1) was used as the outgroup of the tree (its associated characteristics in terms of geographic origin, antimicrobial-resistance genes, and plasmid types are not indicated). Red color on dendrogram indicates nodes with bootstrap support >98%. Light orange rectangle indicates emerging MDR strain. Year of isolation is indicated, together with the travel information (when available) for the isolate, to the right of the tree, because those parameters serve as a proxy for the probable origin of the isolates. Resistance to certain antimicrobial drugs and the presence (black) or absence (white) of antimicrobial-resistance genes (names given along bottom of tree) also are indicated to the right of the tree. The MDR profiles are indicated in red (for profile A; bla_{TEM-1}, *strA*, *strB*, *aadA1*, *sul1*, *sul2*, *dfrA1*, and *tet(B)*) or blue (for profile B; bla_{TEM-1}–like, *strA*, *strB*, *sul2*, *dfrA14*, and *tet(A)*). The presence of plasmid markers is indicated in blue (for IncN) or red (for IncHI1). Scale bar indicates number of nucleotide substitutions per variable site. Information displayed in this figure can be found for each individual strain in Appendix 2 (https://wwwnc.cdc.gov/EID/article/32/10/26-0813-App2.xlsx). AG, aminoglycosides; MDR, multidrug-resistant; PEN, penicillins; QUI, quinolones; SUL, sulfonamides; TET, tetracyclines; TMP, trimethoprim.

study and 40 published genomes [*15*]), including the oldest strain, isolated in Cameroon in 1958 (Appendix 2) from 1,130 single-nucleotide variants. We observed 2 main types of MDR genomes differing in AMR gene content in the phylogenetic tree: MDRA (n = 161) and a second type of MDR genomes, which we named MDRB (n = 11), carrying bla_{TEM-1}–like, *strA*, *strB*, *sul2*, *dfrA14*, and *tet(A)*. Most of the MDRB genomes clustered in the upper clades of the tree and contained a pST3 IncN plasmid (Figure 2). The MDRA genomes were located in the central and lower clades of the tree. Those in the central part contained the pST2 IncHI1 plasmid, and the oldest MDRA strains carrying that plasmid were from Cameroon in 2004. All 154 CIP^R isolates with the *gyrA*_S83F mutation (collected during 2021–2025 and belonging to the emerging MDR strain) clustered tightly together at the bottom of the tree (Figure 2), of which 144 had the MDRA profile. One published MDRA-CIP^R (*gyrA*_S83F) genome from a strain collected in Nigeria in 2019 (National Center for Biotechnology Information Sequence Read Archive [https://www.ncbi.nlm.nih.gov/sra] accession no. SRR10198914) appeared to be the nearest ancestor of this cluster (Figure 2; Appendix 2).

We identified no plasmid in our emerging MDR strain, suggesting that the MDR region of the IncHI1 plasmid had been stably integrated into the chromosome. Long-read sequencing of 2 MDRA-CIP^{R} isolates (202210167 and 202207569) from the emerging MDR strain confirmed that hypothesis, revealing the integration of a 34,664-bp AMR region in the vicinity of chromosomal genes STY2890 and STY2889 (according to reference genome CT18) (Figure 3, panel A). That IS*26*-flanked AMR region contained all 8 AMR genes seen in MDRA isolates. In addition, long-read sequencing of MDRA isolates IPCP (Cameroon, 2006) and 201607514 (Chad, 2021) showed both contained a conjugative pST2 IncHI1 plasmid (188,859-bp pIPCP-1 in IPCP and 187,575-bp p201607514–2 in 201607514) (Appendix 1), indicating that the chromosome-borne AMR region originated from the pST2 IncHI1 plasmid. The region between nucleotides 2824 and 33844 of the AMR region integrated into the chromosome of the epidemic strain (Figure 3, panel B) was 100% identical to region 53376–84396 of the pIPCP-1 plasmid. The *bla*$_{\text{TEM-1}}$ β-lactamase gene (flanked by 2 IS*26* elements) was on the chromosome of the epidemic strain and the IncHI1 plasmid but was not collinear, suggesting secondary rearrangements in the chromosomal AMR region induced by IS*26* elements.

Conclusion

We identified an emerging genotype 2.3.1 MDR *Salmonella* Typhi lineage in patients returning from sub-

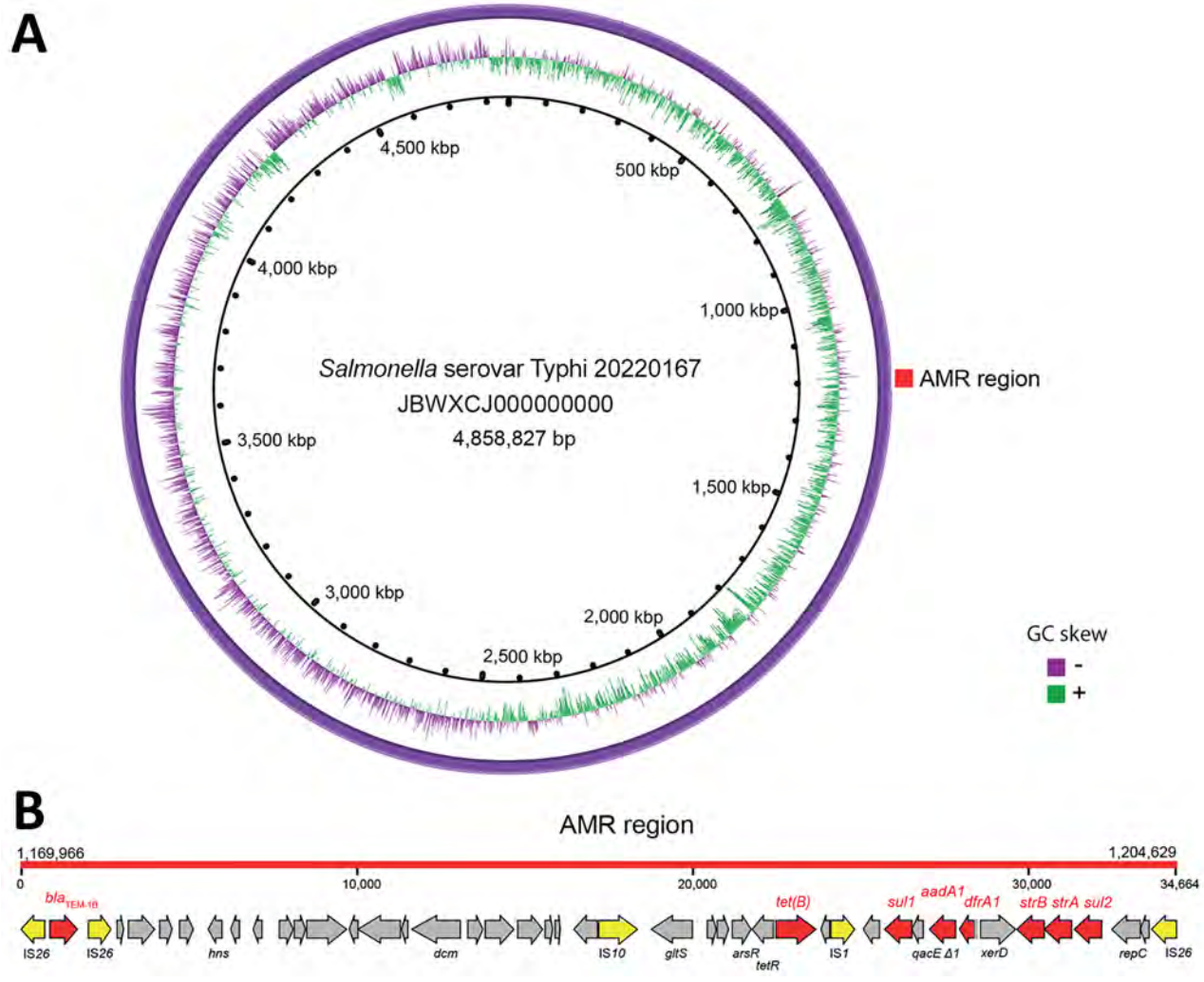

Figure 3. Chromosomal integration of an AMR region derived from an IncHI1 plasmid in study of emergence of genotype 2.3.1 multidrug-resistant *Salmonella enterica* serovar Typhi strain, West Africa, 2021–2025. A) Circular representation of the complete genome of isolate 202210167, a representative isolate of the emerging strain. Red square indicates the chromosomally integrated 34,664-bp AMR region in the external ring. B) Linear representation of the integrated AMR region containing the 8 AMR genes identified in the emerging strain (red indicates AMR genes, yellow indicates insertion sequences, and gray indicates other genes). AMR, antimicrobial resistance.

Saharan Africa, particularly Senegal. This lineage differs from the globally distributed MDR H58 (4.3.1 and derived) lineage originating from South Asia. Genomic analyses revealed the lineage's evolution, including AMR acquisition. First identified in Cameroon in the 1950s, it acquired 2 distinct MDR plasmids during the 2000s. The IncHI1 plasmid was subsequentially lost, but its AMR region is now stably integrated into the bacterial chromosome. Since 2019, this lineage has acquired ciprofloxacin resistance through a chromosomal *gyrA* mutation. That trajectory closely mirrors that of H58, underscoring risk for further resistance development. Continued genomic surveillance is essential to monitor spread and guide control measures to prevent further resistance.

Acknowledgments

We thank all corresponding laboratories of France's National Reference Center for *Escherichia coli*, *Shigella*, and *Salmonella* for their participation in the surveillance of *Salmonella* infections. We thank Magali Ravel, Estelle Serre, Véronique Guibert, and Laëtitia Fabre for technical assistance.

This work was supported by the Institut Pasteur and Santé publique France.

About the Author

Dr. Njamkepo is a research scientist in the Enteric Bacterial Pathogens Unit of the Institut Pasteur. Her research interests include the genomics of several epidemic bacterial pathogens.

References

1. Kuehn R, Rahden P, Hussain HS, Karkey A, Qamar FN, Rupali P, et al. Enteric (typhoid and paratyphoid) fever. Lancet. 2025;406:1283–94. https://doi.org/10.1016/S0140-6736(25)01335-2
2. Murthy S, Hagedoorn NN, Faigan S, Rathan MD, Sharples KJ, Marchello CS, et al. Global typhoid fever incidence: an updated systematic review with meta-analysis. Lancet Infect Dis. 2025;25:1347–62. https://doi.org/10.1016/S1473-3099(25)00359-7
3. Roumagnac P, Weill FX, Dolecek C, Baker S, Brisse S, Chinh NT, et al. Evolutionary history of *Salmonella typhi.* Science. 2006;314:1301–4. https://doi.org/10.1126/science.1134933
4. Goldstein FW, Chumpitaz JC, Guevara JM, Papadopoulou B, Acar JF, Vieu JF. Plasmid-mediated resistance to multiple antibiotics in *Salmonella typhi.* J Infect Dis. 1986;153:261–6. https://doi.org/10.1093/infdis/153.2.261
5. Wain J, Diem Nga LT, Kidgell C, James K, Fortune S, Song Diep T, et al. Molecular analysis of incHI1 antimicrobial resistance plasmids from *Salmonella* serovar Typhi strains associated with typhoid fever. Antimicrob Agents Chemother. 2003;47:2732–9. https://doi.org/10.1128/AAC.47.9.2732-2739.2003
6. Holt KE, Phan MD, Baker S, Duy PT, Nga TVT, Nair S, et al. Emergence of a globally dominant IncHI1 plasmid type associated with multiple drug resistant typhoid. PLoS Negl Trop Dis. 2011;5:e1245. https://doi.org/10.1371/journal.pntd.0001245
7. Parkhill J, Dougan G, James KD, Thomson NR, Pickard D, Wain J, et al. Complete genome sequence of a multiple drug resistant *Salmonella enterica* serovar Typhi CT18. Nature. 2001;413:848–52. https://doi.org/10.1038/35101607
8. Wong VK, Baker S, Connor TR, Pickard D, Page AJ, Dave J, et al.; International Typhoid Consortium. An extended genotyping framework for *Salmonella enterica* serovar Typhi, the cause of human typhoid. Nat Commun. 2016;7:12827. https://doi.org/10.1038/ncomms12827
9. Wong VK, Baker S, Pickard DJ, Parkhill J, Page AJ, Feasey NA, et al. Phylogeographical analysis of the dominant multidrug-resistant H58 clade of *Salmonella* Typhi identifies inter- and intracontinental transmission events. Nat Genet. 2015;47:632–9. https://doi.org/10.1038/ng.3281
10. Carey ME, Thi Nguyen TN, Tran DHN, Dyson ZA, Keane JA, Pham Thanh D, et al. The origins of haplotype 58 (H58) *Salmonella enterica* serovar Typhi. Commun Biol. 2024;7:775. https://doi.org/10.1038/s42003-024-06451-8
11. Klemm EJ, Shakoor S, Page AJ, Qamar FN, Judge K, Saeed DK, et al. Emergence of an extensively drug-resistant *Salmonella enterica* serovar Typhi clone harboring a promiscuous plasmid encoding resistance to fluoroquinolones and third-generation cephalosporins. MBio. 2018;9:e00105–18. https://doi.org/10.1128/mBio.00105-18
12. Baltazar M, Ngandjio A, Holt KE, Lepillet E, Pardos de la Gandara M, Collard JM, et al. Multidrug-resistant *Salmonella enterica* serotype Typhi, Gulf of Guinea Region, Africa. Emerg Infect Dis. 2015;21:655–9. https://doi.org/10.3201/eid2104.141355
13. Wong VK, Holt KE, Okoro C, Baker S, Pickard DJ, Marks F, et al.; International Typhoid Consortium. Molecular surveillance identifies multiple transmissions of typhoid in West Africa. PLoS Negl Trop Dis. 2016;10:e0004781. https://doi.org/10.1371/journal.pntd.0004781
14. Ikhimiukor OO, Oaikhena AO, Afolayan AO, Fadeyi A, Kehinde A, Ogunleye VO, et al. Genomic characterization of invasive typhoidal and non-typhoidal *Salmonella* in southwestern Nigeria. PLoS Negl Trop Dis. 2022;16:e0010716. https://doi.org/10.1371/journal.pntd.0010716
15. Carey ME, Dyson ZA, Ingle DJ, Amir A, Aworh MK, Chattaway MA, et al.; Global Typhoid Genomics Consortium Group Authorship. Global diversity and antimicrobial resistance of typhoid fever pathogens: insights from a meta-analysis of 13,000 *Salmonella* Typhi genomes. eLife. 2023;12:e85867. https://doi.org/10.7554/eLife.85867

Address for correspondence: François-Xavier Weill, Institut Pasteur, Université Paris Cité, Unité des Bactéries pathogènes entériques, 28 Rue du Docteur Roux, 75724 Paris CEDEX 15, France; email: francois-xavier.weill@pasteur.fr

Emergence of *Plasmodium malariae* and Co-endemicity of 3 *Plasmodium* Species Parasites, Khanh Hoa Province, Vietnam, 2023–2025

Tuấn Cường Võ,[1] Chau Van Khanh,[1] Hương Giang Lê,[1] Nguyen Cong Trung Dung, Đăng Thùy Dương Nguyễn, Thu Hằng Nguyễn, Byoung-Kuk Na,[2] Huynh Hong Quang[2]

A large malaria outbreak caused by *Plasmodium malariae* parasites occurred in Khanh Hoa Province, Vietnam, in 2023. Since then, *P. malariae* parasites have persisted in the region alongside *P. falciparum* and *P. vivax* species, changing malaria patterns. Those findings reinforce the need for strengthened surveillance in the region.

Malaria, a mosquitoborne disease caused by *Plasmodium* species parasites, poses a global health burden. Malaria incidence and mortality rates have markedly decreased in Vietnam over the past few decades (*1*); however, the Central Highlands region is a malaria hotspot, accounting for >90% of malaria cases in the country. *P. falciparum* and *P. vivax* are the major parasite species responsible for malaria in the region (*2*,*3*), whereas *P. malariae* cases historically have been rare. However, a large *P. malariae* outbreak occurred in Khanh Hoa Province, Vietnam, in 2023 (*4*), and the epidemic has persisted, further complicating malaria patterns and control efforts in the province. We investigated the epidemiologic characteristics of malaria cases and *Plasmodium* species in Khanh Hoa Province, Vietnam, during January 2023–December 2025, to characterize the epidemic in the province.

The Study

We retrieved epidemiologic data on malaria cases from the Electronic Case-based Disease Surveillance—Malaria and Mosquito-borne Diseases Reporting System, a national electronic reporting system in Vietnam. We performed statistical analyses by using negative binomial regression followed by Tukey-adjusted pairwise comparisons. We calculated incidence rate ratios (IRRs) and 95% CIs and considered $p<0.05$ statistically significant.

During the 3 years studied, we identified a total of 493 symptomatic malaria cases in the province that were confirmed by standard microscopic examination and molecular methods targeting parasite 18S rRNA (*5*). Before 2023, the region had few reported malaria cases annually, just 3 in 2021 and 12 in 2022. However, cases increased sharply in 2023 and peaked in July 2023, when *P. malariae* emerged, gradually declining thereafter (Figure 1, panel A).

Annual malaria cases exhibited typical summer peaks and totaled 209 in 2023, 199 in 2024, and 85 in 2025. During those years, most malaria cases were caused by *P. malariae* (44.8%; n = 221) and *P. falciparum* (36.9%; n = 182), whereas *P. vivax* (17.9%; n = 88) and mixed species (0.4%; n = 2) infections occurred less frequently. Three *Plasmodium* species were co-endemic in 2023 and 2024, but only *P. malariae* and *P. falciparum* were prevalent in 2025. Of the 8 districts and cities in Khanh Hoa Province, Khanh Vinh district had the most (93.1%; n = 459) cumulative malaria cases, whereas the other areas had <15 cases each, fluctuating from 0 in Cam Ranh to 14 in Dien Khanh (Figure 1, panel B). *P. malariae* is reportedly common in mixed co-infections with other species, particularly *P. falciparum* (*6*). However, molecular methods

Author affiliations: Gyeongsang National University College of Medicine and Institute of Health Science, Jinju, South Korea (T.C. Võ, H.G. Lê, D.T.D. Nguyễn, T.H. Nguyễn, B.K. Na); Institute of Malariology, Parasitology, and Entomology, Quy Nhon, Vietnam (C.V. Khanh, N.C.T. Dung, H.H. Quang)

DOI: https://doi.org/10.3201/eid3210.260751

[1]These first authors contributed equally to this article.

[2]These authors were co-principal investigators.

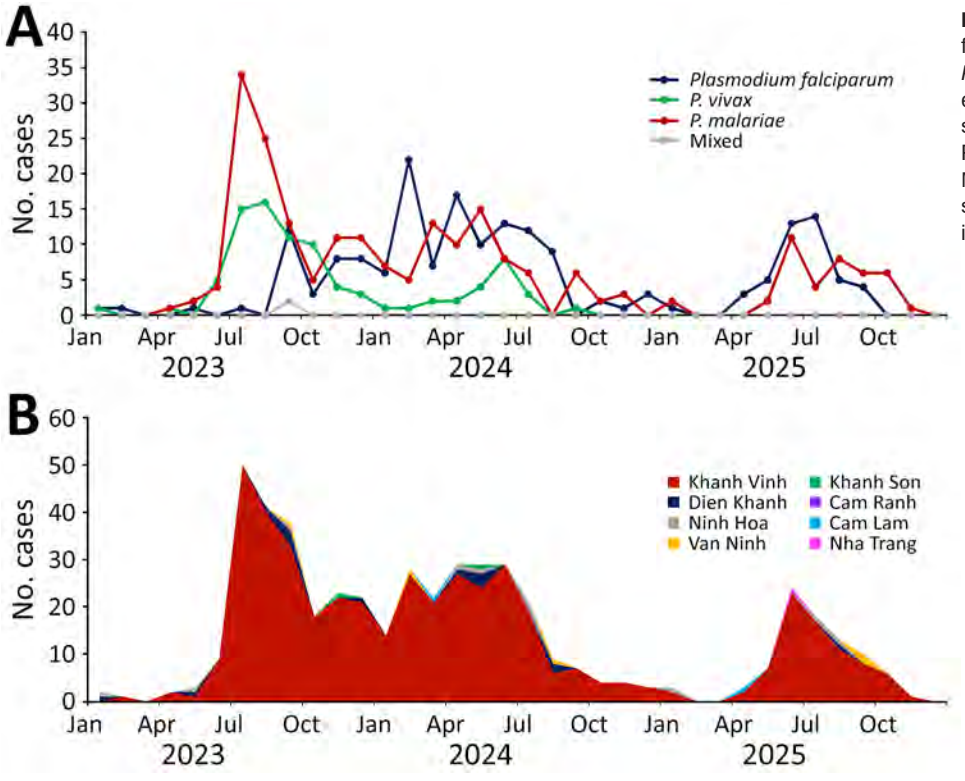

Figure 1. Malaria incidences from a study of emergence of *Plasmodium malariae* and co-endemicity of 3 *Plasmodium* species parasites, Khanh Hoa Province, Vietnam, 2023–2025. A) Monthly incidences by *Plasmodium* species; B) geographic distribution in the province.

confirmed that all *P. malariae* cases in Khanh Hoa Province were monoinfections.

We further investigated the temporal and spatial dynamics of malaria cases in Khanh Vinh district (Figure 2). In 2023, *P. malariae* was most prevalent (104 cases), followed by *P. vivax* (62 cases) and *P. falciparum* (29 cases). Geographic overlap of the 3 species occurred in 6 communes, including Khanh Thuong and Lien Sang, but Khanh Dong, Khanh Phu, Cau Ba, and Khanh Nam had only 1 *Plasmodium* species identified, either *P. falciparum* or *P. malariae*. In 2024, species' geographic distributions changed; *P. falciparum* cases increased in Khanh Dong (n = 53) and Khanh Phu (n = 23), and distribution expanded to other communes. At the same time, overall *P. malariae* cases decreased to 72 (IRR 1.444 [95% CI 0.750–2.782]; p = 0.272), particularly in Son Thai (from 34 in 2023 to 3 in 2024), but no overall distribution changes were evident. Most (n = 40) *P. malariae* cases were detected in Khanh Thuong, but cases were found in most communes, except Khanh Dong and Khanh Trung. Meanwhile, *P. vivax* cases markedly decreased (n = 22; IRR 2.818 [95% CI 2.156–3.685]; p<0.001) in 2024 and had a narrower geographic distribution; most (n = 17) cases were reported in Khanh Thuong. We observed overlap of the 3 species in 3 communes, most notably in Khanh Thuong (Figure 2). In 2025, total malaria cases in Khanh Vinh district declined to 77, and no *P. vivax* cases were detected in the district. However, *P. falciparum* (n = 41) and *P. malariae* (n = 36) still exhibited geographic overlap in 5 communes. Those 3-year epidemiologic data suggested that overall malaria incidence in Khanh Vinh district decreased gradually and that endemic areas also contracted over time. However, *P. malariae* endemicity persists with other *Plasmodium* species.

Among malaria patients in Khanh Vinh district, 338 were male and 121 were female, a 2.8:1 ratio (Figure 3, panel A), and most (n = 344; 75.0%) were >15 years of age (Figure 3, panel B). Ethnic analysis revealed that the Raglai community was the most affected (304 cases; 66.2%), followed by the Kinh (53 cases; 11.6%) and Co Ho (50 cases; 10.9%) populations (Figure 4, panel A). Affected persons largely were forest-goers (n = 314; 68.4%) but also included rangers (n = 29; 6.3%) and government or factory workers (n = 15; 3.3%) (Figure 4, panel B). Heavy dependence on the forest or forest farming for subsistence places the Raglai population at greater risk for malaria infection, and that community accounts for most malaria cases in Central Vietnam (*7*,*8*). We observed no meaningful association between patient demographic characteristics and specific *Plasmodium* species infections.

The cause of the *P. malariae* outbreak in Khanh Hoa Province, particularly in Khanh Vinh district,

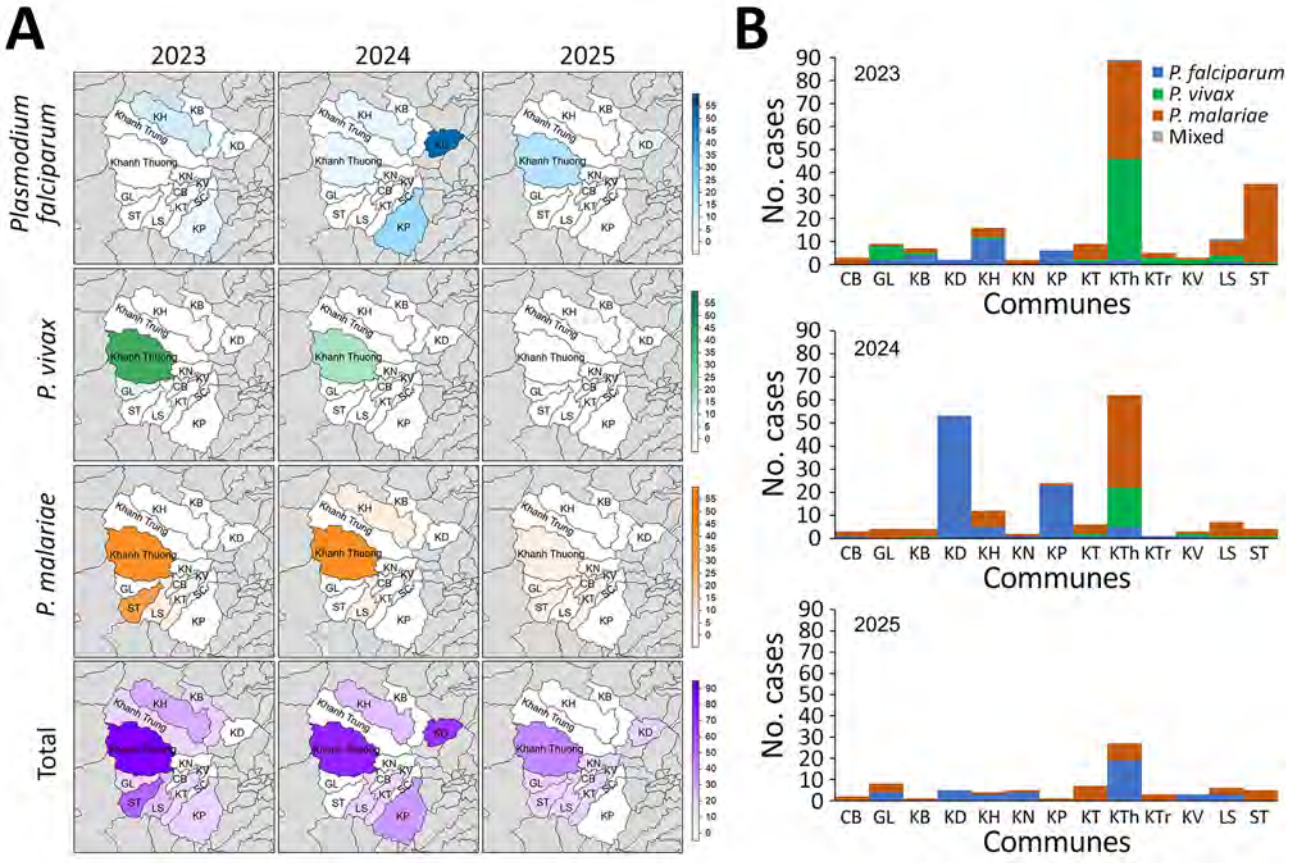

Figure 2. Changing pattern of malaria from a study of emergence of *Plasmodium malariae* and co-endemicity of 3 *Plasmodium* species parasites, Khanh Hoa Province, Vietnam, 2023–2025. A) Geographic distribution of *Plasmodium* species over time; B) annual malaria cases by commune and *Plasmodium* species. CB, Cau Ba; GL, Giang Ly; KB, Khanh Binh; KD, Khanh Dong; KH, Khanh Hiep; KN, Khanh Nam; KP, Khanh Phu; KT, Khanh Thanh; Kth, Khanh Thuong; KTr, Khanh Trung; KV, Khanh Vinh Town; LS, Lien Sang; SC, Song Cau; ST, Son Thai.

remains unclear. Successful interventions targeting *P. falciparum* and *P. vivax* parasites might have inadvertently expanded the ecologic niche of *P. malariae* (*9*). Given the increase in *P. malariae* infections (10 of 12 total malaria cases) in Khanh Hoa Province in 2022, *P. malariae* might have begun to emerge at that time. Persistent asymptomatic infections in the province might also have contributed to the outbreak. Indeed, high rates of asymptomatic and submicroscopic *P. falciparum* and *P. vivax* infections have been identified in Central Vietnam (*10*,*11*). Those hypotheses are supported by our

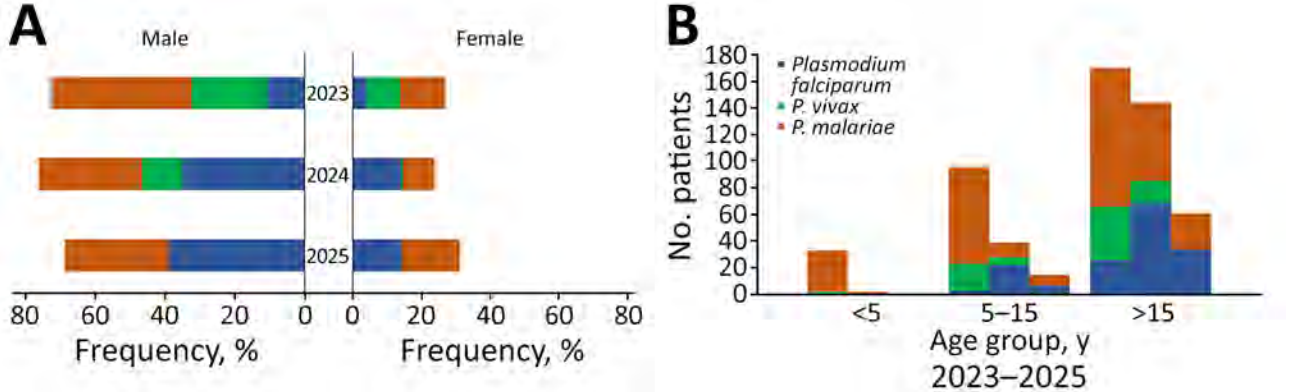

Figure 3. Gender (A) and age (B) demographic characteristics of malaria case-patients in Khanh Vinh district, from a study of emergence of *Plasmodium malariae* and co-endemicity of 3 *Plasmodium* species parasites, Khanh Hoa Province, Vietnam, 2023–2025.

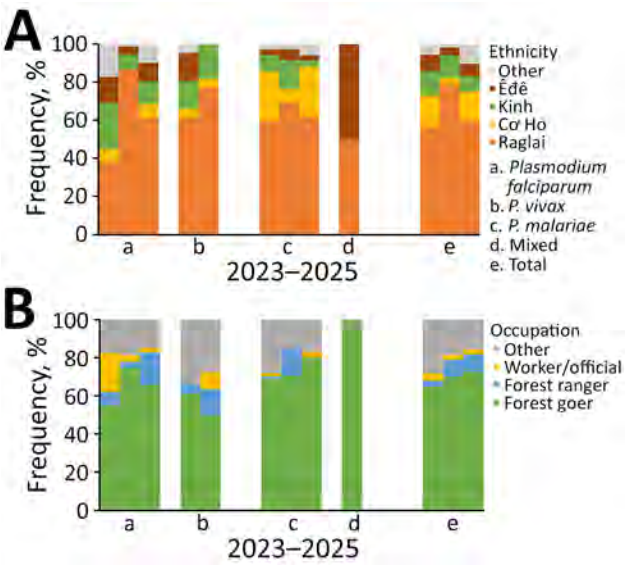

Figure 4. Ethnicity (A) and occupation (B) of malaria case-patients in Khanh Vinh district, from a study of emergence of *Plasmodium malariae* and co-endemicity of 3 *Plasmodium* species parasites, Khanh Hoa Province, Vietnam, 2023–2025.

pilot study on asymptomatic malaria in Khanh Hoa Province (T.C. Võ et al., unpub. data), in which 1.57% of 1,401 residual blood samples collected from 6 communes of Khanh Vinh district during January 2024–April 2025 demonstrated asymptomatic and submicroscopic *P. falciparum* and *P. malariae* infections. The COVID-19 pandemic might also have contributed to that outbreak by straining or fragmenting the health infrastructure, as reported in other countries in Southeast Asia (*12*,*13*).

Genetic analysis of *P. malariae* parasites in Khanh Hoa Province showed notable genetic variations in major polymorphic markers, such as apical membrane antigen 1 and circumsporozoite surface protein (*14*; T.C. Võ et al., unpub. data), despite the homogeneity of the parasite population collected in a limited region over a short period. Although molecular markers of antimalarial drug resistance have not yet been confirmed in *P. malariae* parasites (*15*), molecular analyses of orthologous genes associated with drug resistance in *P. falciparum* and *P. vivax* parasites from Khanh Hoa Province revealed no remarkable mutations associated with antimalarial drug resistance (T.C. Võ et al., unpub. data), which is consistent with no identified clinical drug failure to date in the region. Further genetic studies are underway to elucidate the population structure of *P. malariae* parasites in Khanh Hoa Province and to examine their genetic nature. Studies on mosquito vectors and environmental changes associated with malaria transmission dynamics are also underway.

Conclusions

Co-endemicity of 3 *Plasmodium* species after a recent *P. malariae* outbreak has altered malaria endemicity patterns in Khanh Hoa Province, Vietnam. As of 2025, *P. malariae* cases mainly occurred in Khanh Vinh district, and the epidemic appears to be contained. However, that *P. malariae* outbreak changed the overall malaria epidemic pattern in the province and resulted in the persist, unstable co-endemicity of multiple *Plasmodium* species, suggesting the need for strengthened surveillance and control interventions.

Acknowledgments

We express profound gratitude to the Khanh Hoa Provincial Center for Diseases Control, Khanh Vinh District Health Center, local authorities and collaborators, and study participants for their unwavering support and enthusiastic involvement in our research.

The study protocol was approved by the Institute of Malariology, Parasitology, and Entomology Quy Nhon Institutional Review Board (IMPE-QN, no. 27/CN-QLKH), in compliance with all applicable federal regulations governing the protection of human subjects. The datasets used during the study are not publicly available due to institutional confidentiality but are available from the corresponding author on reasonable request.

This work was supported by the National Research Foundation of Korea grant funded by the government of South Korea (MSIT) (grant no. RS-2025-02413635).

Author contributions: B.K.N. and H.H.Q. conceptualized and designed the study and managed the project; T.C.V., C.V.K., N.C.T.D., H.G.L., T.H.N., and H.H.Q. collected and analyzed data; C.V.K., N.C.T.D., D.T.D.N., and H.H.Q. collected blood and performed experiments; T.C.V. and H.G.L. visualized data; B.K.N. and H.H.Q. obtained funding; T.C.V., C.V.K., H.G.L., and B.K.N. wrote original draft; and N.C.T.D., D.T.D.N., T.H.N., and H.H.Q. reviewed and edited draft. All authors reviewed the manuscript and approved the final version.

About the Author

Dr. Võ is a postdoctoral fellow at Gyeongsang National University, Korea. His research interests include tropical infectious diseases, particularly malaria.

References

1. World Health Organization. World malaria report 2025. Geneva: The Organization; 2025.
2. Võ TC, Lê HG, Kang JM, Naw H, Fan CK, Trinh NTM, et al. Molecular surveillance of malaria in the Central

Highlands, Vietnam. Parasitol Int. 2021;83:102374. https://doi.org/10.1016/j.parint.2021.102374
3. Tam LT, Thinkhamrop K, Suttiprapa S, Clements ACA, Wangdi K, Suwannatrai AT. Bayesian spatio-temporal modelling of environmental, climatic, and socio-economic influences on malaria in Central Vietnam. Malar J. 2024;23:258. https://doi.org/10.1186/s12936-024-05074-y
4. Khanh CV, Lê HG, Võ TC, Quang NX, Nguyen DV, Dung NCT, et al. Unprecedented large outbreak of *Plasmodium malariae* malaria in Vietnam: epidemiological and clinical perspectives. Emerg Microbes Infect. 2025; 14:2432359. https://doi.org/10.1080/22221751.2024.2432359
5. Snounou G, Singh B. Nested PCR analysis of *Plasmodium* parasites. In: Doolan DL ed. Malaria methods and protocols. Totowa (NJ): Humana Press, Inc.; 2002. p. 189–204.
6. Collins WE, Jeffery GM. *Plasmodium malariae*: parasite and disease. Clin Microbiol Rev. 2007;20:579–92. https://doi.org/10.1128/CMR.00027-07
7. Erhart A, Ngo DT, Phan VK, Ta TT, Van Overmeir C, Speybroeck N, et al. Epidemiology of forest malaria in central Vietnam: a large scale cross-sectional survey. Malar J. 2005;4:58. https://doi.org/10.1186/1475-2875-4-58
8. Peeters Grietens K, Xuan XN, Van Bortel W, Duc TN, Ribera JM, Ba Nhat T, et al. Low perception of malaria risk among the Ra-glai ethnic minority in south-central Vietnam: implications for forest malaria control. Malar J. 2010;9:23. https://doi.org/10.1186/1475-2875-9-23
9. Shankar H, Kumar G, Ahmed N, Florentin A. *Plasmodium malariae* is an overlooked malaria parasite with emerging challenges. Commun Med (Lond). 2026;6:95. https://doi.org/10.1038/s43856-025-01360-1
10. San NN, Kien NX, Manh ND, Van Thanh N, Chavchich M, Binh NTH, et al. Cross-sectional study of asymptomatic malaria and seroepidemiological surveillance of seven districts in Gia Lai province, Vietnam. Malar J. 2022;21:40. https://doi.org/10.1186/s12936-022-04060-6
11. Lê HG, Võ TC, Kang JM, Van Khanh C, Trinh NTM, Hanh NTL, et al. Molecular profiles of antimalarial drug resistance in *Plasmodium* species from asymptomatic malaria carriers in Gia Lai Province, Vietnam. Microorganisms. 2025; 13:2101. https://doi.org/10.3390/microorganisms13092101
12. Naserrudin NA, Jiee SF, Habil B, Jantim A, Mohamed AFB, Dony JJF, et al. The public health response to a *Plasmodium malariae* outbreak in Penampang district, Sabah during a COVID-19 movement control order. Malar J. 2023;22:292. https://doi.org/10.1186/s12936-023-04693-1
13. Yek C, Nam VS, Leang R, Parker DM, Heng S, Souv K, et al. The pandemic experience in Southeast Asia: interface between SARS-CoV-2, malaria, and dengue. Front Trop Dis. 2021;2:788590. https://doi.org/10.3389/fitd.2021.788590
14. Nguyên ĐTD, Lê HG, Võ TC, Nguyên TH, Kang JM, Nguyên KO, et al. Genetic polymorphism and natural selection of apical membrane antigen-1 in *Plasmodium malariae* isolated from Vietnam. BMC Infect Dis. 2026;26:476. https://doi.org/10.1186/s12879-026-12935-1
15. Pimpat Y, Saralamba N, Boonyuen U, Pukrittayakamee S, Nosten F, Smithuis F, et al. Genetic analysis of the orthologous *crt* and *mdr1* genes in *Plasmodium malariae* from Thailand and Myanmar. Malar J. 2020;19:315. https://doi.org/10.1186/s12936-020-03391-6

Address for correspondence: Byoung-Kuk Na, Gyeongsang National University School of Medicine, Parasitology and Tropical Medicine, 15 Jinjudaero 816, Jinju 52727, Gyeongsangnamdo, South Korea; email: bkna@gnu.ac.kr

Highly Pathogenic Avian Influenza Virus Subtype 5 in Cetaceans, Brazil

Alanis S. Melgarejo, Mauricio Tavares, Derek B. de Amorim, Sergio C. Estima, Andrine Paiva, Caio R. Soares-Oliveira, Liane A. Dias, Renan C. de Lima, Silvina Botta, Eduardo R. Secchi, Barbara A. Davila, Carlos de Oliveira, Larissa S. Heinzelmann, Martha T. Oliveira, Vitor L. Carvalho, Aline R. Souza, Salvatore Siciliano, Paula Baldassin, Greicy F. Ruenes, Paulo H. Ott, Luciana Sonne, Ana C. Franco, Larissa R. Oliveira

Author affiliations: Universidade Federal do Rio Grande do Sul, Porto Alegre, Brazil (A.S. Melgarejo, M. Tavares, D.B. de Amorim, M.T. Oliveira, L. Sonne, A.C. Franco); Núcleo de Educação e Monitoramento Ambiental, Rio Grande, Brazil (S. C. Estima, A. Paiva, C.R. Soares-Oliveira); Universidade Federal do Rio Grande, Rio Grande (L.A. Dias, R.C. de Lima, S. Botta, E.R. Secchi); Universidade do Vale do Rio dos Sinos, São Leopoldo, Brazil (B.A. Davila, C. de Oliveira, L.S. Heinzelmann); Associação de Pesquisa e Preservação de Ecossistemas Aquáticos, Caucaia, Brazil (V.L. Carvalho, A.R. Souza, L.R. Oliveira); Fundação Oswaldo Cruz, Escola Nacional de Saúde Pública, Rio de Janeiro, Brazil (S. Siciliano); Grupo de Estudos da Região dos Lagos, Rio de Janeiro (S. Siciliano, G.F. Ruenes); Instituto BW para a Conservação e Medicina da Fauna Marinha, Araruama, Brazil (P. Baldassin); Universidade Estadual do Rio Grande do Sul, Osório, Brazil (P.H. Ott); Grupo de Estudos de Mamíferos Aquáticos do Rio Grande do Sul, Porto Alegre, Brazil (P.H. Ott, L.R. Oliveira); Marine Vertebrate Evolution and Conservation Lab, Fortaleza, Brazil (L.R. Oliveira).

DOI: https://doi.org/10.3201/eid3210.260051

We identified highly pathogenic avian influenza virus subtype H5 in stranded dolphins along the coastline of Brazil during 2023–2025. Infected animals included species classified as vulnerable or endangered. Our results highlight the need for ongoing surveillance of cetaceans susceptible to viral infections, which pose an additional threat to threatened species.

Marine ecosystems in Brazil have high biodiversity and support numerous top predators, including marine mammals. Along the coast of Brazil, ≥46 cetacean species have been recorded, several of which are classified as threatened or near threatened (*1*).

Influenza A viruses (IAV) infect a wide range of hosts, including marine mammals (*2*). The highly pathogenic avian influenza (HPAI) H5N1 virus is causing a widespread panzootic, including outbreaks with high mortality rates among birds and pinnipeds (*3*). Reports of IAV in cetaceans remain rare and limited to a few species, and large-scale outbreaks have not been reported (*4*). We screened swab samples from cetaceans stranded along the coast of Brazil during November 2023–August 2025 for IAV by using quantitative reverse transcription PCR (qRT-PCR).

During November 2023–August 2025, we recorded stranded marine mammals along the Brazil coastlines of Rio Grande do Sul (≈485 km), Rio de Janeiro (317 km), and Ceará (573 km) (Figure 1, panels A–D). Moreover, we conducted systematic surveys along the beaches of Rio Grande do Sul and responded to stranding notifications across all coastal regions. For each animal, we recorded standardized data including date, location, species, sex, and decomposition stage (*5*). Ethical approval for this study was granted by the Animal Ethics Committee of the Universidade do Vale do Rio dos Sinos (protocol no. PPECEUA 02.2025).

We collected swab samples exclusively from carcasses in decomposition stages 2–4, which include the bloated stage, active decay, and advanced decay (*5*). We collected and fixed tissue samples (brain, lungs, trachea, spleen, intestine and liver) from carcasses in earlier decomposition stages (*2*,*3*) in 10% buffered formalin and routinely processed the fixed tissues for histology. We extracted total nucleic acids by using the MagMAX CORE Nucleic Acid Purification Kit (Thermo Fisher Scientific, https://www.thermofisher.com) with the KingFisher Flex system (Thermo Fisher Scientific). We performed qRT-PCR amplification of the IAV matrix gene for IAV detection (*6*), and we detected the H5N1 strain by using World Health Organization molecular protocols (*7*). We set the fluorescence threshold at 0.09 and classified samples with cycle threshold (Ct) values ≤37 as positive. We evaluated the sensitivity of the IAV qRT-PCR by using RNA from MDCK cells infected with H1N1, cloned into a plasmid as a positive control. We assessed the sensitivity of the H5N1 qRT-PCR assay by using a pEz plasmid and performed 10-fold serial dilutions to determine the qRT-PCR limit of detection.

We analyzed 45 stranded cetaceans, representing 13 species (Figure 1, panel E; Appendix Table 1, http://wwwnc.cdc.gov/EID/article/32/10/26-0051-App.pdf). We detected the IAV matrix gene RNA in 18 animals, including Franciscana dolphins (*Pontoporia blainvillei*), Lahille's bottlenose dolphins (*Tursiops truncatus gephyreus*), rough-toothed dolphins (*Steno bredanensis*), Clymene dolphins (*Stenella clymene*), dwarf sperm whales (*Kogia sima*), and Fraser's dolphins (*Lagenodelphis hosei*). Samples positive for IAV RNA were from multiple tissues, most frequently blowhole

swab samples, followed by cerebral, oral, anal, intestinal, tracheal, and ocular tissue samples. Overall, viral RNA levels were low, and Ct values ranged from 28–37, corresponding to ≈1.3 × 10^5–8.0 × 10^2 RNA copies/µL (2, panel A), approaching the assay limit of detection (200–2,000 RNA copies/µL). We only detected the H5N1 strain in 2 samples, both with viral RNA levels near the assay limit of detection (Figure 2, panel B; Appendix Table 2). Our histopathologic examination of the 6 samples positive for IAV (animals 11, 16, 17, 35, 37 and 39; Appendix Tables 1, 2) did not reveal lesions associated with influenza infection.

We detected IAV in samples from cetaceans along the coastline of Brazil after large HPAI H5N1 outbreaks that caused high mortality rates in pinnipeds along the coastline of South American were reported in 2023, which suggests enduring viral circulation in the marine environment and interspecies transmission (*3*,*9*). Cetaceans with samples positive for IAV included the Franciscana dolphin, which is classified as vulnerable, and Lahille's bottlenose dolphin, which is classified as endangered (*8*). Our results underscore a new potential threat to species already at risk for extinction along the coast of Brazil, particularly for

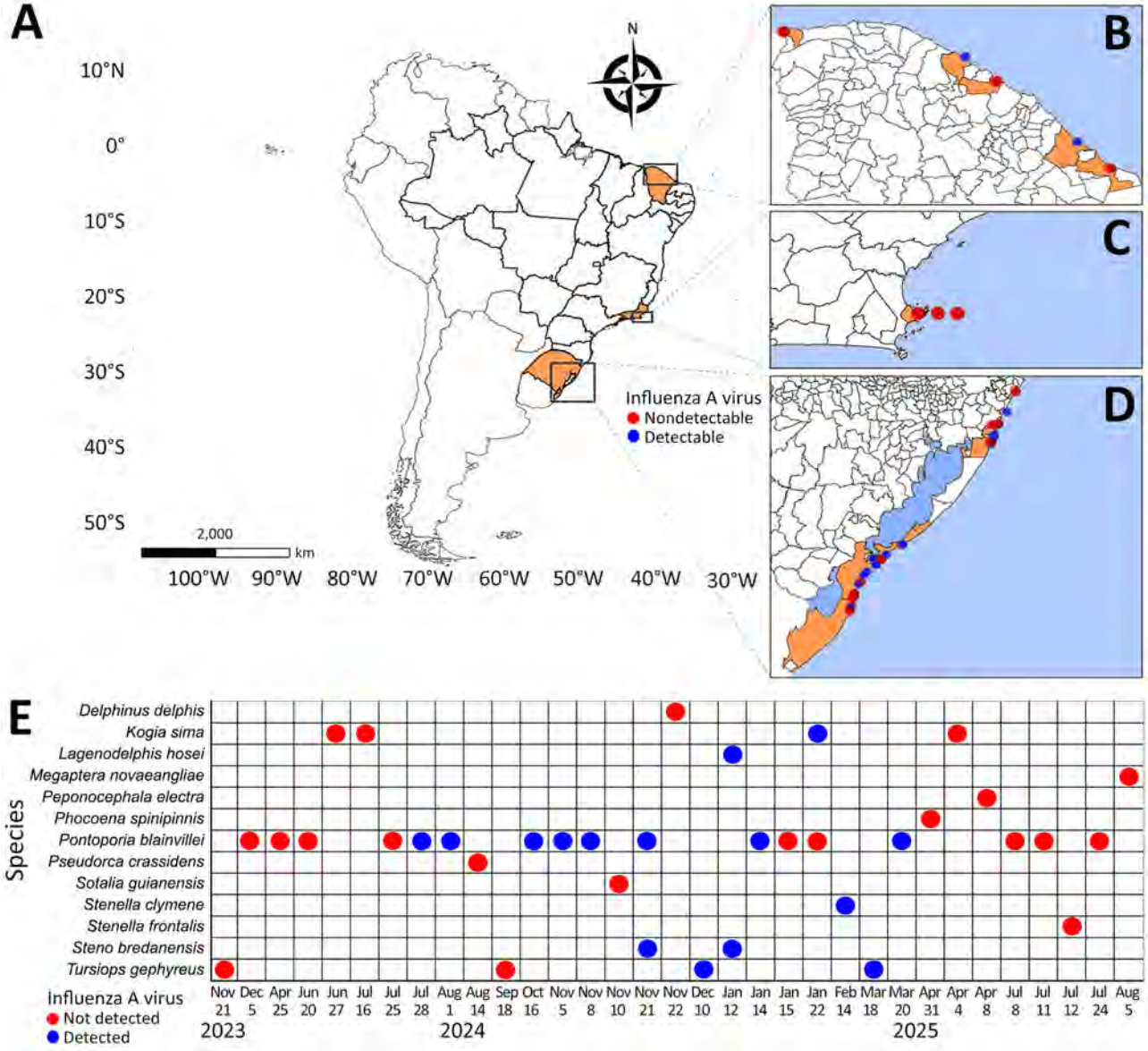

Figure 1. Temporal and spatial distribution of cetacean species collected along the coast of Brazil during a study of influenza A virus from November 2023–August 2025. A–D) Sampling locations along the coast of Brazil. Insets show sampling locations in the states of Ceará (B) Rio de Janeiro (C) and Rio Grande do Sul (D). Each dot represents an analyzed sample from the cetacean. E) Temporal distribution of sampled cetaceans. Each point represents an individual animal; red points indicate detection of influenza A virus matrix gene RNA, and blue points indicate no detectable viral RNA.

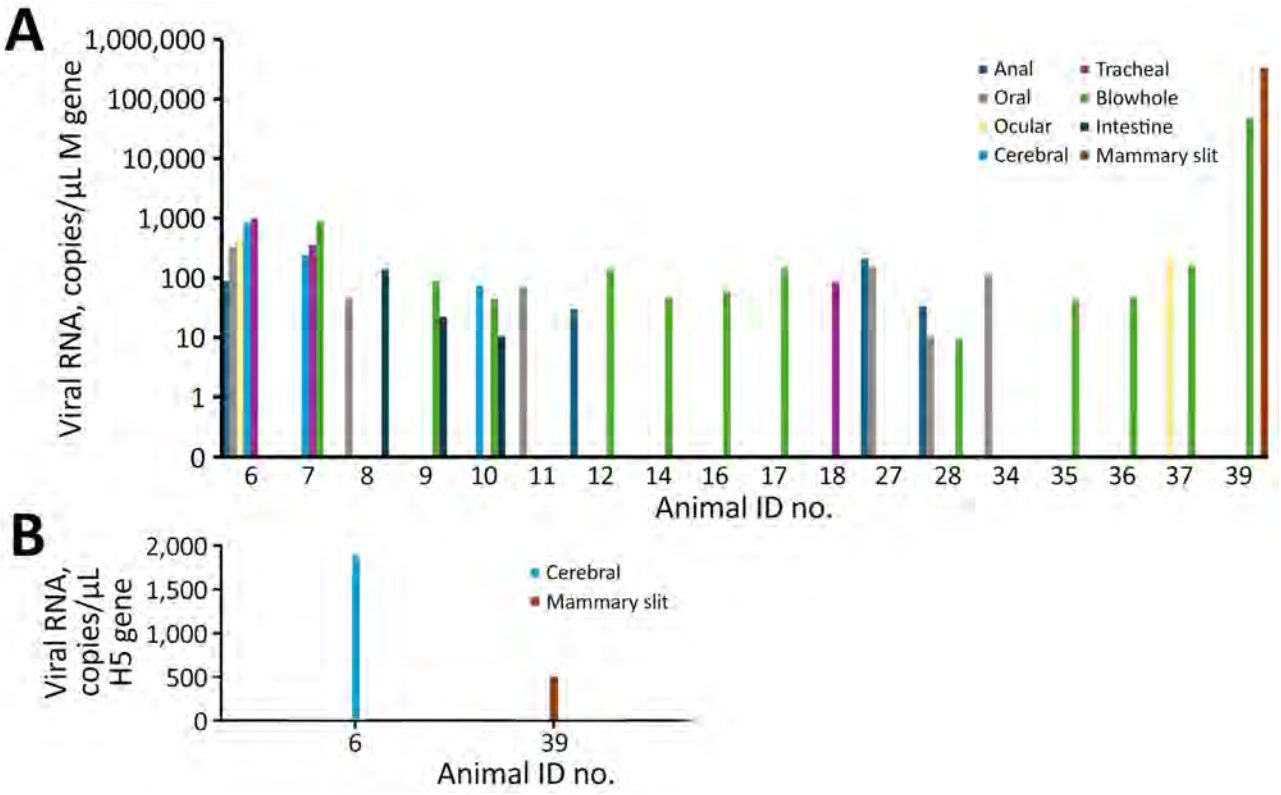

Figure 2. Influenza A viral RNA detected by quantitative reverse transcription PCR in stranded cetaceans from Brazil, November 2023–August 2025. A) Influenza A virus M gene RNA concentration (copies/µL) in positive animals by sample type. B) H5 subtype RNA concentrations (copies/µL) in cetaceans positive for H5 influenza A virus by sample type. ID, identification; M, matrix.

Franciscana and Lahille's bottlenose dolphins, native to the southwestern Atlantic Ocean. Moreover, we detected the HPAI H5N1 strain in Franciscana and Clymene dolphins, highlighting the potential for viral dissemination in coastal and offshore waters.

We observed high Ct values, corresponding with low viral RNA copy numbers. Those results likely reflect RNA degradation associated with postmortem autolysis and advanced carcass decomposition, which can reduce RNA integrity and limit viral detection (*10*). Indeed, the likelihood of identifying lesions associated with influenza infection was likely reduced by the limited number of animals available for histopathologic evaluation because of the advanced stage of decomposition in most of the carcasses analyzed. Environmental contamination from seabirds and shorebirds cannot be excluded in stranded carcasses. However, we detected viral RNA in internal tissues, which indicates true infection rather than surface contamination. Our results underscore the importance of continued and systematic surveillance of marine mammals to understand pathogen dynamics at the wildlife–marine interface.

Acknowledgments

We are very grateful to the staff, students, and volunteers of Universidade do Vale do Rio dos Sinos, Laboratório de Ecologia e Conservação da Megafauna Marinha of Universidade Federal do Rio Grande, Núcleo de Educação e Monitoramento Ambiental, Centro de Estudos Costeiros, Limnológicos e Marinhos of Universidade Federal do Rio Grande do Sul, Centro de Recuperação de Animais Marinhos of Universidade Federal do Rio Grande, Associação de Pesquisa e Preservação de Ecossistemas Aquáticos, and Grupo de Estudos de Mamíferos Marinhos da Região dos Lagos for logistical and field support.

Financial support for fieldwork was provided by the Ministry of Science, Technology and Innovation and the National Council for Scientific and Technological Development (project no. 444448/2023-3: Pathogenicity of avian influenza virus in Brazilian marine mammals), as well as Yaqu Pacha. Research Productivity grants from the National Council for Scientific and Technological Development were awarded to S.B. (grant no. PQ 315365/2020-0), L.S. (grant no. PQ 307277/2021-6), L.R.O. (grant no. 315361/2021-2), and A.C.F. (grant no. PQ 312818/2025-4).

About the Author

Miss Melgarejo is a master's researcher at the Federal University of Rio Grande do Sul, Brazil, working in molecular virology and wildlife disease surveillance. Her research focuses on the surveillance and monitoring of influenza viruses in wildlife, with emphasis on viral detection and public health relevance.

References

1. International Union for Conservation of Nature Marine Mammal Protected Areas Task Force. Final report of the 9th IMMA workshop: important marine mammal area regional workshop for the south west Atlantic Ocean. 2023 [cited 2025 Sep 11]. https://www.marinemammalhabitat.org/immas/workshops/south-west-atlantic-ocean-region
2. Reperant LA, Rimmelzwaan GF, Kuiken T. Avian influenza viruses in mammals. Rev Sci Tech. 2009;28:137–59. https://doi.org/10.20506/rst.28.1.1876
3. Peacock TP, Moncla L, Dudas G, VanInsberghe D, Sukhova K, Lloyd-Smith JO, et al. The global H5N1 influenza panzootic in mammals. Nature. 2025;637:304–13. https://doi.org/10.1038/s41586-024-08054-z
4. Pérez-Sánchez T, Báez JC, Johnstone C. Concern for highly pathogenic avian influenza spillover into cetaceans. Viruses. 2025;17:1536. https://doi.org/10.3390/v17121536
5. Geraci JR, Lounsbury VJ, Yates NS. Marine mammals ashore: a field guide for strandings. 2nd ed. Baltimore (MD): National Aquarium in Baltimore; 2005.
6. Spackman E, Senne DA, Myers TJ, Bulaga LL, Garber LP, Perdue ML, et al. Development of a real-time reverse transcriptase PCR assay for type A influenza virus and the avian H5 and H7 hemagglutinin subtypes. J Clin Microbiol. 2002;40:3256–60. https://doi.org/10.1128/JCM.40.9.3256-3260.2002
7. World Health Organization. WHO information for the molecular detection of influenza viruses. 2017 [cited 2025 May 28]. https://cdn.who.int/media/docs/default-source/influenza/global-influenza-surveillance-and-response-system/related-documents/who_information_for_the_molecular_detection_of_influenza_viruses_20171023_final.pdf
8. International Union for Conservation of Nature. The IUCN Red List of threatened species. Version 2025–2. 2026 [cited 2026 Apr 23]. https://www.iucnredlist.org
9. de Lima RC, Estima SC, Tavares M, Canabarro PL, Botta S, Dias LA, et al. Impacts and lessons learned from the first highly pathogenic avian influenza (H5N1) outbreak in South American pinnipeds along the southern Brazilian coast. Mar Mamm Sci. 2024;41:e13163. https://doi.org/10.1111/mms.13163
10. Hood G, Roche X, Brioudes A, von Dobschuetz S, Fasina FO, Kalpravidh W, et al. A literature review of the use of environmental sampling in the surveillance of avian influenza viruses. Transbound Emerg Dis. 2021;68:110–26. https://doi.org/10.1111/tbed.13633

Address for correspondence: Alanis Silva Melgarejo Federal University of Rio Grande do Sul, Rua Ramiro Barcelos, 2600, Porto Alegre, 90035-003, Rio Grande do Sul, Brazil; email: alanissm97@gmail.com

Evaluation of Trichodysplasia Spinulosa Polyomavirus in Skin Biopsies, United States

Ivan M. Espinal, Gregory W. Charville, Lauren Lawrence, Ryanne A. Brown, Kerri E. Rieger, Sebastian Fernandez-Pol

Author affiliations: Stanford University, Stanford, California, USA (I.M. Espinal, G.W. Charville, R.A. Brown, K.E. Rieger, S. Fernandez-Pol); Guardant Health, Palo Alto, California, USA (L. Lawrence); Stanford Medicine, Stanford (R.A. Brown, K.E. Rieger)

DOI: https://doi.org/10.3201/eid3210.261264

Trichodysplasia spinulosa polyomavirus (TSPyV) has been identified in human endothelial cell tumors. We evaluated 25 clinical cases of various inflammatory dermatoses in California, USA, for TSPyV by using RNAscope in situ hybridization. We did not detect TSPyV in any of the biopsy samples, suggesting that endothelial TSPyV is uncommon in inflammatory dermatoses.

Trichodysplasia spinulosa polyomavirus (TSPyV) typically causes folliculocentric cutaneous eruptions, usually on the face, although the virus has been detected in tonsillar tissue, blood, urine, cerebrospinal fluid, and respiratory specimens (*1*–*4*). Recently, TSPyV was identified within the endothelial cells of tumors from 3 separate patients by analyzing off-target next-generation sequencing reads (*5*). Subsequently, in situ hybridization demonstrated the localization of TSPyV to intratumoral endothelial cells. The significance of TSPyV within endothelial cells in those cases is uncertain. Of note, all 3 patients received corticosteroids immediately before tumor resection.

We hypothesized that TSPyV might be found in vasculitides or other cutaneous inflammatory conditions. We evaluated skin biopsy samples from 25 patients with inflammatory dermatologic conditions. Of the 25 patients, 13 received corticosteroids before skin biopsy. Among those patients, 10 were treated with corticosteroids within 10 days of the biopsy. Three patients had longer intervals between the corticosteroid dose and the biopsy, with intervals of 108 days, 1,494 days, and 1,949 days between the corticosteroid administration and the biopsy. The biopsy samples included leukocytoclastic vasculitis (n = 5), medium-vessel vasculitis (n = 1), interface dermatitis (n = 6), perniosis (n = 2), tumid lupus (n = 1), erythema nodosum (n = 4), calciphylaxis (n = 1), and nonspecific epidermal

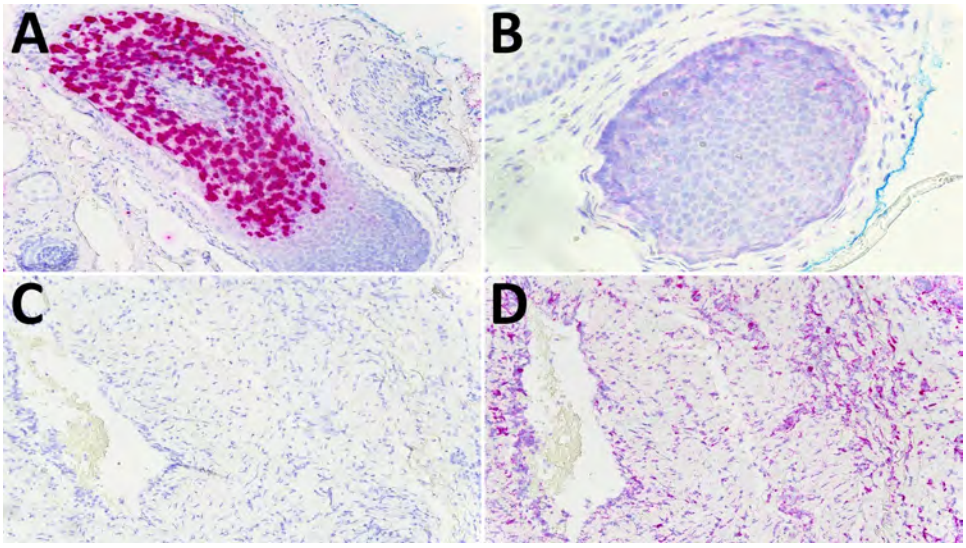

Figure. In situ hybridization (RNAscope) (5) for trichodysplasia spinulosa polyomavirus (TSPyV) in tissue samples, United States. A) Positive control tissue from a case of trichodysplasia spinulosa with staining for TSPyV. Original magnification ×200. B) peptidylprolyl isomerase B (PPIB) RNA probe staining on the same control tissue. Original magnification ×400. C) A representative case of inflammatory dermatosis with no staining for TSPyV RNA. Original magnification ×200. D) PPIB RNA probe staining on the same tissue in (C). Original magnification ×200.

Table. Cases evaluated for trichodysplasia spinulosa polyomavirus using RNAscope in situ hybridization, United States*

Case	Diagnosis	PPIB control probe result	TSPyV probe result	Days from steroid dose to biopsy
Control	Trichodysplasia spinulosa	Positive	Positive	Not applicable
1	Medium vessel vasculitis with epidermal necrosis and fibrinoid degeneration of superficial vessels (favor polyarteritis nodosa)	Positive	Negative	No steroid use
2	Erythema nodosum	Positive	Negative	No steroid use
3	Erythema nodosum	Positive	Negative	No steroid use
4	Erythema nodosum	Positive	Negative	No steroid use
5	Superficial and deep perivascular inflammation with eosinophils (favor resolving erythema nodosum)	Positive	Negative	No steroid use
6	Leukocytoclastic vasculitis	Positive	Negative	No steroid use
7	Leukocytoclastic vasculitis	Positive	Negative	No steroid use
8	Leukocytoclastic vasculitis	Positive	Negative	<1
9	Leukocytoclastic vasculitis	Positive	Negative	<1
10	Leukocytoclastic vasculitis	Positive	Negative	No steroid use
11	Interface dermatitis with eosinophils	Positive	Negative	10
12	Interface dermatitis	Positive	Negative	<1
13	Interface dermatitis with increased dermal mucin	Positive	Negative	No steroid use
14	Interface dermatitis	Positive	Negative	7
15	Interface dermatitis	Positive	Negative	<1
16	Interface dermatitis	Positive	Negative	<1
17	Perniosis	Positive	Negative	1,949
18	Perniosis	Positive	Negative	<1
19	Consistent with calciphylaxis	Positive	Negative	No steroid use
20	Epidermal ulceration with mixed inflammation and background stasis changes	Positive	Negative	No steroid use
21	Vasculopathy with focal calcium deposition (favor vasculopathy)	Positive	Negative	No steroid use
22	Ulceration with dermal necrosis, focal intravascular fibrin, and focal subtle calcium deposits (favor vasculopathy)	Positive	Negative	1
23	Neutrophilic panniculitis with fibrin thrombi and focal vessel wall calcification (favor Sweet syndrome)	Positive	Negative	1,494
24	Tumid lupus	Positive	Negative	108
25	Superficial and deep perivascular and periadnexal lymphocytic infiltrate with focal overlying vacuolar interface change and dyskeratosis, compatible with lupus	Positive	Negative	<1

*PPIB, peptidylprolyl isomerase B RNA; TSPyV, trichodysplasia spinulosa polyomavirus.

dermatoses (n =5). In addition, 1 sample of trichodysplasia spinulosa was included as a positive control.

We performed in situ hybridization by using a custom RNAScope probe (*5*) targeting the complete TSPyV genome on tumor-associated endothelial cells within 25 dermatologic samples representing a range of inflammatory conditions. We used a peptidylprolyl isomerase B RNA probe as a positive control for RNA integrity in all specimens (Figure). We did not detect TSPyV in endothelial cells in any of the 25 inflammatory skin biopsy samples. In contrast, the trichodysplasia spinulosa control had positive staining, and peptidylprolyl isomerase B staining was present in all samples (Table).

We found no evidence of TSPyV infection in endothelial cells in this survey of cutaneous inflammatory conditions, suggesting that TSPyV does not play a role in the cutaneous inflammatory conditions we included. Of note, our cohort is small compared with that of the previous study, which initially led to the identification of TSPyV in 3 cases from 252 specimens (*3*). Therefore, the prevalence of TSPyV infection of endothelial cells might be too low to be detected in a cohort of only 25 cases. Our findings provide evidence that endothelial TSPyV infection is not commonly detected in inflammatory skin biopsy specimens and helps refine the spectrum of tissues and clinical settings in which TSPyV should be considered.

Evaluation and reporting of these cases were performed under research protocols approved by the institutional review board of Stanford University. The patients provided informed consent for the research.

About the Author

Dr. Espinal is a fourth-year anatomic and clinical pathology resident at Stanford University and an incoming gastrointestinal pathology fellow. His research interests include gastrointestinal, hematologic, and microbiologic pathology.

References

1. Lawrence L, Wang A, Charville G, Liu CL, Garofalo A, Alizadeh A, et al. Identification and confirmation via in situ hybridization of Merkel cell polyomavirus in rare cases of posttransplant cutaneous T-cell lymphoma. J Cutan Pathol. 2023;50:835–44. https://doi.org/10.1111/cup.14486
2. Sadeghi M, Aaltonen LM, Hedman L, Chen T, Söderlund-Venermo M, Hedman K. Detection of TS polyomavirus DNA in tonsillar tissues of children and adults: evidence for site of viral latency. J Clin Virol. 2014;59:55–8. https://doi.org/10.1016/j.jcv.2013.11.008
3. van der Meijden E, Horváth B, Nijland M, de Vries K, Rácz EK, Diercks GF, et al. Primary polyomavirus infection, not reactivation, as the cause of trichodysplasia spinulosa in immunocompromised patients. J Infect Dis. 2017;215: 1080–4.4. Borgogna C, Albertini S, Zavattaro E, Veronese F, Peruzzi L, van der Meijden E, et al. Primary trichodysplasia spinulosa polyomavirus infection in a kidney transplant child displaying virus-infected decoy cells in the urine. J Med Virol. 2019;91:1896–900. https://doi.org/10.1002/jmv.25519
5. Lawrence L, Wang A, Charville G, Toland A, Pinsky B, Natkunam Y, et al. Trichodysplasia spinulosa polyomavirus endothelial infection, California, USA. Emerg Infect Dis. 2022;28:1935–7. https://doi.org/10.3201/eid2809.220856

Address for correspondence: Sebastian Fernandez-Pol, Department of Pathology, Stanford University School of Medicine, 300 Pasteur Dr, Rm H2110, Stanford, CA 94305, USA; email: sfernand@stanford.edu

Human Infection with Japanese Encephalitis Virus Genotype V, China, 2025

Wenjing Zou,[1] Yan Peng,[1] Jing Li,[1] Li Cai,[1] Weifeng Tang, Junjing Yang, Xiang Li, Junqiang Xu, Guodong Liang

Author affiliations: Hubei Province Center for Disease Control and Prevention, Wuhan, China (W. Zou, Y. Peng, J. Li, J. Yang, X. Li, J. Xu); Wuhan Center for Disease Control and Prevention, Wuhan (L. Cai, W. Tang); National Key Laboratory of Intelligent Tracking and Forecasting for Infectious Diseases, National Institute for Viral Disease Control and Prevention, Chinese Center for Disease Control and Prevention Chinese Center for Disease Control and Prevention, Beijing, China (G. Liang)

DOI: https://doi.org/10.3201/eid3210.251876

Japanese encephalitis virus genotype V (JEV GV) has caused multiple cases of viral encephalitis in South Korea. We report a human case of JEV GV in China, confirmed by serology, sequencing, and quantitative reverse transcription PCR. We confirm JEV GV infection in China, highlighting the persistent threat of this virus.

Japanese encephalitis virus genotype V (JEV GV) was initially identified in 1952 from viral encephalitis patients in Malaysia and Singapore (*1*). JEV GV was detected again after an ≈60-year hiatus when it was isolated from field-collected *Culex tritaeniorhynchus* mosquitoes in Tibet (Medog County), China,

[1]These authors contributed equally to this article

Figure 1. Timeline of a human case of Japanese encephalitis virus genotype V infection in China, 2025. Timeline spans from birth to death, indicating the timing of specimen collection, specimen types, and corresponding laboratory results. CSF, cerebrospinal fluid; IgM, Japanese encephalitis virus IgM detected by capture ELISA; NGS, next-generation sequencing; qRT-PCR, quantitative reverse transcription PCR; +, positive; –, negative.

in 2009 (*2*). Subsequently, JEV GV has been associated with multiple cases of viral encephalitis in South Korea and is now recognized as an emerging pathogen with considerable public health significance (*3*). Despite its reemergence, surveillance data from mainland China after 2009 had detected exclusively JEV genotype I (GI) in both mosquito populations and human clinical samples, suggesting a possible discontinuity in the circulation of JEV GV in this region (*4*). We report a fatal case of JEV GV infection, highlighting the persistent and evolving threat posed by this genotype.

A male neonate was delivered vaginally on October 6, 2025. Both mother and neonate were in good health at discharge. Neither had a recent history of travel to or residence in a JEV-endemic area outside of Wuhan, China. Laboratory testing in the mother indicated no evidence of recent or past JEV infection (IgM- and IgG-negative and JEV quantitative reverse transcription PCR [qRT-PCR]–negative 3 days after illness onset in infant) and she had not been vaccinated against JE. On day 21 after birth, a high fever (39.3°C) developed, and the neonate was admitted to Wuhan Children's Hospital (Wuhan, China). During hospitalization (October 27–November 6, 2025), clinical manifestations were characterized by persistent high fever (37.8–40.0°C), coma, and convulsions. A diagnosis of suspected viral encephalitis was made, and the neonate unfortunately died on November 7, 2025.

We collected 5 specimens for laboratory testing: 2 cerebrospinal fluid (CSF) samples and 3 serum samples. The initial CSF sample, taken at admission (October 27, 2025), tested positive for JEV nucleic acid by qRT-PCR. Laboratory testing detected JEV-specific IgM in the serum sample collected on day 10 of illness. All other specimens were negative for both JEV RNA and IgM (Figure 1) (*5*).

We conducted next-generation sequencing on the CSF sample collected at admission (*6*). We assembled and designated the complete genome of JEV as the neonate strain (GenBank accession no. PZ393248). Phylogenetic analysis on the basis of the open reading frame sequences of JEV genotypes I–V (GI–GV) revealed that GV segregated into 2 distinct clades. One clade exclusively contained the 1952 prototype strains (Muar from Malaysia and Tengah from Singapore), whereas the other comprised all contemporary isolates, including the neonate strain, the XZ0934 strain (Tibet, China, 2009), and viruses obtained from human cases and mosquitoes in South Korea since 2015 (Figure 2, panel A). The positive qRT-PCR result for JEV in the admission CSF sample, together with the sequencing data, confirmed that the viral encephalitis in this neonate was caused by JEV GV. Further phylogenetic analysis of JEV GV envelope gene sequences revealed that all GV strains fell into 3 distinct evolutionary clades: clade A (the 1952 prototype strains), clade B (including the neonate and XZ0934 strains), and clade C (comprising all South Korea isolates) (Figure 2, panel B). Those results demonstrated a clear phylogeographic pattern of JEV GV, reflecting independent evolution of distinct viral populations in mainland China and South Korea after the reemergence of JEV GV in 2009.

JEV GV has been consistently detected in multiple mosquito species in South Korea, where it has replaced GI as the dominant genotype, and human cases have been reported since 2015 (*2*,*7*). In contrast, since the initial isolation of JEV GV from mosquitoes in Tibet, China, no human cases of JEV GV had been reported in mainland China, nor was it reisolated from vector populations. However, a retrospective serologic analysis of laboratory-confirmed JE cases from 2018–2020 identified 2 patients with possible JEV GV infection in eastern China (Shandong and Zhejiang provinces) (*8*). During previous surveillance in Wuhan in 2009–2010, JEV GI was isolated from mosquitoes, whereas GIII had been detected in earlier mosquito collections (*9*). Together with the identification of the neonate strain in Central China and the earlier detection of the XZ0934 strain in Tibet, our findings confirm the established presence of JEV GV in southwestern, central, and eastern China. Of note, in recent years, JE cases caused by JEV GIV

and GV have been increasing, with geographic expansion into Australia and South Korea (*3*,*10*). The detection of this JEV GV case in mainland China, together with those trends, emphasizes the urgent need to strengthen genotype-based detection and surveillance of JEV for effective Japanese encephalitis prevention and control.

This work was supported by Major Projects of the National Nature Science Foundation of China (project no. 81290342)

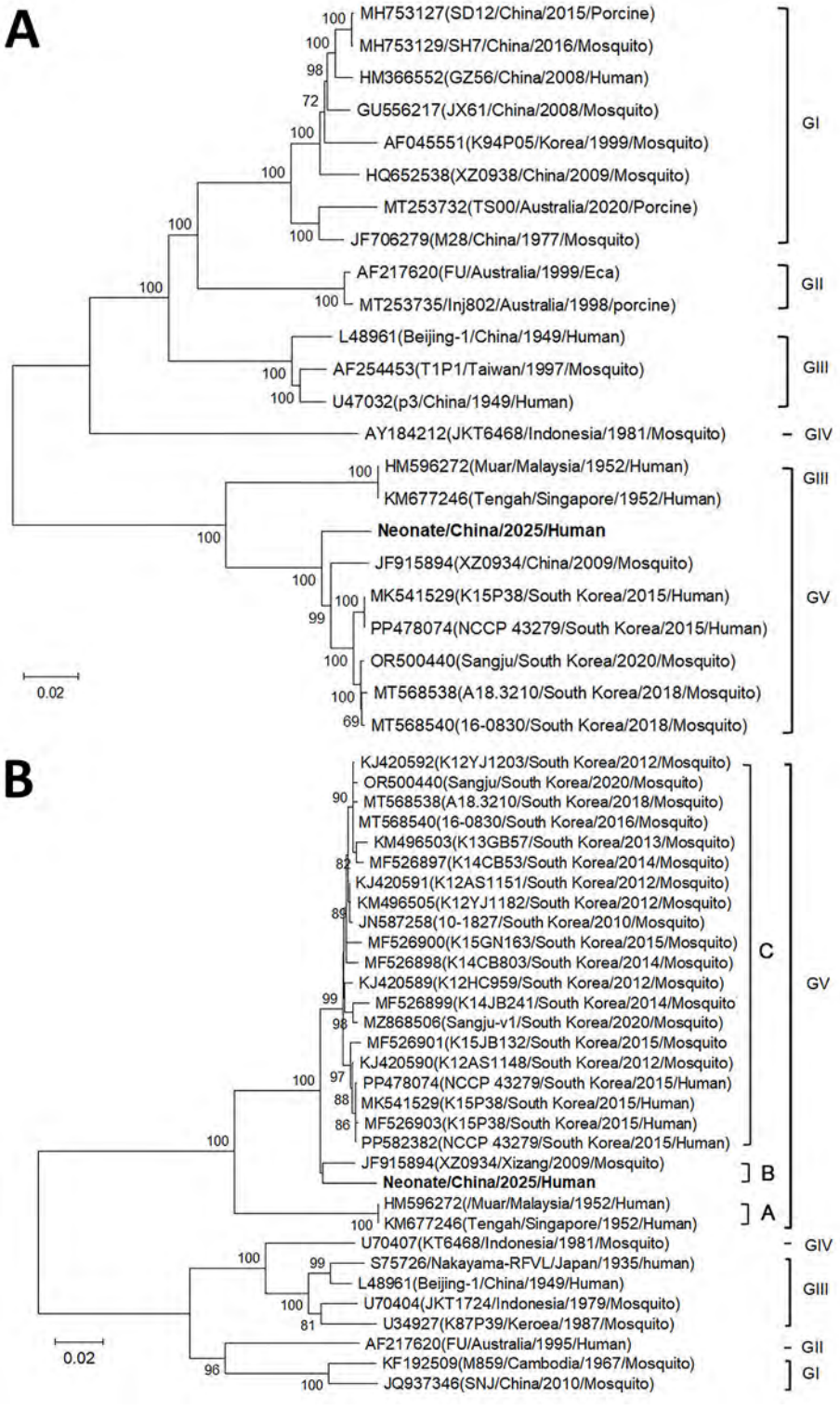

Figure 2. Phylogenetic trees of Japanese encephalitis virus (JEV) genes recovered from a human case in China, 2025. A) Phylogenetic tree built on the basis of the nucleotide sequences of the open reading frame of JEV. B) Phylogenetic tree built on the basis of the nucleotide sequences of the envelope gene of JEV. We constructed the phylogenetic trees by using the neighbor-joining method in MEGA 12.0 software (https://www.megasoftware.net). Neonate sequence from this study is in boldface. Branch numbers indicate percent bootstrap support values. Scale bars indicate nucleotide substitutions per site.

About the Author

Dr. Zou is a professor at the Hubei Provincial Center for Disease Control and Prevention, Wuhan, China, specializing in medical microbiology. Her current research focuses on the detection and diagnosis of mosquitoborne infectious diseases.

References

1. Lee AR, Song JM, Seo SU. Emerging Japanese encephalitis virus genotype V in Republic of Korea. J Microbiol Biotechnol. 2022;32:955–9. https://doi.org/10.4014/jmb.2207.07002
2. Li MH, Fu SH, Chen WX, Wang HY, Guo YH, Liu QY, et al. Genotype V Japanese encephalitis virus is emerging. PLoS Negl Trop Dis. 2011;5:e1231. https://doi.org/10.1371/journal.pntd.0001231
3. Zhang W, Yin Q, Wang H, Liang G. The reemerging and outbreak of genotypes 4 and 5 of Japanese encephalitis virus. Front Cell Infect Microbiol. 2023;13:1292693. https://doi.org/10.3389/fcimb.2023.1292693
4. Liu W, Fu S, Ma X, Chen X, Wu D, Zhou L, et al. An outbreak of Japanese encephalitis caused by genotype Ib Japanese encephalitis virus in China, 2018: a laboratory and field investigation. PLoS Negl Trop Dis. 2020;14:e0008312. https://doi.org/10.1371/journal.pntd.0008312
5. Li W, Feng Y, Zhong H, Jiang M, Zhang J, Lin S, et al. Incongruence between confirmed and suspected clinical cases of Japanese encephalitis virus infection. Front Cell Infect Microbiol. 2024;14:1302314. https://doi.org/10.3389/fcimb.2024.1302314
6. Wang R, Yin Q, Nie K, Li F, Fu S, Cui Q, et al. Is the pathogen spectrum of encephalitis/meningitis changing in China? J Infect. 2025;90:106424. https://doi.org/10.1016/j.jinf.2025.106424
7. Woo JH, Jeong YE, Jo JE, Shim SM, Ryou J, Kim KC, et al. Genetic characterization of Japanese encephalitis virus genotype 5 isolated from patient, South Korea, 2015. Emerg Infect Dis. 2020;26:1002–6. https://doi.org/10.3201/eid2605.190977
8. Zhang WJ, Zhao JR, Yin QK, Liu SH, Wang RC, Fu SH, et al. Serological investigation into the infected genotypes of patients with Japanese encephalitis in the coastal provinces of China. Biomed Environ Sci. 2024;37:716–25.
9. Hu Q, Chen B, Zhu Z, Tian J, Zhou Y, Zhang X, et al. Recurrence of Japanese encephalitis epidemic in Wuhan, China, 2009–2010. PLoS One. 2013;8:e52687. https://doi.org/10.1371/journal.pone.0052687
10. Wang Z, Zhen L, Wei K, Cui B, Wang Z, Farid A, et al. Non-dominant genotypes (GII, GIV and GV) of Japanese encephalitis virus exhibit an elevated evolutionary rate in nature. Microorganisms. 2025;13:2792. https://doi.org/10.3390/microorganisms13122792

Address for correspondence: Junqiang Xu, Hubei Province Center for Disease Control and Prevention, 35 North Zhuodaoquan Rd, Hongshan District, Wuhan 430070, China; email: xjqhbcdc@163.com; or Guodong Liang, National Key Laboratory of Intelligent Tracking and Forecasting for Infectious Diseases, National Institute for Viral Disease Control and Prevention, Chinese Center for Disease Control and Prevention, 155 Chinghai St, Changping District, Beijing 102206, China; email: gdliang@hotmail.com or lianggd@chinacdc.cn

Human Papillomavirus Condylomas of Extragenital Site in Immunocompetent Man, New York, USA, 2025

Sabrina Fong, John G. Zampella

Authors affiliation: New York University Langone Health, Preston Robert Tisch Center for Men's Health, New York, New York, USA

DOI: http://doi.org/10.3201/eid3210.260872

Human papillomavirus types 6 and 11 are associated with mucosal condylomata acuminata, with rare reports of extragenital manifestations. We report a case of condyloma localized to the neck of an immunocompetent heterosexual man, without concurrent anogenital lesions. Our findings challenge theories of the site-specific tropism of these human papillomavirus types.

Human papillomavirus (HPV) types 6 and 11 have long been associated with condylomata acuminata, accounting for 90% of warts affecting the anogenital region (*1*). History of immunosuppression, both primary or secondary, is associated with HPV-related diseases, making affected patients susceptible to development of cutaneous and mucosal warts (2). Reports of extragenital manifestations of condylomas are rare, with previous cases being associated with pediatric populations, men who have sex with men, and persons with a history of HIV. We report a case of HPV types 6 and 11–positive condylomas localized to the lateral neck of an immunocompetent heterosexual man without concurrent anogenital involvement.

In 2025, a heterosexual man in his 40s with an unremarkable medical history sought treatment for a growth on the right side of his neck present for 1 year prior, with reported increase in size. On examination, we noted 6 clustered verrucous-to-mamillated brown papules distributed along the right lateral neck (Figure). Our initial differential diagnosis included inflamed seborrheic keratoses and verruca vulgaris. We treated the lesions with cryotherapy, which provided temporary resolution. The patient returned to our clinic 11 months later for recurrence. We performed a shave biopsy, which showed papillated epidermal hyperplasia with hypergranulosis, compact orthokeratosis, and dilated blood vessels in the papillary dermis. HPV testing by in situ hybridization was positive for HPV types 6 and 11. Screening tests for sexually transmitted infections revealed negative results for gonorrhea, chlamydia, syphilis, and HIV. Complete blood count testing and a comprehensive

metabolic panel also yielded results that were within reference limits. Immunologic screening revealed a positive antinuclear antibody titer of 1:80 (reference <1:40) but unremarkable levels of IgA, IgG, and IgM.

Our case report challenges the traditional paradigm of HPV types 6 and 11 tropism to mucosal skin (*3*). Although reports do exist describing condylomas at extragenital cutaneous sites, those reports have largely involved children, patients with immunosuppression, or persons with concurrent genital involvement (*4*–*6*). One report described a patient with extragenital cutaneous HPV type 6 without genital involvement; however, the patient had a history of HIV (*6*). Although reports of extragenital condylomas and cutaneous HPV types 6 infection exist, cases of HPV types 6 and 11–positive extragenital cutaneous lesions in immunocompetent adults without concurrent anogenital disease are rare.

HPV is known to affect mucosal tissue, particularly of the head and neck, with HPV types 16 accounting for most oropharyngeal squamous cell carcinomas (*7*). Of interest, HPV types 6 and 11 can be co-transmitted with higher-risk types of HPV in genital skin (*8*,*9*). Hypotheses for transmission to this area of the neck include autoinoculation, fomites, skin-to-skin contact with mucosal skin, or even vertical transmission (*10*). A limitation in our case report was the inability to distinguish between HPV types 6 and 11 based on laboratory in situ hybridization technique. Nonetheless, this case highlights the possibility of condylomas in nonanogenital cutaneous sites in immunocompetent hosts, emphasizing that practitioners should consider biopsy with HPV typing in atypical verrucous lesions on cutaneous sites.

About the Authors

Ms. Fong is a research fellow at New York University Grossman School of Medicine. Her research interests include dermatology, infectious diseases, and artificial intelligence applications in medicine.

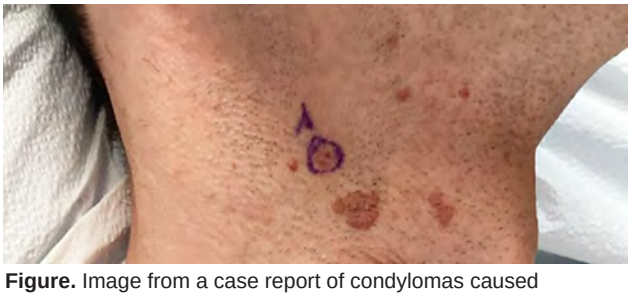

Figure. Image from a case report of condylomas caused by human papillomavirus on extragenital cutaneous site in immunocompetent man, New York, USA, 2025. Brown, clustered, verrucous-to-mamillated papules are shown on the right lateral neck. The circled lesion underwent biopsy.

Dr. Zampella is an associate professor of dermatology at New York University Grossman School of Medicine and a board-certified dermatologist at New York University Langone's Preston Robert Tisch Center for Men's Health. His clinical and academic interests include medical, surgical, and cosmetic dermatology, with particular focus on men's health, LGBTQ+ dermatology, and complex inflammatory skin disease.

References

1. Leslie SW, Sajjad H. Condylomata acuminata (genital warts). In: Kumar S, editor. StatPearls. Treasure Island (FL): StatPearls Publishing; 2025.
2. Hewavisenti RV, Arena J, Ahlenstiel CL, Sasson SC. Human papillomavirus in the setting of immunodeficiency: pathogenesis and the emergence of next-generation therapies to reduce the high associated cancer risk. Front Immunol. 2023;14:1112513. https://doi.org/10.3389/fimmu.2023.1112513
3. Egawa N, Egawa K, Griffin H, Doorbar J. Human papillomaviruses; epithelial tropisms, and the development of neoplasia. Viruses. 2015;7:3863–90. https://doi.org/10.3390/v7072802
4. Blauvelt A, Duarte AM, Pruksachatkunakorn C, Leonardi CL, Schachner LA. Human papillomavirus type 6 infection involving cutaneous nongenital sites. J Am Acad Dermatol. 1992;27:876–9. https://doi.org/10.1016/0190-9622(92)70271-G
5. Achdiat PA, Septharina R, Rowawi R, Dharmadji HP, Puspitosari D, Usman HA, et al. A review and case study of genital and extragenital human papillomavirus type 6 and 11 infections in men who have sex with men accompanied by human immunodeficiency virus infection. HIV AIDS (Auckl). 2024;16:175–82. https://doi.org/10.2147/HIV.S451989
6. Achdiat PA, Larasati R, Hidayah RMN, Avriyanti E, Usman HA, Maharani RH. Atypical HPV typing: detection of genital-associated HPV type 6 in verruca vulgaris of the hands and feet in an HIV-positive patient. Int Med Case Rep J. 2025;18:67–74. https://doi.org/10.2147/IMCRJ.S494454
7. Marur S, D'Souza G, Westra WH, Forastiere AA. HPV-associated head and neck cancer: a virus-related cancer epidemic. Lancet Oncol. 2010;11:781–9. https://doi.org/10.1016/S1470-2045(10)70017-6
8. Chaturvedi AK, Katki HA, Hildesheim A, Rodríguez AC, Quint W, Schiffman M, et al.; CVT Group. Human papillomavirus infection with multiple types: pattern of coinfection and risk of cervical disease. J Infect Dis. 2011;203:910–20. https://doi.org/10.1093/infdis/jiq139
9. Wei X, Zhang J, Mei Y, Dai Q, Yang X, Wang X. Prevalence and genotype distribution of HPV6/11/16/18 infections among 180,276 outpatient females from a Women's and Children's Central Hospital, 2015–2021, Chengdu, China. Sci Rep. 2023;13:22249. https://doi.org/10.1038/s41598-023-48222-1
10. Ardekani A, Taherifard E, Mollalo A, Hemadi E, Roshanshad A, Fereidooni R, et al. Human papillomavirus infection during pregnancy and childhood: a comprehensive review. Microorganisms. 2022;10:1932. https://doi.org/10.3390/microorganisms10101932

Address for correspondence: John G. Zampella, New York University Grossman School of Medicine, 550 1st Ave, New York, NY 10016, USA; email: john.zampella@nyulangone.org

Cocirculation of Human Monkeypox Virus Clade 1b with Varicella Zoster Virus, Uganda

Nicholas Bbosa, Alfred Ssekagiri, Hamidah S. Namagembe, Stella E. Nabirye, Ronald Kiiza, Danstan Kabuuka, Stephen Balinandi, Tom Lutalo, John Kayiwa, Henry Kyobe Bosa, Robert Downing, Michael G. Berg, Mary A. Rodgers, Gavin A. Cloherty, Pontiano Kaleebu, Deogratius Ssemwanga

Author affiliations: Uganda Virus Research Institute, Entebbe, Uganda (N. Bbosa, A. Ssekagiri, S.E. Nabirye, D. Kabuuka, S. Balinandi, T. Lutalo, J. Kayiwa, R. Downing, P. Kaleebu, D. Ssemwanga); Medical Research Council/Uganda Virus Research Institute and London School of Hygiene and Tropical Medicine Uganda Research Unit, Entebbe (N. Bbosa, H.S. Namagembe, R. Kiiza, P. Kaleebu, D. Ssemwanga); Abbott Pandemic Defense Coalition, Abbott Park, Illinois, USA (N. Bbosa, M.G. Berg, M.A. Rodgers, G.A. Cloherty); Uganda Ministry of Health, Kampala, Uganda (H.K. Bosa); Uganda People's Defence Forces, Kampala (H.K. Bosa); Makerere University Lung Institute, Kampala (H.K. Bosa); Abbott Diagnostics, Abbott Park (M.G. Berg, M.A. Rodgers, G.A. Cloherty)

DOI: https://doi.org/10.3201/eid3210.251264

In July 2024, we reported information on the initial human mpox cases in Uganda. Genomic characterization of clinically suspected cases (July–December 2024) revealed cocirculation of several monkeypox virus clade 1b clusters and varicella zoster virus. Our findings highlight the need to refine differential diagnoses by molecular techniques and strengthen surveillance.

In July 2024, human mpox cases were initially reported in Uganda (*1*). As of May 28, 2025, up to 6,479 confirmed mpox cases, including 44 deaths, have been reported (*2*). However, several clinically suspected mpox case-patients tested negative for monkeypox virus (MPXV) by real-time PCR. Mpox can be misdiagnosed as other infections that manifest in rash, especially during the early macule and papule stages of the infection (*3*). Patients with mpox and chickenpox co-infections have been reported in the Democratic Republic of Congo (DRC) (*4*), Burundi (*5*), and Nigeria (*6*). Mpox case-patients frequently experience a febrile prodrome with a high fever 1–4 days before the onset of rash, whereas a low-grade fever is more common in chickenpox patients (*4*). Furthermore, lymphadenopathy is a distinguishing symptom characteristic of mpox infection (*6*) but not chickenpox infection. Here, we describe phylogenetic characterization and mutational analysis of circulating MPXV and other viruses from clinically suspected mpox cases in Uganda.

We conducted real-time PCR on 1,072 samples from patients with clinically suspected MPXV during July–December 2024. A total of 193 persons tested positive for MPXV. Confirmed mpox case-patients were 48.7% male, 51.3% female; cases primarily occurred in persons 16–30 years of age (47.8%) (Appendix 1 Table 1, https://wwwnc.cdc.gov/EID/article/32/10/25-1264-App1.pdf). We obtained 65% of samples from central Uganda. Of the 879 (82%) samples that tested negative for MPXV by PCR, we sequenced a randomly selected subset (127 [14%]) to identify other potential pathogens.

We genotyped 115 MPXV PCR–positive samples using target enrichment NGS (Illumina, https://www.illumina.com; Twist Biosciences, https://www.twistbioscience.com) and the 127 MPXV PCR–negative samples using metagenomic NGS and target enrichment NGS, followed by sequencing on a MiSeq (*1*). We analyzed FASTQ files using UVRI's in-house metagenomic NGS (*1*) and Abbott's DiVir pipelines (*7*) and One Codex software (S.S. Minot et al., unpub. data, https://www.biorxiv.org/content/10.1101/027607v2). We performed phylogenetic tree reconstructions using IQ-TREE (*8*), which showed new Uganda MPXV sequences were clade 1b and genetically close to previous sequences from Uganda and DRC (Figure 1, panel A).

We performed a mutational analysis on Uganda strains (n = 137) using Squirrel software (https://artic.network/software/squirrel), comparing new sequences (n = 115) to previous sequences (n = 22) relative to reference strain Zaire-1979-DQ011155.1 from GenBank. Squirrel infers a maximum-likelihood phylogeny with IQ-TREE2 and performs ancestral state reconstruction to map APOBEC and non-APOBEC mutation events onto individual branches (Figure 1, panel B). TC->TT or GA->AA dinucleotide substitutions were consistent with APOBEC3-mediated cytosine deamination. The reconstructed phylogeny identified 284 mutation events (synonymous, nonsynonymous, intergenic) in Uganda sequences; of those, 118 (41.4%) mutations were APOBEC3-mediated (Appendix 1 Table 2). We observed distinct profiles of affected genes among sequences from this study compared with previously reported Uganda sequences (Appendix

2, https://wwwnc.cdc.gov/EID/article/32/10/25-1264-App2.xlsx). Focusing on nonsynonymous changes, functional annotations of affected genes acquiring APOBEC and non-APOBEC mutations were similar between cohorts. For previous strains, fewer functional annotations were identified related to apoptosis inhibition, viral maturation, and mRNA (de)capping. For strains sequenced in this study, amino acid changes affected proteins involved in inhibition of host responses (inflammasome, T-cell activation) and immune evasion, transcription and RNA metabolism (poly-A polymerase, DNA-dependent RNA polymerase), virion morphogenesis, and viral entry/egress pathways.

We detected varicella zoster virus (VZV) in 106 (83%) of 127 specimens with genome coverage >80% (Figure 2, panel A). VZV sequences were genetically similar to those identified in Nigeria, Ghana, and Guinea-Bissau (Figure 2, panel B). Other pathogens identified included coxsackievirus A6 (9 [7%]), measles virus genotype B3 (7 [6%]), polyomaviruses (5 [4%]), *Cutibacterium acnes*, *Staphylococcus aureus*, *Streptococcus pyogenes,* and *Corynebacterium diphtheriae.* We submitted MPXV sequences (n = 115) to GISAID (https://www.gisaid.org, under EpiPox) in nonsequential installments (Appendix 1) and VZV data (National Center for Biotechnology Information BioProject no. PRJNA1281018) to GenBank (accession nos. PV845252–301).

Genotypic characterization of confirmed mpox cases determined that MPXV sequences belonged to clade Ib and were highly related to previously reported Uganda sequences (*1*), although mutational profiles displayed minimal overlap. Gene ontology suggests recent strains are under selective pressure to evade host responses and increase transmission

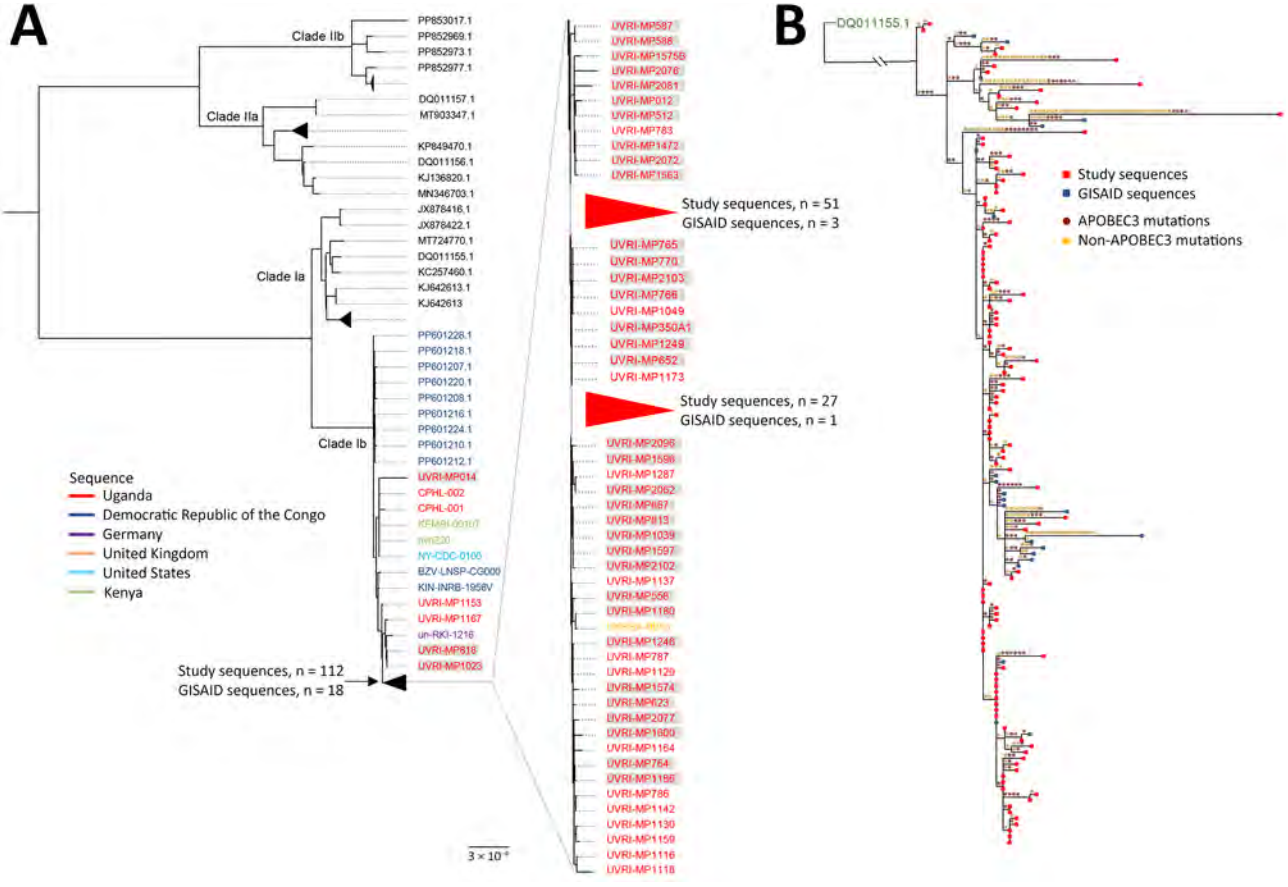

Figure 1. Phylogenetic and mutational characterization of Uganda monkeypox virus (MPXV) strains in study of cocirculation of human MPXV clade 1b with varicella-zoster virus, Uganda. A) Maximum-likelihood phylogenetic tree of MPXV sequences generated with 1,000 bootstrap resampling. Tree includes 115 new sequences from Uganda (highlighted with a gray rectangular background) and 37 clade 1B reference sequences retrieved from GenBank and GISAID (https://www.gisaid.org) (accession numbers provided). Highly similar sequences have been collapsed (denoted by triangle). Scale bar indicates number of nucleotide substitutions per site. B) New (n = 115; red squares) and previously reported (n = 22; blue squares) Uganda sequences were aligned, and Squirrel software was used to infer the maximum-likelihood phylogeny and map APOBEC (brown circle) and non-APOBEC (yellow circle) mutation events. The number of unique mutations from this study and shared mutations distinct from the DQ011155.1 clade I archetype are listed.

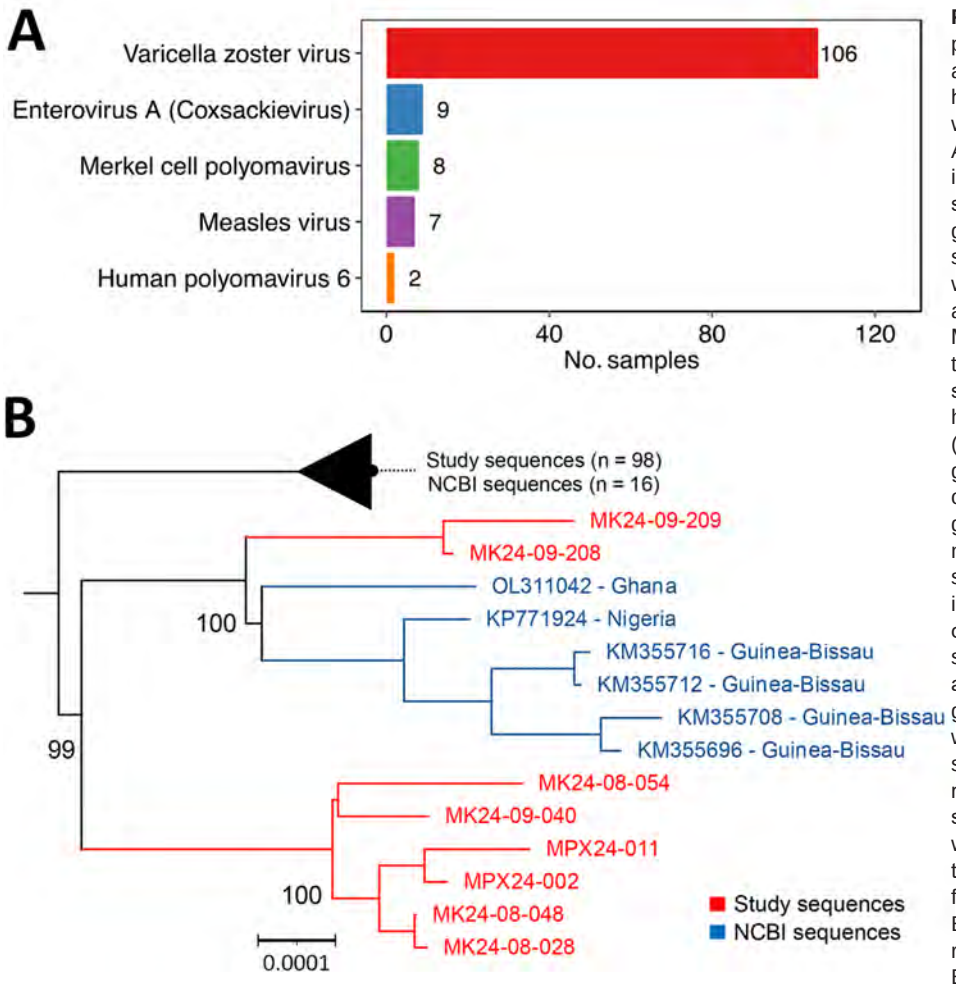

Figure 2. Distribution of viral pathogens and phylogenetic analysis in study of cocirculation of human monkeypox virus clade 1b with varicella-zoster virus, Uganda. A) Viral pathogens detected in monkeypox virus–negative samples by metagenomic next-generation sequencing. Bar plot shows the number of samples in which viruses were identified with a genome coverage ≥80%. B) Maximum-likelihood phylogenetic tree of varicella-zoster virus sequences. The tree includes 106 high-coverage genome sequences (≥80% genome coverage) generated in this study and other publicly available complete genomes from NCBI (accession numbers provided). Most sequences have been collapsed into the triangle at the top, which contains 98 varicella zoster virus sequences generated in this study and 16 publicly available Uganda genomes, together forming a single well-supported clade. Sequences shown individually are those resolving outside that clade: 8 study sequences from Uganda (red), which form 2 distinct lineages, and the 6 publicly available genomes from Ghana, Nigeria and Guinea-Bissau (blue) that are their closest relatives. NCBI, National Center for Biotechnology Information.

through improved replicative and transcriptional fitness. Evidence from Kenya (*9*) and Ethiopia (*10*) indicates that varicella is frequently misdiagnosed as mpox, consistent with DRC (*4*,*11*) and Burundi (*5*) studies that identified VZV in 20 (67%) of 30 samples from clinically suspected persons who tested PCR-negative during an mpox outbreak (*5*). Our study reinforces that mpox can be confused with other febrile, rash-causing illnesses, including varicella. Ongoing MPXV and VZV cocirculation likely explains the increasing number of MPXV PCR–negative results, which in turn could affect case definition criteria for sampling clinically suspected cases in the field. Metagenomic NGS identified MPXV–VZV co-infection in the study's sole fatal mpox case; however, whether the co-infection contributed to the patient's death remains unclear.

Other limitations of our study include presumed underreporting of mpox cases and suboptimal genotyping because of limited sequencing resources. Local, intracountry, and joint regional efforts for cross-border surveillance are essential for curbing the spread of mpox. Cocirculation of MPXV and VZV highlights the need to adhere to clinical case definitions but also incorporate molecular testing to distinguish similarly manifesting infections.

Acknowledgments

We thank the Uganda Ministry of Health, the field teams, and the laboratory staff who participated in the sample collection and laboratory testing. We also thank the scientists and bioinformaticians at the Uganda Virus Research Institute and Medical Research Council/Uganda Virus Research Institute and the London School of Hygiene and Tropical Medicine Uganda Research Unit Sequencing Platform for carrying out the genomic sequencing.

Ethical approval was obtained from the Uganda Virus Research Institute Research Ethics Committee (approval no. GC/127/908) and the Uganda National Council of Science and Technology (approval no. HS2543ES).

About the Author

Dr. Bbosa is an assistant professor at the London School of Hygiene and Tropical Medicine; a senior scientist at the Medical Research Council/Uganda Virus Research Institute and the London School of Hygiene and Tropical Medicine Uganda Research Unit, Entebbe, Uganda; and a project investigator at the Uganda Virus Research Institute in Entebbe. His primary research interests are viral genomics, molecular epidemiology, pathogen phylodynamics, and infectious disease pandemic preparedness and response.

References

1. Bbosa N, Nabirye SE, Namagembe HS, Kiiza R, Ssekagiri A, Munyagwa M, et al. Case reports of human monkeypox virus infections, Uganda, 2024. Emerg Infect Dis. 2025;31:144–8. https://doi.org/10.3201/eid3101.241269
2. Uganda Ministry of Health, Mpox Incident Management Team. National mpox situation report [cited 2025 Jun 15]. https://www.afro.who.int/sites/default/files/2025-05/Ug_Mpox_Sitrep_28May25.pdf
3. Jezek Z, Szczeniowski M, Paluku KM, Mutombo M, Grab B. Human monkeypox: confusion with chickenpox. Acta Trop. 1988;45:297–307.
4. Hughes CM, Liu L, Davidson WB, Radford KW, Wilkins K, Monroe B, et al. A tale of two viruses: coinfections of monkeypox and varicella zoster virus in the Democratic Republic of Congo. Am J Trop Med Hyg. 2020;104:604–11. https://doi.org/10.4269/ajtmh.20-0589
5. Nzoyikorera N, Nduwimana C, Schuele L, Nieuwenhuijse DF, Koopmans M, Otani S, et al. Monkeypox clade Ib virus introduction into Burundi: first findings, July to mid-August 2024. Euro Surveill. 2024;29:2400666. https://doi.org/10.2807/1560-7917.ES.2024.29.42.2400666
6. Mmerem JI, Johnson SM, Iroezindu MO. Monkeypox and chickenpox co-infection in a person living with human immunodeficiency virus. J Infect Dev Ctries. 2024;18:1152–6. https://doi.org/10.3855/jidc.18318
7. Bbosa N, Ssemwanga D, Weiss SL, Kalungi S, Mawanda A, Ssentudde R, et al. Identification of anthrax as the cause of a cluster of unexplained deaths, Uganda, 2023: the role of metagenomic next-generation sequencing and postmortem specimens. Am J Trop Med Hyg. 2025;112:835–9. https://doi.org/10.4269/ajtmh.24-0489
8. Nguyen LT, Schmidt HA, von Haeseler A, Minh BQ. IQ-TREE: a fast and effective stochastic algorithm for estimating maximum-likelihood phylogenies. Mol Biol Evol. 2015;32:268–74. https://doi.org/10.1093/molbev/msu300
9. Onyango C, Hines JZ, Ochieng M, Amon D, Lidechi S, Anguko E, et al. High prevalence of varicella zoster virus infection among persons with suspect mpox cases during an mpox outbreak in Kenya, 2024. Am J Trop Med Hyg. 2025;113:1411–4. https://doi.org/10.4269/ajtmh.25-0308
10. Tayachew A, Kebede N, Alayu M, Onywera H, Kanyerezi S, Agune A, et al. Genomic evidence of varicella-zoster virus among mpox-suspected cases in Ethiopia during the 2022 mpox multi-country outbreak. Sci Rep. 2025;16:148. https://doi.org/10.1038/s41598-025-29116-w
11. Hoff NA, Morier DS, Kisalu NK, Johnston SC, Doshi RH, Hensley LE, et al. Varicella coinfection in patients with active monkeypox in the Democratic Republic of the Congo. EcoHealth. 2017;14:564–74. https://doi.org/10.1007/s10393-017-1266-5

Address for correspondence: Nicholas Bbosa, Medical Research Council/Uganda Virus Research Institute and London School of Hygiene and Tropical Medicine Uganda Research Unit, Plot 51–59 Nakiwogo Rd, Entebbe, Uganda; email: nicholas.bbosa@mrcuganda.org

Age Differences in Pertussis Epidemics, New South Wales, Australia, 2015 and 2024

Ella F. Madden, Sally L. Ellis, Andrea Parisi, Christine E. Selvey, Janaki Amin

Author affiliations: New South Wales Ministry of Health, St. Leonards, New South Wales, Australia (E.F. Madden, S.L. Ellis, A. Parisi, C.E. Selvey, J. Amin); University of Sydney, Sydney, New South Wales, Australia (A. Parisi); Australian National University, Canberra, Australian Capital Territory, Australia (A. Parisi); Macquarie University, Sydney (J. Amin); University of New South Wales, Kensington, New South Wales, Australia (J. Amin).

DOI: https://doi.org/10.3201/eid3210.260332

We compared data from the 2015 and 2024 pertussis epidemics in New South Wales, Australia. In 2024, we found twice as many notifications and a shift in distribution to older children. COVID-19 interventions and lack of circulation of pertussis likely contributed to an age cohort immunity gap and increased infections.

Pertussis (whooping cough) is a highly contagious respiratory disease caused by *Bordetella pertussis* bacteria. Although infants <6 months of age are at greatest risk for severe disease and death (*1*), infections occur across all age groups. Immunity from both immunization and infection wanes over time. Consequently, pertussis remains endemic in New South Wales (NSW), Australia, and causes epidemics every 3–4 years (*2*,*3*).

Pertussis vaccines are funded in Australia under the national immunization program. Since

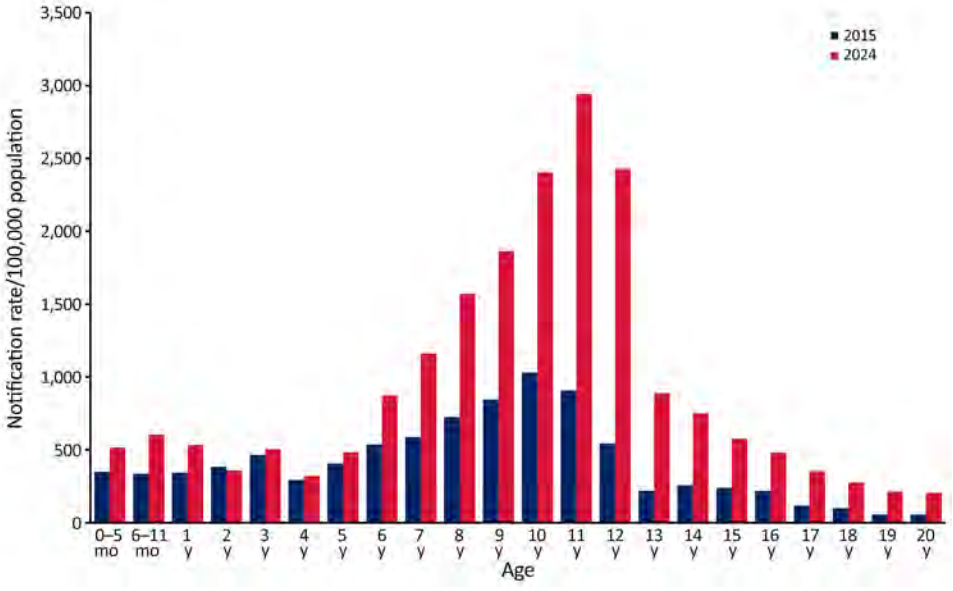

Figure. Age-specific pertussis notification rates per 100,000 population for persons 0–20 years of age, by year notified, New South Wales, Australia, 2015 and 2024. Because no population data were available for children 0–5 months and 6–11 months, the total population estimates for children <1 year of age in 2015 and 2024 was halved. These populations were used for the rate calculations.

2009, pertussis vaccines are administered at 6 weeks, 4 months, 6 months, 18 months, and 4 years of age in NSW; vaccination during pregnancy has been funded since 2015. A booster dose is given at age 12–13 through the NSW school vaccination program (*4*). The COVID-19 pandemic disrupted infection cycles, likely because of widespread nonpharmaceutical interventions that have reduced transmission of multiple respiratory pathogens (*5*). From 2020–2023, NSW reported historically low pertussis activity, with <600 notifications annually (*3*). We describe age- and sex-specific patterns across 2 epidemics in NSW, in 2015 and 2024, and discuss the potential results of pandemic-related interventions and waning immunity as likely contributors to observed pattern changes.

We calculated age-specific rates by using annual NSW population estimates (*6*). Confirmed pertussis cases (*7*) are reported to the NSW notifiable conditions information management system, a statutory public health register of infectious diseases legally notifiable to NSW Health (*8*). Our review of those data reveals NSW experienced a resurgence in 2024, recording the highest annual total since pertussis became notifiable in 1991. After 1991, the most recent NSW epidemic occurred in 2015. During 2015–2024, a total of 68,842 confirmed pertussis cases were reported in NSW, including 12,007 in 2015 and 25,695 in

Table. Demographic characteristics of pertussis cases notified in New South Wales, Australia, 2015 and 2024*

Characteristic	Notifications		Rate, cases/100,000 population†		IRR, 2024 vs. 2015 (95% CI)
	2015	2024	2015	2024	
Age group					
<1 y	336 (2.80)	503 (1.96)	342.47	505.03	1.47 (1.28–1.69)
0–5 mo	171 (1.42)	232 (0.90)	348.58	516.33	1.48 (1.22–1.8)
6–11 mo	165 (1.37)	271 (1.05)	336.35	603.13	1.79 (1.48–2.18)
1–4 y	1,477 (12.30)	1,641 (6.39)	372.04	431.54	1.16 (1.08–1.24)
5–9 y	3,020 (25.15)	5,964 (23.21)	617.39	1,187.25	1.92 (1.84–2.01)
10–14 y	2,666 (22.20)	9,762 (37.99)	594.18	1,904.40	3.21 (3.07–3.35)
15–24 y	981 (8.17)	2,738 (10.66)	99.50	275.72	2.77 (2.58–2.98)
25–34 y	645 (5.37)	859 (3.34)	57.77	73.85	1.28 (1.15–1.42)
35–44 y	905 (7.54)	1,185 (4.61)	87.96	105.64	1.2 (1.1–1.31)
45–54 y	853 (7.10)	1,332 (5.18)	86.51	131.25	1.52 (1.39–1.65)
≥55 y	1,124 (9.36)	1,711 (6.66)	54.41	71.95	1.32 (1.23–1.43)
Sex					
M	5,607 (46.70)	12,883 (50.14)	148.47	317.32	2.14 (2.07–2.21)
F	6,386 (53.19)	12,801 (49.82)	166.32	311.78	1.87 (1.82–1.93)
Unknown/other	13 (0.11)	10 (0.04)	NA	NA	NA
Median age, y (IQR)	11 (7–33)	11 (9–17)	NA	NA	NA
Total cases	12,007 (100.0)	25,695 (100.0)	157.65	314.68	2 (1.95–2.04)

*Values are no. (%) cases except as indicated. IRR, incidence rate ratio. NA, not applicable.
†As no population was available for the groups 0–5 mo and 6–11 mo, the total population estimates for people <1 years of age in 2015 and 2024 respectively was halved. Those populations were then used for rate calculations.

2024. Compared with 2015, notifications in 2024 more than doubled, and the age distribution shifted toward older children, with the greatest proportion of notifications in 10–14-year-olds. The notification rate in 2024 (314.7/100,000 population) was almost double the rate of 2015 (157.7/100,000 population) (Table). The ratio of male to female notifications in 2015 was 0.88; in 2024, the ratio of male to female notifications was 1.08.

In 2015, the highest proportion of cases occurred in children 5–9 years of age (25.2%), followed by those 10–14 years of age (22.2%). By contrast, children 10–14 years of age dominated the 2024 epidemic caseload (38.0%), followed by those 5–9 years of age (23.2%). The percentage of cases in children <5 years of age declined from 15.1% in 2015 to 8.3% in 2024 and in children <6 months of age from 1.4% in 2015 to 0.9% in 2024. Conversely, the notification rate for children 10–14 years of age more than tripled, from 594.2 cases/100,000 population in 2015 to 1,904.4 cases/100,000 population in 2024 (incidence rate ratio [IRR] 3.21 [95% CI 3.07–3.35]) (Table). That increase was not observed to the same extent in other age groups, particularly those ≥25 years of age. The median age at notification remained consistent at 11 years in both epidemics. However, the interquartile range for age narrowed substantially, from 7–33 in 2015 to 9–17 in 2024 (Table), reflecting a more concentrated distribution of cases among school-age children in 2024.

The COVID-19 pandemic likely changed health-seeking and testing behaviors, resulting in a higher proportion of persons with laboratory-confirmed pertussis. That behavior change might have contributed to higher notifications in 2024, but it is unlikely to explain the pronounced shift in age distribution. Several factors possibly contributed. The near absence of circulating pertussis during the pandemic could have disrupted natural immune boosting from exposure to *Bordetella pertussis*. That disruption probably had the greatest effect on children approaching adolescence, as reflected in the age-specific rates (Figure). In 2024, the risk of infection increased with each year of age among school-age children, particularly in those 8–12 years of age, who were several years past their last scheduled vaccine dose and therefore more susceptible to illness because of waning immunity. That immunity gap likely enabled rapid transmission through school populations. In contrast, the relative reduction in the age-specific rates from age 13 years onward, seen in both epidemics but more noticeably in 2024, signals the effect of the adolescent booster and its importance in maintaining immunity (Figure). The NSW pertussis resurgence in 2024 aligns with international observations after the easing of COVID-19 restrictions, with increased incidence among older children reported by several countries (*9*). Those parallels point to global immunity gaps attributable to reduced pathogen circulation during the pandemic.

In conclusion, the 2024 NSW pertussis epidemic differed substantially from the 2015 epidemic in both magnitude and age profile. Waning immunity, exacerbated by reduced natural boosting during the COVID-19 pandemic, likely contributed to the increased effects, particularly in children 8–12 years of age. Future research should explore vaccine effectiveness during extended inter-epidemic periods and the role of adolescent boosters to mitigate transmission. Adjustments should be made to surveillance and outbreak response strategies to prevent and reduce the effects of future outbreaks.

About the Author

Ms. Madden is a senior public health advisor at Health Protection NSW, within the NSW Ministry of Health. Her work focuses on surveillance, reporting, and policy for vaccine-preventable and respiratory diseases.

References

1. Parisi A, Nuñez O, López-Perea N, Masa-Calles J. Reduced pertussis disease severity in infants following the introduction of pertussis vaccination of pregnant women in Spain, 2015–2019. Vaccine. 2024;42:2810–6. https://doi.org/10.1016/j.vaccine.2024.03.028
2. Leong RNF, Wood JG, Turner RM, Newall AT. Estimating seasonal variation in Australian pertussis notifications from 1991 to 2016: evidence of spring to summer peaks. Epidemiol Infect. 2019;147:e155. https://doi.org/10.1017/S0950268818003680
3. NSW Health Communicable Diseases Branch and Centre for Epidemiology and Evidence. Pertussis notifications in NSW residents by year of disease onset and age group. January 2015 to December 2024 [cited 2025 Jul 25]. https://www.health.nsw.gov.au/IDD/#/PERT/periodandagegroup
4. Health NSW. NSW immunisation schedule. 2025 [cited 2025 Sep 22]. https://www.health.nsw.gov.au/immunisation/publications/nsw-immunisation-schedule.pdf
5. van der Kooi S, Beard F, Dey A, McIntyre P, Imai C, Amin J. Pertussis notifications decline in Australia during COVID-19 non-pharmaceutical interventions, 2020–2021. Commun Dis Intell. 2024;48:24. https://doi.org/10.33321/cdi.2024.48.24
6. Australian Bureau of Statistics. Population at 30 June, by sex and single year of age, NSW, from 1971 onwards. June 2025 ed. Canberra (Australia): Australian Government; 2025 [cited 2025 Dec 22]. https://www.abs.gov.au/statistics/people/population/national-state-and-territory-population/jun-2025
7. Australian Centre for Disease Control. Pertussis (whooping cough) surveillance case definition. Canberra (Australia): Australian Government Department of Health; 2025 [cited

2025 Dec 17]. https://www.cdc.gov.au/resources/publications/surveillance-case-definition-pertussis
8. New South Wales Government. Public health act 2010 no. 127 [cited 2025 Feb 25]. https://legislation.nsw.gov.au/view/html/inforce/current/act-2010-127
9. Gorringe A, Cavell B, Beard F, Tsukada K, Otsuka N, Fu P, et al. Global incidence of pertussis after the COVID-19 pandemic. JAMA Netw Open. 2025;8:e2545963. https://doi.org/10.1001/jamanetworkopen.2025.45963

Address for correspondence: Ella Madden, Health Protection NSW, NSW Ministry of Health, Locked Mail Bag 2030, St. Leonards, NSW 1590, Australia; email: ella.madden@health.nsw.gov.au

Estimated Transmissibility and Case Fatality Rate of Bundibugyo Virus, Uganda, 2007

Bianca de Padua and Andrei R. Akhmetzhanov

Authors affiliation: National Taiwan University College of Public Health, Taipei, Taiwan

DOI: https://doi.org/10.3201/eid3210.261175

Because the epidemiology of Bundibugyo virus remains unclear, we reanalyzed the first recognized outbreak (Uganda, 2007). Adjusting for case underascertainment and the effect of control measures, we estimated the effective reproduction number (1.55, falling to <1 after intervention) and case-fatality rate (31%, declining to 25%). The underascertainment rate was 15%.

Bundibugyo virus (BDBV) is 1 of 6 orthoebolaviruses (genus *Orthoebolavirus*), constituting the species *Orthoebolavirus bundibugyoense* (*1*) and causes rare but severe disease in humans (*2*). Two other orthoebolaviruses, Ebola virus (EBOV) and Sudan virus, have caused the largest outbreaks and are highly lethal; case-fatality rates (CFRs) average ≈50% (*2*). BDBV is considered less lethal; CFRs are reported to be 30%–40%, and it has historically caused only small outbreaks (*3*). The ongoing 2026 outbreak in the Democratic Republic of the Congo and Uganda shows a different pattern: first reports in late May 2026 recorded >600 suspected cases, and >2,000 cases were projected within 3 months (*4*). Despite this potential for large outbreaks, the transmissibility and severity of BDBV remain poorly characterized.

Control measures, such as case isolation, active case finding, infection control in hospitals and isolation wards, and safe burial practices, are key to curbing Ebola outbreaks, in part by limiting superspreading and lowering mortality rates (*5*). However, those measures also alter the epidemiologic parameters used to characterize an outbreak: the desirable reduction in the reproduction number can be accompanied by improved case ascertainment and reduced mortality rates. Failing to account for the effect of control measures can bias estimates of transmissibility and severity, whereas adjusting for them yields values closer to the natural history of the virus. In this study, we reanalyzed the first reported BDBV outbreak (Bundibugyo, Uganda, 2007) (*6*) to obtain robust estimates of transmission potential and CFR adjusted for both case underascertainment and the effect of control measures.

We digitized weekly counts of confirmed and probable cases from a 2010 study (*6*), retaining 110 cases (37 deaths) with a known week of symptom onset. We excluded 6 additional cases (2 deaths) lacking onset dates. Those data are consistent with 116 confirmed and probable cases and 39 deaths (crude CFR 34%) reported for the outbreak (*6*). Control measures were initiated in week 48, which we used to define preintervention and postintervention periods. We estimated transmission with a renewal process incorporating intrinsic back-projection to the time of infection (*7*), informed by the incubation period and time from onset to transmission, the latter adapted from EBOV (*8*). That linked the effective reproduction number (R_t) to the time of infection rather than to symptom onset. We modeled the intervention as a step reduction at week 48 in R_t and in case underascertainment, together with a multiplicative reduction in the CFR. We assumed that deaths were fully recorded throughout the outbreak, whereas nonfatal cases that occurred before the intervention could have been missed (*9*). We fitted the model in a Bayesian framework and report posterior means with 95% credible intervals (CrIs) (Appendix, https://wwwnc.cdc.gov/EID/article/32/10/26-1175-App1.pdf).

Before the intervention, BDBV was capable of sustained transmission of R_t of 1.55 (95% CrI 1.02–2.36). The R_t markedly declined to 0.50 (95% CrI 0.17–1.15) after the intervention (Figure; Appendix Figure 1). We estimated that ≈15% (95% CrI 2.7%–31.7%) of cases were under ascertained, corresponding to 20 (95% CrI 3–51) cases predicted to be missed. After adjusting for underascertainment, the preintervention CFR was 31.4% (95% CrI 21.8%–42.8%), which then

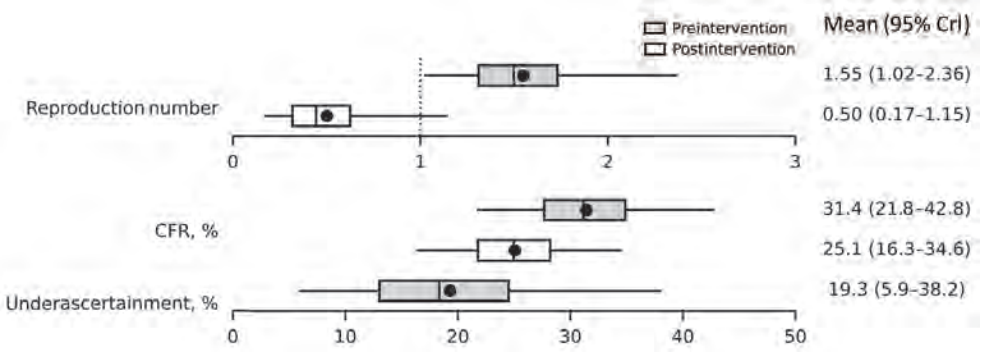

Figure. Estimates of epidemiologic parameters from study of transmissibility and case fatality rate of Bundibugyo virus estimated from first outbreak, Uganda, 2007. Estimates are stratified by preintervention and postintervention periods. Each boxplot displays the interquartile range (box left and right edges), 95% CrI (whiskers), median (vertical line), and mean (solid circle). Dotted vertical line indicates the threshold reproduction number of 1. CFR, case-fatality rate; CrI, credible interval.

decreased to 25.1% (95% CrI 16.3%–34.6%), which translated to an odds ratio of death (postintervention vs. preintervention) of 0.75 (95% CrI 0.40–0.99). Those estimates were robust to the time variation in case-ascertainment during the preintervention period, and posteriors deviated substantially from the priors (Appendix Figures 2–5).

Our findings suggest that BDBV is moderately transmissible; its preintervention reproduction number was ≈1.5 and its CFR ≈31%. That finding places BDBV within the range of other orthoebolaviruses, although with a lower CFR than typical EBOV outbreaks. The R_t fell to <1 after the outbreak response, and the fatality risk also declined (the 95% CrI of the odds ratio excluded 1). A reduction in transmission of ≈35% sufficed to bring the R_t to <1 and was achieved by nonpharmaceutical interventions alone in 2007. Such control measures remain operationally demanding, as the 2026 outbreak shows. A serosurvey among close contacts of survivors conducted 29 months after the 2007 outbreak identified 13 symptomatic infections that had not been recorded (*10*), implying that 21.0% of symptomatic infections were unascertained. That lies within the CrI of our estimate of ≈15% of missed cases, though above our point estimate.

The primary limitation of our study is that it was based on a single small outbreak and used counts digitized from a previously published article, and no BDBV-specific epidemiologic intervals were available. Estimates depended on the assumed time from onset to transmission, the transmission-model structure, and assumptions about death ascertainment. Some CrIs were wide, particularly for the postintervention R_t and the under-ascertainment rate, reflecting the small number of postintervention weeks and the limited information on unascertained cases. Our model also did not reproduce the peak in week 48, which could reflect superspreading (Appendix). Given the scarcity of epidemiologic data on BDBV, our estimates provide a basis for future modeling. Nonetheless, more accurate BDBV-specific estimates of the epidemiologic time intervals and transmission parameters are still needed.

This work was supported by the National Science and Technology Council, Taiwan (NSTC 113-2314-B-002-181-MY3) and National Taiwan University (project no. 115L7869).

About the Author

Ms. de Padua is a graduate of the Global Health Program, College of Public Health, National Taiwan University. Her research interests include modeling of infectious diseases and data analysis. Dr. Akhmetzhanov is an associate professor at National Taiwan University. His research interests include the epidemiology and prevention of infectious disease outbreaks.

References

1. Biedenkopf N, Bukreyev A, Chandran K, Di Paola N, Formenty PBH, Griffiths A, et al. Renaming of genera *Ebolavirus* and *Marburgvirus* to *Orthoebolavirus* and *Orthomarburgvirus*, respectively, and introduction of binomial species names within family Filoviridae. Arch Virol. 2023;168:220. https://doi.org/10.1007/s00705-023-05834-2
2. Towner JS, Sealy TK, Khristova ML, Albariño CG, Conlan S, Reeder SA, et al. Newly discovered Ebola virus associated with hemorrhagic fever outbreak in Uganda. PLoS Pathog. 2008;4:e1000212. https://doi.org/10.1371/journal.ppat.1000212
3. MacNeil A, Farnon EC, Wamala J, Okware S, Cannon DL, Reed Z, et al. Proportion of deaths and clinical features in Bundibugyo Ebola virus infection, Uganda. Emerg Infect Dis. 2010;16:1969–72. https://doi.org/10.3201/eid1612.100627
4. Mooring EQ, Koval WT, Routledge I, Holmdahl I, Hudson K, España G, et al. Modeled scenario projections for the Ebola disease outbreak caused by Bundibugyo virus, 2026. MMWR Morb Mortal Wkly Rep. 2026;75:285–9. https://doi.org/10.15585/mmwr.mm7522e1

5. Osterholm MT, Moore KA, Kelley NS, Brosseau LM, Wong G, Murphy FA, et al. Transmission of Ebola viruses: what we know and what we do not know. mBio. 2015;6:e00137. https://doi.org/10.1128/mBio.00137-15
6. Wamala JF, Lukwago L, Malimbo M, Nguku P, Yoti Z, Musenero M, et al. Ebola hemorrhagic fever associated with novel virus strain, Uganda, 2007–2008. Emerg Infect Dis. 2010;16:1087–92. https://doi.org/10.3201/eid1607.091525
7. Nakajo K, Nishiura H. Estimation of R(t) based on illness onset data: an analysis of 1907–1908 smallpox epidemic in Tokyo. Epidemics. 2022;38:100545. https://doi.org/10.1016/j.epidem.2022.100545
8. Yamin D, Gertler S, Ndeffo-Mbah ML, Skrip LA, Fallah M, Nyenswah TG, et al. Effect of Ebola progression on transmission and control in Liberia. Ann Intern Med. 2015;162:11–7. https://doi.org/10.7326/M14-2255
9. Asai Y, Nishiura H. Joint estimation of the transmissibility and severity of Ebola virus disease in real time. J Biol Syst. 2017;25:587–603. https://doi.org/10.1142/S0218339017400022
10. Clark DV, Kibuuka H, Millard M, Wakabi S, Lukwago L, Taylor A, et al. Long-term sequelae after Ebola virus disease in Bundibugyo, Uganda: a retrospective cohort study. Lancet Infect Dis. 2015;15:905–12. https://doi.org/10.1016/S1473-3099(15)70152-0

Address for correspondence: Andrei R. Akhmetzhanov, Global Health Program & Institute of Epidemiology and Preventive Medicine, College of Public Health, National Taiwan University, No.17 Xuzhou Rd., Zhongzheng District, Taipei 10055, Taiwan; email: akhmetzhanov@ntu.edu.tw

Haemophilus ducreyi Bacteria Causing Cutaneous Ulcer Outbreak in Children, Sierra Leone, December 2025

Jianxu Zhang,[1] Peng Lv,[1] Teng Zhao, Hanji Jiang, James S. Squire, Martin S. Yonnie, Zikan Koroma, Ibrahim F. Kamara, Abdulai A. Jalloh, Guangqian Pei, Yunfei Wang, Hongling Liu, Mohamed B. Jalloh, Zhiqiang Mi

Author affiliations: Changchun Veterinary Research Institute, Chinese Academy of Agricultural Sciences, Changchun, China (J. Zhang); National Key Laboratory of Advanced Biotechnology, Academy of Military Medical Sciences, Beijing, China (P. Lv); State Key Laboratory of Pathogen and Biosecurity, Academy of Military Medical Sciences, Beijing (T. Zhao, H. Jiang, G. Pei, Y. Wang, Z. Mi); University of Sierra Leone, Freetown, Sierra Leone (J.S. Squire); National Public Health Agency, Freetown (J.S. Squire, Z. Koroma, A.A. Jalloh, M.B. Jalloh); Ministry of Health, Bombali DHMT, Makeni, Sierra Leone (M.S. Yonnie); World Health Organization, Health Systems and Services Cluster, Freetown (I.F. Kamara); The Fifth Medical Center of Chinese PLA General Hospital, Beijing (H. Liu); College of Medicine and Allied Health Sciences, University of Sierra Leone, Freetown (M.B. Jalloh)

[1]These authors contributed equally to this article.

DOI: https://doi.org/10.3201/eid3210.260727

We report a cutaneous ulcer outbreak in Sierra Leone in 2025 that predominantly affected ≈403 schoolchildren. The causative agent was confirmed as *Haemophilus ducreyi*, a bacterium traditionally associated with the sexually transmitted infection chancroid but more recently recognized as an emerging cause of lower limb cutaneous ulcers in tropical regions.

Nongenital cutaneous ulcers as a public health problem commonly affect children in many tropical regions, especially in West and Central Africa, the South Pacific, and South Asia (*1*). Yaws, which is caused by *Treponema pallidum* subspecies *pertenue*, has historically been considered the primary causative agent of such ulcers (*2*). In recent years, however, several studies have demonstrated that *Haemophilus ducreyi* is a leading bacterial cause of cutaneous ulcers (lower leg lesions in the absence of genital lesions) in yaws-endemic regions (*3*–*5*).

Beginning on October 29, 2025, several clustered cases of lower limb cutaneous ulcers predominantly affecting schoolchildren in the Kayassie community, Safroko Limba Chiefdom, Bombali District, Sierra Leone, were reported to the National Public Health Agency of Sierra Leone. The infections were originally suspected to be *Bacillus anthracis* infection. Restriction of close student-to-student contact was advised for school management, while immediate laboratory testing for pathogen identification was launched. The outbreak showed sustained transmission: 266 cases by December 24, 2025; 386 cases by January 13, 2026; and 403 cases by February 10, 2026. Patients showed progressive skin ulcerations, sometimes associated with localized edema. The ulcers predominantly occurred on the lower limbs, where opportunistic skin injuries could easily develop, and commonly manifested as a localized lesion with an irregular border. The base of the ulcer was mostly composed of dry and crusted tissue without a purulent exudate (Figure 1). Recovery progressed steadily after case treatment and management (Appendix, https://wwwnc.cdc.gov/

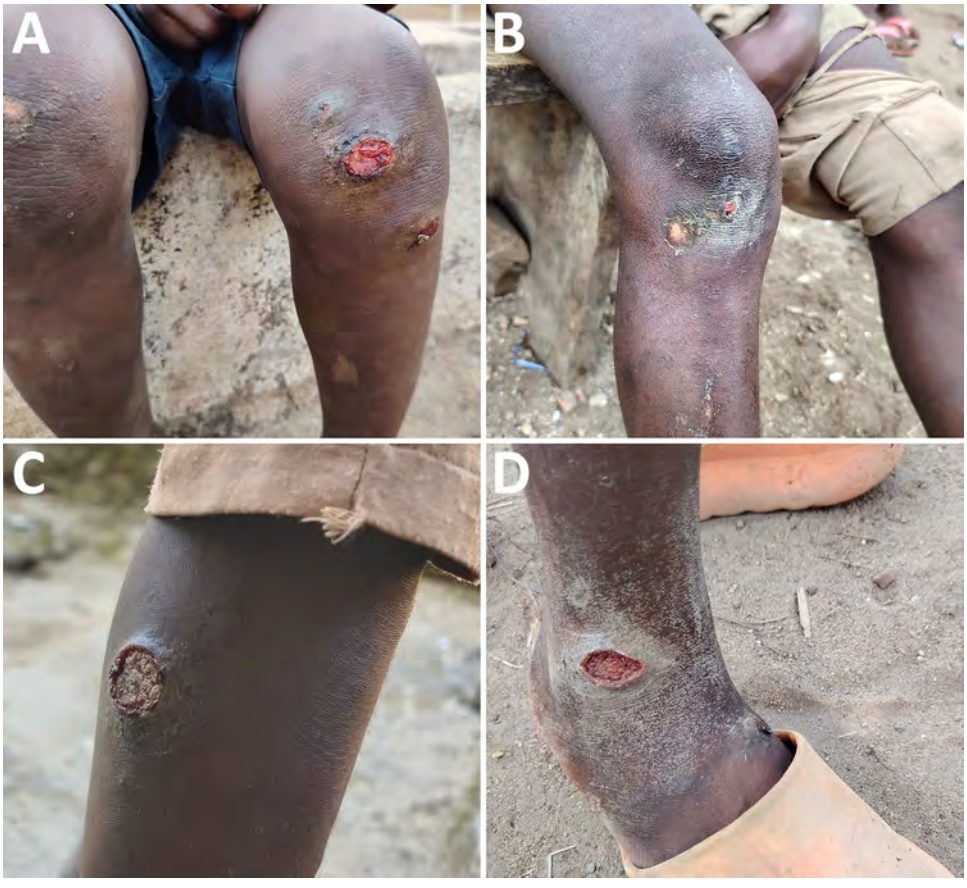

Figure 1. Irregular appearance of cutaneous ulcer lesions from patients in study of *Haemophilus ducreyi* bacteria causing cutaneous ulcer outbreak in children, Sierra Leone, December 2025. A) Lesions over the knee. B) Lesions below the knee. C) Lesions on the mid-lateral aspect of the leg. D) Lesions at the ankle.

EID/article/32/10/26-0727-App1.pdf). Skin swab sample collection was conducted with consent from all participants or their parents or guardians, and the study was conducted using deidentified data derived from routine public health programmatic activities and interventions. The study was also reviewed and approved administratively by the National Public Health Agency of Sierra Leone.

B. anthracis infection was immediately excluded in the first 7 skin swab samples by using quantitative PCR targeting *rpoB*, *pagA*(pXO1), and *capC*(pXO2) (Bio-Perfectus Technologies, https://www.biosearchtech.

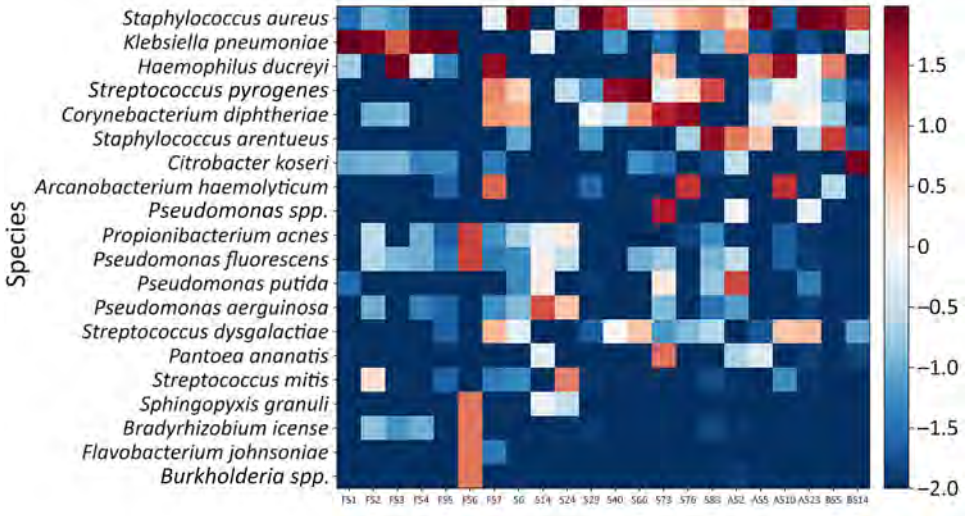

Figure 2. Heatmap of bacterial species investigated from study of *Haemophilus ducreyi* bacteria causing cutaneous ulcer outbreak in children, Sierra Leone, December 2025. Values are shown as $\log_{10}$(abundance + 0.01)%. Metagenomic analysis based on the DNBSEQ-G99 sequencing platform (MGI Tech, https://www.mgi-tech.com). The heatmap revealed that *H. ducreyi*, the third most abundant bacterium, was the most suspected causative agent through 22 skin swab samples. The samples were designated as follows: FS, samples collected on November 18, 2025; S, samples collected on December 12, 2025; AS and BS, samples collected on December 18, 2025.

com). Analysis of metagenomic sequence data produced from MinION (Oxford Nanopore Technologies, https://nanoporetech.com) (Appendix) revealed that *H. ducreyi* sequences were present in 4 of the 7 swab samples; no other relevant pathogens were identified (Appendix Figure 1). To confirm sequencing results, we performed real-time PCR according to a previous report (*6*). All of the first 7 samples tested positive for *H. ducreyi.* Those preliminary results demonstrated that *H. ducreyi* was highly associated with this cutaneous ulcer outbreak.

As the outbreak progressed, another 149 swab samples were collected and shipped to the laboratory for PCR testing. Of the 156 total samples, 96 (61.5%) tested positive for *H. ducreyi*. No DNA evidence of *T. pallidum* subsp. *pertenue*, subsp. *pallidum*, or subsp. *endemicum* bacteria was detected by quantitative PCR in any of the 156 samples (*7*).

To further determine the etiologic agent causing this outbreak, we sequenced genomic DNA from 22 swab samples (12 *H. ducreyi*–positive and 10 *H. ducreyi*–negative) on the DNBSEQ-G99 platform (MGI Tech, https://www.mgi-tech.com) (Appendix). Metagenomic analysis indicated no evidence of *T. pallidum* subsp. *pertenue* in the 22 samples, which is consistent with the PCR result. We identified no other etiologic pathogen associated with cutaneous ulcers in the 22 samples. The most abundant bacterial species were *Staphylococcus aureus* and *Klebsiella pneumoniae* (Figure 2).

To isolate *H. ducreyi*, we immediately inoculated 61 swab samples in the field onto Columbia blood agar base (Thermo Fisher Scientific, https://www.thermofisher.com), supplemented with 2.5% fresh yeast extract, 3 μg/mL of vancomycin, and 30% rabbit blood (*8*). After 96 hours of microaerophilic culture at 33°C, grayish-white pinpoint-sized colonies were picked up (*9*). After 3 consecutive subcultures, we confirmed PCR-positive colonies to be *H. ducreyi* (Appendix Figure 2). Among the 61 inoculated samples, *H. ducreyi* grew from 9 samples. Ambient transport temperature and lack of CO_2 might have reduced isolation.

We sequenced the complete genomes of 9 *H. ducreyi* strains on an Illumina platform (https://www.illumina.com) (Appendix). Phylogenetic analysis demonstrated that the 9 isolates recovered in Sierra Leone formed a cluster with strains from Ghana and were distributed into 2 separate clades (Appendix Figure 3). We submitted short reads for 22 skin swab samples and 9 strains of *H. ducreyi* bacteria to the National Center for Biotechnology Information Sequence Read Archive (https://www.ncbi.nlm.nih.gov/sra; accession no. PRJNA1450830).

To try to determine a source for the outbreak, we tested 60 saline-soaked fly samples, 8 water samples from neighboring ponds, and tissue samples from 2 goats that died during the outbreak by quantitative PCR. No samples were positive for *H. ducreyi*.

This investigation confirmed that *H. ducreyi* was the causative bacterial agent of the cutaneous ulcer outbreak among children in Bombali District, Sierra Leone, in 2025. Sierra Leone is historically classified as a yaws-endemic country (*10*), and national eradication campaigns have been conducted in past decades. This outbreak, in essence, was a protracted, low-severity outbreak of cutaneous *H. ducreyi* infection, yielding no fatalities and leading to gradual resolution under enhanced surveillance and case management. However, the source of *H. ducreyi* in this outbreak remains unclear. Clinicians should be aware of the possibility of cutaneous *H. ducreyi* infection in yaws-endemic regions.

Acknowledgments

We thank all study participants and their parents or legal guardians for their time, the field team from the National Public Health Emergency Operations Centre, the Bombali District Health Management Team, and the World Health Organization Country Office for Sierra Leone. We also thank Shiyang Cao for her constructive suggestions on the culture and isolation of *H. ducreyi*.

About the Author

Dr. Zhang works at the Chinese Academy of Agricultural Sciences, the Changchun Veterinary Research Institute, Changchun, China. His primary research interest is detection, prevention, and control of bacterial pathogens causing zoonotic diseases.

References

1. Fegan D, Glennon MJ, Kool J, Taleo F. Tropical leg ulcers in children: more than yaws. Trop Doct. 2016;46:90–3. https://doi.org/10.1177/0049475515599326
2. Marks M, Mitjà O, Solomon AW, Asiedu KB, Mabey DC. Yaws. Br Med Bull. 2015;113:91–100. https://doi.org/10.1093/bmb/ldu037
3. Mitjà O, Lukehart SA, Pokowas G, Moses P, Kapa A, Godornes C, et al. *Haemophilus ducreyi* as a cause of skin ulcers in children from a yaws-endemic area of Papua New Guinea: a prospective cohort study. Lancet Glob Health. 2014;2:e235–41. https://doi.org/10.1016/S2214-109X(14)70019-1
4. Ndzomo P, Tchatchouang S, Njih Tabah E, Njamnshi T, Tsanga MVN, Bondi JA, et al. Prevalence and risk factors associated with *Haemophilus ducreyi* cutaneous ulcers in Cameroon. PLoS Negl Trop Dis. 2023;17:e0011553. https://doi.org/10.1371/journal.pntd.0011553
5. Simpson SV, Arima H, Behene E, Nundu SS, Hammond J, Atta-Owusu R, et al. Mapping the distribution of yaws and *Haemophilus ducreyi* in the western north region of Ghana.

BMC Infect Dis. 2025;25:1763. https://doi.org/10.1186/s12879-025-12082-z
6. Glatz M, Juricevic N, Altwegg M, Bruisten S, Komericki P, Lautenschlager S, et al. A multicenter prospective trial to asses a new real-time polymerase chain reaction for detection of *Treponema pallidum*, herpes simplex-1/2 and *Haemophilus ducreyi* in genital, anal and oropharyngeal ulcers. Clin Microbiol Infect. 2014;20:O1020–7. https://doi.org/10.1111/1469-0691.12710
7. Chi KH, Danavall D, Taleo F, Pillay A, Ye T, Nachamkin E, et al. Molecular differentiation of *Treponema pallidum* subspecies in skin ulceration clinically suspected as yaws in Vanuatu using real-time multiplex PCR and serological methods. Am J Trop Med Hyg. 2015;92:134–8. https://doi.org/10.4269/ajtmh.14-0459
8. Sottnek FO, Biddle JW, Kraus SJ, Weaver RE, Stewart JA. Isolation and identification of *Haemophilus ducreyi* in a clinical study. J Clin Microbiol. 1980;12:170–4. https://doi.org/10.1128/jcm.12.2.170-174.1980
9. Alfa M. The laboratory diagnosis of *Haemophilus ducreyi*. Can J Infect Dis Med Microbiol. 2005;16:31–4. https://doi.org/10.1155/2005/851610
10. Harding RD. A yaws campaign in Sierra Leone. Trans R Soc Trop Med Hyg. 1949;42:347–66. https://doi.org/10.1016/0035-9203(49)90083-8

Address for correspondence: Mohamed B. Jalloh, National Public Health Agency, 42A Main Motor Rd, Wilberforce Village, Freetown, Sierra Leone; email: boiejalloh@npha.gov.sl; or Zhiqiang Mi, State Key Laboratory of Pathogen and Biosecurity, Academy of Military Medical Sciences, 20 Dongda St, Fengtai District, Beijing, China; email: zhiqiangmi_ime@163.com

In Memoriam: The Enduring Influence of Nancy J. Cox (1948–2026)

Daniel B. Jernigan,[1] Jacueline M. Katz,[1] Keiji Fukuda[1]

In Italian usage, *influenza* refers broadly to influence, which Treccani defines as the "influence or action exerted by the stars on human character and destinies" (*1*). Nancy J. Cox, PhD (Figure), has had an enduring and tremendous influence on the global public health and influenza scientific communities. Over a distinguished career spanning nearly 4 decades, she advanced ideas, systems, and people that shaped contemporary influenza science and practice. Through her work in epidemiology, virology, outbreak response, prevention, vaccinology, surveillance, and One Health, her leadership and diplomacy influenced institutions worldwide. She was recognized with numerous awards and leaves a legacy that will continue to shape future generations of public health scientists.

Early Life and Scientific Foundations

Nancy was born in rural Iowa in 1948 and earned a National Science Foundation scholarship to Iowa State University, completing her degree with highest honors. She then attended Cambridge University as a Marshall Scholar and entered the influenza field in the Division of Virology, Department of Pathology at Cambridge. Her early work examined molecular aspects of influenza virus replication, a foundation that shaped the rest of her career (*2*).

Her focus on the fundamental biology of influenza viruses, especially how they evolved and interacted with the immune system, led her to understand how subtle genetic and antigenic differences affect epidemics. That insight contributed to one of her most enduring public health roles: guiding the selection of influenza viruses for use in the influenza vaccine. Nancy set the standards for how an influenza virus is characterized by using genomic and antigenic testing. As the head of a World Health Organization (WHO) Collaborating Center for Surveillance, Epidemiology, and Control of Influenza at the Centers for Disease Control and Prevention (CDC), she provided globally recognized leadership for the process used for preparing and selecting viruses for updating influenza vaccines.

Over 37 years at CDC, Nancy helped transform a small team of scientists into the preeminent global center for influenza surveillance, epidemiology, research, and preparedness. She authored more than 278 scientific publications and helped define 3 pillars of modern influenza work: quantifying disease burden, characterizing emerging viruses, and using global systems for surveillance and response.

There were 2 settings where Nancy was most comfortable in her professional life. The first was when she was diving deep into the testing of viruses. At weekly meetings, Nancy was always at the head of the table, often wearing a tailored suit jacket, and leading her staff as they reviewed detailed spreadsheets of virus test data. Such gatherings were an odd hybrid of cutting-edge biotechnology and priestly ritual, divining the future of each virus.

The other setting was at small international meetings, where Nancy would engage in deep conversations on virus protein structure with colleagues during the day and then stay up late with the same friends sharing stories and recollections. Nancy understood that the best scientific collaborations were built not only on shared questions and rigorous methods but also on trust, respect, generosity, and genuine care for the people doing the work.

Translating Virology into Public Health Action

Nancy could see the connections between what a virus was doing in the laboratory and how those findings might affect global vaccine policy. She knew the science and she understood the politics. She could see how it all came together, from the genome in the laboratory to the geopolitical in Geneva. She integrated information across disciplines, spanning virus detection to disease prevention, and made it accessible and relevant for a comprehensive global influenza intelligence system.

Nancy loved having things well-categorized, appropriately named, and understandable. She led the development of the Influenza Risk Assessment Tool,

Author affiliations: Johns Hopkins Bloomberg School of Public Health (D. Jernigan); retired (J. Katz, K. Fukuda)

DOI: https://doi.org/10.3201/eid3210.260830

[1]All authors contributed equally to this article.

a structured framework for integrating virologic, epidemiologic, and population-level data to compare the pandemic potential of novel influenza A viruses (*3*). That framework has guided decision-making for novel influenza A viruses and reflects one of her signature approaches: moving from "what is this virus?" to "what should the world do about it?"

Architect of Global Influenza Surveillance and Vaccine Virus Selection

In 1992, Nancy became chief of CDC's Influenza Branch and Director of the WHO Collaborating Center for Surveillance, Epidemiology, and Control of Influenza at CDC. In those roles, she strengthened WHO's Global Influenza Surveillance and Response System (GISRS), a worldwide network of laboratories and public health institutions (*4*,*5*). Now comprising more than 160 National Influenza Centers in 136 countries and 7 Collaborating Centers, GISRS is the world's main system for tracking influenza virus evolution in real time, selecting viruses for annual influenza vaccines and identifying viruses with pandemic potential (*6*).

Nancy foresaw the importance of China's development of influenza monitoring capacities because of the role of China and other countries in the region in the emergence of new influenza virus variants. Collaborating with WHO, she helped expand GISRS and build surveillance and response capabilities in many countries; these systems later proved fundamental during the COVID-19 pandemic. Her efforts expanded the global footprint of the CDC Influenza Division's technical and funding support to national laboratories all around the world. That investment grew substantially over time to fill a critical gap in global surveillance and influenza prevention programs, and created an enduring trust of global partners in CDC, something Nancy championed as a requirement for collaborative responses to influenza threats.

She also oversaw establishment of the Influenza Reagent Resource (later named the International Reagent Resource) to support manufacturing, stockpiling, and distribution of diagnostic reagents and test kits globally. This service fundamentally changed global surveillance by removing costs of core reagents and materials as a roadblock to robust surveillance systems.

Nancy advanced modernization of influenza virus characterization methods. She promoted a "Seq-First" approach, in which genomic sequencing precedes traditional antigenic and serologic testing, enabling laboratories to expand evaluation of new variants for possible incorporation into seasonal influenza vaccines. Her focus on annual global and national vaccine strain selection, in partnership with WHO and the US Food and Drug Administration, was a key contribution to public health.

Figure. Nancy J. Cox (1948–2026) in June 2008. Photograph courtesy of the Centers for Disease Control and Prevention.

Richard Hatchett, chief executive officer of the Coalition for Epidemic Preparedness Innovations, stated, "Nancy was a giant and a tremendous advocate for science, public health, and international partnership. She played a huge role in establishing the international surveillance networks that protect us all, and her dedication to her work and to public service was immense."

Responding to Emerging Threats

Nancy's career spanned the emergence of highly pathogenic avian influenza A(H5N1) in 1997 (*7*), the 2009 influenza A(H1N1) pandemic (*8*), and influenza A(H7N9) in China in 2013 (*9*). In those events, she helped define how animal influenza viruses can cross species barriers to humans, leading her to emphasize integration of animal and human surveillance, an approach central to contemporary One Health strategies.

During the 2009 H1N1 pandemic, she guided US response policies, providing steadiness, clarity, and confidence, and serving as a trusted voice for public and private stakeholders. Her dedication and persistence shone clearly when, early in the pandemic response, her home was struck by lightning and burned down. When most people would have been near a breaking point, Nancy was still driving the response forward, focused on the outcome rather than the obstacle.

Building Bridges through Influenza Diplomacy

Nancy believed in, and exemplified, CDC's longstanding role of assisting countries around the world. She also believed that the United States and the international community were best served when scientific and public health knowledge, experience, and support were shared.

She was recognized internationally as a uniquely authoritative and trusted influenza expert. WHO frequently sought her wisdom and assistance for critical activities, including development and evaluation of new Collaborating Centers, Pandemic Influenza Preparedness Framework negotiations, and international missions to assess complex situations such as influenza A(H7N9) in China and influenza A(H5N1) in Egypt.

Dr. Margaret Chan, former director-general of WHO, wrote: "Your commitment, dedication, scientific attitude and quality of work has inspired everyone in the influenza community and has set an excellent example for the public health. We will miss your brilliant insights, unmatchable expertise, strong leadership and diplomatic skills, as well as your energy, dynamism and grace in our continuous defense against influenza threat."

Mentor and Advocate

Nancy was a mentor and inspiration to scientists within her own team and around the world. Her scientific excellence, tireless work ethic, and collegial attitude inspired respect and admiration and provided a role model for young and senior scientists alike.

Dr. Rebecca J. Garten Kondor, who has taken on the important role of guiding vaccine virus selection in CDC's Influenza Division, recalled, "Early in my career I was fortunate to benefit from Nancy's leadership and mentorship, where I learned the value of bringing multiple disciplines to the table and setting high standards of scientific rigor and integrity. Getting it right—and having confidence in our results—is essential because CDC science is widely respected, and sharing our analysis capabilities and know-how with global partners strengthens influenza surveillance and pandemic preparedness."

Professor Yoshi Kawaoka stated, "So much of my career has been influenced by your work. You leave behind a wonderful footprint — you have touched the lives of and will be missed by many." Professor Guan Yi, University of Hong Kong, China, called her "a scientist of extraordinary vision, a tireless diplomat of public health, and a deeply cherished friend and mentor to so many of us in the global influenza research community."

Upon Nancy's retirement in 2014, then-Senator Tom Harkin (D-Iowa) honored her by stating in the Congressional Record, "During her 37 years at CDC, Dr. Cox has served as mentor, educator, supervisor, and supporter to hundreds of individuals: undergraduates, medical and PhD students, postdoctoral fellows, laboratory and epidemiology staff members, journalists, and visiting researchers" (*10*).

Recognition and Enduring Legacy

Nancy was referred to as a "walking encyclopedia of influenza," and her knowledge of influenza was legendary. She fostered a culture of high quality, scientific excellence, mutual respect, and accountability, and led through example. One former colleague said, "She held our feet to scientific fire, only because she could walk across those coals." Nancy spent her career raising the bar for scientific excellence, an approach needed now more than ever.

Nancy received numerous awards, including the Samuel J. Heyman Service to America Medal as Federal Employee of the Year in 2006 and recognition by Time magazine as one of the 100 most influential people of 2006. Dr. Anthony Fauci, former Director of the National Institute of Allergy and Infectious Diseases at the National Institutes of Health, considered her "one of the leading figures in the influenza research community," whose work "benefitted millions of Americans and people around the world."

Professionally, her legacy is reflected in the systems she helped build: global surveillance networks, vaccine selection processes, and preparedness frameworks that continue to protect populations worldwide. Personally, among those privileged to know and work with her, the deepest impression is her legacy of warmth, generosity, fairness, inclusiveness, and commitment to public health.

Dr. Nancy Cox died on April 23, 2026. She is survived by her husband, daughter, her granddaughter, stepson and wife, three step-grandchildren, and other family members.

About the Author

Dr. Jernigan is a contributing scholar at Johns Hopkins Bloomberg School of Public Health. Formerly, he headed the Influenza Division at CDC's National Center for Immunization and Respiratory Diseases and later served as director of CDC's National Center for Emerging and Zoonotic Infectious Diseases.

References

1. Istituto della Enciclopedia Italiana Fondata da Giovanni Treccani. Vocabolario Treccani. Influenza [in Italian] [cited 2026 May 20]. https://www.treccani.it/vocabolario/influenza
2. Mahy BW, Cox NJ, Armstrong SJ, Barry RD. Multiplication of influenza virus in the presence of cordycepin, an inhibitor of cellular RNA synthesis. Nat New Biol. 1973;243:172–4. https://doi.org/10.1038/newbio243172a0
3. Trock SC, Burke SA, Cox NJ. Development of framework for assessing influenza virus pandemic risk. Emerg Infect Dis. 2015;21:1372–8. https://doi.org/10.3201/eid2108.141086
4. Cox NJ, Brammer TL, Regnery HL. Influenza: global surveillance for epidemic and pandemic variants. Eur J Epidemiol. 1994;10:467–70. https://doi.org/10.1007/BF01719678
5. Ziegler T, Mamahit A, Cox NJ. 65 years of influenza surveillance by a World Health Organization-coordinated global network. Influenza Other Respir Viruses. 2018;12:558–65. https://doi.org/10.1111/irv.12570
6. Centers for Disease Control and Prevention. CDC's World Health Organization (WHO) Collaborating Center for Surveillance, Epidemiology and Control of Influenza. 2024 Sep 12 [cited 2026 Apr 29]. https://www.cdc.gov/flu/php/who-collaboration/index.html
7. Bridges CB, Lim W, Hu-Primmer J, Sims L, Fukuda K, Mak KH, et al. Risk of influenza A (H5N1) infection among poultry workers, Hong Kong, 1997–1998. J Infect Dis. 2002;185:1005–10. https://doi.org/10.1086/340044
8. Garten RJ, Davis CT, Russell CA, Shu B, Lindstrom S, Balish A, et al. Antigenic and genetic characteristics of swine-origin 2009 A(H1N1) influenza viruses circulating in humans. Science. 2009;325:197–201. https://doi.org/10.1126/science.1176225
9. Jernigan DB, Cox NJ. H7N9: preparing for the unexpected in influenza. Annu Rev Med. 2015;66:361–71. https://doi.org/10.1146/annurev-med-010714-112311
10. US Congress. Congressional record of the 113th Congress, 2nd session. Volume 160, Number 140. p. S5984. Recognizing Nancy J. Cox [2014 Nov 13] [cited 2026 May 5]. https://www.congress.gov/113/crec/2014/11/13/CREC-2014-11-13-pt1-PgS5983.pdf

Address for correspondence: Daniel B. Jernigan, Johns Hopkins Bloomberg School of Public Health, 700 E Pratt St, Ste 900, Baltimore, MD 21202, USA; email: djernig3@jhu.edu

etymologia revisited

Dermatophilus congolensis

[dur″mə-tof′-s con-gō-len′sis]

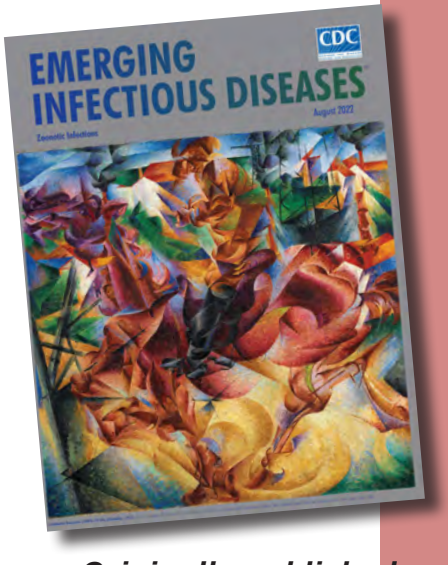

Originally published in August 2022

Dermatophilus congolensis From the Greek *derma* (skin) + *philos* (loving), *Dermatophilus congolensis* is a Gram-positive, aerobic actinomycete, and facultatively anaerobic bacteria. D. congolensis infects the epidermis and produces exudative dermatitis termed dermatophilosis that was previously known as rain rot, rain scald, streptotrichosis, and mycotic dermatitis.

In 1915, René Van Saceghem, a Belgian military veterinarian stationed at a veterinary laboratory in the former Belgian Congo (thus, the species name *congolensis*), reported *D. congolensis* from exudative dermatitis in cattle. Local breeders and veterinarians had observed the disease since 1910, but the causal agent was not identified.

Dermatophilosis affects animals, mainly cattle, and more rarely humans. Outbreaks of *D. congolensis* infection have severe economic implications in the livestock and leather industries.

Sources

1. Amor A, Enríquez A, Corcuera MT, Toro C, Herrero D, Baquero M. Is infection by *Dermatophilus congolensis* underdiagnosed? J Clin Microbiol. 2011;49:449–51. https://doi.org/10.1128/JCM.01117-10
2. Branford I, Johnson S, Chapwanya A, Zayas S, Boyen F, Mielcarska MB, et al. Comprehensive molecular dissection of *Dermatophilus congolensis* genome and first observation of *tet*(z) tetracycline resistance. Int J Mol Sci. 2021;22:7128. https://doi.org/10.3390/ijms22137128
3. Dorland's illustrated medical dictionary. 32nd ed. Philadelphia: Elsevier Saunders; 2012.
4. Van Saceghem R. Contagious skin disease (contagious impetigo) [in French]. Bull Soc Pathol Exot. 1915;8:354–9.

https:// wwwnc.cdc.gov/eid/article/28/8/et-2808_article

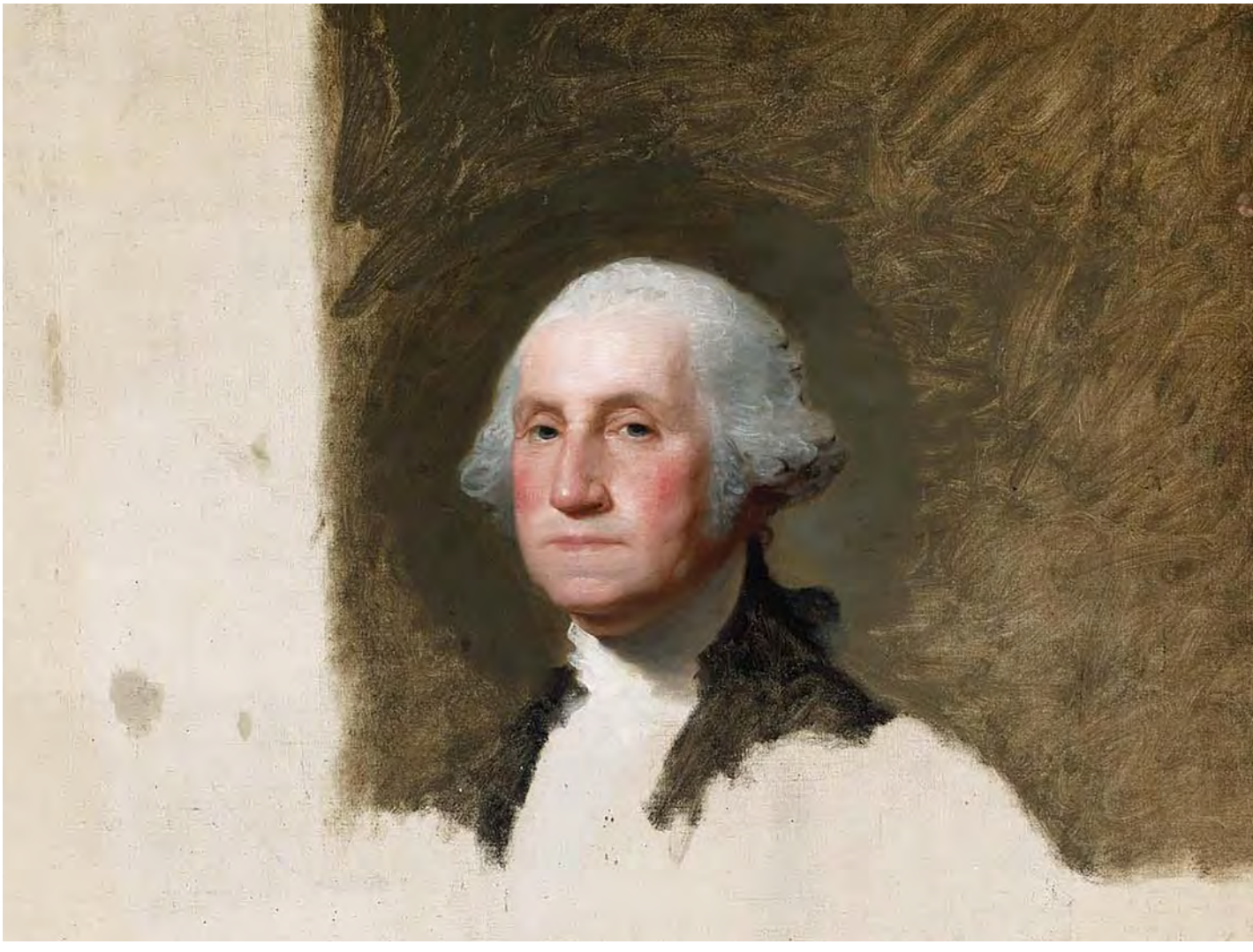

Gilbert Stuart, *George Washington*, 1796 (detail). Oil on canvas. 121.9 cm × 94 cm (48 in × 37 in). Museum of Fine Arts, Boston, Massachusetts, USA. Co-owned by the National Portrait Gallery, Washington, DC, USA.

Smallpox History and Decisive Actions of George Washington

Terence Chorba

As the United States celebrates its semiquincentennial year, the nation's first president, George Washington, is a focal point. On the cover of this month's *Emerging Infectious Diseases* is one of his best-known representations, the second Washington portrait that Gilbert Stuart (1755–1828) painted. This painting was commissioned by Washington's wife, Martha, and begun in 1796. Stuart never wanted to part with this work and hence left it unfinished. This painting later became the template for the engraving of Washington on the US $1 bill.

A Rhode Islander by birth, Stuart had studied portraiture with Benjamin West in London, UK, pursued a brilliant career as a portraitist in Britain and

Author affiliation: Centers for Disease Control and Prevention, Atlanta, Georgia, USA

DOI: https://doi.org/10.3201/eid3210.AC3210

Ireland, and returned to the United States in 1793. In addition to George Washington, he created portraits of Martha Washington (Figure), as well as John Jay, John Adams, Thomas Jefferson, John Quincy Adams, James Madison, and James Monroe, among others.

In 1751, Lawrence Washington, George's elder half-brother, was suffering from tuberculosis and had George accompany him to Barbados as a potential refuge. During that stay, the younger Washington contracted smallpox, enduring an illness lasting several weeks with residual minor facial scarring (*1*). Although the cover painting and others of Washington by Stuart are devoid of smallpox scars, at least one less-idealized Washington portrait rendered by William Joseph Williams from 1794 shows residual pockmarks (*2*). Washington's firsthand familiarity with the progression and consequences of smallpox would later inform his decisions related to the health of the troops, demonstrated in several pieces of correspondence cited in this essay. In a set of general orders written in March 1776 in Boston, Washington observed that "as the enemy with a malicious assiduity, have spread the infection of the smallpox through all parts of the town, nothing but the utmost caution on our part, can prevent that fatal disease from spreading thro' the army, and country, to the infinite detriment of both" (*3*).

As a preventive measure for smallpox, variolation was first promoted in the New World by Puritan minister Cotton Mather in 1721 (*4*). The procedure entailed insertion or rubbing of infectious material from pustules of persons infected with smallpox into the skin of persons who had not previously been infected. That process usually resulted in infection with mild symptoms, but also carried risk for potential spread of infection to others and for severe disease or death (*5*). However, variolation had a much lower associated case-fatality rate than that of naturally acquired smallpox, which was usually 25%–30% (*6*). In a well-documented epidemic in Boston, Massachusetts, in 1752, the reported mortality rate for those with natural smallpox was an unusually low 9%, but the rate was only 1.5% among those who underwent variolation (*4*). In a Charleston, South Carolina, epidemic in 1760, the mortality rate for natural smallpox cases was 34% but only 2.6% among those variolated (*4*).

Washington's evolving stance on variolation reflected consideration of and respect for medical innovation, its attendant hazards, and military necessity. In 1776, as Commander-in-Chief of the Continental Army, he initially prohibited routine variolation. His reasoning was strategic: some soldiers undergoing variolation would be incapacitated for weeks,

Figure. Gilbert Stuart, *Martha Washington*, 1796 (detail). Oil on canvas. 121.9 cm × 94.3 cm (48 in × 37 in). National Portrait Gallery, Washington, DC, USA. Co-owned by the Museum of Fine Arts, Boston, Massachusetts, USA.

potentially leaving the army vulnerable at a critical juncture in the war. He observed, "… should We innoculate generally, the Enemy, knowing it, will certainly take Advantage of our Situation" (*7*). Given the precarious position of the colonial forces, the temporary loss of short-term operational readiness was a risk (*4*). However, smallpox outbreaks threatened losses, and Washington reversed his earlier policy. In February 1777, he ordered the systematic inoculation (i.e., variolation) of Continental troops:

> Finding the Small pox to be spreading… I have determined that the troops shall be inoculated…. Necessity not only authorizes but seems to require the measure, for should the disorder infect the Army in the natural way and rage with its usual virulence we should have more to dread from it than from the Sword of the Enemy (*8*).

In correspondence with John Hancock, Washington justified the decision as necessary, despite its inherent drawbacks: "… I find it impossible to keep it from spreading thro' the whole Army in the natural way. I have therefore determined, not only to innoculate all the Troops now here, that have not had it, but… to innoculate the Recruits as fast as they come in…" (*9*). New recruits would be inoculated upon arrival, recover while being trained and equipped, and then join the ranks immunized and combat-ready.

Elizabeth Fenn, author of *Pox Americana: The Great Smallpox Epidemic of 1775–82*, has noted that, in opting for universal variolation of the troops, "the general had outflanked his enemy" (*10*). By the end of 1777, tens of thousands of soldiers had undergone inoculation. The policy was an effective, organized public health intervention, demonstrating the capacity of centralized authority to manage disease on a large scale (*4*).

In 1796, English physician Edward Jenner identified a safer alternative. Observing that milkmaids who had contracted cowpox appeared resistant to smallpox, Jenner hypothesized that exposure to cowpox could protect against smallpox. His experimental inoculation of a young boy with cowpox material—and the boy's subsequent immunity to smallpox—provided compelling evidence for vaccination (*11*). Inoculations with extracts from cowpox lesions (vaccination) or from horsepox lesions (equination) were safer and averted the onward transmission of smallpox. Vaccination succeeded because the species *Cowpox virus* and *Variola virus* (i.e., smallpox) belong to the same family (Poxviridae) and genus (*Orthopoxvirus*) of viruses, and some *Orthopoxvirus* species generate cross-immunity against infection with others.

In summary, smallpox played a central role in the American Revolution, posing what was perhaps a greater threat than the British to the Continental Army. Washington's variolation program represented not merely a public health decision but a strategic military innovation with far-reaching consequences. That measure established an early precedent for government-led, population-level public health intervention. The intersection of Washington's disease understanding, personal experience, and military leadership resulted in decisive implementation of immunization before there was vaccination; its impact was in the interest of public health and disease control and to the great advantage of the troops.

The author discloses using ChatGPT (OpenAI, https://openai.com) only for locating references for this essay, not in generating content.

References

1. Chernow R. Washington: a life. New York: Penguin Press; 2010.
2. Williams WJ. Portrait of George Washington in Masonic regalia, 1794. Wikimedia Commons [cited 2026 Sep 10]. https://commons.wikimedia.org/wiki/File:Portrait_of_George_Washington_in_Masonic_regalia_by_William_Joseph_Williams,_1794.jpg
3. Washington G. General orders,13 March 1776. Founders Online, National Archives [cited 2026 Sep 10]. https://founders.archives.gov/documents/Washington/03-03-02-0336
4. Wehrman A. The contagion of liberty: the politics of smallpox in the American Revolution. Baltimore (MD): Johns Hopkins University Press; 2022.
5. Hopkins DR. The greatest killer: smallpox in history. Chicago: University of Chicago Press; 2002.
6. Weiss RA, Esparza J. The prevention and eradication of smallpox: a commentary on Sloane (1755) 'An account of inoculation'. Philos Trans R Soc Lond B Biol Sci. 2015;370:20140378. https://doi.org/10.1098/rstb.2014.0378
7. Washington G. To Major General Horatio Gates, 5–6 February 1777. Founders Online, National Archives [cited 2026 Sep 10]. https://founders.archives.gov/documents/Washington/03-08-02-0267
8. Washington G. To William Shippen Jr., 6 February 1777. Founders Online, National Archives [cited 2026 Sep 10]. https://founders.archives.gov/documents/Washington/03-08-02-0281
9. Washington G. To John Hancock, 5 February 1777. Founders Online, National Archives [cited 2026 Sep 10]. https://founders.archives.gov/documents/Washington/03-08-02-0268
10. Fenn EA. Pox Americana: the great smallpox epidemic of 1775–82. New York: Hill and Wang; 2001.
11. Jenner E. An inquiry into the causes and effects of the variolae vaccinae. London: Samson Low; 1798.

Address for correspondence: Terence Chorba, Centers for Disease Control and Prevention, 1600 Clifton Rd NE, Mailstop H24-4, Atlanta, GA 30329-4018, USA; email: tlc2@cdc.gov

EMERGING INFECTIOUS DISEASES®

Upcoming Issue • Measles and Other Respiratory Infections

- Public Health Gains Are Never Permanent—Lessons Learned from Measles Resurgence, Bangladesh, 2026
- Predictors and Patterns of Metastatic *Candidozyma auris* Infection, Spain, 2016–2024
- Importation-Driven Measles Resurgence and the Fragility of Elimination, Japan, 2024–2026
- Subacute Sclerosing Panencephalitis after Measles Outbreaks, Philippines, 2007–2022
- Five-Biomarker Definition for Hypervirulent *Klebsiella pneumoniae* Bloodstream Infection and Abscess Complications, Japan, 2022–2024
- Effects of Antibiotic Use Reduction on *Clostridioides difficile* Colonization in Nursing Homes
- Emergence of Novel *Mycoplasma pneumoniae* Macrolide-resistant Sequence type 3 Subclades during Post–COVID-19 Resurgence in Children
- Microbial Etiology of Postoperative Spinal Fusion Infections and Factors Associated with Gram-Negative Infections
- Invasive Enterovirus and Parechovirus Infections in Adults, Alberta, Canada, 2023–2025
- Global Genomic Surveillance of MERS-CoV
- Middle East Respiratory Syndrome Coronavirus in Camels, Kazakhstan, 2025
- A Dual-Duplex RT-dPCR Approach for Discriminating Avian and Seasonal Influenza Viruses in Wastewater
- Pathotypr: Harmonised MTBC Lineage Assignment and Resistance-Associated Variant Detection for Genomic Surveillance
- Choral Voices, Communal Vulnerability
- *Dirofilaria asiatica* Infections and Asymptomatic Microfilaraemia, Sri Lanka, 2025
- Post–COVID-19 Expansion of M1UK- and M113SNPs-Associated *Streptococcus pyogenes* Lineages Causing Streptococcal Toxic Shock Syndrome, Japan
- Persistent Microfilaraemia with Zoonotic *Dirofilaria asiatica* in a 2-Year-Old Child, Sri Lanka, 2024
- Fatal *Rickettsia parkeri* rickettsiosis in Immunocompromised Pediatric Patient
- Transmission Dynamics of Dengue Virus, Ceará State, Brazil, 2010–2025
- MERS-CoV Serological Testing in the Context of SARS-CoV-2 Cross-Reactive Immune Responses
- Pediatric Deaths during Measles Outbreak, Jerusalem, Israel, 2025–2026
- Serologic assessment of Public Health Action Needed for Trachoma,Coastal Ecuador, 2021–2024
- Systemic *Spiroplasma turonicum* Infection Manifested as Knee Arthritis, France, 2025
- Disseminated Cotrimoxazole-Resistant Nocardiosis in a Renal Transplant Recipient
- Community Transmission of Pneumonic Plague, Fenoarivobe, Madagascar, 2022
- Evidence of Exposure to Highly Pathogenic Avian Influenza H5 Viruses in East Greenland Polar Bears
- Nationwide Surveillance and Control Measures during Large Measles Outbreak, Bangladesh, 2026

Complete list of articles in the November issue at http://www.cdc.gov/eid/#issue-336

Earning CME Credit

To obtain credit, you should first read the journal article. After reading the article, you should be able to answer the following, related, multiple-choice questions. To complete the questions (with a minimum 75% passing score) and earn continuing medical education (CME) credit, please go to http://www.medscape.org/journal/eid. Credit cannot be obtained for tests completed on paper, although you may use the worksheet below to keep a record of your answers.

You must be a registered user on http://www.medscape.org. If you are not registered on http://www.medscape.org, please click on the "Register" link on the right hand side of the website.

Only one answer is correct for each question. Once you successfully answer all post-test questions, you will be able to view and/or print your certificate. For questions regarding this activity, contact the accredited provider, CME@medscape.net. For technical assistance, contact CME@medscape.net. American Medical Association's Physician's Recognition Award (AMA PRA) credits are accepted in the US as evidence of participation in CME activities. For further information on this award, please go to https://www.ama-assn.org. The AMA has determined that physicians not licensed in the US who participate in this CME activity are eligible for *AMA PRA Category 1 Credits*™. Through agreements that the AMA has made with agencies in some countries, AMA PRA credit may be acceptable as evidence of participation in CME activities. If you are not licensed in the US, please complete the questions online, print the AMA PRA CME credit certificate, and present it to your national medical association for review.

Article Title

Meta-Analysis of Maternal and Fetal Outcomes of Crimean-Congo Hemorrhagic Fever during Pregnancy

CME Questions

1. Which of the following statements regarding the epidemiology of Crimean-Congo hemorrhagic fever (CCHF) in the current study is most accurate?

A. Most cases were diagnosed in Russia
B. Most cases were diagnosed in the third trimester
C. Most cases were diagnosed in the first trimester
D. Tick exposure was reported in two-thirds of cases

2. What was the most common presenting symptom among CCHF cases in the current study?

A. Vaginal bleeding
B. Mucosal bleeding
C. Fever
D. Abdominal pain

3. What was the most salient factor associated with maternal mortality due to CCHF in the current study?

A. Age >35 years
B. The presence of gestational diabetes
C. Advancing gestational age
D. The presence of preeclampsia

4. What was the most salient factor associated with fetal loss in the current study?

A. Infection during the first trimester
B. Infection during the third trimester
C. Clinical presentation with mucosal bleeding
D. Living in Africa